seit 1558

Modular polymer-based architectures for light absorption and directional charge transport

Dissertation

(kumulativ)

zur Erlangung des akademischen Grades

doctor rerum naturalium (Dr. rer. nat.)

vorgelegt dem Rat der Chemisch-Geowissenschaftlichen Fakultät

der Friedrich-Schiller-Universität Jena

von Dipl.-Chem. Robert Schroot

geboren am 22.09.1989 in Jena

Gutachter:

1. Prof. Dr. Ulrich S. Schubert – Friedrich-Schiller-Universität Jena
2. Prof. Dr. Benjamin Dietzek – Friedrich-Schiller-Universität Jena
3. Prof. Dr. Mukundan Thelakkat – Universität Bayreuth

Tag der öffentlichen Verteidigung: 07. Februar 2018

Table of contents

Documentation of authorship

This section contains a list of individual authors' contributions to the publications reprinted in this thesis.

P1) "Synthetic approaches towards structurally-defined electrochemically and (photo)redox-active polymer architectures" R. Schroot,[1] M. Jäger,[2] U. S. Schubert,[3] *Chem. Soc. Rev.* **2017**, *46*, 2754-2798.			
Author	1	2	3
Conceptual contribution	x	x	
Preparation of the manuscript	x		
Correction of the manuscript	x	x	x
Supervision of R. Schroot		x	x
Proposal for crediting publication equivalents	0.5		

P2) "Modular assembly of poly(naphthalene diimide) and Ru(II) dyes for an efficient light-induced charge separation in hierarchically controlled polymer architectures" R. Schroot,[1] T. Schlotthauer,[2] U. S. Schubert,[3] M. Jäger,[4] *Macromolecules* **2016***, 49,* 2112-2123.				
Author	1	2	3	4
Conception of the manuscript	x	x		x
Synthesis of monomers, polymers, complexes and dyads	x	x		
Preparation of the manuscript	x	x		
Spectroscopic characterization	x	x		
Correction of the manuscript	x	x	x	x
Supervision of R. Schroot			x	x
Proposal for crediting publication equivalents	1.0	1.0		

P3) "Hydrophilic poly(naphthalene diimide) based acceptor-photosensitizer dyads: Towards water-processible modular photoredox-active architectures" R. Schroot,[1] T. Schlotthauer,[2] M. Jäger,[3] U. S. Schubert,[4] *Macromol. Chem. Phys.* **2017**, *218*, 1600534.				
Author	1	2	3	4
Conception of the manuscript	x		x	
Synthesis and characterization of monomers, polymers, and dyad	x			

Complex synthesis and characterization		x		
Preparation of the manuscript	x	x		
Correction of the manuscript	x	x	x	x
Supervision of R. Schroot			x	x
Proposal for crediting publication equivalents	1.0	0.5		

P4) "Poly(*N*-alkyl-3,6-carbazole)s via Kumada catalyst transfer polymerization: Impact of metal-halogen exchange" R. Schroot,[1] U. S. Schubert,[2] M. Jäger,[3] *Macromolecules* **2016***, 49,* 8801-8811.			
Author	1	2	3
Conceptual contribution	x		x
Synthesis of monomers and polymers	x		
Preparation of the manuscript	x		
Correction of the manuscript	x	x	x
Supervision of R. Schroot		x	x
Proposal for crediting publication equivalents	1.0		

P5) "Poly(*N*-alkyl-3,6-carbazole)s via Suzuki–Miyaura polymerization: From macrocyclization toward end functionalization" R. Schroot,[1] U. S. Schubert,[2] M. Jäger,[3] *Macromolecules* **2017**, *50*, 1319-1330.			
Author	1	2	3
Conceptual contribution	x		x
Synthesis of monomers and polymers	x		
Preparation of the manuscript	x		
Correction of the manuscript	x	x	x
Supervision of R. Schroot		x	x
Proposal for crediting publication equivalents	1.0		

P6) "*Block* copolymer-type architecture with a central Ru^{II} sensitizer core: Conjugated poly(carbazole) for enhanced charge separation" R. Schroot,[1] T. Schlotthauer,[2] B. Dietzek,[3] M. Jäger,[4] U. S. Schubert,[5] submitted.					
Author	1	2	3	4	5
Conception of the manuscript	x			x	
Synthesis and characterization of monomers, polymers, dyad and triad	x				
Complex synthesis and characterization		x			
Transient absorption spectroscopy				x	
Preparation of the manuscript	x	x			
Correction of the manuscript	x	x	x	x	x
Supervision of R. Schroot				x	x
Proposal for crediting publication equivalents	1.0	0.5			

P7) "A *multi*donor-photosensitizer-*multi*acceptor triad for long-lived directional charge separation" T. Schlotthauer,[1] R. Schroot,[2] S. Glover,[3] L. Hammarström,[4] M. Jäger,[5] U. S. Schubert,[6] submitted.						
Author	1	2	3	4	5	6
Conceptual contribution	x	x			x	
Synthesis of monomers and polymers		x				
Complex synthesis	x					
Synthesis and characterization of dyad and triad	x					
Spectroscopic studies			x			
Preparation of the manuscript	x	x			x	
Correction of the manuscript	x	x	x	x	x	x
Supervision of R. Schroot					x	x
Proposal for crediting publication equivalents	1.0	0.5				

Erklärung zu den Eigenanteilen des Promovenden/der Promovendin sowie der weiteren Doktoranden/Doktorandinnen als Koautoren an den Publikationen und Zweitpublikationsrechten bei einer kumulativen Dissertation

Für alle in dieser kumulativen Dissertation verwendeten Manuskripte liegen die notwendigen Genehmigungen der Verlage („Reprint permissions“) für die Zweitpublikation vor.

Die Co-Autoren der in dieser kumulativen Dissertation verwendeten Manuskripte sind sowohl über die Nutzung, als auch über die oben angegebenen Eigenanteile der weiteren Doktoranden/Doktorandinnen als Co-Autoren an den Publikationen und Zweitpublikationsrechten bei einer kumulativen Dissertation informiert und stimmen dem zu (es wird empfohlen, diese grundsätzliche Zustimmung bereits mit Einreichung der Veröffentlichung einzuholen bzw. die Gewichtung der Anteile parallel zur Einreichung zu klären).

Die Anteile des Promovenden sowie der weiteren Doktoranden/Doktorandinnen als Co-Autoren an den Publikationen und Zweitpublikationsrechten bei einer kumulativen Dissertation sind in der Anlage aufgeführt

Name Promovend	Datum	Ort	Unterschrift
Robert Schroot	29.06.2017	Jena	

Ich bin mit der Abfassung der Dissertation als publikationsbasiert, d.h. kumulativ, einverstanden und bestätige die vorstehenden Angaben. Eine entsprechend begründete Befürwortung mit Angabe des wissenschaftlichen Anteils des Doktoranden/der Doktorandin an den verwendeten Publikationen werde ich parallel an den Rat der Fakultät der Chemisch-Geowissenschaftlichen Fakultät richten.

Name Erstbetreuer(in)	Datum	Ort	Unterschrift
Prof. Dr. Ulrich S. Schubert	29.06.2017	Jena	

1. Introduction

In view of the pollution of the environment and the climate change, a sustainable and environmentally friendly energy supply is a major challenge in the 21st century. The use of renewable energy sources, *e.g.*, wind, water or solar energy, represents a promising alternative to the consumption of fossil fuels or nuclear power. In particular, the conversion of light into electrical or chemical bond energy is of special interest in today's research due to the nearly endless amount of light provided by the sun.[1-5]

The energy conversion in photovoltaic, photosynthetic or photocatalytic cells is based on various charge transfer steps after initial light absorption. Finally, the generated charges are collected at an electrode or are consumed in a catalytic reaction.[3-6] The individual steps, *i.e.*, light absorption, charge transfer and charge accumulation, must be precisely tuned to avoid undesired recombination reactions and to achieve a high overall energy conversion efficiency. In case of bulk heterojunction solar cells, the light absorption and charge transport processes occur simultaneously within the active material and at the interfaces. Therefore, a precise tuning of the individual steps is hampered without influencing the whole system. In this regard, a promising approach decouples the processes by the utilization of functional building blocks, *i.e.*, a photosensitizer (P) for light absorption and electron donor (D) and acceptor (A) sites to separate the electron-hole pair by a sequence of charge transfer steps. So, the units can be prepared and optimized individually and the occurring processes can be studied and compared in the building units. The strength of this approach is impressively demonstrated by the highly efficient charge separation in low molar mass D−P−A triads reaching more than 95% charge separation quantum yields.[5] However, in these small molecules, the charges are locally trapped and finally recombine as no further charge transport to an electrode or catalyst is possible.

As an alternative approach, polymers can be utilized as electron donor or acceptor sites in combination with a functional photosensitizer in a modular assembly. As a consequence, additional directional percolation pathways by electron transfer processes in the polymer chain are facilitated and, moreover, a charge accumulation or the assembly of the architectures with a spatial separation of the conducting domains can be achieved. In this regard, polymers with grafted photosensitizers in the side chain[7-15] or surface immobilized structures[13-15] were already reported and demonstrated the potential to achieve a light-induced charge separation. However, these donor-

photosensitizer architectures relied on an inorganic electron acceptor, *e.g.*, TiO_2, to realize a full charge separation. Additionally, defects may occur as a result of an incomplete functionalization of graft polymers. Noteworthy, linear structures, which are expected to increase the spatial separation of the electrochemically active polymers, are not reported. The approach, that is presented in this thesis, is based on the step-wise linkage of functional building blocks, *i.e.*, electron donor and acceptor polymers to suitable Ru(II)-based photosensitizers. This strategy enables a modular construction of highly defined, defect-free linear D_n–P–A_m architectures for a long-lived charge separation. The applied polymers (*vide infra*) are transparent in the visible area, so that the light absorption exclusively occurs by the photosensitizer. Moreover, a detailed analysis of the compounds and of occurring processes upon excitation is guaranteed due to the defined structure of the architectures. Noteworthy, such hierarchical structures may also be utilized as power source in the field of molecular machines to generate local redox gradients by light excitation. This current topic was awarded with the Noble prize for Chemistry in 2016.

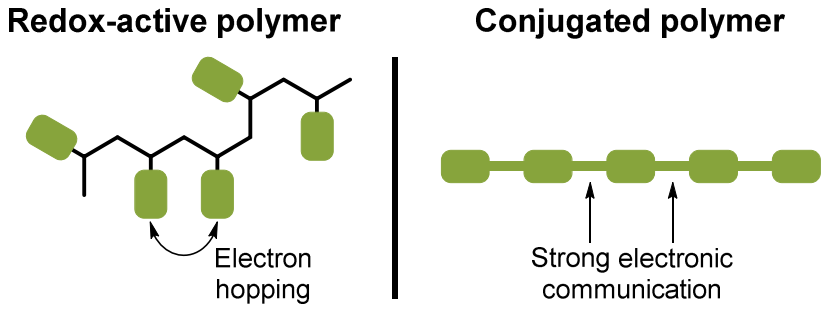

Figure 1.1. Charge transport mechanisms in electrochemically active polymers.

In this regard, modern controlled polymerization techniques represent a powerful synthetic tool box to covalently link multiple functional units for the construction of defined polymer-based architectures. An overview of polymerization techniques for different classes of telechelic electrochemically active polymers and their incorporation in larger systems, *e.g.*, block, comb or end functionalized polymers, is presented in **Chapter 2**. Thereby, the polymers are classified based on the mechanism of the charge transport (Figure 1.1).[16] Redox-active polymers are characterized by isolated redox centers with defined redox potentials. An electron transfer occurs via an electron hopping and, consequently, leads to limited charge carrier mobilities.[16] However, due to their facile preparation by controlled (radical) polymerization techniques, redox-

active polymers represent an intensively investigated class of macromolecules.[17-18] In contrast, conjugated polymers feature a strong electronic communication between the individual active units and, therefore, show in general a higher charge carrier mobility. Nevertheless, the preparation of telechelic conjugated polymers is still challenging and requires advanced synthetic methods, *e.g.*, the Kumada or Suzuki catalyst transfer polymerization.[19-21] Electrochemically active units, which were commonly utilized in redox-active or conjugated polymers, cover triarylamines, carbazoles, thiophenes, naphthalene diimides or fluorenes.

In the diploma thesis, styrenic triarylamines[22] and naphthalene diimides were prepared by nitroxide mediated polymerization and were investigated with respect to their suitability as electron donor and acceptor polymers. For this purpose, the optical and (spectro)electrochemical properties of the compounds were analyzed and the possibility of electron transfer steps between triarylamine polymers in the order of their redox potentials was demonstrated by redox titration experiments.[22] Moreover, the covalent linkage between a ruthenium polypyridyl photosensitizer and a polytriarylamine or a poly(naphthalene diimide) leading to D_n–P and A_m–P dyads was exemplarily conducted. The prepared architectures were investigated towards light-induced charge transfer processes by transient spectroscopic techniques.[23-24] In this regard, the fundamental working principle of the chosen modular approach was verified by the occurring charge separation in an A_m–P dyad.[23] However, only one linking motif for the polymer and the photosensitizer were utilized and no triad was prepared.

Based on these findings new telechelic polymers with tailored properties were designed, *i.e.*, the polarity as well as the electron transfer principle in the polymers were varied. In this regard, the preparation of poly(naphthalene diimide)s with alkyl as well as oligo- and polyethylene glycol side chains is described in **Chapter 3**. Thereby, the variation of the substituents was expected to enable a tuning of the polarity and, thus, the solubility in organic solvents or water. Consequently, the increased hydrophilicity of the polymers may allow a morphology control by self-assembly of the macromolecules and, moreover, the processing in environmentally friendly solvents, *e.g.*, a film formation from water.[25-31] Additionally, the introduction of further reactive end groups at the polymers' α-chain terminus will be discussed. The successful substitution broadens the range of possible linking reactions with appropriate photosensitizers (*vide infra*).

As mentioned before, redox-active polymers, *e.g.*, the polytriarylamines which were prepared during the diploma thesis, feature a limited charge transport due to the hopping

mechanism.[16] In order to increase the charge carrier mobility in the electron donor polymers, the preparation of telechelic conjugated poly(*N*-alkyl-3,6-carbazole)s by Kumada catalyst transfer polymerization (KCTP) and Suzuki-Miyaura polymerization was investigated and is detailed in **Chapter 3**. In the case of the KTCP, the influence of various reagents to activate the monomers by the Grignard metathesis step is presented and limitations with respect to the subsequent polymerization with a Ni catalyst as well as the end group fidelity are identified. Based on these findings, the synthesis of poly(*N*-alkyl-3,6-carbazole)s by Suzuki-Miyaura polymerization benefited from the possibility to utilize purified active monomers and from the higher functional group tolerance. In addition, the application of functional initiators or end capping reagents to synthesize telechelic conjugated polymers is described.

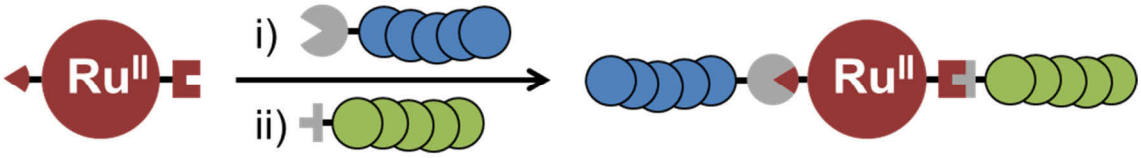

Scheme 1.1. Schematic representation of the modular assembly of photoredox-active A_m–P–D_n triads by orthogonal reaction steps (blue and green balls represent different monomer units, the red ball symbolizes the photosensitizer, grey shapes represent functional end groups).

An overview of the utilization of the prepared telechelic polymers as building blocks to construct photoredox-active architectures is provided in **Chapter 4**. The desired modular assembly of the photosensitizer and the respective polymers guarantees a high flexibility to assemble the final structures (Scheme 1.1). In this regard, three different linking reactions, *i.e.*, two nucleophilic substitutions and the copper-catalyzed azide-alkyne cycloaddition (CuAAC), were utilized to attach a Ru(II) photosensitizer at a poly(naphthalene diimide). The detailed examination of optimized reaction conditions provided a universal synthetic platform to prepare a wide range of A_m–P and D_n–P dyads and, more importantly, D_n–P–A_m triads.

Finally, a detailed spectroscopic characterization covering steady state absorption and emission measurements as well as transient spectroscopic experiments is given in **Chapter 4**. First insights into the occurring charge and energy transfer steps were gained by steady state emission measurements, *i.e.*, the quenching of the photosensitizer's metal-to-ligand charge transfer (MLCT) emission band indicating a charge separation in the A_m–P dyads and the D_n–P–A_m triads is presented. A more

detailed analysis of the occurring processes as well as of the involved species is provided by transient absorption data. Thereby, also the presence of reductive and oxidative quenching pathways could be distinguished (Scheme 1.2). In particular, a possible formation of the charge separated state $D_n^+–P^-$ in the donor dyads and of the fully charge separated state $D_n^+–P–A_m^-$ in the triads was investigated. The experiments revealed additional features in contrast to low molecular mass triads and demonstrated the potential of the chosen approach to generate separated charges in the polymer-based architectures by light absorption.

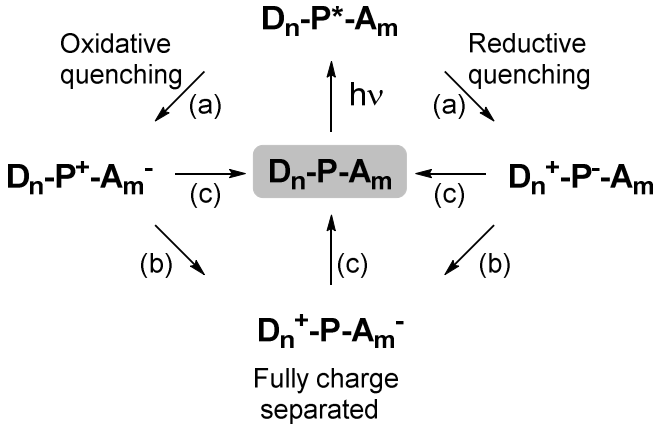

Scheme 1.2. Different steps of charge separation after photo-excitation (hν) of the photosensitizer (P): (a) Oxidative or reductive quenching by a first electron transfer step, (b) formation of fully charge separated state by consecutive second electron transfer step and (c) recombination to the ground state.

Summing up, the utilization of a modular synthetic system (Scheme 1.1) is presented to transfer the light-induced charge separation from low molecular mass D–P–A model systems (Scheme 1.2) to polymer-based architectures ($D_n–P–A_m$). Thereby, modern polymerization techniques and coupling reactions are applied to construct photosystems in which the optical properties of the individual building block are preserved. Finally, time-resolved spectroscopic techniques are utilized to verify the light-induced charge separation in comparison to reference complexes.

2. Structurally well-defined polymer architectures with tunable (opto)electronic properties

Parts of this chapter have been published in P1) R. Schroot, M. Jäger, U. S. Schubert, *Chem. Soc. Rev.* **2017**, *46*, 2754-2798.

This chapter focusses on synthetic approaches and strategies that enable the synthesis of well-defined polymer architectures, *i.e.*, block, comb or end functionalized polymers. These macromolecules are capable to mimic fundamental processes for directional charge transport or light harvesting and allow the construction of multipurpose materials *inter alia* by self-assembly processes.

Functional redox-active, conjugated and photoactive polymers represent a promising class of materials in the field of (opto)electronics and are applied in organic light-emitting diodes, organic field effect transistors or for light harvesting *inter alia* in organic solar cells.[18, 32-35] The polymers promote the task of charge separation, charge transport, charge accumulation or photosensitization in these devices. Their activity and performance is on the one hand dictated by molecular properties, *e.g.*, redox potentials or light absorptivity, but on the other hand also mesoscopic parameters play a crucial role to achieve a stable device morphology, to minimize trap sites or to control the domain sizes. Promising candidates to overcome hitherto existing challenges are covalently linked polymer-based architectures, *e.g.*, block, comb or end functionalized polymers, due to their tailored properties.[36-43] Well-defined (co)polymers with precisely tuned molar masses, end groups and low dispersities may self-assemble in stable and tunable morphologies.[44-46] Additionally, the lowered occurrence of defects and trap sites increases the performance of the materials.[47-49] Consequently, the utilization of these architectures can result in the improvement of the device performance by the formation of ordered self-assembled structures with minimized defect sites.

The construction of functional polymer architectures requires smaller building blocks, *e.g.*, homopolymers with a high fidelity of reactive end groups and defined molar mass. Hence, controlled and “living” polymerization procedures are necessary, which will be initially discussed.

The well-known controlled radical polymerization (CRP) techniques, *e.g.*, nitroxide mediated polymerization (NMP), atom transfer radical polymerization (ATRP) or reversible addition fragmentation chain transfer (RAFT) polymerization, are commonly

applied for the preparation of functional redox-active homopolymers because of commercially available (functional) initiators or transfer agents. The anionic polymerization represents another powerful tool for the synthesis of telechelic polymers due to its living nature – characterized by the absence of termination reactions – and various possible end functionalization reactions, *e.g.*, by the addition of reactive end functionalization reagents like ethylene oxide or fullerenes.[50-52] Interestingly, conjugated polymers can also be prepared by anionic polymerization and subsequent elimination reactions as reported by the groups of Natori or Vanderzande.[53-54] Another often utilized synthetic approach is the ring opening metathesis polymerization (ROMP) of cyclic alkenes, which offers a high functional group tolerance, and, therefore, enables the application of sensitive monomers, *e.g.*, fullerene or radical containing compounds.[55-62] Moreover, ROMP represents also a powerful technique to synthesize telechelic conjugated polymers, *e.g.*, PPVs.[63]

This polymer class is of special interest in the field of (opto)electronis due to the high charge carrier mobility. At the beginning of the 2000s, McCullough and Yokozawa reported the development of the Grignard metathesis (GRIM) or Kumada catalyst transfer polymerization (KCTP) of thiophenes.[64-65] The technique represented a significant advancement in the synthesis of conjugated polymers due to its living character and the associated synthetic possibilities, *i.e.*, the preparation of (co)polymers by sequential monomer addition or the facile end functionalization by the application of functional initiators or end capping reagents.[66]

The presented polymerization techniques for telechelic homopolymers allow the engineering of well-defined architectures, which will be presented in the following. Block copolymers enable the linear combination of two or more different monomer units in distinct sections of a macromolecule to create new materials with unique properties. In particular, electron and hole transporting or hydrophilic and hydrophobic blocks may be incorporated in one polymer chain, hence, allowing a precise tuning of the electrochemical as well as the physical properties, *e.g.*, to control the self-assembly properties and the morphology of the materials.[27, 67-68] In general, four methods for the synthesis of block copolymers can be distinguished (Scheme 2.1).[68-69] In the case of a living polymerization process, *e.g.*, anionic polymerization[70-71] or ROMP,[72-73] block copolymers are prepared by sequential monomer addition (Scheme 2.1A). The polymerization is started with one monomer and a second monomer is added after full consumption and so on. As a consequence, the polymerization is performed as a facile

one pot procedure and an isolation and a purification of the primarily formed homopolymer is not necessary. A successful synthesis, however, requires the addition of the monomers in the right order of reactivity for an efficient crossover reaction and a tuning of the reactivity of the propagating chain may be necessary.[69, 74] In this regard, an interesting example for the anionic polymerization is given by Kang *et al*. by the synthesis of triphenylamine and ethynylpyridine containing block copolymers.[70-71]

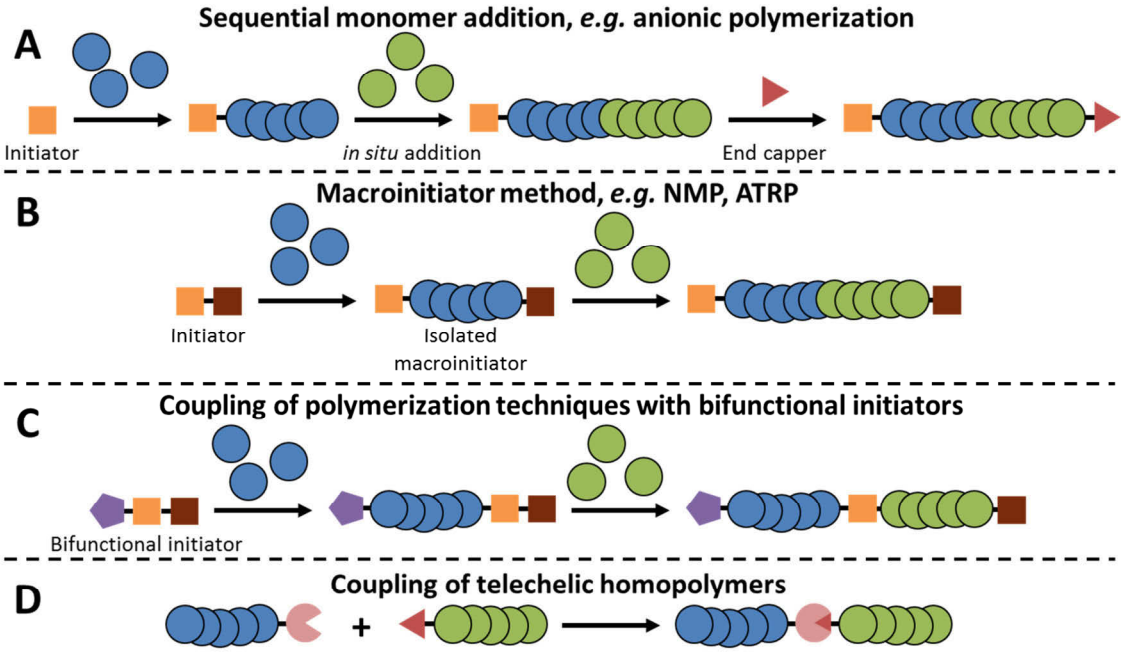

Scheme 2.1. Schematic representation of the main synthetic approaches leading to block copolymers (blue and green balls represent different monomer units, the triangle and the segment of a circle display complementary reactive end groups) (Reproduced from Ref.[43] by permission of The Royal Society of Chemistry).

The second strategy leading to block copolymers relies on the application of macroinitiators or macro-RAFT agents (Scheme 2.1B).[15, 75-77] Primarily, a homopolymer is synthesized that is decorated with the initiating group (or RAFT group). After the removal of residual first monomer, the compound is used to initiate the polymerization of the second monomer. This technique benefits from the modularity because block copolymers with various compositions can be prepared from the same macroinitiator. Similarly, bifunctional initiators[78-79] or end capping and postpolymerization modification approaches can be applied for the synthesis of macroinitiators (Scheme 2.1C). Exemplarily, the *in situ* coupling of P3HT with a NMP initiator is commonly applied.[80] The approach to couple polymerization strategies is of

special interest as a wide scope of monomers and in principle all possible polymerization techniques can be combined. The coupling of telechelic polymer chains is also commonly applied to prepare block copolymers (Scheme 2.1D). The necessary reactive end groups originate from functional initiators, end cappers or postpolymerization reactions. In order to achieve a high yield, very efficient coupling reactions, *e.g.*, the CuAAC reaction,[81] are required. In the case of an incomplete conversion, the separation of the homopolymers and the desired block may be challenging and often requires advanced purification protocols. Nevertheless, the coupling of polymer chains is advantageous with respect to the modularity. The potential of the approach is exemplarily presented by the synthesis of P3HT-*b*-PNIPAM *via* the CuAAC reaction to form thermoresponsive micelles with a LCST behavior in water.[81]

In contrast to block copolymers, graft and comb copolymers combine two or more different monomer units not in a linear order but in the polymer backbone and the side chain. In particular, the optimization of the properties of functional polymers by a side chain modification is of special interest, *e.g.*, to improve the solubility in environmentally benign solvents or to attach additional light-harvesting dyes.[12-14, 82-83] In general, three different techniques to prepare graft copolymers can be distinguished: "Grafting onto" of functional side chain polymers to a polymer backbone, "grafting from" initiating units at the polymer backbone and the "grafting through" of macromonomers. The "grafting onto" approach is preferred for the construction of metal complex containing polymers as the direct polymerization often leads to side reactions with the active propagating species.[84] In this regard, the groups of Schanze and Papanikolas reported the synthesis of light-harvesting polymers with attached Ru(II) complexes by a "Click" chemistry approach.[12-14, 82-83] Grafting approaches are also preferentially used for the preparation of fullerene containing polymers. Due to their instability towards cations, anions and radicals, fullerene containing polymers are in general either prepared by "grafting through" ROMP techniques or by "grafting onto" approaches. In contrast to low molar mass fullerene derivatives, the solubility of the graft copolymers is increased.[41] Noteworthy, the grafting densities of "grafting onto" and "grafting from" approaches is limited due to steric effects.

The end functionalization of polymers with functional units, *e.g.*, photo- or redox-active building blocks, is a promising approach to construct hierarchically defined and directional charge and energy transfer cascades.[23, 85-88] Therefore, this technique was

utilized to prepare photoredox-active dyads and triads during this thesis. In general, two synthetic approaches can be applied for the end functionalization, either the *in situ* or the postpolymerization modification (Scheme 2.2).

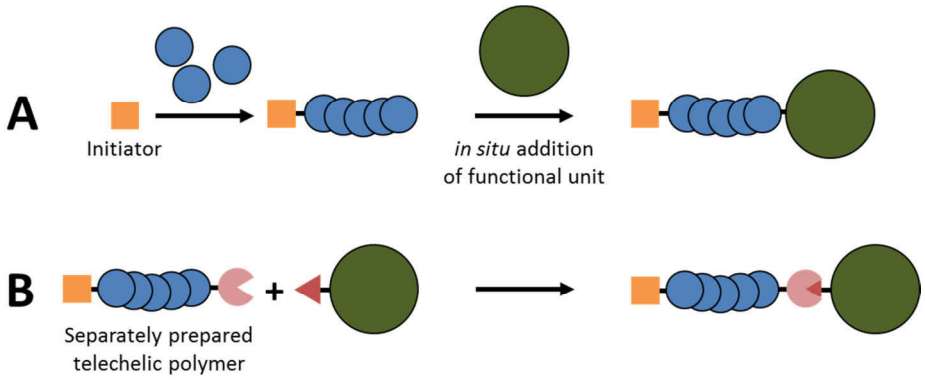

Scheme 2.2. Schematic representation of the two end functionalization approaches: (A) *In situ* functionalization, (B) postpolymerization modification utilizing telechelic polymers (the dark green ball represents a functional unit) (Reproduced from Ref.[43] by permission of The Royal Society of Chemistry).

The *in situ* approach exploits the highly reactive propagating species of the polymerization process by the addition of an end capping reagent. However, this technique prevents a truly modular synthetic concept, *i.e.*, one polymer batch can only be end capped with one functional unit at a time. Typically, this technique is used in combination with an anionic polymerization, *e.g.*, for the end functionalization of styrenic triarylamines with C_{60} fullerene as presented by Natori *et al.*.[52] Moreover, step-growth polycondensations may be quenched by the addition of a functional end capping unit. In this regard, Krebs and Biancardo reported the chain end decoration of P3HT with ruthenium dyes using Stille coupling.[89] In contrast to the *in situ* functionalization, the post polymerization modification enables a modular synthetic approach due to the application of purified telechelic polymers. The required reactive end group is often introduced by a suitable initiator. The construction of Ru(II) photosensitizer decorated donor and acceptor polymers by this technique will be discussed in detail in the Chapters 3 and 4.[87-88, 90] This approach benefits in particular from the high synthetic flexibility due to the modular character, *i.e.*, the same telechelic polymer can be used in several architectures or one building unit can be readily replaced. Fang *et al.* reported an interesting example for the end functionalization utilizing metal complexes.[11] A chromophore-catalyst assembly was prepared *via*

RAFT polymerization followed by side chain as well as chain end modification reactions.

In summary, the presented covalently linked architectures experience an increasing interest in today's research due to their beneficial properties and advantages in comparison to blends, *e.g.*, with respect to structure and morphology control. The steady development of controlled polymerization techniques, functional initiators and coupling reagents is expected to expand the synthetic platform for these architectures.

3. Redox-active and conjugated telechelic polymers

Parts of this chapter have been published in P2) R. Schroot, T. Schlotthauer, U. S. Schubert, M. Jäger, *Macromolecules* **2016***, 49,* 2112-2123. P3) R. Schroot, T. Schlotthauer, M. Jäger, U. S. Schubert, *Macromol. Chem. Phys.* **2017**, *218*, 1600534. P4) R. Schroot, U. S. Schubert, M. Jäger, *Macromolecules* **2016**, *49,* 8801-8811. P5) R. Schroot, U. S. Schubert, M. Jäger, *Macromolecules* **2017**, *50*, 1319-1330.

As mentioned in Chapter 1, the construction of photoredox-active architectures requires telechelic polymers, *i.e.*, polymers with a high fidelity of reactive end groups.[43] In this regard, modern controlled polymerization techniques represent a powerful tool enabling the synthesis of end functionalized polymers. Whereas telechelic redox-active polymers are in general readily prepared by controlled radical polymerization techniques, the synthesis of conjugated polymers is much more challenging. In order to control the molar masses and to achieve a high end group fidelity a transformation of cross coupling reactions from a step-growth to a chain-growth mechanism is necessary. The first part of the following chapter details the nitroxide mediated polymerization (NMP) and the end group modification of various styrenic naphthalene diimides as well as the analysis of the influence of side-chain substitution on the physical and optical properties. Investigations with respect to the eligibility of the Kumada and Suzuki catalyst transfer polymerization (CTP) for the synthesis of telechelic poly(*N*-alkyl-3,6-carbazole)s are presented in the second part of this chapter.

3.1. Redox-active naphthalene diimide based polymers

Naphthalene diimide (NDI) based polymers are intensively investigated as n-type semi-conductors. The pristine NDI unit undergoes two reversible reduction steps. Different substituents on the molecular scaffold enable a tuning of the redox steps as well as of the optical and physical properties.[91-93] The planar π-system is capable for self-organization, *e.g.*, a face-to-face stacking of the units.[94-97] Whereas main-chain conjugated NDI polymers are commonly synthesized by polycondensation reactions, side-chain decorated polymers are conveniently prepared by controlled radical polymerization procedures.[23]

The investigated styrenic naphthalene diimides (NDIs) contained either alkyl or oligo- and polyethylene glycol side chains to tune the solubility and were prepared from 1,4,5,8-naphthalenetetracarboxylic dianhydride by an optimized two-step synthesis compared to a previous reported method (Scheme 3.1).[23] The procedure reduces the number of synthetic steps and requires only one chromatographic purification step, resulting in significantly improved yields (50% compared to 10%): Firstly, the monoimide was prepared by the reaction of the dianhydride with 2-ethylhexylamine, methoxytri- (MTEG) or polyethylene glycol (MPEG 550) amine in DMF under microwave irradiation.[98] The crude products contained approximately 20% bis-functionalized product, but were used without further purification. Next, the styrenic group was introduced by the reaction with an excess of 4-aminostyrene in pyridine in the presence of zinc(II) sulfate as described for similarly functionalized NDIs.[99] The monomers **1** and **2** were isolated by column chromatography using silica gel. Noteworthy, the purification of compound **3** by ordinary column chromatography was hindered due to its high polarity. Instead, the substance was purified by size-exclusion chromatography (SEC) using the Bio-Beads S-X3 resin. Thereby, the separation of the bis-PEGylated species NDI-(MPEG 550)$_2$ from the desired monomer is challenging in larger scales due to overlapping peaks during elution. So, the collected fractions were combined in case of less than 10% impurity (checked by ^{1}H NMR spectroscopy). NDI-(MPEG 550)$_2$ lags a polymerizable group and, thus, is indifferent in the later polymerization.

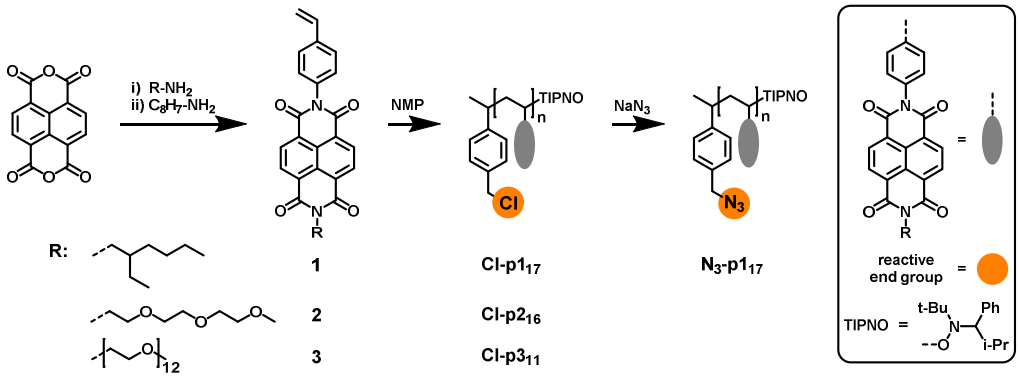

Scheme 3.1. Schematic representation of the synthesis of naphthalene diimide based monomers and the respective polymers by nitroxide mediated polymerization.

The polymerizations were carried out using the commercial functional NMP initiator CMSt-TIPNO, which enables facile modifications of the chloromethyl chain terminus. The ^{1}H NMR spectra of the compounds feature the typical broad NDI resonance at 8.5

ppm and a second broad signal of the phenylene units (7.2 ppm) in the aromatic region. The signal of the chloromethyl group is found at approximately 4.5 ppm and is used to determine the degree of polymerization (DP). The labeling of the polymers (p) is based on the used monomers (**1, 2** or **3**), the functional endgroup (Cl or N_3) and the DP as subscripted number. For example, **N_3-p1$_{17}$** consists of 17 units of monomer **1** and is decorated with an azide end group.

The influence of the MTEG and MPEG 550 substitution on the polymerization behavior was detailed by a kinetic investigation (Figure 3.1). As expected for a controlled NMP, the plot of the evolution of the monomer concentration **2** *versus* $t^{2/3}$ (Figure 3.1, left) shows a linear behavior in the beginning, indicating a reaction in the equilibrium period.[100] However, the graph flattens for reaction times over 24 hours ($t^{2/3} \approx 8$ $h^{2/3}$) which is indicative for a decreasing reaction rate, *i.e.*, the polymerization does not take place in an equilibrium state anymore due to the rise of termination reactions. The slope of the linear fit of the data in the equilibrium region facilitates the calculation of the product of all important rate constants. This value (Figure 3.1) enables the calculation of the reaction times required to reach a certain conversion and molar mass, also in comparison to other monomers (*vide infra*).

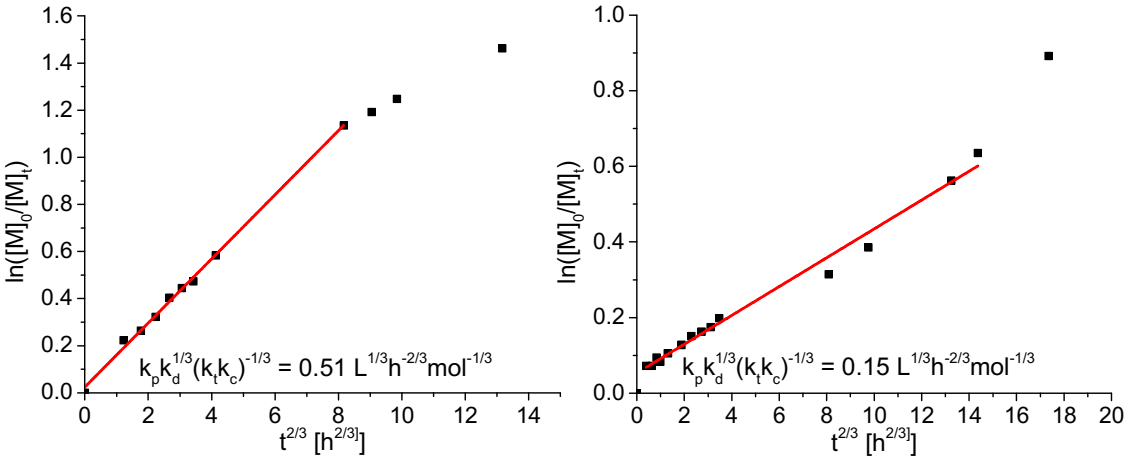

Figure 3.1. Evolution of the monomer concentration *versus* $t^{2/3}$ for the preparation of **Cl-p2$_{16}$** (left) and **Cl-p3$_{11}$** (right). The concentration was determined by ^{1}H NMR spectroscopy. (Reprinted with permission from Ref.[87]. Copyright 2017 John Wiley & Sons, Inc.)

Deviations from the expected behavior (linear increase in the equilibrium period and flattening at the end of the reaction) are observed for graft copolymer **Cl-p3$_{11}$**. In this regard, the occurrence of an induction period at the beginning (approximately 15 to 20 min) followed by the equilibrium range is noticed. Afterwards, the two data points

below the linear fit at approximately 8 and 10 $h^{2/3}$ indicate a decrease of the reaction rate – probably due to more pronounced termination reactions. Finally, a strong increase of the monomer consumption and of the reaction rate is visible. This behavior is very uncommon and it can only be speculated on its origin. Plausible reasons include: 1) Solvent effects, *e.g.*, viscosity changes influence k_d and k_c (similar to the Trommsdorff-Norrish effect in FRP), 2) k_d increases with the degree of polymerization as known for some monomers,[101] or 3) due to side reactions, *e.g.*, decomposition of free nitroxide over the long reaction period, new propagating radicals are formed. This may also explain the increasing dispersity, which was observed by SEC measurements. However, the obtained polymers feature low dispersities (Đ = 1.14 to 1.28) and a defined molar mass (M_n = 14,000 to 17,000 g/mol) despite the deviations from the ideal reaction kinetics. The calculated reaction rate constants are shown in Figure 3.1 and reveal a 3.4 fold decrease of **Cl-p3$_{11}$** *vs.* **Cl-p2$_{16}$**. The considerably lower reaction rate is not surprising due to the presumably induced steric hindrance of the large MPEG 550 side chain which is often observed for the grafting through of comb copolymers.[102-103] In line, the calculated rate constant for the polymerization of **Cl-p2$_{16}$** is already decreased by the factor 1.7 in comparison to the reaction of monomer **1** in DMF under otherwise identical conditions.[104]

In order to increase the possible linkage patterns for D_n−P−A_m systems (see Chapter 4), the chloromethyl group at the chain terminus of **Cl-p1$_{17}$** was converted into the azide functionality. The successful functionalization leading to **N$_3$-p1$_{17}$** was verified by ^{1}H NMR spectroscopy (shift of the respective methylene protons) and IR spectroscopy (azide band at 2100 cm^{-1}).

The hydrophilicity of the polymers containing the monomers **2** or **3** is increased in comparison to **Cl-p1$_{17}$** due to the polar tri- and polyethylene glycol side chains. Thereby, the hydrophilicity and the solubility in polar solvents increase with the number of ethylene glycol units in the side chain. Additionally, an influence of the degree of polymerization of the polymer backbone on the solubility is observed.[105-106]

In this regard, monomer **1** and the respective polymer are only soluble in halogenated solvents or THF. Monomer **2** is additionally soluble in the more polar solvent acetone but not the respective polymer **Cl-p2$_{16}$**. The hydrophilicity of monomer **3** and the respective polymer **Cl-p3$_{11}$** is strongly increased due to the long MPEG 550 side chain and, consequently, these compounds are soluble in polar solvents, *e.g.*, acetone, ethanol, methanol or even water. Thereby, the DP strongly influences the water solubility of the

polymer **Cl-p3$_{11}$**, *i.e.*, above six to eight repeating units only a limited or moderate solubility in water was observed. In conclusion, these polymers represent important materials in order to prepare water-processible architectures and, moreover, are expected to facilitate the self-organization in combination with other building blocks, *e.g.*, hydrophobic electron donors or Ru(II) photosensitizers.

The optical properties of the compounds **N$_3$-p1$_{17}$**, **Cl-p2$_{16}$** and **Cl-p3$_{11}$** were explored by UV/vis absorption and steady state emission spectroscopy. The absorption spectra of the compounds in CH_2Cl_2 are shown in Figure 3.2. The NDI-based polymers feature the typical NDI π-π* absorption bands at 360 and 380 nm. In case of **N$_3$-p1$_{17}$**, the decreased intensity at 380 nm and the peak broadening below 350 nm is tentatively assigned to a slightly changed conformation of the polymer chains in comparison to **Cl-p2$_{16}$** and **Cl-p3$_{11}$**. Noteworthy, in more polar solvents, *e.g.*, MeOH or water, only marginal changes of the absorption spectra were detected for **Cl-p2$_{16}$** and **Cl-p3$_{11}$** implying minor conformational changes.

Upon excitation at 360 nm, the polymer **N$_3$-p1$_{17}$** features a pronounced emission band around 413 nm attributed to interacting NDI units, similar to the reported *J*-aggregates formed in solution.[97] However, **Cl-p2$_{16}$** and **Cl-p3$_{11}$** display no detectable emission suggesting the predominate existence of non-emissive isolated NDI units in the investigated concentration range (10^{-7} M).[94, 97] Probably, this behavior may be a consequence of the steric hindrance of the PEG side chain, *i.e.*, the side chain promotes the formation of rod-like structures with the highest possible distance between the individual NDI units in a single polymer chain.

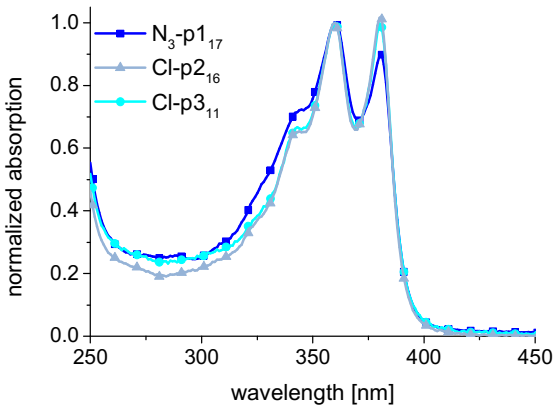

Figure 3.2. Normalized absorption spectra of the polymers **N$_3$-p1$_{17}$**, **Cl-p2$_{16}$** and **Cl-p3$_{11}$** in CH_2Cl_2 showing typical π-π* transitions bands at 360 and 380 nm.

In conclusion, styrenic naphthalene diimide based polymers with hydrophilic and hydrophobic substituents can be readily prepared by nitroxide mediated polymerization. The obtained polymers featured low dispersities and a defined molar mass despite deviations from the ideal reaction kinetics. The introduced side chains enable a tuning of the polarity as well as the solubility of the compounds and, therefore, display a promising approach to influence the assembly in materials. Importantly, the optical absorption properties are not influenced by the modification of the side chains which is desirable to design modular D_n−P−A_m systems (see Chapter 4).

3.2. Kumada and Suzuki catalyst transfer polymerization towards telechelic conjugated poly(*N*-alkyl-3,6-carbazole)s

Triarylamines and related carbazoles represent, among many others, a widely utilized class of hole-conducting materials.[17, 107-109] Whereas styrenic triarylamine based polymers were intensively investigated before,[22] the focus during this work was set on carbazole based materials as an attractive material class,[110-111] due to their facile modification to tune optoelectronic and/or processing properties.[108] Poly(carbazole)s are best divided according to the connectivity between the repeating units, *i.e.*, linking *via* the 2,7- or 3,6-positions of the carbazole resulting in *para*- or *meta*-linked phenylene-conjugation segments, respectively. In consequence, the corresponding poly(2,7-carbazole)s exhibit a high charge carrier mobility, but also an irreversible oxidation process caused by the unprotected reactive 3,6-positions.[108, 112] In contrast, the electrochemical oxidation of poly(3,6-carbazole)s is reversible as the reactive positions are masked.[112] These materials are transparent in the visible light region due to the diminished conjugation segment and are, in particular, commonly used compounds for OLEDs,[113-115] in flash memory devices, OFETs,[116-117] or in devices showing thermally activated delayed fluorescence.[118] The synthesis of suitable substituted monomers is readily achieved from 9H-carbazole, *i.e.*, various solubilizing side chains or substituents at the 3 or 6 position are easily introduced. However, only a very small number of protocols regarding well-defined poly(3,6-carbazole)s by catalyst transfer polymerization have been published. Reported procedures are primarily based on Ni- or Pd-catalyzed Kumada-, Yamamoto-, Negishi- or Suzuki-type step-growth couplings.[119-125] In this regard, the utilization of the polymers in consecutive

functionalization reactions or in assembled materials[126] relies on defined end groups and molar masses, respectively, which are hampered by the prevalent step-growth mechanism. Therefore, the controlled polymerization of 3,6-carbazoles by Kumada and Suzuki-Miyaura CTP to yield polymers with defined molar masses, low dispersities and a high end group fidelity is explored in detail.

The essential steps of the Grignard metathesis (GRIM) and KCTP are shown in Scheme 3.2. The reactive monomer **A** is formed by an initial metal halogen exchange (Scheme 3.2a). Knochel *et al*. investigated the reactivity of various magnesium-based reagents in metal halogen exchange reactions,[127-129] which were successfully applied in the KTCP. In the case of thiophenes, conventional Grignard reagents (^{i}PrMgCl or ^{t}BuMgCl) are adequate for a complete metal halogen exchange, while Grignard reagents with higher reactivity are required for less reactive monomers (fluorenes or 2,7-carbazoles).[125]

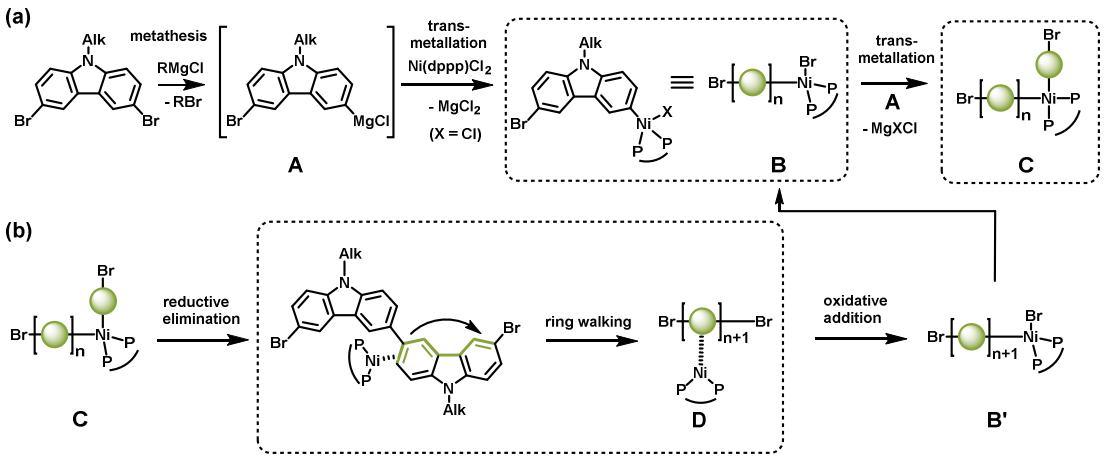

Scheme 3.2. Schematic representation of the ideal chain-growth mechanism exemplified for 3,6-carbazoles (adapted from Ref. [130-132]): (a) Activation of Ni(II) pre-catalyst and monomer addition *via* transmetalation; (b) chain growth step *via* reductive elimination, ring-walking, and oxidative addition at chain terminus. (Adapted with permission from Ref.[133]. Copyright 2016 American Chemical Society)

The activated monomer **A** undergoes a first transmetalation step upon addition of a Ni(II) pre-catalyst, *e.g.*, [Ni(dppp)Cl_2] (dppp is 1,3-bis(diphenylphosphanyl)-propane),[131, 134-135] and **B** is formed. Subsequently, the Ni species (**C**) is generated after a second transmetalation step. Noteworthy, the following reductive elimination yields a polymer chain with the associated catalyst fragment (Scheme 3.2b). The ability of the Ni fragment to migrate along the π-system (ring-walking) towards the chain terminus to form **D** is the key feature to ensure a chain growth mechanism. The species **D** re-enters the catalytic cycle by oxidative addition to form **B'**. Deviations from this ideal

mechanism, *e.g.*, catalyst dissociation and disproportionation, result in a larger dispersity and a decreased end group fidelity.

The polymerization process is typically terminated by the addition of a quenching agent[132] or monofunctional Grignard reagents (end functionalization).[136-137] Besides the termination with mono-functional Grignard reagents, the application of a functionalized Ni pre-catalyst[21, 138] enables the introduction of functional end groups.

Noteworthy, the group of Thelakkat reported chain-chain couplings for P3HT in case of methanol (MeOH) quenching. This leads to Br/Br-terminated polymers with double molar mass, while the protolysis product with strict H/Br end groups was gained by the addition of HCl.[132]

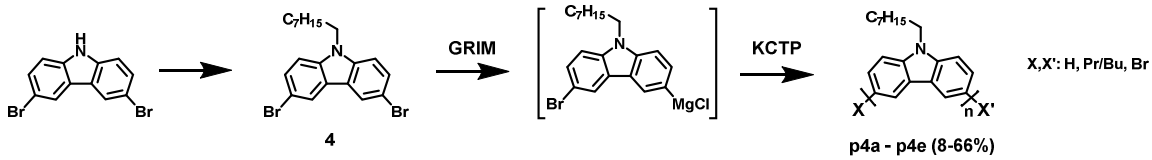

Scheme 3.3. Schematic representation of the general synthesis strategy leading to poly(3,6-carbazole)s by KCTP. (Reprinted with permission from Ref.[133]. Copyright 2016 American Chemical Society)

The synthetic procedure for the preparation of poly(3,6-carbazoles) is outlined in Scheme 3.3. At first, the metal halogen exchange of *N*-alkyl-3,6-dibromocarbazole (**4**) was performed using typical magnesium reagents,[125, 132, 139] followed by the initiation of the polymerization with [Ni(dppp)Cl_2] as pre-catalyst. The progress of the initial GRIM step was analyzed by GC-MS. When a quantitative exchange or no further metathesis progress was detected, the pre-catalyst [Ni(dppp)Cl_2] was added to the monomer solution in analogy to literature reports.[131, 134-135] Finally, the polymerization was quenched by addition of deuterated methanol (MeOD) or various end capping reagents. Noteworthy, chain-chain couplings associated with methanol termination were not observed in preliminary tests, as quenching with HCl and methanol gave identical SEC curves. The application of MeOD was expected to enable a differentiation between deuterated polymer chains with a characteristic M+1 isotope pattern and species, which terminate during the reaction and, therefore, bear a proton end group. The obtained polymers **p4a** to **p4e** are listed in Table 3.1 and were characterized by ^{1}H NMR spectroscopy, SEC and in more detail by mass spectrometry.

Initially, the commonly used Grignard reagents ^{i}PrMgCl (**p4a**) and ^{t}BuMgCl (**p4b**) were applied for the metal halogen metathesis. The reactivity of the reagents was found to be

too low for a complete metal halogen exchange and only minor amounts of polymer were isolated demonstrating the importance of a quantitative GRIM step to obtain poly(3,6-carbazole)s in high yields. The end group analysis revealed mainly Br-decorated chains, accompanied by alkyl- and proton-terminated chains. The occurrence of propyl- or H-termination is reasonable in view of residual Grignard reagent and subsequent β-hydride elimination as no deutered species were found. More importantly, the catalyst dissociation and/or disproportionation reactions are identified by the appearance of Br/Br-decorated polymer chains. Due to these side reactions, the KCTP is less controlled in comparison to the synthesis of poly(3-hexylthiophenes)[132] and, thus, a reduced end group inhomogeneity is obtained.

Table 3.1. Experimental conditions and selected analytical data of the polymers prepared by KCTP using monomer **4**.

Entry	*Poly-mer*	*Grignard reagent*	*Time [h]*	*Temperature*	*M/Br exchange [%]*[a]	*Yield [%]*	M_n *[g/mol]*[b]	$Đ$[b]
1	**p4a**	^{i}PrMgCl	24	65 °C	55	24	4,400	1.53
2	**p4b**	^{t}BuMgCl	24	65 °C	45	5	1,280	1.14
3	**p4c**	$Li^+[(^{i}Pr)MgCl_2]^-$[c]	24	rt	30	8	5,400	1.70
4	**p4d**	$Li^+[(^{i}Pr)MgCl_2]^-$[d]	18	rt	75	35	6,500	1.24
5	**p4e**	$Li^+[^{n}Bu_3Mg]^-$[d]	2	40 °C	Quant.	66	2,300	1.96

[a]Determined by GC-MS, [b]from SEC analysis (Eluent: Chloroform/iso-propanol/triethylamine [94:2:4], PS calibration), [c]formed *in situ*, [d]formed prior to metal halogen exchange.

Based on these findings, reduced side reactions during the polymerization process were expected from an improved metal-halogen exchange. Hence, the so called "Turbo Grignard" – the addition of LiCl – was investigated. In this compound the polymeric aggregates of the Grignard reagent are broken up by the formation of a more reactive $Li^+[(^{i}Pr)MgCl_2]^-$ species.[125, 127-128] In particular, the separately prepared "Turbo Grignard" (**p4d**) enhanced the metal halogen exchange (up to 75%), and also afforded the polymer in slightly increased yield in comparison to the standard reagents and the *in situ* approach (**p4c**). In addition, a general increased reaction rate was observed by the addition of LiCl during KCTP within the series **p4a** to **p4d**. Thereby, the impact on the rates of polymerization seems to be larger compared to the side reactions according to SEC and MALDI-ToF data. Based on isotope analysis mainly Pr- and/or H-terminated species, *i.e.*, Pr/Pr, Pr/H and H/H, were identified, whereas Br-decorated polymer chains were only found in traces.

Finally, the best results regarding the metal-halogen exchange and polymer yield were realized by employing magnesiate complexes ($Li^+[^nBu_3Mg]^-$). A quantitative conversion of **4** in the active monomer was observed within two hours at 40 °C, and after polymerization **p4e** was isolated in good yields (66%). Noteworthy, mainly alkyl terminated chains were obtained similar to the "Turbo Grignard" and probably originate from catalyst dissociation and/or disproportionation. However, poly(3,6-carbazole)s can be efficiently prepared via KCTP using magnesiate complexes although the preparation of telechelic polymers is precluded in the investigated cases. Modifications of the substrate (*ortho*-substituents) and/or improved catalyst systems are promising to disfavor the proposed side reactions and result in an increased chain-growth character combined with an improved control of dispersity and molar masses as well as end group fidelity.[21]

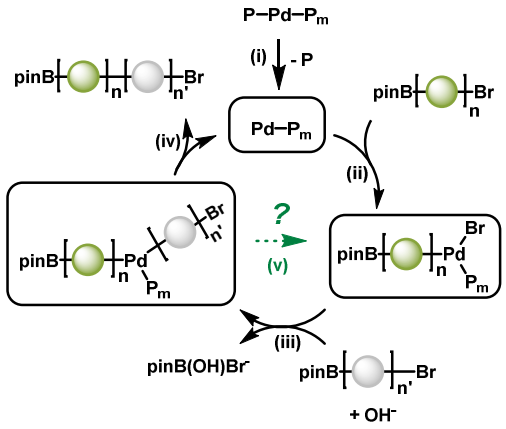

Scheme 3.4. Schematic representation of the Suzuki-Miyaura polymerization illustrating the step-growth character. (i) Formation of the active Pd(0) catalyst (P = phosphine ligand). (ii) Oxidative addition with the monomer (n=1) or polymer (n>1) (in green). (iii) Transmetalation with a second monomer (n'=1) or polymer (n'>1) (in grey). (iv) Reductive elimination and regeneration of active Pd(0) catalyst. (v) Illustration of ring-walking and/or re-insertion at the terminal C-Br bond leading to chain growth (in this case, the new chain length equals n + n'). Note, the shifting of the mechanism *via* step v (chain growth) *vs.* steps iv+i (step growth). (Adapted with permission from Ref.[90]. Copyright 2016 American Chemical Society)

The Suzuki-Miyaura approach is capable to circumvent the limitations caused by the incomplete metal-halogen exchange of the GRIM protocol, because the reactive monomer can be purified and subjected to polymerization afterwards. Hence, the Suzuki-Miyaura coupling polymerization using asymmetric A–B-type monomers was studied in detail. To the best of our knowledge, only one example for the A–B-type monomer is reported to prepare the corresponding homopolymer[140] or a related

triblock copolymer.[141] Therefore, typical activating reagents, catalyst systems as well as reaction conditions were tested and the isolated polymers were characterized in detail by ^{1}H NMR spectroscopy, size exclusion chromatography (SEC) and MALDI-ToF mass spectrometry. The MS data is accompanied by isotope simulations to distinguish various end groups. In addition to the inherent functional groups of the monomer, *i.e* bromo- and boronic ester moieties, additional functionalities were introduced by means of functional initiators and capping agents. In this regard, the end functionalization with an azide-decorated boronic ester was achieved leading to an electron donor building block (see Chapter 4).

The essential steps of the Suzuki-Miyaura coupling polymerization, which alter the mechanism from step to chain-growth similar to KCTP are visualized in Scheme 3.4.[142-143] Initially, the active Pd(0) catalyst is formed by ligand dissociation from a suitable pre-catalyst (step i). In the next step, oxidative addition of the catalyst occurs into the C–Br bond of the monomer or generated polymer (step ii). Subsequently, the C–Pd–C intermediate is formed by transmetalation with the boronic ester group of a second monomer (or polymer) in the presence of a base (step iii). Finally, the cross-coupled compound is released by reductive elimination (step iv) to close the catalytic cycle and to regenerate the active Pd(0) catalyst. This classical reaction sequence results in a step growth mechanism with a free diffusing catalyst and leads to board molar mass distributions (Đ > 2). However, in case of an associated catalyst-polymer pair, the catalyst migrates to the terminal C–Br bond and the mechanism shifts to chain-growth (step v), in analogy to the KCTP of poly(thiophene)s.[21] If both pathways occur simultaneously, intermediate dispersities may be observed.

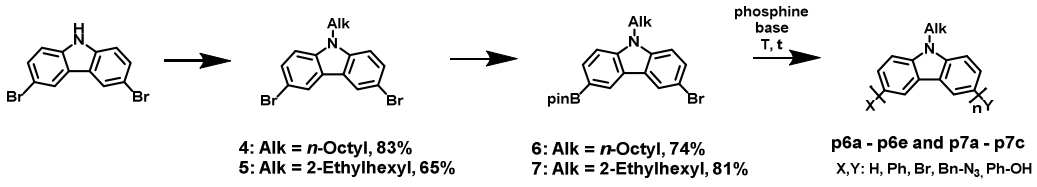

Scheme 3.5. Schematic representation of the monomer synthesis and Suzuki-Miyaura polymerization. (Adapted with permission from Ref.[90]. Copyright 2016 American Chemical Society)

Scheme 3.5 illustrates the synthetic steps of the presented work including the monomer synthesis and the subsequent polymerization. The *N*-alkyl 3,6-dibromocarbazole precursors (**4** or **5**) were prepared in analogy to the KCTP approach.[144-145] Noteworthy,

in case of a linear side chain later experiments revealed a limited re-solubility of the isolated polymers (*vide infra*) and, therefore, the branching of the octyl chain was varied. The monomers **6** and **7** bearing terminal Bpin (pin is pinacolato) and Br-moieties were directly prepared in good yields by reaction with one equivalent *n*-BuLi and subsequent quenching with *iso*-propoxy pinacolato borane. The reaction conditions for the subsequent Suzuki-Miyaura coupling polymerizations of the obtained asymmetric A–B-type monomers were adapted from related thiophenes,[146] fluorenes[147] or phenanthrenes.[148] Thereby, Pd and phosphine pre-catalysts, bases, solvents and temperature regimes were varied. The isolated polymers as well as investigated polymerization conditions are listed in Table 3.2.

Table 3.2. Polymers prepared by Suzuki-Miyaura polymerization including reaction conditions.

Entry	*Poly-mer*	*Base*	*Catalyst*	*Quen-cher*	*T [°C]*	*Yield [%]*	M_n *[g/mol]*[a]	$Đ$[a]
1	**p7a**	Na_2CO_3	$[Pd(PPh_3)_4]$	MeOH	85	52	2,300	1.44
2	**p7b**	K_2CO_3	$[Pd(P^tBu_3)_2]$	MeOH	RT	70	4,000	1.53
3	**p6a**	K_2CO_3	$[Pd(P^tBu_3)_2]$	tol-$B(OH)_2$	RT	72	3,100	1.31
4	**p6b**	CsF 18-C-6	$[(P^tBu_3)Pd(Ph)Br]$	HCl	0	77	3,600	1.61
5	**p6c**	Na_2CO_3	$[(P^tBu_3)Pd(Ph)Br]$	HCl	RT	32	2,700	1.27
6	**p6d**	K_2CO_3	$[(P^tBu_3)Pd(Ph)Br]$	HCl	RT	66	3,300	1.40
7	**p6e**	K_2CO_3	$[Pd(P^tBu_3)_2]$	**8**	RT	77	3,800	1.43
8	**p7c**	K_2CO_3	$[Pd(P^tBu_3)_2]$	**9**	RT	56	3,300	1.59

[a]from SEC analysis (Eluent: chloroform/iso-propanol/triethylamine [94:2:4], PS calibration)

Firstly, the polymerization was performed in a biphasic mixture of toluene and an aqueous Na_2CO_3 solution at 85 °C using $Pd(PPh_3)_4$ as pre-catalyst (Table 3.2, entry 1). The MALDI-ToF mass spectrum of **p7a** featured multiple series and the formation of macrocycles was proved based on isotope simulations in case of $n \geq 4$. The formation and identification of the macrocyclic oligomers are also reported for related Yamamoto coupling reactions and corroborate the assignments.[149-150] A detailed analysis of the macrocyclization is presented for monomer **6** (*vide infra*). The remaining signals at higher molar masses were assigned to H/H-, H/Ph- and Br/Ph-terminated specimen. Whereas the H/H terminated series is attributed to dehalogenation and/or deboronation, the Ph-terminated series can be well explained by the participation of the triphenylphosphine ligand of the catalyst, which is a known side reaction under harsh conditions.[151-153]

Hence, a catalytic system with [Pd(P^tBu_3)$_2$], K_2CO_3 as base and a THF/water mixture at a lower applied reaction temperature (23 °C) was tested to retard the undesired thermal catalyst dissociation from the polymer chain (Table 3.2, entry 2). Additionally, the limitation by macrocycle formation, which is enhanced at high dilution conditions, could be investigated due to the low monomer concentration (27 mM).[150] In comparison to **p7a**, the chemical yield as well as the molar mass were increased for **p7b** significantly, but not the dispersity. Noteworthy, a strongly broadened distribution (higher dispersity) would be expected, if macrocycles were formed to the same extent because of their accumulation in combination with the growing linear chains. This improvement of the polymerization characteristics is tentatively assigned to the lower reaction temperature and, therefore, the polymerization progress under these conditions was investigated in more detail for monomer **6**.

The SEC elugrams for the kinetic study are shown in Figure 3.3. The elution band of the unreacted monomer is found at 11.6 mL (t = 0 min). After 15 min a signal at 10.2 mL elution volume evolved. Notably, during the course of the polymerization this maximum shifted back to higher elution volume (10.4 mL) and an additional shoulder at shorter elution volumes is detected. This observation is attributed to the formation and accumulation of macrocycles in combination with growing linear polymer chains. After 160 min, mainly the linear polymer band continues to evolve while the rise of the macrocycles stops as judged from the virtually superimposing traces.

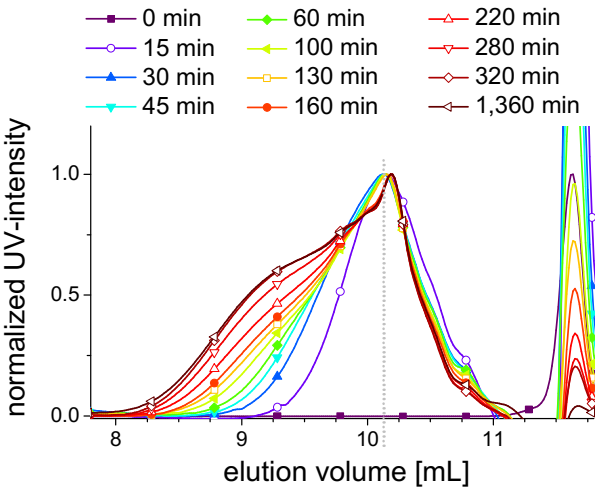

Figure 3.3. Normalized SEC traces of **p6a** sampled at selected times, illustrating the formation of linear polymer and macrocycles (eluent: Chloroform/iso-propanol/triethylamine [94:2:4]). Monomer elutes at 11.6 mL. (Adapted with permission from Ref.[90]. Copyright 2016 American Chemical Society)

The kinetic analysis of **p6a** revealed fast kinetics already at room temperature. After a steady increase of the molar masses up to 90% conversion, an enhanced increase is observed and indicates a step growth mechanism, *i.e.*, high molar masses only occur at high conversion. This observation further suggests that the desired end groups (Br and Bpin) are present to promote the coupling of the oligomer building blocks. Noteworthy, the addition of 4-tolylboronic acid as end capping reagent resulted in a successful yet incomplete end functionalization as judged by mass spectrometry data and ^{1}H NMR analysis.

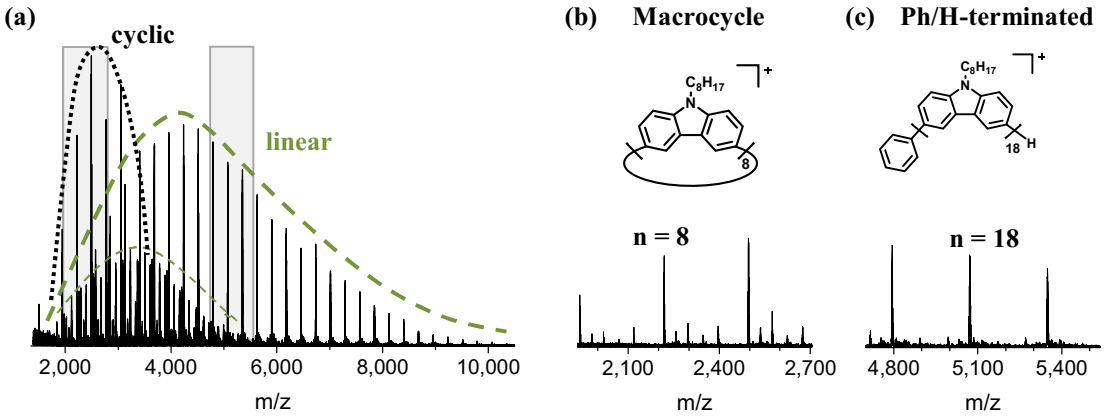

Figure 3.4. (a) MALDI-ToF mass spectrum of **p6b** (matrix: DCTB) showing the macrocycles (black dotted line) and linear domain (green dashed line, singly and doubly-charged). (b and c) Expansions of low molar mass region (b) and high molar mass region (c) with assignment of dominating species. (Adapted with permission from Ref.[90]. Copyright 2016 American Chemical Society)

Based on the previous results, the application of the functionalized Pd catalyst [(P^{t}Bu$_3$)Pd(Ph)Br] in a diluted monomer solution was tested to prepare telechelic polymers and, to simultaneously, trap newly initiated chains as cyclic byproducts. The exact experimental conditions, *e.g.*, CsF, Na_2CO_3 or K_2CO_3 as base, were adapted from related conjugated polymers[146-148] and are listed in Table 3.2 (entry 4 to 6). In all cases, a bimodal distribution that belongs to low molar mass oligomers (around 10 mL) and a varying amount of a high molar mass fraction (< 9 mL), was revealed by SEC data. The main difference in the molar mass distribution of **p6b**, **p6c** and **p6d** is tentatively ascribed to the solubility of the base in THF and the varied reaction times. According to the MALDI-ToF spectra, the apparent dominant series belongs to cyclic oligomers. For inspection of the high molar mass part, a separation by preparative SEC was exemplified for **p6b**. The isolated fraction contained only minor residual amounts of

macrocycles/oligomers, while the Ph/H-decorated polymers dominate the high molar mass region up to 10,000 g/mol (Figure 3.4).

In conclusion, the application of a functionalized initiator at low reaction temperatures yielded for the first time telechelic poly(3,6-carabzole) with high end groups fidelity, even though the inherently formed macrocycles have to be removed. The catalyst dissociation and re-initiation of new chains (*vide supra*) as well as the efficient macrocyclization at high dilution is also confirmed by these observations. At this stage, the influence of other reaction parameters, *i.e.*, the precise role of the base, the monomer concentration, and the reaction temperature, remains to be elucidated as observed differences in the obtained molar mass may arise from different reaction times.

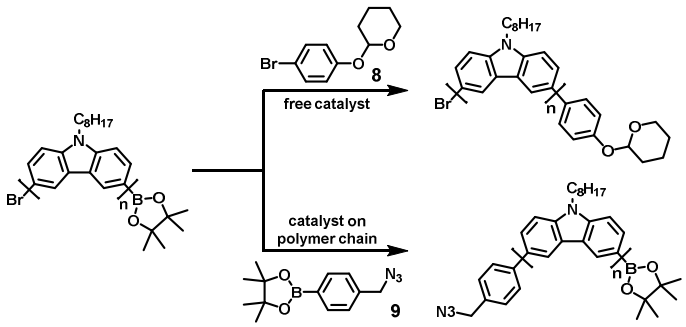

Scheme 3.6. Schematic representation of the end functionalization mechanism using the end cappers **8** and **9**.

As a consequence of the inevitable catalyst dissociation, the scope of termination using functionalized end-capping agents was revisited, as the kinetic study (**p6a**) already showed this opportunity. The general experimental conditions were adapted from **p6a** and the functionalization of both terminal functional groups were explored, *i.e.*, modifying the Bpin-group using tetrahydropyranyl (THP)-protected *para*-bromophenol **8** (**p6e**), as well as the Br-substituent using the pinacol ester of *para*-azido benzyl boronic acid **9** (**p7c**) (Scheme 3.6). The functionalization of the Bpin-terminus requires free Pd(0) catalyst in the reaction mixture for the oxidative addition into the aryl-halogen bond of the end capping agent, hence, a step growth mechanism is inevitable. Notably, the complimentary strategy to use an end capper bearing a boronic ester terminates all active chains in case of a chain-growth mechanism. In the case of **p6e** the functionalization is far from quantitative as observed by ^{1}H NMR spectroscopy and mass spectrometry probably due to partial deboronation (H/Br endcapped series in the MALDI-ToF spectrum) or incomplete conversion. In contrast, the functionalization using the boronic pinacol ester **9** resulted in a much higher degree of functionalization

as verified by ^{1}H NMR spectroscopy as well as MALDI-ToF MS and demonstrates the potential to prepare functional telechelic poly(3,6-carbazole)s by the addition of end cappers.

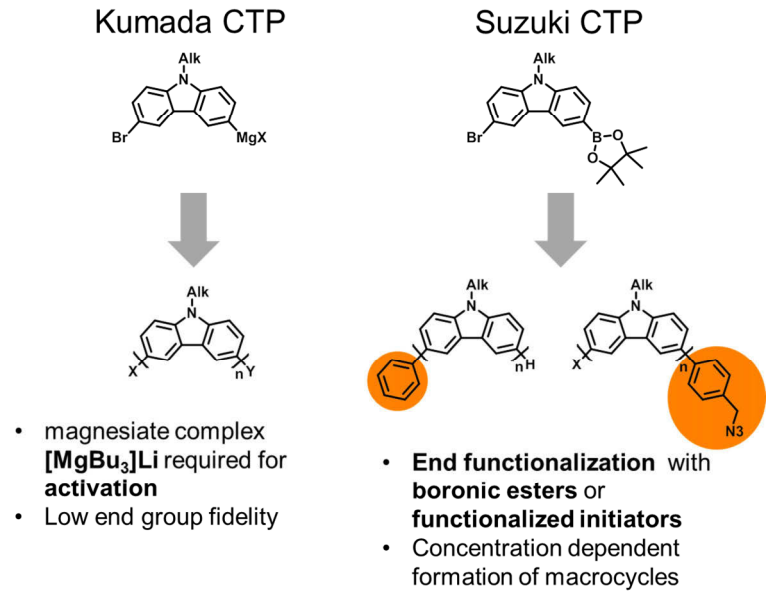

Scheme 3.7. Summary of the most important findings for the preparation of telechelic poly(3,6-carbazole)s by Kumada or Suzuki CTP.

In summary, the polymerization of bifunctional *N-alkyl*-3,6-carbazoles was systematically investigated and analyzed in detail by ^{1}H NMR spectroscopy, SEC and mass spectrometry to prepare telechelic polymers. The most important findings for the synthesis by Kumada or Suzuki CTP are summarized in Scheme 3.7. In the case of KCTP, conventional Grignard reagents yielded incomplete metal halogen exchange so that magnesiate complexes are required. However, the reaction represents a fast and facile approach to prepare H or alkyl-terminated poly(3,6-carbazoles) in a facile one pot reaction. In contrast, the Suzuki-Miyaura coupling proved to be suitable for the introduction of defined reactive end groups capable of further functionalization reactions (see Chapter 4).

4. Modularly assembled photoredox-active dyads and triads

Parts of this chapter have been published in P2) R. Schroot, T. Schlotthauer, U. S. Schubert, M. Jäger, *Macromolecules* **2016***, 49,* 2112-2123. P3) R. Schroot, T. Schlotthauer, M. Jäger, U. S. Schubert, *Macromol. Chem. Phys.* **2017**, *218*, 1600534. P6) R. Schroot, T. Schlotthauer, B. Dietzek, M. Jäger, U. S. Schubert, submitted. P7) T. Schlotthauer, R. Schroot, S. Glover, L. Hammarström, M. Jäger, U. S. Schubert submitted.

The utilization of functional initiators or functional end capping reagents in the polymerization process represents a key requirement for the construction of modularly assembled photoredox-active dyads and triads. The presented telechelic polymers (Chapter 3) enable various synthetic linkages with Ru(II) complexes in order to engineer polymer-based photosystems. The first part of this chapter focusses on the development of a modular assembly strategy based on orthogonal coupling reactions for the step-wise, defect-free construction of photosystems. The modularity of the approach guarantees comparability and reproducibility as one polymer batch can be used for several architectures. Moreover, individual building blocks of the architecture are readily exchanged due to the general scope of the linking reactions. The second part of the chapter details the spectroscopic characterization of the compounds to investigate charge and/or energy transfer steps in the architectures. The steady state absorption and emission properties are explored, followed by time-resolved experiments for selected substances. Noteworthy, also triarylamine based polymers (**Cl-p10$_{15}$**), which were investigated during the diploma thesis,[22] were used as electron donor blocks.

4.1. Modular assembly strategies

The fundamental working principle of the chosen approach to construct linear polymer-based photosystems was already exemplarily demonstrated in previous work (Chapter 1), however, only one linking motif was applied. Hence, initially three different linkage reactions for the synthesized telechelic pNDIs and functionalized ruthenium complexes were investigated with respect to their versatility to construct photoredox-active architectures. A series of P–A$_m$ dyads (Scheme 4.1) were prepared by Williamson ether synthesis from a hydroxyl group (top), quaternization of a pyridine unit (middle), and CuAAC reaction of a terminal alkyne (bottom). Additionally, the corresponding

benzylated complexes (**C1**-**C3**) were synthesized in analogy to the dyads and serve as proper reference complexes for the spectroscopic studies (*vide infra*).

The reaction of the complex $[Ru(dqp)(dqp\text{-}OH)][PF_6]_2$ and pNDI was reported previously,[23] however, the reaction with **Cl-p1$_{17}$** gave only low conversions to the dyad **D1** (Scheme 4.1, top). The reaction progress was monitored by thin-layer chromatography (TLC) and analytical size-exclusion chromotagraphy (SEC). After one day no further conversion was detected. Hence, in analogy to the Finkelstein reaction potassium iodide was added, which resulted in an enhanced reactivity and significantly increased conversion.

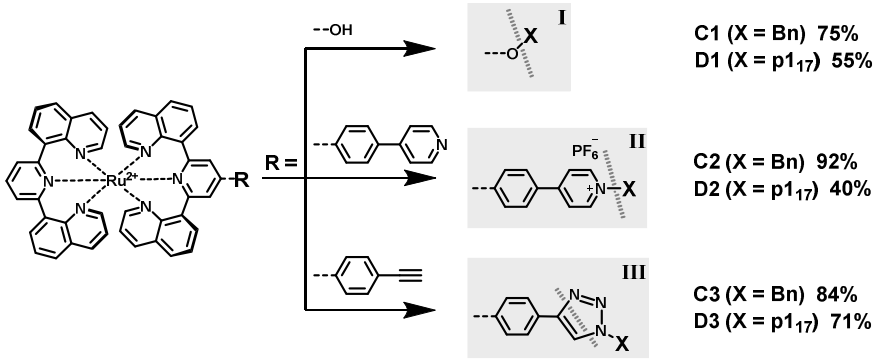

Scheme 4.1. Schematic representation of the investigated linking protocols (I to III) to synthesize the reference complexes **C1** to **C3** and the respective dyads **D1** to **D3**.

The complexes as well as the architectures feature a remarkably increased polarity in contrast to the polymer and, thus, salt containing eluents were required for the purification by column chromatography on silica gel. As a consequence, amino- and diol-functionalized silica gels with a reduced surface polarity were tested in order to achieve a facile purification. These stationary phases can be run with all common solvents (mixtures) as eluents and, indeed, enabled the successful separation. In contrast to salt containing eluents, a counter-ion exchange is not required and, thus, simplifies the purification in comparison to the traditional eluent systems used on silica. The ^{1}H NMR spectrum of **D1** is well resolved, *i.e.*, it clearly confirms the presence of the ligand scaffold of the Ru(II)-fragment and the characteristic shift of the bridging methylene protons in comparison to **Cl-p1$_{17}$** (4.57 ppm to 5.57 ppm). Furthermore, the successful linkage was verified by MALDI-ToF MS analysis. Subsequently, an alternative nucleophilic substitution reaction was investigated for **Cl-p1$_{17}$** and the 4-pyridyl-decorated complex $[Ru(dqp)(dqp\text{-}ph\text{-}py)][PF_6]_2$. The reaction showed almost no conversion after 24 hours at 50 °C. As a consequence, potassium iodide and potassium

hexafluorophosphat (as a source of non-nucleophile counter-ions to prevent the potential cleavage of the pyridinium) were added and the temperature was raised to 70 °C. After two days, the quantitative conversion of the complex [Ru(dqp)(dqp-ph-py)][PF_6]$_2$ was detected by 3D UV/vis SEC and the pure dyad **D2** was isolated. The MALDI-ToF MS spectrum revealed an intense fragmentation of **D2**. The major series shows the typical spacing of the NDI repeating unit and the absence of the Ru fragment is indicated by the narrows peaks. According to isotope simulations, the series is characterized by the typical elimination of the TIPNO group occurring at one polymer chain terminus (as also observed for the non-functionalized polymer), whereas the other chain terminus would correspond to C_7H_8. The latter "end group" is attributed to the fragmentation of the highly charged pyridinium-Ru^{II} subunit (charge +3). Thereby, the linking carbon-nitrogen bond of the benzylpyridinium moiety is cleaved leading to a singly charged polymer fragment (Figure 4.1). Subsequently, a rearrangement and the final elimination of ethyne lead to a cyclopentadienyl cation as the dominant detected species, which is well-known for benzylic compounds.[154]

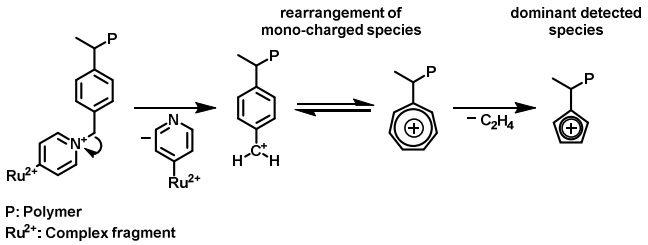

Figure 4.1. Proposed fragmentation of **D2** during MALDI ToF MS including benzyl cleavage resulting in the formation of a singly charged polymer species and subsequent consecutive reactions. (Reprinted with permission from Ref.[88]. Copyright 2016 American Chemical Society)

Finally, the copper(I)-catalyzed azide-alkyne cycloaddition was tested for the preparation of **D3** from **N_3-p1$_{17}$** and [Ru(dqp)(dqp-ph-C≡CH)][PF_6]$_2$. The reaction was carried out using a standard protocol with copper(I) iodide, PMDETA and DMF. Full conversion of the polymer (checked by TLC and SEC) was detected after 16 hours. The dyad **D3** was isolated in good yields (71%) after column chromatography. The reduced yield compared to the observed full conversion of the polymer is attributed to the sampling process in order to monitor the reaction progress. Consistent with the dyads **D1** and **D2**, the successful attachment of the complex at the polymer was proved by ^{1}H NMR spectroscopy, as the signals of the methylene protons of the linker are shifted

from 4.3 ppm to 5.6 ppm. Similar to **D1**, the nitrogen-oxygen bond of the TIPNO end group is cleaved during MS analysis of the dyad **D3**.

The established end functionalization procedures (Scheme 4.1) provided a synthetic platform for the construction of a wide range of dyads and, more importantly, triads (*vide infra*) by orthogonal reaction steps. In this regard, also a hydrophilic polymer – **Cl-p3$_{10}$** – was chain end decorated with the complex [Ru(dqp)(dqp-OH)][PF$_6$]$_2$ to prepare the water-processible dyad **D4**. Notably, this compound was isolated by preparative size-exclusion chromatography using the Toyopearl HW-55F resin and not by the aforementioned functionalized silica gels. The purification according to the hydrodynamic volume avoids typical challenges related to ordinary column chromatography of metal complexes, *e.g.*, adsorption of the analyte on the stationary phase or minor polarity differences. Additionally, a dyad (**D7**) containing the azide end functionalized polycarbazole **N$_3$-p7c** was prepared. All prepared dyads and triads and their respective polymeric building blocks are listed in Table 4.1.

Table 4.1. Overview of the prepared dyads and triads as well as the respective polymeric building blocks (electron acceptors in blue, donors in green) and utilized Ru(II) complexes.

Entry	*Architecture*	*Linking reaction*	*Polymer(s)*	*Complex*
1	**D1**	I	**Cl-p1$_{17}$**	[Ru(dqp)(dqp-OH)][PF$_6$]$_2$
2	**D2**	II	**Cl-p1$_{17}$**	[Ru(dqp)(dqp-ph-py)][PF$_6$]$_2$
3	**D3**	III	**N$_3$-p1$_{17}$**	[Ru(dqp)(dqp-ph-C≡CH)][PF$_6$]$_2$
4	**D4**	I	**Cl-p3$_{10}$**	[Ru(dqp)(dqp-OH)][PF$_6$]$_2$
5	**D5**	I	**Cl-p10$_{15}$**	[Ru(dqp-OH)(dqp-ph-C≡C-TIPS)][PF$_6$]$_2$
6	**D6**	I	**Cl-p1$_{19}$**	[Ru(dqp-OH)(dqp-ph-C≡C-TIPS)][PF$_6$]$_2$
7	**D7**	III	**N$_3$-p7c**	[Ru(dqp)(dqp-ph-C≡CH)][PF$_6$]$_2$
8	**T1**	I + III	**Cl-p10$_{15}$** **N$_3$-p1$_{17}$**	[Ru(dqp-OH)(dqp-ph-C≡C-TIPS)][PF$_6$]$_2$
9	**T2**	I + III	**N$_3$-p7c** **Cl-p1$_{19}$**	[Ru(dqp-OH)(dqp-ph-C≡C-TIPS)][PF$_6$]$_2$

In order to construct D$_n$–P–A$_m$ triads, the bifunctional ruthenium complex [Ru(dqp-OH)(dqp-ph-C≡C-TIPS)][PF$_6$]$_2$ was utilized in a step-wise orthogonal reaction

procedure. At first, one chloromethyl end functionalized polymer was linked by the established nucleophilic substitution to the precursor complex [Ru(dqp-OH)(dqp-ph-C≡C-TIPS)][PF_6]$_2$ to from **D5** or **D6**. In the second step, the TIPS protection group was cleaved and the second block was attached by the CuAAC reaction leading to the photoredox-active D_n–P–A_m architectures **T1** and **T2**. Noteworthy, due to the low observed reaction rate, the reaction temperature was increased to 80 °C for these systems in comparison to the dyads. The prepared triads are depicted in Scheme 4.2. Note, that the polymer **Cl-p10$_{15}$** represents a styrene based butyl substituted polytriarylamine which was prepared during previous work.[22] In analogy to the previous described systems, the purification was achieved by preparative SEC after each coupling step. The covalent linkage of the polymers and the complex was verified by the shift of the respective bridging methylene protons in the ^{1}H NMR spectrum and also by 3D UV/vis SEC analysis.

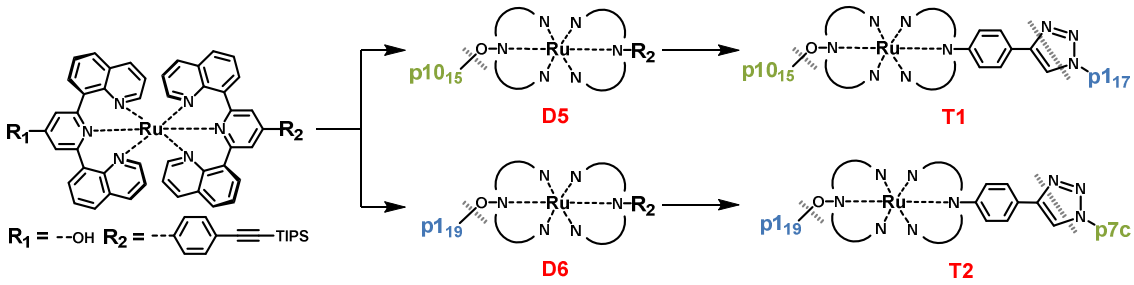

Scheme 4.2. Step-wise modular synthesis leading to the triads **T1** and **T2**.

In summary, the applied modular approach utilizing orthogonal coupling reactions in combination with functional Ru(II) complexes and telechelic polymers enabled a facile construction of various defect-free, highly defined photoredox-active architectures (Table 4.1). Moreover, the developed purification protocols using functionalized silica gels or size-exclusion resins facilitated a straightforward isolation of the compounds.
The potential of the prepared dyads and triads for light-induced charge separation applications was examined by steady state and transient spectroscopic measurements and will be discussed in the next chapter.

4.2. Spectroscopic characterization

The steady state optical properties of the dyads and triads enable the analysis of photo-initiated processes, which will be related to the functional building blocks, *i.e.*, the polymer blocks and the Ru(II) photosensitizer. The absorption spectra contain valuable information on potential interactions (*e.g.*, *H*- or *J*-aggregation)[97] of the building blocks. The emission and excitation data enable the analysis of both the properties as well as the origin of the excited states and are necessary for the discussion of energy or electron transfer steps (*vide infra*).

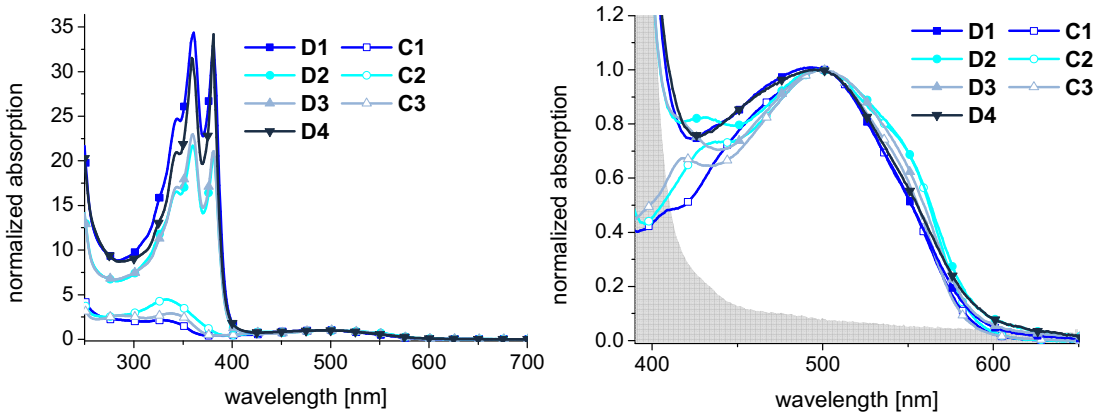

Figure 4.2. Absorption data of the dyads (**D1** to **D4**) and the corresponding model complexes (**C1** to **C3**) in CH_2Cl_2 (normalized at 500 nm). Left: UV-vis spectral region illustrating the dominant UV absorption of the pNDI chains. Right: Inset of the MLCT region illustrating preserved optical properties of the Ru photosensitizers (grey area depicts the low-energy tail of the pNDI absorption).

The absorption spectra of the P−A_m dyads **D1** to **D4** as well as of the reference complexes **C1** to **C3** are depicted in Figure 4.2. The UV region is dominated by the intense absorption bands attributed to the π→π* transitions of the NDI units (Figure 4.2, left) and the spectral shape agrees with the spectrum of individual naphthalene diimide units, *e.g.*, absorption maxima centered at 360 and 380 nm. In line with the isolated polymers, the absence of significant additional detectable features indicates negligible NDI–NDI interactions in solution. The Ru photosensitizer absorption is identified in the visible area (Figure 4.2, right). The model complexes (**C1** to **C3**) exhibit the typical metal-to-ligand charge transfer (MLCT) bands centered at 500 nm, which are preserved upon attachment of the polymer chain. Therefore, the absorption data underline the modular concept of the architectures, *i.e.*, the absorptivity of the individual building blocks is preserved.

The dyads and respective model complexes were investigated by steady state emission spectroscopy under ambient conditions, *i.e.*, in aerated dichloromethane at room temperature using iso-absorbing solutions at 500 nm excitation (Figure 4.3). The model complexes display the typical Ru-based emission from the ^{3}MLCT state between 650 to 700 nm. A minor influence of the substitution pattern on the maximum is observed. In agreement with a previous report,[155] the electron-releasing alkoxy-substitution (**C1**) leads to a bathochromic shift of approximately 15 nm in comparison to the π-extended phenyl-decorated complexes **C2** and **C3**. As the emission decay is more efficient for lower excited state energies within a series (energy gap law),[156] **C1** features a significantly lower absolute quantum yield than the phenyl-decorated congeners. More importantly, the emission spectra of the corresponding dyads differ markedly. In all compounds, the Ru emission is efficiently quenched. Additionally, an emission centered at 550 nm is observed, which is tentatively credited to polymer-based emissive states.[23]

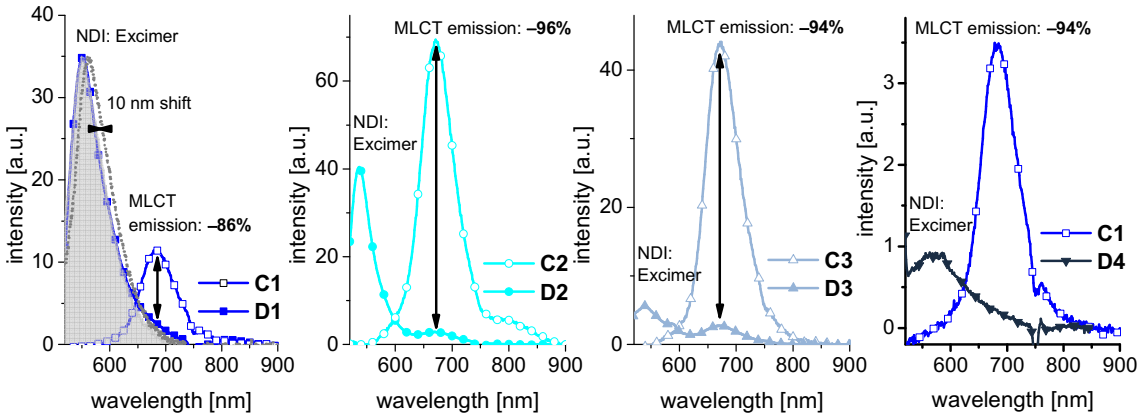

Figure 4.3. Emission data of the model complexes and the corresponding dyads (aerated CH_2Cl_2, room temperature, iso-absorbing solutions at 500 nm excitation). Left: Ether-linked complex **C1** complemented by polymer-based emission (**D1**: Grey area, dotted line: pNDI) to illustrate residual MLCT contribution. Middle left and middle right: Pyridinium- and triazole-linked congeners **D2** and **D3**. Right: Hydrophilic dyad **D4**.

The efficiency of the ^{3}MLCT excited state quenching is calculated from the residual Ru-based emission with respect to the corresponding model complexes. Note, that the contribution of the overlapping polymer-based emission is accounted by subtracting a scaled pNDI spectrum, as depicted in Figure 4.3 (left). Within the experimental errors, the ^{3}MLCT quenching appears to be independent of the solubilizing side chain of the NDI units or the length of the linker as the efficiency is very high in all cases (86% to

96%). Based on our previous analysis, this observation indicates a highly efficient light-induced charge separation for **D1** to **D4**.[23]

The absorption spectra of the triads (**T1** and **T2**) as well as the respective D_n–P dyads (**D5** and **D7**) are depicted in Figure 4.4 and, once again, illustrate the preserved optical properties of the individual building blocks. The spectra of **D5** and **D7** are dominated by the UV absorption of the triarylamine (300 nm, **D5**) or carbazole (312 nm, **D7**) units. In the case of the triads **T1** and **T2**, the broad absorption between 250 and 400 nm is assigned to the overlapping absorption bands of the pNDI (360 and 380 nm) and the respective donor polymers. Additionally, the ^{1}MLCT band of the Ru(II) photosensitizer is observed in all compounds centered at 500 nm.

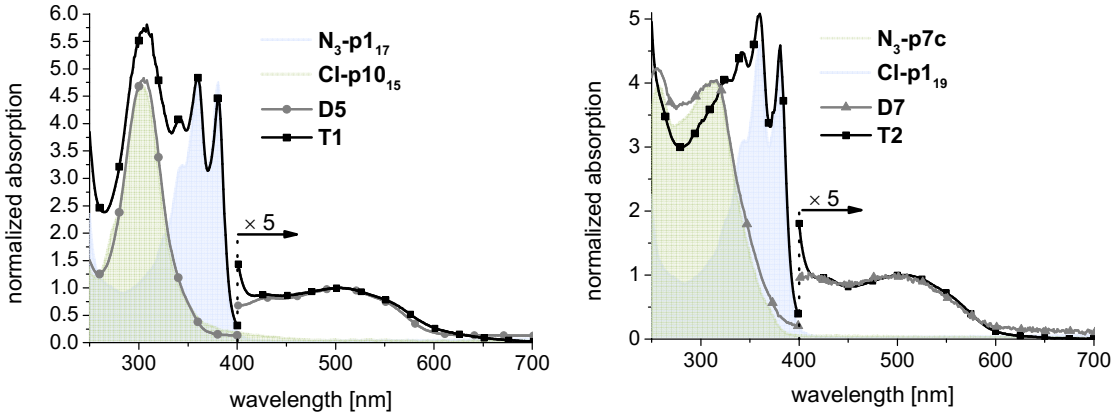

Figure 4.4. Absorption spectra of the prepared triads and their respective D_n–P dyads revealing the modular character of the architectures (normalized at 500 nm, aerated CH_2Cl_2, room temperature)). The green (donor) and blue (acceptor) areas depict the absorption of the polymers. Left: **T1** and **D5**. Right: **T2** and **D7**. Note the scaled absorption (×5) above 400 nm (^{3}MLCT area) to increase visibility.

Light-induced electron and energy transfer processes were detailed by steady state and time-resolved spectroscopic measurements of the triads in comparison to the respective donor dyads and suitable reference complexes. In the case of **D5**, an intense ^{3}MLCT emission band of the photosensitizer centered at 685 nm was observed (Figure 4.5, left). This observation indicates the absence of a charge transfer to the TARA polymer as this reductive quenching is energetically unfavored (+0.20 eV).[23] In contrast, in **T1** the presence of the NDI polymer (**p1$_{17}$**) enables an oxidative quenching (−0.25 eV)[23] and results in an efficient quenching of the photosensitizer's emission (96% efficiency). Further, the formation of the fully charge separated state D_n^+–P–A_m^- was identified by transient spectroscopic measurements. Upon excitation with a laser pulse at 532 nm

(exclusive excitation of the photosensitizer), a spectral trace evolves which resembles the absorption features of the reduced acceptor $pNDI^-$ and the oxidizied donor $pTARA^+$ (Figure 4.6, left). In this regard, absorption bands at 480 nm ($pNDI^-$) and 690 nm ($pTARA^+$) were observed and prove the formation of the fully charge separated state D_n^+–P–A_m^-. The longest life time of a component in the biexponential fit was determined with 2.4 µs, which represents an increase by one order of magnitude in comparison to a reported low molecular mass [Ru(dqp)$_2$]-based triad.[157] This observation is tentatively assigned to the polymer linkage.

Whereas in **D5** and **T1** no reductive quenching was observed, the ^{3}MLCT emission is reduced in **D7** (approximately −25%) compared to the model complex [Ru(dqp)(dqp-ph-tr-bn)][PF$_6$]$_2$, which features the same substitution pattern as **D7** but is linked to a benzyl group. Even though, the quenching is far from quantitative, this observation suggests the partial formation of a reduced complex and an oxidized polymer by a reductive pathway, which was further investigated by transient absorption (TA) spectroscopy. Noteworthy, the formal redox potential of the poly(3,6-carbazole) **p7c** is 0.22 V *vs.* $Fc^{+/0}$, which is 0.14 V less compared to the pTARA donor polymer. Consequently, the driving force for reductive quenching is also less endergonic even without considering the coulombic contribution and the favorable entropic factors. So, this pathway cannot be excluded. In the triad **T2** the linking to the NDI polymer and the supposed formation of a charge separated state is indicated by an efficient emission quenching (96%) (Figure 4.5).

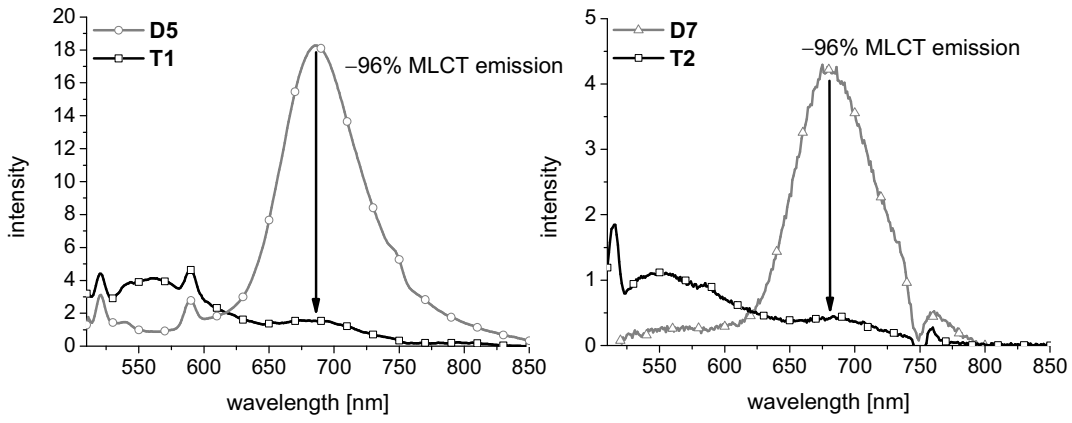

Figure 4.5. Steady state emission data of the triads and respective D_n–P dyads showing an efficient MLCT emission quenching (aerated CH_2Cl_2, room temperature, iso-absorbing solutions at 500 nm). Left: **T1** and **D5**. Right: **T2** and **D7**.

A possible reductive quenching in the dyad **D7** was investigated by determination of the excited state life times of the Ru(II) photosensitizer in the transient absorption or emission spectrum. Based on the fitting of the decay traces of the MLCT bleach (470 nm, transient absorption) and the MLCT emission (700 or 750 nm, transient emission), the life times were calculated to be 3 µs for the reference complex [Ru(dqp)(dqp-ph-tr-bn)][PF_6]$_2$ and 2 µs for the dyad **D7**. Moreover the TA spectrum of **D7** shows an increased absorptivity above 600 nm and a shift of the isosbestic point from 439 to 449 nm which is attributed to the formation of oxidized polycarbazole ($pCarb^+$). Consequently, also the global fit gives a signature which differs from the photosensitizer due to the partial reductive quenching.

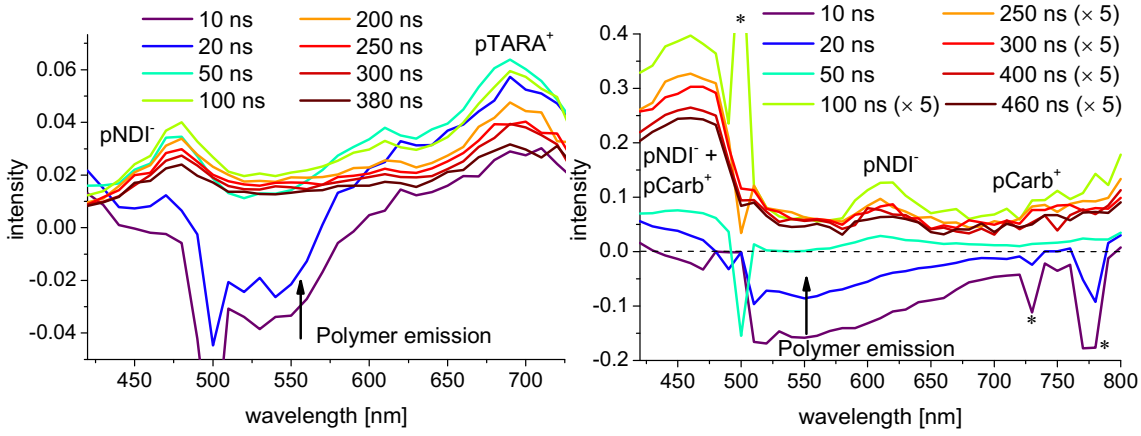

Figure 4.6. Transient absorption data showing the formation of a fully charge separated state upon excitation (purged CH_2Cl_2, optical density approx. 0.1 at 500 nm). Left: **T1**, the reduced acceptor $pNDI^-$ is identified by the evolving absorption band at 480 nm, the oxidized donor $pTARA^+$ displays an absorption at 690 nm (laser pulse at 532 nm). Right: **T2**, the oxidized donor $pCarb^+$ features an absorption at 420 nm and above 600 nm (laser pulse at 500 nm). Note the scaled (×5) traces from 100 ns to 460 ns to increase visibility. Artifacts are marked with an asterisk.

The ground state recovery of the Ru(II) photosensitizer is very fast in the triad **T2** (<10 ns) and, additionally, new absorption features with maxima at 430 to 450 nm and a broad absorption band above 600 nm evolve (Figure 4.6, right). The spectral signatures of the traces from 400 to 460 ns resemble the overlapping absorption spectra of the reduced $pNDI^-$ and the oxidized $pCarb^+$. Consequently, the linking to the pNDI facilitates an oxidative quenching and efficiently results in the formation of a fully charge separated state D_n^+–P–A_m^-. Based on the TA trace at 470 nm the life-time of the charge separated state was determined by a bi-exponential fit and revealed two

processes with life times of 0.7 µs and 7.2 µs, respectively. According to the global fit of the TA data, both processes feature the same spectral signature. The first process is assigned to a direct charge recombination after initial charge separation, the second to combination processes after charge transfer steps in the polymer. Consequently, the application of the conjugated donor polymer results in an one order of magnitude longer life time in comparison to a related low molar mass compound but also a three times increase in comparison to **T1**.[157] This observation is assigned to the electronic coupling within the conjugated polymer leading to a more efficient delocalization of the electron hole and a larger spatial charge separation in comparison to a redox-active electron donor.

Table 4.2. Quenching and charge separation properties of the prepared triads.[a]

compound	Q_{MLCT} *[%]*	$t_{1,CS}$ *[ns]*	$t_{2,CS}$ *[ns] (ratio)*
T1	96	430 (70%)	2400 (30%)
T2	96	700 (83%)	7200 (17%)

[a]Q_{MLCT} is the calculated quenching efficiency compared to the donor dyads, $t_{1,CS}$ and $t_{2,CS}$ are the charge separated state life times of the components of the fit.

A summary of the spectroscopic properties and the occurring processes leading to a charge separation in the triad is given in Table 4.2 and Scheme 4.3. Noteworthy, the inverted linking pattern of **T1** and **T2** has no influence on the charge separation process, which was proved by comparison of **T1** and the respective inverted triad (unpublished results).

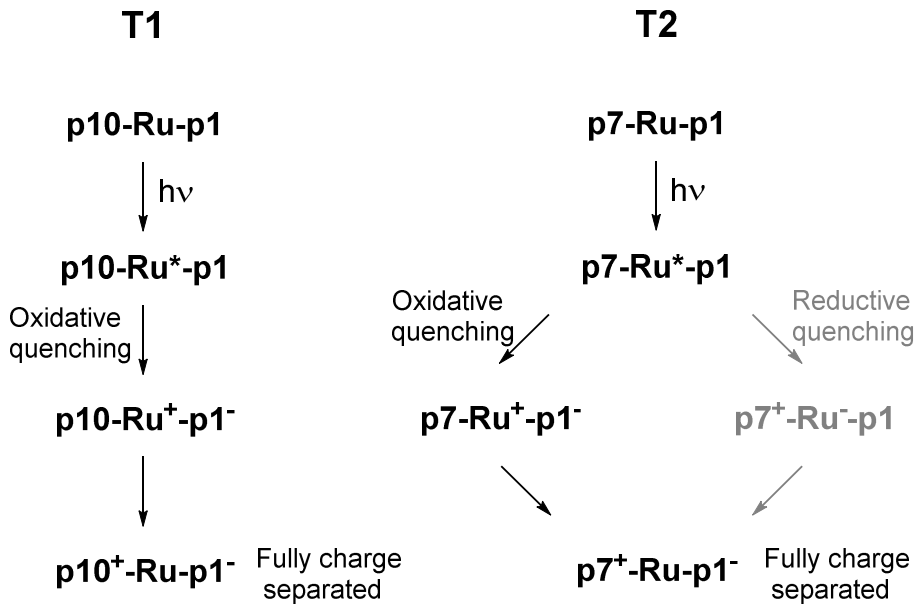

Scheme 4.3. Summary of the occurring processes after excitation of the photosensitizers leading to a charge separation in the triads **T1** and **T2**. Note, that the reductive quenching pathway (grey) was in particular observed in the donor-dyad **D7** but probably also occurs as side reaction in **T2**.

A further improvement of the hitherto presented architectures may be achieved by the utilization of triarylamine based block copolymers with an internal redox gradient as electron donors. TA measurements on the respective compounds revealed a further increased life time due to the formed redox cascade with decreasing oxidation potential. So, a hole transfer in the donor is facilitated but a charge recombination is hampered (unpublished results).

5. Summary

Polymer-based photoredox-active architectures represent an exciting class of materials for the conversion of sun light into electricity or chemical bond energy, *e.g.*, in photovoltaic or photocatalytic cells. These materials consist of a photosensitizer for light absorption, *e.g.*, a Ru(II) polypyridyl complex, as well as electron donor and acceptor sites for the charge separation and charge transport.

In this thesis, the synthesis of redox-active and conjugated telechelic electron acceptor and donor polymers was studied (Scheme 5.1). Moreover, the modular assembly of these polymers to photoredox-active dyads and triads was elucidated. Steady state and transient spectroscopic measurements of architectures revealed the light-induced charge separation.

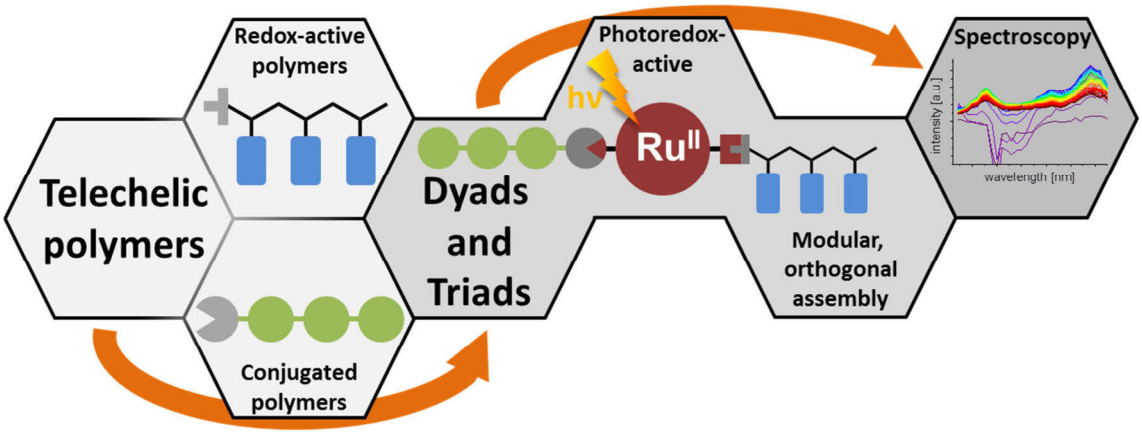

Scheme 5.1. Telechelic redox-active and conjugated polymers as modular building blocks for photoredox-active dyads and triads. Their properties were detailed by spectroscopic measurements.

The synthesis of telechelic hydrophobic and hydrophilic NDI based redox-active polymers was investigated in **Chapter 3.1**. Styrenic monomers with incorporated ethylhexyl, oligo- and polyethylene glycol side chains were prepared by an optimized two-step synthesis including column chromatography with silica or size-exclusion resins in case of the highly polar polyethylene glycol decorated monomer **3**. Subsequently, polymerization utilizing the functional commercial initiator CMSt-TIPNO yielded the polymers **Cl-p1**, **Cl-p2** and **Cl-p3** with defined molar masses, low dispersities ($Đ < 1.3$) and a reactive end group capable of further functionalization. Noteworthy, the polymerization kinetics were analyzed for the monomers with oligo-

and polyethylene glycol side chains (**2** and **3**) and revealed a controlled reaction mechanism up to 80 or 60% conversion, respectively. Deviations from the ideal behavior were in particular found for monomer **3** at prolonged reaction times.

In order to broaden the range of suitable end functionalization reactions with photosensitizers, the functional chloromethyl group of the initiator fragment was substituted to an azidomethyl group for polymer **N_3-p1**. The successful modification was verified by ^{1}H NMR and IR spectroscopy. As a consequence of the polar side chains in **Cl-p2** and **Cl-p3**, the hydrophilicity of these polymers was increased in comparison to **Cl-p1**. In this regard, the solubility in polar solvents increased from **Cl-p1** to **Cl-p3** and a moderate water-solubility was reached for **Cl-p3**, which is decorated with polyethylene glycol side chains. Noteworthy, the optical absorption properties of the polymers did not change due to the variation of the side chains.

Whereas the tuning of the processing properties was of special interest for the pNDI acceptor polymers, the increase of the charge carrier mobility by introduction of a conjugated backbone was a central concern in case of the donor polymers and was presented in **Chapter 3.2**. In this regard, the Kumada catalyst transfer and Suzuki-Miyaura coupling polymerization were studied to prepare telechelic poly(*N*-alkyl-3,6-carbazole)s which feature a transparence in the visible area, a reversible electrochemical oxidation process and are readily accessible from commercial 9H-carbazole. Firstly, the activation of 3,6-dibromo-*N*-octylcarbazole with various Grignard reagents and the subsequent polymerization using [Ni(dppp)Cl_2] was screened. The systematic investigation revealed the necessity to apply magnesiate complexes to achieve a quantitative metal-halogen exchange and, hence, a high conversion during the following polymerization. The end groups of the prepared polymers were analyzed by MALDI-ToF mass spectrometry and indicated an increase of alkyl-terminated chains with increasing reactivity of the applied Grignard reagents. In this regard, ^{i}PrMgCl mainly gave Br-decorated chains, whereas $Li^+[^nBu_3Mg]^-$ resulted in butyl terminated polymer chains as dominant species. These findings imply that an efficient synthesis of poly(3,6-carbazole)s utilizing KCTP and magnesiate complexes is possible if a high functional end group fidelity is not necessary. However, due to the inevitable catalyst dissociation and related side reactions, the preparation of telechelic polymers is precluded with the investigated catalyst systems. Consequently, the scope of the Suzuki-Miyaura polymerization to prepare telechelic poly(*N*-alkyl-3,6-carbazole)s was screened. As the polymerization was carried out with bromo- and boronic ester substituted A−B-type

monomers, limitations caused by the incomplete metal-halogen exchange in case of the KCTP were avoided. Various reaction conditions, *i.e.*, reaction temperatures, concentrations, solvents, bases, catalysts and end capping reagents, were investigated and revealed the strongly concentration dependent formation of cyclic oligomers besides the desired linear polymer. An improvement of the polymerization characteristics, *e.g.*, chemical yield, dispersity and end group fidelity, was achieved by the reduction of the reaction temperature to room temperature or 0 °C even though a catalyst dissociation could not be precluded. The application of the functionalized initiator [(P^{t}Bu$_3$)Pd(Ph)Br] resulted in the formation of poly(3,6-carbazole) with Ph/H decorated chain ends. Noteworthy, unfunctionalized species were trapped as cyclic oligomers due to the high dilution conditions. Furthermore, end capping studies with *para*-azido benzyl boronic acid pinacol ester resulted in a high degree of functionalization of the polymer **N$_3$-p7c** as judged by ^{1}H NMR spectroscopy. In this regard, the end capped polymer **N$_3$-p7c** demonstrated the potential of the Suzuki-Miyaura polymerization to prepare telechelic poly(3,6-carbazole)s and was used for the construction of photoredox-active architectures.

The prepared telechelic redox-active and conjugated polymers were utilized as electron donor and acceptor blocks in combination with various Ru(II) photosensitizers to construct photoredox-active architectures as reported in **Chapter 4.1**. Initially, the polymer **Cl/N$_3$-p1$_{17}$** was chain end decorated with a Ru(II) photosensitizer applying three different linking protocols. The investigated reactions – two nucleophilic substitutions and the CuAAC reaction – gave the desired dyads in good yields. Based on these coupling approaches further architectures, *e.g.*, a hydrophilic A$_m$–P dyad, were prepared. Moreover, the orthogonal character of the reactions enabled the construction of two photoredox-active A$_m$–P–D$_n$ triads, which can be regarded as block copolymers with a central Ru(II) unit. As the isolation of the pure compounds was hampered by ordinary adsorption column chromatography, efficient purification protocols applying amino- and diol-functionalized silica gels and, in particular, size-exclusion resins were developed.

The spectroscopic properties of the prepared architectures were detailed by steady state absorption and emission spectroscopy. In case of the triads and the respective dyads additional transient spectroscopic measurements were performed and are reported in **Chapter 4.2**. The absorption data revealed preserved optical properties upon linkage of the individual building blocks, *i.e.*, the spectra consist of the overlapping individual

absorption bands, and demonstrated the modular character of the synthetic approach. In contrast, energy and charge transfer steps were identified in the A_m–P dyads by an efficient quenching of the photosensitizer's MLCT emission band in the steady state emission spectrum. The quenching was found to be independent of the linking pattern between the pNDI and the Ru(II) complex and the solubilizing side chains of the polymer.

More importantly, the prepared triads **T1** and **T2** showed a very efficient emission quenching (>96%). The formation of a fully charge separated state was proved by transient absorption measurements as absorption bands of new species evolve which resemble the spectra of the oxidized donor and the reduced acceptor. In contrast to low molecular mass triads, the life time of the charge separated state was increased by one order of magnitude and reached the μs-time scale in the triads. In particular, the utilization of the conjugated donor-polymer was beneficial to achieve long lived charge separated states.

In summary, telechelic redox-active and conjugated polymers were synthesized and subsequently utilized as modular functional building blocks for the construction of photoredox-active architectures. The time-resolved spectroscopic investigation revealed an efficient emission quenching and the occurrence of a long-lived light-induced charge separation in the μs-time scale in the triads. Consequently, the potential of the chosen approach to utilize polymers as electron donor and acceptor sites in defect-free linear photosystems is clearly demonstrated. Moreover, the design strategy offers further possibilities with respect to the assembling by self-organization of the hydrophobic and hydrophilic parts of the block copolymer-like structures. Additionally, the prepared architectures may be utilized to realize light-triggered local redox gradients to power molecular machines.

6. Zusammenfassung

Polymerbasierte photoredox-aktive Architekturen stellen eine interessante Materialklasse zur Umwandlung von Sonnenlicht in elektrische oder chemisch gebundene Energie, z.B. in photovoltaischen oder photokatalytischen Zellen, dar. Entsprechende Materialien bestehen aus einem Photosensibilisator zur Lichtabsorption, z.B. einem Ru(II)-Polypyridylkomplex, und Elektronendonor- sowie -akzeptoreinheiten zur Ladungstrennung und zum anschließenden Ladungstransport.

In der vorliegenden Arbeit wurde zu Beginn die definierte Herstellung von telechelen redox-aktiven und konjugierten Polymeren untersucht (Scheme 6.1). Anschließend konnten die Polymere zum modularen Aufbau von photoredox-aktiven Dyaden und Triaden verwendet werden. Das Auftreten einer Licht-induzierten Ladungstrennung in den Architekturen wurde abschließend mittels zeitlich stationärer und zeitaufgelöster spektroskopischer Methoden nachgewiesen.

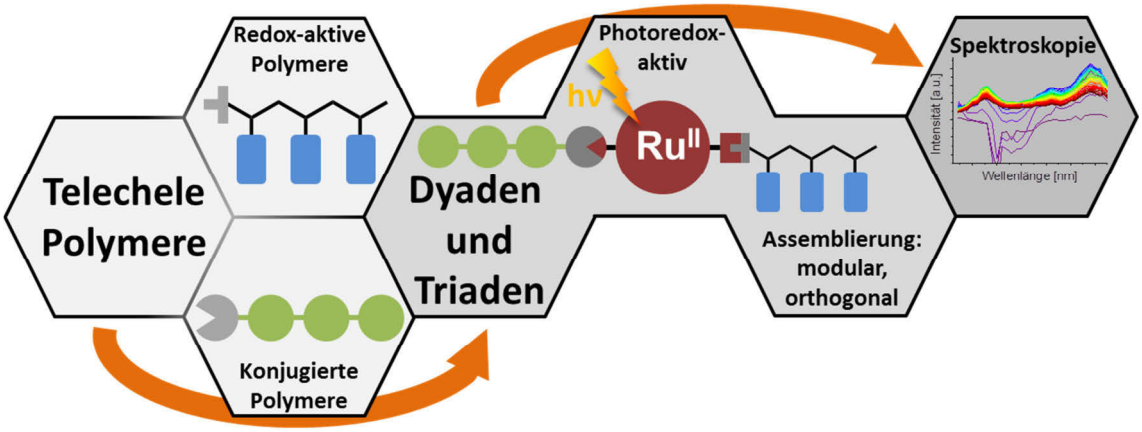

Scheme 6.1. Telechele redox-aktive und konjugierte Polymere als modulare Bausteine für photoredox-aktive Dyaden und Triaden. Die Eigenschaften wurden mittels spektroskopischer Messungen untersucht.

Die Synthese von telechelen hydrophoben und hydrophilen NDI-basierten redox-aktiven Polymeren ist im **Kapitel 3.1** präsentiert. Die entsprechenden Monomere mit Ethylhexyl- sowie Oligo- als auch Polyethylenglykolseitenketten wurden durch eine optimierte Zwei-Stufen-Synthese hergestellt. Die Aufreinigung erfolgte dabei entweder durch Adsorptionschromatographie mit Silikagel oder durch Größenausschluss-chromatographie im Falle des sehr polaren Monomers **3**, welches eine Polyethylenglykolseitenkette trägt. Für die anschließende Polymerisation wurde der kommerziell erhältliche Initiator CMSt-TIPNO verwendet, da er durch seine

Chlormethylgruppe weitere Postpolymerisationsmodifikationen erlaubt. Die hergestellten Polymere **Cl-p1**, **Cl-p2** und **Cl-p3** wurden mit definierter molarer Masse und einer engen Molmassenverteilung, also kleiner Dispersität (Đ < 1.3), isoliert. Zusätzlich konnte durch eine kinetische Studie für die Monomere **2** und **3**, welche aufgrund ihrer Seitenketten über eine erhöhte Polarität verfügen, gezeigt werden, dass bis zu jeweils 80% beziehungsweise 60% Umsatz eine kontrollierte Polymerisation stattfindet. Abweichungen vom idealen Verhalten traten im Besonderen bei sehr langen Reaktionszeiten für Monomer **3** auf.

Um eine breite synthetische Ausgangsplattform zur Kopplung der Polymere mit verschiedenen Photosensibilisatoren zu erhalten, wurde das funktionale Chlormethyl-Initiatorfragment des Polymers **Cl-p1** in eine Azidmethylgruppe überführt (**N_3-p1**). Durch IR-Spektroskopie sowie ^{1}H-NMR-Messungen konnte die quantitative Substitution der Endgruppe belegt werden.

Die Hydrophilie der Polymere **Cl-p2** und **Cl-p3** ist aufgrund der polaren Seitenketten im Vergleich zu **Cl-p1** erhöht, was eine bessere Löslichkeit in polaren Lösungsmitteln bedingt. Außerdem wurde eine moderate Wasserlöslichkeit für **Cl-p3**, das Polyethylenglykolseitenketten trägt, beobachtet. Bemerkenswerterweise änderten sich die optischen Absorptionseigenschaften der Polymere aufgrund der Variation der Seitenketten nicht.

Während für die NDI-basierten Akzeptorpolymere die Beeinflussung der Assemblierungs- und Prozessierungseigenschaften von besonderem Interesse war, stellte die Erhöhung der Ladungsträgerbeweglichkeit im Falle der Donorpolymere ein zentrales Anliegen der Arbeit dar. Dies sollte durch Einführung eines konjugierten Polymerrückgrates realisiert werden, was in **Kapitel 3.2** dargelegt wurde. Die Kumada-Katalysator-Transfer- und die Suzuki-Miyaura-Polymerisation wurden hinsichtlich ihrer Eignung zur Herstellung von telechelen Poly(*N*-alkyl-3,6-carbazol)en untersucht. Diese Polymerklasse weist eine optische Transparenz im sichtbaren Bereich auf, zeigt eine reversible elektrochemische Oxidation und ist leicht von kommerziell erhältlichem 9H-Carbazol herstellbar. Zu Beginn wurde die Aktivierung von 3,6-Dibrom-*N*-octylcarbazol mit verschiedenen Grignard-Reagenzien und die anschließende Polymerisation unter Verwendung von [Ni(dppp)Cl_2] systematisch untersucht. Die Studie zeigte deutlich auf, dass Magnesiatkomplexe für einen quantitativen Metall-Halogen-Austausch und damit verbunden einen hohen Umsatz während der folgenden Polymerisation notwendig sind. Die Endgruppen der hergestellten Polymere wurden

durch MALDI-ToF-Massenspektrometrie analysiert. Dabei zeigte sich eine Zunahme von Alkyl-terminierten Spezies mit zunehmender Reaktivität der verwendeten Grignard-Reagenzien. So resultierte die Aktivierung mit ^{i}PrMgCl hauptsächlich in Br-dekorierten Ketten, während $Li^{+}[^{n}Bu_3Mg]^{-}$ dominant zu Butyl-terminierten Polymerketten als dominante Spezies führte. Diese Erkenntnisse implizieren, dass eine effiziente Synthese von Poly(3,6-carbazol)en mittels KCTP-Technik und Magnesiatkomplexen möglich ist, wenn auf eine hohe Einheitlichkeit von funktionellen Endgruppen verzichtet werden kann. Aufgrund der unvermeidlichen Katalysatordissoziation und damit verbundener Nebenreaktionen wurde die Herstellung von telechelen Polymeren mit den untersuchten Katalysatorsystemen jedoch nicht realisiert. Folglich wurde die Suzuki-Miyaura-Polymerisation zur Herstellung von telechelen Poly(*N*-alkyl-3,6-carbazol)en untersucht. Da die Polymerisation mit Brom- und Boronsäureester-substituierten A-B-Typ-Monomeren durchgeführt wurde, konnten Einschränkungen, die sich aus dem unvollständigen Metall-Halogen-Austausch im Falle der KCTP ergeben, vermieden werden. Verschiedene Reaktionsbedingungen, z.B. die Reaktionstemperatur, Konzentrationen sowie verwendete Lösungsmittel, Basen, Katalysatoren und Endfunktionalisierungsreagenzien, wurden getestet. Dabei trat eine stark konzentrationsabhängige Bildung von zyklischen Oligomeren neben dem gewünschten linearen Polymer auf. Eine Verbesserung wichtiger Polymerisationskenngrößen, z.B. chemische Ausbeute, Dispersität und Endgruppenhomogenität, erfolgte durch die Reduktion der Reaktionstemperatur (Raumtemperatur oder 0 °C). Eine Katalysatordissoziation konnte jedoch nicht ausgeschlossen werden. Die Anwendung des funktionalisierten Initiators [($P^{t}Bu_3$)Pd(Ph)Br] führte im nächsten Schritt zur Bildung von Poly(3,6-carbazol) mit Ph/H-funktionalisierten Kettenenden. Dabei erlaubte die hohe Verdünnung der Reaktionsmischung ein Abfangen von unfunktionalisierten Ketten als zyklische Oligomere. Darüber hinaus führten Endfunktionalisierungsstudien mit *p*-Azidmethylphenylboronsäurepinacolester zu einem hohen Funktionalisierungsgrad des Polymers **N_3-p7c**, was durch ^{1}H-NMR-Spektroskopie nachgewiesen werden konnte. In dieser Hinsicht zeigte das Polymer **N_3-p7c** das Potenzial der Suzuki-Miyaura-Polymerisation zur Herstellung von telechelen Poly(3,6-carbazol)en und diente später als Baustein zur Konstruktion von photoredox-aktiven Architekturen.

Die synthetisierten redox-aktiven und konjugierten Polymere wurden als Elektronen-donor- und -akzeptorbausteine in Kombination mit verschiedenen Ru(II)-

Photosensibilisatoren verwendet, um photoredox-aktive Architekturen aufzubauen. Die Präsentation der entsprechenden Ergebnisse erfolgte in **Kapitel 4.1**. Zunächst wurden drei verschiedene Verknüpfungsmethoden zwischen dem Polymer **Cl/N$_3$-p1$_{17}$** und passend substituierten Ru(II)-Komplexen untersucht. Die Reaktionen – zwei nukleophile Substitutionen und die CuAAC-Reaktion – lieferten die gewünschten Dyaden in guten Ausbeuten und dienten als synthetischer Ausgangspunkt zur Herstellung weiterer Architekturen. So wurde beispielsweise eine hydrophile A_m–P-Dyade auf Basis dieser Kopplungsansätze synthetisiert. Darüber hinaus ermöglichte der orthogonale Charakter der Reaktionen die Konstruktion von zwei photoredox-aktiven D_n–P–A_m-Triaden, welche als Farbstoff-verknüpfte Blockcopolymere betrachtet werden können. Da die Isolierung der reinen Verbindungen durch herkömmliche Adsorptionssäulenchromatographie nicht möglich war, wurden effiziente Reinigungsprotokolle unter Anwendung von Amino- und Diol-funktionalisierten Kieselgelen und insbesondere von Größenausschlussgelen entwickelt.

Die Architekturen wurden durch Absorptions- und Emissionsspektroskopie und im Falle der Triaden und der jeweiligen Dyaden auch durch zeitaufgelöste spektroskopische Messungen charakterisiert, was in **Kapitel 4.2** beschrieben wurde. Die Absorptionsdaten zeigten, dass die optische Eigenschaften bei der Verknüpfung einzelner Bausteine erhalten bleiben, d.h. die Spektren bestehen aus den überlagerten Absorptionsbanden der Einzelkomponenten und zeigen den modularen Charakter des synthetischen Ansatzes. Energie- und Ladungsübertragungsschritte wurden in den A_m–P-Dyaden durch ein effizientes Löschen der MLCT-Emissionsbande des Photosensibilisators im Emissionsspektrum identifiziert. Dabei zeigte sich, dass sowohl das Verknüpfungsmuster zwischen dem pNDI und dem Ru(II)-Komplex als auch die löslichkeitsvermittelnde Seitenkette des Polymers keinen Einfluss auf die Emissionslöschung haben.

Im Falle der Triaden **T1** und **T2** ist die sehr effiziente Emissionslöschung (> 96%) und die damit verbundene Ausbildung eines vollständig ladungsgetrennten Zustands D_n^+–P–A_m^- hervorzuheben. Mittels transienter Absorptionsmessungen konnte die Entstehung neuer Absorptionsbanden nachgewiesen werden, die den Spektren des oxidierten Donor- und des reduzierten Akzeptorpolymers entsprechen. Im Gegensatz zu niedermolekularen Triaden wurde die Lebensdauer des ladungsgetrennten Zustands um eine Größenordnung erhöht und erreichte die µs-Zeitskala in den Triaden. Im

Besonderen die Verwendung des konjugierten Donorpolymers führte hierbei zu ausgesprochen langen Lebenszeiten.

Zusammenfassend erlaubte die Synthese von telechelen redoxaktiven und konjugierten Polymeren deren Verwendung als modulare funktionelle Bausteine für den Aufbau von photoredox-aktiven Architekturen. Die zeitaufgelöste spektroskopische Untersuchung zeigte eine effiziente Emissionslöschung und das Auftreten einer langlebigen lichtinduzierten Ladungstrennung in den Triaden im Bereich einiger Mikrosekunden. Folglich wurde das Potential des gewählten Ansatzes, Polymere als Elektronendonor- und -akzeptoreinheiten in defektfreien linearen Photosystemen zu nutzen, eindeutig unter Beweis gestellt. Darüber hinaus ergeben sich weitere Möglichkeiten hinsichtlich der Assemblierung der Architekturen unter Ausnutzung der Phasenbildungs-eigenschaften der hydrophoben und hydrophilen Teile der blockcopolymerartigen Strukturen. Weiterhin ist die Realisierung von lokalen Licht-stimulierten Redoxgradienten denkbar, um beispielsweise molekulare Maschinen anzutreiben.

7. References

[1] S. Kundu, A. Patra, *Chem. Rev.* **2017**, *117*, 712-757.

[2] L. A. Weinstein, J. Loomis, B. Bhatia, D. M. Bierman, E. N. Wang, G. Chen, *Chem. Rev.* **2015**, *115*, 12797-12838.

[3] V. Balzani, G. Bergamini, P. Ceroni, *Angew. Chem. Int. Ed.* **2015**, *54*, 11320-11337.

[4] J. J. Concepcion, R. L. House, J. M. Papanikolas, T. J. Meyer, *Proc. Natl. Acad. Sci. USA* **2012**, *109*, 15560-15564.

[5] J. H. Alstrum-Acevedo, M. K. Brennaman, T. J. Meyer, *Inorg. Chem.* **2005**, *44*, 6802-6827.

[6] L. Hammarström, *Acc. Chem. Res.* **2015**, *48*, 840-850.

[7] D. M. Ryan, M. K. Coggins, J. J. Concepcion, D. L. Ashford, Z. Fang, L. Alibabaei, D. Ma, T. J. Meyer, M. L. Waters, *Inorg. Chem.* **2014**, *53*, 8120-8128.

[8] D. Ma, S. E. Bettis, K. Hanson, M. Minakova, L. Alibabaei, W. Fondrie, D. M. Ryan, G. A. Papoian, T. J. Meyer, M. L. Waters, J. M. Papanikolas, *J. Am. Chem. Soc.* **2013**, *135*, 5250-5253.

[9] S. E. Bettis, D. M. Ryan, M. K. Gish, L. Alibabaei, T. J. Meyer, M. L. Waters, J. M. Papanikolas, *J. Phys. Chem. C* **2014**, *118*, 6029-6037.

[10] G. Leem, S. Keinan, J. Jiang, Z. Chen, T. Pho, Z. A. Morseth, Z. Hu, E. Puodziukynaite, Z. Fang, J. M. Papanikolas, J. R. Reynolds, K. S. Schanze, *Polym. Chem.* **2015**, *6*, 8184-8193.

[11] Z. Fang, A. Ito, H. Luo, D. L. Ashford, J. J. Concepcion, L. Alibabaei, T. J. Meyer, *Dalton Trans.* **2015**, *44*, 8640-8648.

[12] E. Puodziukynaite, L. Wang, K. S. Schanze, J. M. Papanikolas, J. R. Reynolds, *Polym. Chem.* **2014**, *5*, 2363-2369.

[13] Z. A. Morseth, L. Wang, E. Puodziukynaite, G. Leem, A. T. Gilligan, T. J. Meyer, K. S. Schanze, J. R. Reynolds, J. M. Papanikolas, *Acc. Chem. Res.* **2015**, *48*, 818-827.

[14] G. Leem, Z. A. Morseth, E. Puodziukynaite, J. Jiang, Z. Fang, A. T. Gilligan, J. R. Reynolds, J. M. Papanikolas, K. S. Schanze, *J. Phys. Chem. C* **2014**, *118*, 28535-28541.

[15] L. zur Borg, A. L. Domanski, A. Breivogel, M. Bürger, R. Berger, K. Heinze, R. Zentel, *J. Mater. Chem. C* **2013**, *1*, 1223-1230.

[16] G. Inzelt, in *Conducting Polymers*, Springer Berlin Heidelberg, **2012**, pp. 7-82.

[17] G. Moad, M. Chen, M. Haussler, A. Postma, E. Rizzardo, S. H. Thang, *Polym. Chem.* **2011**, *2*, 492-519.

[18] A. Iwan, D. Sek, *Prog. Polym. Sci.* **2011**, *36*, 1277-1325.

[19] T. Yokozawa, Y. Ohta, *Chem. Rev.* **2016**, *116*, 1950-1968.

[20] L. Verheyen, P. Leysen, M.-P. Van Den Eede, W. Ceunen, T. Hardeman, G. Koeckelberghs, *Polymer* **2017**, *108*, 521-546.

[21] A. Kiriy, V. Senkovskyy, M. Sommer, *Macromol. Rapid Commun.* **2011**, *32*, 1503-1517.

[22] R. Schroot, U. S. Schubert, M. Jäger, *Macromolecules* **2015**, *48*, 1963-1971.

[23] J. Kübel, R. Schroot, M. Wächtler, U. S. Schubert, B. Dietzek, M. Jäger, *J. Phys. Chem. C* **2015**, *119*, 4742-4751.

[24] R. Schroot, C. Friebe, E. Altuntas, S. Crotty, M. Jäger, U. S. Schubert, *Macromolecules* **2013**, *46*, 2039-2048.

[25] F. Mathias, A. Fokina, K. Landfester, W. Tremel, F. Schmid, K. Char, R. Zentel, *Macromol. Rapid Commun.* **2015**, *36*, 959-983.
[26] M. He, F. Qiu, Z. Lin, *J. Mater. Chem.* **2011**, *21*, 17039-17048.
[27] Y. Lee, E. D. Gomez, *Macromolecules* **2015**, *48*, 7385-7395.
[28] E. Moulin, J.-J. Cid, N. Giuseppone, *Adv. Mater.* **2013**, *25*, 477-487.
[29] L. zur Borg, C. Schuell, H. Frey, R. Zentel, *Macromol. Rapid Commun.* **2013**, *34*, 1213-1219.
[30] P. M. Reichstein, S. Gödrich, G. Papastavrou, M. Thelakkat, *Macromolecules* **2016**, *49*, 5484-5493.
[31] Z. He, H. Wu, Y. Cao, *Adv. Mater.* **2014**, *26*, 1006-1024.
[32] A. Facchetti, *Mater. Today* **2013**, *16*, 123-132.
[33] K. Muellen, J. P. Rabe, *Ann. N. Y. Acad. Sci.* **1998**, *852*, 205-218.
[34] A. Facchetti, *Chem. Mater.* **2011**, *23*, 733-758.
[35] Y.-H. Chou, H.-C. Chang, C.-L. Liu, W.-C. Chen, *Polym. Chem.* **2015**, *6*, 341-352.
[36] Y.-L. Li, Y.-S. Cheng, P.-N. Yeh, S.-H. Liao, S.-A. Chen, *Adv. Funct. Mater.* **2014**, *24*, 6811-6817.
[37] S.-H. Liao, Y.-L. Li, T.-H. Jen, Y.-S. Cheng, S.-A. Chen, *J. Am. Chem. Soc.* **2012**, *134*, 14271-14274.
[38] H.-H. Lu, Y.-S. Ma, N.-J. Yang, G.-H. Lin, Y.-C. Wu, S.-A. Chen, *J. Am. Chem. Soc.* **2011**, *133*, 9634-9637.
[39] M. Raissi, H. Erothu, E. Ibarboure, H. Cramail, L. Vignau, E. Cloutet, R. C. Hiorns, *J. Mater. Chem. A* **2015**, *3*, 18207-18221.
[40] S. Miyanishi, Y. Zhang, K. Tajima, K. Hashimoto, *Chem. Commun.* **2010**, *46*, 6723-6725.
[41] M. Hufnagel, M.-A. Muth, J. C. Brendel, M. Thelakkat, *Macromolecules* **2014**, *47*, 2324-2332.
[42] J. U. Lee, J. W. Jung, T. Emrick, T. P. Russell, W. H. Jo, *J. Mater. Chem.* **2010**, *20*, 3287-3294.
[43] R. Schroot, M. Jäger, U. S. Schubert, *Chem. Soc. Rev.* **2017**, *46*, 2754-2798.
[44] A. Walther, A. H. E. Mueller, *Chem. Rev.* **2013**, *113*, 5194-5261.
[45] F. H. Schacher, P. A. Rupar, I. Manners, *Angew. Chem. Int. Ed.* **2012**, *51*, 7898-7921.
[46] E.-K. Fleischmann, R. Zentel, *Angew. Chem. Int. Ed.* **2013**, *52*, 8810-8827.
[47] S. Broll, F. Nuebling, A. Luzio, D. Lentzas, H. Komber, M. Caironi, M. Sommer, *Macromolecules* **2015**, *48*, 7481-7488.
[48] F. Lombeck, H. Komber, D. Fazzi, D. Nava, J. Kuhlmann, D. Stegerer, K. Strassel, J. Brandt, A. D. de Zerio Mendaza, C. Mueller, W. Thiel, M. Caironi, R. Friend, M. Sommer, *Adv. Energy Mater.* **2016**, *6*, 1601232.
[49] D. Schiefer, H. Komber, F. Mugwanga Keheze, S. Kunz, R. Hanselmann, G. Reiter, M. Sommer, *Macromolecules* **2016**, *49*, 7230-7237.
[50] K. Hong, D. Uhrig, J. W. Mays, *Curr. Opin. Solid State Mater. Sci.* **1999**, *4*, 531-538.
[51] J. Jagur-Grodzinski, *J. Polym. Sci., Part A: Polym. Chem.* **2002**, *40*, 2116-2133.
[52] I. Natori, S. Natori, H. Sekikawa, T. Takahashi, H. Sato, *J. Appl. Polym. Sci.* **2011**, *121*, 3433-3438.
[53] I. Natori, S. Natori, K. Tsuchiya, K. Ogino, *Macromolecules* **2010**, *44*, 256-262.
[54] I. Cosemans, J. Wouters, T. Cleij, L. Lutsen, W. Maes, T. Junkers, D. Vanderzande, *Macromol. Rapid Commun.* **2012**, *33*, 242-247.

[55] M. A. Mamo, F. S. Freitas, R. P. Forbes, R. S. Black, A. F. Nogueira, W. A. L. van Otterlo, N. J. Coville, *Fullerenes, Nanotubes, Carbon Nanostruct.* **2013**, *21*, 198-212.
[56] M. Eo, D. Han, M. H. Park, M. Hong, Y. Do, S. Yoo, M. H. Lee, *Eur. Polym. J.* **2014**, *51*, 37-44.
[57] J. Kim, M. H. Yun, J. Lee, J. Y. Kim, F. Wudl, C. Yang, *Chem. Commun.* **2011**, *47*, 3078-3080.
[58] M. Eo, S. Lee, M. H. Park, M. H. Lee, S. Yoo, Y. Do, *Macromol. Rapid Commun.* **2012**, *33*, 1119-1125.
[59] J. A. Paquette, S. Ezugwu, V. Yadav, G. Fanchini, J. B. Gilroy, *J. Polym. Sci., Part A: Polym. Chem.* **2016**, *54*, 1803-1813.
[60] A. de la Escosura, M. V. Martínez-Díaz, T. Torres, R. H. Grubbs, D. M. Guldi, H. Neugebauer, C. Winder, M. Drees , N. S. Sariciftci, *Chem. Asian J.* **2006**, *1*, 148-154.
[61] T. Suga, M. Sakata, K. Aoki, H. Nishide, *ACS Macro Lett.* **2014**, *3*, 703-707.
[62] H.-W. Wang, Z.-C. Liu, C.-H. Chen, T.-S. Lim, W. Fann, C.-G. Chao, J.-Y. Yu, S.-L. Lee, C.-h. Chen, S.-L. Huang, T.-Y. Luh, *Chem. Eur. J.* **2009**, *15*, 5719-5728.
[63] N. Zaquen, L. Lutsen, D. Vanderzande, T. Junkers, *Polym. Chem.* **2016**, *7*, 1355-1367.
[64] R. S. Loewe, S. M. Khersonsky, R. D. McCullough, *Adv. Mater.* **1999**, *11*, 250-253.
[65] R. Miyakoshi, A. Yokoyama, T. Yokozawa, *J. Am. Chem. Soc.* **2005**, *127*, 17542-17547.
[66] C. A. Traina, R. C. Bakus, II, G. C. Bazan, *J. Am. Chem. Soc.* **2011**, *133*, 12600-12607.
[67] P. D. Topham, A. J. Parnell, R. C. Hiorns, *J. Polym. Sci., Part B: Polym. Phys.* **2011**, *49*, 1131-1156.
[68] J. Wang, T. Higashihara, *Polym. Chem.* **2013**, *4*, 5518-5526.
[69] N. Hadjichristidis, M. Pitsikalis, H. Iatrou, in *Block Copolymers I, Vol. 189* (Ed.: V. Abetz), Springer Berlin Heidelberg, **2005**, pp. 1-124.
[70] B.-G. Kang, S. Song, B. Cho, N.-G. Kang, M.-J. Kim, T. Lee, J.-S. Lee, *J. Polym. Sci., Part A: Polym. Chem.* **2014**, *52*, 2625-2632.
[71] B.-G. Kang, Y.-G. Yu, N.-G. Kang, J.-S. Lee, *J. Polym. Sci., Part A: Polym. Chem.* **2013**, *51*, 4233-4239.
[72] C.-Y. Yu, M. Horie, A. M. Spring, K. Tremel, M. L. Turner, *Macromolecules* **2010**, *43*, 222-232.
[73] C.-Y. Yu, J. W. Kingsley, D. G. Lidzey, M. L. Turner, *Macromol. Rapid Commun.* **2009**, *30*, 1889-1892.
[74] H. Hsieh, R. P. Quirk, *Anionic Polymerization: Principles and Practical Applications*, Marcel Dekker, Inc., New York, **1996**.
[75] M. Zorn, S. A. Weber, M. N. Tahir, W. Tremel, H. J. Butt, R. Berger, R. Zentel, *Nano Lett.* **2010**, *10*, 2812-2816.
[76] J. Lim, L. z. Borg, S. Dolezel, F. Schmid, K. Char, R. Zentel, *Macromol. Rapid Commun.* **2014**, *35*, 1685-1691.
[77] L. zur Borg, D. Lee, J. Lim, W. K. Bae, M. Park, S. Lee, C. Lee, K. Char, R. Zentel, *J. Mater. Chem. C* **2013**, *1*, 1722-1726.
[78] Y.-K. Fang, C.-L. Liu, C. Li, C.-J. Lin, R. Mezzenga, W.-C. Chen, *Adv. Funct. Mater.* **2010**, *20*, 3012-3024.
[79] Q. Zhang, A. Cirpan, T. P. Russell, T. Emrick, *Macromolecules* **2009**, *42*, 1079-1082.

[80] M. Sommer, A. S. Lang, M. Thelakkat, *Angew. Chem., Int. Ed.* **2008**, *47*, 7901-7904.
[81] P. Kumari, K. Khawas, S. Hazra, B. K. Kuila, *J. Polym. Sci., Part A: Polym. Chem.* **2016**, *54*, 1785-1794.
[82] L. Wang, E. Puodziukynaite, E. M. Grumstrup, A. C. Brown, S. Keinan, K. S. Schanze, J. R. Reynolds, J. M. Papanikolas, *J. Phys. Chem. Lett.* **2013**, *4*, 2269-2273.
[83] L. Wang, E. Puodziukynaite, R. P. Vary, E. M. Grumstrup, R. M. Walczak, O. Y. Zolotarskaya, K. S. Schanze, J. R. Reynolds, J. M. Papanikolas, *J. Phys. Chem. Lett.* **2012**, *3*, 2453-2457.
[84] K. W. Cheng, C. S. C. Mak, W. K. Chan, A. M. C. Ng, A. B. Djurisic, *J. Polym. Sci., Part A: Polym. Chem.* **2008**, *46*, 1305-1317.
[85] M. J. Robb, D. Montarnal, N. D. Eisenmenger, S.-Y. Ku, M. L. Chabinyc, C. J. Hawker, *Macromolecules* **2013**, *46*, 6431-6438.
[86] L. Wang, Z. Qiao, C. Gao, J. Liu, Z.-G. Zhang, X. Li, Y. Li, H. Wang, *Macromolecules* **2016**, *49*, 3723-3732.
[87] R. Schroot, T. Schlotthauer, M. Jäger, U. S. Schubert, *Macromol. Chem. Phys.* **2017**, *218*, 1600534.
[88] R. Schroot, T. Schlotthauer, U. S. Schubert, M. Jäger, *Macromolecules* **2016**, *49*, 2112-2123.
[89] F. C. Krebs, M. Biancardo, *Sol. Energy Mater. Sol. Cells* **2006**, *90*, 142-165.
[90] R. Schroot, U. S. Schubert, M. Jäger, *Macromolecules* **2017**, *50*, 1319-1330.
[91] S.-L. Suraru, F. Würthner, *Angew. Chem. Int. Ed.* **2014**, *53*, 7428-7448.
[92] C. Huang, S. Barlow, S. R. Marder, *J. Org. Chem.* **2011**, *76*, 2386-2407.
[93] X. Zhan, A. Facchetti, S. Barlow, T. J. Marks, M. A. Ratner, M. R. Wasielewski, S. R. Marder, *Adv. Mater.* **2011**, *23*, 268-284.
[94] S. V. Bhosale, C. H. Jani, S. J. Langford, *Chem. Soc. Rev.* **2008**, *37*, 331-342.
[95] S.-i. Sakurai, J. Areephong, L. Bertone, N.-T. Lin, N. Sakai, S. Matile, *Energy Environ. Sci.* **2011**, *4*, 2409-2416.
[96] O. Yushchenko, D. Villamaina, N. Sakai, S. Matile, E. Vauthey, *J. Phys. Chem. C* **2015**, *119*, 14999-15008.
[97] M. Kumar, S. J. George, *Chem. Eur. J.* **2011**, *17*, 11102-11106.
[98] K. Tambara, N. Ponnuswamy, G. Hennrich, G. D. Pantos, *J. Org. Chem.* **2011**, *76*, 3338-3347.
[99] A. Baron, C. Herrero, A. Quaranta, M.-F. Charlot, W. Leibl, B. Vauzeilles, A. Aukauloo, *Chem. Commun.* **2011**, *47*, 11011-11013.
[100] J. Nicolas, Y. Guillaneuf, C. Lefay, D. Bertin, D. Gigmes, B. Charleux, *Prog. Polym. Sci.* **2013**, *38*, 63-235.
[101] O. Guerret, J.-L. Couturier, F. Chauvin, H. El-Bouazzy, D. Bertin, D. Gigmes, S. Marque, H. Fischer, P. Tordo, in *Advances in Controlled/Living Radical Polymerization, Vol. 854*, American Chemical Society, **2003**, pp. 412-423.
[102] C. Feng, Y. Li, D. Yang, J. Hu, X. Zhang, X. Huang, *Chem. Soc. Rev.* **2011**, *40*, 1282-1295.
[103] H.-i. Lee, J. Pietrasik, S. S. Sheiko, K. Matyjaszewski, *Prog. Polym. Sci.* **2010**, *35*, 24-44.
[104] Reevalution of data from previous reports.
[105] B. A. Miller-Chou, J. L. Koenig, *Prog. Polym. Sci.* **2003**, *28*, 1223-1270.
[106] S. Hocine, M.-H. Li, *Soft Matter* **2013**, *9*, 5839-5861.
[107] T.-T. Bui, F. Goubard, *EPJ Photovolt.* **2013**, *4*, 40402.
[108] J.-F. Morin, M. Leclerc, D. Adès, A. Siove, *Macromol. Rapid Commun.* **2005**, *26*, 761-778.

[109] A. Pron, P. Gawrys, M. Zagorska, D. Djurado, R. Demadrille, *Chem. Soc. Rev.* **2010**, *39*, 2577-2632.
[110] J. Li, A. C. Grimsdale, *Chem. Soc. Rev.* **2010**, *39*, 2399-2410.
[111] J.-P. Lellouche, R. Koner Rik, S. Ghosh, *Rev. Chem. Eng.* **2013**, *29*, 413-437.
[112] U. Geissler, M. L. Hallensleben, A. Rienecker, N. Rohde, *Polym. Adv. Technol.* **1997**, *8*, 87-92.
[113] P.-L. T. Boudreault, S. Beaupre, M. Leclerc, *Polym. Chem.* **2010**, *1*, 127-136.
[114] F. Xu, J.-H. Kim, H. U. Kim, J.-H. Jang, K. S. Yook, J. Y. Lee, D.-H. Hwang, *Macromolecules* **2014**, *47*, 7397-7406.
[115] J. Huang, Y. H. Niu, W. Yang, Y. Q. Mo, M. Yuan, Y. Cao, *Macromolecules* **2002**, *35*, 6080-6082.
[116] G. Pasquinelli, M. C. Vinci, C. Gamberini, C. Orrico, L. Foroni, C. Guarnieri, A. Parenti, M. Gargiulo, F. Ledda, C. M. Caldarera, C. Muscari, *Tissue Eng., Part A* **2009**, *15*, 2751-2762.
[117] S.-J. Liu, W.-P. Lin, M.-D. Yi, W.-J. Xu, C. Tang, Q. Zhao, S.-H. Ye, X.-M. Liu, W. Huang, *J. Mater. Chem.* **2012**, *22*, 22964-22970.
[118] J. Luo, G. Xie, S. Gong, T. Chen, C. Yang, *Chem. Commun.* **2016**, *52*, 2292-2295.
[119] R. Vedarajan, Y. Hosono, N. Matsumi, *Solid State Ionics* **2014**, *262*, 795-800.
[120] A. Iraqi, I. Wataru, *J. Polym. Sci., Part A: Polym. Chem.* **2004**, *42*, 6041-6051.
[121] Z.-B. Zhang, M. Motonaga, M. Fujiki, C. E. McKenna, *Macromolecules* **2003**, *36*, 6956-6958.
[122] Z.-B. Zhang, M. Fujiki, H.-Z. Tang, M. Motonaga, K. Torimitsu, *Macromolecules* **2002**, *35*, 1988-1990.
[123] R.-H. Lee, J.-K. Liu, J.-H. Ho, J.-W. Chang, B.-T. Liu, H.-J. Wang, R.-J. Jeng, *Polym. Int.* **2011**, *60*, 483-492.
[124] L. Beouch, F. Tran Van, O. Stephan, J. C. Vial, C. Chevrot, *Synth. Met.* **2001**, *122*, 351-358.
[125] M. C. Stefan, A. E. Javier, I. Osaka, R. D. McCullough, *Macromolecules* **2009**, *42*, 30-32.
[126] U. Koldemir, S. R. Puniredd, M. Wagner, S. Tongay, T. D. McCarley, G. D. Kamenov, K. Müllen, W. Pisula, J. R. Reynolds, *Macromolecules* **2015**, *48*, 6369-6377.
[127] A. Krasovskiy, B. F. Straub, P. Knochel, *Angew. Chem. Int. Ed.* **2006**, *45*, 159-162.
[128] A. Krasovskiy, P. Knochel, *Angew. Chem. Int. Ed.* **2004**, *43*, 3333-3336.
[129] P. Knochel, W. Dohle, N. Gommermann, F. F. Kneisel, F. Kopp, T. Korn, I. Sapountzis, V. A. Vu, *Angew. Chem. Int. Ed.* **2003**, *42*, 4302-4320.
[130] N. Doubina, A. Ho, A. K. Y. Jen, C. K. Luscombe, *Macromolecules* **2009**, *42*, 7670-7677.
[131] J. A. Bilbrey, S. K. Sontag, N. E. Huddleston, W. D. Allen, J. Locklin, *ACS Macro Lett.* **2012**, *1*, 995-1000.
[132] R. H. Lohwasser, M. Thelakkat, *Macromolecules* **2011**, *44*, 3388-3397.
[133] R. Schroot, U. S. Schubert, M. Jäger, *Macromolecules* **2016**, *49*, 8801-8811.
[134] R. Miyakoshi, A. Yokoyama, T. Yokozawa, *J. Polym. Sci., Part A: Polym. Chem.* **2008**, *46*, 753-765.
[135] N. Doubina, M. Stoddard, H. A. Bronstein, A. K. Y. Jen, C. K. Luscombe, *Macromol. Chem. Phys.* **2009**, *210*, 1966-1972.
[136] M. Jeffries-El, G. Sauvé, R. D. McCullough, *Adv. Mater.* **2004**, *16*, 1017-1019.
[137] W. M. Kochemba, S. M. Kilbey, D. L. Pickel, *J. Polym. Sci., Part A: Polym. Chem.* **2012**, *50*, 2762-2769.

[138] V. Senkovskyy, M. Sommer, R. Tkachov, H. Komber, W. T. S. Huck, A. Kiriy, *Macromolecules* **2010**, *43*, 10157-10161.
[139] H. Wen, Z. Ge, Y. Liu, T. Yokozawa, L. Lu, X. Ouyang, Z. Tan, *Eur. Polym. J.* **2013**, *49*, 3740-3743.
[140] F. Lemasson, N. Berton, J. Tittmann, F. Hennrich, M. M. Kappes, M. Mayor, *Macromolecules* **2012**, *45*, 713-722.
[141] X. Xiao, Y. Q. Fu, M. H. Sun, L. Li, Z. S. Bo, *J. Polym. Sci., Part A: Polym. Chem.* **2007**, *45*, 2410-2424.
[142] E. Elmalem, A. Kiriy, W. T. S. Huck, *Macromolecules* **2011**, *44*, 9057-9061.
[143] R. Tkachov, V. Senkovskyy, T. Beryozkina, K. Boyko, V. Bakulev, A. Lederer, K. Sahre, B. Voit, A. Kiriy, *Angew. Chem. Int. Ed.* **2014**, *53*, 2402-2407.
[144] K. Smith, D. M. James, A. G. Mistry, M. R. Bye, D. J. Faulkner, *Tetrahedron* **1992**, *48*, 7479-7488.
[145] Y. Li, J. Ding, M. Day, Y. Tao, J. Lu, M. D'Iorio, *Chem. Mater.* **2004**, *16*, 2165-2173.
[146] T. Yokozawa, R. Suzuki, M. Nojima, Y. Ohta, A. Yokoyama, *Macromol. Rapid Commun.* **2011**, *32*, 801-806.
[147] A. Yokoyama, H. Suzuki, Y. Kubota, K. Ohuchi, H. Higashimura, T. Yokozawa, *J. Am. Chem. Soc.* **2007**, *129*, 7236-7237.
[148] M. Verswyvel, C. Hoebers, J. De Winter, P. Gerbaux, G. Koeckelberghs, *J. Polym. Sci., Part A: Polym. Chem.* **2013**, *51*, 5067-5074.
[149] L. S. Coumont, J. G. C. Veinot, *Tetrahedron Lett.* **2015**, *56*, 5595-5598.
[150] J. Ostrauskaite, P. Strohriegl, *Macromol. Chem. Phys.* **2003**, *204*, 1713-1718.
[151] S.-Y. Liu, H.-Y. Li, M.-M. Shi, H. Jiang, X.-L. Hu, W.-Q. Li, L. Fu, H.-Z. Chen, *Macromolecules* **2012**, *45*, 9004-9009.
[152] D. F. O'Keefe, M. C. Dannock, S. M. Marcuccio, *Tetrahedron Lett.* **1992**, *33*, 6679-6680.
[153] K. C. Kong, C. H. Cheng, *J. Am. Chem. Soc.* **1991**, *113*, 6313-6315.
[154] M. Hesse, H. Meier, B. Zeeh, *Spectroscopic Methods in Organic Chemistry*, 2nd ed., Georg Thieme Verlag, Stuttgart, **2007**.
[155] M. Jäger, R. J. Kumar, H. Görls, J. Bergquist, O. Johansson, *Inorg. Chem.* **2009**, *48*, 3228-3238.
[156] D. W. Thompson, A. Ito, T. J. Meyer, *Pure Appl. Chem.* **2013**, *85*, 1257-1305.
[157] R. J. Kumar, S. Karlsson, D. Streich, A. Rolandini Jensen, M. Jäger, H.-C. Becker, J. Bergquist, O. Johansson, L. Hammarström, *Chem. Eur. J.* **2010**, *16*, 2830-2842.

List of abbreviations

°C	Degree Celsius
3D	Three-dimensional
A	Acceptor
ATRP	Atom transfer radical polymerization
b	Block
bn	Benzyl
Carb	Carbazole
CMSt-TIPNO	*N*-*tert*-Butyl-O-[1-[4-(chloromethyl)phenyl]ethyl]-*N*-(2-methyl-1-phenylpropyl)hydroxylamine
CRP	Controlled radical polymerization
CS	charge separation
CTP	Catalyst transfer polymerization
CuAAC	Copper(I)-catalyzed Azide-Alkyne Cycloaddition
D	Donor
DMF	*N*,*N*-Dimethylformamide
dqp	2,6-Di(quinolin-8-yl)pyridine
FRP	Free radical polymerization
g	Gram
GC	Gas chromatography
GRIM	Grignard Metathesis
h	Hour
hν	Light energy

IR	Infrared
k_c	Combination reaction rate
KCTP	Kumada catalyst transfer polymerization
k_d	Dissociation reaction rate
LCST	Lower critical solution temperature
MALDI	Matrix-assisted laser desorption ionization
min	Minute
mL	Milliliter
MLCT	Metal-to-ligand charge-transfer
mM	Millimol
M_n	Number average molar mass
MPEG 550	Poly(ethylene glycol) methyl ether, M_n 550 g/mol
MS	Mass spectrometry
MTEG	Triethylene glycol methyl ether
NDI	Naphthalenediimide
nm	Nanometer
NMP	Nitroxide mediated polymerization
NMR	Nuclear magnetic resonance
ns	Nanosecond
OFET	Organic field-effect transistor
OLED	Organic light-emitting diode
P	Photosensitizer
p	Poly

P3HT	Poly(3-hexylthiophene)
PEG	Poly(ethylene glycol)
ph	Phenyl
pin	Pinacolato
PMDETA	*N*,*N*,*N*′,*N*″,*N*″-Pentamethyldiethylenetriamine
PNIPAM	Poly(*N*-isopropylacrylamide)
ppm	Parts per million
py	Pyridyl
RAFT	Reversible addition-fragmentation chain transfer
ROMP	Ring-opening metathesis polymerization
SEC	Size-exclusion chromatography
t	Time
TA	Transient absorption
TARA	Triarylamine
THF	Tetrahydrofuran
TIPS	Triisopropylsilyl
TLC	Thin-layer chromatography
ToF	Time of Flight
tr	Triazole
UV	Ultraviolet
vis	Visible
µs	Microsecond

Curriculum vitae

22/09/1989	Born in Jena, Germany
1996-2000	Elementary school in Krölpa, Germany
2000-2008	Secondary school in Pößneck, Germany Degree: University entrance certification
10/2008-09/2013	Study of chemistry at Friedrich Schiller University Jena, Germany Degree: Diploma
11/2012-09/2013	Diploma thesis in the group of Prof. Dr. Ulrich S. Schubert at the Friedrich Schiller University Jena, Germany Topic: “Polymer architectures for light-induced directional charge transfer cascades”
Since 12/2013	PhD student at the Laboratory of Macromolecular and Organic Chemistry (IOMC) at the Friedrich Schiller University Jena (group of Prof. Dr. Ulrich S. Schubert)
03/2012-09/2013	Scholarship of the Studienstiftung des deutschen Volkes
11/2014	Faculty exam award for diploma thesis

Jena,

Robert Schroot

Publication list

Peer-reviewed publications

[1] R. Schroot, C. Friebe, E. Altuntas, S. Crotty, M. Jäger, U. S. Schubert, "Nitroxide-Mediated Polymerization of Styrenic Triarylamines and Chain-End Functionalization with a Ruthenium Complex: Toward Tailored Photoredox-Active Architectures", *Macromolecules* **2013**, *46*, 2039-2048.

[2] R. Schroot, M. Jäger, U. S. Schubert, "Block Copolymers for Directional Charge Transfer: Synthesis, Characterization, and Electrochemical Properties of Redox-Active Triarylamines", *Macromolecules* **2015**, *48*, 1963-1971.

[3] J. Kübel, R. Schroot, M. Wächtler, U. S. Schubert, B. Dietzek, M. Jäger, "Photoredox-active Dyads Based on a Ru(II) Photosensitizer Equipped with Electron Donor or Acceptor Polymer Chains: A Spectroscopic Study of Light-Induced Processes toward Efficient Charge Separation", *J. Phys. Chem. C* **2015**, *119,* 4742–4751.

[4] R. Schroot, T. Schlotthauer, U. S. Schubert, M. Jäger, "Modular Assembly of Poly(naphthalene diimide) and Ru(II) Dyes for an Efficient Light-Induced Charge Separation in Hierarchically Controlled Polymer Architectures", *Macromolecules* **2016**, *49*, 2112-2123.

[5] R. Schroot, U. S. Schubert, M. Jäger, "Poly(*N*-alkyl-3,6-carbazole)s via Kumada Catalyst Transfer Polymerization: Impact of Metal–Halogen Exchange", *Macromolecules* **2016**, *49*, 8801-8811.

[6] R. Schroot, T. Schlotthauer, M. Jäger, U. S. Schubert, "Hydrophilic Poly(naphthalene diimide)-Based Acceptor–Photosensitizer Dyads: Toward Water-Processible Modular Photoredox-Active Architectures", *Macromol. Chem. Phys.* **2017**, *218*, 1600534.

[7] R. Schroot, U. S. Schubert, M. Jäger, "Poly(*N*-alkyl-3,6-carbazole)s via Suzuki–Miyaura Polymerization: From Macrocyclization toward End Functionalization", *Macromolecules* **2017**, *50*, 1319-1330.

[8] R. Schroot, M. Jäger, U. S. Schubert, "Synthetic approaches towards structurally-defined electrochemically and (photo)redox-active polymer architectures", *Chem. Soc. Rev.* **2017**, *46*, 2754-2798.

[9] R. Schroot, T. Schlotthauer, B. Dietzek, M. Jäger, U. S. Schubert, "Extending Long-lived Charge Separation Between Donor and Acceptor Blocks in Novel Copolymer Architectures Featuring a Sensitizer Core", *Chem. Eur. J.* **2017**, *23*, 16484-16490.

[10] T. Schlotthauer, R. Schroot, S. Glover, L. Hammarström, M. Jäger, U. S. Schubert, "A multidonor–photosensitizer–multiacceptor triad for long-lived directional charge separation", *Phys. Chem. Chem. Phys.* **2017**, *19*, 28572-28578.

Poster presentations

[1] **R. Schroot**, C. Friebe, E. Altuntas, S. Crotty, U. S. Schubert, M. Jäger, *Synthesis of redox-active donor- and acceptor-polymers and coupling to a photoactive complex*, ORCHEM Weimar, Germany, **2012**.

[2] **R. Schroot**, M. Jäger, U. S. Schubert, *Polymer architectures for light-induced directional charge transfer cascades: Synthesis and functionalization of electron donor and acceptor polymers*, JCF Frühjahrssymposium, Jena, Germany, **2014**.

[3] T. Schlotthauer, **R. Schroot**, H. Görls, M. Jäger, U. S. Schubert, *Modular assembly of hierarchical redox-active polymers with Ru(II) dyes for light-induced charge separation*, Polymers and Energy, GDCh Fachgruppentagung Makromolekulare Chemie, Jena, Germany, **2014**.

[4] **R. Schroot**, Ulrich S. Schubert, Michael Jäger, *Polymers for directional light-induced charged transport: Synthesis of electron donor polymers*, European Polymer Congress, Dresden, Germany, **2015**.

[5] **R. Schroot**, T. Schlotthauer, Ulrich S. Schubert, Michael Jäger, *Redox-active and Conjugated Polymers as Modular Building Blocks for Light-induced Directional Charge Transfer Cascades*, Makromolekulares Kolloquium, Freiburg, Germany, **2016**.

[6] **R. Schroot**, T. Schlotthauer, Ulrich S. Schubert, Michael Jäger, *Redox-active and Conjugated Polymers as Modular Building Blocks for Light-induced Directional Charge Transfer Cascades*, Gordon Research Seminar and Conference, Electronic Processes in Organic Materials, Barga, Italy, **2016**.

[7] **R. Schroot**, T. Schlotthauer, Ulrich S. Schubert, Michael Jäger, *Redox-active and Conjugated Polymers as Modular Building Blocks for Light-induced Directional*

Charge Transfer Cascades, 25. Lecture Conference on Photochemistry, Jena, Germany, **2016**.

Acknowledgements / Danksagung

This thesis would not have been possible without the continuous help and support of many people. First of all, I would like to thank Prof. Ulrich S. Schubert for giving me the opportunity to work on this highly interesting topic and to prepare my PhD thesis in his group. His support was crucial for the success of this thesis.

Furthermore, I want to thank Dr. Michael Jäger for supervision, lots of fruitful discussions and for always having an open ear for problems. His support was a great help over the last years. Thank you very much, Michael.

I also thank Tina Schlotthauer for the productive collaboration and lots of helpful discussions. We developed lots of ideas and had a lot of fun in the lab. Moreover, I thank Tina Schlotthauer, Ronny Tepper, Kevin Barthelmes, Dr. Christian Friebe and Dr. Daniel Schmidt for the nice atmosphere and lots of cake and cookies during our coffee breaks.

Furthermore, I would like to thank my Hiwis and lab students Ann-Sophie Lehnert, Adrian Saal and Alexander Kleine, who investigated lots of interesting synthetic questions.

In addition, many people helped with measurements, the discussion of their results or executed other important tasks, *e.g.*, ordered chemicals and lab ware or maintained instruments. In this regard, I thank Dr. Sarah Crotty, Nicole Fritz, Annet Urbanek, Dr. Grit Festag, Sandra Köhn, Beate Lentvogt and Dr. Uwe Köhn. Furthermore, I want to thank the NMR platform IAAC/IOMC, in particular Dr. Wolfgang Günther, Dr. Peter Bellstedt and Gabriele Sentis, for many NMR measurements. All my wishes for special experiments were satisfied quickly which helped me very much during the completion of this thesis.

I would like to thank Dr. Starla Glover and Prof. Dr. Leif Hammarström for a fruitful cooperation and the introductive time-resolved experiments. Moreover, I thank Prof. Dr. Benjamin Dietzek for the opportunity to perform spectroscopic measurements using his equipment.

Finally, I thank my friends and my family for continuous support and encouragement in hard times in the last years. I would not have been able to complete this thesis without you.

Declaration of authorship / Selbstständigkeitserklärung

Ich erkläre, dass ich die vorliegende Arbeit selbständig und unter Verwendung der angegebenen Hilfsmittel, persönlichen Mitteilungen und Quellen angefertigt habe.

I certify that the work presented here is, to the best of my knowledge and belief, original and the result of my own investigations, except as acknowledged, and has not been submitted, either in part or whole, for a degree at this or any other university.

Jena,

_____

Robert Schroot

Publications P1 to P7

P1) R. Schroot, M. Jäger, U. S. Schubert, "Synthetic approaches towards structurally-defined electrochemically and (photo)redox-active polymer architectures", *Chem. Soc. Rev.* **2017**, *46*, 2754-2798. – Reproduced with permission of The Royal Society of Chemistry, Copyright © 2017.

P2) R. Schroot, T. Schlotthauer, U. S. Schubert, M. Jäger, "Modular Assembly of Poly(naphthalene diimide) and Ru(II) Dyes for an Efficient Light-Induced Charge Separation in Hierarchically Controlled Polymer Architectures", *Macromolecules* **2016**, *49*, 2112-2123. – Reproduced with the permission of American Chemical Society, Copyright © 2016.

P3) R. Schroot, T. Schlotthauer, M. Jäger, U. S. Schubert, "Hydrophilic Poly(naphthalene diimide)-Based Acceptor–Photosensitizer Dyads: Toward Water-Processible Modular Photoredox-Active Architectures", *Macromol. Chem. Phys.* **2017**, *218*, 1600534. – Reproduced with the permission of John Wiley & Sons, Inc., Copyright © 2016.

P4) R. Schroot, U. S. Schubert, M. Jäger, "Poly(*N*-alkyl-3,6-carbazole)s via Kumada Catalyst Transfer Polymerization: Impact of Metal–Halogen Exchange", *Macromolecules* **2016**, *49*, 8801-8811. – Reproduced with the permission of American Chemical Society, Copyright © 2016.

P5) R. Schroot, U. S. Schubert, M. Jäger, "Poly(*N*-alkyl-3,6-carbazole)s via Suzuki–Miyaura Polymerization: From Macrocyclization toward End Functionalization", *Macromolecules* **2017**, *50*, 1319-1330. – Reproduced with the permission of American Chemical Society, Copyright © 2017.

P6) R. Schroot, T. Schlotthauer, B. Dietzek, M. Jäger, U. S. Schubert, "*Block* copolymer-type architecture with a central Ru^{II} sensitizer core: Conjugated poly(carbazole) for enhanced charge separation", submitted.

Published P6) R. Schroot, T. Schlotthauer, B. Dietzek, M. Jäger, U. S. Schubert, "Extending Long-lived Charge Separation Between Donor and Acceptor Blocks in Novel Copolymer Architectures Featuring a Sensitizer Core", *Chem. Eur. J.* **2017**, *23*,

16484-16490. – Reproduced with the permission of John Wiley & Sons, Inc., Copyright © 2017.

P7) T. Schlotthauer, R. Schroot, S. Glover, L. Hammarström, M. Jäger, U. S. Schubert, "A *multi*donor-Photosensitizer-*multi*acceptor Triad for Long-Lived Directional Charge Separation", submitted.

Published P7) T. Schlotthauer, R. Schroot, S. Glover, L. Hammarström, M. Jäger, U. S. Schubert, "A multidonor–photosensitizer–multiacceptor triad for long-lived directional charge separation", *Phys. Chem. Chem. Phys.* **2017**, *19*, 28572-28578. – Reproduced with permission of The Royal Society of Chemistry, Copyright © 2017.

Publication P1

Synthetic approaches towards structurally-defined electrochemically and (photo)redox-active polymer architectures

R. Schroot, M. Jäger, U. S. Schubert, *Chem. Soc. Rev.* **2017**, *46*, 2754-2798.

The paper is available online under: doi.org/10.1039/C6CS00811A

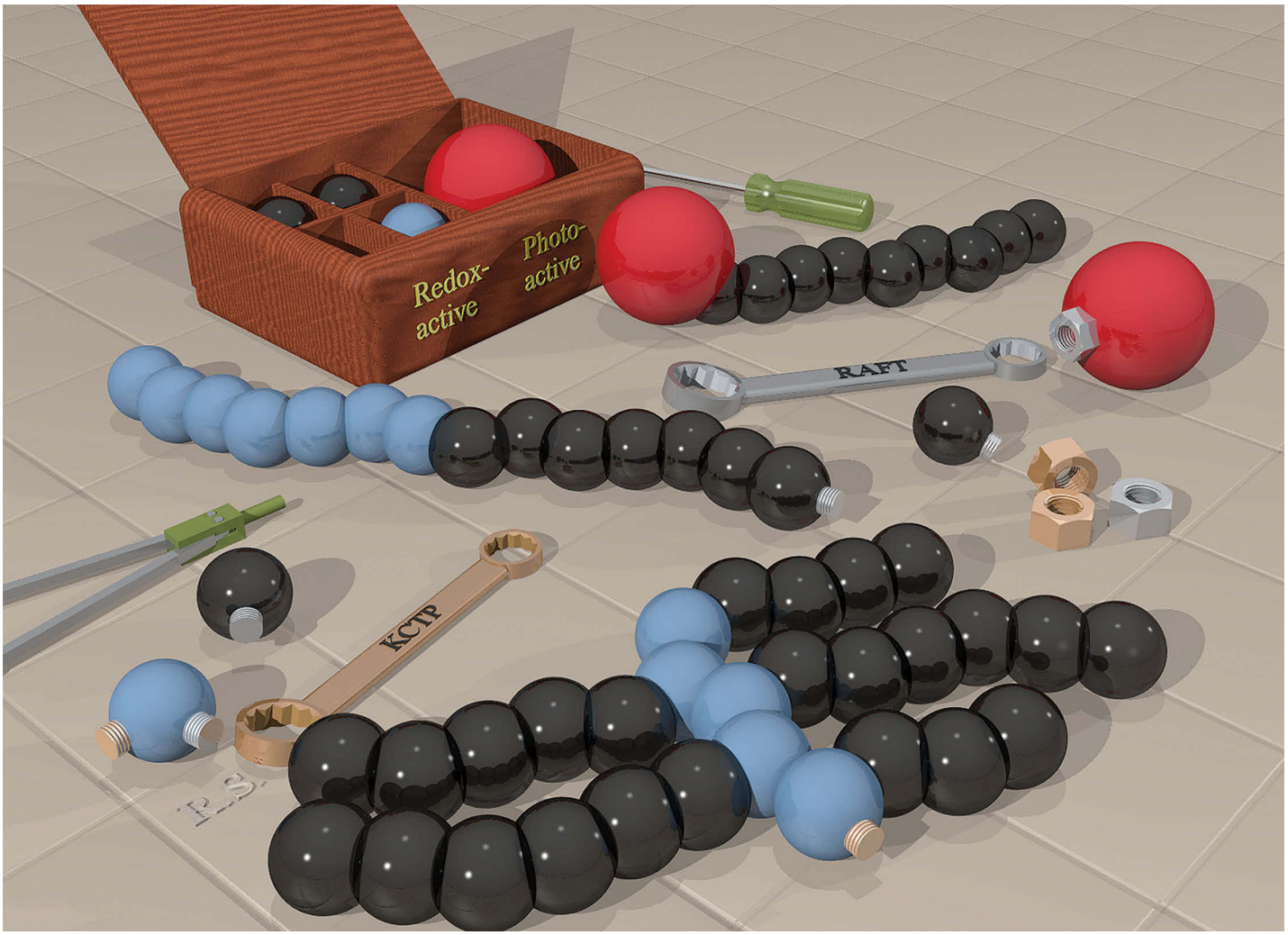

Featuring work from the research group of Professor Ulrich S. Schubert, University of Jena, Germany

Synthetic approaches towards structurally-defined electrochemically and (photo)redox-active polymer architectures

Novel structurally-defined electrochemically and (photo)redox-active polymer architectures, *e.g.* block, graft and end-functionalized (co)polymers, can be designed and prepared from functional building blocks through recent advancements in synthetic methodologies.

As featured in:

See Michael Jäger, Ulrich S. Schubert *et al.*, *Chem. Soc. Rev.*, 2017, **46**, 2754.

ROYAL SOCIETY OF CHEMISTRY

rsc.li/chem-soc-rev

Registered charity number: 207890

Chem Soc Rev

REVIEW ARTICLE

View Article Online
View Journal | View Issue

Cite this: *Chem. Soc. Rev.*, 2017, **46**, 2754

Synthetic approaches towards structurally-defined electrochemically and (photo)redox-active polymer architectures

Robert Schroot,[a] Michael Jäger *[ab] and Ulrich S. Schubert *[ab]

Received 11th November 2016

DOI: 10.1039/c6cs00811a

rsc.li/chem-soc-rev

Electrochemically active polymers are widely used in (opto)electronic applications, *e.g.* organic light-emitting diodes (OLEDs), organic field-effect transistors (OFETs), solar cells or other light harvesting devices. In this regard, the progress in controlled polymerization techniques opens new possibilities to construct covalently linked polymer architectures, *e.g.* block copolymers or graft copolymers, from defined building blocks. These architectures represent promising candidates for application in (opto)electronic devices as they allow control of the morphology through self-assembly processes and, furthermore, are capable of mimicking fundamental processes for directional charge transport or light harvesting. This review details synthetic approaches to prepare functional redox-active and conjugated homopolymers as well as the construction of covalently linked well-defined architectures thereof, *e.g.* block copolymers, graft copolymers or chain end functionalized assemblies.

1. Introduction

Functional redox-active, conjugated or photoactive polymers are valuable materials in the field of (opto)electronics, *i.e.* they are applied in organic light-emitting diodes, organic field effect transistors or for light harvesting *inter alia* in organic solar cells. In these devices the polymers fulfill the tasks of charge transport, charge separation, charge accumulation or photosensitization. The activity and performance of the polymers in a device is on the one hand determined by the molecular properties, *e.g.* redox potentials or light absorptivity, but on the other hand also by physical parameters, *e.g.* device morphology, morphology stability, trap sites or domain sizes, *etc.* (*vide infra*). In this regard, covalently bound polymer based architectures,

[a] *Laboratory of Organic and Macromolecular Chemistry (IOMC), Friedrich Schiller University Jena, Humboldtstraße 10, 07743 Jena, Germany. E-mail: michael.jager.iomc@uni-jena.de, ulrich.schubert@uni-jena.de*
[b] *Center for Energy and Environmental Chemistry Jena (CEEC Jena), Friedrich Schiller University Jena, Philosophenweg 7a, 07743 Jena, Germany*

Robert Schroot

Robert Schroot was born in Jena (Germany) in 1989. He studied chemistry at the Friedrich Schiller University Jena (Germany). Since 2013 he has been a PhD student in the group of Prof. Schubert at the Friedrich Schiller University Jena. His research interests cover redox-active and conducting polymers as well as their modular and covalent incorporation into photoredox-active architectures.

Michael Jäger

Michael Jäger was born in 1979 in Jena (Germany). He studied chemistry at the Friedrich Schiller University Jena (Germany) and the McGill University (Canada). For his PhD studies, he moved to Uppsala University (Sweden) to gain further insight into fundamental photosynthetic principles. After a short research stay with J.-P. Sauvage in Strasbourg (France), he finished his PhD thesis in 2009. His research interests cover photoactive compounds and the controlled modular assembly of functional molecules in (polymeric) architectures.

e.g. block, comb or end functionalized polymers, represent promising candidates to overcome hitherto existing challenges.[1–7] Well-defined copolymers, *i.e.*, with tailored molar masses, dispersity and end groups, are capable of self-organization into stable and tunable morphologies.[8–10] Moreover, a high end group fidelity is beneficial for the controlled alignment of the macromolecules.[11] Additionally, the occurrence of defects and trap sites lowers the performance of the materials.[12–14] As a consequence, the application of well-defined architectures is expected to improve the device performance through the formation of ordered self-assembled structures with minimized defect sites. Due to the progress in polymer science, *i.e.* the development of a number of controlled polymerization techniques, numerous well-defined architectures are readily accessible and are gaining increasing attention in the field of (opto)electronics.[15,16]

This review focuses on synthetic approaches and strategies enabling the synthesis of well-defined polymer based architectures, *i.e.* the aforementioned block, comb or end functionalized polymers, which enable control of the morphology through self-assembly processes and which are furthermore capable of mimicking fundamental processes for directional charge transport or light harvesting and allow the construction of multipurpose materials. The main focus is set on developments in the last ten years and covers synthetic procedures as well as strategies, whereas the application in devices consisting of these materials as well as their working principle, *e.g.* solar cells, is not presented but is partly discussed in other reviews.[17–19] The preparation of alternating donor–acceptor polymers, dye-decorated polymers,[20] coordination polymers,[21] and more-dimensional polymers[22,23] are intensively discussed elsewhere. While individual polymerization techniques and single architectures,[24,25] which are part of this contribution, were discussed in the respective reviews in the last few years, the here given overview of a wide range of techniques as well as architectures should be in particular helpful for synthetic chemists. The classification of the presented electrochemically active polymers is based on the mechanism of charge transport (Fig. 1).[26] Redox-active polymers consist of monomer units with isolated redox centers with pristine redox potentials. Charge transport in these materials occurs by an electron hopping process. As a consequence, the charge carrier mobilities are limited. Nevertheless, redox-active polymers have been widely investigated and benefit from their facile preparation by controlled (radical) polymerization techniques. In contrast, the preparation of telechelic conjugated polymers is much more challenging and requires advanced techniques, *e.g.* Kumada catalyst transfer polymerization (*vide infra*). The active units in conjugated polymers strongly influence each other leading to broad oxidation or reduction ranges and much higher charge carrier mobilities compared to redox-active polymers. Commonly applied electrochemically active units comprise, for example, triarylamines, carbazoles, fluorenes, thiophene, naphthalene diimides or fullerenes.

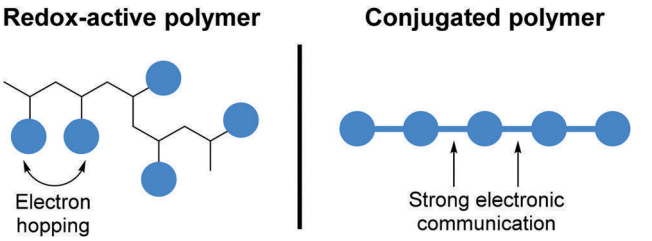

Fig. 1 Classification of electrochemically active polymers based on the mechanism of charge transport.

At the beginning of this contribution, the most important controlled polymerization techniques allowing for the synthesis of different classes of electrochemically active polymers are introduced. In particular, the preparation of telechelic polymers, *i.e.* polymers with defined reactive end groups capable of further functionalization, is of special interest for the later application in complex architectures and represents a central point for the discussion. After this initial introduction of the polymerization techniques, the following sections detail the construction of certain architectures, *i.e.* block copolymers, graft copolymers or chain end decorated polymers. In this regard, synthetic approaches based on the initially introduced techniques as well as combinations thereof are presented. Compelling and detailed examples demonstrate the resultant possibilities to influence the domain sizes and morphology in devices, whereas enumerated reports illustrate the band width of the synthetic methods.

To avoid misunderstandings of often used and recurring terms in this review, they will be shortly defined and the meaning of symbols will be shortly explained in the following paragraph. The term architecture refers to macromolecules based on covalent bonds which comprise more than one segment, *e.g.* block or comb copolymers as well as polymers decorated with a terminal functional unit. In this regard a functional unit or a functional building block is a molecule which fulfills a certain task in the final architecture, *e.g.* light absorption by metal complexes or charge accumulation by fullerene units. In contrast, a functional group or a reactive group is applied in modification reactions and has no particular task in the end product.

Ulrich S. Schubert

Ulrich S. Schubert was born in Tübingen (Germany) in 1969. He studied chemistry in Frankfurt and Bayreuth (both Germany) and at the Virginia Commonwealth University, Richmond (USA). His PhD studies were performed at the Universities of Bayreuth and South Florida. After postdoctoral training with J.-M. Lehn at the University of Strasbourg (France), he moved to the TU Munich (Germany) and obtained his Habilitation degree in 1999. During 1999–2000 he was a Professor at the University of Munich, and during 2000–2007 he was a Full-Professor at the TU Eindhoven (the Netherlands). Since 2007, he has been a Full-Professor at the Friedrich Schiller University Jena, Germany.

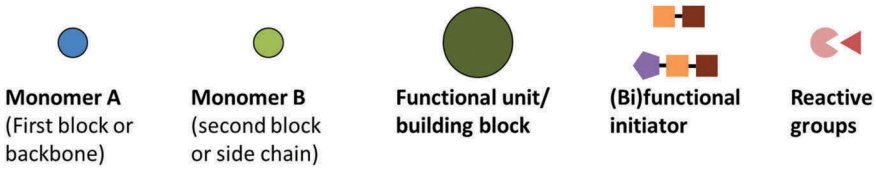

Fig. 2 Symbols used in schemes and figures and their meaning.

A telechelic polymer features well-defined functional end groups which originate from initiators or termination reagents.[27] For completion, an overview of the symbols that are used in the schemes and figures in the later parts of this review is given in Fig. 2.

Noteworthily, the available characterization data of the polymers are partly very limited, in particular with respect to yields, initiation efficiencies and necessary purification steps. If no data are given for a tabulated polymer in this review, then to the best of our knowledge it was not reported in the original literature. Depending on the polymer class, the most useful characterization data are given, *e.g.* initiating and end capping efficiencies for telechelic homopolymers and grafting efficiencies for graft copolymers.

The number average molar masses and dispersities (M_n, $Đ$) of the polymers in the review are mainly based on SEC investigations with a polystyrene calibration. Due to the application of different instruments and solvents, a comparison of the values is hardly possible and, moreover, in the case of stiff polymers the deviation in the SEC molar mass and the actual molar mass can be rather large. Nevertheless, the data provide an overview of the level of control which is reached with the different polymerization techniques.

2. Synthesis of functional homopolymers

The construction of functional polymer architectures from smaller building blocks, *e.g.* homopolymers, requires preparation techniques leading to macromolecules with well-defined molar masses as well as a high fidelity of reactive end groups, *i.e.* controlled and "living" polymerization procedures. In this section various polymerization techniques fulfilling these criteria are shortly presented and essential characteristics will be discussed with respect to electrochemically active polymers as the basis for subsequent applications in extended architectures.

2.1. Redox-active polymers by controlled radical polymerization (CRP) techniques

The established controlled radical polymerization (CRP) techniques, *e.g.* nitroxide mediated polymerization (NMP), atom transfer radical polymerization (ATRP) or reversible addition-fragmentation chain transfer (RAFT) polymerization, are suitable for the preparation of functional homopolymers bearing redox-active units in the side chain. The advantages and limitations regarding commercially available monomers and initiators, functional group tolerance or end functionalization of the individual methods are extensively described in the respective literature references[28–32] and will not be discussed here in detail. Instead, relevant examples to prepare functional redox-active homopolymers which are capable of further functionalization reactions as building blocks will be presented in this section. The utilization of the respective polymers in larger systems, *e.g.* in block copolymers or chain end functionalization with functional units, will be discussed in the later sections (*vide infra*).

Nitroxide-mediated polymerization is based on a thermally-balanced equilibrium between an active radical and an inactive dormant species (nitroxide)[33] (Scheme 1) and is predestinated for the polymerization of styrene and MMA based monomers, *e.g.* triaryl amine (TARA)[34–37] derivatives or perylene diimides (PDIs).[35] Due to the commercial availability of (functional) initiators and the easy procedure, a screening of the influence of various substituents on the electrochemical properties and charge carrier mobility can be readily conducted.[34,35] Typically reached number average molar masses range from 3000 to 40 000 g mol^{-1} and in general the dispersity increases with the molar mass, *i.e.* small homopolymers with a dispersity $Đ \approx 1.10$[34] and large block or homopolymers with $Đ \approx 1.40$ to 1.97[34–37] were reported. In addition, a large variety of functional initiators can be easily prepared by coupling with (2,2,6,6-tetramethylpiperidin-1-yl)oxyl (TEMPO) or 1,1-dimethylethyl-2-methyl-1-phenylpropyl nitroxide (TIPNO) or a commercially available one can be used to introduce functional units into the

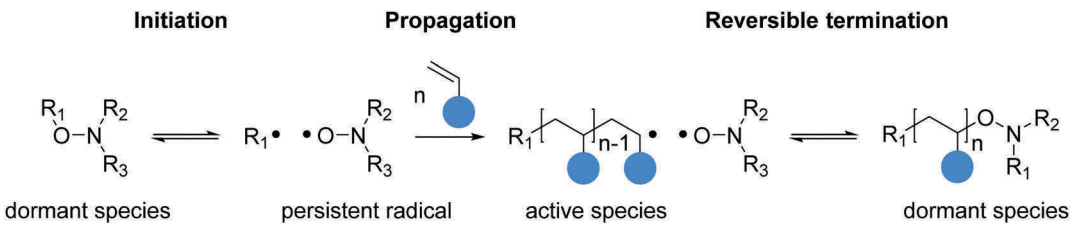

Scheme 1 Simplified polymerization mechanism of the nitroxide-mediated polymerization based on a thermal equilibrium between active and dormant species.

Table 1 Schematic representation of selected functional NMP initiators and comments

Entry	Structure	Comment	Ref.	Entry	Structure	Comment	Ref.
1	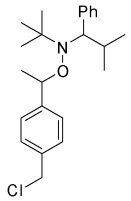	Commercially available Substitution of Cl with N_3 after polymerization	34 and 37 39 and 40	3	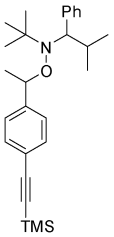	Suitable for CuAAC	41
2	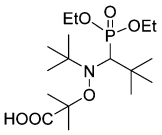	Commercially available	42	4	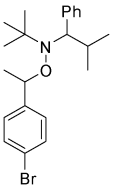	Suitable for cross couplings or activation with Mg (see KCTP)	38, 43 and 44

polymer.[28,31,38] Selected examples of functional initiators are listed in Table 1.

Atom transfer radical polymerization (ATRP) is also based on the equilibrium between a dormant and an active species. The activation occurs by a metal catalyst in a one electron transfer process (Scheme 2).[45] Major advantages are commercially available cheap initiators (alkyl halides), catalysts (copper complexes) and ligands (pyridine based). In addition, the functionalization of surfaces, *e.g.* silicon, with redox-active polymers can be readily achieved by the attachment of initiators in a self-assembling monolayer and subsequent polymerization.[46] Nevertheless, the polymerization of coordinating monomers, *e.g.* pyridine or metal complex based monomers, is precluded due to interactions with the metal catalyst and requires the utilization of "protected" monomers which can be transferred in the desired species by polymer analogous reactions. This approach was used by Fang *et al.* to prepare ruthenium polypyridyl decorated polystyrene by amide coupling.[47] Although high conversions were reached (≈90% based on NMR data), it is not possible to construct defect-free materials by this method. In addition, traces of remaining metal catalysts in the final product may limit the applications in (opto)electronics.

The most applied CRP technique is the reversible addition-fragmentation chain transfer (RAFT) polymerization due to the mild reaction conditions, high reaction rates and wide range of suitable monomers.[48–50] The controlled character of the polymerization relies on fast reversible chain transfer steps involving chain transfer agents, *e.g.* dithioesters, thiocarbamates and xanthates, so that the propagation rate of all chains is equal. Partly these RAFT agents are commercially available. A simplified mechanism is depicted in Scheme 3 and illustrates primary initiation, propagation and pre equilibration steps as well as the dominating main equilibrium step.

The diversity of polymerizable monomers is illustrated by the feasibility to directly incorporate metal complexes or dyes into polymers.[51–53] Furthermore, the well-defined end groups of RAFT polymers can be utilized by further functionalization reactions. A prominent example is the cleavage of dithioesters to generate a polymer decorated with a thiol group at the ω-end. The conversion of the modification can be quantified by UV/vis analysis (disappearance of the C=S band at 310 nm) or ^{1}H NMR spectroscopy.[54] Subsequently the thiol can be applied in a thiol–ene click reaction[49] or can be directly used for the attachment to gold surfaces.[54] The modification of the α-chain terminus is also possible by application of reactive RAFT agents, *i.e.* reactive esters with pentafluorophenyl groups can be readily modified with amines. In this way, the group of Zentel introduced photocleavable anchor groups into TARA polymers to stabilize nanoparticles[55] and further prepared disulfide bearing carbazole based polymers to result in hybrid materials with quantum dots.[56] The RAFT agent enabled the preparation of polymers with dispersities in the range of 1.1 to 1.2 and molar masses from 5000 to 12 000 g mol^{-1}.

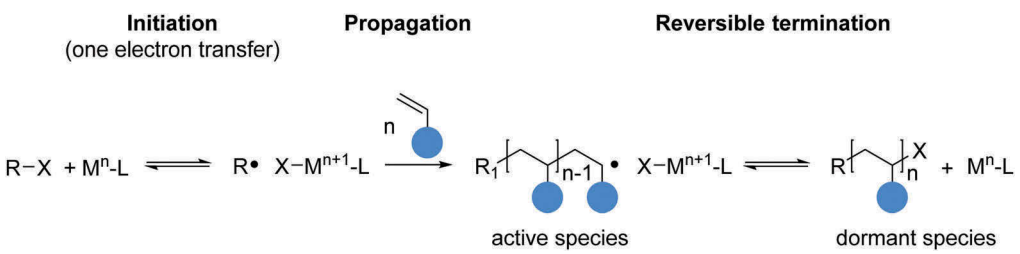

Scheme 2 Simplified polymerization mechanism of the atom transfer radical polymerization based on equilibrium between active and dormant species catalyzed by a one electron transfer process.

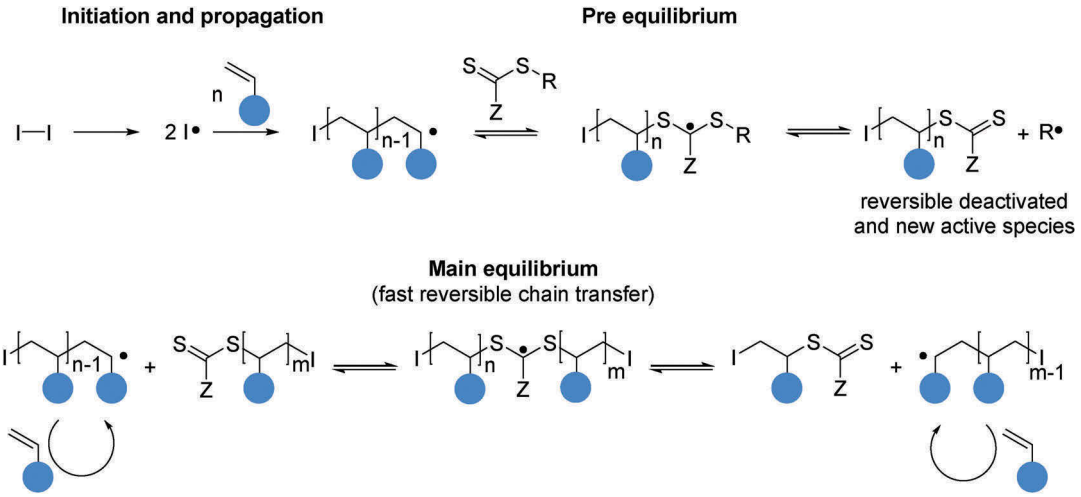

Scheme 3 Simplified mechanism of RAFT polymerization including fast and reversible chain transfer as a source of the controlled reaction process. I is initiator; the Z group, *e.g.* Ph, influences the stability of the C=S bond.

The quantitative substitution of the pentafluorophenyl group was verified by ^{19}F NMR spectroscopy. Moreover, surface-initiated approaches enable the construction of electroactive films.[57] RAFT polymerization (as well as the NMP process) is also the method of choice for the preparation of methacrylate based liquid crystalline polymers with discotic side groups for hierarchical self-assembled materials.[58,59]

For completeness, also other CRP techniques, *e.g.* iniferter polymerization,[60] can be suitable to prepare functional redox-active polymers but are much less frequently utilized.

2.2. Redox-active and conjugated polymers by anionic polymerization techniques

Anionic polymerization enables a truly living reaction process in case of absent termination reactions. In addition the chain end functionalization is readily achieved by the addition of end capping agents to quench the reactive species, *e.g.* by the addition of ethylene oxide.[61,62] The method requires a very high purity of the used chemicals and solvents to avoid termination reactions; as a consequence, it is less frequently used in comparison to CRP to prepare polymers for optoelectronics. However, a few interesting synthetic examples including chain end functionalization with fullerenes[63] are reported for triarylamine derivatives leading to polymers with number average molar masses from 2000 to 20 000 g mol^{-1} and dispersities from 1.05 to 1.2 according to SEC investigations.[63,64] Moreover, Higashihara and Mitsuru described the precise synthesis of block copolymers utilizing bifunctional initiators or functional coupling reagents, *i.e.* modified poly(3-hexylthiophene).[65] The preparation of block copolymers by sequential monomer addition of styrene or MMA as a second block gave very high conversions (>99%), low $Đ$ values (1.04–1.07) and high molar masses (25 000–39 000 g mol^{-1}) without further purification. In contrast, end capping with modified bifunctional poly-(3-hexylthiophene) required the removal of residual homopolymer by Soxhlet extraction to yield a product with high molar mass (26 000 g mol^{-1}) and low dispersity ($Đ$ = 1.15).

Conjugated polymers can also be prepared by anionic polymerization and subsequent elimination reactions. In this way Natori *et al.* synthesized a conjugated polymer consisting of *p*-phenylene, *p*-phenylenevinylene and styrylamine structures by copolymerization of cyclohexadiene and a styrenic triarylamine (Scheme 4).[66] Whereas the polymerization yield ranged

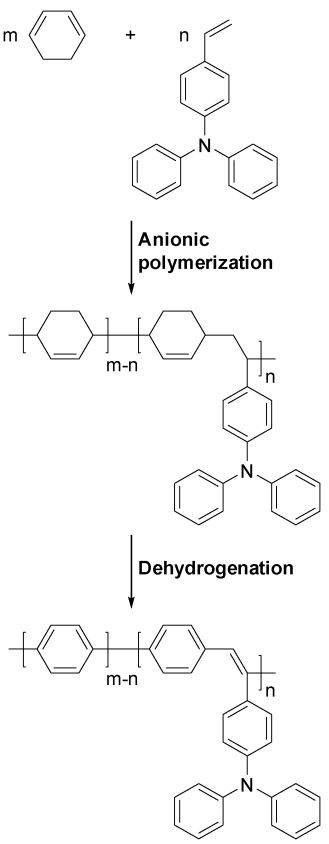

Scheme 4 Anionic polymerization and subsequent dehydrogenation leading to semiconducting polymers with *p*-phenylene, *p*-phenylenevinylene and styrylamine substructures (adapted from ref. 66).

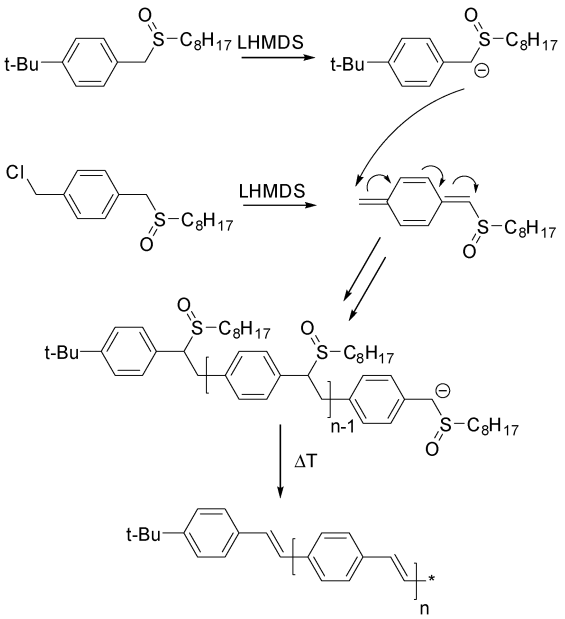

Scheme 5 Anionic polymerization using the sulfinyl precursor route leading to PPV after thermal treatment (adapted from ref. 67).

from 76% to 98% depending on the ratio of the monomers, the final dehydrogenation was apparently quantitative (based on ^{1}H NMR data) and yielded the conjugated polymers. Interestingly, this approach avoids the partly complicated introduction of functional groups necessary for the preparation of the respective polymers by cross coupling reactions.

Moreover, the group of Vanderzande reported the preparation of PPV polymers by the so-called sulfinyl precursor route (Scheme 5).[67] In this approach a *p*-quinodimethane derivative is used as a monomer and the obtained non-conjugated polymer is transformed into PPV by thermal elimination (Scheme 5). The reaction is very fast and an almost quantitative conversion of the monomer is reached within seconds. Although the reported dispersities are high for a controlled process ($Đ > 1.7$), the molar mass can be controlled by the amount of added initiator and varied from 4000 to 20 000 g mol^{-1}. Noteworthily, this technique yields polymers with high end group fidelity and functional groups may be introduced with the initiator.[67]

2.3. Redox-active and conjugated polymers by ring opening metathesis polymerization (ROMP) approaches

The ring opening metathesis polymerization of cyclic alkenes (Scheme 6) offers high functional group tolerance and, therefore, enables the application of sensitive monomers, *e.g.* fullerene or radical containing compounds (Fig. 3).[68–75] The reaction is most commonly catalyzed by Grubbs catalysts, *i.e.* ruthenium complexes, and enables end functionalization as well as the preparation of block copolymers. In general, high conversions are reached in less than one hour due to the high reaction rate and dispersities smaller than 1.10 could be observed.[72,74,75] Depending on the kind of monomer, either conjugated or redox-active polymers may be synthesized.

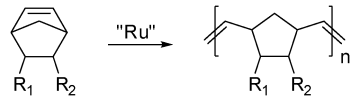

Scheme 6 Schematic representation of the general ROMP polymerization process of norbornene derivatives. R_1 and R_2 represent moieties to attach functional units (see Fig. 3).

Due to their established preparation methods and easy functionalization, norbornene derivatives (Scheme 6) are of special interest for the preparation of redox-active polymers. In particular, they exclusively allow direct polymerization of fullerene derivatives. The conformational freedom of the fullerene in the side chain is adjusted by the utilized linker between the backbone and fullerene, and examples applying long flexible linkers as well as rigid monomers can be found.[68–71] Typically, molar masses between 6500 and 17 000 g mol^{-1} were reached. Due to intensive optimization of the polymerization conditions by Kim *et al.*,[70] the dispersity of a dendritic polymer was improved ($Đ = 1.08$) and the fullerene density was significantly increased in comparison to other fullerene containing polymers, which feature a much broader molar mass distribution ($Đ > 1.8$).[71,73]

As mentioned in the beginning of this section, ROMP is also a powerful technique to synthesize telechelic conjugated polymers, *i.e.* PPVs.[76] Suitable monomers leading to PPV derivatives include [2.2]paracyclophanes,[77–83] [2.2.2]paracyclophanes[84,85] or derived compounds[86] (Scheme 7). The synthesis of [2.2]paracyclophanes succeeds through a multi-step reaction involving a nucleophilic ring closing reaction of benzylic dithiols and benzylic dibromides as the first step. The obtained [3.3]dithiacyclophanes are transferred into the monomers by either Stevens or Pummerer rearrangement and subsequent reactions.[78,87] In contrast, [2.2.2]paracyclophanes can be prepared from a phenylene–ethynylene backbone by a ring-closing intramolecular McMurry reaction as the last step.[84] The kind of monomer dictates the substitution pattern of the later (co)polymer which is depicted in Fig. 4. Noteworthily, the polymers are obtained as a *cis*/*trans* mixture after the reaction but isomerization to the all *trans* isomer is achieved by exposure to UV light in solution. The ROMP process follows the characteristics of a living polymerization so that the preparation of block copolymers[88,89] (*vide infra*) or an end functionalization[77,83,90] is readily possible. Typically, molar masses between 5000 and 60 000 g mol^{-1} and dispersities $Đ \approx 1.2$–1.4 are reached for [2.2]paracyclophanes combined with high monomer conversion (>90%). In contrast, [2.2.2]paracyclophanes and related thiophene derivatives yield polymers with higher dispersities ($Đ = 1.4$ to 1.9) and the monomer conversion is lower.[84–86] End functionalization or termination reagents are commonly based on substituted alkenes, *e.g.* functional vinyl ether derivatives. Remarkable functionalization examples include supramolecular recognition units, which were prepared by Elacqua and Weck to fabricate supramolecular polymers,[77] or α-bromo esters as macroinitiators for ATRP as prepared by Lidster *et al.*[83,90] The end functionalization efficiency was calculated to be above 90%.

Besides PPVs, also polyacetylenes can be prepared by ROMP utilizing cyclooctatetraene as the monomer. In this regard the

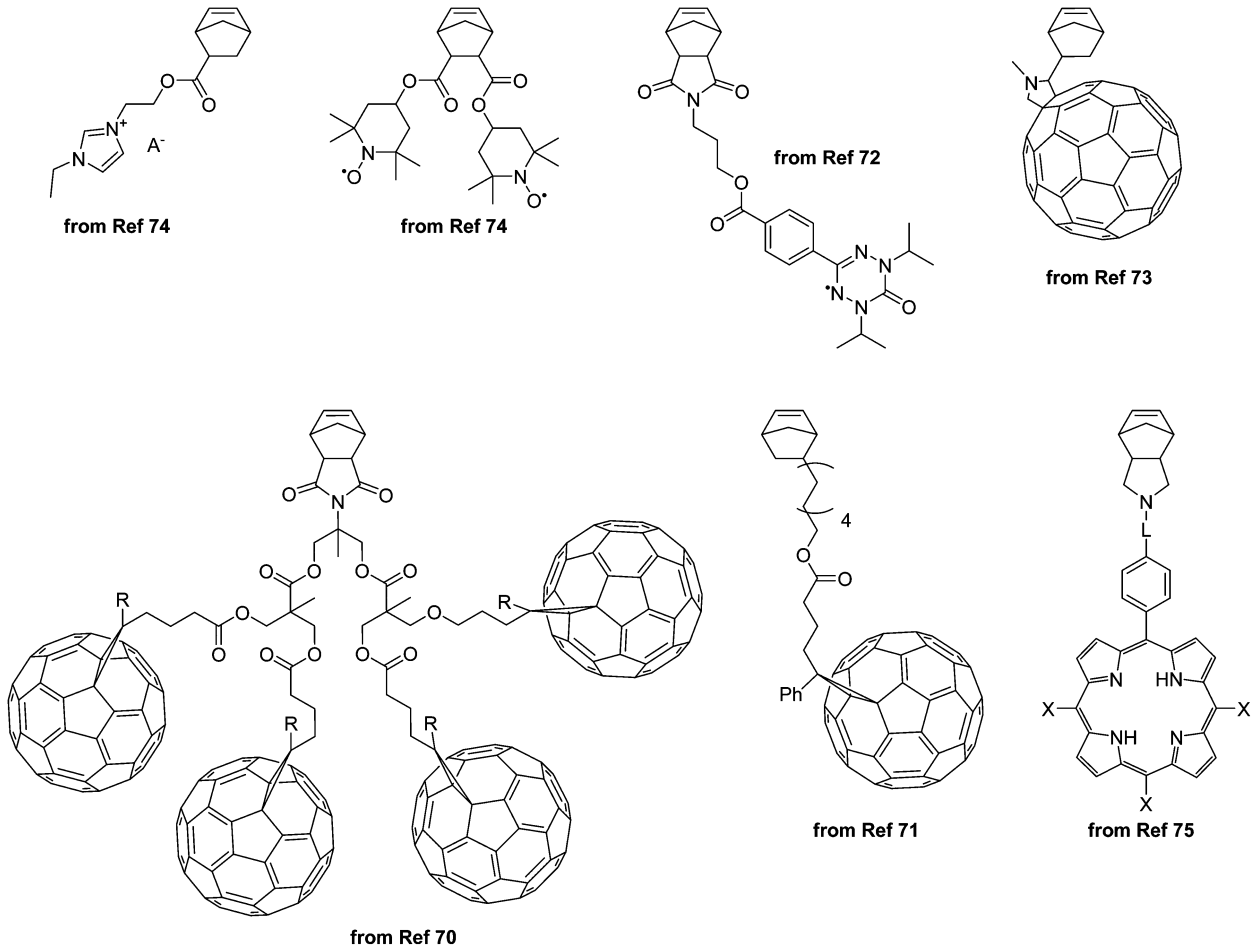

Fig. 3 Schematic representation of norbornene based monomers containing redox- or photoactive monomer units commonly used for the preparation of homopolymers.

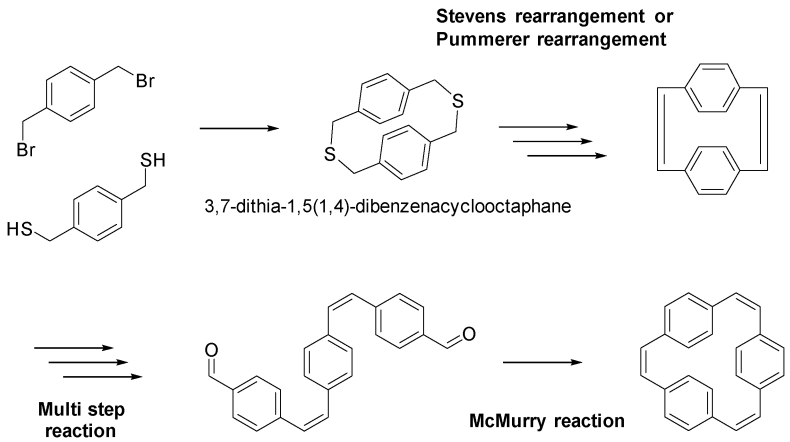

Scheme 7 Schematic representation of the simplified synthesis leading to [2.2]paracyclophanes[78] and [2.2.2]paracyclophanes.[84]

group of Choi demonstrated the potential of the *in situ* formation of nanoparticles consisting of polyacetylene copolymers. Polyacetylene is almost insoluble in all common solvents and directly leads to self-assembly of the copolymer during the synthesis due to the collapsing of the PA segment.[91,92] Moreover, poly(*o*-phenylene ethynylene)s are also accessible by the ROMP of strained cyclic alkynes.[93] Interestingly, the structure of the respective macromolecules, *i.e.* cyclic or linear, was shown to be dependent on the catalyst used.[93]

For the sake of completeness it should be mentioned that also acyclic diene metathesis polymerization can yield redox-active polymers as shown by Song *et al.*[94]

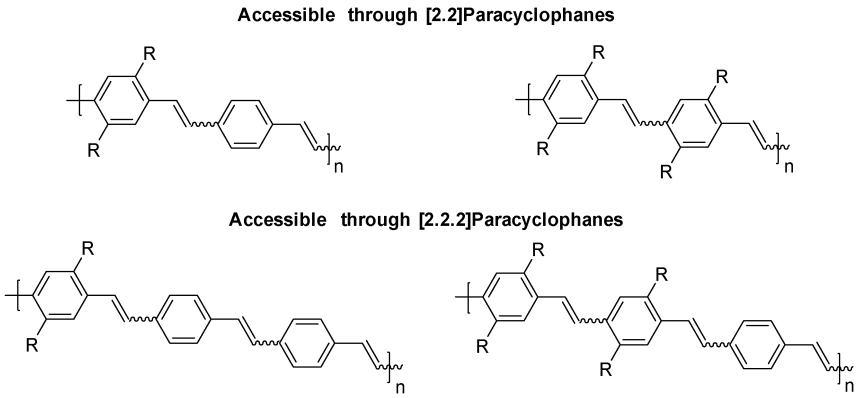

Fig. 4 Reported substitution pattern of PPVs depending on the monomer used to influence the properties of the polymers.

2.4. Conjugated polymers by catalyst transfer polycondensation (CTP) techniques

The classical approaches to prepare a multitude of conjugated polymers are step-growth based polymerization procedures leading to polymers with a broad molar mass distribution and low end group fidelity. In the beginning of the 2000s the development of the Grignard metathesis (GRIM) and/or Kumada catalyst transfer polymerization (KCTP) of thiophenes by McCullough and Yokozawa represented a significant advancement due to its living character and the associated novel synthetic possibilities, *i.e.* the preparation of (co)polymers with defined functional end groups and a narrow molar mass distribution.[39,95–102] A detailed overview of the mechanism of this chain growth polymerization process and the scope of monomers, which nowadays cover more than thiophenes, is found in recent reviews detailing the Kumada catalyst transfer polymerization.[103–108] In the following only a short introduction with a focus on the end functionalization possibilities will be provided.

Telechelic polymers may either be prepared by the application of functional initiators,[100,102,109–115] *in situ* end capping reagents[97,99,109,116–118] or a post polymerization approach.[101,119,120] An overview of various functional initiators and introduced end groups is given in Tables 2 and 3. The efficiency of the initiation or end functionalization, *i.e.* the amount of the desired end groups in the product, is also given in the tables. Noteworthily, the end functionalization using Grignard reagents with triple or double bonds partly leads to difunctionalized polymers (Table 3). In addition, the living character also facilitates the polymer linkage to surfaces or nanoparticles by grafting from a surface with incorporated starting units[121] or attachment of the polymers *via* functional end groups.[101,119]

Besides magnesium, zinc is also a suitable metal for the activation of the monomers and subsequent polymerization, in particular for thiophene or related perylene and naphthalene diimide derivatives.[122–124,125] In line with the classical KCTP approach various (functionalized) nickel[102,126,127] or palladium catalysts[128–130] represent suitable initiators. Palladium catalysts are in general more stable but increase the tendency for a break of the catalyst/polymer π complex especially with monomers different from thiophene.[130] Nevertheless a remarkable protocol, which did not rely on the π complexation of the metal catalyst for polymerization control, was developed by Verswyvel *et al.*[129] The reported catalyst system using Pd/Ruphos and monomers which are deactivated for oxidative addition resulted in a controlled polymerization process.[129]

The activation with zinc further enables the application of monomers with alkyl halide moieties without any side reactions, so that these functionalities are available for subsequent post polymerization reactions (see Section "Graft and comb polymers").[131]

A major challenge of the GRIM approach utilizing zinc or magnesium is the required base stability of the monomer and the necessity of an almost quantitative metal/halogen exchange to preclude side and termination reactions. In order to expand the field of accessible polymers the catalyst transfer approach was transferred to various metal catalyzed cross coupling polymerization procedures in the past few years.[103] Today, Suzuki, Heck or Sonogashira cross coupling polymerizations can also be carried out under mild conditions in a nearly ideal chain growth mechanism. As an advantage of these CTP techniques in contrast to Kumada CTP, the required substituted AB monomers are prepared separately, *i.e.* they can be purified, isolated and stored. The investigated suitable monomers for Suzuki CTP include fluorene,[132] *para*-phenylene,[133] or thiophenes.[134,135] Noteworthily, also the polymerization of *para*-phenylenevinylene,[136] phenanthrene[137] or pyridine[138] was studied but an ideal chain growth mechanism was not found as an intermolecular catalyst transfer or side reactions, *e.g.* disproportionation or dehalogenation, occurred. End functionalization of the respective polymers can be realized using functional Pd catalysts[132,133,135–146] (Tables 4 and 5) or functional end capping reagents, *i.e.* substituted boronic acids or esters (Table 6).[140,141,144,145] Deviations from the ideal chain growth mechanism decrease the initiation efficiency of the externally prepared functional initiators, *e.g.* in the case of *para*-phenylenevinylene instead of thiophene as the monomer (Table 4, entry 2) or at very high conversions (typically conversions ≈ 50% were aimed for).[136,140] In contrast to the usual reported synthetic routine applying the externally prepared initiators (Table 4), Zhang *et al.* synthesized a broad range of polymers utilizing functional catalysts which were *in situ* generated from a catalyst precursor and an aryl halide and result in a high fidelity of the

Table 2 Schematic representation of functional initiators for KCTP[a]

Entry	Structure	Efficiency[b]	Ref.	Entry	Structure	Efficiency[b]	Ref.
1	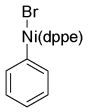	Quant.	109	8	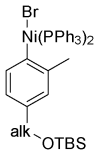	95%	100 and 111
2	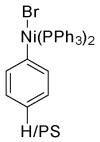	n.d.	100 and 112	9	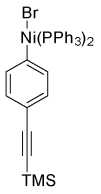	90%	100
3	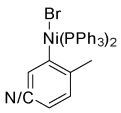	80–95%	100 and 113	10	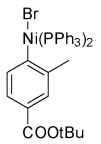	Quant.	102
4		Quant.	110	11	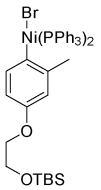	>50%	102
5	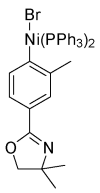	n.d.	102	12	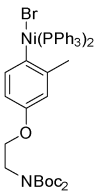	Quant.	102
6	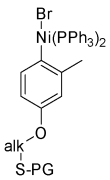	Quant.	114	13	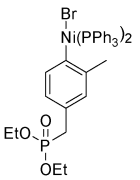	Quant.	113
7	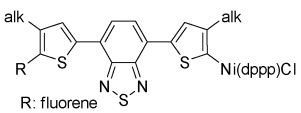	Main product	110				

[a] PS = polystyrene, PG = protecting group, TBS = *tert*-butyldimethylsilyl, TMS = trimethylsilyl, n.d. = not determined, dppe = 1,2-bis-(diphenylphosphino)ethane, dppp = 1,3-Bis(diphenylphosphino)propane. [b] Based on the amount of initiator groups found in the final product (when mentioned) by MALDI-TOF MS.

desired end group (Table 5).[142–144,146] The application of end capping reagents is also an appropriate way to introduce functional end groups in good yields (Table 6). The ability to prepare bi-telechelic polymers is impressively documented by Elmalem *et al.*, who synthesized a library of heterobisfunctionalized polyfluorenes.[140]

The transfer of the CTP approach to the Sonogashira cross coupling route gives access to poly(*p*-phenyleneethynylene)s which are interesting materials due to their rigid structure.[147] The respective synthesis including kinetic studies to reveal the ideal chain growth mechanism was documented by Kang *et al.*[147] Similar to the Suzuki polymerization, end functionalization or attachment on surfaces is also feasible by functionalized initiators.[147] Recently, efforts were undertaken to perform Heck coupling in a catalyst transfer fashion to prepare PPVs in a straight-forward approach.[148]

Noteworthily, the atom economy of the described synthetic routes is unsatisfactory for preparation on large scales, *e.g.* the mass loss during the polymerization of 2,5-dibromo-3-hexylthiophene is 49%. Therefore strategies using direct arylation are currently being extensively studied.[14,149–157] A comprehensive review of direct (hetero)arylation polymerization covering current developments as well as challenges and limitations was recently published by the group of Leclerc.[158]

Table 3 Schematic representation of reported end groups introduced by *in situ* end capping (entries 1 to 9) or postpolymerization modification (entries 10 to 14)

Entry	Structure	Efficiency[a]	Ref.	Entry	Structure	Efficiency[a]	Ref.
1		91%	97 and 99	8	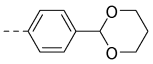	Mainly di-capped	97
2		86% + 14%[b]	97, 99 and 109	9	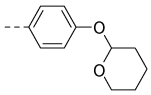	12% + 75%[b]	97 and 99
3		86%	97 and 99	10		95%	101
4		24% + 76%[b]	97 and 99	11	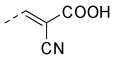	95%	101
5	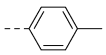	20% + 80%[b]	97 and 118	12		Quant.	116
6		20% + 80[b]	97 and 99	13	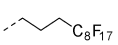	Quant.	117
7	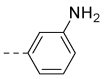	Mainly mono-capped	97	14		n.d.	120

[a] Based on the amount of end groups found in the final product (when mentioned) by MALDI-TOF MS. [b] End capping at both chain ends.

Table 4 Schematic representation of externally prepared initiators for Suzuki coupling polymerization

Entry	Catalyst	Efficiency[a]	Ref.	Entry	Catalyst	Efficiency[a]	Ref.
1	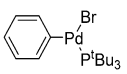	Quant.	132	6	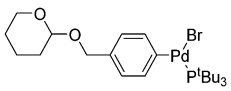	Quant.	145
2	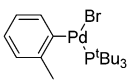	<50%[b]	136	7	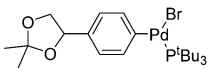	Quant.	145
3	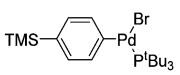	Quant.	141	8	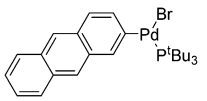	>95%	140
4	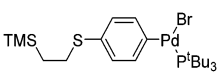	Quant.	141	9	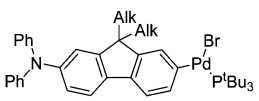	>95%	140
5	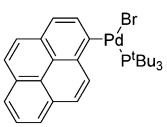	>95%	140	10	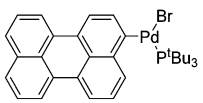	>95%	140

[a] Based on the amount of end groups found in the final product (when mentioned) by MALDI-TOF MS. [b] Also di-capped product observed due to chain couplings.

3. Block copolymers

Block copolymers allow the linear combination of two or more different monomer units in distinct sections of a macromolecule to create new materials with tailored properties, *e.g.* electron and hole transporting as well as hydrophilic and hydrophobic blocks can be incorporated into one polymer chain. Thus the electrochemical as well as the physical properties can be precisely tuned, *e.g.* to control the morphology and self-assembly properties of the materials.[24,159,160] In the context of organic solar cells, especially, improved stability of the device morphology and reduced sintering[161] is expected from the application of block copolymers. Based on their behavior in solution, polymers are differentiated either as coil or as rod polymers. Whereas coil polymers are characterized by a flexible backbone, rod polymers are rigid as a result of a restricted conformational freedom. Due to the different structures of these polymers, the combination of the two types in a block copolymer represents a promising and often used approach to control the microphase separation (*vide infra*).

In general four methods for the synthesis of block copolymers can be distinguished, which are depicted in Scheme 8.[160,162] In the case of a living polymerization, *e.g.* anionic polymerization or ROMP, block copolymers are prepared by sequential monomer addition, *i.e.* the polymerization is started with one monomer and after full consumption a second monomer is added and so on.

Table 5 Schematic representation of aryl halides applied for the *in situ* generation of functional catalysts by Zhang *et al.*[142–144,146]

Entry	Compound	Efficiency[a]	Ref.	Entry	Compound	Efficiency[a]	Ref.	Entry	Compound	Efficiency[a]	Ref.
1	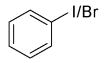	Quant.	143 and 146	8	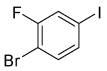	n.d.	143	15	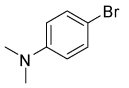	Quant.	142
2	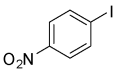	Quant.	142 and 143	9	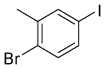	n.d.	143	16	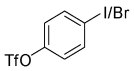	90–99%	144
3	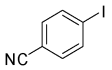	Quant.	142 and 143	10	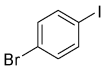	n.d.	146	17	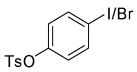	Quant.[b]	144
4	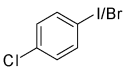	Quant.	144 and 146	11		Quant.	142 and 146	18	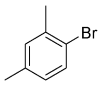	Quant.	142
5	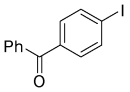	Quant.	142 and 143	12	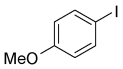	Quant.	142 and 146	19	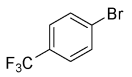	Quant.	142
6	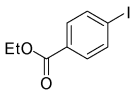	Quant.	143 and 146	13	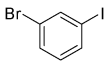	n.d.	143	20	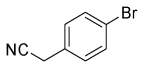	Quant.	142
7	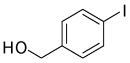	Quant.	143	14		n.d.	143	21	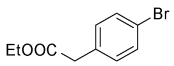	Quant.	142

[a] Based on the amount of end groups found in the final product (when mentioned) by MALDI-TOF MS. [b] Quantitative initiation but partly cleavage to alcohol during isolation and/or ionization.

Table 6 Schematic representation of reported end capping reagents – applied as boronic acids/esters – for the Suzuki CTP. The dashed line indicates the bond to the respective polymer

Entry	Structure	Efficiency[a]	Ref.	Entry	Structure	Efficiency[a]	Ref.
1		99%	144	7	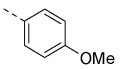	Quant.	140
2	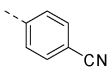	Quant.	140	8	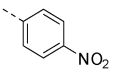	Quant.	140
3		99%	144	9	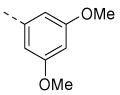	Quant.	140
4	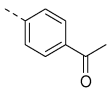	99%	144	10	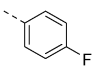	99%	144
5	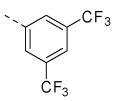	Quant.	140	11	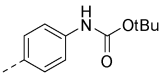	Quant.	140
6	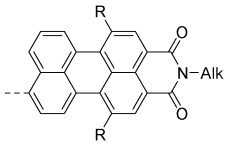	95%	145	12	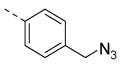	85%	141

[a] Based on the amount of end groups found in the final product (when mentioned) by MALDI-TOF MS.

Consequently the polymerization is carried out in a facile one pot procedure and isolation and purification of the primarily formed homopolymer is not possible but also generally not necessary. Very precise control of the final structure is achieved. A successful synthesis, however, requires an efficient crossover reaction, the addition of the monomers in the right order of reactivity and possibly tuning of the reactivity of the propagating chain by additives.[162,163] The synthesis of block copolymers by CRP or similar techniques cannot be accomplished by sequential monomer addition due to the emergence of termination reactions at high monomer conversions. As a consequence, the second strategy leading to block copolymers is based on the

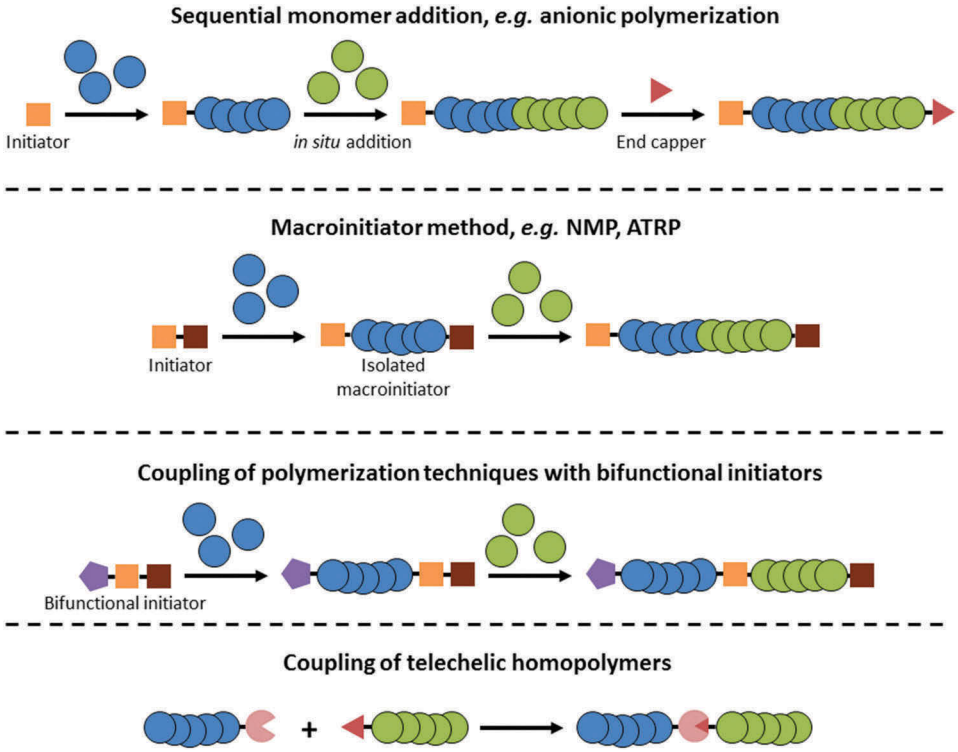

Scheme 8 Main synthetic approaches leading to block copolymers.

use of macroinitiators or macro-RAFT agents. In the first step, a homopolymer still bearing the initiating group (or RAFT group) is synthesized. After purification, *i.e.* the removal of unreacted monomers, the compound may be used to initiate the polymerization of the second monomer. In contrast to the sequential monomer addition, this technique enables a modular approach as the macroinitiator can be utilized for varying block copolymers. In a similar way bifunctional initiators capable of initiating two or more different polymerization processes may be applied to construct macroinitiators and, subsequently, block copolymers. This coupling of polymerization strategies is of special interest as a wide scope of monomers and in principle all possible polymerization techniques may be combined. The last common approach leading to block copolymers is the coupling of telechelic polymer chains. The required end groups are introduced by functional initiators, end cappers or postpolymerization reactions (see Section "Synthesis of functional homopolymers"). In order to achieve high conversion during coupling, very efficient reactions, *e.g.* the copper(I)-catalyzed azide–alkyne cycloaddition (CuAAC) reaction, are required. In the case of incomplete conversion, separation of the block and homopolymers may be challenging. Nevertheless the coupling of polymer chains is beneficial with respect to a modular synthetic approach.

3.1. Block copolymers by CRP and anionic polymerization

Controlled radical polymerization techniques are well suited for the synthesis of block copolymers due to the high fidelity of the reactive end groups (see Section "Synthesis of functional homopolymers"). For this purpose, at first a homopolymer is synthesized and is then utilized as a macroinitiator (NMP and ATRP) or as a macro-RAFT agent (RAFT polymerization) to prepare the block copolymer. Ideally the so obtained block copolymer can also be further used for the synthesis of triblock terpolymers and so on.

In the simplest case, one block of the copolymer is electrochemically active, *e.g.* poly(*N*-vinyl carbazole) or poly(vinyl-*m*-triphenylamine), and the second one is only used to control the self-assembly properties of the material, *e.g.* poly(*N*-vinyl pyrrolidone) or PMMA.[164,165] An interesting example for the preparation of block copolymers in which the second block fulfills an additional task is reported by the group of Zentel. The authors prepared copolymers which contained triarylamine derivatives in the first and pentafluorophenyl acrylate in the second block (Scheme 9).[166–169] The activated ester of the second block is readily substituted so that anchor groups for the attachment of the polymer on quantum dots,[168] nanorods[166] or tetrapods[167] can be introduced (Fig. 5). Moreover, the approach is applicable for decoration with photosensitizers or dye molecules, which can be used for the construction of donor–photosensitizer–acceptor (D–P–A) nanocomposites (Fig. 5).[166,169] Whereas bulky units are not quantitatively linked to the polymer backbone due to steric hindrance, small molecules result in a quantitative conversion as judged from ^{19}F NMR spectroscopy. For example, Zorn *et al.* achieved 30% conversion of the ester with a perylene diimide and full conversion with dopamine.[166]

In a similar approach, Brendel *et al.* exploited the possibility to selectively modify one block of a copolymer to construct amphiphilic block copolymers consisting of a triarylamine and

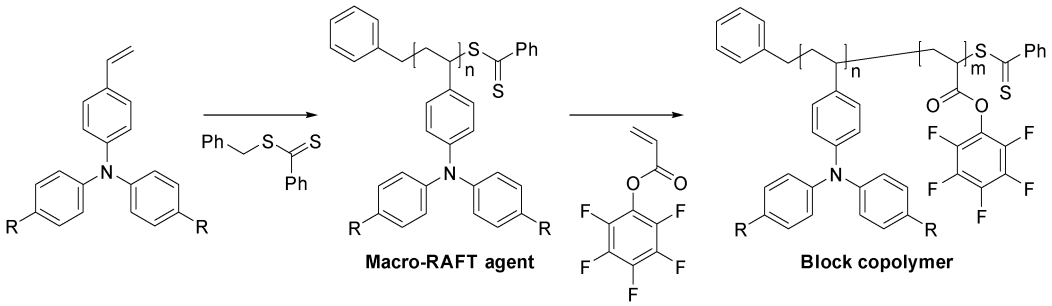

Scheme 9 Schematic representation of the preparation of triarylamine based block copolymers with a reactive pentafluorophenyl acrylate block by RAFT polymerization.[166–169]

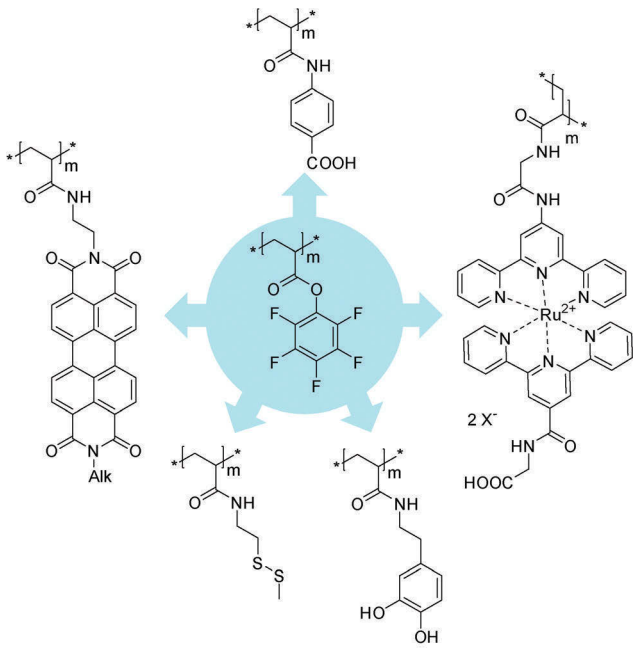

Fig. 5 Schematic representation of reported substitution reactions of pentafluorophenyl acrylate used to introduce metal complexes, anchor groups or dyes into the respective block copolymers.[166–169]

a hydrophilic polystyrene sulfonate block.[170] Interestingly, a small part of the macro-RAFT agent was inactive, so that a separation of the desired block copolymer and the residual macro RAFT agent by preparative SEC was necessary and resulted in a narrow molar mass distribution with $Đ$ = 1.08 (before purification $Đ \approx 1.3$). This material gave micelles in aqueous solution which were decorated with nanorods leading to nanocomposites.[170] Due to the application of water as a solvent, this approach displays a promising "green" alternative for the construction of hybrid solar cells with controlled domain sizes.[170]

Besides these examples comprising copolymers with one block, which is not electrochemically active, also block copolymers with two active blocks are reported in the literature. For instance, the incorporation of monomers with varying redox potentials yields block copolymers with an internal redox gradient for directed charge transport.[34,171] In this regard, Schroot *et al.* reported the preparation of triarylamine block copolymers with number average molar masses between 25 000 and 39 000 g mol^{-1} and low dispersities ($Đ$ = 1.20 to 1.42) using standard NMP conditions.[34] In contrast RAFT polymerization to yield block copolymers of triarylamine derivatives required an intensive optimization to achieve a significant increase in the molar mass and low dispersities ($Đ < 1.60$).[171] Moreover, donor–acceptor block copolymers are readily prepared by CRP, *e.g.* NMP.[172,173] The combination of amorphous triphenylamine and perylene bisimide, which is capable of π–π stacking due to a flexible linker, produced nanostructured materials leading to higher yields of long-lived free charges in comparison to blends of the homopolymers.[172,173]

The anionic polymerization is predestinated for the synthesis of block copolymers by sequential monomer addition. Due to the absence of termination reactions in the ideal case, it is possible to achieve the full consumption of a monomer and afterwards add a second monomer to obtain a second block.[174,175] In this regard, a comprehensive example is given by Kang *et al.* by the synthesis of triphenylamine and ethynylpyridine containing copolymers.[176,177] In their work the influence of the cation on polymerization is described and strategies to tune the reactivity of the active species are presented. After optimization of the reaction conditions, block copolymers with narrow molar mass distributions ($Đ$ = 1.10 to 1.15) and molar masses between 8000 and 20 000 g mol^{-1} were observed under full conversion. Noteworthily, the application of potassium naphthalenide also allowed for the synthesis of BAB triblock copolymers (Scheme 10).[176,178]

The preparation of PPV and PA containing block copolymers by sequential monomer addition utilizing the sulfinyl precursor route is reported by Cosemans *et al.*[179] However, besides block copolymer formation, the authors also observed a homopolymer at the end of the reaction which made a purification step by preparative SEC necessary.[179] In addition, so far no other second block could be introduced, *e.g.* styrene did not lead to a polymer.

3.2. Block copolymers by ROMP

Ring-opening metathesis polymerization, similar to anionic polymerization, is a living process and therefore well suited for the preparation of block copolymers by sequential monomer addition. In particular the wide scope of cyclic monomers

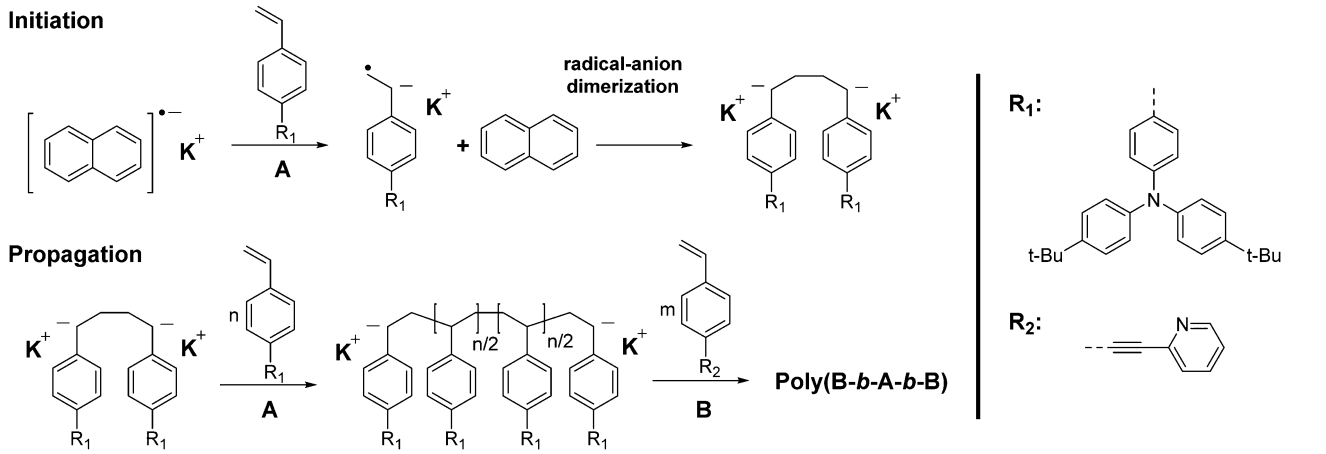

Scheme 10 Schematic representation of anionic polymerization using potassium naphthalenide as an initiator leading to BAB triblock copolymers.[176,178]

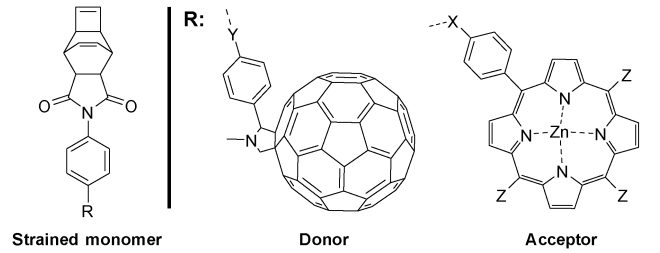

Fig. 6 Schematic representation of tricyclo[4.2.2.0^{2,5}]deca-3,7-diene based monomers for the preparation of donor–acceptor block copolymers by sequential monomer addition.[182]

enables a multiplicity of different structures and will be presented in the following section.

A facile approach to prepare block copolymers by ROMP is the use of substituted norbornenes[180,181] or related compounds, *e.g.* tricyclo[4.2.2.0^{2,5}]deca-3,7-diene derivatives,[182] with varying substituents. For instance, Gu *et al.* synthesized polyelectrolytic copolymers containing blocks with different metallocene derivatives with low dispersities ($Đ$ = 1.07) with quantitative conversion of each monomer.[180,181,183]

In a similar approach, the incorporation of porphyrin and fullerene moieties was achieved by Charvet *et al.* (Fig. 6).[182] The obtained photoconductive films featured nanowire-like self-assembly with well segregated domains which were tailorable by the size of the block copolymer.

The synthesis of PPV block copolymers with various substitution and linking patterns is reported by Yu *et al.*[88,89] The sequential monomer addition of strained cyclophanedienes allowed the incorporation of 1,4-phenylenevinylene and 1,3-phenylenevinylene repeating units. Due to the different structures of the blocks, phase separation was observed and, moreover, energy transfer between the blocks could also be observed by photoluminescence measurements.[89] The variation of the cyclophane building block, *i.e.* by introduction of cyclopentadithiophene-vinylene or dithienobenzothiadiazole-vinylene moieties as underlying units, was used to construct donor–acceptor block copolymers as shown by Chang and Masaki (Scheme 11).[184] The observed dispersities ($Đ$ = 1.51 to 1.85) are higher than for PPVs by the ROMP of cyclophanedienes ($Đ$ = 1.2 to 1.5).[184] However, by the variation of the monomer units, various backbone structures can potentially be realized in order to tune the HOMO–LUMO levels or the UV/vis absorptivity.

The so far presented examples utilized monomers, which were, respectively, based on the same chemical structure to construct block copolymers. However, it is also possible to synthesize block copolymers by ROMP consisting of structurally different monomer units. In this regard the group of Choi reported the synthesis of polynorbornene-*b*-polyacetylene by sequential monomer addition and the *in situ* nanoparticlization of the conjugated polymer leading to the formation of nanocaterpillars.[92] Based on the large reactivity differences of the monomers, the authors additionally developed a one-step preparation method leading to block-like copolymers.[91] A further compelling example is given by Menk *et al.* by the synthesis of block copolymers containing PPVs and polynorbornenes.[185] At first, the polymerization of norbornene derivatives was initiated with a Grubbs catalyst and after consumption of the first monomer, a substituted paracyclophanediene was added to form the second block of the polymer with narrow molar mass distribution ($Đ$ = 1.29, 17 000 g mol^{-1}). This example is of special interest as various substituents, *e.g.* PEG chains or reactive esters, were introduced in the non-conjugated block and enabled self-assembly into micelles as well as post-polymerization modification to introduce anchor groups for attachment to quantum dots.[185] Therefore the combination of various strategies to design macromolecular hierarchical architectures is appealingly demonstrated.

3.3. Block copolymers by CTP

Various "classical approaches", *i.e.* step growth polymerization techniques, can be utilized to prepare block copolymers. For example, the synthesis of PPV derivatives by Horner–Emmons coupling leading to multiblock copolymers[186] and the Hartwig–Buchwald coupling to prepare donor–acceptor triblock copolymers[187,188] should be mentioned in this context. However, the control over the molar mass distribution and the degree of polymerization is limited by these techniques.

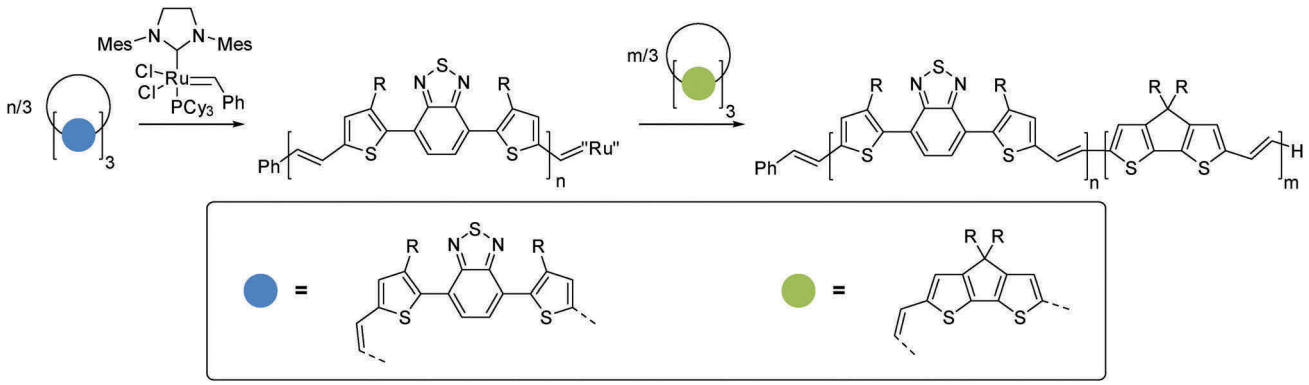

Scheme 11 Schematic representation of donor–acceptor block copolymer synthesis using ROMP and the sequential monomer addition technique.[184]

In contrast, the Kumada catalyst transfer polymerization and related CTP protocols allow the preparation of well-defined block copolymers by sequential monomer addition.[189–222] An overview of various synthesized polymers, molar masses and dispersities is provided in Table 7. Noteworthily, the conversion of the individual monomers is in general higher than 90% but the yields of the final polymer (when given in the report) are normally lower due to losses upon purification, *e.g.* by extraction.

Table 7 Schematic representation of block polymers prepared by CTP protocols utilizing the sequential monomer addition method

Entry	Polymer	M_n[a] [kg mol^{-1}] $Đ$	Ref.	Entry	Polymer	M_n[a] [kg mol^{-1}] $Đ$	Ref.
1	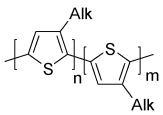	4–22 1.10–1.69	189–191	14	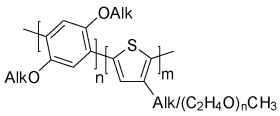	5–26 1.10–1.40	192–194
2	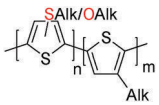	8–13 1.70	195 and 196	15	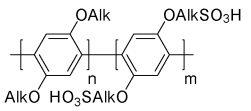	26–82 1.11–1.32	197
3	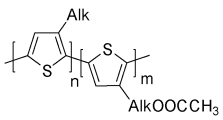	9–10 1.29–1.49	198	16	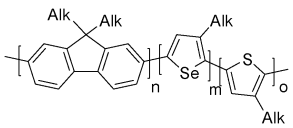	8–17 1.40–1.70	199
4	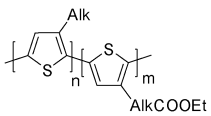	8–10 1.10–1.18	198	17	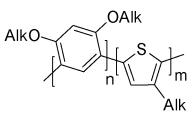	16 1.15	200
5	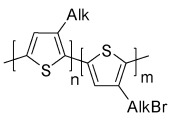	11 1.07	201	18	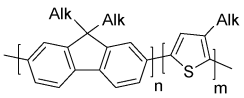	8–46 1.24–1.30	202 and 203
6	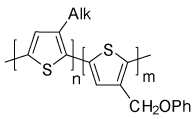	12–35 1.13–1.20	204	19	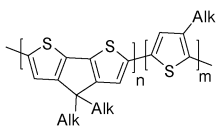	7[b] 1.45	205
7	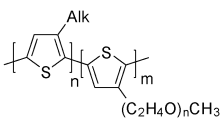	10–18 1.10–1.73	206–209	20	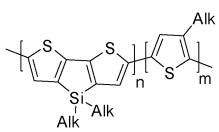	6–31 1.3–3.3	210
8	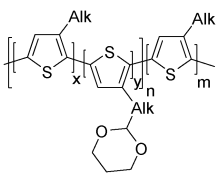	37 1.6	211	21	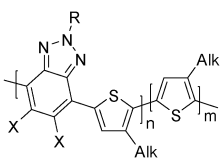	11–18 1.31–1.6	212

Table 7 (*continued*)

Entry	Polymer	M_n[a] [kg mol^{-1}] $Đ$	Ref.	Entry	Polymer	M_n[a] [kg mol^{-1}] $Đ$	Ref.
9	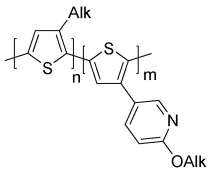	20 1.22	213	22	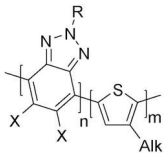	19–21 1.39–1.74	212 and 214
10	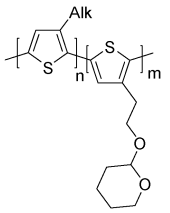	5–15 1.1–1.2	215 and 216	23	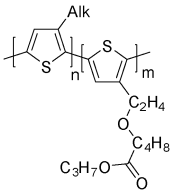	17 1.16	217
11	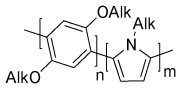	16 1.13	218	24	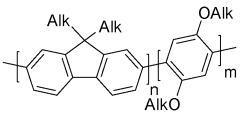	6–9 1.45–2.01[c]	203
12	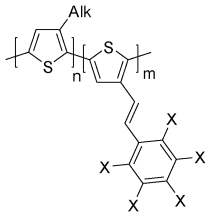	2–3 1.38–1.58	219	25	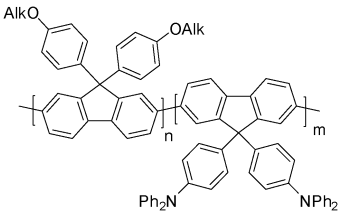	18 1.31	202
13	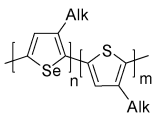	18–29 1.15–1.36	220 and 221	26	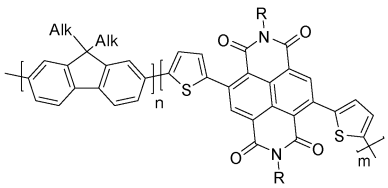	49 3.9	222

[a] Based on SEC (data are only given, when mentioned in the report). [b] From ^{1}H NMR data. [c] The lower dispersity value was observed with PPP as the first block.

Moreover, initiation with an externally prepared initiator (*vide supra*) should be preferred to preclude B–A–B triblock formation which can occur in particular in small blocks or in the case of a second monomer with a less electron-rich character (weaker complexing ability of the Ni catalyst).[205] However, this issue is rarely investigated or commented on in publications. Block copolymers consisting of different substituted thiophene units were reported and can be used to achieve self-assembly into nanowires (entry 1),[189] to introduce functionalized side chains (entry 4)[198] or to tune the energy levels in a donor–donor block copolymer for application in solar cells (entry 2).[195] Furthermore, functional side chains are attractive to attach additional functional units (covalent or supramolecular), *e.g.* fullerene derivatives (entries 5, 8 and 9).[201,211,213] Besides thiophene, also derived monomers, *e.g.* selenothiophene, were applied in block copolymers. In this regard, Palermo and McNeil investigated the influence of the copolymer structure, *i.e.* random, block or gradient, on polythiophene-*b*-polyselenophene (entry 13).[221] In a similar approach the group of Seferos obtained thermostable fiber-like nanostructures for solar cell applications from polythiophene-*b*-polyselenophene block copolymers.[220] Other blocks which were combined with polythiophene leading to donor–donor polymers are poly(*p*-phenylene) (entry 14)[192] or polyfluorene (entry 16).[199] Interestingly, Verswyvel *et al.* prepared triblock terpolymers in all possible orders from fluorene, thiophene and selenophene monomers which were activated with zinc using a palladium catalyst (entry 16).[199] Surprisingly, the authors observed an unusual independence of the monomer sequence in contrast to common sequential monomer addition protocols (*vide supra*). Nevertheless, the removal of residual homopolymer by extraction was hindered in these examples.

Along with donor–donor, also donor–acceptor block copolymers were prepared by KCT polymerization or related procedures. A first example was presented by Seferos' group (entry 22).[214] The block copolymer was synthesized utilizing thiophene and benzotriazole as monomers and a Ni(II) diimine complex as a catalyst. The controlled polymerization of electron-rich as well as electron-deficient compounds is attributed to strong association of the catalyst.[214] In a similar approach, Todd *et al.* synthesized P3HT-*b*-PFBTzHT(=poly(3-hexylthiophene)-block-poly(5,6-difluorobenzotriazole-alt-4-hexylthiophene) by sequential monomer addition.[212] A further example

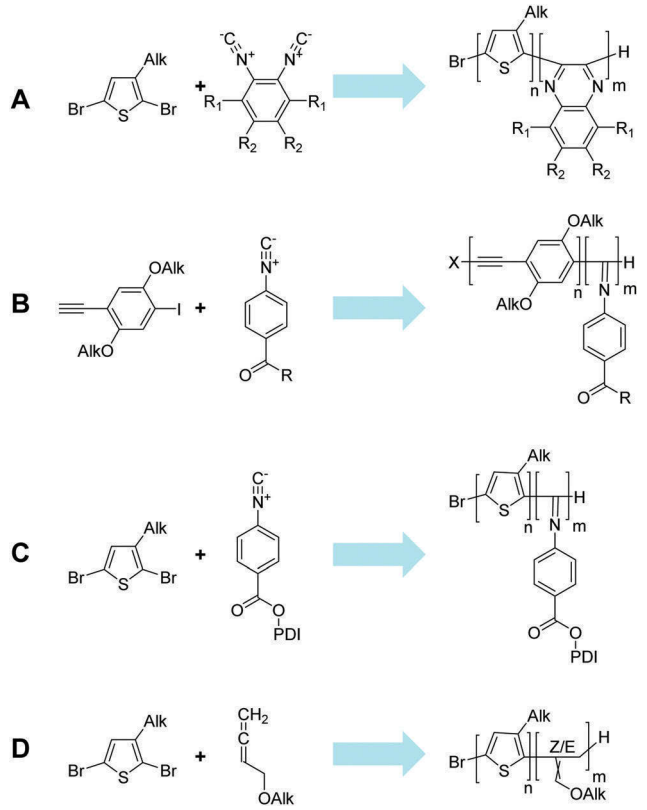

Scheme 12 Schematic representation of monomers and respective block copolymers prepared with one initiator system but following mechanistically distinct procedures.[224–229]

discussing donor–acceptor copolymers is reported by Tkachov *et al.* (entry 26).[222] Due to the much faster polymerization of a fluorenic monomer than a bis(thiopenyl)naphthalene diimide derivative, the authors were able to obtain block-like copolymers in a one pot procedure under simultaneous addition of the two monomers.[222] The dibrominated monomers were activated with zinc or zinc compounds and palladium was used as a metal catalyst.[222] Although the reported polymerization did not yield a well-defined block copolymer (broad dispersity), the approach represents an important step towards a facile and rapid protocol for the preparation of conjugated donor–acceptor block copolymers.[222]

Besides the sequential monomer addition method, block copolymers may also be synthesized from separately prepared homopolymers and a final Kumada coupling step. Following this approach Ananthakrishnan *et al.* reported the synthesis of poly(3-hexylthiophene)-*block*-oligo(anthracene-9,10-diyl).[223]

Modern synthesis protocols further enable the sequential block copolymerization of monomers by mechanistically distinct procedures in a living fashion.[224–227] Remarkable examples include donor–acceptor copolymers consisting of P3HT[224,225,228,229] and PPE[226] in one block and isocyanide (Scheme 12A–C)[224,226,227,229] or allene (Scheme 12D)[225,228] derivatives as well as a range of vinyl monomers[225] in the other block. The catalytic systems are based on nickel[224,225,228,229] or palladium[226] and establish novel facile pathways to interesting polymer classes. The obtained polymers featured a narrow molar mass distribution (1.1 to 1.4), controllable molar masses between 4000 to 31 000 g mol^{-1} and yields up to 60–90%.

3.4. Block copolymers by coupling of polymerization techniques

The coupling of different polymerization techniques represents a very valuable tool to synthesize block copolymers of intensively studied electrochemically active monomer units which are not compatible with just one polymerization process. As stated in the beginning of this section, mainly two strategies are applied to couple polymerization techniques. Either a bi- or multifunctional initiator is used and the block copolymer is step-wise synthesized or two independently prepared telechelic polymer chains are coupled together by an efficient linking reaction, most commonly the CuAAC "Click" reaction. Noteworthily, the reviewed work in the following section concentrates on block copolymers in which predominantly at least one block consists of a conjugated polymer.

3.4.1 Coupling of conjugated polymers with CRP. The covalent connection of conjugated polymers with non-conjugated polymers, which were prepared by CRP, is either achieved by the coupling of telechelic blocks or, more commonly, by the utilization of macroinitiators and macro-RAFT agents. An overview of the respective reported linking reactions and initiators is given in Scheme 13 and Table 8. In the case of coupling of well-defined telechelic homopolymers, the molar mass and the dispersity can be tuned by the used individual blocks.[230,231] Reported yields are in the range of 50 to 80% and the removal of residual homopolymers is often achieved by extraction to exploit solubility differences or by preparative SEC.

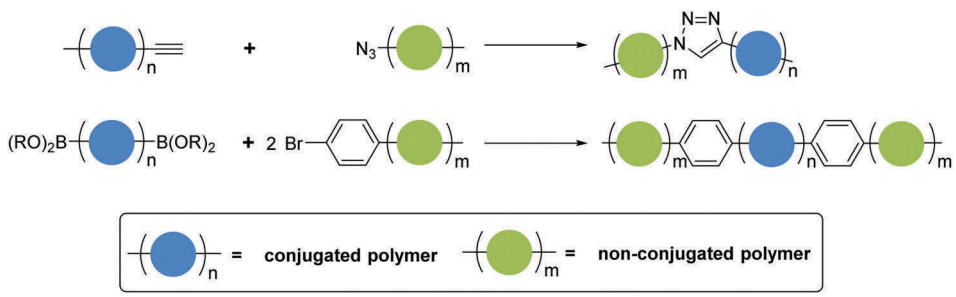

Scheme 13 Schematic representation of reported coupling reactions involving telechelic conjugated polymers and non-conjugated polymers prepared by CRP.[232–237]

Table 8 Schematic representation of macroinitiators and macro-RAFT agents for CRP decorated with conjugated polymers

Entry	Structure	CRP	Ini. yield[a] [%]	Efficiency/polymer yield[b] [%]	Ref.	Entry	Structure	CRP	Ini. yield[a] [%]	Efficiency/polymer yield[b] [%]	Ref.
1	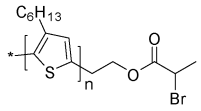	ATRP	n.d.	47–57	250	7	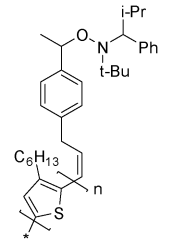	NMP	96	42	44
2	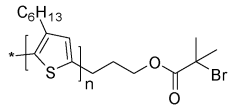	ATRP	n.d.	76	240	8	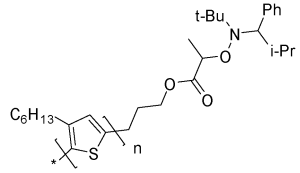	NMP	n.d.	n.d.	243
3	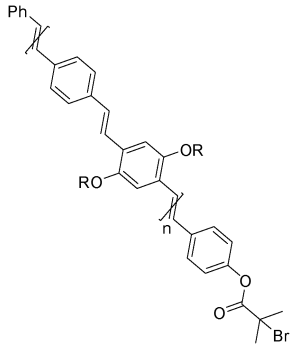	ATRP	83–90	Quant.	90	9	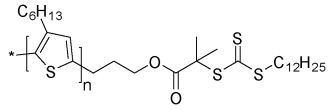	RAFT	90–95	n.d.	239
4	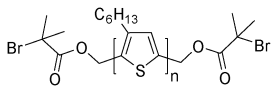	ATRP	n.d.	n.d.	241	10	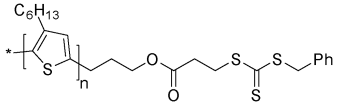	RAFT	n.d.	n.d.	242 and 243
5	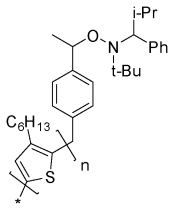	NMP	84	30–50	244	11	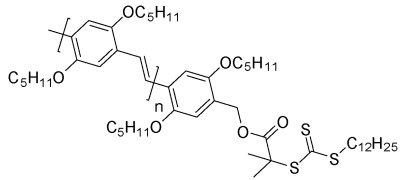	RAFT	Quant.	25	251 and 252

Table 8 (*continued*)

Entry	Structure	CRP	Ini. yield[a] [%]	Efficiency/polymer yield[b] [%]	Ref.
6	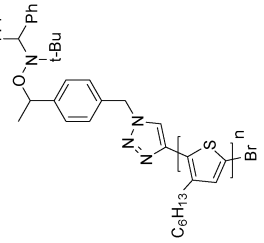	NMP	Quant.	Not quant.	238

[a] Yield of the macroinitiator (when given in the publication). [b] Initiation efficiency of the macroinitiator or yield of the isolated block copolymer.

Entry	Structure	CRP	Ini. yield[a] [%]	Efficiency/polymer yield[b] [%]	Ref.

P3HT is the most often used conjugated polymer which is combined with hydrophilic,[232,233,238,239] thermoresponsive[232] or manipulable liquid crystalline[240,241] monomers as well as units capable of metal coordination[238,239,242] to prepare block copolymers. In this regard, Kumari *et al.* synthesized P3HT-*b*-PNIPAM by the CuAAC reaction in good yields (60 to 75%) and formed thermoresponsive micelles which revealed LCST behavior in water.[232] A further example is introduced by the group of Zhao by utilizing KCTP and ATRP to design block copolymers in which the surface- and photoinduced orientation of azobenzene mesogens was applied in order to tune the self-assembly behavior.[240] The incorporation of P4VP in block copolymers containing P3HT is also suitable to induce microphase separation.[238] Moreover, acetylene terminated P3HT was coupled with bifunctional PMA by the CuAAC reaction leading to thermoplastic elastomers which may be useful for the production of stretchable electronics.[235] Besides these examples utilizing telechelic homopolymers for the coupling to block copolymers, also the application of P3HT based macroinitiators for NMP or macro-RAFT agents for RAFT polymerization has been reported and was utilized for the fabrication of nanofibrils consisting of P3HT-*b*-PS or P3HT-*b*-PIP block copolymers.[243]

A large number of donor–acceptor copolymers consist of a conjugated electron-rich polymer, *e.g.* P3HT, and non-conjugated acceptors, *e.g.* fullerenes[40,43,234] or liquid crystalline perylene bisimide[244–249] units. In this regard, a common synthetic approach is the coupling of P3HT with a NMP initiator either by *in situ* end capping[43,244,245,247,248] or postpolymerization modification[44,246,249] leading to a macroinitiator. Naturally, the transformation of the polymer into the macroinitiator is not necessarily quantitative and the denoted yields range from approximately 80%[244] to quantitative conversions.[44,238] Nevertheless, an incomplete functionalization is not problematic as a purification step is necessary anyway after the synthesis of the second block. The systems involving P3HT and perylene bisimide revealed a tunable microphase separation and self-assembly behavior as acrylate based perylene bisimide monomers with a long and flexible side chain are liquid crystalline.[244–249]

As fullerenes are sensitive towards radicals, direct incorporation with appropriate substituted monomers is not possible, so a monomer with a reactive functional group is primarily incorporated into the block copolymers and the fullerene is attached in a postpolymerization modification reaction (*vide infra*).[40,43,234] In analogy, Yao *et al.* applied the ATRP procedure for the coupling of P3HT with polymers containing reactive side groups. Subsequently side chain decoration with a perylene bisimide was achieved.[236]

Furthermore, the preparation of poly(3-hexylthiophene)-*b*-poly(vinylphenyl oxadiazole) by a combination of Kumada CTP and ATRP was reported.[250]

The coupling of other conjugated polymers besides P3HT with a second block prepared by CRP is much less studied and only very few literature examples are described.[252] However, an outstanding example is presented by the group of Zentel.[252] The authors synthesized PPV by Siegrist polycondensation and used a comprehensive postpolymerization approach to transform the

polymer into a macro-RAFT agent, which was used to polymerize pentafluorophenyl acrylate. This active ester was subsequently substituted with dopamine as an anchor group for the decoration of TiO_2 nanoparticles to form hybrid materials.[252] The Suzuki coupling of bi-endfunctional polyfluorene with fullerene-substituted PS derivatives leading to ABA triblock copolymers is described by Bicciocchi *et al.*[237]

PPVs which were prepared by ROMP can also be decorated with reactive end groups serving as initiators for CRP. For instance, Lidster *et al.* applied this approach to prepare monotelechelic PPVs by ROMP and the corresponding block copolymers with PMMA by ATRP using a PPV macroinitiator.[90]

3.4.2 Coupling reactions involving anionic polymerization techniques. Basically, two routes were applied to combine anionic polymerization with other polymerization techniques leading to electrochemically active polymers. Either the reactivity of the propagating anion is *in situ* exploited by end capping with a reactive reagent[253–255] (Scheme 14) or telechelic end functionalized polymers, *e.g.* PEG-OH derivatives, are applied in a post-polymerization approach to be linked to a second block[256–262] or are utilized as a macroinitiator.[263–265] In particular, the preparation of PPV by anionic polymerization using the so-called sulfinyl precursor approach is of high interest from a synthetic point of view.[263] Cosemans *et al.* presented the preparation of block copolymers using a bifunctional initiator suitable for SET-LRP (single electron transfer living radical polymerization) and anionic polymerization. This approach yielded defined block copolymers in contrast to their previous work applying the sequential monomer addition technique.[179] The obtained PPV precursor polymer was readily transformed into PPV by elimination at elevated temperatures.[263]

An elegant *in situ* endcapping approach is presented by Sary *et al.*[253,254] The authors prepared P4VP by anionic polymerization and utilized aldehyde terminated PPV[254] or P3HT[253] as end capping agents leading to block copolymers capable of self-assembly processes (Scheme 14A and B). Moreover, the P4VP block experiences weak supramolecular interactions with PCBM and assists the separation of donor and acceptor units.[253] Furthermore, alkyl halides represent valuable end capping reagents. In this regard the preparation of AB and ABA rod-coil block copolymers consisting of alkyl halide terminated P3HT and phenylethynyl styrene derivatives is reported (Scheme 14C).[266] Noteworthily, also 1,1-diphenylethylene derivatives can be used as end capping reagents (Scheme 14D).

A very stimulating example for the combination of KCTP and anionic polymerization is provided by the group of Coulembier.[267] The authors individually prepared alkyne terminated P3HT by KCTP polymerization and azide terminated polyphthalaldehyde by anionic polymerization and covalently linked the units by the CuAAC reaction. These block copolymers were isolated in good yields (>80%), featured low dispersities ($Đ$ = 1.26 to 1.34) and molar masses between 9000 and 17 000 g mol^{-1}, and could be assembled into fibrillary nanostructures and upon thermal treatment the thermo-sacrificial polyphthalaldehyde block could be removed leading to nanoporous P3HT (Scheme 15).[267]

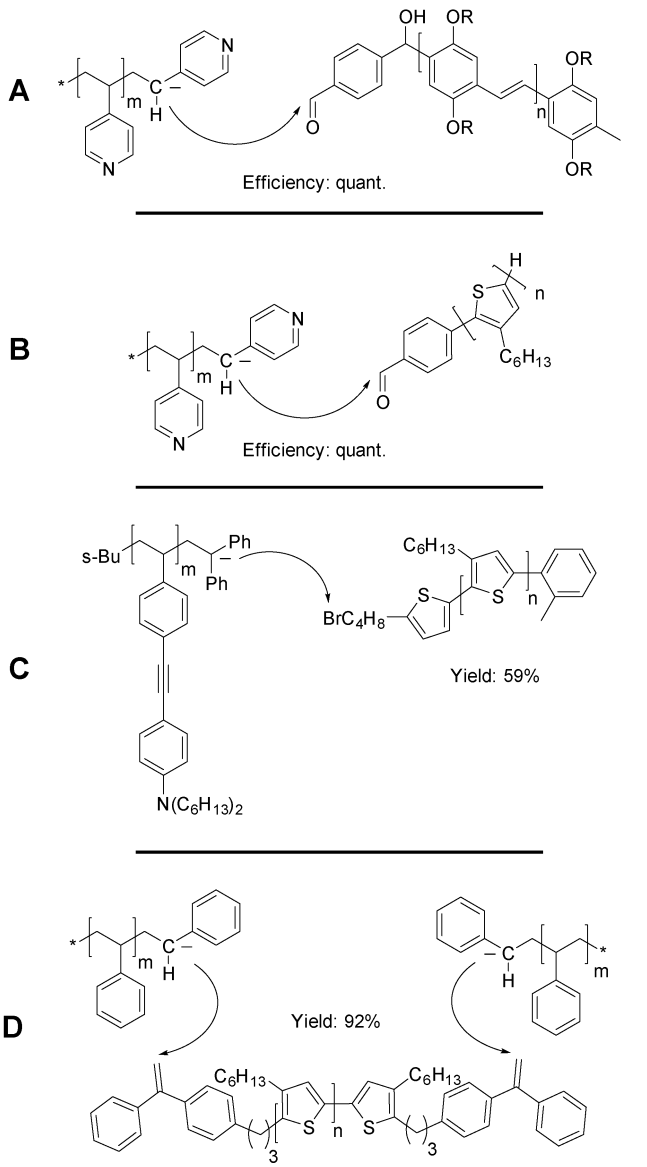

Scheme 14 Schematic representation of reported examples of *in situ* end capping of anionic polymers with conjugated polymers, and reported yields and coupling efficiencies.[253–255,266]

3.4.3 Combination of metal catalyzed cross coupling polymerization techniques. Fully conjugated block copolymers are commonly prepared either by sequential monomer addition techniques (*vide supra*), by the coupling of telechelic blocks with complementary end groups or by the application of macroinitiators. In particular, the last two approaches broaden the scope of accessible polymers in comparison to sequential monomer addition techniques. Noteworthily, P3HT is most commonly used as one of the building blocks due to its established synthetic procedures and beneficial properties.

The functional groups, which are necessary to covalently link the individual blocks, can be introduced by functional initiators. In this regard, Smeets *et al.* synthesized polythiophene block copolymers using KCTP and functionalized Ni(II) catalysts

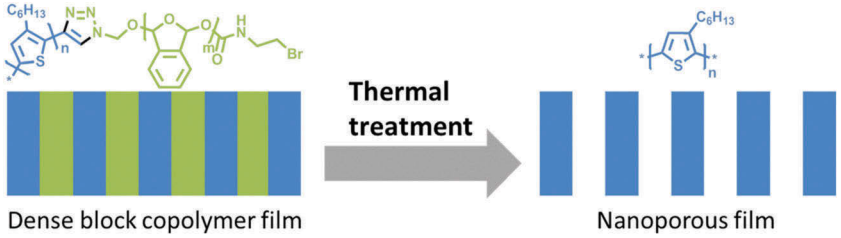

Scheme 15 Preparation of nanoporous films by utilization of thermo-sacrificial segments.[267]

enabling the introduction of azide or acetylene end groups for a connection utilizing the CuAAC reaction.[102] In addition, also the Suzuki–Miyaura coupling polymerization applying functional initiators is established and was used to decorate the chain terminus of polyfluorene with substituents enabling the construction of block copolymers by coupling of individual chains.[268] Moreover, the bromine decorated chain terminus of P3HT prepared by KCTP is often applied as a starting or end capping unit for subsequent cross coupling reactions, *e.g.* Suzuki polycondensation.[269–272] In general, two synthetic approaches to prepare the second block can be devised either relying on the polymerization of AA/BB-type (Scheme 16) or AB-type monomers (Scheme 17) (A = Br, B = $B(OR)_2$, SnR_3, ZnCl, Br). The polymerization of two complementary monomers (AA/BB-type) is widely utilized to prepare alternating copolymers, but the obtained polymers generally feature a broader molar mass distribution compared to AB-type systems. An overview of reported examples for both approaches is provided in Tables 9 and 10.

The combination of KCTP and Stille coupling polymerization is commonly used in particular for the preparation of donor–acceptor copolymers, as it is very challenging to prepare electron-deficient polymers by classical KCTP protocols. In contrast, Stille coupling enables facile preparation of the electron acceptor block as successfully shown in the synthesis of NDI (=naphthalene diimide) containing block copolymers with an acceptable dispersity.[275–277] In this regard, the P3HT[277] as well as the NDI[275,276] containing block were applied as macroinitiators. Additionally, other acceptor building blocks, *e.g.* PCDTBT, were utilized in combination with P3HT as a macroinitiator.[273,274,278,279]

For completion, it is stated that the combination of KCTP with Yamamoto[280–282] or Negishi[283] coupling is also reported for the preparation of AB or ABA donor–acceptor polymers. In particular for Yamamoto coupling, the control of the polymerization process is low and the formation of byproducts, *e.g.* homopolymer, in larger amounts is reported (entry 4, Table 10).

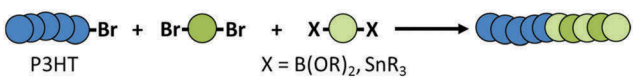

Scheme 16 Preparation of block copolymers utilizing AA/BB-type monomers for the second block in combination with P3HT as the first block.

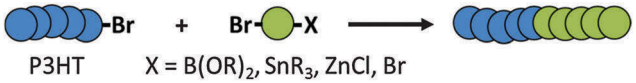

Scheme 17 Preparation of block copolymers utilizing AB-type monomers for the second block in combination with P3HT as the first block.

3.4.4 Other combined techniques. Although fullerenes are usually sensitive towards typical polymerization conditions, *e.g.* anions, cations, strong bases or radicals, examples for multiblock copolymers synthesized by step-growth polymerization techniques are reported. In this regard, successful incorporation relies on the mild reaction conditions of the nucleophilic substitution[284] or imine condensation processes.[285]

The combination of KCTP polymerization and ROMP of cyclooctene with subsequent hydrogenation leading to P3HT-*b*-PE block copolymers is described by Radano *et al.*[286] The resulting tough, semiconducting crystalline–crystalline block copolymers may be useful for the fabrication of flexible electronic components.[287] Last but not least, hydroxyl terminated P3HT is also capable of initiating the ring-opening polymerization of lactide.[288]

4. Graft and comb polymers

Graft and comb polymers consist of a linear polymer backbone and covalently connected side chains of one or more different species.[27,289,290] Thus, these copolymers allow the incorporation of functional units besides the backbone to optimize the properties and functions of polymer architectures, *e.g.* to improve the solubility or to attach additional antenna dyes in light harvesting systems. After introduction of the basic principles to construct graft polymers, the following section presents concrete examples to illustrate the possible scope of photo- and electrochemically active graft copolymers.

In general, the preparation of graft copolymers is possible by three construction principles: grafting onto, grafting from and grafting through (Scheme 18).[289–291] The grafting onto approach is based on the reaction of functional units in the backbone of the main chain polymer A with the end groups of the telechelic side chain polymer B. As the main chain polymer and the side chain units are synthesized separately, both blocks can be prepared by appropriate methods and the molar mass and dispersity of the parts can be controlled. As a limitation, the realization of a high grafting density is restricted by steric hindrance and additionally requires a high yield coupling reaction, *e.g.* the nitroxide radical coupling reaction[292] or the CuAAC reaction.[289,290] Noteworthily, the separation of unreacted side chains and the graft copolymer can be challenging.

Table 9 Schematic representation of examples of AA/BB-type monomers for the synthesis of block copolymers in combination with P3HT as the first block

Entry	Br–●–Br	X–●–X	Coupling	M_n[a] [kg mol^{-1}] $Đ$	Yield [%]	Ref.
1	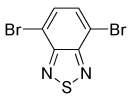	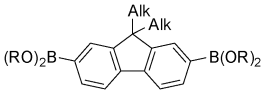	Suzuki	19–168 1.43–3.61	80	269 and 270
2	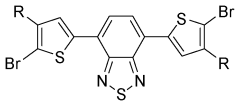	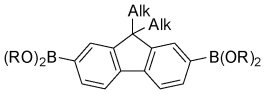	Suzuki	13–66 1.14–1.52	54	271–273
3	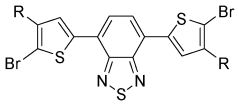	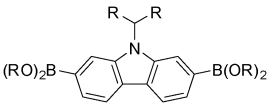	Suzuki	16–36 1.51–2.51	89–94	274
4	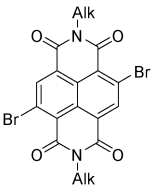	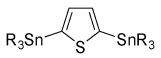	Stille	26–47 1.15–1.86	75–93	275–277
5	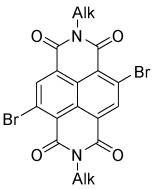	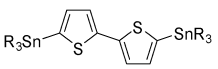	Stille	16 1.24	76	276
6	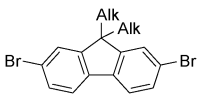	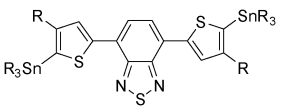	Stille	20 1.37	70	273
7	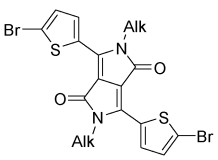	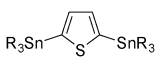	Stille	60–134 1.58–1.91	85–97	278

[a] Based on SEC data.

The grafting from strategy grows the side chains directly from the initiating units of the polymer backbone. The initiating group either originates from the monomer of the main chain polymer or is introduced in the main chain by a polymer analogous reaction. Major advantages of the approach are the facile purification due to the absence of unreacted macromolecules (*vide supra*) and the decrease of the steric effect compared to the grafting onto and grafting through approaches.[289]

The grafting through strategy involves the polymerization of macromonomers with a polymerizable end group.[289,290] Technically, this technique also includes the preparation of homopolymers featuring large solubilizing groups in the side chains, *e.g.* long alkyl or ethylene glycol chains. Advantageously, the molar mass of the later side chains can be well-defined as the macromonomer is prepared separately. The grafting density that can be reached is 100% but steric hindrance can influence the polymerization and more importantly due to an incomplete conversion of the macromonomers a challenging purification step can be necessary.

The hydrodynamic volume of graft polymers differs from linear polymers, so the SEC molar masses and dispersities are only of very limited use for comparison and will not be reported. Instead grafting densities and yields are given in the tables.

4.1. Conjugated graft copolymers with electrochemically active side chains

The side chain functionalization of conjugated polymers represents a promising approach to introduce a further functionality, *e.g.* electron acceptors[293,295,297] or donors,[294,296,298] in the respective polymer. An overview of reported graft copolymers containing acceptor or donor side chains is displayed in Table 11 including reported grafting densities and yields. As it can be seen, the grafting densities and yields for "grafting onto" approaches are limited.

Besides polymer based side chains, also the attachment of discrete electrochemically active units was reported (Table 11, entries 1 to 4). In this regard, a donor–acceptor assembly based on a grafting through approach is reported by Marder's

Table 10 Schematic representation of examples of AB-type monomers for the synthesis of block copolymers in combination with P3HT as the first block

Entry	Br-●-X	Coupling	M_n[a] [kg mol^{-1}] $Đ$	Yield [%]	Ref.
1	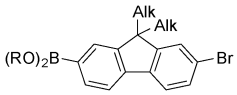	Suzuki	17 1.31	n.d.	270
2	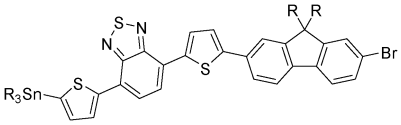	Stille	15 1.30	33[b]	279
3	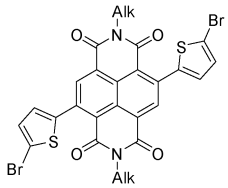	Yamamoto	22–26 1.28–1.60	85[c]	281 and 282
4	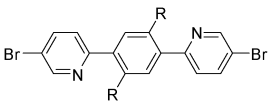	Yamamoto	26–30 1.55–2.11	96[c]	280
5	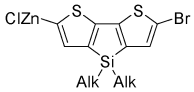	Negishi	8–12 1.30–1.5	20	283

[a] Based on SEC data. [b] Mixture of block and homopolymers. [c] A–B–A triblock copolymer + varying amounts of homopolymers and diblock copolymers.

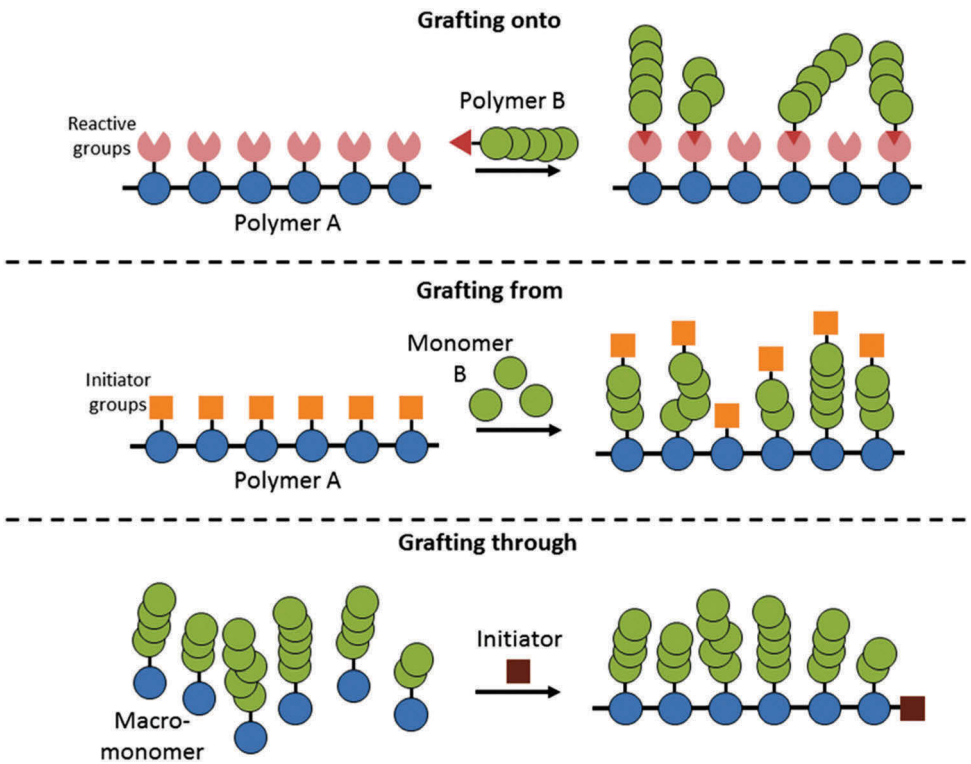

Scheme 18 Synthetic methods for the synthesis of graft copolymers.

group (entry 4).[297] The compounds, which were prepared by copolymerization of perylene diimide functionalized dibromocarbazoles and fluorene derivatives, revealed long-lived charge separated states. Polythiophenes are also applied

Table 11 Schematic representation of graft copolymers containing a conjugated backbone and conjugated electron acceptor or donor side chains

Entry	Compound	Method	Grafting efficiency[a] [%]	Yield [%]	Ref.	Entry	Compound	Method	Grafting efficiency[a] [%]	Yield [%]	Ref.
1	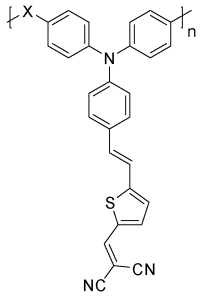	Through, polymer anal. reaction	100[b]	83–91	293	5	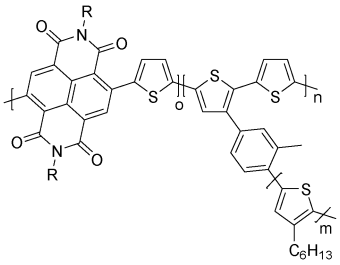	From	n.d.	87–95	294
2	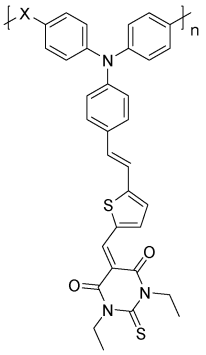	Through, polymer anal. reaction	100[b]	91–95	293	6	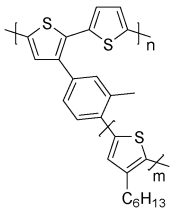	From	n.d.	88	294
3	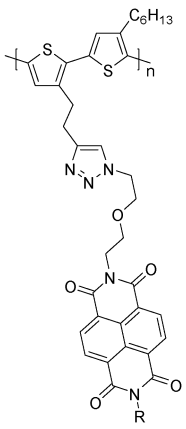	Onto	100[b]	57	295	7	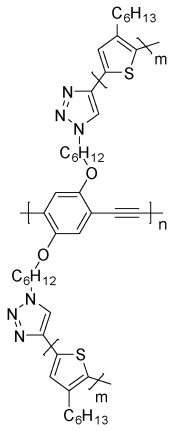	Onto	10–50[b]	13–20	296
4	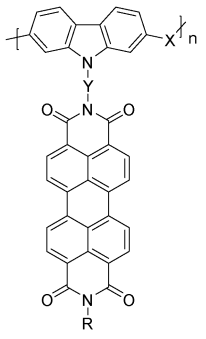	Through	100	80–83	297	8	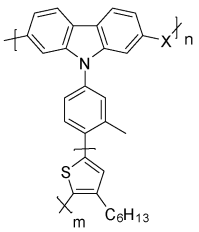	Through	100	69–83	298

[a] Amount of functionalized units on the backbone. [b] Determined by ^{1}H NMR data.

as side chains in graft polymers. The respective materials can be prepared by any of the introduced methods. A grafting from approach is reported by Higashihara's group (entry 5).[294] The authors prepared various conjugated polymers containing 3-(4′-chloro-3′-tolyl)thiophene units by Stille reaction and subsequently converted the materials into macroinitiators by addition of nickel complexes. These macroinitiators are suitable to graft polythiophene side chains from the polymer backbone (entry 6).

Telechelic polythiophenes can also be grafted onto suitable polymers, *e.g.* PPE (entry 7).[296] In this regard the already mentioned CuAAC reaction represents a very powerful tool for functionalization even though a grafting density of 100% is not reached. Moreover, grafting through of P3HT based macromonomers is possible (entry 8).[298] For this purpose a functionalized Nickel catalyst is used (*vide supra*) to initiate the polymerization of P3HT and the so obtained telechelic macromonomer is applied to construct the polymer backbone.

4.2. Graft copolymers containing a saturated main chain

Graft copolymers of conjugated and non-electrochemically active units either contain a non-conjugated backbone or non-conjugated side chains. In the first case, the backbone often fulfills a structural function, whereas in the case of modified side chains the physical properties can be modified, *e.g.* the solubility. The first scenario will be discussed in the following section and relevant examples are depicted in Table 12.

Polystyrene displays a readily available and easily modifiable polymer backbone, which can be used in combination with P3HT for grafting from (Table 12, entries 2 and 3)[300,302] and onto approaches (entry 4 and 7).[304,309] The resulting graft copolymers are characterized by a good solubility[304] and the ability to form stable films on surfaces.[300,302] Besides, PS is also utilized in donor and/or acceptor graft polymers, in which the active units are grafted onto the backbone by hydrosilylation (entry 5)[306] or CuAAC reactions (entry 6).[308] Another suitable polymer backbone is polynorbonene which can be prepared by the ROMP process in high yields from telechelic P3HT macromonomers (entries 9, 13 and 15).[299,307,310] The obtained bottlebrush architecture resulted in an increased π–π interaction and, therefore, a strong aggregation of the P3HT side chains.[310] Surface immobilized polynorbonene was used in a grafting from strategy for the step-by-step construction of ordered heterojunctions (entry 11).[303] Moreover, after hydrogenation of the backbone an increased electric field breakdown strength was observed, making the materials promising candidates for dielectrics.[307] Interestingly, the group of Nishide prepared radical containing graft copolymers by a combination of anionic polymerization and ROMP (entry 16).[312] In the first step, the anionic polymerization of a TEMPO-based monomer yielded a norbornene-substituted macromonomer, which was subsequently polymerized with a Grubbs catalyst. Due to the functional group tolerance, high yields (>94% for each step) and high radical concentrations (0.95 radicals per monomer unit) were reached.

The anionic polymerization of glycidyl derivatives and the subsequent grafting of active units onto the main chain represent an additional method for the construction of electrochemically active graft polymers (entry 10).[301] Interestingly, poly(vinyl alcohol) (PVA) can be modified with TEMPOL leading to a macroinitiator for NMP with vinyl naphthalene by a grafting from approach (entry 12).[305] As the hydroxyl groups of the PVA stay intact during polymerization, a water soluble graft copolymer is obtained despite the hydrophobicity of the side chains. However, the grafting density is low. Last but not least, an example featuring polyacrylamide as the main chain will be shortly presented (entry 8). The group of Meijer reported the grafting of porphyrins onto a modified poly(pentafluorophenyl acrylate) by amidation leading to single-chain polymeric nanoparticles. These particles act as photosensitizers and can produce singlet oxygen.[311]

The before mentioned acyclic diene metathesis polymerization (see Section "Redox-active and conjugated polymers by ring opening metathesis polymerization") was also applied to prepare perylene bisimide-substituted polyethylene (entry 1).[94]

4.3. Tuning the physical properties with the side chains

The side chain functionalization or manipulation of conjugated polymers represents an efficient way to tune *inter alia* the self-assembly behavior,[251,329] solubility,[109] processability[330,333] or energy levels of polymers.[328] An overview of the modified polymers is provided in Table 13. All reported polymers feature very high grafting efficiencies but the isolated yield is commonly lower due to losses upon purification.

The first reported method enabling the side chain modification of P3HT applied 2,5-dibromo-3-(ω-bromoalkyl)thiophene as the monomer.[315,317,334] Surprisingly, the halogen substituted side chain was not affected by the Grignard reagents and was further functionalized by nucleophilic substitution, *e.g.* with glucose derivatives[315] (Table 13, entry 3) or units capable of hydrogen bonding (entries 4 and 26).[317] Furthermore, tuning of the solubility was accomplished by varying the side chains. As a consequence, a good solubility in organic solvents can be readily achieved by the introduction of long solubilizing groups, *e.g.* polyisobutylene (entry 18).[316] In contrast, the introduction of polar side groups results in a good solubility in polar solvents, *e.g.* water or alcohol (entries 1 and 30).[109,331,332,335] The influence of linear or branched polyether side chains on the assembly of PPV-based block copolymers was investigated by Zentel's group (entry 14).[251] The applied grafting onto approach allowed modular construction of the compounds, *i.e.* various side chains were attached on the same starting copolymer by amidation. On the basis of TEM images, different structures were observed, depending on the side chains. Wittmeyer *et al.* pursued a similar approach as they prepared water-soluble PPPs with ethylene oxide based side chains by a grafting through strategy (entries 5 and 6).[319] An additional increase of the polarity of the branched chains was accomplished by the incorporation of ionic groups leading to a class of polyelectrolytes (entries 2, 7, 15, 16, 19 and 20).[131,313,318,321] The respective ionic groups result from the modification of ω-bromoalkyl side chains, *i.e.* in general by quaternization with amines.[131,313,321] Besides the good solubility of these materials and, thus, an improved processability, *e.g.* in water as an environmentally friendly solvent,[313] also surfactochromic properties[131] and a high charge density can be achieved.[318] Interestingly, the group of Chen reported various conjugated polymers with crown ether decorated side chains for the complexation of potassium ions (entries 12, 13, 22, 24 and 25).[1–3] The polymers were applied as electron transport layers in polymer solar cells and resulted in an increased power conversion efficiency. This improvement is *inter alia* based on an optical interference effect, the enhanced

Table 12 Schematic representation of graft copolymers containing a saturated backbone and electro- or photoactive functional side chains

Entry	Compound	Method	Grafting efficiency[a] [%]	Yield [%]	Ref.	Entry	Compound	Method	Grafting efficiency[a] [%]	Yield [%]	Ref.
1	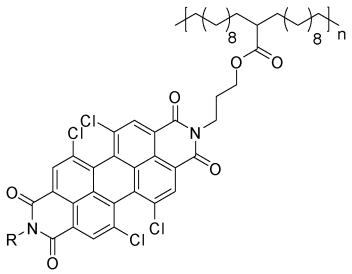	Through	100	89–99	94	9	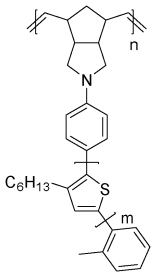	Through	100	n.d.[c]	299
2	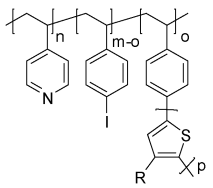	From	n.d.	n.d.[b]	300	10	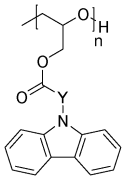	Onto	100	72	301
3	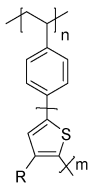	From	n.d.	n.d.[b]	302	11	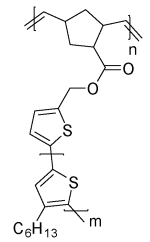	From	n.d.	n.d.[b]	303
4	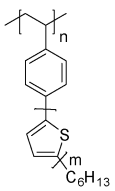	Onto	96	n.d.	304	12	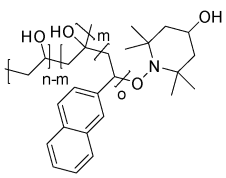	From	4	n.d.	305
5	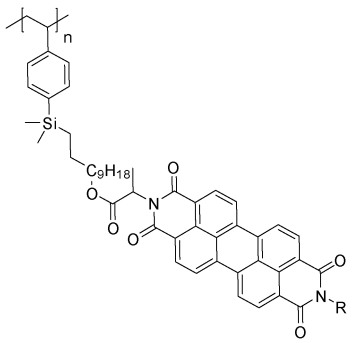	Onto	100	89	306	13	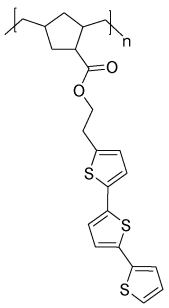	Through	100	99	307

Table 12 (*continued*)

Entry	Compound	Method	Grafting efficiency[a] [%]	Yield [%]	Ref.	Entry	Compound	Method	Grafting efficiency[a] [%]	Yield [%]	Ref.
6	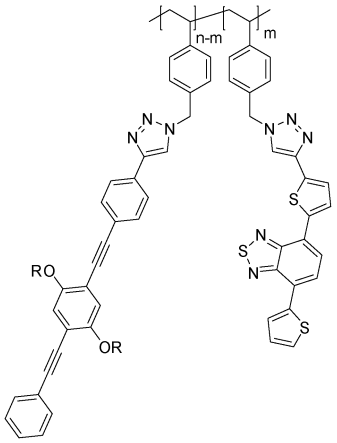	Onto	100	86	308	14	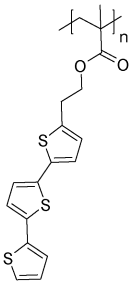	Through	100	n.d.	307
7	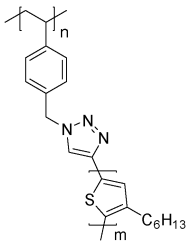	Onto	97–99	77–85	309	15	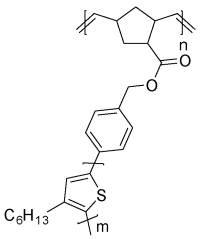	Through	100	86–98	310
8	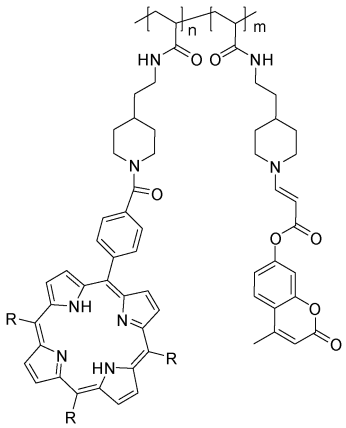	Onto	n.d.	n.d.	311	16	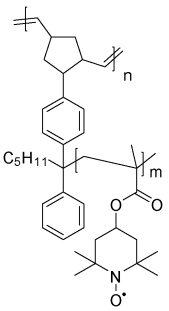	Through	100	99	312

[a] Amount of functionalized units on the backbone. [b] Immobilized on the substrate. [c] Yield not given, but purity between 78–92%.

electron conduction and the blocking of electron–hole combination at the interface with the cathode.[1,2]

Moreover, adequate side chains can be utilized for crosslinking reactions to enhance the mechanical properties in polymer films (entry 18).[316] For this purpose, H-bond crosslinkable units,[316] UV-crosslinkable moieties, *e.g.* azides (entry 8)[322] or 4-hydroxy-2,5-dimethylbenzophenone/maleimide (entry 9),[324] or thermal crosslinkable hydroxyl (entry 21)[320] moieties, are introduced in the monomer units, *e.g.* in the alkyl side chain of thiophene. After film formation, the polymer is then crosslinked by the external stimuli. Alternatively, the crosslinking can be achieved by the addition of a multidentate crosslinker, which reacts with functional groups of the polymer to form a network, *e.g.* by the thiol–ene "Click" reaction (entry 17)[314] or by the reaction of diisocyanates with hydroxyl or amine groups (entries 10 and 23).[323]

The side chain decoration of polyfluorene with P2VP represents a suitable approach to control the morphology in ordered nanostructures similar to block copolymers as shown by Lee *et al.* (entry 11).[325] The variation of the volume fractions of the P2VP side chain led to well-ordered cylinders or lamellae.

4.4. Graft copolymers containing metal complexes

Metal complexes are an important class of photosensitizers and catalysts for light harvesting materials. Their incorporation into polymer side chains enables structural control to construct

Table 13 Schematic representation of side chain modified conjugated polymers to tune physical properties

Entry	Compound	Method	Grafting efficiency[a] [%]	Yield [%]	Ref.	Entry	Compound	Method	Grafting efficiency[a] [%]	Yield [%]	Ref.
1	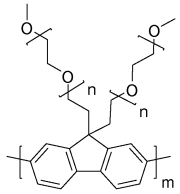	Through	100	53	109	16	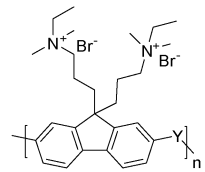	Through, polymer anal. reaction	100	85	313
2	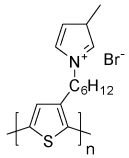	Through, polymer anal. reaction	n.d.	80	131	17	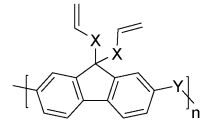	Through	100	84–97	314
3	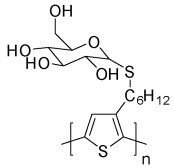	Through, polymer anal. reaction	100	84–90	315	18	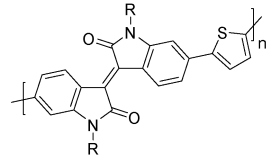 R = poly(isobutylene) **or** 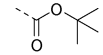	Through	100	n.d.	316
4	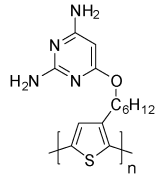	Through, polymer anal. reaction	100	n.d.	317	19	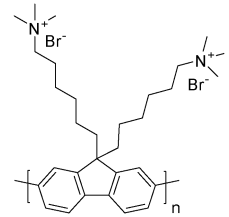	Through, polymer anal. reaction	90	n.d.	318
5	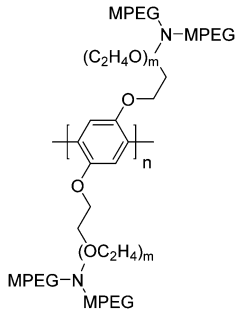	Through	100	68–93	319	20	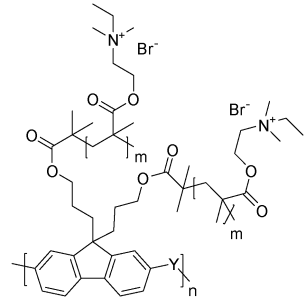	From, polymer anal. reaction	95	n.d.	318

Table 13 (*continued*)

Entry	Compound	Method	Grafting efficiency[a] [%]	Yield [%]	Ref.	Entry	Compound	Method	Grafting efficiency[a] [%]	Yield [%]	Ref.
6	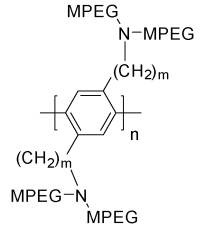	Through	100	32–85	319	21	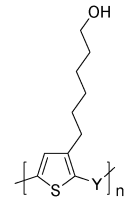	Through	100	63	320
7	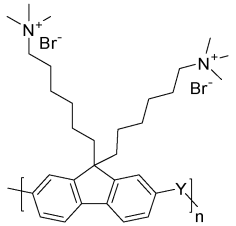	Through, polymer anal. reaction	n.d.	n.d.	321	22	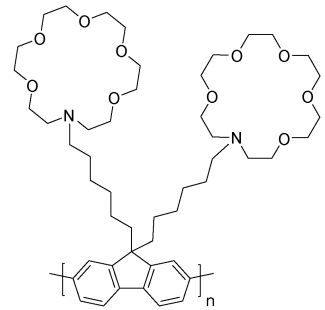	Through	100	62	1 and 3
8	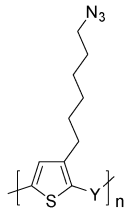	Through	100	43–93	322	23	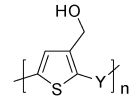	Through, polymer anal. reaction	100	91	323
9	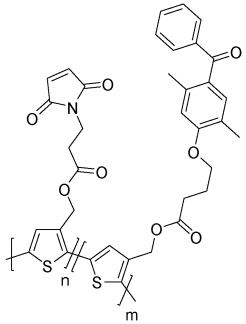	Onto	>90	n.d.	324	24	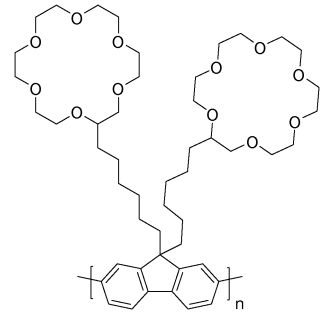	Through	100	63	1

Table 13 (*continued*)

Entry	Compound	Method	Grafting efficiency[a] [%]	Yield [%]	Ref.	Entry	Compound	Method	Grafting efficiency[a] [%]	Yield [%]	Ref.
10	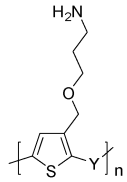	Through, polymer anal. reaction	100	78	323	25	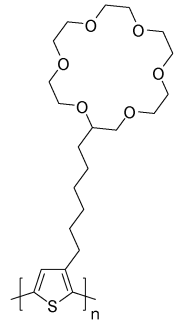	Through	100	43	1
11	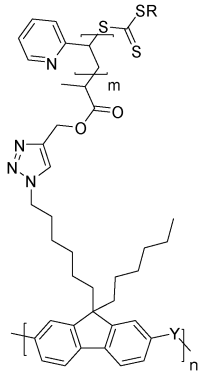	Onto	100	n.d.	325	26	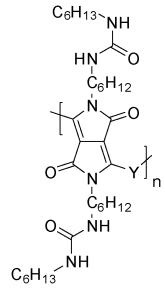	Through	100	82	326
12	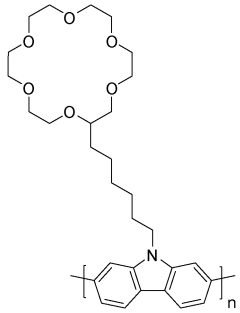	Through	100	57	1	27	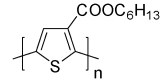	Through	100	20–69	327

Table 13 (*continued*)

Entry	Compound	Method	Grafting efficiency[a] [%]	Yield [%]	Ref.	Entry	Compound	Method	Grafting efficiency[a] [%]	Yield [%]	Ref.
13	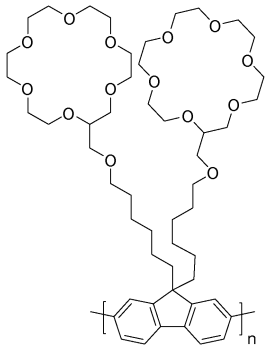	Through	100	63	2	28	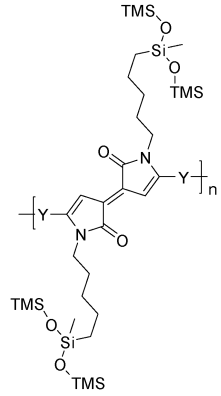	Through	100	83–91	328
14	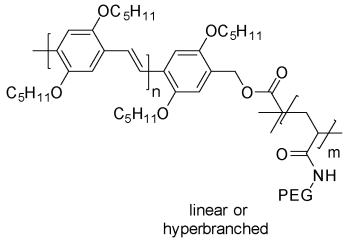	Onto	100	n.d.	251	29	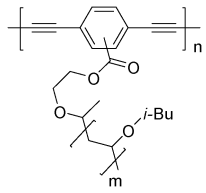	Through	100	35	329
15	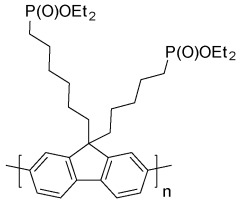	Through	100	n.d.	330	30	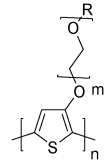	Through	100	59–66	331 and 332

[a] Amount of functionalized units on the backbone.

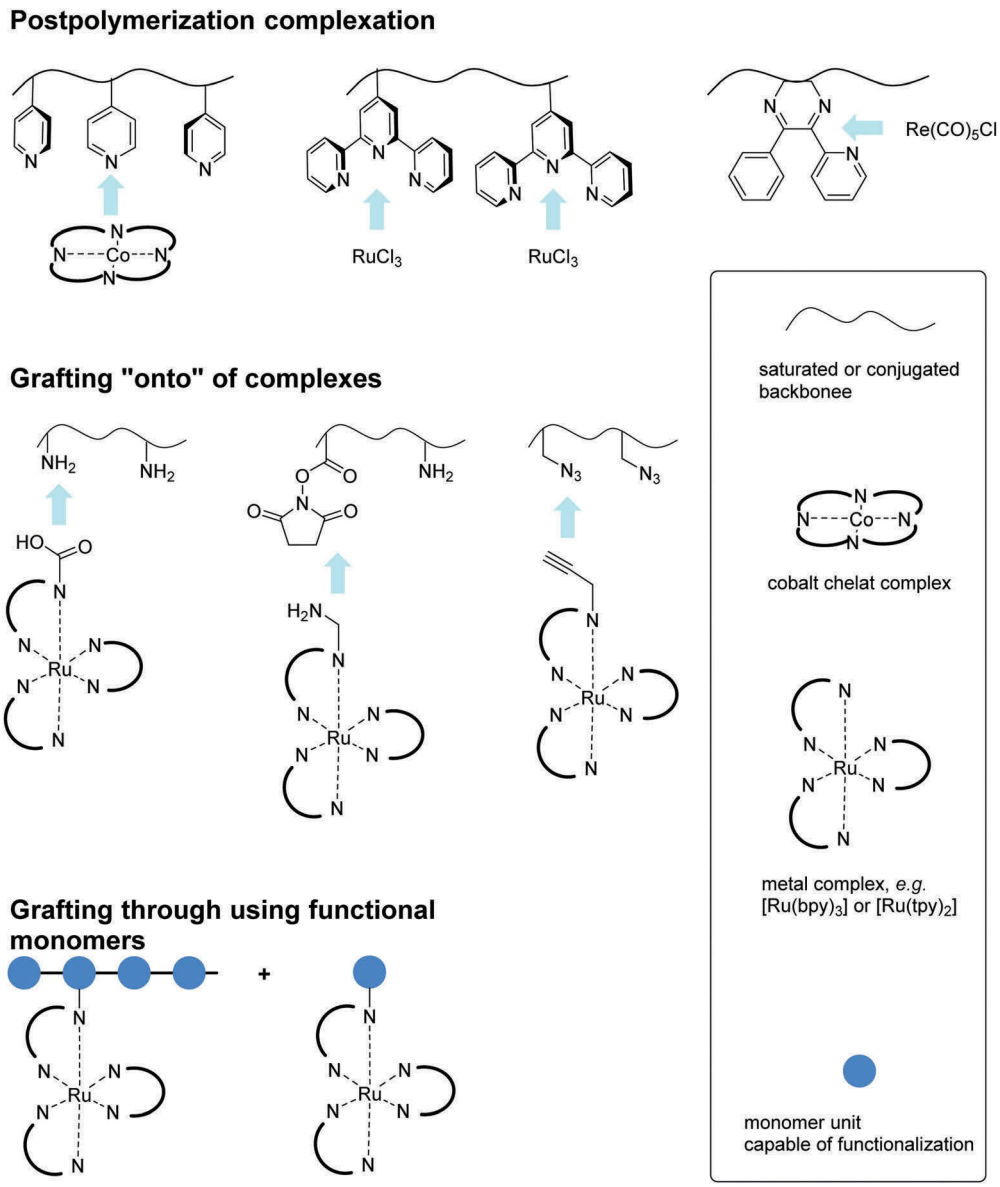

Scheme 19 Schematic representation of reported preparation methods for graft polymers containing metal complexes.

light harvesting antennas and in the case of electrochemically active polymers, additionally light induced charge separation can be realized within such an assembly. In general, the polymerization of metal containing monomers is impractical due to possible side reactions with the active propagating species[336] so that preferential "grafting onto" approaches are applied in the literature (Scheme 19).

Polystyrene and PMA derivatives are readily available by CRP and represent often used polymers to provide a structure for the attachment of photosensitizers.[47,337–341] Suitable linking reactions to decorate the polymer backbone are shown in Scheme 19 and include the CuAAC reaction[339–342] or amidation reactions.[47,337,338] Noteworthily, the azide functionality – necessary for the CuAAC reaction – is introduced in a postpolymerization reaction by nucleophilic substitution as general azides are not compatible with common polymerization conditions.[339–342] The conversion of the subsequent CuAAC reaction is reported to be quantitative. Monomers with NHS ester moieties are directly polymerized and side chain decorated with the respective amino-substituted Ru(II) photosensitizer with loadings up to 90% in good yields (75%).[47,338] Interestingly, poly(4-vinylpyridine) (P4VP) can directly act as a monodentate ligand for metal complexes without further modification. Hence, the functionalization of surface bound P4VP with hydrogen production cobalt catalysts is readily achieved and increased the performance of the photocathode in devices.[343]

Besides the presented PS and PMA based photosensitizer-polymer assemblies, a very exciting grafting through approach for a light harvesting graft polymer based on an amino acid backbone was introduced by the group of Meyer.[344] The authors prepared an oligoproline by solid-phase peptide synthesis (SPPS) applying modified monomers bearing Ru(II) complexes

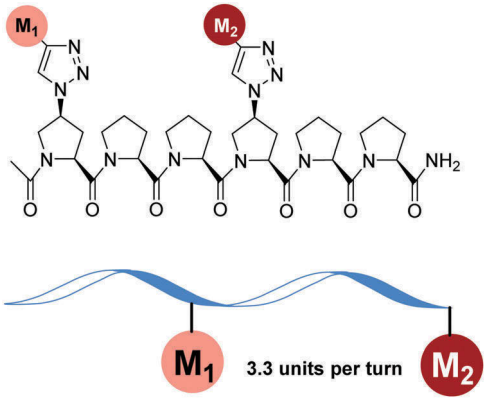

Fig. 7 Schematic representation of the chemical structure of metal complex substituted polyproline and of the resulting helical structure with 3.3 monomer units per turn (adapted from ref. 345 and 346).

as a chromophore or phenothiazine moieties as an electron donor (Fig. 7). The yields for coupling steps between unmodified prolines were 97 to 99% and 20 to 30% for the modified analogs. Therefore, the crude products had to be purified by HPLC to isolate the pure assemblies with 16, 17, 18 or 19 amino acids. The observed helical architecture of the polymer backbone provides a structurally well-defined environment for the photo-redox-active assembly and enables distance dependent analysis of electron transfer processes. Furthermore, by the defined incorporation of Ru(II) and Os(II) complexes in the assemblies also an antenna system with a secondary structure could be obtained and the distance dependence of excited state energy transfer processes was studied.[345] Modularity was additionally accomplished in the systems by combination with "Click" chemistry, *i.e.* azido functionalized prolines were utilized in the SPPS and were subsequently functionalized with metal complexes to allow a high variability.[346–348] These structurally well-defined assemblies represent promising model compounds for photoelectrosynthesis cells as they can be immobilized on surfaces using complexes with anchor groups[346–348] and the modular approach allows for the application of several different metal complexes, *e.g.* to incorporate water oxidation catalysts.[347,348] Noteworthily, the modification of the polymer backbone, *i.e.* the utilization of other amino acids besides proline, resulted in a much less ordered architecture.[349]

In addition to providing a structural backbone, the application of conjugated polymers enables the realization of charge transport processes or additional light absorption in metal complex containing graft polymers. One of the earliest examples of such an approach is reported by Cheng *et al.* by the preparation of substituted poly(phenylenethiophene)s and poly(fluorenethiophene)s with ruthenium terpyridine trithiocyanato complexes.[336] For this purpose, terpyridine functionalized dibromobenzene and dibromofluorene were synthesized and subsequently polymerized with thiophenediboronic acid by Suzuki coupling. The complexation with ruthenium was afterwards realized in a "grafting to" approach consisting of two reaction steps with yields of 99% and 89%, respectively, and quasi-quantitative functionalization. Noteworthily, the direct polymerization of ruthenium containing monomers did not lead to any polymer.

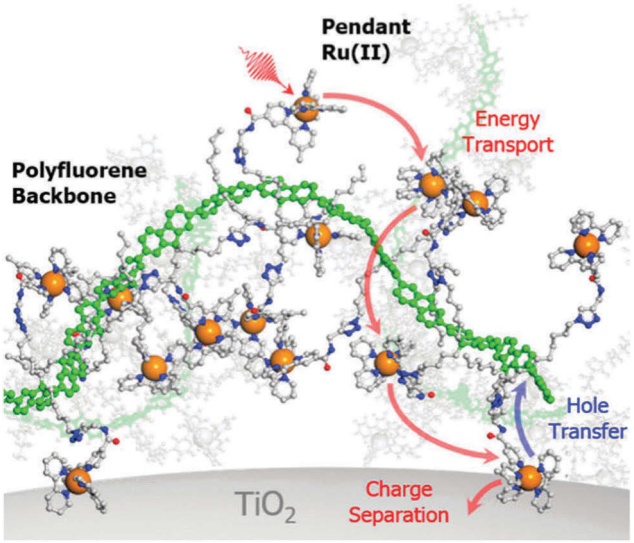

Fig. 8 Polyfluorene based metal decorated architecture bound to TiO_2 for light harvesting and charge separation (reprinted with permission from ref. 350, Copyright 2014 American Chemical Society).

A series of light-harvesting polymers loaded with Ru(II) complexes by a grafting onto approach utilizing "Click" chemistry is reported by the groups of Schanze and Papanikolas.[350–354] The introduction of azide functionalities into suitable substituted polyfluorenes,[350,351,354] polythiophenes[353] or their respective copolymers[351,352] enabled efficient coupling with Ru(II) photosensitizers by the CuAAC reaction (quantitative conversion, yields above 80%). Immobilization of these photo-redox-active assemblies onto TiO_2 was also realized by the introduction of anchor groups on the complex' ligand scaffold (Fig. 8).[351,353] The polymer–metal complex hybrid materials showed fast energy and electron transfer processes resulting in the formation of long-lived charge separated states (>100 μs).

Also other metals besides ruthenium, *e.g.* rhenium,[355] may be applied in the described architectures, however their usage is much less frequently investigated.

4.5. Graft copolymers containing fullerenes

As discussed previously, fullerenes are reactive towards cations, anions and radicals so common fullerene containing monomers are not polymerized directly except by the ROMP process. As a consequence, the grafting of these compounds to a separately prepared polymer with functional side groups is very common. In contrast to low molar mass fullerene derivatives, incorporation into homopolymers[6,356,357] leads to an increased solubility and may result in the formation of homogenous films.[6] Additionally, fullerenes also represent promising candidates for donor–acceptor polymers due to their electron accepting properties. These compounds are either introduced as electron accepting side chains of conducting polymers, *e.g.* PPV,[358] or are more prominent in block copolymers as electron acceptor blocks.[5,43,234,237,359–362] In general, two approaches leading to fullerene grafted block copolymers can

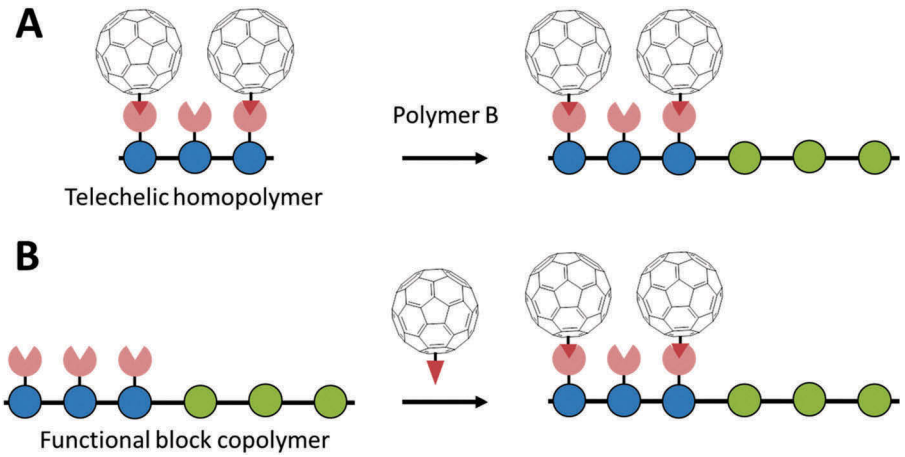

Scheme 20 Schematic representation of synthetic approaches leading to fullerene decorated block copolymers.

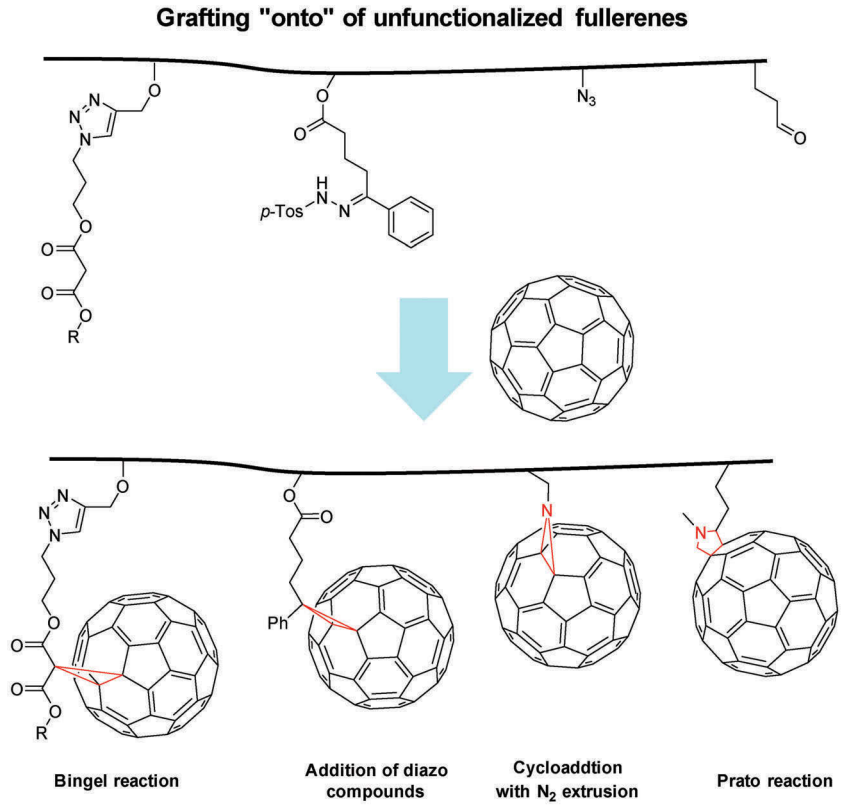

Scheme 21 Schematic representation of synthetic methods for the side chain decoration of polymers with unfunctionalized fullerenes (the formed linking motif is marked in red).

be distinguished. Either a telechelic homopolymer is fullerene decorated and coupled with the second block (Scheme 20A) or the block copolymer is prepared first and the fullerene is introduced in the second step (Scheme 20B).

Suitable polymer backbones, which are often used for a later fullerene substitution, include PS[6,40,43,234,237,357,359,361] and PMA/PA[356,360,362] derivatives as they can be readily prepared with CRP techniques using functional initiators or macroinitiators leading to defined reactive end groups capable of further reactions (see Section ''Block copolymers''). Suitable reactions for the attachment of fullerenes on the polymer are shown in Scheme 21. As it can be seen, the Prato reaction,[358] the Bingel reaction,[357] cycloadditions with subsequent nitrogen extrusion[43,361,363] and the addition of diazo compounds[237] can be performed with pristine fullerenes if the monomer units in the polymer feature the appropriate functional groups. On the one hand, these approaches are straightforward as unfunctionalized fullerenes are commercially available but potentially

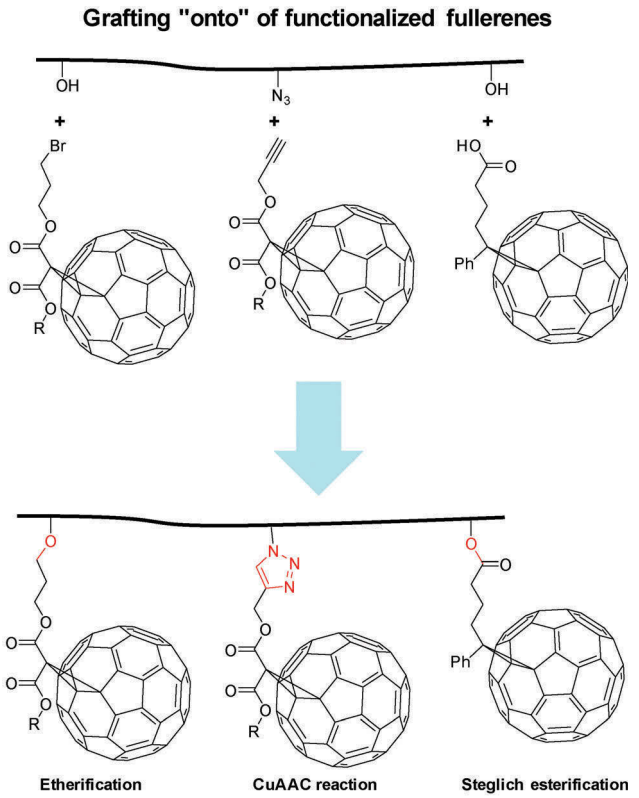

Scheme 22 Schematic representation of synthetic methods for the side chain decoration of polymers with functionalized fullerenes (the formed linking motif is marked in red).

cross-linking is possible due to multiple reactions of one single fullerene molecule and therefore these reactions require the application of a large excess of fullerene.[237] In contrast, the application of functionalized fullerene derivatives and their subsequent incorporation into the polymer side chains avoids the cross-linking issue. Suitable reactions for this approach include Steglich esterifaction,[6,40,234,362] the CuAAC reaction[5,356] or etherification reactions (Scheme 22).[359] In general, fullerene containing block copolymers are rod–coil copolymers and are expected to improve the morphological control in organic solar cells, *e.g.* as compatibilizers or stabilizers. In contrast to blends, the polymers are able to show microphase separation without undesired macrophase separation.[5,6,234,237,356,359,362] Moreover, improved long-term stability of the structures and reduced agglomeration behavior is also expected resulting in higher efficiencies of organic solar cells.[5,6,237,360] The grafting density of the polymers is typically below 100% as the fullerene is sterically hindered. The calculation of the mass fraction of the attached fullerene is often hampered as very weak NMR signals have to be quantified and, therefore, often relies on TGA analysis.

A more comprehensive discussion of polymers containing fullerenes and related reactions is not possible at this point due to the scope of the review. Therefore we would like to refer to reviews detailing these respective topics.[364–366]

5. Chain end functionalization with functional building blocks

The initially introduced polymerization techniques produce telechelic polymers, whose reactive end groups are by definition capable of further reactions and, therefore, enable the attachment of functional units, *e.g.* substituents to influence the assembly properties or photo- or redox-active moieties.[11,367]

The determination of the end functionalization efficiency and the separation of non-functionalized and functionalized polymers are challenging and are not always mentioned in reports.

Basically, two different approaches leading to end functionalization can be differentiated, *in situ* functionalization and post polymerization functionalization (Scheme 23). *In situ* functionalization (Scheme 23A) exploits the high reactivity of the propagating species that is formed during a polymerization process. In a typical approach an end capping reagent is added to quench the active species and to simultaneously introduce a functional unit. This technique is often utilized in anionic polymerizations. For instance, Natori *et al.* prepared styrenic triarylamines and functionalized the obtained polymer by the addition of C_{60} fullerene, which readily reacts with the

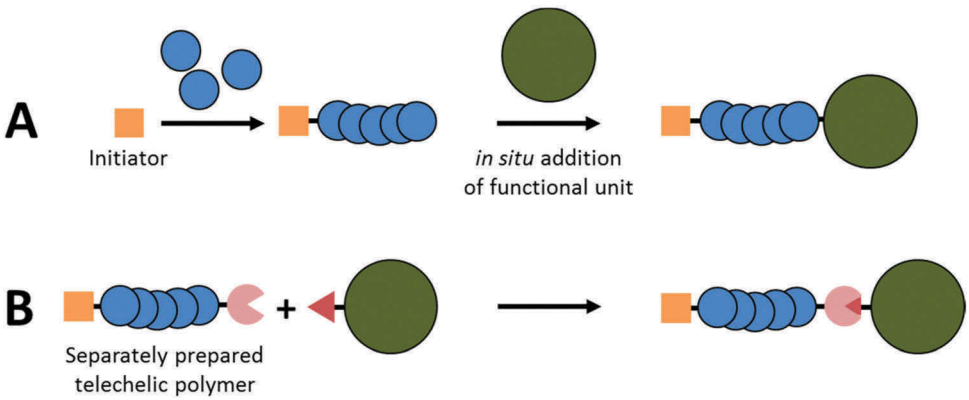

Scheme 23 Schematic representation of synthetic approaches towards chain end decoration with functional units, either by *in situ* functionalization (A) or postpolymerization modification of telechelic polymers (B).

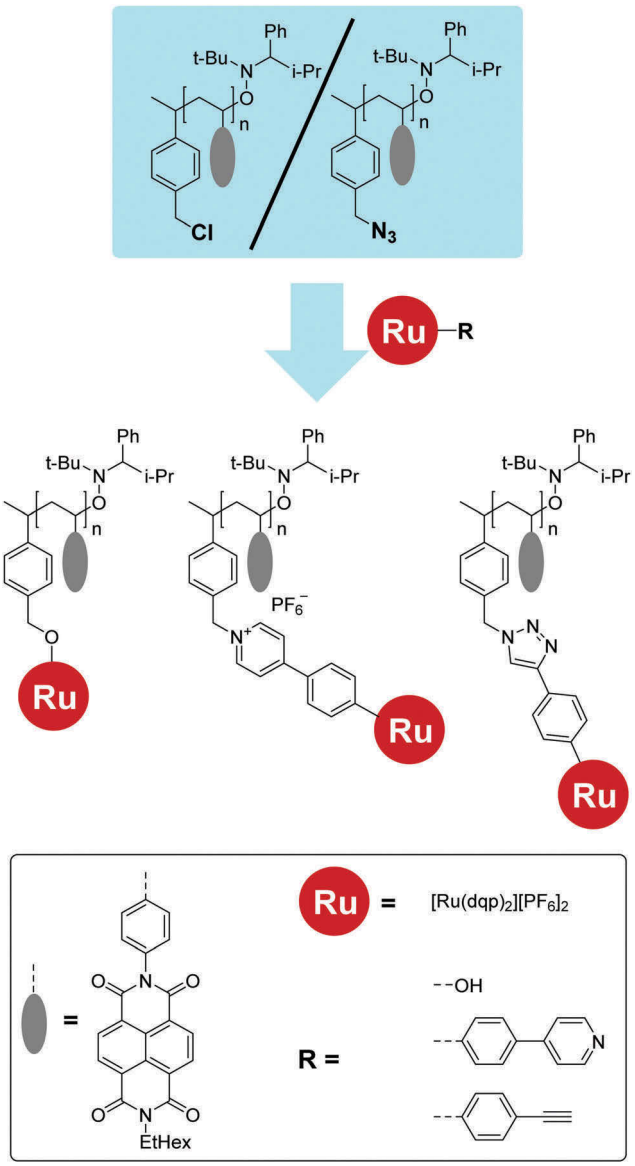

Scheme 24 Schematic representation of telechelic polymers as a modular basis for the synthesis of acceptor–photosensitizer dyads.[372]

anionic species.[63,368] The *in situ* approach is also suitable for the chain end decoration of conjugated polymers. Classical step growth polycondensation reactions with AA/BB type monomers can be quenched by an excess of the desired functional unit, which is either modified with the reactive group A or B. A compelling example is provided by Robb *et al.* as the authors synthesized a PDPP2FT donor–acceptor polymer by Stille coupling and introduced bromine bearing perylene diimide (PDI) as an end capper to terminate the propagating chains resulting in more than 50% bisfunctionalized chains.[369] The functionalized polymer revealed an efficient charge transfer between the main polymer chain and the PDI moieties as a result of the covalent linkage.[369] A second example is given by the group of Wang by *in situ* end capping of donor–acceptor copolymers with porphyrin complexes during Stille coupling polymerization.[370] The obtained materials featured an enhancement of light absorption and improved power conversion efficiency (by 50%). A similar approach utilizing AB monomers is presented by Krebs and Biancardo, who attached ruthenium dyes on P3HT by Stille coupling to prepare materials for dye sensitized solar cells.[371] However, full conversion was not reached in the P3HT–Ru-complex dyad that still contained residual unfunctionalized homopolymer.

In contrast to the *in situ* functionalization procedure, the end functionalization approach by a post polymerization reaction (Scheme 23B) is characterized by the usage of a purified telechelic polymer in a consecutive reaction after the actual polymerization. The required reactive end group capable of further functionalization is often introduced by utilization of a suitable initiator. A major advantage of the procedure is the modularity, so that a large batch of the prepared polymer can be decorated with different functional units and, thus, a good comparability and reproducibility is ensured when the influence of various end groups, *e.g.* metal complexes, on the polymer properties is investigated (Scheme 24).[372] The end functionalization of redox-active polymers prepared by NMP with photoactive ruthenium complexes was elaborately investigated by Schroot *et al.*[37,372,373] The presented modular assembly of donor–photosensitizer and acceptor–photosensitizer dyads was accomplished by nucleophilic reactions and the CuAAC reaction of the NMP initiator's starting group and suitable substituted metal complexes in yields between 40 and 71%. Besides, a simplified purification protocol by modified silica gels was developed to ensure the complete removal of unfunctionalized polymer and excess metal complex. Moreover, the detected charge transfer within the architectures illustrated the eligibility of the chosen approach.[374] Another interesting example for the end functionalization using a metal complex is reported by Fang *et al.* (Scheme 25).[340] The combination of RAFT polymerization, CuAAC click reaction and subsequent esterification allowed the construction of a chromophore–catalyst assembly consisting of Ru(II) polypyridyl-derivatized polypropylacrylate and a terminal water oxidation catalyst with a good yield of 63% for the last two steps. Interestingly, this example combines chain end as well as side chain functionalization reactions and underlines the versatility of the RAFT process. The presented approaches also enable directional energy or charge transfer as a result of the linear prepared architecture.

As discussed in previous sections, cross coupling reactions may also lead to telechelic polymers capable of further modification reactions. The synthesis of C_{60} end capped P3HT is described by Lee *et al.*[7] In a first step, *in situ* end capping with allylmagnesium bromide yielded telechelic P3HT, which was converted in hydroxypropyl-terminated P3HT by hydroboration. Finally Steglich esterification gave the desired fullerene end capped polymer (end capping efficiency >90%), which acts as a compatibilizer and increases the stability of bulk heterojunction solar cells.[7] A second example for the end functionalization of conjugated telechelic polymers is the decoration of ethynyl end group bearing polyfluorene by the CuAAC reaction with bio-targeting

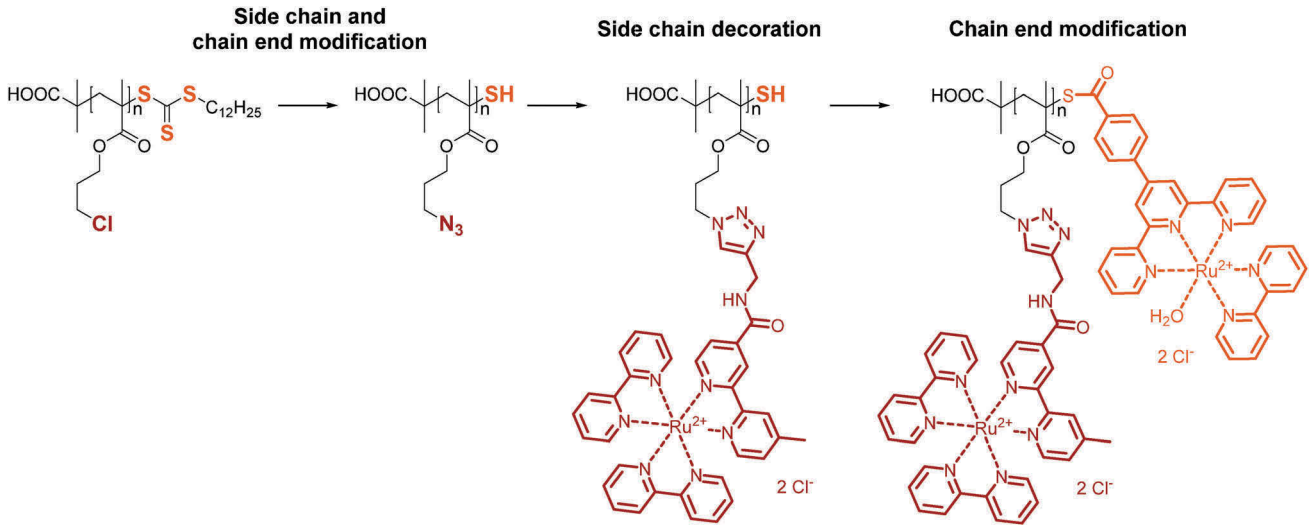

Scheme 25 Schematic representation of the construction of terminal water oxidation catalyst decorated polypyridyl Ru(II)-derivatized polypropylacrylate by RAFT polymerization applying side chain as well as chain end functionalization techniques.[340]

groups for sensing applications.[109] However, the amount of functionalized polymer chains was not determined.

Although this review focuses on electrochemically active polymers, the decoration of non-electrochemically active polymers with photo- or redox-active units can be desired to tune and improve the mechanical and optical properties, *e.g.* absorption maxima, film forming properties or mechanical stability.[4,375,376] The improvement of device stability and efficiency is demonstrated by Raissi *et al.* by end capping of P3HT-*b*-PS with C_{60} fullerene utilizing atom transfer radical addition.[4] Subsequently the material was applied as a compatibilizer in bulk heterojunction solar cells and improved the efficiency as well as the stability by inducing interpenetrating domains.

In summary, the chain end functionalization of telechelic electrochemically active polymers with functional units is of special interest for architectures including light harvesting units as the decoration of the chain end ensures a linear architecture and directional energy or charge transport processes.

6. Conclusion

Synthetic approaches leading to well-defined polymer based architectures with tunable (opto)electronic properties were reviewed. The utilization of these tailor-made architectures facilitates new possibilities with regard to important physical parameters, *e.g.*, morphology control and morphology stability, and enables the construction of multipurpose materials.

The controlled synthesis of redox-active and conjugated polymers represents a key step for the construction of these macromolecules. Modern polymerization methods for redox-active polymers, *e.g.* controlled anionic or radical polymerization or ROMP techniques, and conjugated polymers, *e.g.* Kumada catalyst transfer polymerization and related techniques, provide the fundamental basis for the covalent incorporation of various polymers in larger architectures. Thus a large number of different telechelic polymers can be readily prepared and further applied to prepare block or comb polymers as well as end functionalized polymers. The combination of two or more different monomer units in these macromolecules enables the realization of donor–acceptor polymers, photoredox-active dyads and triads or tuning of physical properties.

The synthesis of block copolymers can be achieved by the initially discussed polymerization techniques by application of the sequential monomer addition approach, the macroinitiator approach or the coupling of polymerization techniques (bifunctional initiator or telechelic homopolymers). Graft and comb polymers are readily prepared by grafting onto, from or through approaches utilizing the aforementioned polymerization techniques as well as highly efficient coupling reactions, *e.g.* the CuAAC reaction. The coupling reactions are also of fundamental importance for the construction of directional end functionalized architectures, *e.g.* light harvesting antennas or donor–photosensitizer–acceptor assemblies. However, challenges remain as often functionalization reactions are not quantitative or rather hard to quantify by analytical methods and challenging purification and fractionation steps may be necessary.

In the future the steadily increasing number of functional initiators and coupling reagents as well as the development of polymerization techniques will further expand the number of well-defined covalently linked architectures.

Acknowledgements

Financial support by the Carl-Zeiss-Foundation, the Friedrich Schiller University Jena (“Nachwuchsförderung”) and the Thüringer Ministerium für Wirtschaft, Wissenschaft und Digitale Gesellschaft (TMWWDG) is kindly acknowledged.

References

1 Y.-L. Li, Y.-S. Cheng, P.-N. Yeh, S.-H. Liao and S.-A. Chen, *Adv. Funct. Mater.*, 2014, **24**, 6811–6817.
2 S.-H. Liao, Y.-L. Li, T.-H. Jen, Y.-S. Cheng and S.-A. Chen, *J. Am. Chem. Soc.*, 2012, **134**, 14271–14274.
3 H.-H. Lu, Y.-S. Ma, N.-J. Yang, G.-H. Lin, Y.-C. Wu and S.-A. Chen, *J. Am. Chem. Soc.*, 2011, **133**, 9634–9637.
4 M. Raissi, H. Erothu, E. Ibarboure, H. Cramail, L. Vignau, E. Cloutet and R. C. Hiorns, *J. Mater. Chem. A*, 2015, **3**, 18207–18221.
5 S. Miyanishi, Y. Zhang, K. Tajima and K. Hashimoto, *Chem. Commun.*, 2010, **46**, 6723–6725.
6 M. Hufnagel, M.-A. Muth, J. C. Brendel and M. Thelakkat, *Macromolecules*, 2014, **47**, 2324–2332.
7 J. U. Lee, J. W. Jung, T. Emrick, T. P. Russell and W. H. Jo, *J. Mater. Chem.*, 2010, **20**, 3287–3294.
8 A. Walther and A. H. E. Mueller, *Chem. Rev.*, 2013, **113**, 5194–5261.
9 F. H. Schacher, P. A. Rupar and I. Manners, *Angew. Chem., Int. Ed.*, 2012, **51**, 7898–7921.
10 E.-K. Fleischmann and R. Zentel, *Angew. Chem., Int. Ed.*, 2013, **52**, 8810–8827.
11 U. Koldemir, S. R. Puniredd, M. Wagner, S. Tongay, T. D. McCarley, G. D. Kamenov, K. Muellen, W. Pisula and J. R. Reynolds, *Macromolecules*, 2015, **48**, 6369–6377.
12 S. Broll, F. Nuebling, A. Luzio, D. Lentzas, H. Komber, M. Caironi and M. Sommer, *Macromolecules*, 2015, **48**, 7481–7488.
13 F. Lombeck, H. Komber, D. Fazzi, D. Nava, J. Kuhlmann, D. Stegerer, K. Strassel, J. Brandt, A. D. de Zerio Mendaza, C. Mueller, W. Thiel, M. Caironi, R. Friend and M. Sommer, *Adv. Energy Mater.*, 2016, 1601232.
14 D. Schiefer, H. Komber, F. Mugwanga Keheze, S. Kunz, R. Hanselmann, G. Reiter and M. Sommer, *Macromolecules*, 2016, **49**, 7230–7237.
15 K. Muellen and W. Pisula, *J. Am. Chem. Soc.*, 2015, **137**, 9503–9505.
16 K. Muellen and J. P. Rabe, *Ann. N. Y. Acad. Sci.*, 1998, **852**, 205–218.
17 Y.-H. Chou, H.-C. Chang, C.-L. Liu and W.-C. Chen, *Polym. Chem.*, 2015, **6**, 341–352.
18 A. Facchetti, *Chem. Mater.*, 2011, **23**, 733–758.
19 Y. He, W. Hong and Y. Li, *J. Mater. Chem. C*, 2014, **2**, 8651–8661.
20 A. M. Breul, M. D. Hager and U. S. Schubert, *Chem. Soc. Rev.*, 2013, **42**, 5366–5407.
21 X. Zhang, W. Wang, Z. Hu, G. Wang and K. Uvdal, *Coord. Chem. Rev.*, 2015, **284**, 206–235.
22 A. Bousquet, H. Awada, R. C. Hiorns, C. Dagron-Lartigau and L. Billon, *Prog. Polym. Sci.*, 2014, **39**, 1847–1877.
23 X. Guo, M. Baumgarten and K. Muellen, *Prog. Polym. Sci.*, 2013, **38**, 1832–1908.
24 P. D. Topham, A. J. Parnell and R. C. Hiorns, *J. Polym. Sci., Part B: Polym. Phys.*, 2011, **49**, 1131–1156.
25 J. K. Kallitsis, C. Anastasopoulos and A. K. Andreopoulou, *MRS Commun.*, 2015, **5**, 365–382.
26 G. Inzelt, *Conducting Polymers*, Springer Berlin Heidelberg, 2012, ch. 2, pp. 7–82.
27 A. D. McNaught and A. Wilkinson, *IUPAC Compendium of Chemical Terminology (the "Gold Book")*, Blackwell Scientific Publications, Oxford, 2nd edn, 1997.
28 U. Mansfeld, C. Pietsch, R. Hoogenboom, C. R. Becer and U. S. Schubert, *Polym. Chem.*, 2010, **1**, 1560–1598.
29 L. Wu, U. Glebe and A. Boeker, *Polym. Chem.*, 2015, **6**, 5143–5184.
30 G. Moad, M. Chen, M. Haussler, A. Postma, E. Rizzardo and S. H. Thang, *Polym. Chem.*, 2011, **2**, 492–519.
31 J. Nicolas, Y. Guillaneuf, C. Lefay, D. Bertin, D. Gigmes and B. Charleux, *Prog. Polym. Sci.*, 2013, **38**, 63–235.
32 K. Matyjaszewski, *Macromolecules*, 2012, **45**, 4015–4039.
33 R. B. Grubbs, *Polym. Rev.*, 2011, **51**, 104–137.
34 R. Schroot, U. S. Schubert and M. Jaeger, *Macromolecules*, 2015, **48**, 1963–1971.
35 E. M. Barea, G. Garcia-Belmonte, M. Sommer, S. Huettner, H. J. Bolink and M. Thelakkat, *Thin Solid Films*, 2010, **518**, 3351–3354.
36 S. King, M. Sommer, S. Huettner, M. Thelakkat and S. A. Haque, *J. Mater. Chem.*, 2009, **19**, 5436–5441.
37 R. Schroot, C. Friebe, E. Altuntas, S. Crotty, M. Jaeger and U. S. Schubert, *Macromolecules*, 2013, **46**, 2039–2048.
38 S. Koyuncu, H.-W. Wang, F. Liu, K. B. Toga, W. Gu and T. P. Russell, *J. Mater. Chem. A*, 2014, **2**, 2993–2998.
39 R. H. Lohwasser and M. Thelakkat, *Macromolecules*, 2011, **44**, 3388–3397.
40 M. Hufnagel, M. Fischer, T. Thurn-Albrecht and M. Thelakkat, *Macromolecules*, 2016, **49**, 1637–1647.
41 S. Fleischmann, H. Komber, D. Appelhans and B. I. Voit, *Macromol. Chem. Phys.*, 2007, **208**, 1050–1060.
42 D. Gigmes, J. Vinas, N. Chagneux, C. Lefay, T. N. T. Phan, T. Trimaille, P.-E. Dufils, Y. Guillaneuf, G. Carrot, F. Boué and D. Bertin, *Controlled/Living Radical Polymerization: Progress in RAFT, DT, NMP & OMRP*, American Chemical Society, 2009, vol. 1024, ch. 16, pp. 245–262.
43 F. Richard, C. Brochon, N. Leclerc, D. Eckhardt, T. Heiser and G. Hadziioannou, *Macromol. Rapid Commun.*, 2008, **29**, 885–891.
44 Q. Zhang, A. Cirpan, T. P. Russell and T. Emrick, *Macromolecules*, 2009, **42**, 1079–1082.
45 K. Matyjaszewski and J. Xia, *Chem. Rev.*, 2001, **101**, 2921–2990.
46 A. A. Golriz, T. Kaule, M. B. Untch, K. Kolman, R. Berger and J. S. Gutmann, *ACS Appl. Mater. Interfaces*, 2013, **5**, 2485–2494.
47 Z. Fang, A. Ito, S. Keinan, Z. Chen, Z. Watson, J. Rochette, Y. Kanai, D. Taylor, K. S. Schanze and T. J. Meyer, *Inorg. Chem.*, 2013, **52**, 8511–8520.
48 G. Moad, E. Rizzardo and S. H. Thang, *Polymer*, 2008, **49**, 1079–1131.
49 G. Moad, E. Rizzardo and S. H. Thang, *Aust. J. Chem.*, 2005, **58**, 379–410.
50 G. Moad, J. Chiefari, Y. K. Chong, J. Krstina, R. T. A. Mayadunne, A. Postma, E. Rizzardo and S. H. Thang, *Polym. Int.*, 2000, **49**, 993–1001.

51 B. Happ, J. Schaefer, R. Menzel, M. D. Hager, A. Winter, J. Popp, R. Beckert, B. Dietzek and U. S. Schubert, *Macromolecules*, 2011, **44**, 6277–6287.
52 A. M. Breul, J. Schaefer, E. Altuntas, M. D. Hager, A. Winter, B. Dietzek, J. Popp and U. S. Schubert, *J. Inorg. Organomet. Polym. Mater.*, 2013, **23**, 74–80.
53 A. M. Breul, I. Rabelo de Moraes, R. Menzel, M. Pfeffer, A. Winter, M. D. Hager, S. Rau, B. Dietzek, R. Beckert and U. S. Schubert, *Polym. Chem.*, 2014, **5**, 2715–2724.
54 M. Aqil, A. Aqil, F. Ouhib, A. El Idrissi, C. Detrembleur and C. Jerome, *RSC Adv.*, 2015, **5**, 85035–85038.
55 F. Mathias, M. N. Tahir, W. Tremel and R. Zentel, *Macromol. Chem. Phys.*, 2014, **215**, 604–613.
56 A. Fokina, Y. Lee, J. H. Chang, L. Braun, W. K. Bae, K. Char, C. Lee and R. Zentel, *Polym. Chem.*, 2016, **7**, 101–112.
57 M. C. Tria, K.-S. Liao, N. Alley, S. Curran and R. Advincula, *J. Mater. Chem.*, 2011, **21**, 10261–10264.
58 B. Mu, B. Wu, S. Pan, J. Fang and D. Chen, *Macromolecules*, 2015, **48**, 2388–2398.
59 P. Kohn, L. Ghazaryan, G. Gupta, M. Sommer, A. Wicklein, M. Thelakkat and T. Thurn-Albrecht, *Macromolecules*, 2012, **45**, 5676–5683.
60 K. Wolski, A. Gruszkiewicz and S. Zapotoczny, *Polym. Chem.*, 2015, **6**, 7505–7513.
61 K. Hong, D. Uhrig and J. W. Mays, *Curr. Opin. Solid State Mater. Sci.*, 1999, **4**, 531–538.
62 J. Jagur-Grodzinski, *J. Polym. Sci., Part A: Polym. Chem.*, 2002, **40**, 2116–2133.
63 I. Natori, S. Natori, H. Sekikawa, T. Takahashi and H. Sato, *J. Appl. Polym. Sci.*, 2011, **121**, 3433–3438.
64 B.-G. Kang, N.-G. Kang and J.-S. Lee, *Macromolecules*, 2010, **43**, 8400–8408.
65 T. Higashihara and M. Ueda, *Macromolecules*, 2009, **42**, 8794–8800.
66 I. Natori, S. Natori, K. Tsuchiya and K. Ogino, *Macromolecules*, 2010, **44**, 256–262.
67 I. Cosemans, J. Wouters, T. Cleij, L. Lutsen, W. Maes, T. Junkers and D. Vanderzande, *Macromol. Rapid Commun.*, 2012, **33**, 242–247.
68 M. A. Mamo, F. S. Freitas, R. P. Forbes, R. S. Black, A. F. Nogueira, W. A. L. van Otterlo and N. J. Coville, *Fullerenes, Nanotubes, Carbon Nanostruct.*, 2013, **21**, 198–212.
69 M. Eo, D. Han, M. H. Park, M. Hong, Y. Do, S. Yoo and M. H. Lee, *Eur. Polym. J.*, 2014, **51**, 37–44.
70 J. Kim, M. H. Yun, J. Lee, J. Y. Kim, F. Wudl and C. Yang, *Chem. Commun.*, 2011, **47**, 3078–3080.
71 M. Eo, S. Lee, M. H. Park, M. H. Lee, S. Yoo and Y. Do, *Macromol. Rapid Commun.*, 2012, **33**, 1119–1125.
72 J. A. Paquette, S. Ezugwu, V. Yadav, G. Fanchini and J. B. Gilroy, *J. Polym. Sci., Part A: Polym. Chem.*, 2016, **54**, 1803–1813.
73 A. de la Escosura, M. V. Martínez-Díaz, T. Torres, R. H. Grubbs, D. M. Guldi, H. Neugebauer, C. Winder, M. Drees and N. S. Sariciftci, *Chem. – Asian J.*, 2006, **1**, 148–154.
74 T. Suga, M. Sakata, K. Aoki and H. Nishide, *ACS Macro Lett.*, 2014, **3**, 703–707.
75 H.-W. Wang, Z.-C. Liu, C.-H. Chen, T.-S. Lim, W. Fann, C.-G. Chao, J.-Y. Yu, S.-L. Lee, C.-h. Chen, S.-L. Huang and T.-Y. Luh, *Chem. – Eur. J.*, 2009, **15**, 5719–5728.
76 N. Zaquen, L. Lutsen, D. Vanderzande and T. Junkers, *Polym. Chem.*, 2016, **7**, 1355–1367.
77 E. Elacqua and M. Weck, *Chem. – Eur. J.*, 2015, **21**, 7151–7158.
78 M. Montanari, A. Bugana, A. K. Sharma and D. Pasini, *Org. Biomol. Chem.*, 2011, **9**, 5018–5020.
79 F. Menk, M. Mondeshki, D. Dudenko, S. Shin, D. Schollmeyer, O. Ceyhun, T.-L. Choi and R. Zentel, *Macromolecules*, 2015, **48**, 7435–7445.
80 C.-Y. Yu, M. Helliwell, J. Raftery and M. L. Turner, *Chem. – Eur. J.*, 2011, **17**, 6991–6997.
81 C.-Y. Yu and M. Turner, *Angew. Chem., Int. Ed.*, 2006, **45**, 7797–7800.
82 A. M. Spring, C.-Y. Yu, M. Horie and M. L. Turner, *Chem. Commun.*, 2009, 2676–2678.
83 B. J. Lidster, D. R. Kumar, A. M. Spring, C.-Y. Yu and M. L. Turner, *Polym. Chem.*, 2016, **7**, 5544–5551.
84 D. Maeker, C. Maier, K. Broedner and U. H. F. Bunz, *ACS Macro Lett.*, 2014, **3**, 415–418.
85 D. Maeker and U. H. F. Bunz, *Macromol. Rapid Commun.*, 2014, **35**, 2096–2100.
86 M. Horie, I. W. Shen, S. M. Tuladhar, H. Leventis, S. A. Haque, J. Nelson, B. R. Saunders and M. L. Turner, *Polymer*, 2010, **51**, 1541–1547.
87 B. J. Lidster, D. R. Kumar, A. M. Spring, C.-Y. Yu, M. Helliwell, J. Raftery and M. L. Turner, *Org. Biomol. Chem.*, 2016, **14**, 6079–6087.
88 C.-Y. Yu, M. Horie, A. M. Spring, K. Tremel and M. L. Turner, *Macromolecules*, 2010, **43**, 222–232.
89 C.-Y. Yu, J. W. Kingsley, D. G. Lidzey and M. L. Turner, *Macromol. Rapid Commun.*, 2009, **30**, 1889–1892.
90 B. J. Lidster, J. M. Behrendt and M. L. Turner, *Chem. Commun.*, 2014, **50**, 11867–11870.
91 S. Shin, K.-Y. Yoon and T.-L. Choi, *Macromolecules*, 2015, **48**, 1390–1397.
92 K.-Y. Yoon, I.-H. Lee, K. O. Kim, J. Jang, E. Lee and T.-L. Choi, *J. Am. Chem. Soc.*, 2012, **134**, 14291–14294.
93 S. von Kugelgen, D. E. Bellone, R. R. Cloke, W. S. Perkins and F. R. Fischer, *J. Am. Chem. Soc.*, 2016, **138**, 6234–6239.
94 W. Song, J. Wu, G. Yang, H. Han, M. Xie and X. Liao, *RSC Adv.*, 2015, **5**, 68765–68772.
95 M. C. Stefan, A. E. Javier, I. Osaka and R. D. McCullough, *Macromolecules*, 2009, **42**, 30–32.
96 R. Miyakoshi, A. Yokoyama and T. Yokozawa, *J. Am. Chem. Soc.*, 2005, **127**, 17542–17547.
97 M. Jeffries-El, G. Sauve and R. D. McCullough, *Macromolecules*, 2005, **38**, 10346–10352.
98 M. C. Iovu, E. E. Sheina, R. R. Gil and R. D. McCullough, *Macromolecules*, 2005, **38**, 8649–8656.
99 M. Jeffries-El, G. Sauvé and R. D. McCullough, *Adv. Mater.*, 2004, **16**, 1017–1019.

100 A. Smeets, K. Van den Bergh, J. De Winter, P. Gerbaux, T. Verbiest and G. Koeckelberghs, *Macromolecules*, 2009, **42**, 7638–7641.
101 R. A. Krueger, T. J. Gordon, T. Baumgartner and T. C. Sutherland, *ACS Appl. Mater. Interfaces*, 2011, **3**, 2031–2041.
102 A. Smeets, P. Willot, J. De Winter, P. Gerbaux, T. Verbiest and G. Koeckelberghs, *Macromolecules*, 2011, **44**, 6017–6025.
103 R. Grisorio and G. P. Suranna, *Polym. Chem.*, 2015, **6**, 7781–7795.
104 M. C. Stefan, M. P. Bhatt, P. Sista and H. D. Magurudeniya, *Polym. Chem.*, 2012, **3**, 1693–1701.
105 T. Yokozawa, Y. Nanashima, H. Kohno, R. Suzuki, M. Nojima and Y. Ohta, *Pure Appl. Chem.*, 2013, **85**, 573–587.
106 T. Yokozawa, Y. Nanashima and Y. Ohta, *ACS Macro Lett.*, 2012, **1**, 862–866.
107 A. Kiriy, V. Senkovskyy and M. Sommer, *Macromol. Rapid Commun.*, 2011, **32**, 1503–1517.
108 T. Yokozawa and Y. Ohta, *Chem. Rev.*, 2016, **116**, 1950–1968.
109 C. A. Traina, R. C. Bakus, II and G. C. Bazan, *J. Am. Chem. Soc.*, 2011, **133**, 12600–12607.
110 V. Senkovskyy, M. Sommer, R. Tkachov, H. Komber, W. T. S. Huck and A. Kiriy, *Macromolecules*, 2010, **43**, 10157–10161.
111 K. Van den Bergh, P. Willot, D. Cornelis, T. Verbiest and G. Koeckelberghs, *Macromolecules*, 2011, **44**, 728–735.
112 X. Yu, K. Xiao, J. Chen, N. V. Lavrik, K. Hong, B. G. Sumpter and D. B. Geohegan, *ACS Nano*, 2011, **5**, 3559–3567.
113 F. Monnaie, W. Brullot, T. Verbiest, J. De Winter, P. Gerbaux, A. Smeets and G. Koeckelberghs, *Macromolecules*, 2013, **46**, 8500–8508.
114 F. Monnaie, L. Verheyen, J. De Winter, P. Gerbaux, W. Brullot, T. Verbiest and G. Koeckelberghs, *Macromolecules*, 2015, **48**, 8752–8759.
115 H. Komber, V. Senkovskyy, R. Tkachov, K. Johnson, A. Kiriy, W. T. S. Huck and M. Sommer, *Macromolecules*, 2011, **44**, 9164–9172.
116 B. Yameen, N. Zydziak, S. M. Weidner, M. Bruns and C. Barner-Kowollik, *Macromolecules*, 2013, **46**, 2606–2615.
117 J. Ma, Y. Geng, K. Hashimoto and K. Tajima, *Macromol. Chem. Phys.*, 2013, **214**, 1326–1331.
118 W. M. Kochemba, S. M. Kilbey and D. L. Pickel, *J. Polym. Sci., Part A: Polym. Chem.*, 2012, **50**, 2762–2769.
119 J. Zhang, H. Yang, S. Xu, L. Yang, Y. Song, L. Jiang and Y. Dan, *Appl. Catal., B*, 2015, **174–175**, 193–202.
120 H. Rathnayake, N. Wright, A. Patel, J. Binion, L. E. McNamara, D. J. Scardino and N. I. Hammer, *Nanoscale*, 2013, **5**, 3212–3215.
121 F. Boon, D. Moerman, D. Laurencin, S. Richeter, Y. Guari, A. Mehdi, P. Dubois, R. Lazzaroni and S. Clement, *Langmuir*, 2014, **30**, 11340–11347.
122 R. S. Loewe, P. C. Ewbank, J. S. Liu, L. Zhai and R. D. McCullough, *Macromolecules*, 2001, **34**, 4324–4333.
123 V. Senkovskyy, R. Tkachov, H. Komber, A. John, J.-U. Sommer and A. Kiriy, *Macromolecules*, 2012, **45**, 7770–7777.
124 W. Liu, R. Tkachov, H. Komber, V. Senkovskyy, M. Schubert, Z. Wei, A. Facchetti, D. Neher and A. Kiriy, *Polym. Chem.*, 2014, **5**, 3404–3411.
125 The activation of thiophene substituted perylene and naphthalene diimides relies on the formation of radical anions rather than on a metathesis.
126 E. Goto, S. Nakamura, S. Kawauchi, H. Mori, M. Ueda and T. Higashihara, *J. Polym. Sci., Part A: Polym. Chem.*, 2014, **52**, 2287–2296.
127 S.-H. Kim, *Macromol. Res.*, 2014, **22**, 859–863.
128 P. Willot, J. Steverlynck, D. Moerman, P. Leclere, R. Lazzaroni and G. Koeckelberghs, *Polym. Chem.*, 2013, **4**, 2662–2671.
129 M. Verswyvel, P. Verstappen, L. De Cremer, T. Verbiest and G. Koeckelberghs, *J. Polym. Sci., Part A: Polym. Chem.*, 2011, **49**, 5339–5349.
130 R. Tkachov, V. Senkovskyy, T. Beryozkina, K. Boyko, V. Bakulev, A. Lederer, K. Sahre, B. Voit and A. Kiriy, *Angew. Chem., Int. Ed.*, 2014, **53**, 2402–2407.
131 M. Knaapila, R. C. Evans, A. Gutacker, V. M. Garamus, N. K. Szekely, U. Scherf and H. D. Burrows, *Soft Matter*, 2011, **7**, 6863–6872.
132 A. Yokoyama, H. Suzuki, Y. Kubota, K. Ohuchi, H. Higashimura and T. Yokozawa, *J. Am. Chem. Soc.*, 2007, **129**, 7236–7237.
133 T. Yokozawa, H. Kohno, Y. Ohta and A. Yokoyama, *Macromolecules*, 2010, **43**, 7095–7100.
134 T. Yokozawa, R. Suzuki, M. Nojima, Y. Ohta and A. Yokoyama, *Macromol. Rapid Commun.*, 2011, **32**, 801–806.
135 Y. Yao, J. Gao, F. Bao, S. Jiang, X. Zhang and R. Ma, *RSC Adv.*, 2015, **5**, 42754–42761.
136 M. Nojima, Y. Ohta and T. Yokozawa, *J. Polym. Sci., Part A: Polym. Chem.*, 2014, **52**, 2643–2653.
137 M. Verswyvel, C. Hoebers, J. De Winter, P. Gerbaux and G. Koeckelberghs, *J. Polym. Sci., Part A: Polym. Chem.*, 2013, **51**, 5067–5074.
138 Y. Nanashima, R. Shibata, R. Miyakoshi, A. Yokoyama and T. Yokozawa, *J. Polym. Sci., Part A: Polym. Chem.*, 2012, **50**, 3628–3640.
139 E. Elmalem, A. Kiriy and W. T. S. Huck, *Macromolecules*, 2011, **44**, 9057–9061.
140 E. Elmalem, F. Biedermann, K. Johnson, R. H. Friend and W. T. S. Huck, *J. Am. Chem. Soc.*, 2012, **134**, 17769–17777.
141 J. K. Lee, S. Ko and Z. Bao, *Macromol. Rapid Commun.*, 2012, **33**, 938–942.
142 H.-H. Zhang, W. Peng, J. Dong and Q.-S. Hu, *ACS Macro Lett.*, 2016, 656–660.
143 H.-H. Zhang, C.-H. Xing, Q.-S. Hu and K. Hong, *Macromolecules*, 2015, **48**, 967–978.
144 H.-H. Zhang, Q.-S. Hu and K. Hong, *Chem. Commun.*, 2015, **51**, 14869–14872.
145 C. S. Fischer, M. C. Baier and S. Mecking, *J. Am. Chem. Soc.*, 2013, **135**, 1148–1154.
146 H.-H. Zhang, C.-H. Xing and Q.-S. Hu, *J. Am. Chem. Soc.*, 2012, **134**, 13156–13159.
147 S. Kang, R. J. Ono and C. W. Bielawski, *J. Am. Chem. Soc.*, 2013, **135**, 4984–4987.
148 M. Nojima, R. Saito, Y. Ohta and T. Yokozawa, *J. Polym. Sci., Part A: Polym. Chem.*, 2015, **53**, 543–551.

149 K. Fujita, Y. Sumino, K. Ide, S. Tamba, K. Shono, J. Shen, T. Nishino, A. Mori and T. Yasuda, *Macromolecules*, 2016, **49**, 1259–1269.
150 A. Mori, K. Ide, S. Tamba, S. Tsuji, Y. Toyomori and T. Yasuda, *Chem. Lett.*, 2014, **43**, 640–642.
151 A. Balasubramanian, T.-C. Ku, H.-P. Shih, A. Suman, H.-J. Lin, T.-W. Shih and C.-C. Han, *Polym. Chem.*, 2014, **5**, 5928–5941.
152 K. Fuji, S. Tamba, K. Shono, A. Sugie and A. Mori, *J. Am. Chem. Soc.*, 2013, **135**, 12208–12211.
153 S. Tamba, K. Shono, A. Sugie and A. Mori, *J. Am. Chem. Soc.*, 2011, **133**, 9700–9703.
154 Q. Wang, R. Takita, Y. Kikuzaki and F. Ozawa, *J. Am. Chem. Soc.*, 2010, **132**, 11420–11421.
155 J.-R. Pouliot, M. Wakioka, F. Ozawa, Y. Li and M. Leclerc, *Macromol. Chem. Phys.*, 2016, **217**, 1493–1500.
156 C.-H. Tsai, A. Fortney, Y. Qiu, R. R. Gil, D. Yaron, T. Kowalewski and K. J. T. Noonan, *J. Am. Chem. Soc.*, 2016, **138**, 6798–6804.
157 F. Livi, N. S. Gobalasingham, B. C. Thompson and E. Bundgaard, *J. Polym. Sci., Part A: Polym. Chem.*, 2016, **54**, 2907–2918.
158 J.-R. Pouliot, F. Grenier, J. T. Blaskovits, S. Beaupré and M. Leclerc, *Chem. Rev.*, 2016, **116**, 14225–14274.
159 Y. Lee and E. D. Gomez, *Macromolecules*, 2015, **48**, 7385–7395.
160 J. Wang and T. Higashihara, *Polym. Chem.*, 2013, **4**, 5518–5526.
161 Macrophase separation of polymer blends (in particular with fullerene derivatives) may lead to a sintering of the active layer and reduced efficiencies due to decreased boundary interface.
162 N. Hadjichristidis, M. Pitsikalis and H. Iatrou, in *Block Copolymers I*, ed. V. Abetz, Springer Berlin Heidelberg, 2005, vol. 189, ch. 5, pp. 1–124.
163 H. Hsieh and R. P. Quirk, *Anionic Polymerization: Principles and Practical Applications*, Marcel Dekker, Inc., New York, 1996.
164 Y. Xiang, H. Cong, L. Li and S. Zheng, *J. Polym. Sci., Part A: Polym. Chem.*, 2016, **54**, 1852–1863.
165 S. E. Mastroianni, J. P. Patterson, R. K. O'Reilly and I. I. I. T. H. Epps, *Soft Matter*, 2013, **9**, 10146–10154.
166 M. Zorn, S. A. Weber, M. N. Tahir, W. Tremel, H. J. Butt, R. Berger and R. Zentel, *Nano Lett.*, 2010, **10**, 2812–2816.
167 J. Lim, L. z. Borg, S. Dolezel, F. Schmid, K. Char and R. Zentel, *Macromol. Rapid Commun.*, 2014, **35**, 1685–1691.
168 L. zur Borg, D. Lee, J. Lim, W. K. Bae, M. Park, S. Lee, C. Lee, K. Char and R. Zentel, *J. Mater. Chem. C*, 2013, **1**, 1722–1726.
169 L. zur Borg, A. L. Domanski, A. Breivogel, M. Buerger, R. Berger, K. Heinze and R. Zentel, *J. Mater. Chem. C*, 2013, **1**, 1223–1230.
170 J. C. Brendel, H. Burchardt and M. Thelakkat, *J. Mater. Chem.*, 2012, **22**, 24386–24393.
171 P. E. Williams, A. O. Moughton, J. P. Patterson, S. Khodabakhsh and R. K. O'Reilly, *Polym. Chem.*, 2011, **2**, 720–729.
172 S. King, M. Sommer, S. Huettner, M. Thelakkat and S. A. Haque, *J. Mater. Chem.*, 2009, **19**, 5436–5441.
173 S. M. Lindner, N. Kaufmann and M. Thelakkat, *Org. Electron.*, 2007, **8**, 69–75.
174 M. Szwarc, *J. Polym. Sci., Part A: Polym. Chem.*, 1998, **36**, IX–XV.
175 N. Hadjichristidis, M. Pitsikalis, S. Pispas and H. Iatrou, *Chem. Rev.*, 2001, **101**, 3747–3792.
176 B.-G. Kang, S. Song, B. Cho, N.-G. Kang, M.-J. Kim, T. Lee and J.-S. Lee, *J. Polym. Sci., Part A: Polym. Chem.*, 2014, **52**, 2625–2632.
177 B.-G. Kang, Y.-G. Yu, N.-G. Kang and J.-S. Lee, *J. Polym. Sci., Part A: Polym. Chem.*, 2013, **51**, 4233–4239.
178 *Controlled and Living Polymerizations: From Mechanisms to Applications*, ed. K. Matyjaszewski and A. H. E. Mueller, Wiley-VCH Verlag GmbH & Co. KGaA, Weinheim, 2009.
179 I. Cosemans, J. Vandenbergh, V. S. D. Voet, K. Loos, L. Lutsen, D. Vanderzande and T. Junkers, *Polymer*, 2013, **54**, 1298–1304.
180 H. Gu, R. Ciganda, R. Hernandez, P. Castel, P. Zhao, J. Ruiz and D. Astruc, *Macromol. Rapid Commun.*, 2016, **37**, 630–636.
181 H. Gu, R. Ciganda, R. Hernandez, P. Castel, A. Vax, P. Zhao, J. Ruiz and D. Astruc, *Polym. Chem.*, 2016, **7**, 2358–2371.
182 R. Charvet, S. Acharya, J. P. Hill, M. Akada, M. Liao, S. Seki, Y. Honsho, A. Saeki and K. Ariga, *J. Am. Chem. Soc.*, 2009, **131**, 18030–18031.
183 H. B. Gu, R. Ciganda, P. Castel, J. Ruiz and D. Astruc, *Macromolecules*, 2016, **49**, 4763–4773.
184 S.-W. Chang and M. Horie, *Chem. Commun.*, 2015, **51**, 9113–9116.
185 F. Menk, S. Shin, K.-O. Kim, M. Scherer, D. Gehrig, F. Laquai, T.-L. Choi and R. Zentel, *Macromolecules*, 2016, **49**, 2085–2095.
186 C. Zhang, S. Choi, J. Haliburton, T. Cleveland, R. Li, S.-S. Sun, A. Ledbetter and C. E. Bonner, *Macromolecules*, 2006, **39**, 4317–4326.
187 E. N. Hooley, D. J. Jones, N. C. Greenham, K. P. Ghiggino and T. D. M. Bell, *J. Phys. Chem. B*, 2015, **119**, 7266–7274.
188 C. Yan, A. J. Cadby, A. J. Parnell, W. Tang, M. W. A. Skoda, D. Mohamad, S. P. King, L. X. Reynolds, S. A. Haque, T. Wang, S. R. Parnell, A. B. Holmes, R. A. L. Jones and D. J. Jones, *J. Polym. Sci., Part B: Polym. Phys.*, 2013, **51**, 1705–1718.
189 P.-T. Wu, G. Ren, C. Li, R. Mezzenga and S. A. Jenekhe, *Macromolecules*, 2009, **42**, 2317–2320.
190 Y. Zhang, K. Tajima, K. Hirota and K. Hashimoto, *J. Am. Chem. Soc.*, 2008, **130**, 7812–7813.
191 M. Verswyvel, F. Monnaie and G. Koeckelberghs, *Macromolecules*, 2011, **44**, 9489–9498.
192 Y.-H. Lee, Y.-P. Lee, C.-J. Chiang, F.-K. Wei, C.-H. Wu, W.-C. Chen, C. Shen, H.-A. Jeng, L. Wang, M.-W. Liu, Y.-F. Chen, T. Yokozawa and C.-A. Dai, *J. Mater. Chem. A*, 2014, **2**, 14600–14612.
193 X. Q. Zhang, W. W. Yang, F. Kong, H. Yang and B. P. Lin, *Polym. Int.*, 2013, **62**, 204–209.

194 Y.-H. Lee, W.-C. Chen, Y.-L. Yang, C.-J. Chiang, T. Yokozawac and C.-A. Dai, *Nanoscale*, 2014, **6**, 5208–5216.
195 L. M. Kozycz, D. Gao, J. Hollinger and D. S. Seferos, *Macromolecules*, 2012, **45**, 5823–5832.
196 K. Van den Bergh, I. Cosemans, T. Verbiest and G. Koeckelberghs, *Macromolecules*, 2010, **43**, 3794–3800.
197 K. Umezawa, T. Oshima, M. Yoshizawa-Fujita, Y. Takeoka and M. Rikukawa, *ACS Macro Lett.*, 2012, **1**, 969–972.
198 S. Kudret, N. Van den Brande, M. Defour, B. Van Mele, L. Lutsen, D. Vanderzande and W. Maes, *Polym. Chem.*, 2014, **5**, 1832–1837.
199 M. Verswyvel, J. Steverlynck, S. Hadj Mohamed, M. Trabelsi, B. Champagne and G. Koeckelberghs, *Macromolecules*, 2014, **47**, 4668–4675.
200 K. Ohshimizu, A. Takahashi, T. Higashihara and M. Ueda, *J. Polym. Sci., Part A: Polym. Chem.*, 2011, **49**, 2709–2714.
201 S.-H. Chan, C.-S. Lai, H.-L. Chen, C. Ting and C.-P. Chen, *Macromolecules*, 2011, **44**, 8886–8891.
202 A. Sui, X. Shi, S. Wu, H. Tian, Y. Geng and F. Wang, *Macromolecules*, 2012, **45**, 5436–5443.
203 A. E. Javier, S. R. Varshney and R. D. McCullough, *Macromolecules*, 2010, **43**, 3233–3237.
204 K. Ohshimizu and M. Ueda, *Macromolecules*, 2008, **41**, 5289–5294.
205 P. Willot, S. Govaerts and G. Koeckelberghs, *Macromolecules*, 2013, **46**, 8888–8895.
206 T. Higashihara, K. Ohshimizu, Y. Ryo, T. Sakurai, A. Takahashi, S. Nojima, M. Ree and M. Ued, *Polymer*, 2011, **52**, 3687–3695.
207 J. Kim, A. Siva, I. Y. Song and T. Park, *Polymer*, 2011, **52**, 3704–3709.
208 I. Y. Song, J. Kim, M. J. Im, B. J. Moon and T. Park, *Macromolecules*, 2012, **45**, 5058–5068.
209 T. Yokozawa, I. Adachi, R. Miyakoshi and A. Yokoyama, *High Perform. Polym.*, 2007, **19**, 684–699.
210 F. Boon, N. Hergue, G. Deshayes, D. Moerman, S. Desbief, J. De Winter, P. Gerbaux, Y. H. Geerts, R. Lazzaroni and P. Dubois, *Polym. Chem.*, 2013, **4**, 4303–4307.
211 F. Ouhib, A. Khoukh, J.-B. Ledeuil, H. Martinez, J. Desbrieres and C. Dagron-Lartigau, *Macromolecules*, 2008, **41**, 9736–9743.
212 A. D. Todd and C. W. Bielawski, *ACS Macro Lett.*, 2015, **4**, 1254–1258.
213 Y.-C. Lai, K. Ohshimizu, A. Takahashi, J.-C. Hsu, T. Higashihara, M. Ueda and W.-C. Chen, *J. Polym. Sci., Part A: Polym. Chem.*, 2011, **49**, 2577–2587.
214 C. R. Bridges, H. Yan, A. A. Pollit and D. S. Seferos, *ACS Macro Lett.*, 2014, **3**, 671–674.
215 F. Ouhib, S. Desbief, R. Lazzaroni, J. De Winter, P. Gerbaux, C. Jerome and C. Detrembleur, *Macromolecules*, 2012, **45**, 6796–6806.
216 F. Ouhib, S. Desbief, R. Lazzaroni, S. Melinte, C. A. Dutu, C. Jerome and C. Detrembleur, *Polym. Chem.*, 2013, **4**, 4151–4161.
217 C. Suspene, L. Miozzo, J. Choi, R. Gironda, B. Geffroy, D. Tondelier, Y. Bonnassieux, G. Horowitz and A. Yassar, *J. Mater. Chem.*, 2012, **22**, 4511–4518.
218 A. Yokoyama, A. Kato, R. Miyakoshi and T. Yokozawa, *Macromolecules*, 2008, **41**, 7271–7273.
219 S. Clement, F. Meyer, J. De Winter, O. Coulembier, C. M. L. V. Velde, M. Zeller, P. Gerbaux, J.-Y. Balandier, S. Sergeyev, R. Lazzaroni, Y. Geerts and P. Dubois, *J. Org. Chem.*, 2010, **75**, 1561–1568.
220 D. Gao, J. Hollinger and D. S. Seferos, *ACS Nano*, 2012, **6**, 7114–7121.
221 E. F. Palermo and A. J. McNeil, *Macromolecules*, 2012, **45**, 5948–5955.
222 R. Tkachov, H. Komber, S. Rauch, A. Lederer, U. Oertel, L. Haeussler, B. Voit and A. Kiriy, *Macromolecules*, 2014, **47**, 4994–5001.
223 S. J. Ananthakrishnan, J. Strain, N. Neerudu Sreeramulu, A. Mitul, L. E. McNamara, A. Iefanova, N. I. Hammer, Q. Qiao and H. Rathnayake, *J. Polym. Sci., Part A: Polym. Chem.*, 2016, **54**, 3032–3045.
224 R. J. Ono, A. D. Todd, Z. Hu, D. A. Vanden Bout and C. W. Bielawski, *Macromol. Rapid Commun.*, 2014, **35**, 204–209.
225 L.-M. Gao, Y.-Y. Hu, Z.-P. Yu, N. Liu, J. Yin, Y.-Y. Zhu, Y. Ding and Z.-Q. Wu, *Macromolecules*, 2014, **47**, 5010–5018.
226 M. Su, N. Liu, Q. Wang, H. Wang, J. Yin and Z.-Q. Wu, *Macromolecules*, 2016, **49**, 110–119.
227 Z.-Q. Wu, D.-F. Liu, Y. Wang, N. Liu, J. Yin, Y.-Y. Zhu, L.-Z. Qiu and Y.-S. Ding, *Polym. Chem.*, 2013, **4**, 4588–4595.
228 Z.-P. Yu, C.-H. Ma, Q. Wang, N. Liu, J. Yin and Z.-Q. Wu, *Macromolecules*, 2016, **49**, 1180–1190.
229 Y.-Y. Zhu, T.-T. Yin, J. Yin, N. Liu, Z.-P. Yu, Y.-W. Zhu, Y.-S. Ding, J. Yin and Z.-Q. Wu, *RSC Adv.*, 2014, **4**, 40241–40250.
230 C. M. Preuss and C. Barner-Kowollik, *Macromol. Theory Simul.*, 2011, **20**, 700–708.
231 C. Barner-Kowollik, *Macromol. Rapid Commun.*, 2009, **30**, 1625–1631.
232 P. Kumari, K. Khawas, S. Hazra and B. K. Kuila, *J. Polym. Sci., Part A: Polym. Chem.*, 2016, **54**, 1785–1794.
233 H. Erothu, J. Kolomanska, P. Johnston, S. Schumann, D. Deribew, D. T. W. Toolan, A. Gregori, C. Dagron-Lartigau, G. Portale, W. Bras, T. Arnold, A. Distler, R. C. Hiorns, P. Mokarian-Tabari, T. W. Collins, J. R. Howse and P. D. Topham, *Macromolecules*, 2015, **48**, 2107–2117.
234 M. Hufnagel, M. Fischer, T. Thurn-Albrecht and M. Thelakkat, *Polym. Chem.*, 2015, **6**, 813–826.
235 R. Peng, B. Pang, D. Hu, M. Chen, G. Zhang, X. Wang, H. Lu, K. Cho and L. Qiu, *J. Mater. Chem. C*, 2015, **3**, 3599–3606.
236 Y. Tao, B. McCulloch, S. Kim and R. A. Segalman, *Soft Matter*, 2009, **5**, 4219–4230.
237 E. Bicciocchi, M. Haeussler, E. Rizzardo, A. D. Scully and K. P. Ghiggino, *J. Polym. Sci., Part A: Polym. Chem.*, 2015, **53**, 888–903.
238 R. H. Lohwasser and M. Thelakkat, *Macromolecules*, 2012, **45**, 3070–3077.
239 M. R. Kern and S. G. Boyes, *J. Polym. Sci., Part A: Polym. Chem.*, 2014, **52**, 3575–3585.
240 D. Han, X. Tong, Y. Zhao and Y. Zhao, *Angew. Chem., Int. Ed.*, 2010, **49**, 9162–9165.

241 T. M. S. K. Pathiranage, H. D. Magurudeniya, M. P. Bhatt, E. A. Rainbolt, M. C. Biewer and M. C. Stefan, *Polymer*, 2015, **72**, 317–326.
242 K. Palaniappan, N. Hundt, P. Sista, H. Nguyen, J. Hao, M. P. Bhatt, Y.-Y. Han, E. A. Schmiedel, E. E. Sheina, M. C. Biewer and M. C. Stefan, *J. Polym. Sci., Part A: Polym. Chem.*, 2011, **49**, 1802–1808.
243 M. C. Iovu, C. R. Craley, M. Jeffries-El, A. B. Krankowski, R. Zhang, T. Kowalewski and R. D. McCullough, *Macromolecules*, 2007, **40**, 4733–4735.
244 M. Sommer, A. S. Lang and M. Thelakkat, *Angew. Chem., Int. Ed.*, 2008, **47**, 7901–7904.
245 M. Sommer, S. Huettner, U. Steiner and M. Thelakkat, *Appl. Phys. Lett.*, 2009, **95**, 183308.
246 R. H. Lohwasser, G. Gupta, P. Kohn, M. Sommer, A. S. Lang, T. Thurn-Albrecht and M. Thelakkat, *Macromolecules*, 2013, **46**, 4403–4410.
247 S. Huettner, M. Sommer, J. Hodgkiss, P. Kohn, T. Thurn-Albrecht, R. H. Friend, U. Steiner and M. Thelakkat, *ACS Nano*, 2011, **5**, 3506–3515.
248 S. Huettner, J. M. Hodgkiss, M. Sommer, R. H. Friend, U. Steiner and M. Thelakkat, *J. Phys. Chem. B*, 2012, **116**, 10070–10078.
249 G. Gupta, C. R. Singh, R. H. Lohwasser, M. Himmerlich, S. Krischok, P. Mueller-Buschbaum, M. Thelakkat, H. Hoppe and T. Thurn-Albrecht, *ACS Appl. Mater. Interfaces*, 2015, **7**, 12309–12318.
250 Y.-K. Fang, C.-L. Liu, C. Li, C.-J. Lin, R. Mezzenga and W.-C. Chen, *Adv. Funct. Mater.*, 2010, **20**, 3012–3024.
251 L. zur Borg, C. Schuell, H. Frey and R. Zentel, *Macromol. Rapid Commun.*, 2013, **34**, 1213–1219.
252 L. zur Borg, A. L. Domanski, R. Berger and R. Zentel, *Macromol. Chem. Phys.*, 2013, **214**, 975–984.
253 N. Sary, F. Richard, C. Brochon, N. Leclerc, P. Leveque, J.-N. Audinot, S. Berson, T. Heiser, G. Hadziioannou and R. Mezzenga, *Adv. Mater.*, 2010, **22**, 763–768.
254 N. Sary, L. Rubatat, C. Brochon, G. Hadziioannou, J. Ruokolainen and R. Mezzenga, *Macromolecules*, 2007, **40**, 6990–6997.
255 T. Higashihara, K. Ohshimizu, A. Hirao and M. Ueda, *Macromolecules*, 2008, **41**, 9505–9507.
256 W. Wu, H. Xu, D. Shen, T. Qiu and L.-J. Fan, *J. Polym. Sci., Part A: Polym. Chem.*, 2013, **51**, 1636–1644.
257 J. Park, K. S. Lee, C. Choi, J. Kwak, H. C. Moon and J. K. Kim, *Macromolecules*, 2016, **49**, 3647–3653.
258 A. E. Javier, S. N. Patel, D. T. Hallinan, V. Srinivasan and N. P. Balsara, *Angew. Chem., Int. Ed.*, 2011, **50**, 9848–9851.
259 Z. Gu, T. Kanto, K. Tsuchiya, T. Shimomura and K. Ogino, *J. Polym. Sci., Part A: Polym. Chem.*, 2011, **49**, 2645–2652.
260 H. Erothu, A. A. Sohdi, A. C. Kumar, A. J. Sutherland, C. Dagron-Lartigau, A. Allal, R. C. Hiorns and P. D. Topham, *Polym. Chem.*, 2013, **4**, 3652–3655.
261 J. Chen, X. Yu, K. Hong, J. M. Messman, D. L. Pickel, K. Xiao, M. D. Dadmun, J. W. Mays, A. J. Rondinone, B. G. Sumpter and S. M. Kilbey Ii, *J. Mater. Chem.*, 2012, **22**, 13013–13022.
262 P. M. Reichstein, S. Goedrich, G. Papastavrou and M. Thelakkat, *Macromolecules*, 2016, **49**, 5484–5493.
263 I. Cosemans, J. Vandenbergh, L. Lutsen, D. Vanderzande and T. Junkers, *Polym. Chem.*, 2013, **4**, 3471–3479.
264 T. Higashihara, C.-L. Liu, W.-C. Chen and M. Ueda, *Polymers*, 2011, **3**, 236–251.
265 Y. Wu, H. Hu, J. Hu, T. Liu, G. Zhang and S. Liu, *Langmuir*, 2013, **29**, 3711–3720.
266 H. Fujita, T. Michinobu, M. Tokita, M. Ueda and T. Higashihara, *Macromolecules*, 2012, **45**, 9643–9656.
267 L. Pessoni, J. De Winter, M. Surin, N. Hergué, N. Delbosc, R. Lazzaroni, P. Dubois, P. Gerbaux and O. Coulembier, *Macromolecules*, 2016, **49**, 3001–3008.
268 K. A. Smith, D. L. Pickel, K. Yager, K. Kisslinger and R. Verduzco, *J. Polym. Sci., Part A: Polym. Chem.*, 2014, **52**, 154–163.
269 Y.-H. Lin, K. A. Smith, C. N. Kempf and R. Verduzco, *Polym. Chem.*, 2013, **4**, 229–232.
270 R. Verduzco, I. Botiz, D. L. Pickel, S. M. Kilbey, K. Hong, E. Dimasi and S. B. Darling, *Macromolecules*, 2011, **44**, 530–539.
271 C. Guo, Y.-H. Lin, M. D. Witman, K. A. Smith, C. Wang, A. Hexemer, J. Strzalka, E. D. Gomez and R. Verduzco, *Nano Lett.*, 2013, **13**, 2957–2963.
272 M. Sommer, H. Komber, S. Huettner, R. Mulherin, P. Kohn, N. C. Greenham and W. T. S. Huck, *Macromolecules*, 2012, **45**, 4142–4151.
273 J. W. Mok, Y.-H. Lin, K. G. Yager, A. D. Mohite, W. Nie, S. B. Darling, Y. Lee, E. Gomez, D. Gosztola, R. D. Schaller and R. Verduzco, *Adv. Funct. Mater.*, 2015, **25**, 5578–5585.
274 F. Lombeck, H. Komber, A. Sepe, R. H. Friend and M. Sommer, *Macromolecules*, 2015, **48**, 7851–7860.
275 J. Wang, M. Ueda and T. Higashihara, *ACS Macro Lett.*, 2013, **2**, 506–510.
276 J. Wang, M. Ueda and T. Higashihara, *J. Polym. Sci., Part A: Polym. Chem.*, 2014, **52**, 1139–1148.
277 S. Wang, Y. Guo, J. Yang, Y. Tao and W. Huang, *Chin. J. Chem.*, 2015, **33**, 865–872.
278 S.-Y. Ku, M. A. Brady, N. D. Treat, J. E. Cochran, M. J. Robb, E. J. Kramer, M. L. Chabinyc and C. J. Hawker, *J. Am. Chem. Soc.*, 2012, **134**, 16040–16046.
279 R. C. Mulherin, S. Jung, S. Huettner, K. Johnson, P. Kohn, M. Sommer, S. Allard, U. Scherf and N. C. Greenham, *Nano Lett.*, 2011, **11**, 4846–4851.
280 D. Izuhara and T. M. Swager, *Macromolecules*, 2011, **44**, 2678–2684.
281 K. Nakabayashi and H. Mori, *J. Nanomater.*, 2015, **2015**, 1–8.
282 K. Nakabayashi and H. Mori, *Macromolecules*, 2012, **45**, 9618–9625.
283 T. Erdmann, J. Back, R. Tkachov, A. Ruff, B. Voit, S. Ludwigs and A. Kiriy, *Polym. Chem.*, 2014, **5**, 5383–5390.
284 R. C. Hiorns, E. Cloutet, E. Ibarboure, A. Khoukh, H. Bejbouji, L. Vignau and H. Cramail, *Macromolecules*, 2010, **43**, 6033–6044.
285 L. Perrin, M. Legros and R. Mercier, *Macromolecules*, 2015, **48**, 323–336.

286 C. P. Radano, O. A. Scherman, N. Stingelin-Stutzmann, C. Mueller, D. W. Breiby, P. Smith, R. A. J. Janssen and E. W. Meijer, *J. Am. Chem. Soc.*, 2005, **127**, 12502–12503.
287 C. Mueller, S. Goffri, D. W. Breiby, J. W. Andreasen, H. D. Chanzy, R. A. J. Janssen, M. M. Nielsen, C. P. Radano, H. Sirringhaus, P. Smith and N. Stingelin-Stutzmann, *Adv. Funct. Mater.*, 2007, **17**, 2674–2679.
288 B. W. Boudouris, C. D. Frisbie and M. A. Hillmyer, *Macromolecules*, 2008, **41**, 67–75.
289 C. Feng, Y. Li, D. Yang, J. Hu, X. Zhang and X. Huang, *Chem. Soc. Rev.*, 2011, **40**, 1282–1295.
290 H.-i. Lee, J. Pietrasik, S. S. Sheiko and K. Matyjaszewski, *Prog. Polym. Sci.*, 2010, **35**, 24–44.
291 R. Verduzco, X. Li, S. L. Pesek and G. E. Stein, *Chem. Soc. Rev.*, 2015, **44**, 2405–2420.
292 D. Yang, C. Feng and J. Hu, *Polym. Chem.*, 2013, **4**, 2384–2394.
293 C. Duan, K.-S. Chen, F. Huang, H.-L. Yip, S. Liu, J. Zhang, A. K. Y. Jen and Y. Cao, *Chem. Mater.*, 2010, **22**, 6444–6452.
294 J. Wang, C. Lu, T. Mizobe, M. Ueda, W.-C. Chen and T. Higashihara, *Macromolecules*, 2013, **46**, 1783–1793.
295 T. L. Benanti, A. Kalaydjian and D. Venkataraman, *Macromolecules*, 2008, **41**, 8312–8315.
296 J. Steverlynck, J. De Winter, P. Gerbaux, R. Lazzaroni, P. Leclère and G. Koeckelberghs, *Macromolecules*, 2015, **48**, 8789–8796.
297 C. Huang, M. M. Sartin, M. Cozzuol, N. Siegel, S. Barlow, J. W. Perry and S. R. Marder, *J. Phys. Chem. A*, 2012, **116**, 4305–4317.
298 D. F. Zeigler, K. A. Mazzio and C. K. Luscombe, *Macromolecules*, 2014, **47**, 5019–5028.
299 D. van As, J. Subbiah, D. J. Jones and W. W. H. Wong, *Macromol. Chem. Phys.*, 2016, **217**, 403–413.
300 N. Khanduyeva, V. Senkovskyy, T. Beryozkina, M. Horecha, M. Stamm, C. Uhrich, M. Riede, K. Leo and A. Kiriy, *J. Am. Chem. Soc.*, 2009, **131**, 153–161.
301 S. Jung, W. Kwon, D. Wi, J. Kim, B. J. Ree, Y. Y. Kim, W. J. Kim and M. Ree, *Macromolecules*, 2016, **49**, 1369–1382.
302 N. Khanduyeva, V. Senkovskyy, T. Beryozkina, V. Bocharova, F. Simon, M. Nitschke, M. Stamm, R. Groetzschel and A. Kiriy, *Macromolecules*, 2008, **41**, 7383–7389.
303 J. Yan, Q. Ye, X. Han and F. Zhou, *RSC Adv.*, 2013, **3**, 166–171.
304 Z. Hu and E. Reichmanis, *J. Polym. Sci., Part A: Polym. Chem.*, 2011, **49**, 1155–1162.
305 M. Rymarczyk-Machal, S. Zapotoczny and M. Nowakowska, *J. Polym. Sci., Part A: Polym. Chem.*, 2006, **44**, 2675–2683.
306 F. Guo, B. Wang, H. Ma, T. Li and Y. Li, *J. Polym. Sci., Part A: Polym. Chem.*, 2016, **54**, 735–739.
307 X. Yin, Y. Qiao, M. R. Gadinski, Q. Wang and C. Tang, *Polym. Chem.*, 2016, **7**, 2929–2933.
308 Z. Chen, E. M. Grumstrup, A. T. Gilligan, J. M. Papanikolas and K. S. Schanze, *J. Phys. Chem. B*, 2014, **118**, 372–378.
309 X. Pang, L. Zhao, C. Feng, R. Wu, H. Ma and Z. Lin, *Polym. Chem.*, 2013, **4**, 2025–2032.
310 S. K. Ahn, D. L. Pickel, W. M. Kochemba, J. H. Chen, D. Uhrig, J. P. Hinestrosa, J. M. Carrillo, M. Shao, C. Do, J. M. Messman, W. M. Brown, B. G. Sumpter and S. M. Kilbey, *ACS Macro Lett.*, 2013, **2**, 761–765.
311 Y. Liu, T. Pauloehrl, S. I. Presolski, L. Albertazzi, A. R. A. Palmans and E. W. Meijer, *J. Am. Chem. Soc.*, 2015, **137**, 13096–13105.
312 T. Sukegawa, I. Masuko, K. Oyaizu and H. Nishide, *Macromolecules*, 2014, **47**, 8611–8617.
313 Z. Wu, C. Sun, S. Dong, X.-F. Jiang, S. Wu, H. Wu, H.-L. Yip, F. Huang and Y. Cao, *J. Am. Chem. Soc.*, 2016, **138**, 2004–2013.
314 A. R. Davis and K. R. Carter, *Macromolecules*, 2015, **48**, 1711–1722.
315 C. Xue, F.-T. Luo and H. Liu, *Macromolecules*, 2007, **40**, 6863–6870.
316 Z.-H. Guo, N. Ai, C. R. McBroom, T. Yuan, Y.-H. Lin, M. Roders, C. Zhu, A. L. Ayzner, J. Pei and L. Fang, *Polym. Chem.*, 2016, **7**, 648–655.
317 J. De Girolamo, P. Reiss and A. Pron, *J. Phys. Chem. C*, 2007, **111**, 14681–14688.
318 Z. Zhang, X. Lu, Q. Fan, W. Hu and W. Huang, *Polym. Chem.*, 2011, **2**, 2369–2377.
319 P. Wittmeyer, S. Traser, R. Sander, K. B. Sondergeld, A. Ungefug, R. Weiss and M. Rehahn, *Macromol. Chem. Phys.*, 2016, **217**, 1473–1487.
320 X. Yang, J. Ge, M. He, Z. Ye, X. Liu, J. Peng and F. Qiu, *Macromolecules*, 2016, **49**, 287–297.
321 C. Xing, L. Liu, Z. Shi, Y. Li and S. Wang, *Adv. Funct. Mater.*, 2010, **20**, 2175–2180.
322 C. J. Mueller, T. Klein, E. Gann, C. R. McNeill and M. Thelakkat, *Macromolecules*, 2016, **49**, 3749–3760.
323 B. A. G. Hammer, F. A. Bokel, R. C. Hayward and T. Emrick, *Chem. Mater.*, 2011, **23**, 4250–4256.
324 E. Blasco, B. Yameen, A. S. Quick, P. Krolla-Sidenstein, A. Welle, M. Wegener and C. Barner-Kowollik, *Macromolecules*, 2015, **48**, 8718–8728.
325 W. Lee, J.-S. Kim, H. J. Kim, J. M. Shin, K. H. Ku, H. Yang, J. Lee, J. G. Bae, W. B. Lee and B. J. Kim, *Macromolecules*, 2015, **48**, 5563–5569.
326 J. Yao, C. Yu, Z. Liu, H. Luo, Y. Yang, G. Zhang and D. Zhang, *J. Am. Chem. Soc.*, 2016, **138**, 173–185.
327 Y. Qiu, J. C. Worch, A. Fortney, C. Gayathri, R. R. Gil and K. J. T. Noonan, *Macromolecules*, 2016, **49**, 4757–4762.
328 S.-F. Yang, Z.-T. Liu, Z.-X. Cai, H.-W. Luo, P.-L. Qi, G.-X. Zhang and D.-Q. Zhang, *Macromolecules*, 2016, **49**, 5857–5865.
329 J. Motoyanagi, T. Ishikawa and M. Minoda, *J. Polym. Sci., Part A: Polym. Chem.*, 2016, **54**, 3318–3325.
330 B. Zhang, Z. Xie and L. Wang, *Polym. Bull.*, 2012, **68**, 829–845.
331 Y.-S. Yoon, H.-S. Sohn and J.-C. Lee, *Polymer*, 2009, **50**, 1395–1402.
332 H. Zhao, B. Zhu, J. Sekine, S.-C. Luo and H.-h. Yu, *ACS Appl. Mater. Interfaces*, 2012, **4**, 680–686.
333 C. B. Nielsen, A. Giovannitti, D.-T. Sbircea, E. Bandiello, M. R. Niazi, D. A. Hanifi, M. Sessolo, A. Amassian, G. G. Malliaras, J. Rivnay and I. McCulloch, *J. Am. Chem. Soc.*, 2016, **138**, 10252–10259.

334 L. Zhai, R. L. Pilston, K. L. Zaiger, K. K. Stokes and R. D. McCullough, *Macromolecules*, 2003, **36**, 61–64.
335 C. B. Nielsen, A. Giovannitti, D.-T. Sbircea, E. Bandiello, M. R. Niazi, D. A. Hanifi, M. Sessolo, A. Amassian, G. G. Malliaras, J. Rivnay and I. McCulloch, *J. Am. Chem. Soc.*, 2016, **138**, 10252–10259.
336 K. W. Cheng, C. S. C. Mak, W. K. Chan, A. M. C. Ng and A. B. Djurisic, *J. Polym. Sci., Part A: Polym. Chem.*, 2008, **46**, 1305–1317.
337 C. N. Fleming, M. K. Brennaman, J. M. Papanikolas and T. J. Meyer, *Dalton Trans.*, 2009, 3903–3910.
338 Z. Fang, A. Ito, A. C. Stuart, H. Luo, Z. Chen, K. Vinodgopal, W. You, T. J. Meyer and D. K. Taylor, *ACS Nano*, 2013, **7**, 7992–8002.
339 G. Leem, S. Keinan, J. Jiang, Z. Chen, T. Pho, Z. A. Morseth, Z. Hu, E. Puodziukynaite, Z. Fang, J. M. Papanikolas, J. R. Reynolds and K. S. Schanze, *Polym. Chem.*, 2015, **6**, 8184–8193.
340 Z. Fang, A. Ito, H. Luo, D. L. Ashford, J. J. Concepcion, L. Alibabaei and T. J. Meyer, *Dalton Trans.*, 2015, **44**, 8640–8648.
341 Y. Sun, Z. Chen, E. Puodziukynaite, D. M. Jenkins, J. R. Reynolds and K. S. Schanze, *Macromolecules*, 2012, **45**, 2632–2642.
342 Z. Chen, H.-Y. Hsu, M. Arca and K. S. Schanze, *J. Phys. Chem. B*, 2015, **119**, 7198–7209.
343 D. Cedeno, A. Krawicz, P. Doak, M. Yu, J. B. Neaton and G. F. Moore, *J. Phys. Chem. Lett.*, 2014, **5**, 3222–3226.
344 W. S. Aldridge, III, B. J. Hornstein, S. Serron, D. M. Dattelbaum, J. R. Schoonover and T. J. Meyer, *J. Org. Chem.*, 2006, **71**, 5186–5190.
345 M. K. Brennaman, C. N. Fleming, C. A. Slate, S. A. Serron, S. E. Bettis, B. W. Erickson, J. M. Papanikolas and T. J. Meyer, *J. Phys. Chem. B*, 2013, **117**, 6352–6363.
346 D. Ma, S. E. Bettis, K. Hanson, M. Minakova, L. Alibabaei, W. Fondrie, D. M. Ryan, G. A. Papoian, T. J. Meyer, M. L. Waters and J. M. Papanikolas, *J. Am. Chem. Soc.*, 2013, **135**, 5250–5253.
347 S. E. Bettis, D. M. Ryan, M. K. Gish, L. Alibabaei, T. J. Meyer, M. L. Waters and J. M. Papanikolas, *J. Phys. Chem. C*, 2014, **118**, 6029–6037.
348 D. M. Ryan, M. K. Coggins, J. J. Concepcion, D. L. Ashford, Z. Fang, L. Alibabaei, D. Ma, T. J. Meyer and M. L. Waters, *Inorg. Chem.*, 2014, **53**, 8120–8128.
349 K. Hanson, D. J. Wilger, S. T. Jones, D. P. Harrison, S. E. Bettis, H. Luo, J. M. Papanikolas, M. L. Waters and T. J. Meyer, *Biopolymers*, 2013, **100**, 25–37.
350 G. Leem, Z. A. Morseth, E. Puodziukynaite, J. Jiang, Z. Fang, A. T. Gilligan, J. R. Reynolds, J. M. Papanikolas and K. S. Schanze, *J. Phys. Chem. C*, 2014, **118**, 28535–28541.
351 Z. A. Morseth, L. Wang, E. Puodziukynaite, G. Leem, A. T. Gilligan, T. J. Meyer, K. S. Schanze, J. R. Reynolds and J. M. Papanikolas, *Acc. Chem. Res.*, 2015, **48**, 818–827.
352 E. Puodziukynaite, L. Wang, K. S. Schanze, J. M. Papanikolas and J. R. Reynolds, *Polym. Chem.*, 2014, **5**, 2363–2369.
353 L. Wang, E. Puodziukynaite, E. M. Grumstrup, A. C. Brown, S. Keinan, K. S. Schanze, J. R. Reynolds and J. M. Papanikolas, *J. Phys. Chem. Lett.*, 2013, **4**, 2269–2273.
354 L. Wang, E. Puodziukynaite, R. P. Vary, E. M. Grumstrup, R. M. Walczak, O. Y. Zolotarskaya, K. S. Schanze, J. R. Reynolds and J. M. Papanikolas, *J. Phys. Chem. Lett.*, 2012, **3**, 2453–2457.
355 C. S. K. Mak, W. K. Cheung, Q. Y. Leung and W. K. Chan, *Macromol. Rapid Commun.*, 2010, **31**, 875–882.
356 J. Li and B. C. Benicewicz, *J. Polym. Sci., Part A: Polym. Chem.*, 2013, **51**, 3572–3582.
357 M. Heuken, H. Komber and B. Voit, *Macromol. Chem. Phys.*, 2012, **213**, 97–107.
358 Y. Chen, T. Midorikawa, J. Bai, Y. Liu, Y. Araki and O. Ito, *Polymer*, 2005, **46**, 9803–9809.
359 M. Heuken, H. Komber, T. Erdmann, V. Senkovskyy, A. Kiriy and B. Voit, *Macromolecules*, 2012, **45**, 4101–4114.
360 C. Yang, J. K. Lee, A. J. Heeger and F. Wudl, *J. Mater. Chem.*, 2009, **19**, 5416–5423.
361 S. Barrau, T. Heiser, F. Richard, C. Brochon, C. Ngov, K. van de Wetering, G. Hadziioannou, D. V. Anokhin and D. A. Ivanov, *Macromolecules*, 2008, **41**, 2701–2710.
362 J. U. Lee, A. Cirpan, T. Emrick, T. P. Russell and W. H. Jo, *J. Mater. Chem.*, 2009, **19**, 1483–1489.
363 E. Şennik, B. Şennik, O. Alev, N. Kılınç, F. Yilmaz and Z. Ziya Oeztuerk, *J. Appl. Polym. Sci.*, 2016, **133**, 43641.
364 M. Yamada, T. Akasaka and S. Nagase, *Chem. Rev.*, 2013, **113**, 7209–7264.
365 N. Martín, F. Giacalone and M. Prato, *Fullerene Polymers: Synthesis, Properties and Applications*, Wiley-VCH Verlag GmbH & Co. KGaA, Weinheim, Germany, 2009.
366 F. Giacalone and N. Martín, *Chem. Rev.*, 2006, **106**, 5136–5190.
367 The application of end cappers or initiators leading to reactive end groups is introduced in Section 1. The discussion in this section is limited to the attachment of functional units, *i.e.* moieties fullfilling a defined task in the final architecture.
368 I. Natori, S. Natori, A. Kanasashi, K. Tsuchiya and K. Ogino, *J. Appl. Polym. Sci.*, 2013, **128**, 4212–4216.
369 M. J. Robb, D. Montarnal, N. D. Eisenmenger, S.-Y. Ku, M. L. Chabinyc and C. J. Hawker, *Macromolecules*, 2013, **46**, 6431–6438.
370 L. Wang, Z. Qiao, C. Gao, J. Liu, Z.-G. Zhang, X. Li, Y. Li and H. Wang, *Macromolecules*, 2016, **49**, 3723–3732.
371 F. C. Krebs and M. Biancardo, *Sol. Energy Mater. Sol. Cells*, 2006, **90**, 142–165.
372 R. Schroot, T. Schlotthauer, U. S. Schubert and M. Jaeger, *Macromolecules*, 2016, **49**, 2112–2123.
373 R. Schroot, T. Schlotthauer, M. Jäger and U. S. Schubert, *Macromol. Chem. Phys.*, 2017, 1600534.
374 J. Kuebel, R. Schroot, M. Waechtler, U. S. Schubert, B. Dietzek and M. Jaeger, *J. Phys. Chem. C*, 2015, **119**, 4742–4751.
375 M. Schulze, M. Jaeger and U. S. Schubert, *Macromol. Rapid Commun.*, 2012, **33**, 579–584.
376 I. Natori, S. Natori, A. Kanasashi, K. Tsuchiya and K. Ogino, *J. Polym. Sci., Part B: Polym. Phys.*, 2013, **51**, 368–375.

Publication P2

Modular assembly of poly(naphthalene diimide) and Ru(II) dyes for an efficient light-Induced charge separation in hierarchically controlled polymer architectures

R. Schroot, T. Schlotthauer, U. S. Schubert, M. Jäger, *Macromolecules* **2016***, 49,* 2112-2123.

The paper as well as the supporting information (free of charge) are available online under: doi.org/10.1021/acs.macromol.5b02717

Macromolecules

Article

pubs.acs.org/Macromolecules

Modular Assembly of Poly(naphthalene diimide) and Ru(II) Dyes for an Efficient Light-Induced Charge Separation in Hierarchically Controlled Polymer Architectures

Robert Schroot,[†,#] Tina Schlotthauer,[†,#] Ulrich S. Schubert,[*,†,‡] and Michael Jäger[*,†,‡]

[†]Laboratory of Organic and Macromolecular Chemistry (IOMC) and [‡]Center for Energy and Environmental Chemistry Jena (CEEC Jena), Friedrich Schiller University Jena, 07743 Jena, Germany

Supporting Information

ABSTRACT: Hierarchically well-defined multielectron acceptor−photosensitizer (A_n−P) assemblies were prepared by nitroxide-mediated polymerization of a styrenic naphthalene diimide and subsequent decoration of the chain terminus by a $[Ru(dqp)_2]^{2+}$ photosensitizer (dqp is 2,6-di(quinolin-8-yl)-pyridine). In view of a facile modular design, three synthetic linkage procedures were explored aiming at tailored light-initiated energy and electron transfer processes. The polymers were conveniently purified by column chromatography using amino- or diol-functionalized silica gels and were characterized in detail by NMR, MS, and UV−vis-SEC measurements. The electrochemical and absorption data confirmed the preserved individual redox and optical properties of the building blocks. The detailed steady-state emission measurements revealed an efficient quenching of the photosensitizer exceeding 86−96% with respect to reference complexes and the partial sensitization of/by polymer-based excited states. The results demonstrate the general versatility to construct photoredox-active macromolecules from tailored building blocks.

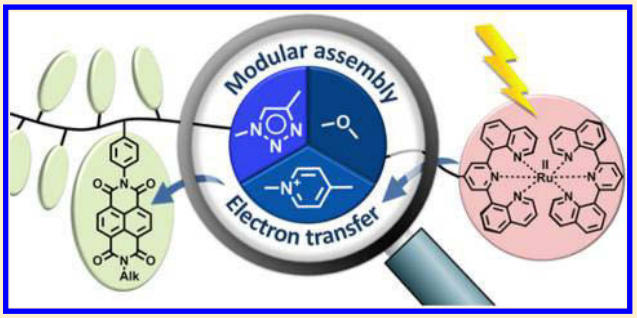

INTRODUCTION

The conversion of light energy into electrical energy and/or chemical bond energy is a key process for an environmentally friendly and sustainable power supply,[1] i.e., in photovoltaics and photosynthesis. Thereby, the latter process relies on the utilization of the generated charge carriers in coupled catalytic processes and thereby enables the storage as fuels with high energy density.[2,3] The energy conversion process is initiated by photon absorption to generate an excited state, followed by the primary charge separation, subsequent charge translocation, and ultimately the collection on an electrode (photovoltaics) or the consumption in catalytic reactions (photosynthesis). In order to obtain a high overall efficiency, all forward steps should be well tuned to minimize any undesired recombination processes.

One promising approach on a molecular level utilizes functional building blocks, i.e., electron donors (D), acceptors (A), and photosensitizer (P), which can be connected to form defined architectures with more complex functionality, i.e., photoinitiated charge separation. The strength of this (supramolecular) strategy is demonstrated by the highly efficient charge separation in molecular triad (D−P−A) systems reaching unit quantum efficacy.[4] Nevertheless, the photogenerated charges are locally trapped in such model compounds because a directional percolation pathway is essential to utilize the charge carriers in photovoltaic or photosynthetic applications. In this regard, the recent advances in polymer chemistry provide an invaluable synthetic platform to overcome the challenge of connecting multiple functional (redox-active) units. In particular, modern controlled radical polymerization techniques (e.g., NMP or RAFT polymerization processes)[5−8] enable the facile preparation of redox-active polymers (D_n and/or A_m) with a controlled degree of polymerization and dispersity ($Đ$). The utilization of functional monomers assures the formation of the fully functionalized polymer, which is often challenging to reach in a grafting approach. In addition, the facile preparation of telechelic polymers enables a postpolymerization functionalization specifically at the chain terminus, which can fulfill two important tasks with respect to efficient charge separation: First, the decoration with a terminal photosensitizer leads to *hierarchically* controlled polymer architectures, as demonstrated for D_n−P and P−A_m dyads.[9,10] Second, the simple modular assembly of the functional building blocks (D_n, P, A_m) assures a high variability to design and synthesis to explore new assembly generations.

Polymers based on naphthalene diimide (NDI) are intensively investigated as n-type semiconductors. The NDI unit exhibits reversible reduction steps, which are as well as the optical and physical properties tunable by different substituents on the molecular scaffold.[11−13] Additionally, their sizable planar π-system is capable for self-organization, e.g., a face-to-face

Received: December 16, 2015
Revised: February 15, 2016
Published: March 3, 2016

DOI: 10.1021/acs.macromol.5b02717
Macromolecules 2016, 49, 2112−2123

stacking of the units.[14−17] Main-chain conjugated NDI polymers are typically prepared by polycondensation and reach high charge charier mobilities,[18,19] whereas side-chain decorated polymers are conveniently prepared by controlled radical polymerization procedures.[10] Ruthenium polypyridyl complexes are widely used photosensitizer due to their metal-to-ligand charge transfer (MLCT) character of the excited state.[20−22] In addition to the ubiquitous $[Ru(bpy)_3]^{2+}$ complexes (bpy is 2,2′-bipyridine), e.g. in polymer-based architectures,[4,23−25] similar complexes based on 2,6-di-(quinolin-8-yl)pyridine (dqp) ligands have received increasing attention. This photosensitizer subclass displays comparably long excited states (microsecond time scale) combined with a red-shifted absorption (up to 550 nm) for an enhanced coverage of the solar spectrum.[26−28] Moreover, the parent complex $[Ru(dqp)_2]^{2+}$ was shown to exhibit an enhanced photostability in comparison to $[Ru(bpy)_3]^{2+}$.[28] Notably, very efficient photoinitiated charge separation (>95%) was achieved in D−P−A triads based on the $[Ru(dqp)_2]^{2+}$ core,[29] whereas the effective primary charge separation was recently demonstrated for a polymer-based P−A_m dyad by time-resolved spectroscopy,[10] irrespective of the highly flexible unsaturated linkage.

In this contribution, various linkage patterns are explored to prepare acceptor-photosensitizer (P−A_m) dyads based on poly(naphthalene diimides) (pNDI) and $[Ru(dqp)_2]^{2+}$-based complexes. Both functional building blocks (A_m, P) are individually synthesized and subsequently connected by nucleophilic substitution or by the application of the copper-(I)-catalyzed azide−alkyne cycloaddition (CuAAC) reaction. Chromatographic purification protocols were developed to facilitate the challenging purification of the macromolecular structures. The building blocks and dyads were characterized in detail by NMR spectroscopy, mass spectrometry, electrochemistry, and optical spectroscopy. The second part addresses the energy- and electron-transfer processes for the various linkages by steady-state absorption and emission spectroscopy. First, the quenching efficiency of the Ru-based emission was determined between the dyads and suitable reference complexes. Hence, complexes with the same substitution pattern at the ligand framework were synthesized to account for the (unknown) differences in the MLCT excited state character, i.e., emission quantum yield. Second, excitation spectra were recorded to shed light on the origin and fate of the polymer-based emission.[10] Hence, the steady-state optical characterization will provide first insights into energy- and electron-transfer pathways. In combination with the investigated synthetic procedures, the presented work and the results show the suitability of the various orthogonal linkages to ensure efficient Ru emission quenching. The facile modular assembly is believed to assist the design and synthesis of future architectures, e.g., D_n−P−A_m triads.

EXPERIMENTAL SECTION

Materials. All reagents were purchased from ABCR, Acros Organics, Alfa Aesar, Apollo Scientific, Sigma-Aldrich, or TCI Chemicals and were used without further purification unless otherwise noted. Dry pyridine and dry *N*,*N*-dimethylformamide (DMF) were commercially available. All solvents were degassed before use. THF was dried using a PureSolv-EN solvent purification system (Innovative Technology). $[Ru(dqp)(dqp\text{-}OH)][PF_6]_2$ (**3**, dqp is 2,6-di(quinolin-8-yl)pyridine, dqp-OH is 4-hydroxy-2,6-di(quinolin-8-yl)pyridine), 4-bromophenyl-2,6-di(quinolin-8-yl)pyridine (dqp-ph-Br), $[Ru(dqp)(dqp\text{-}ph\text{-}Br)][PF_6]_2$, and $[Ru(dqp)(CH_3CN)_3][PF_6]_2$ were prepared as previously described.[9,30,31] dba is dibenzylidene acetone. SPhos is 2-dicyclohexylphosphino-2′,6′-dimethoxybiphenyl. PMDETA is *N*,*N*,*N*′,*N*″,*N*″-pentamethyldiethylenetriamine.

*N-(2-Ethylhexyl)naphthalene-1,8-dicarboxyanhydride-4,5-dicarboxyimide (Adopted from Ref 32) (**1**).* Five microwave vials were each charged with 1,4,5,8-naphthalenetetracarboxylic dianhydride (0.800 g, 2.980 mmol), 2-ethylhexylamine (0.480 mL, 2.980 mmol), and dry DMF (20 mL). After the vials were capped and flushed with nitrogen for 10 min, the brown suspension was homogenized by ultrasound sonication. Subsequently, the vials were heated using microwave irradiation to 75 °C for 5 min and then to 140 °C for 15 min. The batches were combined, and the excess of solvent was removed under reduced pressure; the brown residue was resuspended in acetone (100 mL) and added dropwise to 1 M aqueous HCl (150 mL). The solid was filtered off and washed with water. The crude product was used without further purification (5.430 g, 96%, purity approximately 80% by ^{1}H NMR). ^{1}H NMR (300 MHz, $CDCl_3$): δ 8.83 (s, 4H, NaphH), 4.35−4.00 (m, 2H, CH_2), 2.12−1.86 (m, 1H, CH), 1.51−1.17 (m, 8H, 4 × CH_2), 1.06−0.69 (m, 6H, 2 × CH_3).

*N-(2-Ethylhexyl)-N′-(4-vinylphenyl)-naphthalene-1,4,5,8-dicarboxydiimide (Adopted from Ref 33) (**2**).* Crude **1** (5.430 g, 1 equiv), 4-aminostyrene (2.040 g, 1.2 equiv, 17.120 mmol), and $ZnSO_4 \cdot 1H_2O$ (1.540 g, 0.6 equiv, 8.560 mmol) were dissolved in dry pyridine (100 mL) under nitrogen. The mixture was heated to reflux for 4 h. Then the black reaction mixture, which contained white solids, was added dropwise to 1 M aqueous HCl (800 mL). After filtration the residue was dissolved in CH_2Cl_2 and washed with brine and water. The organic layer was dried over $MgSO_4$. Subsequently, the crude product was purified by two flash column chromatography runs (silica, eluent: CH_2Cl_2) to yield a yellow solid (3.300 g, 60%). ^{1}H NMR (250 MHz, $CDCl_3$): δ 8.81 (s, 4H, NaphH), 7.61 (d, J = 8.5 Hz, 2H, ArH), 7.29 (d, J = 8.5, 2H, ArH), 6.81 (dd, J = 17.5, 11.0 Hz, 1H, C**H**═CH_2), 5.84 (d, J = 17.5 Hz, 1H, CH═C**H**$_2$-trans), 5.37 (d, J = 11.0 Hz, 1H, CH═C**H**$_2$-cis), 4.32−4.02 (m, 2H, CH_2), 2.07−1.84 (m, 1H, CH), 1.49−1.21 (m, 8H, 4 × CH_2), 1.02−0.82 (m, 6H, 2 × CH_3). ^{13}C NMR (101 MHz, $CDCl_3$): δ 163.2, 163.0, 138.6, 136.0, 133.8, 131.4, 131.1, 128.6, 127.3, 127.1, 127.0, 126.9, 126.7, 115.5, 44.7, 38.0, 30.7, 28.6, 24.1, 23.0, 14.1, 10.6. Elem anal. calcd for $C_{30}H_{28}N_2O_4$: C, 74.98%; H, 5.87%; N, 5.83%; found: C, 75.10%; H, 5.75%; N, 5.69%. MS (ESI-ToF) m/z: 481.280 ($[M + H]^+$). T_d = 230 °C.

*$[Ru(dqp)(dqp\text{-}ph\text{-}C{\equiv}C{-}H)][PF_6]_2$ (**4**).* A vial was charged with $[Ru(dqp)(dqp\text{-}ph\text{-}Br)][PF_6]_2$ (0.030 g, 0.025 mmol) and $Pd(PPh_3)_4$ (0.003 g, 0.003 mmol). The vial was sealed and purged with nitrogen. Then dry DMF (3.0 mL), a fine suspension of copper(I) iodide (0.0005 g, 0.003 mmol) in DMF (0.078 mL), triethylamine (1.5 mL), and triisopropylsilylacetylene (0.006 mL) were added. Subsequently, the reaction mixture was heated to 60 °C for 16 h. Afterward, the reaction was cooled to room temperature and was precipitated in aqueous NH_4PF_6. The red precipitate was extracted from the aqueous phase with CH_2Cl_2, and the organic extracts were washed with water, dried over Na_2SO_4, and concentrated under reduced pressure. The crude product was purified by column chromatography using a mixture of acetonitrile/H_2O/$KNO_{3(aq)}$ (40/4/1) as eluent. The product fractions were combined, and the anion exchange was performed by precipitation in an aqueous NH_4PF_6 solution (0.029 g, 91%).

Deprotection. The complex (0.016 g, 0.012 mmol) was deprotected by stirring with tetrabutylammonium fluoride (0.003 g, 0.012 mmol) in a mixture of THF (2.0 mL) and MeOH (1.0 mL) overnight. The reaction mixture was quenched with water. Subsequently, the solvent was evaporated under reduced pressure, and the crude product was redissolved in a minimum amount of acetonitrile and precipitated in an aqueous NH_4PF_6 solution. The product was filtered, washed with water, and dried to yield **4** as an red solid (0.014 g, 98%). ^{1}H NMR (600 MHz, CD_3CN): δ 8.17 (t, J = 8.0 Hz, 1H), 8.12 (dd, J = 5.2, 1.4 Hz, 2H), 8.11 (s, 2H), 8.09−8.07 (m, 4H), 8.07 (s, 2H), 7.95 (m, 2H), 7.91−7.87 (m, 4H), 7.74 (dd, J = 7.4, 1.1 Hz, 2H), 7.72−7.65 (m, 6H), 7.47 (dd, J = 16.0, 8.4 Hz, 4H), 7.11−7.00 (m, 4H), 3.58 (s, 1H). ^{13}C NMR (151 MHz, CD_3CN): δ 159.5, 159.4, 158.1, 157.7, 149.4, 147.6, 147.4, 139.1, 138.6, 138.5, 137.3, 134.4, 133.9, 133.8, 132.8, 132.7, 131.6 (2×), 128.9, 128.6,

DOI: 10.1021/acs.macromol.5b02717
Macromolecules 2016, 49, 2112−2123

127.8 (2×), 127.6, 127.5, 126.2, 124.8, 123.0, 122.9, 83.4, 81.2. HR-ESI ($[C_{54}H_{34}N_6Ru]^{2+}$) *m/z*: calcd 434.0939, found: 434.0966. Error: 4.6 ppm.

*[Ru(dqp)(dqp-ph-py)][PF$_6$]$_2$ (**5**).* A microwave vial was charged with [Ru(dqp)(dqp-ph-Br)][PF$_6$]$_2$ (0.090 g, 0.098 mmol), 4-pyridylboronic acid (0.014 g, 0.114 mmol), Pd(dba)$_2$ (0.003 g, 0.006 mmol), SPhos (0.007 g, 0.018 mmol), and K_2CO_3 (0.040 g, 0.293 mmol). Then acetonitrile (3.0 mL) and water (1.5 mL) were added, and the vial was sealed. The solution was purged with nitrogen for 10 min and heated to 100 °C for 16 h. Afterward, the reaction mixture was allowed to cool to room temperature; subsequently, the mixture was added into an aqueous NH_4PF_6 solution. The fine suspension was extracted three times with CH_2Cl_2, and the combined organic layers were washed with water and brine. After drying over Na_2SO_4 the solvent was evaporated under reduced pressure, and the crude product was purified by flash column chromatography (diol-functionalized silica, eluent: CH_2Cl_2/acetonitrile 95/5). Finally, diffusion-controlled crystallization (diethyl ether into acetonitrile solution) gave the desired complex **5** (0.060 g, 67%). ^{1}H NMR (400 MHz, CD_3CN): δ 8.69 (d, J = 5.9 Hz, 2H), 8.25−8.15 (m, 3H), 8.17−8.13 (m, 2H), 8.12−8.06 (m, 8H), 8.00−7.94 (m, 2H), 7.94−7.88 (m, 4H), 7.74 (dd, J = 7.4, 1.2 Hz, 2H), 7.71 (ddd, J = 8.1, 3.3, 1.2 Hz, 6H), 7.48 (dd, J = 15.9, 8.4 Hz, 4H), 7.13−7.01 (m, 4H). ^{13}C NMR (101 MHz, CD_3CN): δ 159.5 (2×), 158.1, 157.8, 151.4, 149.7, 147.6, 147.5, 140.7, 139.2, 138.6, 138.5, 137.6, 134.5, 134.0, 132.8 (2×), 131.6, 129.2, 128.9 (2×), 127.8 (2×), 127.6, 127.5, 126.3, 123.1, 122.9, 122.4. HR-ESI ($[C_{57}H_{37}N_7Ru]^{2+}$) *m/z*: calcd: 460.6071, found: 460.6075. Error: 0.8 ppm.

Polymerization (Adopted from Ref 9) and Azide Functionalization. *Chloro-End-Functionalized Poly(naphthalene diimide) Cl-**p2**$_{17}$.* A glass tube equipped with a septum, and an external overhead flushing with nitrogen was used for the polymerization (see Supporting Information). The reaction vessel was charged with **2** (0.500 g, 1.040 mmol), *N*-(*tert*-butyl)-*O*-(1-(4-(chloromethyl)-phenyl)ethyl)-*N*-(2-methyl-1-phenylpropyl)hydroxylamine (CMSt-TIPNO) (0.019 g, 0.052 mmol), and anisole (4.0 mL), purged with nitrogen for 20 min, and placed in a preheated oil bath (120 °C). After 17 h the reaction mixture was diluted with CH_2Cl_2 and was precipitated in cold MeOH. Unreacted monomer was removed by preparative SEC (Bio-Beads S-X1, CH_2Cl_2). The polymer was obtained as a bright yellow powder after precipitation in MeOH. Yield: 0.400 g. SEC ($CHCl_3$/IPA/NEt_3 94/2/4, PS calibration): M_n = 6400 g/mol, $Đ$ = 1.11. ^{1}H NMR (300 MHz, $CDCl_3$): δ 9.04−7.98 (br), 7.78−6.66 (br), 4.73−4.42 (br), 4.36−3.60 (br), 2.92−1.71 (br), 1.51−1.05 (br), 1.05−0.45 (br). MS (MALDI-ToF, DCTB + NaTFA) *m/z*: 7,384 ($[(C_{30}H_{28}N_2O_4)_{15}C_9H_{10}Cl + Na]^+$).

*Azide-End-Functionalized Poly(naphthalene diimide) N$_3$-**p2**$_{17}$.* *Safety advice: sodium azide is very toxic; personal protection precautions should be taken. Heavy metal azides are explosive. Do not use metal spatula.* A glass vial was charged with Cl-**p2**$_{17}$ (0.033 g, 0.005 mmol, 1 equiv) and sodium azide (0.001 g, 0.016 mmol, 3 equiv), capped, and placed under a nitrogen atmosphere. Dry DMF (1 mL) was added, and the reaction mixture was immersed in an oil bath at 60 °C at which the polymer dissolved. After 48 h CH_2Cl_2 and water were added to the formed suspension, and the layers were separated. The aqueous layer was extracted two times with CH_2Cl_2. The combined organic layers were washed with brine and dried over Na_2SO_4. After removal of the solvent under reduced pressure, a yellow solid was obtained. Yield: 0.033 g. SEC ($CHCl_3$/IPA/NEt_3 94/2/4, PS calibration): M_n = 6300 g/mol, $Đ$ = 1.08. ^{1}H NMR (300 MHz, $CDCl_3$): δ 9.04−7.98 (br), 7.78−6.66 (br), 4.56−4.22 (br), 4.23−3.60 (br), 2.83−1.65 (br), 1.51−1.05 (br), 1.05−0.45 (br). MS (MALDI-ToF, DCTB + NaTFA) *m/z*: 7,391 ($[(C_{30}H_{28}N_2O_4)_{15}C_9H_{10}N_3 + Na]^+$). IR (KBr): $\tilde{\nu}$ [cm^{-1}] = 2100 (w, $\nu_{as}(N_3)$).

*End-Functionalization Procedures (Dyads and Reference Complexes). [Ru(dqp)(dqp-O-**p2**$_{17}$)][PF$_6$]$_2$ (**D1**).* A vial was charged with Cl-**p2**$_{17}$ (0.062 g, 0.009 mmol, 2 equiv), K_2CO_3 (0.001 g, 0.009 mmol, 2 equiv), and **3** (0.005 g, 0.009 mmol, 1 equiv), sealed, and placed under a nitrogen atmosphere. Dry DMF (1.0 mL) was added, and the resulting solution was heated to 60 °C. The reaction progress was monitored by TLC (aluminum oxide, CH_2Cl_2/MeOH 95/5) and analytical size exclusion chromatography (DMAc + 0.08% NH_4PF_6, diode array detection). After 24 h only little conversion was noticed; thus, potassium iodide (0.002 g, 0.001 mmol, 2 equiv) was added as catalyst. After an additional 24 h and TLC analysis, further base and potassium iodide were added. The reaction was continued until no further conversion was monitored by TLC (in total 72 h). The mixture was diluted with a minimum amount of THF and precipitated into aqueous NH_4PF_6 solution. The red precipitate was filtered off and washed with water. Unreacted complex **3** was recovered by column chromatography (diol-functionalized silica; eluent: CH_2Cl_2 to CH_2Cl_2/MeOH 95/5). The polymer-containing product was purified from excess polymer Cl-**p2**$_{17}$ by column chromatography (aluminum oxide; eluent: CH_2Cl_2 to CH_2Cl_2/MeOH 95/5). The dyad **D1** was obtained as a red powder after drying (0.020 g, 55%). ^{1}H NMR (600 MHz, $CDCl_3$): δ 8.89−8.00 (br, **p2**$_{17}$), 8.06 (br, Ru), 8.00 (br, Ru), 7.92 (br, Ru), 7.84 (br, Ru), 7.77 (br, Ru), 7.65 (br, Ru). 7.54 (br, Ru), 7.48 (br, Ru), 7.57−6.37 (br, **p2**$_{17}$), 5.67−5.40 (br, linker), 4.25−3.71 (br, **p2**$_{17}$), 3.07−1.70 (br, **p2**$_{17}$), 1.47−1.04 (br, **p2**$_{17}$), 0.99−0.47 (br, **p2**$_{17}$).

*[Ru(dqp)(dqp-ph-py-**p2**$_{17}$)][PF$_6$]$_3$ (**D2**).* Cl-**p2**$_{17}$ (0.013 g, 0.002 mmol, 2 equiv) and **5** (0.001 mg, 0.001 mmol, 1 equiv) were dissolved in a mixture of $CHCl_3$ and CH_3CN (0.32 and 0.07 mL), and the resulting solution was heated to 50 °C. After 48 h the conversion was very low as monitored by TLC (aluminum oxide, CH_2Cl_2/MeOH 95/5) and analytical size exclusion chromatography (DMAc + 0.08% NH_4PF_6, diode array detection). Subsequently, KPF_6 (0.37 mg, 0.002 mmol, 2 equiv) and potassium iodide (0.33 mg, 0.002 mmol, 2 equiv) were added, and the reaction mixture was heated to 70 °C until the complex was fully converted (48 h, reaction progress monitored by TLC). The solvent was removed under reduced pressure, and the excess of polymer was removed by column chromatography (aluminum oxide; eluent: CH_2Cl_2 to CH_2Cl_2/MeOH 95/5). The desired product was dissolved in a minimal amount of THF and was precipitated into aqueous NH_4PF_6 solution, filtered off, and washed with water. After drying the dyad **D2** was obtained as a red powder (isolated yield: 0.003 g, 40%). ^{1}H NMR (600 MHz, CD_2Cl_2): δ 9.06−8.14 (br, **p2**$_{17}$), 8.10 (br, Ru), 8.00 (br, Ru), 7.82 (br, Ru), 7.69 (br, Ru), 7.54 (br, Ru), 7.48 (br, Ru), 7.65−6.68 (br, **p2**$_{17}$), 6.21−5.91 (br, linker), 4.46−3.76 (br, **p2**$_{17}$), 3.18−1.70 (br, **p2**$_{17}$), 1.47−1.00 (br, **p2**$_{17}$), 0.99−0.51 (br, **p2**$_{17}$).

*[Ru(dqp)(dqp-ph-tr-**p2**$_{17}$)][PF$_6$]$_2$ (**D3**).* A microwave vial was charged with N$_3$-**p2**$_{17}$ (0.015 g, 0.003 mmol, 1 equiv) and **4** (0.009 g, 0.008 mmol, 3 equiv), sealed, and place under a nitrogen atmosphere. Then dry DMF (1.0 mL), a solution of copper(I) bromide (0.001 g, 0.005 mmol, 2 equiv) in DMF (0.1 mL), and a solution of PMDETA (0.02 mL, 0.24 M in DMF) were added. Subsequently, the reaction mixture was stirred at room temperature. The reaction progress was monitored by TLC (aluminum oxide, CH_2Cl_2/MeOH 95/5) and analytical size exclusion chromatography (DMAc + 0.08% NH_4PF_6, diode array detection). After 16 h the solution was concentrated under reduced pressure, and the crude product was redissolved in CH_2Cl_2 and water. The organic layer was separated, and the aqueous layer was extracted two times with CH_2Cl_2. The organic extracts were combined, excess of solvent was removed under reduced pressure, and the crude product was purified by column chromatography (amino-functionalized silica; eluent: CH_2Cl_2/MeOH 98/2). The dyad **D3** was obtained as red solid (0.013 g, 71%). ^{1}H NMR (600 MHz, CD_2Cl_2): δ 8.67−8.14 (br, **p2**$_{17}$), 8.23 (br, Ru), 8.02 (br, Ru), 7.94 (br, Ru), 7.90 (br, Ru), 7.86 (br, Ru), 7.74 (br, Ru), 7.62 (br, Ru), 7.46 (br, Ru), 7.14 (br, Ru), 7.08 (br, Ru), 7.04 (br, Ru), 7.51−6.90 (br, **p2**$_{17}$), 5.57−5.40 (br, linker), 4.10−3.74 (br, **p2**$_{17}$), 2.11−1.62 (br, **p2**$_{17}$), 1.62−1.39 (br, **p2**$_{17}$), 1.36−0.97 (br, **p2**$_{17}$), 0.90−0.60 (br, **p2**$_{17}$).

*[Ru(dqp)(dqp-O-bn)][PF$_6$]$_2$ (**C1**).* A microwave vial was charged with [Ru(dqp)(dqp-OH)][PF$_6$]$_2$ (0.008 g, 0.007 mmol), potassium iodide (0.005 g, 0.030 mmol), and K_2CO_3 (0.004 g, 0.030 mmol), sealed, and placed under a nitrogen atmosphere. Subsequently, dry DMF (1 mL) and a solution of benzyl chloride in DMF (0.082 mL, 0.27 M) were added via a syringe. The resulting mixture was stirred at

DOI: 10.1021/acs.macromol.5b02717
Macromolecules 2016, 49, 2112−2123

Scheme 1. Synthesis of Monomer 2 and Subsequent Polymerization and Postpolymerization Modification[a]

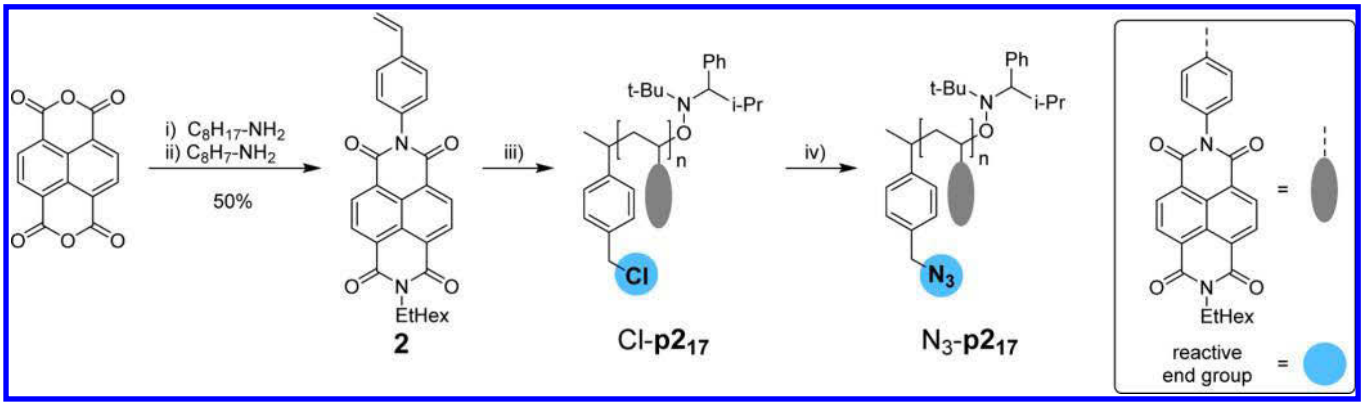

[a]Reagents and conditions: (i) DMF, microwave irradiation, N_2, 75 °C (5 min), 140 °C (15 min); (ii) 4-aminostyrene, $ZnSO_4 \cdot 1H_2O$, pyridine, reflux, 4 h; 50% over both steps; (iii) CMSt-TIPNO, anisole, N_2, 120 °C, 17 h; (iv) NaN_3, DMF, N_2, 60 °C, 48 h.

60 °C, until TLC analysis (silica, eluent: acetonitrile/H_2O/$KNO_{3\ (aq)}$ 40/4/1) showed complete conversion. After 16 h, the reaction mixture was allowed to cool to room temperature and was precipitated into an aqueous NH_4PF_6 solution. The red precipitate was filtered off, washed with water, and redissolved in acetonitrile. Then the solvent was evaporated under reduced pressure, and the crude product was purified by flash column chromatography (diol-functionalized silica; eluent: CH_2Cl_2/MeOH 95/5). Finally, diffusion-controlled crystallization with acetonitrile and diethyl ether gave the desired complex (0.007 g, 75%). ^{1}H NMR (600 MHz, CD_3CN): δ 8.15 (t, J = 8.0 Hz, 1H), 8.12 (dd, J = 5.1, 1.3 Hz, 2H), 8.10−8.04 (m, 6H), 7.87 (d, J = 8.0 Hz, 2H), 7.73 (ddd, J = 17.5, 7.4, 1.1 Hz, 4H), 7.68 (ddd, J = 8.2, 5.0, 1.0 Hz, 4H), 7.54−7.49 (m, 4H), 7.49−7.40 (m, 7H), 7.06 (ddd, J = 9.1, 8.2, 5.2 Hz, 4H), 5.40 (d, J = 11.4 Hz, 1H), 5.31 (d, J = 11.4 Hz, 1H). ^{13}C NMR (151 MHz, CD_3CN): δ 167.2, 159.6, 159.5, 158.6, 157.9, 147.7, 147.5, 138.9, 138.6, 138.4, 136.4, 134.1, 133.9, 132.9, 132.6, 131.7, 131.5, 129.9, 129.7, 129.1, 128.9, 127.8, 127.6, 123.0, 122.9, 116.0, 72.2. HR-ESI ($[C_{53}H_{36}N_6ORu]^{2+}$) m/z: calcd: 437.0992; found: 437.1020. Error: 4.9 ppm.

Note: the methylene protons of the benzyl group cause two doublets (5.40 and 5.31 ppm), which is assigned to a restricted conformational freedom and a resulting nonequivalence of the protons.

[Ru(dqp)(dqp-ph-py-bn)](PF$_6$)$_3$ ***(C2)***. A microwave vial was charged with [Ru(dqp)(dqp-ph-py)][PF_6]$_2$ (0.010 g, 0.008 mmol), potassium iodide (0.003 g, 0.017 mmol), and acetonitrile (0.5 mL), sealed, and placed under a nitrogen atmosphere. Subsequently, a solution of benzyl chloride in DMF (0.062 mL, 0.27 M) was added via a syringe, and the reaction mixture was heated to 70 °C, until TLC analysis (silica; eluent: acetonitrile/H_2O/$KNO_{3\ (aq)}$ 40/4/1) showed complete conversion. After 16 h, the reaction was allowed to cool to room temperature and was precipitated into an aqueous NH_4PF_6 solution. The aqueous solution was extracted three times with dichloromethane, and the combined organic layers were washed with water and brine. After drying over Na_2SO_4 the solvent was evaporated under reduced pressure, and the crude product was purified by flash column chromatography (amine-functionalized silica; eluent: CH_2Cl_2/MeOH 95/5). The desired complex was isolated as a dark red solid (0.011 g, 92%). ^{1}H NMR (600 MHz, CD_3CN): δ 8.80 (d, J = 7.0 Hz, 2H), 8.35 (d, J = 7.0 Hz, 2H), 8.22−8.16 (m, 4H), 8.14 (dd, J = 5.1, 1.4 Hz, 2H), 8.12 (s, 1H), 8.11−8.07 (m, 7H), 7.92 (m, 4H), 7.75 (dd, J = 7.4, 1.1 Hz, 2H), 7.74−7.68 (m, 4H), 7.55−7.43 (m, 10H), 7.12−7.03 (m, 4H), 5.74 (s, 2H). ^{13}C NMR (151 MHz, CD_3CN): δ 159.5 (2×), 158.3, 157.7, 156.6, 148.8, 147.6, 147.5, 145.5, 140.6, 139.2, 138.6 (2×), 136.2, 134.5, 134.1 (2×), 134.0, 132.8, 132.7, 131.7, 131.6, 130.8, 130.5, 130.2, 130.1, 130.0, 129.7, 129.0, 127.8 (2×), 127.6, 127.5, 126.5, 126.4, 123.1, 123.0, 64.7. HR-ESI ($[C_{64}H_{44}N_7Ru]^{3+}$) m/z: calcd: 337.4228, found: 337.4250. Error: 4.7 ppm.

[Ru(dqp)(dqp-ph-tr-bn)][PF$_6$]$_2$ ***(C3)***. A microwave vial was charged with [Ru(dqp)(dqp-ph-C≡C−H)] (0.008 g, 0.007 mmol) and copper(I) bromide (0.002 g, 0.014 mmol), sealed, and placed under a nitrogen atmosphere. Subsequently, dry DMF (1 mL), a solution of PMDETA in DMF (0.058 mL, 0.24 M), and a solution of benzyl azide in CH_2Cl_2 (0.028 mL, 0.5 M) were added via a syringe. Then the reaction mixture was heated at 60 °C, until TLC analysis (silica; eluent: acetonitrile/H_2O/$KNO_{3\ (aq)}$ 40/4/1) showed complete conversion. After 16 h, the reaction mixture was allowed to cool to room temperature and precipitated into an aqueous NH_4PF_6 solution. The red precipitate was filtered off, washed with water, and redissolved in acetonitrile. Subsequently the solvent was evaporated under reduced pressure, and the crude product was purified via flash column chromatography (amine-functionalized silica; eluent: CH_2Cl_2/MeOH 95/5). The complex was isolated as a dark red solid (0.008 g, 84%). ^{1}H NMR (600 MHz, CD_3CN): δ 8.26 (s, 1H), 8.17 (dd, J = 9.3, 6.7 Hz, 1H), 8.15 (s, 2H), 8.14 (dd, J = 5.1, 1.3 Hz, 2H), 8.08 (dd, J = 2.3, 1.3 Hz, 3H), 8.07 (s, 3H), 8.06−8.01 (m, 4H), 7.90 (dt, J = 7.9, 1.9 Hz, 4H), 7.74 (dd, J = 7.4, 1.1 Hz, 2H), 7.72−7.68 (m, 4H), 7.52−7.43 (m, 4H), 7.44−7.35 (m, 4H), 7.06 (ddd, J = 8.7, 7.5, 4.8 Hz, 4H), 5.62 (s, 2H). ^{13}C NMR (151 MHz, CD_3CN): δ 159.5, 159.4, 158.0, 157.7, 149.9, 147.6, 147.5, 147.3, 139.1, 138.5 (2×), 136.7, 136.2, 134.4, 133.9 (2×), 132.8 (2×), 131.5 (2×), 129.9, 129.4, 129.0, 128.9, 127.8, 127.7, 127.6, 127.5, 127.1, 126.0, 123.0, 122.9, 122.6, 54.5. HR-ESI ($[C_{61}H_{41}N_9Ru]^{2+}$) m/z: calcd: 500.6259, found: 500.6272. Error: 1.0 ppm.

RESULTS AND DISCUSSION

The modular assembly of the dyads relies on two stages, i.e., the individual preparation of the functional building blocks and their covalent coupling by polymer-analogous reactions.

Preparation of Building Blocks. The styrenic naphthalene diimide (NDI) **2** was prepared from 1,4,5,8-naphthalenetetracarboxylic dianhydride by an optimized two-step synthesis compared to our previous reported method (Scheme 1).[10] The procedure requires fewer synthetic steps and only one chromatographic purification step, which results in significantly improved yields (50% compared to 10%): First, the monoimide was prepared by the reaction of the dianhydride with 2-ethylhexylamine in DMF under microwave irradiation.[32] The crude product **1** contained approximately 20% bis-alkylated product but was used without further purification. Next, the styrenic group was introduced by the reaction of compound **1** with an excess of 4-aminostyrene in pyridine in the presence of zinc(II) sulfate as described for similarly functionalized NDIs.[33]

The styrenic monomer **2** was polymerized by nitroxide-mediated polymerization (NMP) using the functional initiator CMSt-TIPNO (Scheme 1) as reported previously.[10] Because of the similar solubility of monomer and polymer, the removal of

DOI: 10.1021/acs.macromol.5b02717
Macromolecules 2016, 49, 2112−2123

Scheme 2. Synthesis of Functional Ruthenium Complexes 4 and 5[a]

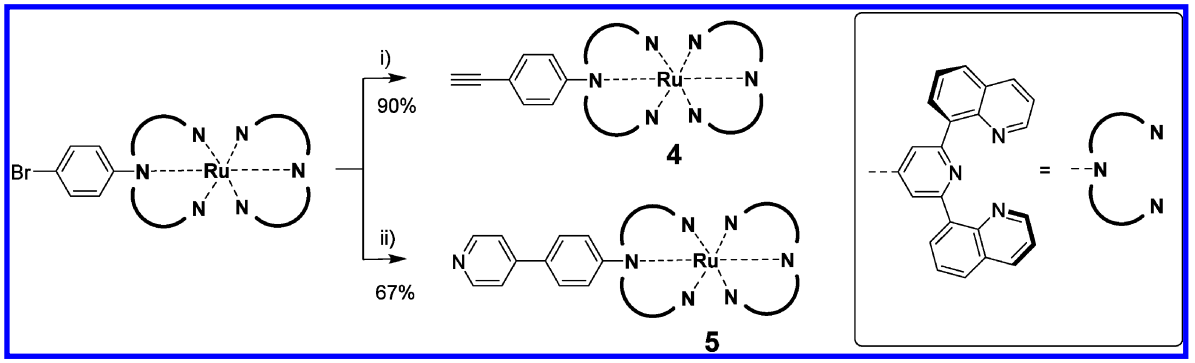

[a]Reagents and conditions: (i) TIPS−C≡C−H, $Pd(PPh_3)_4$, CuI, Et_3N, DMF, N_2, 60 °C, 16 h, Bu_4NF, THF, MeOH, RT, overnight, 90% isolated yield; (ii) 4-pyridineboronic acid, $Pd(dba)_2$, SPhos, K_2CO_3, CH_3CN, H_2O, 100 °C, 16 h, 67% isolated yield.

Scheme 3. Synthesis of Reference Complexes C1−C3 and the Respective Dyads D1−D3[a]

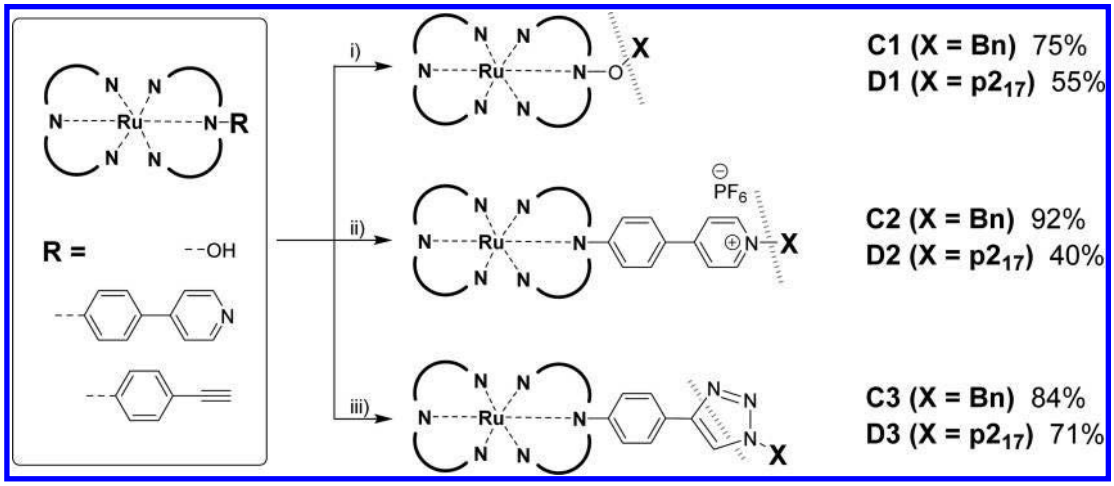

[a]Reagents and conditions: (i) K_2CO_3, KI, DMF, N_2, 60 °C, 72 h; (ii) KI, KPF_6, $CHCl_3$, CH_3CN, N_2, 70 °C, 96 h; (iii) CuBr, PMDETA, DMF, N_2, RT, 16 h. Gray dashed line illustrates the newly formed bond.

unreacted monomer was performed by preparative size-exclusion chromatography (Bio-Beads S-X1). The obtained polymer was characterized by analytical size exclusion chromatography and revealed a molar mass of 6400 g/mol (PS calibration) with a low dispersity ($Đ$ = 1.11). The ^{1}H NMR spectrum shows the typical broad NDI resonances in the aromatic region, whereby the resonance of the distinct chloromethyl group (around 4.6 ppm) enables the determination of the degree of polymerization and to monitor the progress of the functionalization reactions (*vide infra*). The chloromethyl group of Cl-**p2**$_{17}$ (the subscripted number represents the degree of polymerization according to NMR) was converted into the azide functionality. Note that **p2**$_{17}$ refers in the following to the polymer with the initiator's benzyl unit except the end group (chlorine, azide, or a ruthenium fragment; *vide infra*). The reaction was performed with sodium azide in DMF at 60 °C, resulting in a quantitative substitution of the chloride as judged from the shift of the methylene proton resonances in the ^{1}H NMR of N_3-**p2**$_{17}$ (from 4.6 to 4.4 ppm). The azide functionality was further confirmed by IR data, showing the appearance of the typical band at 2100 cm^{-1} (see Supporting Information). The analysis of pNDIs by mass spectrometry proved to be challenging applying standard conditions.[10] However, tuning the MALDI conditions enabled the identification of a characteristic series with the NDI repeating unit (480 amu). The centers of the unresolved isotope peaks can be assigned to specimen formed by nitroxide cleavage; i.e., the fragments carry the characteristic end groups (Cl or N_3) for the corresponding polymers (see Supporting Information). The comparison of the SEC data revealed negligible differences in molar mass and dispersity and, thus, indicates the absence of polymer degradation and undesired couplings during the azide functionalization (see Supporting Information).

The hydroxyl-decorated Ru complex (**3**) was synthesized according to a literature procedure,[9] whereas the functional complexes **4** and **5** were prepared by a "chemistry-on-the-complex" approach (Scheme 2). This methodology allows a simple preparation from reported [Ru(dqp)(dqp-ph-Br)]-$[PF_6]_2$. The alkyne functionality was introduced by Sonogashira cross-coupling in DMF/Et_3N with $Pd(PPh_3)_4$ as catalyst. After deprotection with tetrabutylammonium fluoride, the desired complex **4** was obtained in excellent yield (90%). The corresponding pyridine-equipped complex **5** was prepared by Suzuki cross-coupling using 4-pyridineboronic acid in 67% yield. The apparent lower yield of **5** is attributed to losses during purification and isolation of the pure product. Both new complexes were characterized by 1D and 2D NMR spectroscopy and HR-MS (see Supporting Information).

DOI: 10.1021/acs.macromol.5b02717
Macromolecules 2016, 49, 2112−2123

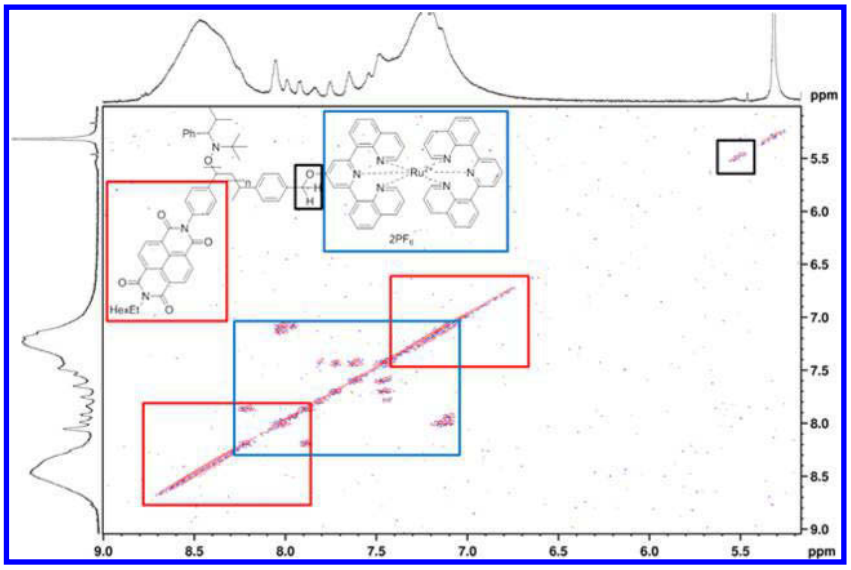

Figure 1. COSY NMR (600 MHz, CD_2Cl_2) of **D1** with typical resonances of the polymer (red), the complex's ligand scaffold (blue), and the linker (black).

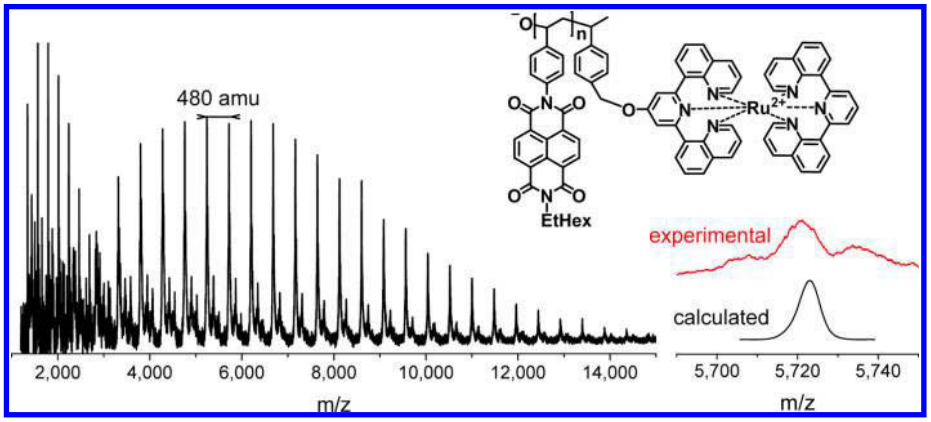

Figure 2. MALDI-ToF MS of **D1** with proposed structure of the fragments and with experimental (red) and calculated (black) isotopic pattern (matrix: dithranol + NaTFA).

Modular Assembly. Three different linkage reactions were investigated for the synthesized telechelic polymers and functionalized ruthenium complexes. A series of P−A_m dyads (Scheme 3) were prepared, i.e., Williamson ether synthesis from a hydroxyl group (top), quaternization of a pyridine unit (middle), and CuAAC reaction of a terminal alkyne (bottom). Additionally, the corresponding benzylated complexes (**C1**−**C3**) were synthesized analogously to the dyads, in order to serve as proper reference complexes for the quantitative emission quenching studies (*vide infra*). The comparable yields of the latter references complexes indicate the efficiency of the postpolymerization reactions, which will be detailed in the following paragraph.

Method Development (Nucleophilic Substitutions). The reaction of complex **3** and pNDI was reported previously;[10] however, the reaction with Cl-$\mathbf{p2}_{17}$ gave only low conversions to dyad **D1** and a more complicated purification procedure upon applying the reported conditions (Scheme 3, top). The reaction progress was monitored by thin-layer chromatography (TLC) and analytical size-exclusion chromotagraphy (SEC), which revealed no further conversion after 1 day. Hence, potassium iodide was added to enhance the reactivity in analogy to the Finkelstein reaction, which led to significantly increased conversion. Surprisingly, the reported purification protocol resulted in an incomplete separation of **D1** from complex **3**. This observation is rationalized by a decreased net polarity difference, which shifts the subtle balance between solubilization (promoted by the pNDI fragment) and retention (caused by the dicationic Ru complex fragment) unfavorably. Consequently, the shorter polymer chains of $\mathbf{p2}_{17}$ (6400 g/mol) vs. reported pNDI (9000 g/mol)[10] would lead to a dominating contribution of the Ru^{II}, in line with the aforementioned difficulties to remove complex **3**. Although the excess of nonfunctionalized polymer is readily removed by column chromatography on aluminum oxide (eluent: CH_2Cl_2/MeOH 18/1), the corresponding chromatography on silica revealed as nonsuitable. Organic solvent mixtures as used previously lead to no elution, which is attributed to the stronger interaction of the dicationic Ru^{II} fragment to silica. Using typical eluent systems for Ru^{II} complexes (a mixture of acetonitrile and aqueous potassium nitrate) resulted in severe streaking and coelution (attributed to solubility issues of the pNDI). Hence, we tested amino- and diol-functionalized silica gels, which are commercially available and benefit from a reduced surface polarity. This stationary phase can be run with all common solvents (mixtures) as eluents and, indeed, allowed

DOI: 10.1021/acs.macromol.5b02717
Macromolecules 2016, 49, 2112−2123

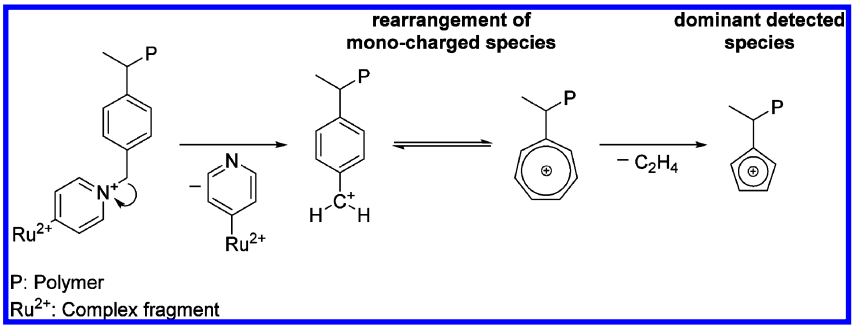

Figure 3. Proposed fragmentation of **D2** including benzyl cleavage, resulting in the formation of a singly charged polymer species and subsequent consecutive reactions.

the successful separation. Notably, no counterion exchange is necessary and thus facilitates the purification over the traditional eluent systems used on silica.[34] The ^{1}H NMR spectrum of **D1** is well resolved and agrees with the previous report;[10] i.e., it clearly confirms the characteristic shift of the bridging methylene protons in comparison to Cl-**p2**$_{17}$ (4.57 ppm to 5.57 ppm) and the presence of the ligand scaffold of the Ru(II) fragment (Figure 1).

Further reoptimization of the mass spectrometry conditions led to the successful analysis by MALDI-ToF MS (Figure 2). The spectrum shows a peak distribution with the mass difference (Δm = 480 g/mol) of a naphthalene diimide unit. Although no isotope-resolved spectra could be obtained, the peaks can be assigned to a species generated by the fragmentation of the TIPNO group (see also Supporting Information).

An alternative nucleophilic substitution reaction was investigated for Cl-**p2**$_{17}$ and the 4-pyridyl-decorated complex (**5**). As stated above, the reaction showed almost no conversion after 24 h at 50 °C. Therefore, potassium iodide and potassium hexafluorophosphate (as a source of non-nucleophile counterions to prevent the potential cleavage of the pyridinium) were added, and the temperature was raised to 70 °C. After 2 days, the quantitative conversion of complex **5** was achieved according to 3D SEC (see Supporting Information). The excess of polymer was removed by column chromatography on aluminum oxide to yield **D2** (40%). The apparent low yield arises from the small reaction scale and losses upon sampling.[35] The ^{1}H NMR spectrum confirmed the successful linkage on the basis of the shifts of the bridging methylene protons to 6 ppm (see Supporting Information). An intense fragmentation of **D2** was detected in the MALDI-ToF MS spectrum (see Supporting Information). The major series displays the typical spacing of the NDI repeating unit indicating the absence of the Ru fragment, as judged from the narrow peaks. This series can be rationalized by the typical elimination of the TIPNO group occurring at one polymer chain terminus (as also observed for the nonfunctionalized polymer), whereas the other chain terminus would correspond to C_7H_8. The latter fragment can be explained by the fragmentation of the pyridinium–Ru^{II} subunit (+3). Thereby, the carbon–nitrogen bond of the benzylpyridinium moiety is cleaved, and a singly charged polymer fragment is formed (Figure 3). Subsequently the rearrangement and the elimination of ethyne lead to a cyclopentadienyl cation as the dominant detected species, which is well-known for benzylic compounds.[36] Additionally, a second series appears at low molar masses in the mass spectrum. Surprisingly, this distribution indicates doubly charged specimen (Δm = 240 g/mol) and is tentatively assigned to the dyad after cleavage of the nitrogen–oxygen bond of the TIPNO (see Supporting Information).

Linkage via Triazole Formation. The dyad **D3** was prepared by copper(I)-catalyzed azide–alkyne cycloaddition of complex **4** with the azide-functionalized polymer N_3-**p2**$_{17}$. The reaction was carried out using a standard protocol with copper(I) iodide, PMDETA, and DMF. After 16 h the reaction showed full conversion of the polymer (checked by TLC and SEC), and the dyad **D3** was isolated in good yields (71%) after column chromatography (*vide supra*). The yield compared to the observed full conversion of the polymer is attributed to losses due to samples which were taken to monitor the reaction progress. Consistent with the dyads **D1** and **D2**, the successful attachment of the complex at the polymer was proved by ^{1}H NMR spectroscopy, as the signals of the methylene protons of the linker are shifted from 4.3 to 5.6 ppm. The dyad **D3** exhibits the same fragmentation behavior in the MALDI-ToF MS as **D1**, i.e., the nitrogen–oxygen bond of the TIPNO end group is cleaved (see Supporting Information).

Table 1. Electrochemical Data from Cyclovoltammetry[a]

	E_{red} [V] (NDI^0/NDI$^-$)	E_{red} [V] (NDI$^-$/NDI^{2-})	E_{ox} [V] (Ru^{III}/Ru^{II})	E_{red} [V] (L^0/L$^-$)	E_{red} [V] (L$^-$/$^{2-}$)
D1	−1.05	−1.51	+0.54	−1.83	n.d.
D2	−1.05	−1.50	+0.51	−1.74	−1.94
D3	−1.05	−1.52	+0.51	−1.79	−1.97

[a] $E_{1/2}$ vs. Fc$^{+/0}$ in DMF containing 0.1 M TBAPF$_6$ using a scan rate of 200 mV/s.

Electrochemistry. The electrochemical properties of the dyads were analyzed by cyclic voltammetry using a standard three-electrode setup. The first cycle of each experiment was used for the analysis of the electrochemical processes. This approach ensures a clean electrode surface and prevents contaminations from side products, which may influence the measurement or alter the electrode's surface due to irreversible reactions.[37−39] A detailed analysis of the raw electrochemical data is further complicated due to the background signals; thus, a correction by subtraction of a blank measurement was executed to allow a more comprehensive analysis. The deviations from the ideal peak shape, particularly of the weak signals of the ruthenium fragment, are tentatively attributed to additional contributing parameters, e.g., different electron transfer rates, reorientation of the polymer chain upon accumulative charging, adsorption, etc. (see Figure 4 (left) and Supporting Information). More importantly, the redox couples can be assigned to the corresponding units and are summarized in Table 1 (reported vs. Fc$^+$/Fc^0). The cyclo-

DOI: 10.1021/acs.macromol.5b02717
Macromolecules 2016, 49, 2112−2123

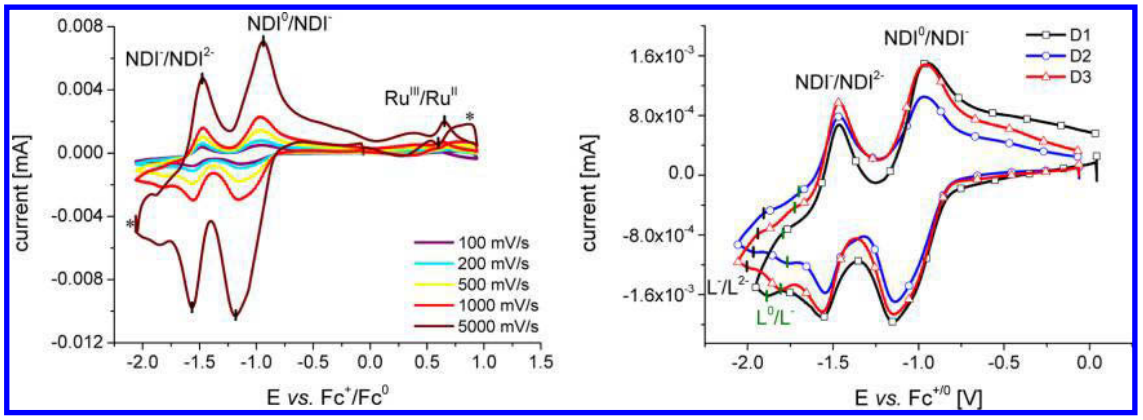

Figure 4. Left: background corrected cyclovoltammogram of **D1** showing two quasi-reversible reduction steps corresponding to the polymer (NDI^0/NDI^- and NDI^-/NDI^{2-}) and one reversible oxidation attributed to the ruthenium (Ru^{III}/Ru^{II}). Right: background corrected data of the negative potential range enabling the detection of the reduction of the ligand scaffold (L^0/L^- and L^-/L^{2-}) (0.1 M $TBAPF_6$, DMF, 500 mV/s). All shown spectra were smoothed using a 10-point moving average filter to remove a systematic noise pattern. Artifacts and displacements (marked with an asterisk) are caused by the applied analysis procedure (subtraction of the blank spectra without analyte).

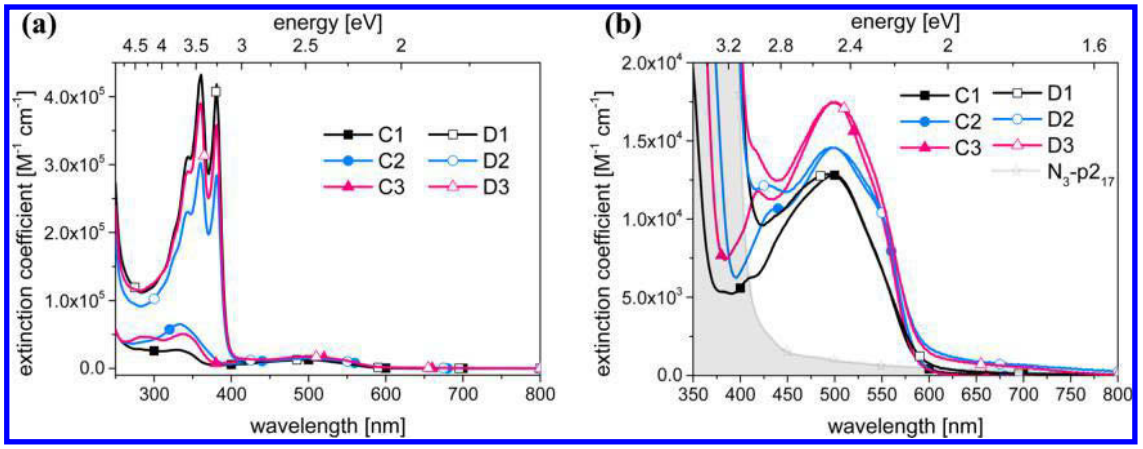

Figure 5. Absorption data of the reference complexes (**C1**−**C3**) and the corresponding dyads (**D1**−**D3**) in dichloromethane. (a) UV−vis spectral region illustrating the dominant UV absorption of the pNDI chains. (b) Inset of the MLCT region illustrating preserved optical properties of the Ru photosensitizer (gray area depicts the low-energy tail of the pNDI absorption).

voltammogram of **D3** is exemplarily shown in Figure 4 (left) with various scan rates. Two quasi-reversible reduction steps at −1.0 and −1.5 V were clearly detected corresponding to the naphthalene diimide units of the polymer. The asymmetry of the reduction peaks is assigned to kinetic effects besides the diffusion-controlled electron transfer, e.g., conformational changes within the polymer. The tailing of the anodic wave, i.e., upon reoxidation of the NDI^- units, is more pronounced for faster scan rates and indicates the kinetic effects of the accumulative charging. In fact, any deviations become less pronounced at slower scan rates (<500 mV/s). The reversible oxidation of the ruthenium center was detected as a small signal centered around 0.5 V. Interestingly, the respective potentials are similar for all prepared dyads, indicating that the nature of the linker has only a minor influence on the electrochemical properties of the metal center. Additional redox waves were observed at potentials below −1.51 V (Figure 4, right) and are assigned to the reduction of the complex fragment. The first ligand-centered reduction occurs at typical electrochemical potentials, i.e., between −1.74 and −1.83 V. Consequently, the exact potential is more strongly influenced by the substituent, i.e., the electron-donating ether bridge decreases the potential (−1.83 V), while the electron-deficient pyridinium moiety leads to less negative potentials (−1.74 V). The same trend is found for the second reduction step; however, this redox process was not determined for **D1** due to the necessary strong negative potential. In the case of **D2** an additional reduction of the pyridinium unit is expected around −1.4 to −1.5 V, which is probably overlapped by the intense NDI reduction.

Optical Spectroscopy. The steady-state optical properties of the dyads enable the analysis of photoinitiated processes, which will be related to the constituting functional building blocks, i.e., the pNDI block and the Ru^{II} photosensitizer. Thereby, the absorption spectra yield valuable information on potential interactions (e.g., H- or J-aggregation), while emission and excitation data detail both the properties as well as the origin of the excited states and enable the discussion of energy or electron transfer steps (*vide infra*). Previous studies have identified the formation of the charge-separated state and the quenching of the ^{3}MLCT emission, accompanied by additional polymer-based emissive states.[10] More importantly, the emission quantum yield serves as quantitative measure for the efficiency of light-induced processes, e.g., charge separation.

Absorption Spectroscopy. The absorption spectra of the model complexes (**C1**−**C3**) and the corresponding dyads (**D1**−**D3**) are depicted in Figure 5. The UV region is dominated by the intense absorption bands attributed to the $\pi \rightarrow \pi^*$ transitions of the NDI units (panel a). The spectral

DOI: 10.1021/acs.macromol.5b02717
Macromolecules 2016, 49, 2112−2123

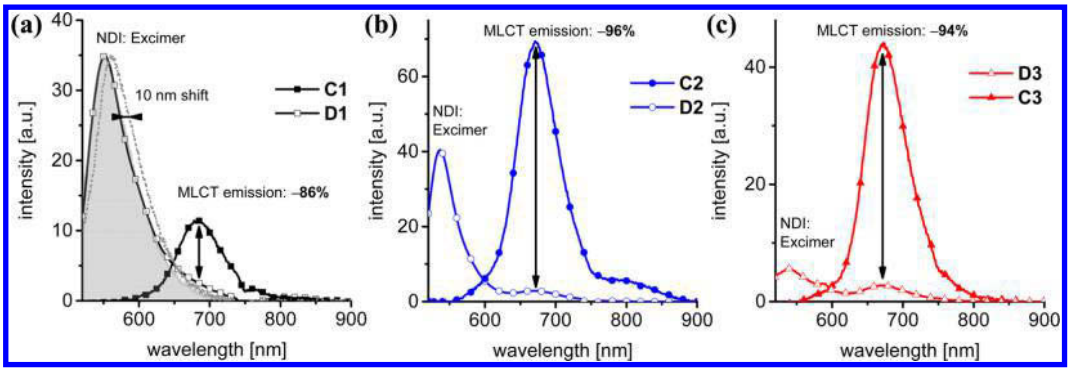

Figure 6. Emission data of the reference complexes and the corresponding dyads (aerated dichloromethane, room temperature, iso-absorbing solutions at 500 nm excitation). Arrows indicate quenching of the ^{3}MLCT emission (in %) of the dyad vs. the reference complex, respectively. Note the lower emission intensity of **C1** compared to **C2** and **C3** caused by a lower intrinsic quantum yield (not reported). (a) Ether-linked complex **C1** complemented by polymer-based emission (**D1**: gray area; dotted line: pNDI) to illustrate residual MLCT contribution. (b, c) Pyridinium- and triazole-linked congeners.

shape resembles the spectrum of individual naphthalene diimide units, e.g., absorption maxima centered at 360 and 380 nm. In line with a previous report, the absence of additional detectable features indicates negligible NDI–NDI interactions in solution, as expected upon aggregate formation in solution.[10] The visible region is governed by the Ru photosensitizer (panel b). The reference complexes (**C1**–**C3**) exhibit the typical metal-to-ligand charge transfer (MLCT) bands centered at 500 nm. The enhanced absorptivity of complexes **C2** and **C3** are attributed to the ligand's extend π-system, in agreement with a previous report.[31] More importantly, the spectral characteristics are preserved upon attachment of the polymer chain. These findings corroborate the electrochemical data and confirm the modular character of the photosensitizer–polymer assemblies, i.e., preserved optical properties of the individual building blocks (see Supporting Information).

Emission Spectroscopy. The reference complexes and respective dyads were investigated by steady-state emission spectroscopy under ambient conditions, i.e., in aerated dichloromethane at room temperature using iso-absorbing solutions at 500 nm excitation (Figure 6). The reference complexes display the typical Ru-based emission from the ^{3}MLCT state between 650 and 700 nm, which is slightly affected by the substitution pattern. In agreement with a previous report,[31] the electron-releasing alkoxy substitution (**C1**) leads to a bathochromic shift of approximately 15 nm in comparison to the π-extended phenyl-decorated complexes **C2** and **C3**. In agreement with the energy gap law, i.e., the emission decay is more efficient for lower excited state energies within a series,[22] the absolute quantum yield of **C1** is also significantly lower than for the phenyl-decorated congeners. More importantly, the emission spectra of the corresponding dyads differ markedly from the reference complexes. In all cases, the Ru emission is quenched and an additional emission centered at 550 nm is observed. A similar profile of the high-energy emission band is observed for the pristine pNDI and is therefore attributed to polymer-based emissive states (*vide infra*).[10] The efficiency of the ^{3}MLCT excited state quenching (Q_{MLCT}) is calculated from the residual Ru-based emission with respect to the corresponding reference complexes (Table 2). Noteworthy, the contribution of the overlapping polymer-based emission is accounted by subtracting a scaled pNDI spectrum, as depicted in Figure 6a. Following this procedure, the quenching efficiency was averaged between 650 and 700 nm (see Supporting Information) to yield reliable values for **C1** (86%), **C2** (96%), and **C3** (94%). Within the experimental errors, the ^{3}MLCT quenching appears to be independent of the length of the linker.

Table 2. UV–Vis Data of the Reference Complexes and Dyads[a]

	λ_{Abs} (MLCT) [nm]	λ_{Em} (MLCT) [nm]	Q_{MLCT} [%]
C1	500	684	
C2	500	670	
C3	500	670	
D1	496	684	86
D2	499	669	96
D3	500	669	94

[a] λ_{Abs} (MLCT) is the absorption maximum of the MLCT, λ_{Em} (MLCT) is the emission maximum of the MLCT, and Q_{MLCT} is the calculated quenching efficiency compared to the respective reference complex.

The origin of the polymer-based emission was investigated in more detail using diluted samples to circumvent inner filter effects in the previous data (*vide supra*). The UV–vis absorption spectra of monomer **2**, the nonfunctionalized pNDI, and the Ru-decorated polymer retain the typical absorption bands at 360 and 380 nm (Figure 7, panel a). In comparison to the monomer, both polymer compounds show decreased absorption at 380 nm as well as a slight tailing of the bathochromic shoulder. In addition, significant spectral shifts are observed at shorter wavelength, i.e., decreased absorption (<280 nm) and increased absorption (280–340 nm). These observations suggest that a certain fraction of the NDI chromophores experience a different local environment, e.g., solvent excluded volume within the polymer. In addition, the high local concentration and the spatial proximity of the NDI units may lead to partial (transient) aggregation or stacking of NDI units as commonly observed in solution.[15,40–46] This assignment is corroborated by the steady-state emission data (Figure 7b). Upon excitation at 360 nm, the monomer displays no detectable emission in line with related derivatives,[14] whereas the corresponding polymer displays a pronounced emission band around 413 nm. This observation is attributed to interacting NDI units, similar to the reported J-aggregates formed in solution.[15] Additionally, the emission band around 550 nm is detected at high polymer concentrations (×30)

DOI: 10.1021/acs.macromol.5b02717
Macromolecules 2016, 49, 2112–2123

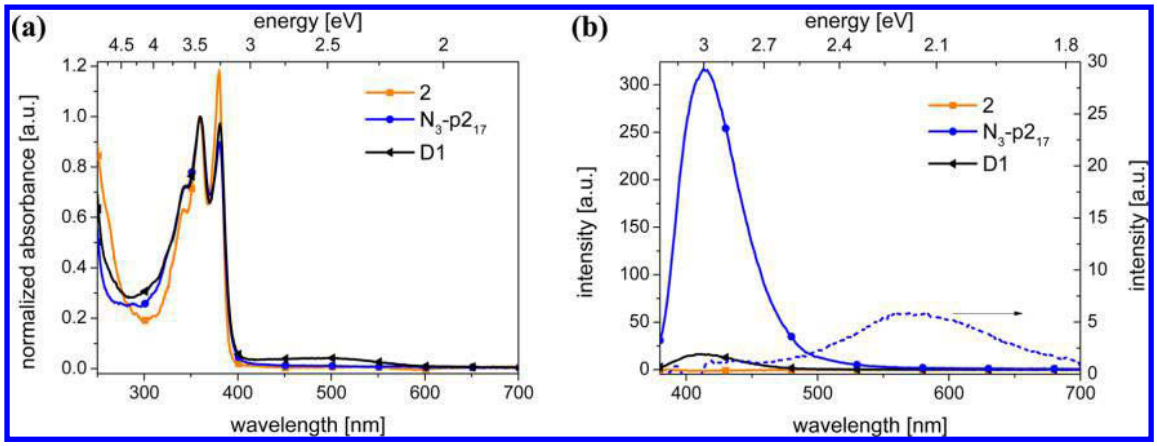

Figure 7. (a) Normalized absorption spectra (at 360 nm, optical density approximately 0.1) of **2**, N_3-**p2**$_{17}$, and **D1** in dichloromethane. (b) Emission spectra (excitation at 360 nm) showing emission bands centered at 413 nm (solid line, left axis) and 550 nm (concentrated sample of N_3-**p2**$_{17}$, optical density at 360 nm 2.5, dashed line refers to right axis as indicated by arrow, excitation at 360 nm).

(Figure 7, right inset, or see Supporting Information), which is reported for naphthalene diimide dimers (excimers) and their subsequent emission.[14,15,47−53] Apparently, upon higher concentrations more aggregated NDI specimen are formed and, thus, result in an apparent bathochromic emission shift. The corresponding excitation spectra recorded at 413 and 550 nm detection, respectively, yield spectral profiles that are significantly broadened with respect to the absorption spectrum (see Supporting Information). On the basis of all presented experimental data, the absorption of a UV photon in the nonfunctionalized polymer leads to either an excited NDI state (in a stack or aggregate, emission at 413 nm) or an excimer state (emission at 550 nm), which can undergo secondary processes to populate emissive states that are not accessible for isolated NDI units. For completion, the two-dimensional excitation−emission plots corroborate the made assignments; i.e., both polymer-based emissions show small Stokes shifts in contrast to the substantial spectral shift arising from the Ru emission (Supporting Information). In the case of the dyad (**D1**), the emission intensity at 413 nm is decreased significantly in comparison to the nonfunctionalized polymer, which is assigned to additional energy transfer processes involving the Ru fragment. However, any Ru sensitization is difficult to discern due to the subsequent charge separation on the basis of the steady-state data. Nevertheless, the quenching of the UV-emission and the occurrence of the polymer-based emission (*vide supra*) may open attractive avenues to sensitize the Ru dye. Time-resolved measurements are in due course to detail the associated rate constants for energy and electron transfer. Noteworthy, the higher emission energy of the polymer-based emission vs the MLCT emission corroborate our previous detailed analysis of electron-transfer from the energetically most favorable Ru-based excited state.[10]

CONCLUSION

The use of a commercial NMP initiator enabled the synthesis of a well-defined telechelic poly(naphthalene diimide). The chain end was subsequently functionalized with a ruthenium(II) photosensitizer employing three different reactions—two nucleophilic substitutions and the CuAAC reaction. In addition to the high conversion, the straightforward purification of the functional architectures using functionalized silica allowed the facile isolation in good yields. All compounds were fully characterized by NMR, MS, and SEC measurements, including three reference complexes to detail the spectroscopic properties of the prepared dyads.

The electrochemical potentials of the building blocks redox processes are retained in the corresponding dyads; i.e., the polymer shows two large quasi-reversible reduction waves at −1.0 and −1.5 V, respectively. Additionally the reversible oxidation of the ruthenium center was detected around +0.5 V, whereas the reduction potential of the ligand scaffold is influenced by the electron-deficient or electron-donating nature of the linker. The absorption spectra of the A_n−P dyads display intense absorption bands centered at 360 and 380 nm, which are based on the $\pi \rightarrow \pi^*$ transitions of the NDI units, and the typical MLCT band of the ruthenium photosensitizer at 500 nm. Steady-state emission spectroscopy revealed that the MLCT emission of the ruthenium dye is efficiently quenched in the dyads, attributed to charge separation between the Ru^{II} center and a NDI acceptor. A quenching efficiency of >86% was determined for the series of linkage pattern with respect to corresponding reference complexes. Furthermore, additional energy transfer processes involving the polymer and the ruthenium dye were observed, which may be exploited for future light harvesting processes.

In conclusion, the presented modular assembly of hierarchically defined A_n−P dyads was achieved by efficient coupling reactions. More importantly, the long-lived excited state of the photosensitizer is exploited to promote efficient charge separation irrespective of the flexible saturated linkage pattern. Because of the orthogonality of the presented methods, future functional photoredox-active A_n−P−D_m architectures can be envisioned and readily synthesized, including facile purification protocols.

ASSOCIATED CONTENT

Supporting Information

The Supporting Information is available free of charge on the ACS Publications website at DOI: 10.1021/acs.macromol.5b02717.

Additional instrumental details and analytical data (NMR, MS, SEC, UV−vis, and cyclic voltammetry) are provided for completion (PDF)

DOI: 10.1021/acs.macromol.5b02717
Macromolecules 2016, 49, 2112−2123

AUTHOR INFORMATION

Corresponding Authors

*E-mail ulrich.schubert@uni-jena.de (U.S.S.).
*E-mail michael.jager.iomc@uni-jena.de (M.J.).

Author Contributions

#R.S. and T.S. contributed equally to this work. All authors have given approval to the final version of the manuscript.

Funding

M.J. was financially supported by the Carl-Zeiss Foundation and the Friedrich Schiller University Jena ("Nachwuchsförderung").

Notes

The authors declare no competing financial interest.

ACKNOWLEDGMENTS

We thank Sarah Crotty for MALDI-ToF analysis, Nicole Fritz for ESI-ToF analysis, Annett Urbanek for MALDI-TOF measurements, and Dr. Peter Bellstedt for help with the NMR measurements.

ABBREVIATIONS

PMDETA, *N,N,N′,N′,N″*-pentamethyldiethylenetriamine; IPA, isopropyl alcohol.

REFERENCES

(1) Lewis, N. S.; Nocera, D. G. *Proc. Natl. Acad. Sci. U. S. A.* **2006**, *103* (43), 15729−15735.
(2) Concepcion, J. J.; House, R. L.; Papanikolas, J. M.; Meyer, T. J. *Proc. Natl. Acad. Sci. U. S. A.* **2012**, *109* (39), 15560−15564.
(3) Gust, D.; Moore, T. A.; Moore, A. L. *Acc. Chem. Res.* **2009**, *42* (12), 1890−1898.
(4) Alstrum-Acevedo, J. H.; Brennaman, M. K.; Meyer, T. J. *Inorg. Chem.* **2005**, *44* (20), 6802−6827.
(5) Nicolas, J.; Guillaneuf, Y.; Lefay, C.; Bertin, D.; Gigmes, D.; Charleux, B. *Prog. Polym. Sci.* **2013**, *38* (1), 63−235.
(6) Rizzardo, E.; Solomon, D. H. *Aust. J. Chem.* **2012**, *65* (8), 945−969.
(7) Moad, G.; Rizzardo, E.; Thang, S. H. *Aust. J. Chem.* **2005**, *58* (6), 379−410.
(8) Hadjichristidis, N.; Iatrou, H.; Pitsikalis, M.; Mays, J. *Prog. Polym. Sci.* **2006**, *31* (12), 1068−1132.
(9) Schroot, R.; Friebe, C.; Altuntas, E.; Crotty, S.; Jäger, M.; Schubert, U. S. *Macromolecules* **2013**, *46* (6), 2039−2048.
(10) Kübel, J.; Schroot, R.; Wächtler, M.; Schubert, U. S.; Dietzek, B.; Jäger, M. *J. Phys. Chem. C* **2015**, *119* (9), 4742−4751.
(11) Suraru, S.-L.; Würthner, F. *Angew. Chem., Int. Ed.* **2014**, *53* (29), 7428−7448.
(12) Huang, C.; Barlow, S.; Marder, S. R. *J. Org. Chem.* **2011**, *76* (8), 2386−2407.
(13) Zhan, X.; Facchetti, A.; Barlow, S.; Marks, T. J.; Ratner, M. A.; Wasielewski, M. R.; Marder, S. R. *Adv. Mater.* **2011**, *23* (2), 268−284.
(14) Bhosale, S. V.; Jani, C. H.; Langford, S. J. *Chem. Soc. Rev.* **2008**, *37* (2), 331−342.
(15) Kumar, M.; George, S. J. *Chem. - Eur. J.* **2011**, *17* (40), 11102−11106.
(16) Sakurai, S.-i.; Areephong, J.; Bertone, L.; Lin, N.-T.; Sakai, N.; Matile, S. *Energy Environ. Sci.* **2011**, *4* (7), 2409−2416.
(17) Yushchenko, O.; Villamaina, D.; Sakai, N.; Matile, S.; Vauthey, E. *J. Phys. Chem. C* **2015**, *119* (27), 14999−15008.
(18) Zhou, W.; Wen, Y.; Ma, L.; Liu, Y.; Zhan, X. *Macromolecules* **2012**, *45* (10), 4115−4121.
(19) Sommer, M. *J. Mater. Chem. C* **2014**, *2* (17), 3088−3098.
(20) Juris, A.; Balzani, V.; Barigelletti, F.; Campagna, S.; Belser, P.; Vonzelewsky, A. *Coord. Chem. Rev.* **1988**, *84*, 85−277.
(21) Campagna, S.; Puntoriero, F.; Nastasi, F.; Bergamini, G.; Balzani, V. Photochemistry and photophysics of coordination compounds: Ruthenium. In *Photochemistry and Photophysics of Coordination Compounds I*; Balzani, V., Campagna, S., Eds.; Springer-Verlag: Berlin, 2007; Vol. *280*, pp 117−214.
(22) Thompson, D. W.; Ito, A.; Meyer, T. J. *Pure Appl. Chem.* **2013**, *85* (7), 1257−1305.
(23) Fang, Z.; Ito, A.; Keinan, S.; Chen, Z.; Watson, Z.; Rochette, J.; Kanai, Y.; Taylor, D.; Schanze, K. S.; Meyer, T. J. *Inorg. Chem.* **2013**, *52* (15), 8511−8520.
(24) Puodziukynaite, E.; Wang, L.; Schanze, K. S.; Papanikolas, J. M.; Reynolds, J. R. *Polym. Chem.* **2014**, *5* (7), 2363−2369.
(25) Sun, Y.; Chen, Z.; Puodziukynaite, E.; Jenkins, D. M.; Reynolds, J. R.; Schanze, K. S. *Macromolecules* **2012**, *45* (6), 2632−2642.
(26) Abrahamsson, M.; Jäger, M.; Österman, T.; Eriksson, L.; Persson, P.; Becker, H.-C.; Johansson, O.; Hammarström, L. *J. Am. Chem. Soc.* **2006**, *128* (39), 12616−12617.
(27) Jäger, M.; Kumar, R. J.; Görls, H.; Bergquist, J.; Johansson, O. *Inorg. Chem.* **2009**, *48* (7), 3228−3238.
(28) Abrahamsson, M.; Jäger, M.; Kumar, R. J.; Österman, T.; Persson, P.; Becker, H.-C.; Johansson, O.; Hammarström, L. *J. Am. Chem. Soc.* **2008**, *130* (46), 15533−15542.
(29) Kumar, R. J.; Karlsson, S.; Streich, D.; Jensen, A. R.; Jäger, M.; Becker, H.-C.; Bergquist, J.; Johansson, O.; Hammarström, L. *Chem. - Eur. J.* **2010**, *16* (9), 2830−2842.
(30) Jäger, M.; Eriksson, L.; Bergquist, J.; Johansson, O. *J. Org. Chem.* **2007**, *72* (26), 10227−10230.
(31) Jäger, M.; Kumar, R. J.; Görls, H.; Bergquist, J.; Johansson, O. *Inorg. Chem.* **2009**, *48* (7), 3228−3238.
(32) Tambara, K.; Ponnuswamy, N.; Hennrich, G.; Pantos, G. D. *J. Org. Chem.* **2011**, *76* (9), 3338−3347.
(33) Baron, A.; Herrero, C.; Quaranta, A.; Charlot, M.-F.; Leibl, W.; Vauzeilles, B.; Aukauloo, A. *Chem. Commun.* **2011**, *47* (39), 11011−11013.
(34) The fair yield (55%) for **D1** is attributed to an incomplete conversion. However, the starting material can be recovered and is available for further reactions. Furthermore, under optimized conditions (addition of KI at the reaction start) yields up to 75% were reached for similar systems (unpublished results).
(35) At least five samples with an approximated volume of 20−40 μL were taken during the reaction. With respect to the reaction scale (volume: 0.4 mL; see Experimental Section) the amount of lost material due to sampling has to be considered and causes the apparent low yield although a full conversion was detected.
(36) Hesse, M.; Meier, H.; Zeeh, B. *Spectroscopic Methods in Organic Chemistry*, 2nd ed.; Georg Thieme Verlag: Stuttgart, 2007.
(37) Nicholson, R. S.; Shain, I. *Anal. Chem.* **1964**, *36* (4), 706−723.
(38) Van Benschoten, J. J.; Lewis, J. Y.; Heineman, W. R.; Roston, D. A.; Kissinger, P. T. *J. Chem. Educ.* **1983**, *60* (9), 772.
(39) Bard, A. J. F.; Larry, R. *Electrochemical Methods*, 2nd ed.; Wiley: New York, 2001.
(40) Ganesan, P.; van Lagen, B.; Marcelis, A. T. M.; Sudhölter, E. J. R.; Zuilhof, H. *Org. Lett.* **2007**, *9* (12), 2297−2300.
(41) Bell, T. D. M.; Bhosale, S. V.; Forsyth, C. M.; Hayne, D.; Ghiggino, K. P.; Hutchison, J. A.; Jani, C. H.; Langford, S. J.; Lee, M. A. P.; Woodward, C. P. *Chem. Commun.* **2010**, *46* (27), 4881−4883.
(42) Licchelli, M.; Orbelli Biroli, A.; Poggi, A. *Org. Lett.* **2006**, *8* (5), 915−918.
(43) Rajdev, P.; Molla, M. R.; Ghosh, S. *Langmuir* **2014**, *30* (8), 1969−1976.
(44) Kar, H.; Molla, M. R.; Ghosh, S. *Chem. Commun.* **2013**, *49* (39), 4220−4222.
(45) Das, A.; Ghosh, S. *Macromolecules* **2013**, *46* (10), 3939−3949.
(46) Shao, H.; Seifert, J.; Romano, N. C.; Gao, M.; Helmus, J. J.; Jaroniec, C. P.; Modarelli, D. A.; Parquette, J. R. *Angew. Chem., Int. Ed.* **2010**, *49* (42), 7688−7691.
(47) Kumar, M.; George, S. J. *Nanoscale* **2011**, *3* (5), 2130−2133.
(48) Barros, T. C.; Brochsztain, S.; Toscano, V. G.; Filho, P. B.; Politi, M. J. *J. Photochem. Photobiol., A* **1997**, *111* (1−3), 97−104.

DOI: 10.1021/acs.macromol.5b02717
Macromolecules 2016, 49, 2112−2123

(49) Kulkarni, C.; George, S. J. *Chem. - Eur. J.* **2014**, *20* (16), 4537−4541.
(50) Licchelli, M.; Linati, L.; Orbelli Biroli, A.; Perani, E.; Poggi, A.; Sacchi, D. *Chem. - Eur. J.* **2002**, *8* (22), 5161−5169.
(51) Tu, S.; Kim, S. H.; Joseph, J.; Modarelli, D. A.; Parquette, J. R. *J. Am. Chem. Soc.* **2011**, *133* (47), 19125−19130.
(52) Molla, M. R.; Gehrig, D.; Roy, L.; Kamm, V.; Paul, A.; Laquai, F.; Ghosh, S. *Chem. - Eur. J.* **2014**, *20* (3), 760−771.
(53) Lasitha, P.; Prasad, E. *RSC Adv.* **2015**, *5* (52), 41420−41427.

DOI: 10.1021/acs.macromol.5b02717
Macromolecules 2016, 49, 2112−2123

Publication P3

Hydrophilic poly(naphthalene diimide) based acceptor-photosensitizer dyads: Towards water-processible modular photoredox-active architectures

R. Schroot, T. Schlotthauer, M. Jäger, U. S. Schubert, *Macromol. Chem. Phys.* **2017**, *218*, 1600534.

The paper as well as the supporting information (free of charge) are available online under: doi.org/10.1002/macp.201600534

Volume 218 • Number 6 • March 20, 2017

www.mcp-journal.de

Macromolecular Chemistry and Physics

Founded by Hermann Staudinger

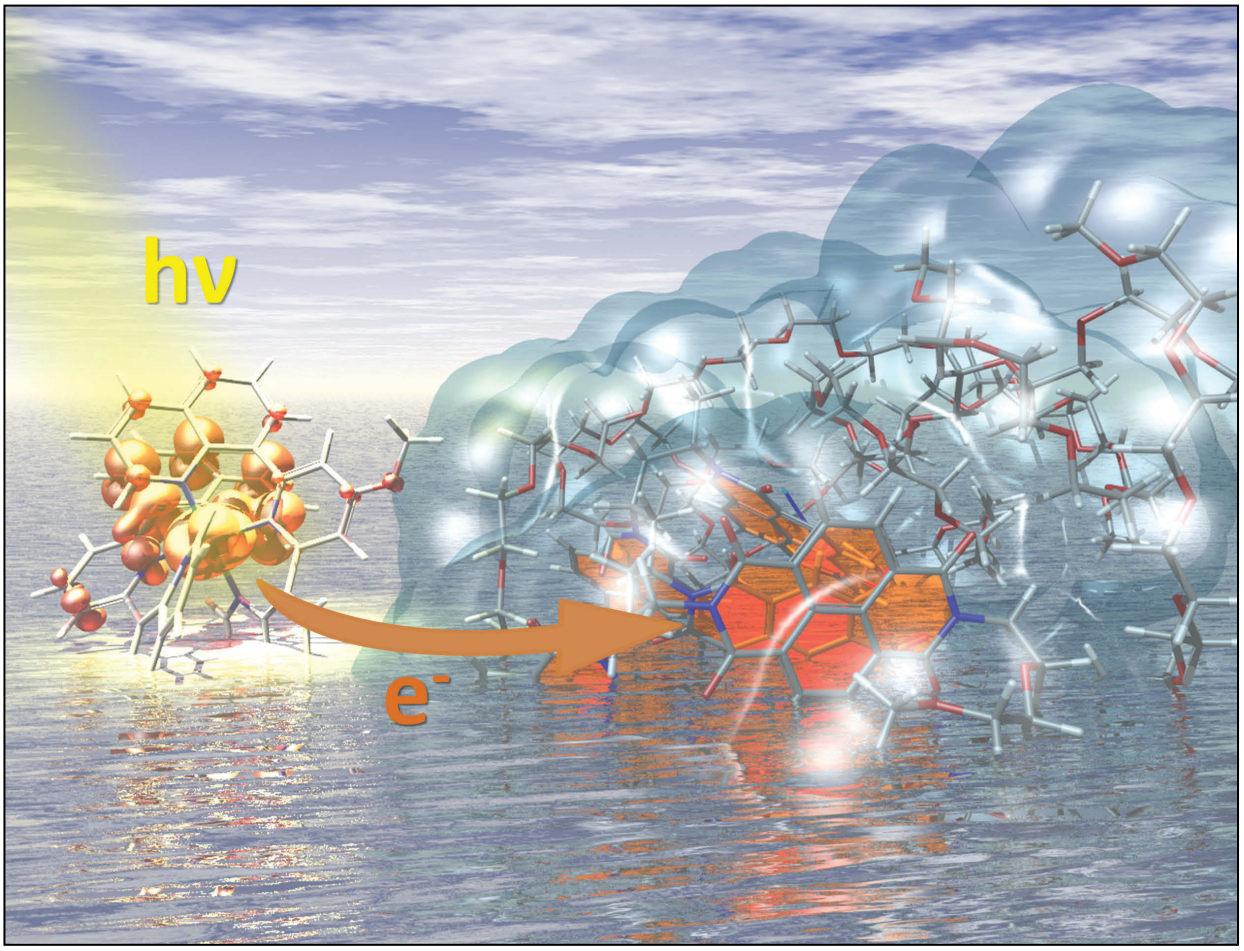

6/2017

WILEY-VCH

Macromolecular Journals

Macromolecular Chemistry and Physics

Hydrophilic Poly(naphthalene diimide)-Based Acceptor–Photosensitizer Dyads: Toward Water-Processible Modular Photoredox-Active Architectures

Robert Schroot, Tina Schlotthauer, Michael Jäger,* Ulrich S. Schubert*

Hydrophilic naphthalene diimide based acceptor polymers are prepared by the incorporation of triethylene glycol or poly(ethylene glycol) side chains in the monomers and subsequent nitroxide-mediated polymerization (NMP). The kinetic investigation of the polymerization reveals a controlled chain growth as well as a narrow molar mass distribution. Due to the utilization of a functional NMP initiator, a single Ru(II) photosensitizer unit is readily attached at the polymers chain terminus by a modular approach to construct water soluble photoredox-active acceptor–photosensitizer dyads. The analysis of the optical properties by steady-state absorption and emission spectroscopy reveals preserved optical absorption properties of the individual building blocks, and, more importantly, an efficient quenching of the Ru(II) emission assigned to intramolecular charge transfer from the complex to the acceptor polymer. The results demonstrate the versatility of side chain modifications to prepare water-processible photoredox-active architectures under preservation of the modular character known from hydrophobic systems.

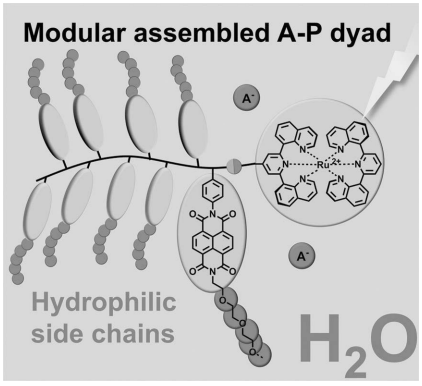

1. Introduction

The conversion of sunlight into storable energy forms, e.g., electrical or chemical bond energy, can be realized in photoredox-active architectures consisting of light harvesting and charge transport units.[1] In such devices the initial light absorption of the photosensitizer (P) leads to an excited state, followed by a primary charge separation and an additional separation and transport of the generated charges in the attached donor or acceptor moieties, i.e., p - or n-conducting building blocks. Finally, the generated charges are collected at an electrode or are consumed in a catalytic reaction.[2,5]

The presented approach toward photoredox-active architectures is based on a modular design, e.g., a ruthenium-based photosensitizer and electron acceptor or donor polymers, which can be prepared separately and finally linked together. Hence, the individual parts can be optimized and a high flexibility in the final architecture is achieved. Recently, we demonstrated the suitability of this modular approach by the preparation of a series of

R. Schroot, T. Schlotthauer, Dr. M. Jäger, Prof. U. S. Schubert
Laboratory of Organic and Macromolecular Chemistry (IOMC)
Friedrich Schiller University Jena
Humboldtstraße 10, 07743 Jena, Germany
E-mail: michael.jager.iomc@uni-jena.de;
ulrich.schubert@uni-jena.de
R. Schroot, T. Schlotthauer, Dr. M. Jäger, Prof. U. S. Schubert
Center for Energy and Environmental Chemistry Jena (CEEC Jena)
Friedrich Schiller University Jena
Philosophenweg 7a, 07743 Jena, Germany

acceptor–photosensitizer dyads[6] and, in addition, the desired charge separation was proved by spectroscopic studies.[7]

Besides the optical and electrochemical properties, the processability and the control of the morphology play a crucial role with respect to the fabrication of working devices. Therefore, the introduction of hydrophilic phase-forming moieties in the applied polymers is a potent strategy to guarantee the solubility in environmentally friendly polar solvents, e.g., water or alcohols,[8–13] to allow the application of orthogonal solvents in the layer-by-layer processes[11] and to control the morphology by self-assembly of the macromolecules.[14–19]

In this contribution, the synthesis of oligo- and poly(ethylene glycol) (PEG) decorated naphthalene diimide (NDI)-based styrenic polymers is presented in order to increase the hydrophilicity of acceptor–photosensitizer dyads and, thereby, the solubility and processability in polar solvents in comparison with the alkyl-substituted analogs.[6] The versatility of the general scope is demonstrated by kinetic investigations of the nitroxide-mediated polymerization (NMP) polymerization and the modular construction of a hydrophilic acceptor–photosensitizer dyad (A–P dyad) using a ruthenium(II) complex. The influence of the PEG substitution on the synthetic procedure as well as the physical and optical properties is investigated with respect to the preservation of the modular character.

2. Experimental Section

All reagents were purchased from ABCR, Acros Organics, Alfa Aesar, Apollo Scientific, Sigma-Aldrich, or TCI chemicals, and were used without further purification unless otherwise noted. Dry pyridine and dry *N*-*N*-dimethylformamide (DMF) were commercially available. All solvents were degassed before use. Methoxytriethylene glycol amine (MTEG-NH_2) was prepared according to literature procedures following a Gabriel synthesis protocol[20,21] and subsequent hydrazinolysis.[21,22] Methoxypoly(ethylene glycol) amine 550 (MPEG-NH_2 550) was prepared by Staudinger reaction according to the literature.[23] [Ru(dqp)(dqpOH)][PF_6]$_2$[24] (dqp is 2,6-di(quinolin-8-yl)pyridine, dqp-OH is 4-hydroxy-2,6-di(quinolin-8-yl)pyridine) and [Ru(dqp)$_2$][PF_6]$_2$[25] were prepared as described previously.

2.1. *N*-(MTEG)-naphthalene-1,8-dicarboxyanhydride-4,5-dicarboxyimide (3)

A vial was charged with 1,4,5,8-naphthalenetetracarboxylic dianhydride (0.657 g, 2.451 mmol), methoxytriethylene glycol amine (0.400 g, 2.451 mmol), and dry DMF (17 mL). After the vial was capped and flushed with nitrogen for 20 min, the brown suspension was homogenized by ultrasound sonication for 10 min. Afterward, the vial was heated 5 min at 75 °C and 15 min at 140 °C under microwave irradiation. Subsequently, the solvent was removed under reduced pressure and CH_2Cl_2 as well as water were added and the phases were separated. The aqueous phase was extracted five times with CH_2Cl_2 (5 × 50 mL). The combined organic layers were concentrated and the crude product was used without further purification (0.870 g, 86%, purity ≈80% according to NMR, impurities by bisfunctionalized diimide). ^{1}H NMR (300 MHz, $CDCl_3$): δ 8.82 (s, 4H, NaphH), 4.55–4.41 (m, 2H, CH_2), 3.90–3.82 (m, 2H, CH_2), 3.76–3.68 (m, 2H, CH_2), 3.68–3.53 (m, 4H, CH_2), 3.53–3.43 (m, 2H, CH_2), 3.32 (s, 3H, CH_3).

2.2. *N*-(MTEG)-*N*′-(vinylphenyl)-naphthalene-1,4,5,8-dicarboxydiimide (1)

Crude *N*-(MTEG)-naphthalene-1,8-dicarboxyanhydride-4,5-dicarboxyimide (0.870 g, 1 eq.), 4-aminostyrene (0.301 g, 1.2 eq, 2.530 mmol), and $ZnSO_4 \cdot 1H_2O$ (0.227 g, 0.6 eq, 1.263 mmol) were dissolved in dry pyridine (15 mL) under nitrogen. The mixture was heated to reflux for 4 h. The crude product was precipitated in 1 M HCl (120 mL), filtered off, and washed with water. The solid was redissolved in CH_2Cl_2, washed with water as well as brine, dried over Na_2SO_4, and the solvent was removed under reduced pressure. Purification by column chromatography (silica, CH_2Cl_2) gave the product as bright yellow solid (0.585 g, 54%). ^{1}H NMR (300 MHz, $CDCl_3$): δ 8.79 (s, 4H, NaphH), 7.61 (d, J = 8.4 Hz, 2H, ArH), 7.30 (d, J = 8.4 Hz, 2H, ArH), 6.81 (dd, J = 17.6, 10.9 Hz, 1H, C**H** = CH_2), 5.84 (d, J = 17.6 Hz, 1H, CH = C**H**$_2$-trans), 5.37 (d, J = 10.9 Hz, 1H, CH = C**H**$_2$-cis), 4.48 (t, J = 5.9 Hz, 2H, CH_2), 3.87 (t, J = 5.8 Hz, 2H, CH_2), 3.67–3.55 (m, 4H, CH_2), 3.53–3.44 (m, 2H, CH_2), 3.33 (s, 3H, CH_3). ^{13}C NMR (63 MHz, $CDCl_3$): δ 163.1, 163.0, 138.7, 136.1, 134.0, 131.5, 131.2, 128.7, 127.4, 127.2, 127.0, 126.9, 115.6, 72.0, 70.8, 70.7, 70.3, 67.9, 59.0, 39.8. HR-ESI ([$C_{29}H_{26}N_2O_7$]Na^+) *m/z*: calc: 537.1632, found: 537.1629, Error: 0.7 ppm.

2.3. *N*-(MPEG 550)-naphthalene-1,8-dicarboxyanhydride-4,5-dicarboxyimide (4)

A vial was charged with 1,4,5,8-naphthalenetetracarboxylic dianhydride (0.488 g, 1.818 mmol), MPEG-NH_2 550 (1.000 g, 1.818 mmol), and dry DMF (20 mL). After the vial was capped and flushed with nitrogen for 20 min, the brown suspension was homogenized by ultrasound sonication for 10 min. Afterward, the vial was heated 5 min at 75 °C and 15 min at 140 °C under microwave irradiation. Subsequently, the solvent was removed under reduced pressure, CH_2Cl_2 and water were added, and the phases were separated. The aqueous phase was extracted five times with CH_2Cl_2. The combined organic layers were concentrated and the crude product was used without further purification (1.600 g, quantitative, purity ≈75% according to NMR, impurities by DMF and bisfunctionalized diimide). ^{1}H NMR (300 MHz, $CDCl_3$): δ 8.82 (s, 4H, NaphH), 4.57–4.37 (m, 2H, CH_2), 3.90–3.82 (m, 2H, CH_2), 3.79–3.41 (m, 48H, CH_2), 3.38 (s, 3H, CH_3).

2.4. *N*-(MPEG 550)-*N*′-(vinylphenyl)-naphthalene-1,4,5,8-dicarboxydiimide (2)

Crude *N*-(MPEG 550)-naphthalene-1,8-dicarboxyanhydride-4,5-dicarboxyimide (1.000 g, 1 eq.), 4-aminostyrene (0.174 g, 1.2 eq, 1.463 mmol), and $ZnSO_4 \cdot 1H_2O$ (0.131 g, 0.6 eq, 0.732 mmol) were dissolved in dry pyridine (30 mL) under nitrogen. The mixture

Macromol. Chem. Phys. **2017**, DOI: 10.1002/macp.201600534

Table 1. Prepared polymers as well as experimental conditions and analytical data.

Entry	Polymer[a)]	Monomer	*M/I*	M_n [g mol^{-1}][b)]	*Đ*
1	**Cl-P1**$_8$	**1**	20	4900	1.11
2	**Cl-P1**$_{16}$	**1**	20	7900	1.13
3	**Cl-P2**$_{10}$	**2**	20	16 000	1.26
4	**Cl-P2**$_8$	**2**	20	14 000	1.14
5	**Cl-P2**$_{11}$	**2**	20	16 700	1.28

[a)]All reactions were carried out in anisole with CMSt-TIPNO as initiator, the subscripted number represents the degree of polymerization determined by ^{1}H NMR; [b)]Determined by SEC (chloroform/*iso*-propanol/triethylamine [94:2:4], PS calibration).

was heated to reflux overnight. The crude product was diluted with CH_2Cl_2, filtered, and concentrated under reduced pressure. Due to the high polarity of the compounds, the pure product (dark green to brown oil) was isolated by preparative size-exclusion chromatography (SEC) (Bio-Beads S-X3) and not by a silica column (0.690 g, 62%). ^{1}H NMR (300 MHz, $CDCl_3$): δ 8.78 (s, 4H, NaphH), 7.60 (d, J = 8.5 Hz, 2H, ArH), 7.29 (d, J = 8.5 Hz, 2H, ArH), 6.80 (dd, J = 17.5, 11.0 Hz, 1H, C**H** = CH_2), 5.84 (d, J = 17.5 Hz, 1H, CH = C**H**$_2$-trans), 5.35 (d, J = 11.0 Hz, 1H, CH = C**H**$_2$-cis), 4.54–4.36 (m, 2H, CH_2), 4.01–3.79 (m, 2H, CH_2), 3.79–3.46 (m, 42H, CH_2), 3.37 (s, 3H, CH_3). ^{13}C NMR (101 MHz, $CDCl_3$): δ 163.0, 162.8, 138.6, 136.0, 133.8, 131.4, 131.1, 128.6, 127.3, 127.0, 126.9, 126.8, 115.5, 71.9, 70.6 (2×), 70.5, 70.1, 67.8, 59.0, 39.6. MS (matrix-assisted laser desorption/ionization time-of-flight (MALDI-TOF), dithranol) *m/z*: 933.4 ([$C_{22}H_{11}N_2O_4(C_2H_4O)_{12}CH_3$]+Na$^+$). Note that some batches still contained NDI-(MPEG 550)$_2$ as minor impurity, as this side product is hard to separate from the monomer in larger batches (see the Results and Discussion section and Figure S14 in the Supporting Information). This byproduct was expected and proved to be inert in the polymerization (vide infra).

2.5. General Polymerization Procedure

A glass tube equipped with a septum and an external overhead flushing with nitrogen was used for the polymerizations (Figure S1, Supporting Information). The reaction vessel was charged with monomer, initiator and solvent, purged with nitrogen for 20 min and placed in a preheated oil bath (120 °C). The purification is described for each polymer. Experimental conditions and analytical data are given in Table 1.

Cl-P1$_8$ was prepared according to the general procedure using **1** (0.200 g, 0.389 mmol), *N*-(*tert*-butyl)-*O*-(1-(4-(chloromethyl) phenyl)ethyl)-*N*-(2-methyl-1-phenylpropyl)hydroxylamine (CMSt-TIPNO) (0.007 g, 0.019 mmol) and anisole (1.2 mL). After 24 h the reaction mixture was diluted with CH_2Cl_2 and unreacted monomer was removed by preparative SEC (Bio-Beads S-X1, CH_2Cl_2). The polymer was obtained as brown solid after precipitation in MeOH. Yield: 0.050 g. SEC ($CHCl_3$/*i*-PrOH /NEt_3 94/2/4, polystyrene (PS) calibration): M_n = 4900 g mol^{-1}, *Đ* = 1.11. ^{1}H NMR (300 MHz, $CDCl_3$): δ 9.14–8.09 (br), 7.90–6.73 (br), 4.87–4.09 (br), 3.90–3.70 (br), 3.70–3.60 (br), 3.60–3.45 (br), 3.45–3.35 (br), 3.35–3.11 (br). 2.96–0.13 (br).

Cl-P1$_{16}$ was prepared according to the general procedure using **1** (0.286 g, 0.556 mmol), CMSt-TIPNO (0.010 g, 0.028 mmol), and anisole (1.65 mL). Samples were taken for SEC and NMR analysis. After 48 h the reaction mixture was diluted with CH_2Cl_2 and unreacted monomer was removed by preparative SEC (Bio-Beads S-X1, CH_2Cl_2). Yield: 0.125 g. SEC ($CHCl_3$/*i*-PrOH/NEt_3 94/2/4, PS calibration): M_n = 7900 g mol^{-1}, *Đ* = 1.13.

Cl-P2$_{10}$ was prepared according to the general procedure using **2** (0.120 g, 0.130 mmol), CMSt-TIPNO (0.002 g, 0.006 mmol), and anisole (0.5 mL). After 25 h the reaction mixture was diluted with CH_2Cl_2 and unreacted monomer was removed by preparative SEC (Bio-Beads S-X1, CH_2Cl_2). The polymer was obtained as brown solid after precipitation in pentane. Yield: 0.062 g. SEC ($CHCl_3$/*i*-PrOH/NEt_3 94/2/4, PS calibration): M_n = 16 000 g mol^{-1}, *Đ* = 1.26. ^{1}H NMR (300 MHz, $CDCl_3$): δ 9.28–8.01 (br), 8.01–6.70 (br), 4.95–4.09 (br), 4.09–3.45 (br), 3.45–3.15 (br), 2.96–0.67 (br).

Cl-P2$_8$ was prepared according to the general procedure using **2** (0.420 g, 0.457 mmol), CMSt-TIPNO (0.009 g, 0.023 mmol), and anisole (1.0 mL). After 18 h the reaction mixture was diluted with CH_2Cl_2 and unreacted monomer was removed by preparative SEC (Bio-Beads S-X1, CH_2Cl_2). The polymer was obtained as brown solid after precipitation in pentane. Yield: 0.152 g. SEC ($CHCl_3$/*i*-PrOH/NEt_3 94/2/4, PS calibration): M_n = 14 000 g mol^{-1}, *Đ* = 1.14.

Cl-P2$_{11}$ was prepared according to the general procedure using **2** (containing 8% NDI-(MPEG 550)$_2$,[26] 0.700 g, 0.685 mmol), CMSt-TIPNO (0.013 g, 0.034 mmol), and anisole (2.5 mL). Samples were taken for SEC and NMR analysis. After 72 h the reaction mixture was diluted with CH_2Cl_2 and unreacted monomer was removed by preparative SEC (Bio-Beads S-X1, CH_2Cl_2). The polymer was obtained as brown solid after precipitation in pentane. Yield: 0.110 g. SEC ($CHCl_3$/*i*-PrOH/NEt_3 94/2/4, PS calibration): M_n = 16 700 g mol^{-1}, *Đ* = 1.28.

2.6. End Functionalization Procedure

Ru-P2$_{10}$**.** A vial was charged with **Cl-P2**$_{10}$ (0.020 g, 0.0015 mmol, 1 eq.), K_2CO_3 (0.001 g, 0.006 mmol, 4 eq.), KI (0.001 g, 0.006 mmol, 4 eq.), and [Ru(dqp)(dqpOH)][PF_6]$_2$ (0.003 g, 0.003 mmol, 2 eq.). Then, the vial was sealed, evacuated, and flushed with nitrogen. Dry DMF (0.5 mL) was added and the resulting solution was heated to 60 °C. The reaction progress was monitored by thin layer chromatography (TLC) (aluminum oxide, CH_2Cl_2/MeOH 95/5) and analytical size exclusion chromatography (DMAc + 0.08% NH_4PF_6, diode array detection). The reaction was continued until no further conversion was monitored (96 h). The mixture was diluted with a minimum amount of tetrahydrofuran (THF). The following precipitation into aqueous NH_4PF_6 solution was not successful. For this purpose, the solvent was removed under

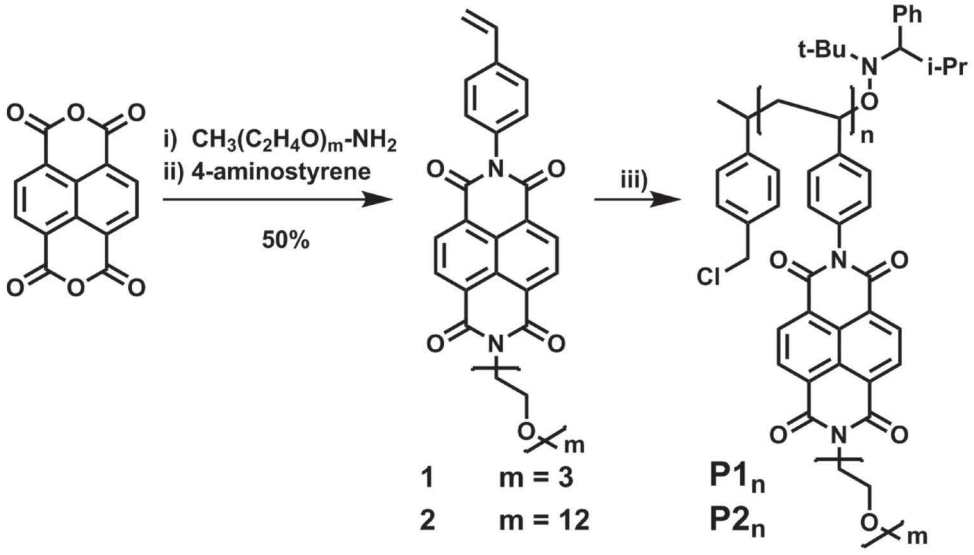

Scheme 1. Schematic representation of the synthesis of monomers 1 and 2 as well as subsequent polymerization. Conditions: i) DMF, microwave irradiation, N2, 75 °C (5 min), 140 °C (15 min); ii) 4-aminostyrene, $ZnSO_4 \cdot 1H_2O$, pyridine, reflux, 4 h; 50% over both steps. iii) CMSt-TIPNO, anisole, N2, 120 °C.

reduced pressure and the residual solid was redissolved in CH_2Cl_2 and filtered. The resulting clear solution was transferred onto a preparative size-exclusion chromatography column (Toyopearl HW-55F, CH_2Cl_2/MeOH 95/5) to give the dyad **Ru-P2**$_{10}$ as red solid (0.015 g, 70%). ^{1}H NMR (300 MHz, CD_2Cl_2): δ 9.03–8.16 (br, **P2**$_{10}$), 8.05 (br, Ru), 7.97 (br, Ru), 7.89 (br, Ru), 7.73 (br, Ru), 7.65 (br, Ru), 7.48 (br, Ru), 7.60–6.57 (br, **P2**$_{10}$), 5.58–5.41 (br, linker), 4.63–4.02 (br, **P2**$_{10}$), 3.96–3.38 (br, **P2**$_{10}$), 3.32 (s, **P2**$_{10}$), 2.96–0.70 (br, **P2**$_{10}$).

3. Results and Discussion

3.1. Monomer Synthesis and Polymerization

The monomers **1** and **2** were prepared by a two-step synthesis from 1,4,5,8-naphthalenetetracarboxylic dianhydride in analogy to previously described NDIs (Scheme 1).[6] In the first step, the respective monoimide was prepared by reaction with MTEG-NH_2 or MPEG-NH_2 550 in DMF under microwave irradiation. The obtained crude product, containing minor impurities of unfunctionalized and bis-functionalized compounds, was used without further purification. The subsequent reaction with 4-aminostyrene gave the product in good yields. Noteworthily, the isolation of **2** was precluded by ordinary column chromatography due to the high polarity of the compound. As a consequence, the monomer was purified by SEC using the Bio-Beads S-X3 resin. Thereby, in particular the separation of the desired monomer and the bis-PEGylated species NDI-(MPEG 550)$_2$ in larger scales is challenging due to overlapping peaks during elution. All collected fractions were checked with ^{1}H NMR and were combined in case of less than 10% impurity of this side product (Figure S14, Supporting Information). The side product is expected to be indifferent in the later polymerization as it contains no polymerizable group.

The polymerizations were carried out in anisole at 120 °C with the commercial functional NMP initiator CMSt-TIPNO. The unreacted monomer was subsequently removed by preparative SEC (Bio-Beads S-X1). The isolated polymers as well as the experimental conditions and analytical data are listed in Table 1. The labeling of the polymers (P) is based on the used monomers (**1** or **2**), the functional endgroup (Cl), and the degree of polymerization (DP) as subscripted number. The ^{1}H NMR spectra show the typical broad NDI resonance at 8.5 ppm and a second broad signal of the phenylene units (7.2 ppm) in the aromatic region. The signal of the chloromethyl group, which is used to determine the DP, appears at ≈4.5 ppm (see chapter NMR data in the Supporting Information). The MTEG and MPEG 550 protons were found as overlapping signals between 4.0 and 3.0 ppm. All polymers were characterized by analytical SEC and revealed narrow dispersities.

3.2. Kinetic Investigations

In order to prepare polymers with tailored molar masses the knowledge of the reaction kinetics and rate constants is required. Therefore, we performed kinetic studies for the polymerization of monomers **1** and **2**.

The nitroxide-mediated polymerization deviates from the ideal living polymerization process due to reversible and (irreversible) termination reactions. Considering all these processes—reversible dissociation (k_d)

Macromol. Chem. Phys. **2017**, DOI: 10.1002/macp.201600534

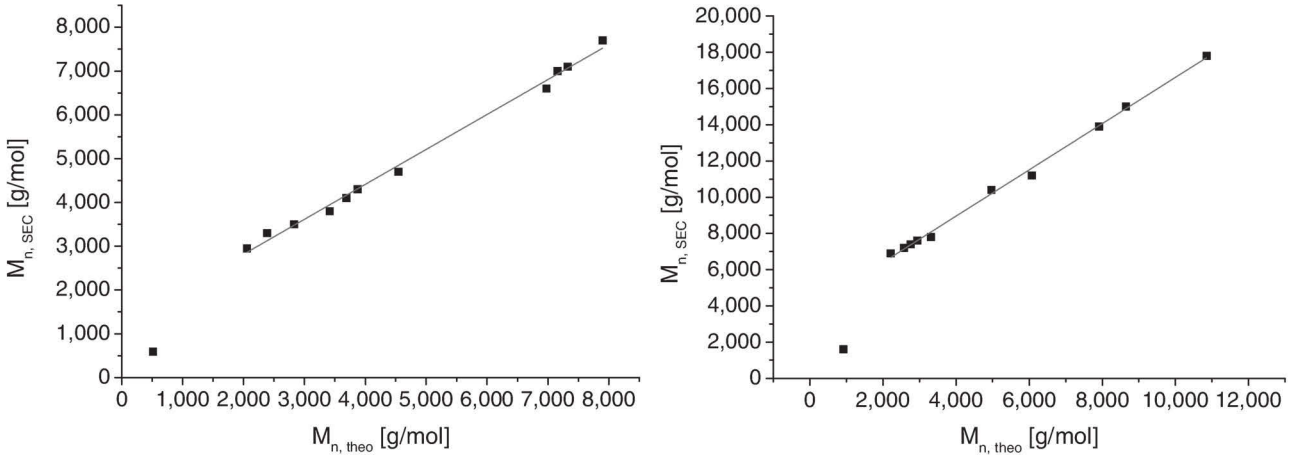

Figure 1. Plot of the molar mass determined by SEC (eluent: chloroform/*iso*-propanol/triethylamine [94:2:4], PS calibration) versus the theoretical molar mass based on the conversion (^{1}H NMR). Left: Cl-P1$_{16}$; right: Cl-P2$_{11}$.

and recombination (k_c) and irreversible termination (k_t) leading to the accumulation of persistent radicals—the evolution of the monomer concentration after an induction period is given by Equation (1)[27–29]

$$\ln\frac{[M]_o}{[M]_t}=\frac{3}{2}k_p\left(\frac{k_d[I]_o}{3k_tk_c}\right)^{1/3}t^{2/3} \quad (1)$$

Consequently, in the case of a controlled NMP mechanism the plot of $\ln[M]_0/[M]_t$ versus time to the power of two-thirds should result in a straight line. Whether the equation applies for the polymerization processes of **1** and **2** will be discussed in the following chapter.

The conversion of the polymerization reactions was determined by ^{1}H NMR based on the ratio of the vinyl groups compared to the aromatic NDI resonances and by UV–vis SEC based on the integral of the monomer and the polymer peak. Importantly, both methods gave values in the same range (Figure S26, Supporting Information). Therefore, the assumption that the monomer is exclusively converted into polymer can be made and enables the calculation of theoretical molar masses based on NMR conversion, *M*/*I* ratio, and the molar mass of the monomer.

In the case of **Cl-P1**$_{16}$, the plot of the theoretical and the SEC molar mass values reveals a linear relationship for molar masses above 2 000 g mol^{-1} (Figure 1, left). Moreover, the molar masses of the PS calibration are in the same range as the theoretical ones, suggesting a solution behavior of the polymer similar to PS, i.e., as a random coil. In contrast, a large discrepancy between the SEC molar mass and the theoretical value was observed for **Cl-P2**$_{11}$ (Figure 1, right). Apparently, the solution behavior of the polymer **Cl-P2**$_{11}$ differs strongly from a PS random coil. As the SEC data overestimate the molar mass (PS calibration) and **Cl-P2**$_{11}$ can be described as comb polymer with poly(ethylene glycol) side chains, one can tentatively assume that the polymer tends to form a rod-like structure in solution.[30]

The kinetic plots and the SEC elugrams for the preparation of **Cl-P1**$_{16}$ are shown in Figure 2 and Figure S29 (Supporting Information), respectively. As expected for a controlled polymerization the plot of the evolution of the monomer concentration versus $t^{2/3}$ (Figure 2, left) shows a linear behavior in the beginning indicating a reaction in the equilibrium period as described by Equation (1). However, a flatten of the graph is seen for reaction times over 24 h ($t^{2/3}$ = 8 h$^{2/3}$), which represents a decreasing reaction rate, i.e., termination reactions gain significance and the polymerization does not take place in an equilibrium state anymore. The slope *m* of the linear fit of the data in the equilibrium region enables the calculation of the product of all important rate constants (Equation (2)). With this value in hand (Table 2), reaction times required to reach a certain conversion can be calculated, also in comparison to other monomers (vide infra). The controlled character of the polymerization process is, additionally, revealed by the linear increase of the molar mass with the conversion and, moreover, also the dispersity decreases until 70% conversion (Figure 2, right). The slight increase in dispersity at even higher conversions is, again, an indicator for rising termination reactions.

$$\frac{k_pk_d^{1/3}}{k_t^{1/3}k_c^{1/3}}=\frac{\frac{2}{3}m\cdot 3^{1/3}}{[I]_o^{1/3}} \quad (2)$$

The experimental conditions for the polymerization leading to **Cl-P2**$_{11}$ are shown in Table 1 and Table 2. As it can be seen, most parameters, i.e., applied initiator, solvent, and *M*/*I* ratio, were identical to the preparation of **Cl-P1**$_{16}$. The only difference is a slightly higher dilution of the reaction mixture due to solubility reasons.

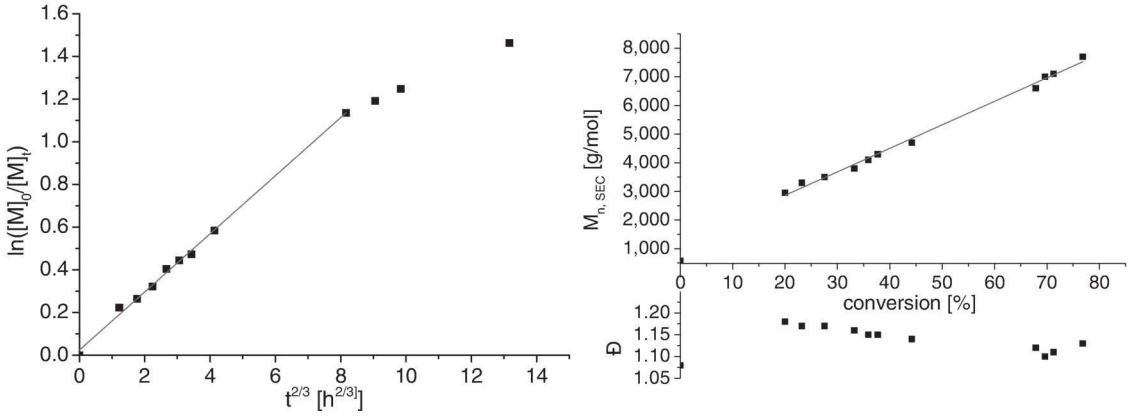

Figure 2. Kinetic data for the polymerization leading to Cl-P1$_{16}$. Left: Evolution of the monomer concentration versus $t^{2/3}$. The concentration was determined by ^{1}H NMR. Right: Data plots of the molar mass and dispersity versus conversion showing a linear increase of the molar mass. Molar masses and dispersity were determined by SEC (eluent: chloroform/*iso*-propanol/triethylamine [94:2:4], PS calibration), the conversion by ^{1}H NMR.

The reaction progress, i.e., the growth of the polymer chains, is clearly visualized by the plot of the SEC elugrams (Figure 3, left). Apparently, the reaction rate is low and only minor amounts of polymer are formed during the first hours of the reaction. Then a steady increase of the molar mass is observed and a satisfying conversion is reached after 72 h. Noteworthily, the low-molar mass tailing and the broadening of the polymer's SEC signal are indicative for increasing termination/side reactions at longer reaction times. The linear increase of the molar mass with the conversion but also the slightly increasing dispersity is additionally demonstrated by the respective plots (Figure 3, right).

The plot of the evolution of the monomer concentration versus $t^{2/3}$ enables a detailed analysis of the influence of the MPEG 550 side chains on the polymerization kinetic (Figure 4). At the first sight, deviations from the expected behavior (linear increase in the equilibrium period and flattening at the end of the reaction) are noticed. In this way, an induction period occurs at the beginning (≈15–20 min) followed by the equilibrium range. Afterward, the reaction rate decreases as indicated by the two data points below the linear fit at ≈8 and 10 $h^{2/3}$—probably due to more pronounced termination reactions—but finally an increase of the reaction rate is detected. This rise is very unusual and at the moment we can only speculate on its origin. However, in our opinion three different reasons may be plausible: (1) Solvent effects, e.g., viscosity changes, influence k_d and k_c (similar to the Trommsdorff–Norrish effect in free radical polymerization (FRP)); (2) k_d increases with the degree of polymerization as known for some monomers;[31] or (3) due to side reactions, e.g., decomposition of free nitroxide over the long reaction period, new propagating radicals are formed, which probably also explains the increasing dispersity seen by SEC. Despite these deviations from the ideal reaction kinetics, the obtained polymer features a narrow molar mass distribution and a defined molar mass.

Table 2. Initiator concentration and calculated rate constants for the investigated polymerizations leading to Cl-P1$_{16}$ and Cl-P2$_{11}$ as well as reevaluated data of p(EtHex-NDI) from previous reports.[7]

Entry	Polymer	$[I]_0$ [mmol L^{-1}]	$k_p k_d^{1/3}(k_t k_c)^{-1/3}$ [L$^{1/3}$ h$^{-2/3}$ mol$^{-1/3}$]
1	Cl-P1$_{16}$	16.85	0.51
2	Cl-P2$_{11}$	13.70	0.15
3	p(EtHex-NDI)	16.50	0.87

A comparison of the calculated reaction rate constants (Equation (2), Table 2) between **Cl-P1**$_{16}$ and **Cl-P2**$_{11}$ reveals a 3.4× smaller value for the latter one, i.e., the polymerization proceeds much slower. This finding is not surprising as the large MPEG 550 side chain presumably induces a sterical hindrance as often observed for the grafting through of comb copolymers.[32,33] Noteworthily, the reaction rate constant of **Cl-P1**$_{16}$ is already decreased by the factor 1.7 in comparison to the polymerization of the 2-ethylhexyl substituted monomer (Table 2, entry 3)[6,7] in DMF under otherwise identical conditions (Figure S27, Supporting Information).

3.3. End Functionalization with Ru(II) Dye

The end functionalization of polymer **Cl-P2**$_{10}$ with [Ru(dqp)(dqpOH)][PF$_6$]$_2$ leading to the dyad **Ru-P2**$_{10}$ was accomplished by nucleophilic substitution of the initiator's chloromethyl group in analogy to reported procedures (Scheme 2).[6] Noteworthily, in case of chain–chain couplings during the polymerization, a decoration with two Ru(II) complexes could be possible due to the availability of two reactive end groups. However, this side reaction was avoided by the relatively low polymerization conversion (60%) and, in addition, this highly charged side product

Macromol. Chem. Phys. **2017**, DOI: 10.1002/macp.201600534

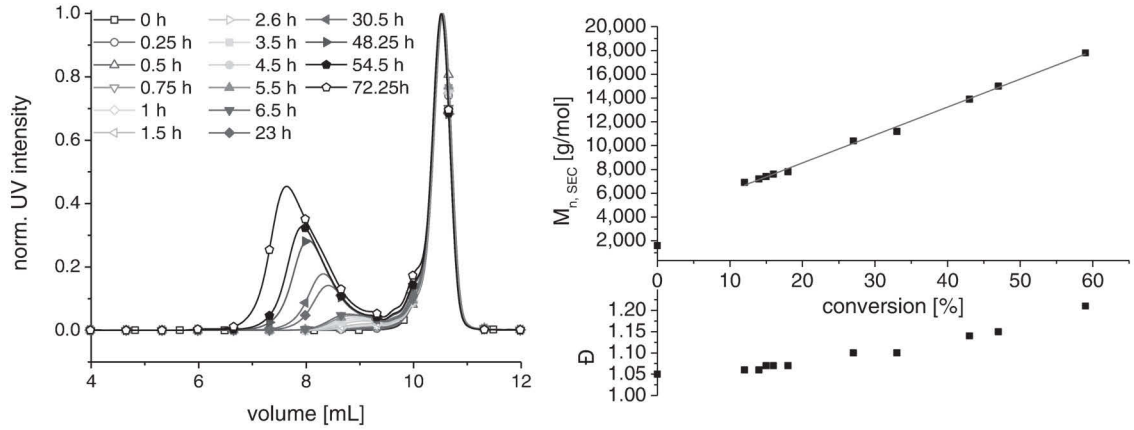

Figure 3. Left: UV–vis–SEC traces (340 nm) for the preparation of Cl-P2$_{11}$ showing the polymer growth with increasing reaction time. The traces are normalized to the monomer signal. Noteworthily, the small initial shoulder of the monomer signal is assigned to traces of NDI-(MPEG 550)$_2$. Right: Data plots of the molar mass and dispersity versus conversion. Molar masses and dispersity were determined by SEC (eluent: chloroform/*iso*-propanol/triethylamine [94:2:4], PS calibration), the conversion by ^{1}H NMR.

(+4) would be readily detected by TLC or UV–vis SEC. Due to the increased hydrophilicity of the polymer, the usual precipitation of the crude product in aqueous NH_4PF_6 solution to remove inorganic salts was not successful. Instead, these impurities were removed by filtration of a CH_2Cl_2 solution of the crude product. Subsequently, the pure polymer dyad was isolated by the established purification by preparative size-exclusion chromatography using the Toyopearl HW-55F resin.

3.4. Solubility of the Polymers and the Dyad

The hydrophilicity of the polymers **Cl-P1**$_8$ and **Cl-P2**$_{10}$ is increased compared to the alkyl substituted analogs due to the polar tri- and poly(ethylene glycol) side chain. Thereby, the hydrophilicity increases with the size of the side chain and, consequently, also the solubility in polar solvents.

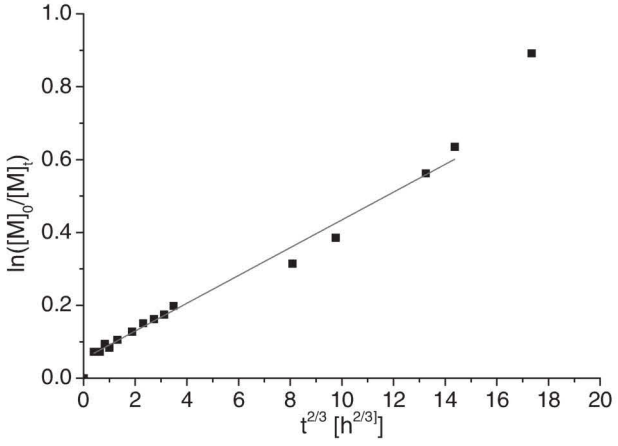

Figure 4. Evolution of the monomer concentration versus $t^{2/3}$ for the preparation of Cl-P2$_{11}$. The concentration was determined by ^{1}H NMR.

Additionally, a dependence of the solubility on the degree of polymerization of the copolymer is expected.[34,35]

In this regard the monomer **1** is soluble in halogenated solvents and also in acetone, whereas the respective polymer **Cl-P1**$_8$ is not soluble in acetone. In contrast, the MPEG 550 decorated monomer and the respective polymers are much more hydrophilic and are soluble in polar solvents, e.g., acetone, ethanol, methanol, or water. The water solubility of the polymer **Cl-P2**$_{10}$ strongly depends on the degree of polymerization, i.e., polymers with a degree of polymerization above six to eight are only limited or moderately soluble in water. The dyad **Ru-P2**$_{10}$ is highly soluble in common organic solvents, e.g., THF, CH_2Cl_2, or $CHCl_3$, and is also moderately soluble in water, enabling an assembly in a wide range of solvents with different polarity. Noteworthily, the water solubility of the compound is expected to be further increased by substitution of the hexafluorophosphate counterion with chloride. As a consequence, these materials represent an important step toward water-processible architectures and, moreover, are expected to allow a self-assembly in combination hydrophobic building blocks, e.g., electron donors. In this regard, preliminary tests showed the possibility to prepare water-based solutions of the dyad **Ru-P2**$_{10}$, which were used for drop casting of thin films (Figure S35, Supporting Information). Further investigations with respect to other film-forming techniques, e.g., spin coating or doctor blading and a detailed characterization of the films are ongoing and will be reported in due course.

3.5. Optical Spectroscopy

The optical properties of the compounds **Cl-P1**$_8$, **Cl-P2**$_{11}$, and **Ru-P2**$_{10}$ as well as the contingent influence of

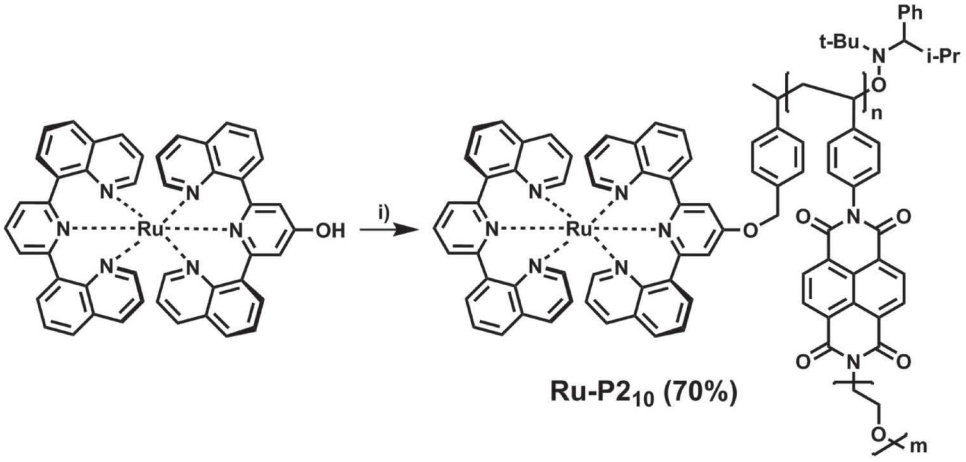

Scheme 2. Schematic representation of the synthesis of the dyad Ru-P2$_{10}$. Reagents and conditions: **Cl-P2$_{10}$**, K2CO3, KI, DMF, N2, 60 °C, 94 h.

various solvents were explored by UV–vis absorption and steady-state emission spectroscopy. The absorption spectra of the compounds in various solvents are shown in Figure 5. The NDI-based polymers feature the typical absorption bands at 360 and 380 nm. The metal-to-ligand charge transfer (MLCT) absorption band of the ruthenium dye is additionally visible around 500 nm in the spectrum of **Ru-P2$_{10}$**. An increasing polarity of the solvent results in changes of the absorption spectrum, i.e., decreased absorption at 380 nm as well as a slight bathochromic shift and increased absorptivity at shorter wavelengths (250 to 340 nm). This behavior is in particular pronounced for **Cl-P1$_8$**. These observations imply conformational changes, i.e., the chemical environment of the NDI chromophores changes induced by the solvents polarity. In solutions of small NDI molecules similar observations are associated with a stacking of individual units and the formation of J or H aggregates.[36–45] Consequently, high polar solvents may lead to a partial aggregation of NDI units in the polymer. The changes in the solution behavior seem to be most prominent for **Cl-P1$_8$** and less significant for **Cl-P2$_{11}$** and **Ru-P2$_{10}$** as the spectral changes are marginal in comparison to the literature examples.[36] In the case of **Cl-P1$_8$**, which is not soluble in pure MeOH, the broadening of the absorption band may additionally be attributed to a partial collapsing of the solvated polymer coil and the formation of aggregates.

As the stacking of NDI units is accompanied by major changes of the emission properties, a comprehensive study of the prepared compounds was conducted by steady-state emission spectroscopy. However, the expected intensive emission of stacked NDI units upon excitation at 360 nm could not be detected in any solvent (Figures S30–S32, Supporting Information). Consequently, the predominate existence of nonemissive isolated NDI units can be assumed in the investigated concentra-

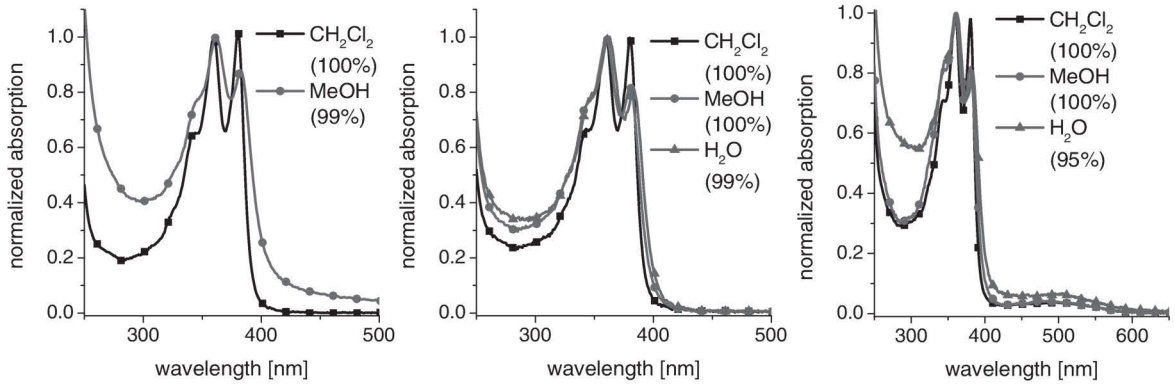

Figure 5. Left: UV–vis absorption spectra of Cl-P1$_8$ in various solvents. Middle: UV–vis absorption spectra of Cl-P2$_{11}$ in various solvents. Right: UV–vis absorption spectra of Ru-P2$_{10}$ in various solvents. Stock solutions in CH_2Cl_2 or MeOH were used. The noted percentages indicate the fraction of pure solvent, while the rest represents the volume fraction of the stock solution (aerated solutions, ≈10^{-7} M, absorbance <0.1, no inner filter effects).

Macromol. Chem. Phys. **2017**, DOI: 10.1002/macp.201600534

tion range (10^{-7} M).[36,46] This observation is somehow surprising as previously reported alkyl-chain decorated poly(naphthalene diimide)s feature an emission at 413 nm despite the restricted conformational freedom of the polystyrene backbone (Figure S33, Supporting Information).[6] In our opinion, this observation may be a consequence of the sterical hindrance of the PEG side chain, i.e., the side chain promotes the formation of rod-like structures (vide supra) with the highest possible distance between the individual NDI units in a single polymer chain. In the case of **Cl-P1**$_8$, a very weak feature was detected between 500 and 600 nm (Figure S30, Supporting Information), which may be tentatively attributed to the very weak formation of intermolecular excimers as described in the literature.[45]

Last but not least, we were interested whether the polymer is capable of quenching the dye's MCLT emission as reported for related systems, i.e., whether the compounds are suitable for light-induced charge separation applications.[6] The respective graph illustrating the recorded emission spectra of **Ru-P2**$_{10}$ and the reference complex $[Ru(dqp)_2][PF_6]_2$ upon excitation at 500 nm is shown in Figure 6. The comparison of the spectra clearly reveals the quantitative MLCT emission quenching and corroborates an electron transfer from the energetically most favorable Ru-based excited state to the NDI polymer.[6] Please note that the complex $[Ru(dqp)_2][PF_6]_2$ shows spectral properties very similar to the complex $[Ru(dqp)(dqp\text{-}O\text{-}Bn)][PF_6]_2$,[6] which features the same substitution pattern as the dyad **Ru-P2**$_{10}$ (Figure S34, Supporting Information). The detected emission around 560 nm is attributed to NDI excimer formation due to the high concentration of the solution (more than ten times higher as for the analysis of the optical properties of the polymers).

In summary, the introduction of hydrophilic MPEG side chains does not change the desired optical properties of the dyad, i.e., the absorptivity of the individual building blocks is preserved and the emission quenching is not influenced.

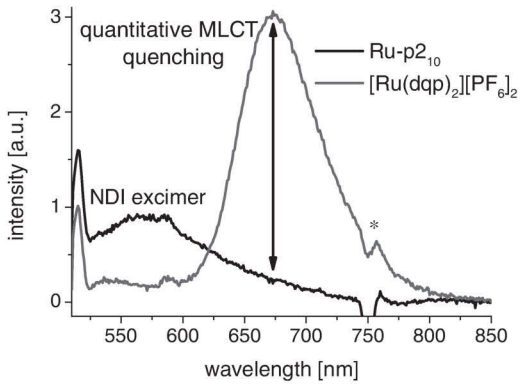

Figure 6. Emission data of the reference complex and the dyad Ru-P2$_{10}$ (aerated dichloromethane, room temperature, isoabsorbing solutions at 500 nm excitation, ≈10^{-6} M). Artefacts are marked with an asterisk.

4. Conclusions

Two styrenic naphthalene diimide based monomers with methyltriethylene or methylpoly(ethylene glycol) side chains were synthesized and subsequently polymerized using a functional commercial NMP initiator. The polymerization kinetics was analyzed for both monomers and revealed the controlled formation of well-defined telechelic polymers up to a conversion of 80 or 60%, respectively. For the MTEG substituted analog, the reaction rate decreases upon higher conversions due to the accumulation of persistent radicals. In contrast, the MPEG decorated pNDI revealed an increase of the reaction rate after longer reactions times, probably caused by secondary initiation reactions or kinetic effects.

The MPEG decorated telechelic polymer was examplarily functionalized with a Ru(II) photosensitizer on the chain terminus to construct a hydrophilic acceptor–photosensitizer dyad by nucleophilic substitution. The dyad was readily purified by preparative size-exclusion chromatography.

Due to the polar side chains, the monomers, the respective polymers, and the dyad feature an increased hydrophilicity and an improved solubility in polar solvents. Therefore, the MPEG substituted polymer and the respective dyad are well soluble in protic solvents, e.g., methanol or ethanol, and even paartially soluble in water. Thereby, the solubility in water decreases with an increasing DP.

The optical properties of the polymers and the dyad as well as a possible solvent influence were analyzed by steady-state absorption and emission spectroscopy. Whereas no strong influence of the solvent on the optical properties was found, the dyad showed an efficient emission quenching due to a proposed electron transfer from the ruthenium complex to the NDI polymer.

In conclusion, the incorporation of hydrophilic poly(ethylene glycol) side chains can be readily achieved and leads to an increase of the solubility of the polymers in polar solvents, while the desired modular character of the architecture with respect to the synthetic approach and the optical properties is preserved. The high hydrophilicity is beneficial for assembly of the materials in water-based solvents and, moreover, is expected to assist the assembly in combination with hydrophobic counterparts, e.g., in thin films or materials. The assembly of the hydrophilic dyads and the construction of amphiphilic donor–photosensitizer–acceptor triads by the utilization of bifunctional photosensitizers is under current investigation.

Macromol. Chem. Phys. **2017**, DOI: 10.1002/macp.201600534

Supporting Information

Supporting Information is available from the Wiley Online Library or from the author.

Acknowledgements: The authors thank Annett Urbanek for MALDI-ToF measurements as well as Dr. Peter Bellstedt and the NMR platform of the IAAC/IOMC for help with the NMR measurements. Financial support by the Carl-Zeiss-Foundation, the Friedrich Schiller University Jena ("Nachwuchsförderung"), and the Thüringer Ministerium für Wirtschaft, Wissenschaft und Digitale Gesellschaft (TMWWDG), is kindly acknowledged.

Received: November 14, 2016; Revised: December 20, 2016; Published online: ; DOI: 10.1002/macp.201600534

Keywords: functional building blocks; light induced charge transfer; modular synthesis; nitroxide-mediated polymerization; ruthenium(II) polypyridyl complex

[1] N. S. Lewis, D. G. Nocera, *Proc. Natl. Acad. Sci. USA* **2006**, *103*, 15729.
[2] L. Hammarström, *Acc. Chem. Res.* **2015**, *48*, 840.
[3] V. Balzani, G. Bergamini, P. Ceroni, *Angew. Chem., Int. Ed.* **2015**, *54*, 11320.
[4] J. J. Concepcion, R. L. House, J. M. Papanikolas, T. J. Meyer, *Proc. Natl. Acad. Sci. USA* **2012**, *109*, 15560.
[5] J. H. Alstrum-Acevedo, M. K. Brennaman, T. J. Meyer, *Inorg. Chem.* **2005**, *44*, 6802.
[6] R. Schroot, T. Schlotthauer, U. S. Schubert, M. Jäger, *Macromolecules* **2016**, *49*, 2112.
[7] J. Kübel, R. Schroot, M. Wächtler, U. S. Schubert, B. Dietzek, M. Jäger, *J. Phys. Chem. C* **2015**, *119*, 4742.
[8] A. Facchetti, *Chem. Mater.* **2011**, *23*, 733.
[9] Z. He, H. Wu, Y. Cao, *Adv. Mater.* **2014**, *26*, 1006.
[10] J. C. Brendel, H. Burchardt, M. Thelakkat, *J. Mater. Chem.* **2012**, *22*, 24386.
[11] Z. Wu, C. Sun, S. Dong, X.-F. Jiang, S. Wu, H. Wu, H.-L. Yip, F. Huang, Y. Cao, *J. Am. Chem. Soc.* **2016**, *138*, 2004.
[12] P. Wittmeyer, S. Traser, R. Sander, K. B. Sondergeld, A. Ungefug, R. Weiss, M. Rehahn, *Macromol. Chem. Phys.* **2016**, *217*, 1473.
[13] C.-C. Hung, H.-C. Wu, Y.-C. Chiu, S.-H. Tung, W.-C. Chen, *J. Polym. Sci. Polym. Chem.* **2016**, *54*, 3224.
[14] F. Mathias, A. Fokina, K. Landfester, W. Tremel, F. Schmid, K. Char, R. Zentel, *Macromol. Rapid Commun.* **2015**, *36*, 959.
[15] M. He, F. Qiu, Z. Lin, *J. Mater. Chem.* **2011**, *21*, 17039.
[16] Y. Lee, E. D. Gomez, *Macromolecules* **2015**, *48*, 7385.
[17] E. Moulin, J.-J. Cid, N. Giuseppone, *Adv. Mater.* **2013**, *25*, 477.
[18] L. zur Borg, C. Schuell, H. Frey, R. Zentel, *Macromol. Rapid Commun.* **2013**, *34*, 1213.
[19] P. M. Reichstein, S. Gödrich, G. Papastavrou, M. Thelakkat, *Macromolecules* **2016**, *49*, 5484.
[20] S. Kohmoto, E. Mori, K. Kishikawa, *J. Am. Chem. Soc.* **2007**, *129*, 13364.
[21] C. Wendeln, S. Rinnen, C. Schulz, T. Kaufmann, H. F. Arlinghaus, B. J. Ravoo, *Chem. Eur. J.* **2012**, *18*, 5880.
[22] J. D. Revell, D. Gantenbein, P. Krattiger, H. Wennemers, *Pept. Sci.* **2006**, *84*, 105.
[23] P. A. Ledin, N. Kolishetti, G.-J. Boons, *Macromolecules* **2013**, *46*, 7759.
[24] R. Schroot, C. Friebe, E. Altuntas, S. Crotty, M. Jäger, U. S. Schubert, *Macromolecules* **2013**, *46*, 2039.
[25] M. Abrahamsson, M. Jäger, R. J. Kumar, T. Österman, P. Persson, H.-C. Becker, O. Johansson, L. Hammarström, *J. Am. Chem. Soc.* **2008**, *130*, 15533.
[26] This side product is indifferent in the later polymerization.
[27] G. Gryn'ova, C. Y. Lin, M. L. Coote, *Polym. Chem.* **2013**, *4*, 3744.
[28] J. Nicolas, Y. Guillaneuf, C. Lefay, D. Bertin, D. Gigmes, B. Charleux, *Prog. Polym. Sci.* **2013**, *38*, 63.
[29] D. Bertin, D. Gigmes, S. R. A. Marque, P. Tordo, *Chem. Soc. Rev.* **2011**, *40*, 2189.
[30] A. M. Striegel, W. W. Yau, J. J. Kirkland, D. D. Bly, in *Modern Size-Exclusion Liquid Chromatography*, John Wiley & Sons, Inc., Hoboken, NJ, USA **2009**, pp. 92–115.
[31] O. Guerret, J.-L. Couturier, F. Chauvin, H. El-Bouazzy, D. Bertin, D. Gigmes, S. Marque, H. Fischer, P. Tordo, in *Advances in Controlled/Living Radical Polymerization*, Vol. *854*, American Chemical Society, Ed: K. Matyjaszewski, Washington, DC **2003**, pp. 412–423.
[32] C. Feng, Y. Li, D. Yang, J. Hu, X. Zhang, X. Huang, *Chem. Soc. Rev.* **2011**, *40*, 1282.
[33] H.-I. Lee, J. Pietrasik, S. S. Sheiko, K. Matyjaszewski, *Prog. Polym. Sci.* **2010**, *35*, 24.
[34] B. A. Miller-Chou, J. L. Koenig, *Prog. Polym. Sci.* **2003**, *28*, 1223.
[35] S. Hocine, M.-H. Li, *Soft Matter* **2013**, *9*, 5839.
[36] M. Kumar, S. J. George, *Chem. Eur. J.* **2011**, *17*, 11102.
[37] P. Rajdev, M. R. Molla, S. Ghosh, *Langmuir* **2014**, *30*, 1969.
[38] M. R. Molla, D. Gehrig, L. Roy, V. Kamm, A. Paul, F. Laquai, S. Ghosh, *Chem. Eur. J.* **2014**, *20*, 760.
[39] S. Tu, S. H. Kim, J. Joseph, D. A. Modarelli, J. R. Parquette, *J. Am. Chem. Soc.* **2011**, *133*, 19125.
[40] H. Shao, J. Seifert, N. C. Romano, M. Gao, J. J. Helmus, C. P. Jaroniec, D. A. Modarelli, J. R. Parquette, *Angew. Chem., Int. Ed.* **2010**, *49*, 7688.
[41] T. C. Barros, S. Brochsztain, V. G. Toscano, P. B. Filho, M. J. Politi, *J. Photochem. Photobiol. A* **1997**, *111*, 97.
[42] T. D. M. Bell, S. V. Bhosale, C. M. Forsyth, D. Hayne, K. P. Ghiggino, J. A. Hutchison, C. H. Jani, S. J. Langford, M. A. P. Lee, C. P. Woodward, *Chem. Commun.* **2010**, *46*, 4881.
[43] X. Zhan, A. Facchetti, S. Barlow, T. J. Marks, M. A. Ratner, M. R. Wasielewski, S. R. Marder, *Adv. Mater.* **2011**, *23*, 268.
[44] S. Basak, N. Nandi, A. Baral, A. Banerjee, *Chem. Commun.* **2015**, *51*, 780.
[45] M. Kumar, S. J. George, *Nanoscale* **2011**, *3*, 2130.
[46] S. V. Bhosale, C. H. Jani, S. J. Langford, *Chem. Soc. Rev.* **2008**, *37*, 331.

Publication P4

Poly(*N*-alkyl-3,6-carbazole)s via Kumada catalyst transfer polymerization: Impact of metal-halogen exchange

R. Schroot, U. S. Schubert, M. Jäger, *Macromolecules* **2016***, 49,* 8801-8811.

The paper as well as the supporting information (free of charge) are available online under: doi.org/10.1021/acs.macromol.6b02088

Macromolecules

Article

pubs.acs.org/Macromolecules

Poly(*N*-alkyl-3,6-carbazole)s via Kumada Catalyst Transfer Polymerization: Impact of Metal−Halogen Exchange

Robert Schroot,[†] Ulrich S. Schubert,*[,†,‡] and Michael Jäger*[,†,‡]

[†]Laboratory of Organic and Macromolecular Chemistry (IOMC) and [‡]Center for Energy and Environmental Chemistry Jena (CEEC Jena), Friedrich Schiller University Jena, 07743 Jena, Germany

Supporting Information

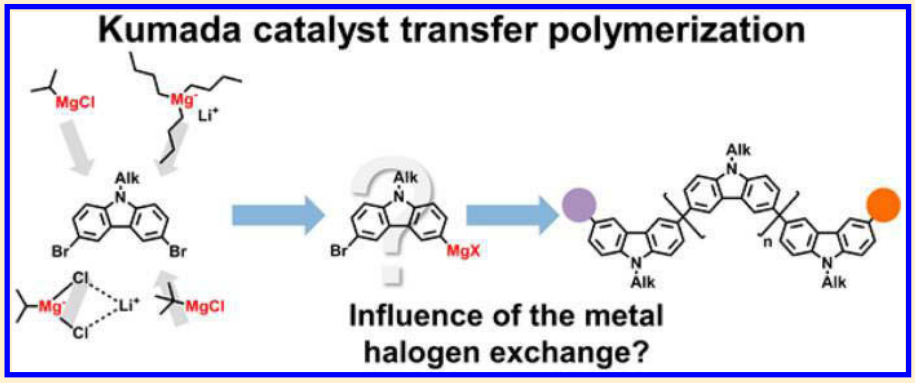

ABSTRACT: The preparation of poly(3,6-carbazole) via Kumada catalyst transfer polymerization (KCTP) is investigated and analyzed in detail by mass spectrometry to explore the scope of the applied protocols. Namely, common magnesium reagents were screened for the initial Grignard metathesis (GRIM) step and subsequently polymerized using [Ni(dppp)Cl_2] (dppp is 1,3-bis(diphenylphosphanyl)propane). The metal−halogen exchange was monitored by GC, while the polymers were characterized by size exclusion chromatography (SEC) and ^{1}H NMR spectroscopy. More importantly, the polymer end groups were investigated by means of mass spectrometry and isotope analysis, which revealed significant deviation from the chain-growth character of related poly(3-hexylthiophene). It was found that standard Grignard reagents led to incomplete GRIM even under extended reaction times and elevated temperatures, while the presence of LiCl greatly accelerated the metal−halogen exchange and also the KCTP. According to end-group analysis of the obtained polymers, side reactions occur that are attributed and explained in terms of catalyst dissociation and/or disproportionation. Namely, the replacement of the bromo-substituents by either alkyl groups via transmetalation or hydrogen via β-hydride elimination was observed. Finally, quantitative metal−halogen exchange was achieved using a magnesiate reagent, which also afforded the corresponding polymer in good isolated yield (66%). The end-group scrambling, dispersity, and observed molar masses support the proposed role of catalyst dissociation and/or disproportionation, even in the absence of excess of residual Grignard reagent.

INTRODUCTION

The discovery of high electrical conductivity in doped polyacetylene in 1977 by Shirakawa, Heeger, and MacDiarmid initiated the interest in conjugated polymers as active materials for optoelectronic applications, e.g., organic light-emitting diodes (OLEDs), organic field-effect transistors (OFETs), and organic photovoltaic cells and/or sensors. The practical value of conjugated polymers benefits from their adjustable properties, e.g., defined optical and electrical characteristics, their ability for phase separation and self-assembly, and/or the cost-effective production and processing techniques.[1−3] The majority of conjugated polymers are based on thiophene,[4−8] phenylene,[9,10] fluorene,[11−16] or 2,7-carbazole,[17,18] which are conveniently obtained via metal-catalyzed polycondensation reactions. Hence, relatively high conversions are required to obtain high molar masses, concomitant with relatively high dispersity ($Đ \geq 2$) and often undefined end groups. Notably, the control of the end-group fidelity has received recent attention, e.g., to precisely adjust the electronic levels (trap sites)[19] or to utilize the terminal functional group to construct defined polymer architectures—as demonstrated by the control of the morphology in block copolymer films,[20] postpolymerization functionalization of the chain terminus,[21,22] or the grafting onto a specific surface.[23] In this regard, the seminal work by Yokozawa and McCullough on the Kumada catalyst transfer polymerization (KCTP)—also known as Grignard metathesis (GRIM) polymerization—constituted a breakthrough to synthesize polymers with defined molar masses, low dispersities, and defined end groups under mild reaction conditions as they follow a chain-growth mechanism.[24−26]

Received: September 27, 2016
Revised: November 7, 2016
Published: November 18, 2016

DOI: 10.1021/acs.macromol.6b02088
Macromolecules 2016, 49, 8801−8811

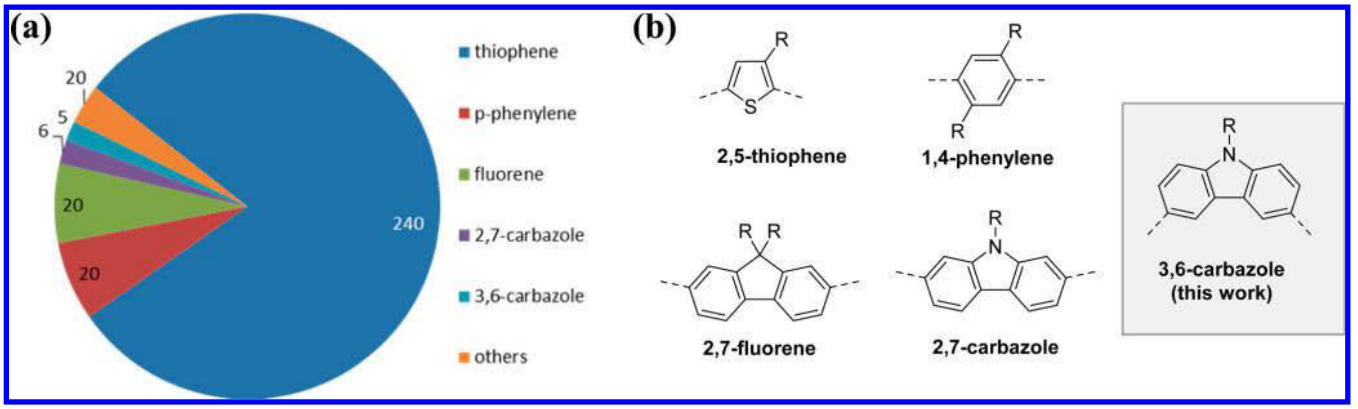

Figure 1. (a) Number of reports investigating the controlled metal-catalyzed polymerization of common bifunctional monomers.[27] (b) Schematic representation of the structures of the respective monomer units (dashed lines indicate the linking pattern).

Table 1. Experimental Conditions and Selected Analytical Data of the Polymers Prepared by KCTP Using Monomer 1

		metal–halogen exchange				polymerization[a]		analytical characterization		
entry	polymer	Grignard reagent	time [h]	temp	M/Br exchange[b] [%]	quencher	isolated yield [%]	M_n [g/mol][c]	$Đ$[c]	end-group analysis[d]
1	**p1**	^{i}PrMgCl	24	65 °C	55	CD_3OD	24	4400	1.53	Br/Br > Br/H ≫ Br/Pr
2	**p2**	^{t}BuMgCl	24	65 °C	45	CD_3OD	5	1280	1.14	Br/Br + nonassigned series
3	**p3**	$Li^+[(^{i}Pr)MgCl_2]^-$	24	rt	30	(i) HC≡CMgBr; (ii) HCl[e]	8	5400	1.70	Pr/Pr > Pr/H > Br/Br
4	**p4**	$Li^+[(^{i}Pr)MgCl_2]^-$[f]	18	rt	75	CD_3OD	35	6500	1.24	Pr/Pr > Pr/H ≫ H/H
5	**p5**	$Li^+[n\text{-}Bu_3Mg]^-$[g]	2	40 °C	quant	CD_3OD	66	2300	1.96	
	p5a[h]							5000	1.25	Bu/Bu > Bu/H > Bu/Br ≈ H/H
	p5b[h]							2900	1.24	Bu/Bu > Bu/H > Bu/Br ≈ H/H

[a]Conditions: [Ni(dppp)Cl_2], room temperature, 2–4 h. [b]Determined by GC-MS. [c]From SEC analysis (eluent: chloroform/isopropanol/triethylamine [94:2:4], applying PS calibration). [d]Most intense series according to MALDI-ToF MS analysis. [e]HCl was added after 1 h at room temperature. [f]Formed *in situ*. [g]Formed prior to metal–halogen exchange. [h]Polymer fractions after preparative size exclusion chromatography.

Among semiconducting polymers (Figure 1), triarylamines and the related carbazoles are widely utilized as hole-conducting materials.[2,28−30] In particular, carbazole-based materials constitute an attractive material class,[31,32] owing to the facile syntheses to achieve tailored optoelectronic and/or processing properties.[2] Polycarbazoles can be distinguished by the degree of conjugation, which arises from the connectivity between the repeating units. The linkage via the 2,7- or 3,6-positions of the carbazole leads to a *para*- or *meta*-linked phenylene backbone, respectively. Hence, the corresponding poly(2,7-carbazole)s feature a large conjugation segment length and high hole mobility. Notably, the chemical instability vs oxidation processes arises from the reactive 3,6-positions[2,33] and requires encapsulation for their use in photovoltaic applications.[3] Alternatively, poly(3,6-carbazole)s feature the inherent blocking of the reactive positions and, thus, exhibit electrochemically stable oxidation processes.[33] Because of the diminished conjugation, such materials are transparent in the visible light region and are particularly attractive materials for OLEDs,[3,34,35] in flash memory devices or OFETs,[36,37] or in devices showing thermally activated delayed fluorescence.[38] Despite the facile preparation of the monomers starting from 9*H*-carbazole, the preparation of well-defined poly(3,6-carbazole)s is not intensively studied by KCTP and mainly relies on Ni- or Pd-catalyzed Kumada-, Yamamoto-, Negishi-, or Suzuki-type couplings.[18,39−44] Notably, the step-growth conditions of the applied protocols may hamper their utility in subsequent functionalization reactions and in assembled materials,[19] and relatively little is reported regarding the end groups analysis.

In this contribution, the controlled polymerization of 3,6-carbazoles via KCTP is explored and systematically analyzed. It has been noted that the GRIM step of carbazoles is more challenging than for thiophene or fluorene[18] as well as that the extent of residual Grignard reagent interferes in the KCTP.[6] Hence, we set out to investigate prominent protocols for the metal–halogen exchange and analyzed the impact on the polymers obtained by subsequent KCTP. In the first part, we present a detailed end-group analysis and discussion of the proposed pathways by means of mass spectrometry and end-group analysis. The second part describes the efforts to enhance the GRIM step and to improve the KCTP performance in terms of yield, molar masses, dispersity, and end-group fidelity. The synthesized monomers and polymers were characterized by GC, ^{1}H NMR spectroscopy, size exclusion chromatography (SEC), and in more detail by MALDI-ToF mass spectrometry (see Supporting Information for procedural details on SEC and MS analysis). The latter technique revealed important details concerning the end groups by virtue of isotope simulations, which lead to the efficient preparation of poly(3,6-carbazoles).

■ EXPERIMENTAL SECTION

All reagents were purchased from ABCR, Acros Organics, Alfa Aesar, Apollo Scientific, Sigma-Aldrich, or TCI Chemicals and were used

DOI: 10.1021/acs.macromol.6b02088
Macromolecules 2016, 49, 8801−8811

Scheme 1. Schematic Representation of the Ideal Chain-Growth Mechanism Illustrated for 3,6-Carbazoles (Adapted from Refs 6, 50, and 54)[a]

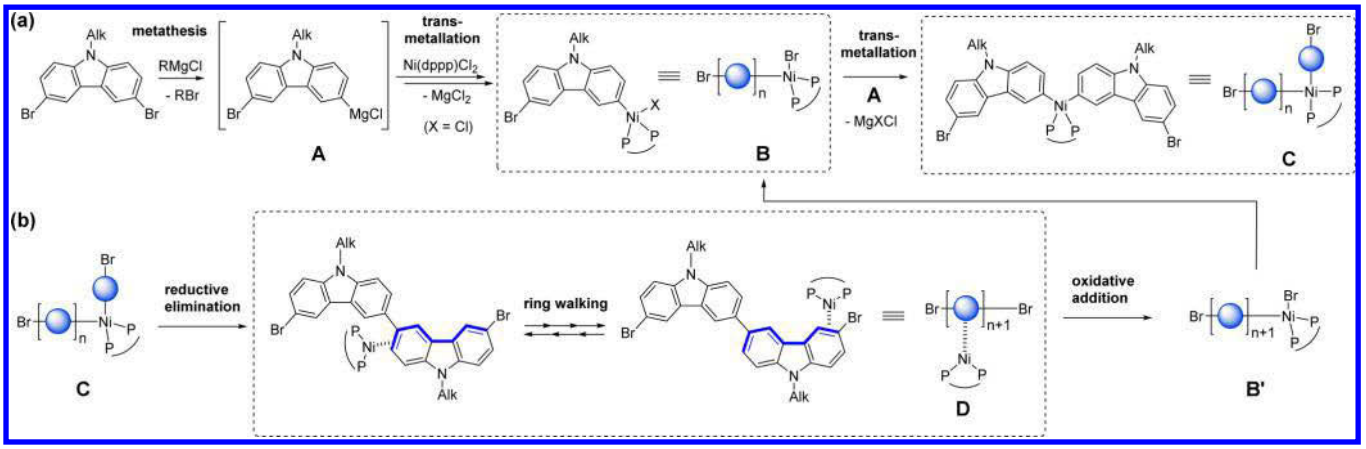

[a]Activation of Ni(II) precatalyst and monomer addition via transmetalation (a) and chain growth step via reductive elimination, ring-walking, and oxidative addition at chain terminus (b).

without further purification unless otherwise noted. Fresh bottles of the commercial Grignard reagents were used without previous titration. All solvents were degassed before use. THF was distilled from sodium/benzophenone. 3,6-Dibromocarbazole[45] was prepared according to literature procedures. It has been advised that commercial Grignard reagents should always be titrated prior usage to determine the exact concentration. However, this extra step was omitted during our screening, as the results unambiguously identified the limitation of GRIM in terms of reactivity rather than stoichiometry (*vide infra*).

3,6 Dibromo-9-octyl-9H-carbazole (*1*). The compound was prepared by an adopted literature procedure.[46] 3,6-Dibromocarbazole (4.580 g, 14.09 mmol) and 1-bromooctane (4.080 g, 21.14 mmol) were dissolved in DMSO (28 mL). Subsequently a 50% solution of NaOH in water (14 mL) was added and the resulting suspension was stirred overnight at room temperature. Then water was added and the mixture was extracted three times with diethyl ether. The organic solution was dried over $Na2SO_4$, filtered and concentrated under reduced pressure. Purification by column chromatography (silica, CH_2Cl_2/hexane 5/95) gave the product as colorless oil (5.10 g, 83%). ^{1}H NMR (300 MHz, $CDCl_3$): δ 8.15 (d, J = 1.8 Hz, 2H, ArH), 7.56 (dd, J = 8.7, 1.8 Hz, 2H, ArH), 7.28 (d, J = 8.7 Hz, 2H, ArH), 4.25 (t, J = 7.3 Hz, 2H, CH_2), 1.91−1.75 (m, 2H, CH_2), 1.48−1.01 (m, 10H, 5 × CH_2), 1.01−0.75 (m, 3H, CH_3).

Kumada Catalyst Transfer Polymerization. A tabulated overview of all prepared polymers is given in Table 1 (see also Results and Discussion section).

p1. A microwave vial was charged with **1** (0.500 g, 1.14 mmol, 1 equiv), sealed, evacuated, and flushed with nitrogen. Subsequently dry THF (2.20 mL) and ^{i}PrMgCl (0.572 mL, 2 M in THF, 1 equiv) were added, and the reaction mixture was heated to reflux. After 24 h no further reaction progress was observed (conversion 55%), and [Ni(dppp)Cl_2] (0.005 g, 0.01 mmol, 0.008 equiv) was added as suspension in THF (0.15 mL) at room temperature. The reaction was quenched by addition of CD_3OD (2 mL) after 2 h, and the mixture was precipitated in MeOH. The crude product (0.075 g) was purified by fractionated precipitation (nonsolvent addition method,[47] THF, MeOH). The solid of the first precipitation was further analyzed (0.037 g) (see text and Supporting Information).

p2. A microwave vial was charged with **1** (0.500 g, 1.14 mmol, 1 equiv), sealed, evacuated, and flushed with nitrogen. Subsequently dry THF (2.20 mL) and ^{t}BuMgCl (1.14 mL, 1 M in THF, 1 equiv) were added, and the reaction mixture was heated to reflux. After 24 h no further reaction progress was observed (conversion 45%), and [Ni(dppp)Cl_2] (0.005 g, 0.01 mmol, 0.008 equiv) was added as suspension in THF (0.15 mL) at room temperature. After 2 h the reaction was quenched by addition of CD_3OD (2 mL), and the mixture was precipitated in MeOH, filtered, and the off-white solid was washed with MeOH and water (0.010 g) (see text and Supporting Information).

p3.[17] A microwave vial was charged with LiCl (0.050 g, 1.19 mmol, 1.04 equiv), sealed, evacuated, and flushed with nitrogen. Then a solution of **1** (0.500 g, 1.14 mmol, 1 equiv) in dry THF (6.25 mL) was added. The reaction vessel was cooled to 0 °C, and ^{i}PrMgCl (0.572 mL, 2 M in THF, 1 equiv) was added dropwise. Subsequently the mixture was stirred at room temperature. After 24 h the conversion was checked by GC-MS (below 30%), and [Ni(dppp)Cl_2] (0.006 g, 0.0144 mmol, 0.01 equiv) was added as solution in THF (6.2 mL). After stirring for 3 h at room temperature ethynylmagnesium bromide (0.69 mL, 0.5 M in THF, 0.3 equiv) was used to quench the reaction, and stirring was continued for 1 h before 1 N HCl (1 mL) was added. Subsequently the solution was precipitated in MeOH, filtered, and the off-white solid was washed with MeOH and water. The crude product (0.025 g) was purified by fractionated precipitation (nonsolvent addition method,[47] THF, MeOH). The solid of the first precipitation was further analyzed (0.008 g) (see text and Supporting Information).

p4.[18] A microwave vial was charged with LiCl (0.049 g, 1.14 mmol, 1 equiv), sealed, evacuated, and flushed with nitrogen. Subsequently dry THF (1.15 mL) and ^{i}PrMgCl (0.572 mL, 2 M in THF, 1 equiv) were added, and the resulting solution was stirred at room temperature for 6 h. Then a solution of **1** (0.500 g, 1.14 mmol, 1 equiv) in dry THF (1.10 mL) was added. The progress of the metal−halogen exchange was monitored by GC-MS, and after 18 h (at least 75% conversion) [Ni(dppp)Cl_2] (0.005 g, 0.01 mmol, 0.008 equiv) was added as suspension in THF (0.15 mL). The reaction was quenched by addition of CD_3OD (2 mL) after 2 h, and the mixture was precipitated in MeOH. The crude product (0.110 g) was purified by fractionated precipitation (nonsolvent addition method,[47] THF, MeOH). The solid of the first precipitation was further analyzed (0.060 g) by ^{1}H NMR, SEC, and MALDI-ToF MS (see text and Supporting Information).

p5.[18] A three-neck flask with septum and nitrogen inlet was heated under vacuum with a heat gun and filled with nitrogen. After cooling to room temperature, toluene (4.1 mL) was added, and the reaction vessel was cooled to −10 °C. Subsequently, ^{n}BuLi (0.915 mL, 2.5 M in hexane, 0.67 equiv) and ^{n}BuMgCl (0.572 mL, 2 M in THF, 0.33 equiv) were added with a syringe forming a white suspension. After stirring for 1 h at −10 °C, a solution of **1** (1.500 g, 3.43 mmol, 1 equiv) in dry THF (10.25 mL) was added at room temperature. The resulting clear yellow solution was stirred at 40 °C, and the progress of the metal−halogen exchange was monitored by GC-MS. After quantitative conversion (approximately 2 h), [Ni(dppp)Cl_2] (0.021 g, 0.04 mmol, 0.01 equiv) was added at room temperature, and the solution was stirred for additional 4 h at ambient temperature. The reaction was quenched by addition of CD_3OD and subsequently

DOI: 10.1021/acs.macromol.6b02088
Macromolecules 2016, 49, 8801−8811

Scheme 2. Schematic Representation of the General Synthesis Strategy Leading to Poly(3,6-carbazole)s[a]

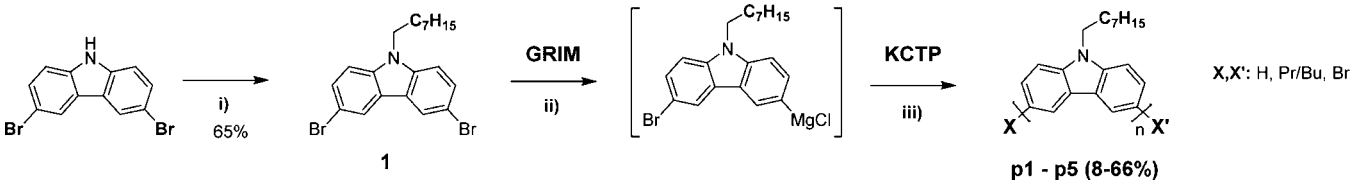

[a]Conditions: (i) octyl bromide, DMSO, NaOH, RT, overnight; (ii) Grignard reagent, THF (see Table 1 and Experimental Section for details and conditions); (iii) [Ni(dppp)Cl_2], RT, N_2, 2−4 h.

precipitated in MeOH. The crude product (1.100 g) was purified by fractionated precipitation (nonsolvent addition method,[47] THF, MeOH). The solids of the first (**p5a**, 0.303 g) and the second precipitation (**p5b**, 0.150 g) were further analyzed by ^{1}H NMR, SEC, and MALDI-ToF MS (see text and Supporting Information).

RESULTS AND DISCUSSION

In this contribution, we set out to explore the preparation of poly(3,6-carbazoles) via Grignard metathesis (GRIM) and subsequent Kumada catalyst transfer polymerization (KCTP). The aim of this work is to systematically investigate the effect of the applied experimental parameters, namely the kind of Grignard reagent and reaction conditions during GRIM, and the outcome of end groups of the KCTP. In order to provide a foundation for the interpretation of our results, we begin the discussion with a brief review of the essential steps of GRIM and KCTP, which have been analyzed in great depth for poly(3-hexylthiophene), P3HT.[24,48−53]

Mechanistic Aspects of KCTP. In a recent review, Kiriy and co-workers emphasized the control in KCTP of this particular important polymer due to the beneficial effect of the *ortho*-substituent substrates and the efficient ring-walking ability of the catalyst fragment even across the oligothiophene subunits.[48] The resulting retardation of disproportionation and catalyst dissociation leads to the chain-growth character including excellent end-group homogeneity.[6,48]

Scheme 1 briefly depicts the essential steps involved in the GRIM and KCTP: The initial metal−halogen metathesis step yields the reactive monomer **A** (Scheme 1a). Knochel et al. explored in detail the reactivity of various magnesium reagents in metal−halogen exchange reactions,[55−57] which assisted their successfully application in the KCTP. Notably, thiophenes readily undergo a metal−halogen exchange employing conventional Grignard reagents, e.g., ^{i}PrMgCl or ^{t}BuMgCl, while other monomers, e.g. fluorenes or 2,7-carbazoles, are much less reactive and require Grignard reagents with higher reactivity (*vide infra*).[18] Upon addition of a Ni(II) precatalyst, e.g., [Ni(dppp)Cl_2] (dppp is 1,3-bis(diphenylphosphanyl)-propane),[49−51] the Grignard intermediate **A** undergoes the first transmetalation to generate **B**. After a second transmetalation step, the bis-aryl Ni complex (**C**) is formed. Notably, this species undergoes reductive elimination, whereby the catalyst fragment stays associated with the polymer chain (Scheme 1b). Hence, the Ni fragment can migrate along the π-system (ring-walking) toward the chain terminus to form species **D**, which re-enters the catalytic cycle by oxidative addition to form **B′**. The termination occurs typically via monofunctional Grignard reagents or deactivation of the active Ni species by a quencher.[6] In the case of the P3HT, Thelakkat and co-workers identified chain−chain coupling upon addition of MeOH to account for the Br/Br-terminated polymers, while addition of HCl yielded the protolysis product with strict H/Br end groups.[6] In addition, defined end groups beyond the bromo substituent can be introduced by means of a functionalized Ni precatalyst[48,58] or by the addition of a monofunctional Grignard reagent to terminate the polymerization.[25,59] Hence, the analysis of the end groups gives valuable insights into potential side reactions and assist the systematic exploration of the scope of the synthetic protocols.

Synthetic Strategy. The synthetic sequence presented in this work is outlined in Scheme 2 and involves the metal−halogen exchange of *N*-alkyl-3,6-dibromocarbazole (**1**) using typical magnesium reagents,[6,17,18] followed by KCTP utilizing [Ni(dppp)Cl_2] as precatalyst. At selected times, samples were taken and analyzed by GC-MS to follow the course of the initial GRIM step. Upon quantitative exchange or ceased metathesis progress, the precatalyst [Ni(dppp)Cl_2] was added to the monomer solution in analogy to literature reports.[49−51] The polymerization was finally quenched by addition of various end-capping reagents, and the obtained polymers **p1**−**p5** were characterized by ^{1}H NMR spectroscopy (Figures S2−S6), SEC (Figures S8 and S9), and in more detail by mass spectrometry (Figures S11−S19). Procedural details on the analysis and interpretation of the SEC and MS data can be found in the Supporting Information (sections 3 and 4). It has been reported in the case of P3HT that methanol may lead to chain couplings during quenching.[6,60] However, a control experiment using monomer **1** revealed identical SEC traces irrespective of the nature of the terminating agent (MeOH or HCl, Figure S7), and thus, subsequent experiments were conducted with methanol. We further applied deuterated methanol (CD_3OD) in order to identify active Grignard species and catalyst fragments, which would give rise to the characteristic M + 1 isotope pattern.

Conventional Grignard Reagents (Entries 1 and 2). Our investigation of the KCTP starts with the evaluation of typical Grignard reagents known from P3HT, i.e., ^{i}PrMgCl or ^{t}BuMgCl.[55−57] The metal−halogen exchange was tested for monomer **1** (Table 1, entries 1 and 2). In agreement with reports on related fluorenes and carbazoles,[18] the metal−halogen exchange of **1** in refluxing THF was incomplete using either Grignard reagent. GC-MS monitoring revealed no further progress (55% for ^{i}PrMgCl, 45% for ^{t}BuMgCl), but high enough conversion to attempt the polymerization step applying [Ni(dppp)Cl_2] as precatalyst at room temperature for 2−4 h. In agreement with the incomplete GRIM step, the isolated yields of the respective polymers **p1** (24%) and **p2** (5%) were very low. The SEC analysis revealed a fairly large dispersity for **p1** ($Đ$ = 1.53) with an apparent molar mass of 4400 g/mol on the basis of a PS calibration (Figure S8), which indicates substantial side reactions. The polymer **p2** featured significantly lower molar masses (1200 g/mol) with a narrower

DOI: 10.1021/acs.macromol.6b02088
Macromolecules 2016, 49, 8801−8811

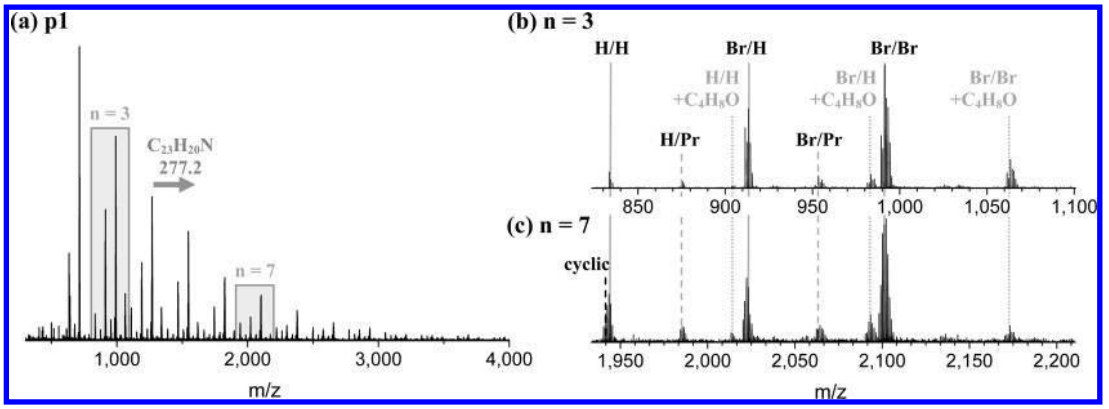

Figure 2. (a) MALDI-ToF mass spectrum of **p1** (matrix: DCTB + NaCl). Arrow indicates the carbazole repeating unit and associated molar mass. Boxes indicate selected repeat units for n = 3 (see b) and n = 7 (see c). (b, c) Expansion and assigned end groups from isotope simulation. Mass regions are aligned to indicate corresponding specimen (vertical lines): Dominant series of Br/Br, Br/H, and H/H (gray solid lines) and the corresponding formal THF adducts (gray dotted lines; cf. text) and minor series of Br/Pr and H/Pr (dashed lines). Note the missing macrocycle (n = 3) but its occurrence for n = 7 (black dashed line). For more details cf. Figure S12.

Scheme 3. Schematic Representation of Assigned Side Reactions during KCTP[a]

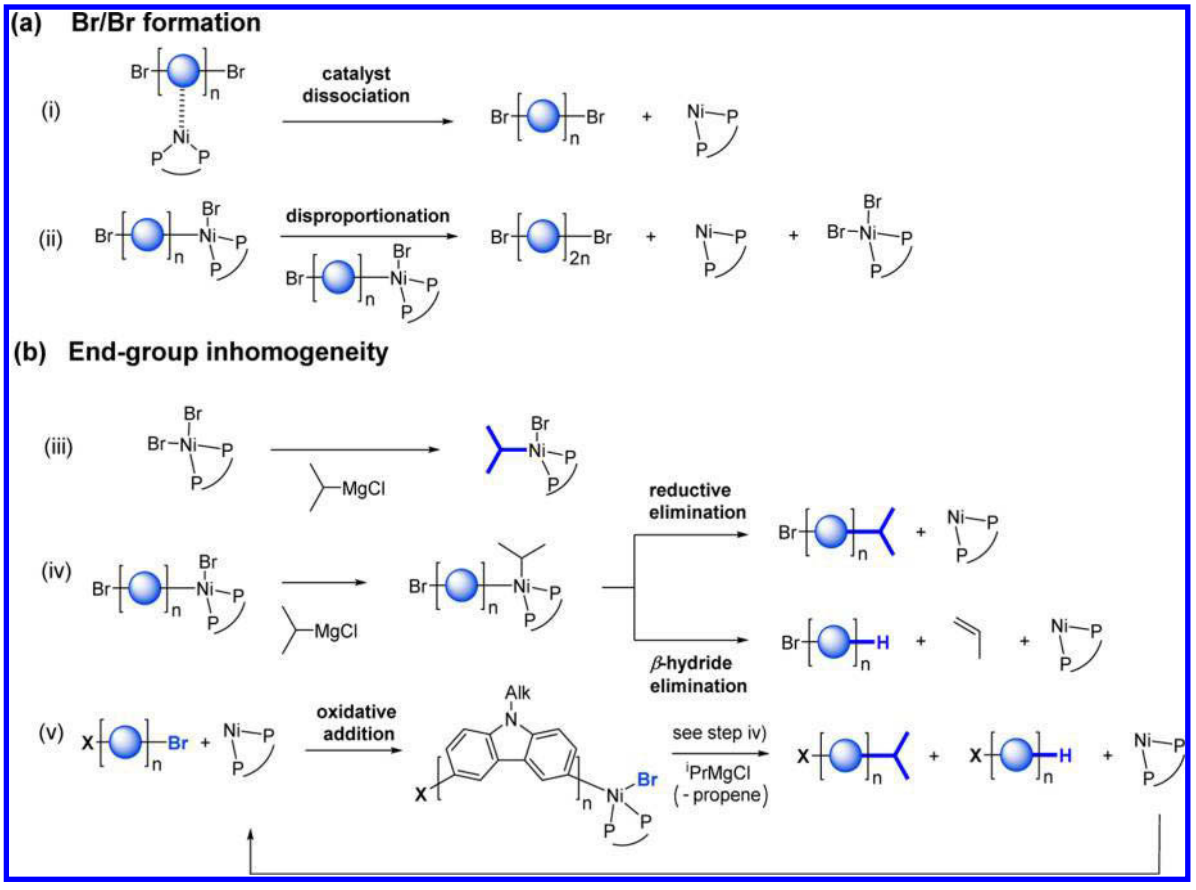

[a](a) Formation of Br/Br-terminated polymers and active Ni(0) and Ni(II) complexes via (i) catalyst dissociation or (ii) disproportionation. (b) End-group inhomogeneity due to residual Grignard reagent via (iii) KCTP initiation, (iv) transmetalation and reductive elimination and β-hydride elimination, and Br → Pr, H exchange by released Ni(0) complexes during steps i, ii, and iv, respectively. Note the catalytic character of step v with respect to Ni(0).

dispersity ($Đ$ = 1.14), as expected due to termination by the excess of Grignard reagent.[61]

The MALDI-ToF analysis of **p1** revealed several polymer series with the characteristic mass difference of the carbazole (Figure 2a). The corresponding end groups were assigned according to isotope simulations (Figure S12) and will be exemplified in more detail for the 3-mer series (n = 3, Figure 2b) and the 7-mer series (n = 7, Figure 2c). The dominating series belong to the Br/Br-, Br/H-, and H/H-decorated polymers. Interestingly, the corresponding series with an additional C_4H_8O fragment was identified, which is tentatively assigned to side reactions with THF during the GRIM and/or KCTP step. A similar formal incorporation of solvent molecules has been reported in the case of P3HT and methanol,[6] whereby

DOI: 10.1021/acs.macromol.6b02088
Macromolecules 2016, 49, 8801−8811

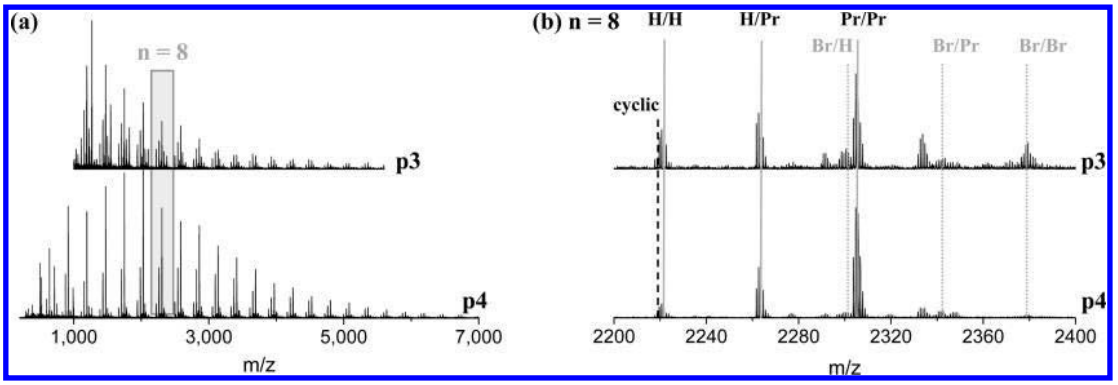

Figure 3. (a) MALDI-ToF mass spectra (matrix: DCTB + NaCl) of **p3** (top) and **p4** (bottom). Box indicates selected repeat unit for n = 8 (see panel b). (b) Expansion and assigned end groups from isotope simulation of **p3** (top) and **p4** (bottom). Dominant series of Pr/Pr, H/Pr, and H/H (gray solid lines) and minor series of Br/Br, Br/Pr, and Br/H (dashed lines) and occurrence of the macrocycle (black dashed line). For more details cf. Figures S15–S17.

the exact structure and mechanism is not yet understood to the best of our knowledge. In our case, the forcing conditions during metal–halogen metathesis may lead to a ring-opening of THF and subsequent interference of the formed products during polymerization. However, this series was hardly detected in latter experiments applying less forcing conditions during GRIM (*vide infra*). In addition to the aforementioned specimen, also the corresponding Br/Pr- and H/Pr-terminated polymers were detectable, along with the formation of macrocycles for $n \geq 4$ (Figure 2c). These observations can be reasoned on the basis of a detailed report on P3HT: In the case of perfect catalyst association during KCTP, termination with HCl leads exclusively to the H/Br series from the active chains, while methanol further gives the Br/Br series. The formation of the latter is assigned to chain–chain coupling, which is further supported by a characteristic shoulder in the SEC with double molar mass.[6,48] However, we observed no difference in the SEC profiles between quenching with methanol or HCl (Figure S7). In addition, we employed deuterated methanol (CD_3OD) for quenching, which is expected to yield the corresponding M + 1 peaks of any metalated specimen upon quenching. However, we could not discern any deuteron end group, which suggests that the Br/Br series has formed and accumulated already during KCTP. As the dominant chain–chain coupling during quenching is ruled out, the Br/Br series must have formed during KCTP, which implies catalyst dissociation or disproportionation reactions (Scheme 3a, steps i and ii). More importantly, both processes release active Ni(0) catalysts and/or Ni(II) precatalysts, which can undergo secondary side reactions and explain the end-group inhomogeneity.

The occurrence of propyl (Pr)- or H-terminated specimen is reasonably explained by residual Grignard reagent (Scheme 3). The first possibility of formation arises from simple initiation of the Ni(II) precatalyst (step iii). Note that the required Ni(II) can also be regenerated during KCTP by the proposed disproportionation of two active chains. The second possibility of Pr-terminated polymers involves the transmetalation of the active chain (step iv), in analogy to the typical termination of KCTP by monofunctional Grignard reagents. However, β-hydride elimination of related Ni complexes are also known[62,63] and has been recently reported as a side reaction for poly(3-(2-pyridyl)thiophenes)[64] or poly(2,5-pyridine) to form H-terminated chains.[52] It should be noted that the steric differences of the investigated poly(carbazole) vs P3HT differ and, thus, may facilitate or block each pathway, in analogy to the known reactivity differences between the 2- and 3-regioisomers of the transmetalated hexylthiophene formed during McCullough's route to P3HT.[6] Hence, we tentatively assign the occurrence of H-terminated specimen to transmetalation and subsequent β-hydride elimination (step iv).

The previous assignments explain the occurrence of the Br, H, and Pr end groups, but there are further implications from the release of Ni(0) (steps i, ii, or iv). The active catalyst can undergo oxidative addition of any bromine substituents and, thus, leads potentially to the conversion of any Br terminus into the Pr- and H-congeners, as long as residual Grignard reagent is present. Hence, these side reactions should preferentially occur in the early stage of KCTP, leading to terminated oligomers. We attempted to estimate the extent of these side reactions by comparison of the relative peak ratios for different degrees of polymerization, e.g. of the 3-mer vs 7-mer series (Figure 2b,c) and up to the signal detection limit (11-er, Figure S12). However, the data showed no marked difference between the Pr- and H-terminated series, yet revealed a lower intensity of the THF-containing side products for higher oligomers (*vide supra*) and a higher intensity of the Br/Br species for shorter oligomers. The former is explained by the formation during the early stage, while the latter seems counterintuitive at first sight. However, the incomplete GRIM also implies residual amounts of Br/Br-decorated monomer, which can undergo oxidative addition with Ni(0), and thus, the new chain contains the Br/Br end groups. Hence, such species would be constantly formed during the KCTP. In summary, the MS data suggest that H-termination exceeds the Pr-termination, as shown for H/H vs H/Pr or Br/H vs Br/Pr. Furthermore, the Br/Br dominates each series and, thus, implies the large extent of catalyst dissociation or disproportionation. With this first MS analysis of **p1** in hand, in particular the importance of complete GRIM,[6] we analyzed the effect of using ^{t}BuMgCl under similar conditions. The lower isolated yields of **p2**, as well as the SEC and MS data, are in line with the lower extent of metal–halogen exchange. Furthermore, the side reactions become even more detrimental, as revealed by the significant decreased end-group homogeneity (Figure S13). The absence of Pr-terminated species and the occurrence of the related butyl-species corroborate the previous assignments for **p1**, i.e., the negative effect of incomplete metal–halogen exchange leading to severe termination reactions.

DOI: 10.1021/acs.macromol.6b02088
Macromolecules 2016, 49, 8801–8811

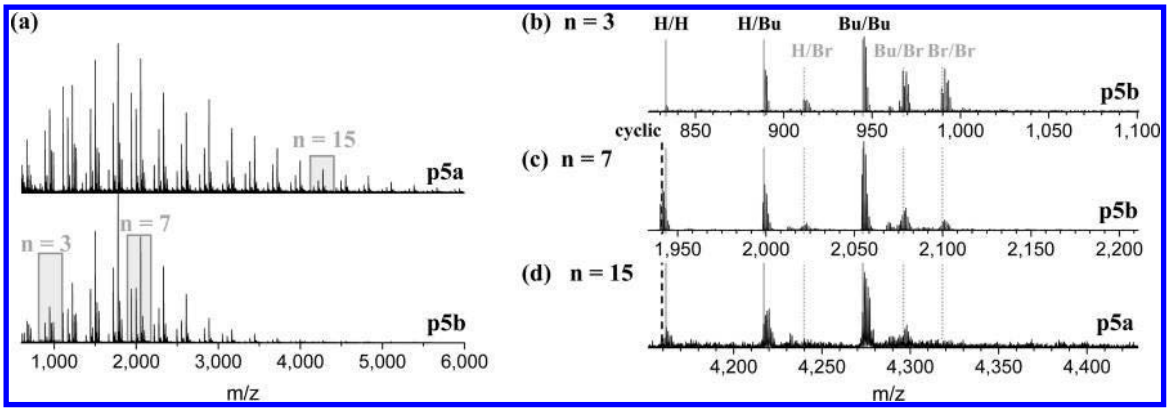

Figure 4. (a) MALDI-ToF spectra of **p5a** (top) and **p5b** (bottom) (matrix: DCTB + NaCl). Boxes indicate selected repeat units for n = 3 (see b), n = 7 (see c), and n = 15 (see d). (b–d) Expansion and assigned end groups from isotope simulation. Mass regions are aligned to indicate corresponding specimen (vertical lines): Dominant series of Bu/Bu, H/Bu, and H/H (gray solid lines) and minor series of Br/Br, Bu/Br, and H/Br (dashed lines). Note the missing macrocycle (n = 3) but its occurrence for n > 3 (black dashed line). For more details cf. Figures S18 and S19.

Turbo Grignard. Based on these first observations, an improved metal–halogen exchange was expected to decrease the side reactions during the polymerization process. Hence, the addition of LiCl was investigated ("Turbo Grignard"), which is known to break the polymeric aggregates of Grignard reagents by formation of a more reactive $Li^+[(^iPr)MgCl_2]^-$ species.[18,55,56] Two different procedures were tested: the first one taken from 3,6-carbazoles[17] and the second one being adapted from 2,7-fluorenes and 2,7-carbazoles.[18] In the former case, the Turbo Grignard is formed *in situ* from a solution containing LiCl and the monomer in THF, followed by addition of ^{i}PrMgCl to perform the GRIM at room temperature (entry 3).[17] However, our attempts applying identical conditions gave only minor metal–halogen exchange (<30%). Nevertheless, we performed the polymerization, followed by quenching with ethynylmagnesium bromide and after one additional hour by termination with HCl. Irrespective of the low extend of GRIM, this methodology addresses the opportunity to utilize LiCl for rate acceleration in KCTP—as reported for related poly(3-hexylthiophene).[6] Secondly, the utilization of a monofunctional Grignard reagent and subsequent definite termination by HCl are expected to give more insights into the termination reactions. Unfortunately, the literature work on 3,6-carbazole does not report isolated yields or mass spectrometry data.[17] In line with the low degree of metal–halogen exchange (entry 3), also the isolated yield of the corresponding polymer **p3** was very low (8%).

In contrast to the low yield, the SEC and mass spectrometry data (Figure 3) revealed a significantly higher degree of polymerization (M_n = 5400 g/mol, $Đ$ = 1.70), which suggests a higher rate of polymerization during KCTP. The isotope analysis identified the dominating Pr- and/or H-terminated species, i.e., Pr/Pr, Pr/H, and H/H, while only a minor amount of Br-decorated species was found. This fact supports a general rate enhancement by LiCl in KCTP;[6] i.e., also the side reactions leading to end group inhomogeneity are enhanced—because the related **p1** and **p2** did not show the dominant alkyl end groups (*vide supra*). Noteworthy, no end-functionalized polymer bearing the ethynyl terminus could be detected, which suggest that the chain termination again occurred during KCTP and before the addition of the end-capper. The second attempt employed the Turbo Grignard as adapted from 2,7-fluorenes.[18] For this purpose, $Li^+[(^iPr)MgCl_2]^-$ was prepared separately, followed by addition of a solution of monomer **1** in THF (entry 4). This method enabled the highest metal–halogen exchange so far (75%). The subsequent polymerization (**p4**) was quenched by addition of CD_3OD in order to trap any active metal terminus as their deuterated analogues. Consistent with previous interpretation, the higher metal–halogen exchange is also reflected in higher polymer yields (35%), while the side reactions of excessive Grignard reagent should be lower—as reflected by a higher degree of polymerization (M_n = 6500 g/mol) and significantly lower dispersity ($Đ$ = 1.24). However, the MALDI-ToF analysis identified a similar end-group distribution as for **p3**, i.e., mainly Pr/Pr- and Pr/H-terminated chains were found (Figure 3). In summary of both experiments using the "Turbo" Grignard, the presence of LiCl was attributed to greatly accelerate the KCTP, as previously also reported for poly(3-hexylthiophene).[6] In addition to the hitherto established trend, that a lower metal–halogen exchange gives also a lower degree of polymerization (e.g., **p1** vs **p2** and **p3** vs **p4**), the presence of LiCl seems to accelerate the polymerization more than the termination reactions. This is reflected by the fact that the even lower metal–halogen exchange observed for **p3** leads to higher molar masses (vs **p1** or **p2**) but almost complete Br → Pr, H replacement.

Magnesiate Complex. The enhanced metal–halogen exchange in the case of $Li^+[(i\text{-Pr})MgCl_2]^-$ prompted us to test magnesium ate complexes (entry 5), which were already successfully applied in the preparation of poly(2,7-carbazole)s.[18] Notably, the reactive complex $Li^+[n\text{-}Bu_3Mg]^-$ contains no charge-stabilizing Mg–Cl bond and, consequently, features a significantly enhanced nucleophilicity of the alkyl groups. Up to 3 equiv are released during metathesis, and thus, a stoichiometry of 1:3 in relation to the bifunctional monomer (**1**) is used.[57,65,66] Indeed, quantitative metal–halogen exchange was observed at 40 °C within 2 h. The subsequent polymerization with $[Ni(dppp)Cl_2]$ gave polymer **p5** in good yields (66%, entry 5). The SEC analysis of **p5** revealed an intermediate apparent molar mass with a broad dispersity ($Đ$ = 2.0), which indicates the deviation from the ideal chain-growth mechanism. The crude polymer was fractionated for further analysis (Figure S9), in particular in view of end-group analysis by ^{1}H NMR spectroscopy and mass spectrometry of the higher molar mass fraction (**p5a**).

The main polymer distributions of both fractions consist mainly of Bu-terminated chains (Figure 4). In line with our previous findings, no deuterated species but H-terminated were

DOI: 10.1021/acs.macromol.6b02088
Macromolecules 2016, 49, 8801–8811

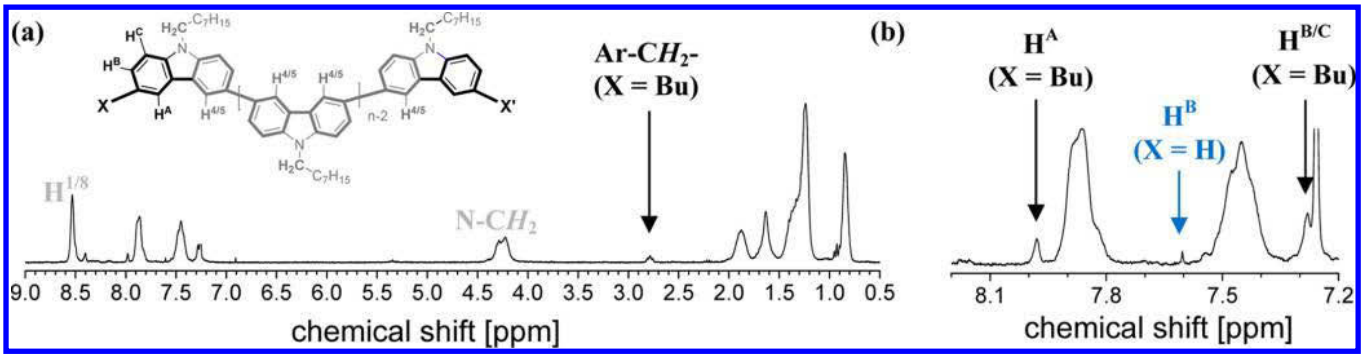

Figure 5. (a) ^{1}H NMR spectrum (300 MHz, $CDCl_3$) of **p5a** and with assignment of characteristic protons including a chemical representation emphasizing the two terminal benzoid subunits shown in black (X, X′) vs the polymer backbone (gray). Corresponding protons are labeled for X (H^A, H^B, H^C) and the backbone protons ($H^{4/5}$) as well as the side-chain protons (N−CH_2). = bearing variable end groups X/X′. Characteristic benzylic protons (X = B) are assigned and labeled by arrow. (b) Expansion of aromatic region showing the set of protons for X = Bu (black) and a characteristic proton for X = H (blue).

detected, which is tentatively assigned to *β*-hydride elimination (*vide supra*). Figure 4 depicts the comparison of the 3-mer (panel b), 7-mer (panel c), and 15-mer series (panel d). Notably, a decreasing content of Br-containing polymers is noticed with increasing degree of polymerization; i.e., the relative ratios of the Bu/Br-, Br/Br-, and H/Br- vs Bu/Bu-decorated chains are larger. This observation is qualitatively explained by termination of the propagating chain by butyl groups (*vide infra*). However, the extent of Bu-decorated polymers seems unexpected because it requires an exhaustive termination and/or replacement of distal Br groups by Bu groups (Scheme 3b, steps iii−v). In contrast to the previous polymers (**p1**−**p4**), a full conversion of the dibromocarbazole was observed, and thus, also the consumption of equivalent amounts of the Grignard reagent is assumed. Although a residual slight excess of $Li^+[n\text{-}Bu_3Mg]^-$ cannot be ruled out, it appears unlikely to account for all H- and Bu-decorated chains—so that an alternative pathway may be operable based on the following assumptions: (a) The hitherto derived analysis on polycarbazoles supports the significant liberation of low-valent Ni(0) by dissociation and/or disproportionation during KCTP (Scheme 3a, steps i and ii). (b) The metal−halogen exchange generates equivalent amounts of alkyl bromide (i.e., *n*-BuBr), which have been shown to undergo oxidative addition with Ni(0) even at room temperature.[63] Hence, even in the absence of the Grignard reagent, Bu-decorated chain may be initiated. (c) The disproportionation of Ni−aryl complexes without *ortho*-substituents has been addressed,[48,67] which can account for this significant difference in end-group homogeneity of poly(3,6-carbazole) vs P3HT.[6] As a consequence of disproportionation, the Bu/Bu-decorated chains can form, while the concomitant generation of Ni(0) and Ni(II) re-enters the KCTP sequence (Scheme 1).

The ^{1}H NMR spectrum of **p5a** is shown in Figure 5 and is complemented by end-group analysis. The proton assignment is based on *N*-alkylcarbazoles bearing alkyl, bromo, or hydrogen groups in the 3,6-positions.[61] The spectrum is dominated by the carbazole protons centered at 8.55, 7.85, and 7.45 ppm and below 2 ppm by the alkyl side chain protons. Notably, the N−CH_2 moiety is well resolved and serves to estimate the degree of polymerization with respect to the benzylic protons of the terminal Bu substituent, which is identified by the characteristic signal and coupling pattern at 2.85 ppm.[61] The numerical ratio is 10:1 (see Figure S6), so that the lower bound of the average degree of polymerization is approximately 5 (assuming complete chain end termination by butyl groups). However, the mass spectrometry clearly shows also H- and Br-terminated polymers, whose ratio further varies with the degree of polymerization (*vide supra*). A reasonable guess is derived from the 7-mer series, in which the Bu-containing species account for approximately 50% of the total signal. Despite the crudeness of this estimate, the degree of polymerization (n = 10) is in reasonable agreement with the mass spectrometry data, while the overestimation by the SEC data (5000 g/mol by PS calibration, $n \approx 20$) is attributed to the stiffness of the polymer vs the polystyrene standard.

In summary, the utilization of magnesiate complexes enabled a quantitative and mild metal−halogen exchange for the first time (2 h, 40 °C), while the subsequent KCTP afforded the corresponding polymer (**p5**) in good yields (66%). The dispersity by SEC analysis and the dominant Bu and H end groups indicate side reaction during KCTP and, thus, deviation, from the ideal chain-growth mechanism. The origin is assigned to catalyst dissociation and/or disproportionation for the studied polycarbazoles, which is reported for various Ni−aryl complexes bearing no *ortho*-substituents.[67]

CONCLUSION

The scope of polymerization of 3,6-dibromocarbazole via GRIM and KCTP was investigated, and the obtained polymers were analyzed in detail by NMR spectroscopy, SEC analysis, and particularly mass spectrometry, including isotope analysis for end-group determination. The screening of various conventional KCTP protocols demonstrated that a quantitative metal−halogen exchange is crucial to obtain poly(3,6-carbazole)s in high yields. The reactivity of standard Grignard reagents, i.e., ^{i}PrMgCl (**p1**) or ^{t}BuMgCl (**p2**), is found to be too low (<55%) for complete metal−halogen exchange but afforded minor amounts of polymers with dominant Br-decorated chains, accompanied by alkyl- and proton-terminated chains. More importantly, the occurrence of Br/Br-decorated polymers strongly supports catalyst dissociation and/or disproportionation reactions. Consequently, the KCTP becomes less well behaved as examined in detail for poly(3-hexylthiophenes)[6] and, thus, accounts for the end-group inhomogeneity. The utilization of LiCl during metathesis (**p3** and **p4**) enhanced the metal−halogen exchange (up to 75%) and also afforded the polymer in somewhat increased yield. In addition, the comparison within the series **p1**−**p4** revealed also a general rate acceleration by LiCl during KCTP, with a larger

DOI: 10.1021/acs.macromol.6b02088
Macromolecules 2016, 49, 8801−8811

impact on the rates of polymerization vs side reactions according to SEC and MALDI-ToF data. Finally, the best results were found employing magnesiate complexes. Quantitative metal−halogen exchange was achieved within 2 h at 40 °C, and subsequent polymerization afforded **p5** in good isolated yield (66%). Noteworthy, similar end-group distributions were obtained as before, which are tentatively assigned to the catalyst dissociation and/or disproportionation. In summary, poly(3,6-carbazole) can be efficiently prepared via KCTP using magnesiate complexes. In view of improving the chain-growth character of 3,6-carbazoles by KCTP, modifications of the substrate (*ortho*-substituents) and/or improved catalyst systems are attractive to disfavor the proposed catalyst dissociation and/or disproportionation (Scheme 3a),[48] which would lead to a higher control of dispersity and molar masses as well as end-group fidelity.

■ ASSOCIATED CONTENT

Supporting Information

The Supporting Information is available free of charge on the ACS Publications website at DOI: 10.1021/acs.macromol.6b02088.

Additional instrumental details and analytical data (NMR, MS, SEC) are provided for completion (PDF)

■ AUTHOR INFORMATION

Corresponding Authors

*E-mail ulrich.schubert@uni-jena.de (U.S.S.).
*E-mail michael.jager.iomc@uni-jena.de (M.J.).

ORCID

Michael Jäger: 0000-0003-0400-1812

Funding

M.J. for financial support by the Carl-Zeiss-Foundation and the Friedrich Schiller University Jena ("Nachwuchsförderung").

■ ACKNOWLEDGMENTS

We thank Annett Urbanek for MALDI-ToF measurements, Tina Schlotthauer for ESI-ToF measurements, and Dr. Peter Bellstedt and the NMR platform IAAC/IOMC for help with the NMR measurements.

■ REFERENCES

(1) Shirakawa, H.; Louis, E. J.; MacDiarmid, A. G.; Chiang, C. K.; Heeger, A. J. Synthesis of electrically conducting organic polymers: halogen derivatives of polyacetylene, $(CH)_x$. *J. Chem. Soc., Chem. Commun.* **1977**, *16*, 578−580.

(2) Morin, J.-F.; Leclerc, M.; Adès, D.; Siove, A. Polycarbazoles: 25 Years of Progress. *Macromol. Rapid Commun.* **2005**, *26* (10), 761−778.

(3) Boudreault, P.-L. T.; Beaupre, S.; Leclerc, M. Polycarbazoles for plastic electronics. *Polym. Chem.* **2010**, *1* (2), 127−136.

(4) Yokozawa, T.; Suzuki, R.; Nojima, M.; Ohta, Y.; Yokoyama, A. Precision Synthesis of Poly(3-hexylthiophene) from Catalyst-Transfer Suzuki-Miyaura Coupling Polymerization. *Macromol. Rapid Commun.* **2011**, *32* (11), 801−806.

(5) Lee, J. K.; Ko, S.; Bao, Z. In Situ Hetero End-Functionalized Polythiophene and Subsequent "Click" Chemistry With DNA. *Macromol. Rapid Commun.* **2012**, *33* (10), 938−942.

(6) Lohwasser, R. H.; Thelakkat, M. Toward Perfect Control of End Groups and Polydispersity in Poly(3-hexylthiophene) via Catalyst Transfer Polymerization. *Macromolecules* **2011**, *44* (9), 3388−3397.

(7) Kosaka, K.; Ohta, Y.; Yokozawa, T. Influence of the Boron Moiety and Water on Suzuki−Miyaura Catalyst-Transfer Condensation Polymerization. *Macromol. Rapid Commun.* **2015**, *36* (4), 373−377.

(8) Zeigler, D. F.; Mazzio, K. A.; Luscombe, C. K. Fully Conjugated Graft Copolymers Comprising a P-Type Donor-Acceptor Backbone and Poly(3-hexylthiophene) Side Chains Synthesized Via a "Graft Through" Approach. *Macromolecules* **2014**, *47* (15), 5019−5028.

(9) Miyakoshi, R.; Shimono, K.; Yokoyama, A.; Yokozawa, T. Catalyst-transfer polycondensation for the synthesis of poly(p-phenylene) with controlled molecular weight and low polydispersity. *J. Am. Chem. Soc.* **2006**, *128* (50), 16012−16013.

(10) Yokoyama, A.; Suzuki, H.; Kubota, Y.; Ohuchi, K.; Higashimura, H.; Yokozawa, T. Chain-growth polymerization for the synthesis of polyfluorene via Suzuki-Miyaura coupling reaction from an externally added initiator unit. *J. Am. Chem. Soc.* **2007**, *129* (23), 7236−7237.

(11) Elmalem, E.; Kiriy, A.; Huck, W. T. S. Chain-Growth Suzuki Polymerization of n-Type Fluorene Copolymers. *Macromolecules* **2011**, *44* (22), 9057−9061.

(12) Elmalem, E.; Biedermann, F.; Johnson, K.; Friend, R. H.; Huck, W. T. S. Synthesis and Photophysics of Fully pi-Conjugated Heterobis-Functionalized Polymeric Molecular Wires via Suzuki Chain-Growth Polymerization. *J. Am. Chem. Soc.* **2012**, *134* (42), 17769−17777.

(13) Tkachov, R.; Senkovskyy, V.; Beryozkina, T.; Boyko, K.; Bakulev, V.; Lederer, A.; Sahre, K.; Voit, B.; Kiriy, A. Palladium-Catalyzed Chain-Growth Polycondensation of AB-type Monomers: High Catalyst Turnover and Polymerization Rates. *Angew. Chem., Int. Ed.* **2014**, *53* (9), 2402−2407.

(14) Javier, A. E.; Varshney, S. R.; McCullough, R. D. Chain-Growth Synthesis of Polyfluorenes with Low Polydispersities, Block Copolymers of Fluorene, and End-Capped Polyfluorenes: Toward New Optoelectronic Materials. *Macromolecules* **2010**, *43* (7), 3233−3237.

(15) Fischer, C. S.; Baier, M. C.; Mecking, S. Enhanced Brightness Emission-Tuned Nanoparticles from Heterodifunctional Polyfluorene Building Blocks. *J. Am. Chem. Soc.* **2012**, *135* (3), 1148−1154.

(16) Fischer, C. S.; Jenewein, C.; Mecking, S. Conjugated Star Polymers from Multidirectional Suzuki−Miyaura Polymerization for Live Cell Imaging. *Macromolecules* **2015**, *48* (3), 483−491.

(17) Wen, H.; Ge, Z.; Liu, Y.; Yokozawa, T.; Lu, L.; Ouyang, X.; Tan, Z. Efficient synthesis of well-defined polycarbazoles via catalyst-transfer Kumada coupling polymerization. *Eur. Polym. J.* **2013**, *49* (11), 3740−3743.

(18) Stefan, M. C.; Javier, A. E.; Osaka, I.; McCullough, R. D. Grignard Metathesis Method (GRIM): Toward a Universal Method for the Synthesis of Conjugated Polymers. *Macromolecules* **2009**, *42* (1), 30−32.

(19) Koldemir, U.; Puniredd, S. R.; Wagner, M.; Tongay, S.; McCarley, T. D.; Kamenov, G. D.; Müllen, K.; Pisula, W.; Reynolds, J. R. End Capping Does Matter: Enhanced Order and Charge Transport in Conjugated Donor−Acceptor Polymers. *Macromolecules* **2015**, *48* (18), 6369−6377.

(20) He, M.; Qiu, F.; Lin, Z. Conjugated rod-coil and rod-rod block copolymers for photovoltaic applications. *J. Mater. Chem.* **2011**, *21* (43), 17039−17048.

(21) Traina, C. A.; Bakus, R. C., II; Bazan, G. C. Design and Synthesis of Monofunctionalized, Water-Soluble Conjugated Polymers for Biosensing and Imaging Applications. *J. Am. Chem. Soc.* **2011**, *133* (32), 12600−12607.

(22) Raissi, M.; Erothu, H.; Ibarboure, E.; Cramail, H.; Vignau, L.; Cloutet, E.; Hiorns, R. C. Fullerene-capped copolymers for bulk heterojunctions: device stability and efficiency improvements. *J. Mater. Chem. A* **2015**, *3* (35), 18207−18221.

(23) Yameen, B.; Zydziak, N.; Weidner, S. M.; Bruns, M.; Barner-Kowollik, C. Conducting Polymer/SWCNTs Modular Hybrid Materials via Diels-Alder Ligation. *Macromolecules* **2013**, *46* (7), 2606−2615.

(24) Miyakoshi, R.; Yokoyama, A.; Yokozawa, T. Catalyst-transfer polycondensation. Mechanism of Ni-catalyzed chain-growth polymerization leading to well-defined poly(3-hexylthiophene). *J. Am. Chem. Soc.* **2005**, *127* (49), 17542−17547.

DOI: 10.1021/acs.macromol.6b02088
Macromolecules 2016, 49, 8801−8811

(25) Jeffries-El, M.; Sauvé, G.; McCullough, R. D. In-Situ End-Group Functionalization of Regioregular Poly(3-alkylthiophene) Using the Grignard Metathesis Polymerization Method. *Adv. Mater.* **2004**, *16* (12), 1017−1019.
(26) Yokoyama, A.; Yokozawa, T. Converting step-growth to chain-growth condensation polymerization. *Macromolecules* **2007**, *40* (12), 4093−4101.
(27) Literature search using Scifinder, 13/06/2016.
(28) Bui, T.-T.; Goubard, F. Recent advances in small molecular, non-polymeric organic hole transporting materials for solid-state DSSC. *EPJ Photovoltaics* **2013**, *4*, 40402.
(29) Pron, A.; Gawrys, P.; Zagorska, M.; Djurado, D.; Demadrille, R. Electroactive materials for organic electronics: preparation strategies, structural aspects and characterization techniques. *Chem. Soc. Rev.* **2010**, *39* (7), 2577−2632.
(30) Moad, G.; Chen, M.; Haussler, M.; Postma, A.; Rizzardo, E.; Thang, S. H. Functional polymers for optoelectronic applications by RAFT polymerization. *Polym. Chem.* **2011**, *2* (3), 492−519.
(31) Li, J.; Grimsdale, A. C. Carbazole-based polymers for organic photovoltaic devices. *Chem. Soc. Rev.* **2010**, *39* (7), 2399−2410.
(32) Lellouche, J.-P.; Koner, R. R.; Ghosh, S. N-Substituted carbazole heterocycles and derivatives as multipurpose chemical species: at the interface of chemical engineering, polymer and materials science. *Rev. Chem. Eng.* **2013**, *29* (6), 413−437.
(33) Geissler, U.; Hallensleben, M. L.; Rienecker, A.; Rohde, N. Polyarylenes on the basis of alkylpyrrole and alkylcarbazole derivatives and their oligomeric model systems. *Polym. Adv. Technol.* **1997**, *8* (2), 87−92.
(34) Xu, F.; Kim, J.-H.; Kim, H. U.; Jang, J.-H.; Yook, K. S.; Lee, J. Y.; Hwang, D.-H. Synthesis of High-Triplet-Energy Host Polymer for Blue and White Electrophosphorescent Light-Emitting Diodes. *Macromolecules* **2014**, *47* (21), 7397−7406.
(35) Huang, J.; Niu, Y. H.; Yang, W.; Mo, Y. Q.; Yuan, M.; Cao, Y. Novel electroluminescent polymers derived from carbazole and benzothiadiazole. *Macromolecules* **2002**, *35* (16), 6080−6082.
(36) Li, Z. A.; Liu, Y.; Yu, G.; Wen, Y.; Guo, Y.; Ji, L.; Qin, J.; Li, Z. A New Carbazole-Constructed Hyperbranched Polymer: Convenient One-Pot Synthesis, Hole-Transporting Ability, and Field-Effect Transistor Properties. *Adv. Funct. Mater.* **2009**, *19* (16), 2677−2683.
(37) Liu, S.-J.; Lin, W.-P.; Yi, M.-D.; Xu, W.-J.; Tang, C.; Zhao, Q.; Ye, S.-H.; Liu, X.-M.; Huang, W. Conjugated polymers with cationic iridium(III) complexes in the side-chain for flash memory devices utilizing switchable through-space charge transfer. *J. Mater. Chem.* **2012**, *22* (43), 22964−22970.
(38) Luo, J.; Xie, G.; Gong, S.; Chen, T.; Yang, C. Creating a thermally activated delayed fluorescence channel in a single polymer system to enhance exciton utilization efficiency for bluish-green electroluminescence. *Chem. Commun.* **2016**, *52* (11), 2292−2295.
(39) Vedarajan, R.; Hosono, Y.; Matsumi, N. π-Conjugated polycarbazole-boron complex as a colorimetric fluoride ion sensor. *Solid State Ionics* **2014**, *262*, 795−800.
(40) Iraqi, A.; Wataru, I. 3,6-linked 9-alkyl-9H-carbazole main-chain polymers: Preparation and properties. *J. Polym. Sci., Part A: Polym. Chem.* **2004**, *42* (23), 6041−6051.
(41) Zhang, Z.-B.; Motonaga, M.; Fujiki, M.; McKenna, C. E. The First Optically Active Polycarbazoles. *Macromolecules* **2003**, *36* (19), 6956−6958.
(42) Zhang, Z.-B.; Fujiki, M.; Tang, H.-Z.; Motonaga, M.; Torimitsu, K. The First High Molecular Weight Poly(N-alkyl-3,6-carbazole)s. *Macromolecules* **2002**, *35* (6), 1988−1990.
(43) Lee, R.-H.; Liu, J.-K.; Ho, J.-H.; Chang, J.-W.; Liu, B.-T.; Wang, H.-J.; Jeng, R.-J. Synthesis of quaternized ammonium iodide-containing conjugated polymer electrolytes and their application in dye-sensitized solar cells. *Polym. Int.* **2011**, *60* (3), 483−492.
(44) Beouch, L.; Tran Van, F.; Stephan, O.; Vial, J. C.; Chevrot, C. Optical and electrochemical properties of soluble N-hexylcarbazole-co-3,4-ethylenedioxythiophene copolymers. *Synth. Met.* **2001**, *122* (2), 351−358.
(45) Smith, K.; James, D. M.; Mistry, A. G.; Bye, M. R.; Faulkner, D. J. A new method for bromination of carbazoles, β-carbolines and iminodibenzyls by use of N-bromosuccinimide and silica gel. *Tetrahedron* **1992**, *48* (36), 7479−7488.
(46) Li, Y.; Ding, J.; Day, M.; Tao, Y.; Lu, J.; D'Iorio, M. Synthesis and Properties of Random and Alternating Fluorene/Carbazole Copolymers for Use in Blue Light-Emitting Devices. *Chem. Mater.* **2004**, *16* (11), 2165−2173.
(47) Cantow, M. J. R. *Polymer Fractionation*, 1st ed.; Academic Press Inc.: New York, 1967.
(48) Kiriy, A.; Senkovskyy, V.; Sommer, M. Kumada Catalyst-Transfer Polycondensation: Mechanism, Opportunities, and Challenges. *Macromol. Rapid Commun.* **2011**, *32* (19), 1503−1517.
(49) Miyakoshi, R.; Yokoyama, A.; Yokozawa, T. Development of catalyst-transfer condensation polymerization. Synthesis of π-conjugated polymers with controlled molecular weight and low polydispersity. *J. Polym. Sci., Part A: Polym. Chem.* **2008**, *46* (3), 753−765.
(50) Bilbrey, J. A.; Sontag, S. K.; Huddleston, N. E.; Allen, W. D.; Locklin, J. On the Role of Disproportionation Energy in Kumada Catalyst-Transfer Polycondensation. *ACS Macro Lett.* **2012**, *1* (8), 995−1000.
(51) Doubina, N.; Stoddard, M.; Bronstein, H. A.; Jen, A. K. Y.; Luscombe, C. K. The Effects of Binding Ligand Variation on the Nickel Catalyzed Externally Initiated Polymerization of 2-Bromo-3-hexyl-5-iodothiophene. *Macromol. Chem. Phys.* **2009**, *210* (22), 1966−1972.
(52) Nanashima, Y.; Shibata, R.; Miyakoshi, R.; Yokoyama, A.; Yokozawa, T. Investigation of catalyst-transfer condensation polymerization for the synthesis of n-type π-conjugated polymer, poly(2-dioxaalkylpyridine-3,6-diyl). *J. Polym. Sci., Part A: Polym. Chem.* **2012**, *50* (17), 3628−3640.
(53) Bryan, Z. J.; McNeil, A. J. Evidence for a preferential intramolecular oxidative addition in Ni-catalyzed cross-coupling reactions and their impact on chain-growth polymerizations. *Chem. Sci.* **2013**, *4* (4), 1620−1624.
(54) Doubina, N.; Ho, A.; Jen, A. K. Y.; Luscombe, C. K. Effect of Initiators on the Kumada Catalyst-Transfer Polycondensation Reaction. *Macromolecules* **2009**, *42* (20), 7670−7677.
(55) Krasovskiy, A.; Straub, B. F.; Knochel, P. Highly Efficient Reagents for Br/Mg Exchange. *Angew. Chem., Int. Ed.* **2006**, *45* (1), 159−162.
(56) Krasovskiy, A.; Knochel, P. A LiCl-Mediated Br/Mg Exchange Reaction for the Preparation of Functionalized Aryl- and Heteroarylmagnesium Compounds from Organic Bromides. *Angew. Chem., Int. Ed.* **2004**, *43* (25), 3333−3336.
(57) Knochel, P.; Dohle, W.; Gommermann, N.; Kneisel, F. F.; Kopp, F.; Korn, T.; Sapountzis, I.; Vu, V. A. Highly Functionalized Organomagnesium Reagents Prepared through Halogen−Metal Exchange. *Angew. Chem., Int. Ed.* **2003**, *42* (36), 4302−4320.
(58) Senkovskyy, V.; Sommer, M.; Tkachov, R.; Komber, H.; Huck, W. T. S.; Kiriy, A. Convenient Route To Initiate Kumada Catalyst-Transfer Polycondensation Using Ni(dppe)Cl2 or Ni(dppp)Cl2 and Sterically Hindered Grignard Compounds. *Macromolecules* **2010**, *43* (23), 10157−10161.
(59) Kochemba, W. M.; Kilbey, S. M.; Pickel, D. L. End-group composition of poly(3-hexylthiophene)s prepared by in situ quenching of the grignard metathesis polymerization: Influence of additives and reaction conditions. *J. Polym. Sci., Part A: Polym. Chem.* **2012**, *50* (14), 2762−2769.
(60) Miyakoshi, R.; Yokoyama, A.; Yokozawa, T. Synthesis of Poly(3-hexylthiophene) with a Narrower Polydispersity. *Macromol. Rapid Commun.* **2004**, *25* (19), 1663−1666.
(61) Park, M.; Buck, J. R.; Rizzo, C. J. A convenient synthesis of 3,6-substituted carbazoles via nickel catalyzed cross-coupling. *Tetrahedron* **1998**, *54* (42), 12707−12714.
(62) Grubbs, R. H.; Miyashita, A.; Liu, M.-I. M.; Burk, P. L. The preparation and reactions of nickelocyclopentanes. *J. Am. Chem. Soc.* **1977**, *99* (11), 3863−3864.

DOI: 10.1021/acs.macromol.6b02088
Macromolecules 2016, 49, 8801−8811

(63) Rudolph, A.; Lautens, M. Secondary Alkyl Halides in Transition-Metal-Catalyzed Cross-Coupling Reactions. *Angew. Chem., Int. Ed.* **2009**, *48* (15), 2656−2670.
(64) Takagi, K.; Kawagita, E.; Kouchi, R. Synthesis and Characterization of Polythiophene Derivatives with Nitrogen Heterocycles on the Side Chain. *J. Polym. Sci., Part A: Polym. Chem.* **2014**, *52* (15), 2166−2174.
(65) Dumouchel, S.; Mongin, F.; Trécourt, F.; Quéguiner, G. Synthesis and reactivity of lithium tri(quinolinyl)magnesates. *Tetrahedron* **2003**, *59* (43), 8629−8640.
(66) Iida, T.; Wada, T.; Tomimoto, K.; Mase, T. Tributylmagnesium ate complex-mediated novel bromine−magnesium exchange reaction for selective monosubstitution of dibromoarenes. *Tetrahedron Lett.* **2001**, *42* (29), 4841−4844.
(67) Doubina, N.; Paniagua, S. A.; Soldatova, A. V.; Jen, A. K. Y.; Marder, S. R.; Luscombe, C. K. Steric Effects of the Initiator Substituent Position on the Externally Initiated Polymerization of 2-Bromo-5-iodo-3-hexylthiophene. *Macromolecules* **2011**, *44* (3), 512−520.

DOI: 10.1021/acs.macromol.6b02088
Macromolecules 2016, 49, 8801−8811

Publication P5

Poly(*N*-alkyl-3,6-carbazole)s via Suzuki–Miyaura polymerization: From macrocyclization toward end functionalization

R. Schroot, U. S. Schubert, M. Jäger, *Macromolecules* **2017**, *50*, 1319-1330.

The paper as well as the supporting information (free of charge) are available online under: doi.org/10.1021/acs.macromol.7b00144

Macromolecules

Article

pubs.acs.org/Macromolecules

Poly(*N*-alkyl-3,6-carbazole)s via Suzuki–Miyaura Polymerization: From Macrocyclization toward End Functionalization

Robert Schroot,[†] Ulrich S. Schubert,*[,†,‡] and Michael Jäger*[,†,‡]

[†]Laboratory of Organic and Macromolecular Chemistry (IOMC) and [‡]Center for Energy and Environmental Chemistry Jena (CEEC Jena), Friedrich Schiller University Jena, 07743 Jena, Germany

Supporting Information

ABSTRACT: The metal-catalyzed polymerization of 3,6-carbazoles is explored with emphasis of end-group fidelity of the telechelic polymers. The Suzuki–Miyaura coupling polymerization using asymmetric bifunctional (AB-type) monomers was selected to circumvent the inherent polycondensation character of symmetric (AA/BB-type) monomers. Common synthetic protocols were screened to facilitate the chain growth vs step growth character during the polymerization, e.g., several activation reagents for the boronic ester and various catalytic systems and their associated reaction conditions. The reactions were analyzed in detail by size exclusion chromatography (SEC), ^{1}H NMR spectroscopy, and mass spectrometry including isotope analysis for end-group determination. It was found that the intermediate oligomers are susceptible for macrocycle formation, particularly at low concentration, while longer polymer chains continue to polymerize. The synthetic methodology was extended to utilize functionalized precatalysts and functional terminating agents in order to explore the scope of chain growth vs step growth. The concomitant formation of macrocycles was observed, which indicates the catalyst dissociation and, thus, also the polycondensation pathway. Importantly, the applied low concentration leads to trapping of the undesired nonfunctionalized chains as macrocycles, which can be readily removed from the telechelic linear polymer. In summary, the developed protocols demonstrate the versatility to prepare telechelic poly(3,6-carbazole)s via Suzuki–Miyaura coupling. The azide-decorated poly(carbazole) exemplifies the potential to serve as building blocks for further copper-mediated azide–alkyne cycloaddition reactions.

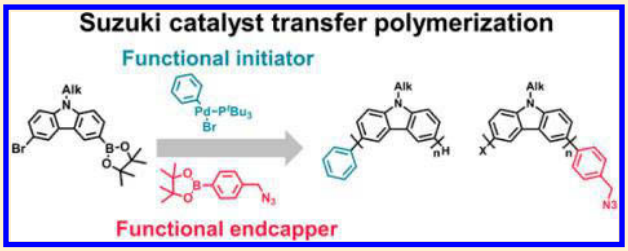

INTRODUCTION

Semiconducting polymers have gained enormous attention since the ground-breaking work by Shirakawa, Heeger, and MacDiarmid four decades ago. Since then, this material class has matured immensely and entered successfully various application fields, e.g. organic light-emitting diodes (OLEDs), organic field-effect transistors (OFETs), and organic photovoltaic cells and/or sensors. The ongoing research is fueled by the almost unlimited opportunity to adjust the optical and electrical characteristics by means of their constituting subunits and linkage pattern as well as phase separation and self-assembly by virtue of side-chain modifications.[1−3] Among others, the majority of hitherto explored polymers comprises electron-rich thiophene,[4−8] phenylene,[9,10] fluorene,[11−16] and 2,7-carbazole[17,18] subunits, which are often complemented by alternating electron-poor heterocyclic subunits to tailor the optical and electrical band gaps.[19] Such conjugated alternating copolymers are conveniently prepared by polycondensation of the two corresponding symmetric bifunctional (A–A/B–B-type, A and B denote complementary functional groups for linkage) monomers, which further offers great opportunities to readily synthesize polymer libraries. Because of the inherent step-growth mechanism, the precise control of molar mases and low dispersities, as well as end-group fidelity, is challenging. An alternative strategy utilizes the asymmetric bifunctional A–B-type monomer, which can in principle follow a chain growth mechanism. A prominent example is given by the Kumada chain transfer polymerization (KCTP),[20] in particular for the preparation of telechelic poly(3-hexylthiophene) (P3HT). While the KCTP has been optimized for P3HT,[20] other monomers often lack such high control, which has been traced to the instability of the active species against disproportionation in order to control end-group fidelity[6,21] as well as the importance of an associated catalyst–polymer pair vs catalyst dissociation to sustain the chain growth mechanism vs polycondensation.[20] Notably, such features were also reported for Suzuki–Miyaura coupling, which considerably expands the scope of suitable monomers.[10,22,23] Note that the employed boronic esters are less nucleophilic than their corresponding Grignard reagents, which extends the scope of available end groups introduced by functional precatalysts.

In addition to the control of the polymerization process itself, current work is devoted to develop (facile) synthetic procedures for defined telechelic macromolecular architectures. Such advanced materials offer the opportunity to control important device parameters on a molecular level, e.g., to control trap sites at the chain terminus,[24] to utilize the phase

Received: January 19, 2017
Published: February 8, 2017

DOI: 10.1021/acs.macromol.7b00144
Macromolecules 2017, 50, 1319−1330

segregation and stability of morphology by means of block copolymers, or to achieve adherence to specific surfaces by virtue of a grafting approach.[25,26] One underlying synthetic challenge is to efficiently prepare and utilize the end groups in subsequent postpolymerization reactions, and thus, the progress in synthetic routes toward telechelic polymers with tunable optical and electrical properties is expected to provide a powerful platform to design functional macromolecules.

Among many others, triarylamine-based semiconducting polymers are widely utilized as hole transporter.[2,27−29] In particular, carbazole-derived materials constitute an attractive material class,[30,31] owing to the facile syntheses and optoelectronic and/or processing properties.[2] Two major classes of polycarbazoles can be assigned, depending on the position of connectivity. The linkage through the 2,7-positions of carbazole—which resembles *p*-phenylene—assures a high degree conjugation and a large conjugation segment length. Hence, such materials are particularly attractive for applications requiring low optical and electrochemical band gaps. The connectivity via the 3,6-positions leads to a *meta*-linked phenylene backbone. As consequence, the corresponding poly(3,6-carbazole)s feature lower charge carrier mobilities but exhibit distinct benefits, e.g., electrochemically stable oxidation processes[32] and transparency in the visible light region. These properties render poly(3,6-carbazole)s particularly attractive for OLED applications,[3,33,34] flash memory devices, or OFETs[35,36] as well as devices with thermally activated delayed fluorescence.[37] The synthesis of telechelic 3,6-carbazole-based homopolymers mainly relies on Ni- or Pd-mediated cross-couplings without detailed end-group analysis.[18,38−46] Typically, the polymerizations involve the *in situ* activation of the symmetric bifunctional precursors, e.g., *N*-alkyl-3,6-dibromocarbazoles by elemental Mg[39,40] or Zn,[41] or Yamamoto coupling using stoichiometric amounts of Ni(0),[42−45] as well as polycondensation reactions of A−A/B−B-type monomers, particularly employing boronic ester derivatives.[39,47] The latter strategy has been successfully employed to prepare a variety of donor−acceptor polymers.[33,34,37,39,47] Recently, we investigated the preparation of poly(3,6-carbazole) via KCTP, which identified the importance of metal−halogen exchange and the associated side reactions that precluded the formation of telechelic polymers.[48]

In this contribution, we investigate the preparation of telechelic poly(3,6-carbazole)s with controlled molar masses, including end-group analysis and a mechanistic interpretation of their formation. Hence, we focus on the Suzuki−Miyaura coupling polymerization using asymmetric A−B-type monomers as well as the *in situ* activation using a diboron reagent similar to the GRIM-KCTP approach. To the best of our knowledge, there is only one scientific report for usage of the A−B-type monomer to prepare the corresponding homopolymer[39] or a related triblock copolymer,[46] while the *in situ* activation of *N*-alkyl-3,6-dibromocarbazole is unpreceded but for related poly(2,7-carbazole).[49] The polymerization was conducted using typical activating reagents, catalyst systems, and reaction conditions. The obtained polymers were characterized by ^{1}H NMR spectroscopy, by size exclusion chromatography (SEC), and in more detail by MALDI-ToF mass spectrometry (see Supporting Information for procedural details on SEC and MS analysis). The MS data are further analyzed by isotope simulations to discern the desired end-group fidelity. The second part addresses the utilization of functionalized initiator and termination reagents, which extend the set of available functional groups beyond bromo- and boronic ester moieties. In this regard, the preparation of an azide-functionalized poly(3,6-carbazole) is presented, which can serve as a building block applying azide−alkyne cycloaddition reactions.

EXPERIMENTAL SECTION

All reagents were purchased from ABCR, Acros Organics, Alfa Aesar, Apollo Scientific, Sigma-Aldrich, or TCI Chemicals and were used without further purification unless otherwise noted. All solvents were degassed before use. THF and toluene were distilled from sodium/benzophenone. 3,6-Dibromocarbazole,[50] 3,6-dibromo-9-octyl-9*H*-carbazole (**1**),[51] 2-(4-(azidomethyl)phenyl)-4,4,5,5-tetramethyl-1,3,2-dioxaborolane (**6**),[5] and [(P^tBu_3)Pd(Ph)Br][10] were prepared according to literature procedures.

3,6-Dibromo-9-ethylhexyl-9*H*-carbazole (2). The compound was prepared by an adopted literature procedure.[51] 3,6-Dibromocarbazole (8.320 g, 25.60 mmol) and 3-(bromomethyl)heptane (9.890 g, 51.20 mmol) were dissolved in DMSO (50 mL). Subsequently a 50% solution of NaOH in water (25 mL) was added, and the resulting suspension was stirred overnight at room temperature. Then water was added, and the mixture was extracted three times with diethyl ether. The organic solution was dried over Na_2SO_4, filtered, and concentrated under reduced pressure. Purification by column chromatography (silica, CH_2Cl_2/hexane 5/95) gave the product as colorless oil (7.32 g, 65%). ^{1}H NMR (300 MHz, $CDCl_3$): δ 8.15 (d, J = 1.7 Hz, 2H, ArH), 7.55 (dd, J = 8.7, 1.7 Hz, 2H, ArH), 7.26 (d, J = 8.7 Hz, 2H, ArH), 4.12 (d, J = 7.6 Hz, 2H, CH_2), 2.18−1.82 (m, 1H, CH), 1.48−1.15 (m, 8H, 4 × CH_2), 1.00−0.79 (m, 6H, 2 × CH_3).

3-Bromo-9-octyl-6-(4,4,5,5-tetramethyl-1,3,2-dioxaborolan-2-yl)-9*H*-carbazole (3). The compound was prepared by an adopted literature procedure.[39] A Schlenk tube was charged with **1** (1.150 g, 2.63 mmol) and flushed with nitrogen. Then dry THF (25 mL) was added with a syringe, and the solution was cooled to −78 °C. *n*-BuLi (1.05 mL, 2.63 mmol, 2.5 M in hexane) was added dropwise, and the yellow solution was stirred for 30 min at −78 °C. Subsequently, 2-isopropoxy-4,4,5,5-tetramethyl-1,3,2-dioxaborolane (0.538 g, 2.89 mmol) was added. The formed suspension was slowly warmed to room temperature overnight. Afterward, water was added, and the mixture was extracted three times with ethyl acetate. The organic solution was dried over Na_2SO_4, filtered, and concentrated under reduced pressure. Purification by column chromatography (silica, ethyl acetate/hexane 4/96) gave the product as colorless oil which crystallized in the freezer (0.940 g, 74%). *Note: The compound tends to decomposition during chromatography, which decreases the yield. In this case, the addition of 1% Et_3N to the eluent increases the stability of the compound.* ^{1}H NMR (300 MHz, $CDCl_3$): δ 8.56 (s, 1H, ArH), 8.25 (s, 1H, ArH), 7.94 (d, J = 8.1 Hz, 1H, ArH), 7.54 (d, J = 8.5 Hz, 1H, ArH), 7.39 (d, J = 8.1 Hz, 1H, ArH), 7.28 (d, J = 8.5 Hz, 1H, ArH), 4.27 (t, J = 7.0 Hz, 2H, CH_2), 1.96−1.73 (m, 2H, CH_2), 1.41 (s, 12H, 4 × CH_3), 1.38−1.12 (m, 10H, 5 × CH_2), 1.00−0.77 (m, 3H, CH_3).

3-Bromo-9-(2-ethylhexyl)-6-(4,4,5,5-tetramethyl-1,3,2-dioxaborolan-2-yl)-9*H*-carbazole (4). The compound was prepared analogously to **3** using **2** (0.500 g, 1.14 mmol) as starting material. Purification by column chromatography gave **4** as colorless oil (0.450 g, 81%). *Note: The compound tends to decompose during chromatography, which decreases the yield. In this case, the addition of 1% Et_3N to the eluent increases the stability of the compound.* ^{1}H NMR (300 MHz, $CDCl_3$): δ 8.59 (s, 1H, ArH), 8.27 (d, J = 1.8 Hz, 1H, ArH), 7.96 (dd, J = 8.3 Hz, 0.9 Hz, 1H, ArH), 7.54 (dd, J = 8.6 Hz, 1.8 Hz, 1H, ArH), 7.38 (d, J = 8.3 Hz, 1H, ArH), 7.24 (d, J = 8.6 Hz, 1H, ArH), 4.10 (d, J = 7.2 Hz, 2H, CH_2), 2.12−1.91 (m, 1H, CH), 1.43 (s, 12H, 4 × CH_3), 1.40−1.13 (m, 8H, 4 × CH_2), 1.00−0.80 (m, 6H, 2 × CH_3). ^{13}C NMR (100 MHz, $CDCl_3$): δ 143.3, 139.6, 132.7, 128.3, 128.1, 124.9, 123.3, 121.6, 112.1, 110.5, 108.7, 83.7, 47.5, 39.3, 31.0, 28.8, 25.0, 24.4, 23.1, 14.1, 11.0. HR-ESI ([$C_{26}H_{35}BBrNO_2$ + H]$^+$) m/z: calcd: 484.2017; found: 484.2009. Error: 2.5 ppm.

4-(2-Tetrahydropyranyloxy)bromobenzene (5). A flask was charged with 4-bromophenol (5.000 g, 28.90 mmol), 3,4-dihydro-2*H*-pyran

DOI: 10.1021/acs.macromol.7b00144
Macromolecules 2017, 50, 1319−1330

Table 1. Experimental Conditions for the Suzuki–Miyaura Polymerization[a]

entry	polymer	monomer	base	catalyst	quencher	solvents	c_M[b] [mM]	T [°C]	t [h]	isolated yield [%]
A	**p1**[52]	**1**	K_2CO_3	[Pd_2dba_3], BuAdP	H_2O	DMF/H_2O[c]	364	90	24	44
B	**p2**[39]	**4**	Na_2CO_3	[$Pd(PPh_3)_4$]	MeOH	PhMe/H_2O	67	85	48	52
C	**p3**	**4**	K_2CO_3	[$Pd(P^tBu_3)_2$]	MeOH	THF/H_2O	27	RT	24	70
D	**p4**	**3**	K_2CO_3	[$Pd(P^tBu_3)_2$]	tol-B(OH)$_2$	THF/H_2O	25	RT	5.4[d]	72
E	**p5**[4]	**3**	CsF 18-crown-6	[$(P^tBu_3)Pd(Ph)Br$]	HCl	THF/H_2O	14	0	24	77
F	**p6**[10]	**3**	Na_2CO_3	[$(P^tBu_3)Pd(Ph)Br$]	HCl	THF/H_2O	23	RT	0.5	32
G	**p7**[53]	**3**	K_2CO_3	[$(P^tBu_3)Pd(Ph)Br$]	HCl	THF/H_2O	20	RT	24	66
H	**p8**	**3**	K_2CO_3	[$Pd(P^tBu_3)_2$]	5	THF/H_2O	25	RT	6	77
I	**p9**	**4**	K_2CO_3	[$Pd(P^tBu_3)_2$]	6	THF/H_2O	27	RT	6	56

[a]See the Supporting Information for analytical data including molar masses and dominant end group series. [b]Concentration of the monomer (in the organic phase in the case of biphasic reactions). [c]*In situ* borylation with bis(pinacolato)diboron in DMF and then addition of water to initiate polymerization. dba is dibenzylideneacetone, and BuAdP is diadamantyl-*n*-butyl-phosphine. [d]After 5.4 h, *p*-tolylboronic acid was added, and the reaction continued for 17.3 h.

(4.860 g, 57.80 mmol), and CH_2Cl_2 (50 mL). 4-Methylbenzenesulfonic acid (0.004 g, 0.12 mmol) was added, and the solution was stirred overnight at room temperature. The reaction was quenched with water (100 mL), and the mixture was extracted with CH_2Cl_2. The organic solution was dried over Na_2SO_4, filtered, and concentrated under reduced pressure. Purification by column chromatography (silica, ethyl acetate/hexane 5/95) gave the product as with solid (6.000 g, 81%). ^{1}H NMR (300 MHz, $CDCl_3$): δ 7.38 (d, J = 8.8 Hz, 2H, ArH), 6.95 (d, J = 8.8 Hz, 2H, ArH), 5.38 (t, J = 3.2 Hz, 1H, CH), 4.11–3.72 (m, 1H, CH_2), 3.72–3.31 (m, 1H, CH_2), 2.21–1.91 (m, 1H, CH_2), 1.91–1.80 (m, 2H, CH_2), 1.80–1.47 (m, 3H, CH_2).

Suzuki–Miyaura Coupling Polymerization. An overview of all prepared polymers is given in Table 1, followed by the exact conditions for each entry.

p1.[52] A vial was charged with **1** (0.500 g, 1.15 mmol), bis(pinacolato)-diboron (0.290 g, 1.15 mmol), potassium acetate (0.337 g, 3.43 mmol), butyl-di-1-adamantylphosphine (BuAdP) (0.012 g, 0.03 mmol), [$Pd_2(dba)_3$] (0.010 g, 0.01 mmol), and dry DMF (2 mL). The vial was sealed, purged with nitrogen, and heated to 90 °C for 1 h. Subsequently, an aqueous solution of K_2CO_3 (1.14 mL, 4 M) was added with a syringe, and the reaction mixture was stirred at 90 °C overnight. The next day, water was added to the suspension, and the mixture was extracted with CH_2Cl_2 (three times). The organic phases were combined, washed with water and brine, dried over Na_2SO_4, filtered, and concentrated under reduced pressure to yield a yellow solid. Fractionated precipitation (nonsolvent addition method,[54] THF, MeOH) gave two main fractions, which were further analyzed (**p1a**: 0.085 g; **p1b**: 0.050 g).

p2.[39] A nitrogen-flushed flask was charged with **4** (0.450 g, 0.93 mmol), dry toluene (14 mL), and an aqueous Na_2CO_3 solution (14 mL, 1 M). The mixture was purged with nitrogen for 0.5 h before [$Pd(PPh_3)_4$] (0.022 g, 0.02 mmol) was added. Subsequently, the biphasic solution was heated to 85 °C for 48 h. After cooling to room temperature the mixture was precipitated in MeOH (120 mL). The solid was filtered off and was washed with water and MeOH. After drying the compound was obtained as bright yellow solid (0.135 g).

p3. A nitrogen-flushed Schlenk tube was charged with **4** (0.225 g, 0.47 mmol), dry THF (15 mL), and a purged aqueous solution of K_2CO_3 (0.95 mL, 4 M). Subsequently, [$Pd(P^tBu_3)_2$] (0.012 g, 0.023 mmol) was added as solution in THF (2.00 mL), and the resulting yellow mixture was stirred at room temperature overnight. The solution was precipitated in MeOH and filtered, and the off-white solid was washed with MeOH as well as water and dried (0.100 g).

p4. A nitrogen-flushed Schlenk tube was charged with **3** (0.330 g, 0.68 mmol), dry THF (23 mL), and a purged aqueous solution of K_2CO_3 (1.40 mL, 4 M). Subsequently, [$Pd(P^tBu_3)_2$] (0.017 g, 0.03 mmol) was added as solution in THF (2.25 mL), and the resulting mixture was stirred at room temperature. Samples were taken for SEC and MALDI analysis and were quenched with DCl in THF. After 5.4 h, 4-tolylboronic acid (0.093 g, 0.68 mmol) was added as solution in dry THF (1.50 mL), and the reaction was continued at room temperature overnight. The reaction was quenched by addition of 2 M DCl in THF (15 mL). The mixture was precipitated in MeOH and filtered, and the off-white solid was washed with MeOH as well as water and dried (0.137 g).

p5.[4] A Schlenk tube was charged with CsF (0.361 g, 2.34 mmol) and 18-crown-6 (1.138 g, 4.3 mmol), evacuated, and flushed with nitrogen. Then **3** (0.250 g, 0.52 mmol) was added as solution in dry THF (5 mL), and additional THF (30 mL) was added. Subsequently, the reaction mixture was cooled to 0 °C, and N_2-purged water (2.25 mL) was added. Afterward, [$(P^tBu_3)Pd(Ph)Br$] (0.007 g, 0.015 mmol) was added as solution in THF (0.93 mL), the yellow reaction solution was stirred overnight, and the reaction mixture was slowly allowed to come to room temperature. After 24 h the reaction was quenched by addition of 6 M HCl (5.00 mL); the mixture was precipitated in MeOH and filtered, and the off-white solid was washed with MeOH and water (0.110 g). A small amount of the polymer was fractionated by preparative SEC (Bio-Beads S-X3, CH_2Cl_2; Toyopearl HW-50F, CH_2Cl_2/MeOH 95/5) to analyze the high molar mass fraction of the polymer.

p6.[10] A nitrogen-flushed Schlenk tube was charged with **3** (0.250 g, 0.52 mmol), dry THF (22 mL), and a purged aqueous solution of Na_2CO_3 (10.40 mL, 2 M). Subsequently, [$(P^tBu_3)Pd(Ph)Br$] (0.007 g, 0.02 mmol) was added as solution in THF (0.93 mL), and the resulting biphasic mixture was stirred at room temperature for 30 min. Then the reaction solution was precipitated in a mixture of 2 M HCl (10 mL) and MeOH (40 mL). The precipitate was filtered off, washed with water as well as MeOH, and dried (0.045 g).

p7.[53] A nitrogen-flushed Schlenk tube was charged with **3** (0.250 g, 0.52 mmol), dry THF (21 mL), and a purged aqueous solution of K_2CO_3 (1.05 mL, 4 M). Subsequently, [$(P^tBu_3)Pd(Ph)Br$] (0.007 g, 0.02 mmol) was added as solution in THF (0.93 mL), and the resulting mixture was stirred at room temperature overnight. The reaction was quenched by addition of 2 M HCl in THF (10 mL). The mixture was precipitated in MeOH and filtered, and the off-white solid was washed with MeOH as well as water and dried (0.094 g).

Polymerization Including End-Capping Reagents. p8. A nitrogen-flushed Schlenk tube was charged with **3** (0.250 g, 0.52 mmol), dry THF (21 mL), and a purged aqueous solution of K_2CO_3 (1.05 mL, 4 M). Subsequently, [$Pd(P^tBu_3)_2$] (0.013 g, 0.03 mmol) was added as solution in THF (2.00 mL), and the resulting yellow mixture was stirred at room temperature for 6 h. Then 4-(2-tetrahydropyranyloxy)bromobenzene (**5**) (0.133 g, 0.52 mmol) was added as solution in dry THF (1.00 mL). After stirring overnight the mixture was precipitated in MeOH and filtered, and the off-white solid was washed with MeOH as well as water and dried (0.110 g).

p9. A nitrogen-filled Schlenk tube was charged with **4** (0.225 g, 0.47 mmol), dry THF (15 mL), and a purged aqueous solution of K_2CO_3 (0.95 mL, 4 M). Subsequently, [$Pd(P^tBu_3)_2$] (0.012 g, 0.02 mmol) was added as solution in THF (2.00 mL), and the

DOI: 10.1021/acs.macromol.7b00144
Macromolecules 2017, 50, 1319–1330

resulting yellow mixture was stirred at room temperature for 6 h. Then 2-(4-(azidomethyl)phenyl)-4,4,5,5-tetramethyl-1,3,2-dioxaborolane (**6**) (0.120 g, 0.47 mmol) was added as solution in dry THF (1.00 mL). After stirring overnight the mixture was precipitated in MeOH and filtered, and the off-white solid was washed with MeOH as well as water and dried (0.080 g).

RESULTS AND DISCUSSION

In this contribution, we present the preparation and analysis of asymmetric telechelic poly(3,6-carbazoles). The article is organized as follows: The first part briefly summarizes recent conceptional strategies and challenges to prepare conjugated telechelic polymers via Pd-catalysis beyond polythiophenes,[11,20] which serves as basis for the detailed analysis of the experimental results as well as for our chosen synthetic strategy. The experimental part starts with the exploration of general synthetic procedures using the Suzuki–Miyaura coupling polymerization, including a SEC and MS study to detail the course of the polymerization. The end groups are assigned by means of MALDI-ToF mass spectrometry, and the telechelic polymers will be denoted in the article as X/Y-terminated, e.g., Ph/H corresponds to one phenyl and one hydrogen end group. The third part details the scope of controlled initiation via a functionalized Pd catalyst as well as termination through macrocyclization or functionalized end-capping reagents to yield telechelic polymers.

Scheme 1. Schematic Representation of the Suzuki–Miyaura Polymerization Illustrating the Step Growth Character[a]

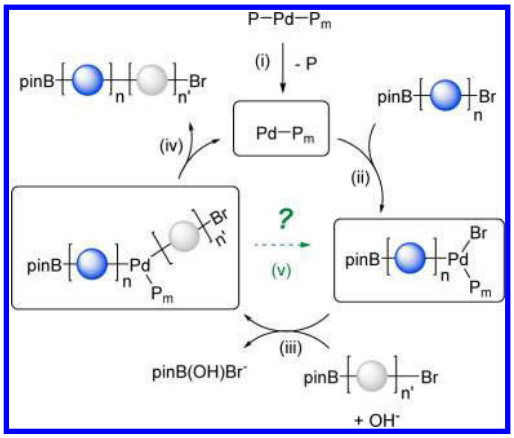

[a](i) Formation of the active Pd(0) catalyst from Pd precatalyst. (ii) Oxidative addition of the active Pd(0) catalyst into the monomer (n = 1) or formed polymer (n > 1) (in blue). (iii) Transmetalation step with a second monomer (n' = 1) or polymer (n' > 1) (in gray) in the presence of base (OH^-). (iv) Reductive elimination to release the coupled organic fragments and regeneration of active Pd(0) catalyst. (v) Illustration of the consequence of ring-walking and/or reinsertion at the terminal C–Br bond (in this case, the new chain length equals $n + n'$). Note: the altered polymerization character via step v (chain growth) vs steps iv + ii (step growth).

Suzuki–Miyaura Coupling Polymerization and Synthetic Strategy. Scheme 1 depicts the essential features of the Suzuki–Miyaura coupling polymerization, which are desired to achieve a controlled polymerization with end-group fidelity as well as shifting the mechanism toward chain-growth similar to KCTP.[11,13] The catalytic cycle begins with the formation of the active Pd(0) catalyst from a suitable precatalyst upon ligand loss (step i). Next, oxidative addition into the C–Br bond of the monomer—or subsequently generated polymer—leads to the C–Pd–Br species (step ii). The transmetalation with the boronic ester group of a second monomer (or polymer), which requires a base for activation, affords the C–Pd–C intermediate (step iii). The catalytic cycle is typically closed upon reductive elimination (step iv) to release the cross-coupled product and to regenerate the active Pd(0) catalyst. This sequence explains the typical step growth character leading to relatively high dispersities ($Đ$ > 2), if the catalyst is free to diffuse. However, if the catalyst stays associated with the chain, and undergoes oxidative addition at the terminal C–Br bond, the mechanism shifts to chain-growth (step v), as observed for the KCTP using Ni catalysts to prepare poly(thiophene)s.[20] In reality, both pathways may be operable leading to intermediate dispersities. Notably, polymerizations relying on A–A/B–B-type couplings are not capable to sustain the chain growth because the added unit during transmetalation carries *a priori* the wrong functionality, which does not permit the oxidative addition step (Scheme 1, step v). However, the benefits of the Suzuki–Miyaura cross-coupling originate from a broader functional group tolerance compared to GRIM/KCTP, the possibility to isolate and purify the monomers, and to apply advanced catalyst systems (e.g., Pd precatalyst and phosphine). Notably, the possibility to utilize purified bifunctional monomers precludes the side reactions that originate from incomplete *in situ* activation, which is reported to be challenging via GRIM.[18,48]

The synthetic steps of this work are outlined in Scheme 2, illustrating the monomer synthesis and the subsequent polymerization of the asymmetric A–B-type monomers. The required *N*-alkyl 3,6-dibromocarbazole precursor (**1** or **2**) was readily prepared by adopted literature procedures.[50,51] Note that the branching of the octyl side chain was varied because later experimental results revealed a lower solubility of the isolated polymers in the case of a linear side chain (*vide infra*). A similar low solubility was noted during the preparation of a triblock copolymer with two peripheral poly(3,6-carbazole) segments, so that the concomitant homopolymerization lead only to low molar masses.[46] The asymmetric monomers (**3** and **4**) were directly prepared without the need of transesterfication by one-fold lithiation and subsequent quenching with isopropoxypinacolato borane in good yields. The obtained asymmetric A–B-type monomers bearing terminal Bpin (pin is pinacolato) and Br moieties were used in the subsequent Suzuki–Miyaura coupling polymerization reactions adapted from related thiophenes,[4] fluorenes,[10] or phenanthrenes.[53] The variations comprise popular Pd and phosphine precatalysts, bases, solvents, and temperature regimes. The investigated polymerization conditions are provided in Table 2 (screening) and Table 3 (functionalized catalysts) and will be discussed in more detail in the following sections.

General Scope Poly(3,6-carbazole) via Suzuki–Miyaura Coupling. We begin our screening by applying the *in situ* activation of the 3,6-dibromocarbazole (**1**) with a diboron reagent (Table 2, entry 1). The initial borylation step is performed in nonaqueous dimethylformamide (DMF) with the weak base (KOAc) for 1 h at 90 °C; the subsequent Suzuki–Miyaura polymerization is initiated by addition of water in the second stage. The catalyst system is composed of $[Pd_2(dba)_3]$ as precatalyst (0.5% per C–Br moiety), which forms the active catalyst by ligand exchange/loss with butyldiadamamtylphosphine (BuAdP) as shown in Scheme 1 (step i).[52] This special ligand was selected, as a recent study revealed the selectivity toward borylation, which is desired

DOI: 10.1021/acs.macromol.7b00144
Macromolecules 2017, 50, 1319–1330

Scheme 2. Schematic Representation of the Monomer Synthesis and Polymerization[a]

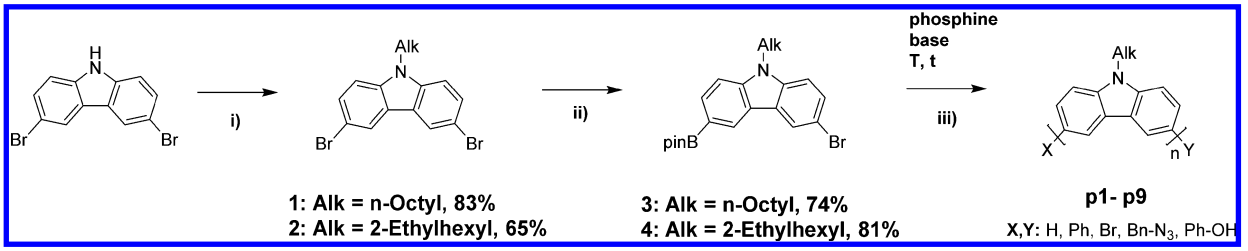

[a]Conditions: (i) alkyl bromide, DMSO, NaOH, RT, overnight; (ii) *n*-BuLi (1 equiv), 2-isopropoxy-4,4,5,5-tetramethyl-1,3,2-dioxaborolane, THF, − 78 °C, N_2, overnight. (iii) Pd^0, phosphine, base, solvent. Essential parameters are indicated above the reaction arrow (phosphine, base, temperature, time). See Experimental Section and Table 1 for details.

Table 2. Initial Polymerizations To Test the Scope of Suzuki−Miyaura Coupling

entry	polymer	monomer	base	catalyst	quencher	solvent	c_M [mM]	T [°C]	t [h]	isolated yield [%]
1	**p1**[52]	**1**	K_2CO_3	[Pd_2dba_3], BuAdP	H_2O	DMF/H_2O[b]	364	90	24	44
2	**p2**[39]	**4**	Na_2CO_3	[$Pd(PPh_3)_4$]	MeOH	PhMe/H_2O	67	85	48	52
3	**p3**	**4**	K_2CO_3	[$Pd(P^tBu_3)_2$]	MeOH	THF/H_2O	27	RT	24	70
4	**p4**	**3**	K_2CO_3	[$Pd(P^tBu_3)_2$]	tol-B(OH)$_2$	THF/H_2O	25	RT	5.4[c]	72

[a]Concentration of the monomer (in the organic phase in the case of biphasic reactions). [b]*In situ* borylation with bis(pinacolato)diboron in DMF and then addition of water to initiate polymerization. dba is dibenzylideneacetone, and BuAdP is diadamantyl-*n*-butylphoshine. [c]After 5.4 h, *p*-tolylboronic acid was added, and the reaction continued for 17.3 h.

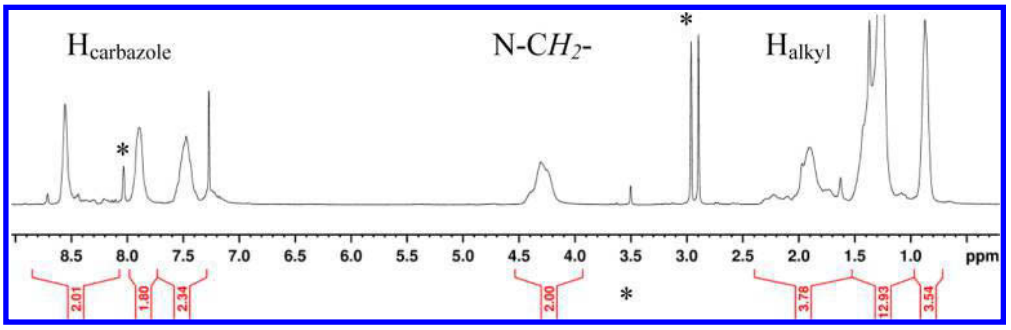

Figure 1. ^{1}H NMR spectrum (300 MHz, $CDCl_3$) of **p1** showing the typical signals of the carbazole backbone centered at 8.55, 7.90, and 7.50 ppm as well as the N−CH_2 group around 4.30 ppm and remaining alkyl proton signals below 2.3 ppm. Residual solvent signals (DMF, MeOH, $CHCl_3$) are marked by an asterisk.

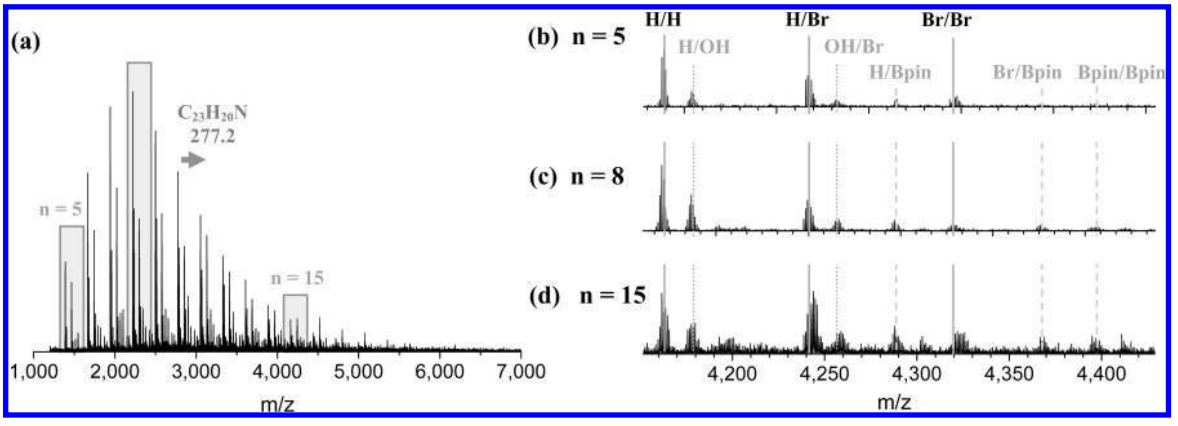

Figure 2. (a) MALDI-ToF spectrum of **p1b** (matrix: DCTB + NaCl). Arrow indicates the carbazole repeating unit and associated molar mass. Boxes indicate selected repeat units for n = 5, 8, and 15. (b−d) Expansion and assigned end groups from isotope simulation. Mass regions are aligned to indicate corresponding specimen (vertical lines): dominant series of H/H, H/Br, and Br/Br (gray solid lines), H/OH and OH/Br (gray dotted lines), and minor series of H/Bin, Br/Bin, and Bpin/Bpin (gray dashed lines). The end groups are found on the general order H > OH ≈ Br > Bpin (cf. text and Figure S29 for more details).

to achieve a high degree of monofunctionalization. The reaction was quenched with water, and the polymer **p1** was isolated in 44% yield.

The ^{1}H NMR spectrum of **p1** is shown in Figure 1, which reveals three broad signals in the aromatic region, the characteristic N−CH_2−group around 4.30 ppm, and the remaining

DOI: 10.1021/acs.macromol.7b00144
Macromolecules 2017, 50, 1319−1330

alkyl signal in the aliphatic region. The SEC data (Figure S20) indicate the polycondensation behavior, as reflected by the high dispersity values (M_n = 3900 g/mol, $Đ$ = 1.77). Hence, the polymer was purified further by fractionated precipitation.[45,54] Both obtained fractions (**p1a** and **p1b**) are characterized by lower dispersity values ($Đ \approx 1.4$) and higher molar masses ($M_n \approx 6000$ g/mol). Note that the higher molar mass fraction (**p1a**) showed a decreased tendency to redissolve, so that the subsequent analysis was performed on **p1b**, instead.

The MALDI-ToF mass spectrum of **p1b** (Figure 2) is composed of multiple series with the characteristic repeating unit of the *N*-alkylcarbazole (277.2 g/mol) of up to 20 repeating units. Note that the semiquantitative analysis of MS intensity data throughout this article is based on the assumption that specimen with the same degree of polymerization ionizes with equal probability; i.e., the desorption process is governed by the polymer and that end groups have only an inferior impact. The end groups were further analyzed by isotope simulation (Figure S29). Figure 2b shows three representative series from the low molar mass region (5-mer, panel b), the most abundant specimen (8-mer, panel c), and the high molar mass tail (15-mer, panel d). The corresponding mass regions are aligned to assist the comparison of the corresponding specimen (vertical lines). The major series belong to the H/H- and Br/H-decorated polymers as well as the corresponding H/OH- and Br/OH-terminated species. Small signals were also detected for the boronic esters, i.e., the H/Bpin, Br/Bpin and Bpin/Bpin. The relative contributions are comparable among the 5-mer, 8-mer, and 15-mer series, so that the distribution of end groups of **p1b** is best summarized by the following order: H > OH ≈ Br > Bpin. Note that also each subseries (denoted by underline) obey the same order, e.g., H/H > H/OH ≈ H/Br > H/Bpin (H-series) or H/Br > OH/Br ≈ Br/Br > Br/Bpin (Br series). The hitherto observed end-group distribution suggests substantial H and OH termination, along with the desired Br and Bpin substitution pattern. The occurrence of all combinations is tentatively assigned to the catalyst dissociation from the chain, which enables the transformation also of the distal functional groups, e.g., by deboronation and dehalogenation under the aqueous alkaline conditions.[55,56] Note that such side reactions are typically of minor importance for small organic molecules but lead in the case of polymerization to termination and thus accumulation of such specimen. More importantly, this example confirms the practical utility of diboron reagents for the convenient homopolymerization of *N*-alkyl 3,6-dibromocarbazole, which leads to molar masses comparable to those from related KCTP protocols.[17,18] It should be noted that the unknown extent of borylation can lead also to Br/Br, Br/Bpin, and Bpin/Bpin decorated building blocks, which favors a polycondensation mechanism and, thus, may explain the high dispersity of **p1**.

Hence, we focused on the asymmetric A−B-type monomers, which can be readily synthesized and isolated prior to polymerization. In fact, this possibility is a strategic advantage of boron derivatives in comparison to more sensitive Grignard reagents. Hence, we tested the reported protocol utilizing the AB-type monomer **4**.[39] The polymerization is performed at 5-fold monomer dilution in a biphasic mixture of toluene and aqueous Na_2CO_3 solution at 85 °C using $Pd(PPh_3)_4$ as precatalyst (Table 2, entry 2). The isolated polymer **p2** (52%) showed a more complex ^{1}H NMR spectrum (Figure S11), while the SEC data revealed a bimodal distribution (~90:10 peak intensity). The major series (M_n = 2300 g/mol) is in good agreement with the literature report,[39] whereas the minor distribution corresponds to an apparent molar mass of 40 000 g/mol (Figure S21). The origin of the high molar mass fraction is unclear, but chain chain couplings are unlikely to account for this unusually high (20-fold) molar mass and would not result in such distinctly separated distributions. We tentatively assign the observation to the possible formation of charged polymer, which would be repelled by the column material and, thus, interfer with the size-exclusion separation principle (see Section 3 in the Supporting Information).[57] The MALDI-ToF mass spectrum shows multiple series and revealed the formation of macrocycles with $n \geq 4$ on the basis of isotope simulations (Figures S30 and S31). This assignment is corroborated by the results from related Yamamoto coupling reactions, which reports the formation and identification of the macrocyclic oligomers.[45,58] The macrocyclization will be analyzed in more detail for monomer **3** and by means of a functionalized initiator (*vide infra*). The analysis of the remaining signals at higher molar masses revealed also H/H-, H/Ph-, and Br/Ph-terminated specimen. Whereas the H/H-terminated series can be explained by dehalogenation and/or deboronation, the occurrence of Ph-terminated series requires the participation of the PPh_3 ligand of the catalyst, which is somewhat surprising but a known side reaction under harsh conditions.[59−61]

Hence, we further tested $[Pd(P^tBu_3)_2]$, K_2CO_3 as base, and a THF/water mixture but applied lower reaction temperature (23 °C) to retard undesired thermal catalyst dissociation. The monomer concentration was kept low (25 mM) in order to screen the inherent limitation by macrocycle formation, which is enhanced at high dilution conditions.[45] Polymer **p3** was isolated in good yield (70%), and the SEC analysis (Figure S22) gave typical molar masses (M_n = 4000 g/mol) and dispersity values ($Đ$ = 1.53). This result is remarkable in view of the previous runs because the 13-fold dilution (vs **p1**) did not lead to dominant macrocycle formation, as would be anticipated.[45,58] Instead, a higher yield of isolated polymer was obtained, which featured comparable molar masses but lower dispersity. In comparison to **p2**, the polymer **p3** was isolated in higher chemical yield, increased molar mass but not a lower dispersity. The latter would be expected if macrocycles form to the same extent because their accumulation in combination with the growing linear chains would result in a severely broadened distribution (higher dispersity). The MALDI-ToF analysis of **p3** revealed the presence of macrocycles in the low molar mass region (around 2000 g/mol), while the higher molar mass region (>4000 g/mol) showed additionally the H/H-, H/Br-, and Br/Br-terminated polymers (Figures S32 and S33). We tentatively assign this improvement of the polymerization characteristics to the lower reaction temperature and decided to investigate the polymerization progress in more detail for monomer **3** by SEC and MS analysis, i.e., taking samples at selected times and quench the polymerization by addition of equimolar amounts of a monofunctional end-capper.

The SEC elugrams are shown in Figure 3a. The unreacted monomer elutes at 11.6 mL (t = 0 min), whereas after 15 min a band at 10.2 mL elution volume was detected. Notably, the maximum shifted back during the course of polymerization to higher elution volume (10.4 mL), whereas the shoulder at shorter elution volumes evolved. This behavior is well explained by the formation and accumulation of macrocycles in combination with growing linear polymer chains. After 160 min,

DOI: 10.1021/acs.macromol.7b00144
Macromolecules 2017, 50, 1319−1330

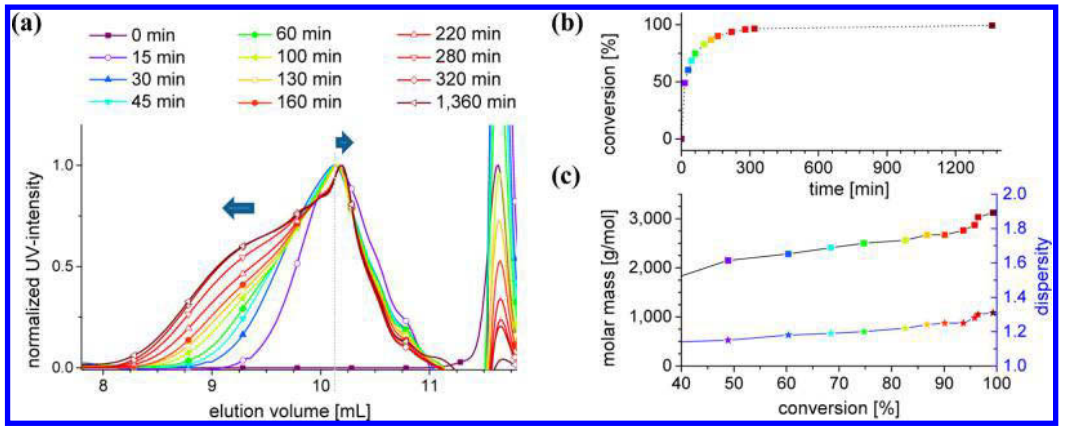

Figure 3. (a) Normalized SEC traces of **p4** sampled at selected times, illustrating the formation of linear polymer and macrocycles (eluent: chloroform/isopropanol/triethylamine [94:2:4]). Arrows indicate evolution of peak maximum from 10.2 to 10.4 mL and concomitant growth of high molar mass shoulder. Monomer elutes at 11.6 mL. (b, c) Kinetic analysis: (b) conversion vs time and (c) molar mass (squares, left axis) and dispersity (stars, right axis) vs conversion. See (a) for color code of data points.

the rise of the macrocycles stops as judged from the virtually superimposing traces, while the linear polymer bands continue to evolve. The plot of conversion vs reaction time (Figure 3b) reveals a fast polymerization, i.e., the monomer conversion of 50% within 15 min, 90% after 160 min, and 97% after 320 min. At that time, the end-capping reagent tolylboronic acid was added and allowed to react overnight to reach full conversion. The evolution of molar mass and dispersity is shown in Figure 3c. Within the first 15 min, molar masses of 2200 g/mol were reached with low dispersity ($Đ$ = 1.15). Note that the measured unusual high dispersity of the (monodisperse) monomer ($Đ$ = 1.10) suggests secondary interactions during SEC analysis, so that all given dispersity values of the polymers reflect an upper bound and the real distributions should be in fact much narrower. More importantly, the increase of molar masses and dispersities is steady up to 90%, whereafter an enhanced increase is observed. This observation is well explained by the step growth mechanism, which features high molar masses only at high conversion and suggests further that the desired end groups (Br and Bpin) are present to promote the coupling of the oligomer building blocks. In line, the addition of the end-capping reagent terminates further chain couplings, as expressed by the comparable final molar masses (M_n = 3100 g/mol) and dispersity ($Đ$ = 1.31). The polymerization progress was also monitored by MALDI-ToF MS (Figure S34). The data confirm the formation and growth of the polymer and/or the macrocycles. However, a discrimination of high molar mass species was observed, based on the comparison with the SEC data (showing the evolution of polymers >160 min, *vide supra*) and the very similar corresponding MALDI-ToF profiles. Hence, we limit our interpretation to the low molar mass region (<2500 g/mol) and the identity of the detected specimen at higher molar masses (>4000 g/mol). The temporal evolution of the 8-mer series (Figure S35) revealed the dominating 8-mer macrocycle and various linear oligomeric species assigned to Br/H-, Bpin/H-, Bpin/Br-decorated polymers. As expected, the contribution of the macrocycle vs linear chains increases at later times due to their accumulation and the growth of the linear chains. The latter is confirmed upon inspection of the high molar mass region as exemplified for the 16-mer series (Figure S36), which revealed the preferential formation of the Br-decorated series. This result is in perfect agreement with the final MS analysis of **p1b** (*vide supra*). Notably the relative distribution of the various oligomeric macrocycles stays comparable, which is reasonable in view of the entropic factors that disfavor large macrocycles. After end-capping with 4-tolylboronic acid (tol-B(OH)$_2$), the MALDI-ToF spectrum (Figure S37) confirmed the formation of the H/tol-decorated polymer, but also the residual signal of Br/H-decorated polymer, which indicates incomplete functionalization at the given conditions (*vide infra*). The successful but partial functionalization is further corroborated by the ^{1}H NMR data of purified **p4** (Figure S13), which revealed the typical proton signal of the benzyl group at 2.4 ppm.

In summary of the benchmarking study, end-functionalized poly(3,6-carbazole) and/or the corresponding macrocycles can be prepared in high yields via *in situ* generation of the monomer (**p1**) or employing the Br/Bpin-functionalized monomers (**p2**–**p4**). The analysis confirms[45] that high dilution conditions favor the formation of macrocycles (e.g., **p1** vs **p4**), which accumulate during the course of the polymerization and, thus, dominate in the final product. The kinetic analysis of **p4** revealed fast kinetics already at room temperature, and the MS analysis confirmed the possibility to terminate the polymerization by an end-capping reagent. The large discrepancy in the molar mass between **p3** and **p4**, which were prepared under comparable reaction conditions, is tentatively assigned to the sampling during the kinetic analysis, which may trigger detrimental termination reactions by e.g. introduced O_2.

Initiation by Functionalized Pd Catalyst. The previous results and the published data indicate that macrocycle formation is an inherent side reaction, particularly at low concentrations. Hence, we decided to prepare a functionalized Pd catalyst prior to polymerization[10] in order to prevent macrocycle formation. In this regard, the presence of the modified initiator also becomes a valuable diagnostic tool for end-group analysis. In addition, we anticipated that lower reaction temperatures may help to diminish thermal dissociation of the active catalyst during polymerization and, thus, may sustain the ring-walking necessary for the chain growth mechanism. Finally, we selected low concentrations of the monomers due to the following arguments: If the active catalyst is released, it will initiate new chains with complementary Br/Bpin functionality. In this case, the high dilution conditions will trap such oligomeric side products by their favored macrocyclization, which can be readily removed by precipitation,

DOI: 10.1021/acs.macromol.7b00144
Macromolecules 2017, 50, 1319–1330

Scheme 3. Preparation of Ph-Functionalized Pd(II) Initiator for Subsequent Polymerization[a]

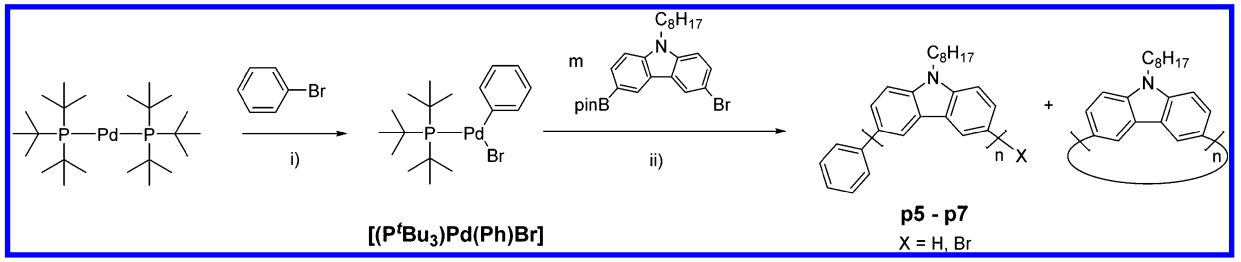

[a]Conditions: (i) neat, 70 °C, 2.5 h;[10] (ii) base, solvent. See Experimental Section and Table 3 for details.

Table 3. Polymers Prepared from Phenyl-Functionalized Initiators

entry	polymer	monomer	base	catalyst	quencher	solvent	c_M [mM]	T [°C]	t [h]	isolated yield [%]
1	**p5**[4]	**3**	CsF/18-crown-6	[(P^{t}Bu$_3$)Pd(Ph)Br]	HCl	THF/H$_2$O	14	0	24	77
2	**p6**[10]	**3**	Na_2CO_3	[(P^{t}Bu$_3$)Pd(Ph)Br]	HCl	THF/H$_2$O	23	RT	0.5	32
3	**p7**[53]	**3**	K_2CO_3	[(P^{t}Bu$_3$)Pd(Ph)Br]	HCl	THF/H$_2$O	20	RT	24	66

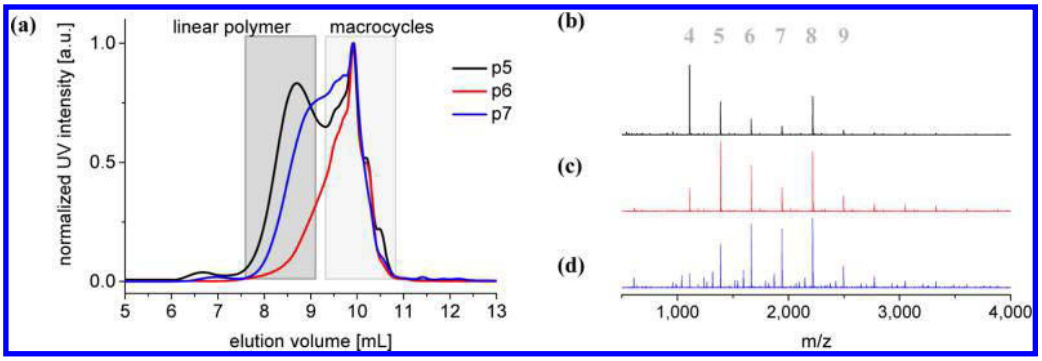

Figure 4. (a) Normalized SEC traces (eluent: chloroform/isopropanol/triethylamine [94:2:4]) of **p5**, **p6**, and **p7** showing the formation of macrocycles (9.3–10.7 mL, light gray box) and varying amounts of linear polymer (7.5–9.2 mL). Signals <7.5 mL are attributed to artifacts arising from charged polymers. (b–d) MALDI-ToF spectra of **p5** (b), **p6** (c), and **p7** (d) illustrating macrocycle formation ($n \geq 4$) in the low molar mass region. Note the potential suppression of higher molar mass specimen, which are present according to the corresponding SEC data (a).

preparative size exclusion chromatography or Soxhlet extraction.[45,58]

The active Ph-decorated Pd(II) catalyst was prepared and purified prior to the polymerization of monomer **3** (Scheme 3), which is performed under milder reaction conditions than before (*vide supra*). In particular, lower temperatures (0 °C or rt) and high dilution of the monomer (14–23 mM) were applied in order to diminish catalyst dissociation and to trap any undesired initiated chains as their macrocycles (*vide supra*). The exact experimental conditions were adapted from related conjugated polymers[4,10,53] and are compiled in Table 3. The first run utilizes the base CsF in a THF/water mixture at 0 °C, including the masking of the cation by 18-crown-6 to enhance the Lewis basicity of the fluoride, which is required to achieve Suzuki–Miyaura cross-coupling (**p5**, entry 1).[4] The second and third runs apply Na_2CO_3 (**p6**) or K_2CO_3 (**p7**) as bases in a mixture of THF and water at room temperature.[10,53] The main difference is tentatively ascribed to the solubility of the base in THF and the significantly shorter reaction time for **p6** (entry 2) vs **p7** (entry 3). The three polymerization reactions were quenched by HCl and the crude polymers were isolated by precipitation in MeOH.

The ^{1}H NMR spectra of the **p5**–**p7** (Figures S14–S16) show the presence of the typical polymer-related signals as well as additional sharp signals sets in the aromatic region. The comparison of the SEC data is shown in Figure 4a and revealed a bimodal distribution, which belong to low molar mass oligomers (around 10 mL) and a varying amount of a high molar mass fraction (<9 mL). The MALDI-ToF spectra of all three polymers (Figure 4b) revealed the same dominant series with molar masses up to 2500 g/mol, whereby the spectrum of **p7** shows additional series. For all polymers, the major series was identified by isotope simulation as macrocycles (Figures S38–S42). The large discrepancy between SEC data (substantial formation of polymers) and the MALDI-ToF data (dominantly oligomeric macrocycles) prompted us to reinspect the MS data in more detail. The analysis of the 8-mer and 16-mer series of **p5**–**p7** is provided in Figure S43 and revealed the formation of the Ph/H- and Ph/Br-decorated species, which form via protolysis during work-up and/or catalyst dissociation during polymerization, respectively. The latter process releases active Pd(0) catalysts, which are capable to initiate new chains, and thus explains the occurrence of the related Bpin-containing specimen (Bpin/Br and Bpin/H) as well as the macrocycles via intramolecular termination under the applied high dilution conditions (*vide supra*).[45] Furthermore, the comparison of the MALDI-ToF data and isolated yields for **p6** vs **p7** suggests that macrocycle formation already occurs in the early stage of the polymerization (0.5 h vs 24 h) or low conversion (32% vs 66% yield)—in agreement with the kinetic study. More importantly, the apparent mass discrimination led us to purify polymer **p5** by preparative size exclusion chromatography because it showed the highest content of linear polymers vs macrocycles according to SEC. Several fractions

DOI: 10.1021/acs.macromol.7b00144
Macromolecules 2017, 50, 1319–1330

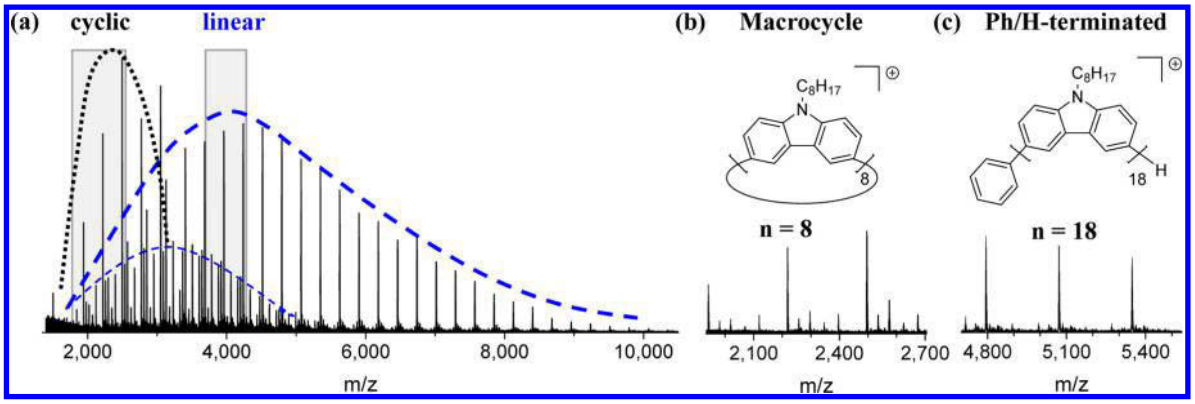

Figure 5. (a) MALDI-ToF mass spectrum of **p5a** (matrix: DCTB) showing the macrocycles (black dotted line) and linear domain (blue dashed line, singly and doubly charged). (b, c) Expansions of low molar mass region (b) and high molar mass region (c) with assignment of dominating species, i.e., cyclic octamer (b) and Ph/H-decorated linear monomer.

were collected and analyzed by MALDI-ToF (Figure S44). The high molar mass fraction contained only small residual amounts of macrocycles/oligomers, as exemplified for **p5a** by to SEC analysis (Figure S24) and MALDI-ToF data (Figure 5). The low molar mass region of **p5a** reveals residual macrocycles, while the high molar mass region is dominated by the Ph/H-decorated polymers up to 10 000 g/mol. According to the peak areas of the SEC traces of crude **p5** (Figure S24), the ratio of linear polymers to macrocycles corresponds to approximately 60:40.

In conclusion, the investigated methodology to apply a functionalized initiator at reduced reaction temperatures and monomer concentration afforded for the first time telechelic poly(3,6-carabzole) with high end-group fidelity but required removal of the inherently formed macrocyclic side products. The occurrence of the latter confirms catalyst dissociation and reinitiation of new chains (*vide supra*, Scheme 1) but also the efficient macrocyclization at high dilution. On the basis of the UV-SEC trace, approximately 60% of the polymer accounts for the telechelic homopolymers (Figure S24). Notably, the removal of undesired macrocycles can be conveniently achieved, as demonstrated by size exclusion chromatography or by reported extraction methods.[39,45] The isolated telechelic polymer (**p5a**) displays a fairly narrow distribution ($Đ \approx 1.25$) by SEC analysis and a molar mass reaching up to 10 000 g/mol including high end-group fidelity according to MALDI-ToF analysis. Note that the true molar masses may be even higher considering the observed mass discrimination effect, while the values from SEC data applying PS calibration are likely overestimated in case of stiffened polymer backbones (see Sections 3 and 4 in the Supporting Information). At this stage, the precise role of the base, the monomer concentration, the reaction temperature, and particularly the catalyst system remains to be elucidated, and the reaction conditions may be further optimized, which is beyond the scope of this study.

Termination by Functionalized Reagents. As a consequence of the inevitable catalyst dissociation, the scope of termination using functionalized end-capping agents was revisited (Scheme 4), as our initial test (**p4**) already indicated this possibility. Hence, the general experimental conditions were adapted from **p4** to explore the functionalization of both terminal moieties, i.e., modifying the Bpin-group using tetrahydropyranyl(THP)-protected *p*-bromophenol (**p8**) as well as the Br-substituent using the pinacol ester of *p*-azidobenzylboronic acid (**p9**). In the former case, the capping of the Bpin

Scheme 4. Preparation of End-Capped Poly(3,6-carbazole)s[a]

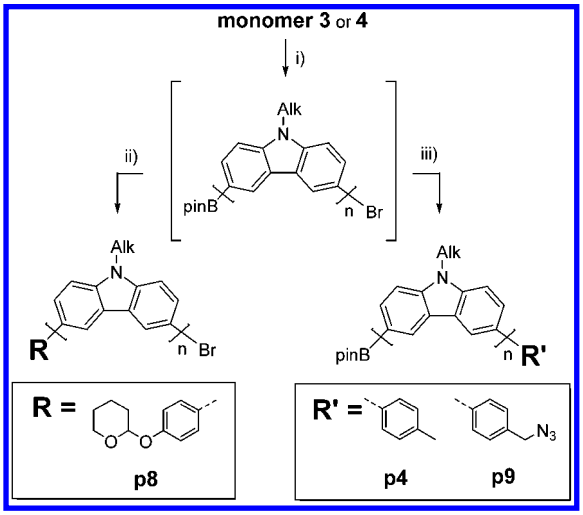

[a]Conditions: (i) $[Pd(P^tBu_3)_2]$, K_2CO_3, THF/H_2O, rt, 6 h (except **p4**: 24 h); (ii) *p*-tolylboronic acid or **5**, 18 h, rt; (iii) **6**, 18 h, rt. See Experimental Section for details.

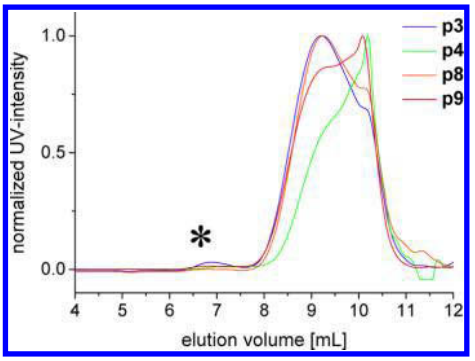

Figure 6. Normalized SEC trace of **p3**, **p4**, **p8**, and **p9** (eluent: chloroform/isopropanol/triethylamine [94:2:4]). Artifact marked by an asterisk (see Results and Discussion for explanation).

terminus requires free Pd(0) catalyst in the reaction mixture, which would be capable of oxidative addition into the aryl–halogen bond of the end-capping agent and, subsequently, of Suzuki–Miyaura coupling with Bpin-decorated polymer chains. Hence, this methodology would sustain the chain growth mechanism as long as the catalyst stays associated with

DOI: 10.1021/acs.macromol.7b00144
Macromolecules 2017, 50, 1319–1330

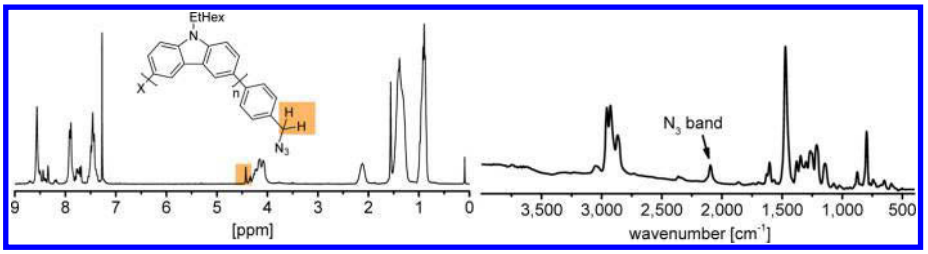

Figure 7. Left: NMR spectrum (300 MHz, $CDCl_3$) of **p9** with resonance assigned to methylene protons next to the azide. Right: IR spectrum (KBr pellet) with characteristic N_3 band at approximately 2100 cm^{-1}.

the growing chain. In contrast, the reverse strategy to use an end-capper bearing a boronic ester would terminate effectively the growing chains, which precludes the coupling of chains to reach high molar masses at high conversions (*vide supra*). These features can explain the observed systematic differences in the SEC data of **p3** or **p8** vs **p4** or **p9** (Figure 6), respectively.

The partial end decoration of **p8** is indicated by ^{1}H NMR analysis (Figure S18) by the weak signal at 6.85 ppm, which is characteristic for a phenolic unit that forms via deprotection of the THP group under the acidic conditions. The MALDI-ToF mass spectrum (Figure S46) is dominated by macrocycles, but it also revealed PhOH-decorated chains (Figure S47): At low molar masses (4-mer series), the occurrence of PhOH-decorated chains can be reasoned by the initiation of the added reagent and subsequent oligomerization of residual monomer. In the intermediate mass region, the spectrum is dominated by the accumulated macrocycles, as discussed before. More interestingly, the presence of PhOH-decorated chains at high molar masses indirectly confirms the presence of Bpin-decorated polymer chains. However, these specimen are only detected in trace amounts, which parallels the results from the ^{1}H NMR analysis and previous MS results; i.e., the functionalization is far from quantitative due to substantial deboronation leading to the H/Br series. Hence, the complementary strategy for end-functionalization was investigated, i.e., employing azidomethylphenylboronic pinacol ester for derivatization of the bromine terminus (**p9**). Indeed, the ^{1}H NMR spectrum displays a broad singlet at approximately 4.4 ppm, which is characteristic for methylene protons next to the azide functionality (Figure 7). Additionally, the IR spectrum indicates the successful functionalization due to the appearance of a diagnostic signal for azide (around 2100 cm^{-1}). Unfortunately, the end functionalization could not be further verified by MALDI- or ESI-ToF MS analysis under various conditions, which is tentatively attributed to the known instability of the azide group during ionization.[62,63] Hence, only macrocycles or undefined fragments were detected. Nevertheless, the ^{1}H NMR and IR data—in conjunction with the disappearance of typical MS peaks—suggest the successful preparation of telechelic poly(3,6-carbazole).

CONCLUSION

The polymerization of bifunctional 3,6-carbazole was systematically investigated (Table 1) and analyzed in detail by ^{1}H NMR spectroscopy, SEC, and mass spectrometry, which are compiled in the Supporting Information. The latter technique enabled the detailed analysis of end groups and supported the identification of limiting processes, which are discussed in terms of the mechanism of the catalytic cycle. It was found that no strict end-group control is observed during the regular Suzuki–Miyaura coupling polymerization, despite the facile preparation of the polymers in good isolated yields. In addition, macrocyclization of the oligomers was identified as an accompanying process, particularly at low monomer concentrations. Although undesired, this side reaction can be utilized to prepare telechelic poly(3,6-carbazoles) using prefunctionalized initiators: The regularly initiated chains grow and cannot undergo macrocyclization, while the portion of dissociated catalyst can reinitiate new chains. Importantly, the complementary functionality (Bpin/Br) and the high dilution conditions ensure the trapping as oligomeric macrocycles. Accordingly, the linear polymers are obtained as the major product and can be separated from the macrocycles by preparative size exclusion chromatography or extraction methods. Alternatively, the decoration with terminating agents is possibly, in particular by the application of functionalized boronic esters. The further optimization of reaction conditions and utilization of the telechelic poly(carbazoles) is beyond this initial study and will be reported in due course. In summary, the Pd-catalyzed Suzuki–Miyaura coupling polymerization represents a versatile alternative to Ni-based couplings, e.g., the KCTP or Yamamoto coupling. If the end groups are not of importance, a simple diboron reagent can be utilized for homocoupling (**p1**), while the macrocycles can be selectively obtained using the bifunctional A–B type monomer working under high dilution conditions. More importantly, the utilization of functional Pd(II) initiators or monofunctional boronic esters as end-capping reagents are a potent approach to yield telechelic poly(*N*-alkyl-3,6-carbazoles).

ASSOCIATED CONTENT

Supporting Information

The Supporting Information is available free of charge on the ACS Publications website at DOI: 10.1021/acs.macromol.7b00144.

Additional instrumental details and analytical data (NMR, MS, and SEC) (PDF)

AUTHOR INFORMATION

Corresponding Authors

*E-mail ulrich.schubert@uni-jena.de (U.S.S.).
*E-mail michael.jager.iomc@uni-jena.de (M.J.).

ORCID

Ulrich S. Schubert: 0000-0003-4978-4670
Michael Jäger: 0000-0003-0400-1812

Funding

M.J. for financial support by the Carl-Zeiss-Foundation and the Friedrich Schiller University Jena ("Nachwuchsförderung").

Notes

The authors declare no competing financial interest.

DOI: 10.1021/acs.macromol.7b00144
Macromolecules 2017, 50, 1319–1330

■ ACKNOWLEDGMENTS

We thank Annett Urbanek for MALDI-ToF measurements, Tina Schlotthauer for ESI-ToF measurements, and Dr. Peter Bellstedt and the NMR platform IAAC/IOMC for help with the NMR measurements.

■ REFERENCES

(1) Shirakawa, H.; Louis, E. J.; MacDiarmid, A. G.; Chiang, C. K.; Heeger, A. J. Synthesis of electrically conducting organic polymers: halogen derivatives of polyacetylene, $(CH)_x$. *J. Chem. Soc., Chem. Commun.* **1977**, No. 16, 578−580.
(2) Morin, J.-F.; Leclerc, M.; Adès, D.; Siove, A. Polycarbazoles: 25 Years of Progress. *Macromol. Rapid Commun.* **2005**, *26* (10), 761−778.
(3) Boudreault, P.-L. T.; Beaupre, S.; Leclerc, M. Polycarbazoles for plastic electronics. *Polym. Chem.* **2010**, *1* (2), 127−136.
(4) Yokozawa, T.; Suzuki, R.; Nojima, M.; Ohta, Y.; Yokoyama, A. Precision Synthesis of Poly(3-hexylthiophene) from Catalyst-Transfer Suzuki-Miyaura Coupling Polymerization. *Macromol. Rapid Commun.* **2011**, *32* (11), 801−806.
(5) Lee, J. K.; Ko, S.; Bao, Z. In Situ Hetero End-Functionalized Polythiophene and Subsequent "Click" Chemistry With DNA. *Macromol. Rapid Commun.* **2012**, *33* (10), 938−942.
(6) Lohwasser, R. H.; Thelakkat, M. Toward Perfect Control of End Groups and Polydispersity in Poly(3-hexylthiophene) via Catalyst Transfer Polymerization. *Macromolecules* **2011**, *44* (9), 3388−3397.
(7) Kosaka, K.; Ohta, Y.; Yokozawa, T. Influence of the Boron Moiety and Water on Suzuki−Miyaura Catalyst-Transfer Condensation Polymerization. *Macromol. Rapid Commun.* **2015**, *36* (4), 373−377.
(8) Zeigler, D. F.; Mazzio, K. A.; Luscombe, C. K. Fully Conjugated Graft Copolymers Comprising a P-Type Donor-Acceptor Backbone and Poly(3-hexylthiophene) Side Chains Synthesized Via a "Graft Through" Approach. *Macromolecules* **2014**, *47* (15), 5019−5028.
(9) Miyakoshi, R.; Shimono, K.; Yokoyama, A.; Yokozawa, T. Catalyst-transfer polycondensation for the synthesis of poly(p-phenylene) with controlled molecular weight and low polydispersity. *J. Am. Chem. Soc.* **2006**, *128* (50), 16012−16013.
(10) Yokoyama, A.; Suzuki, H.; Kubota, Y.; Ohuchi, K.; Higashimura, H.; Yokozawa, T. Chain-growth polymerization for the synthesis of polyfluorene via Suzuki-Miyaura coupling reaction from an externally added initiator unit. *J. Am. Chem. Soc.* **2007**, *129* (23), 7236−7237.
(11) Elmalem, E.; Kiriy, A.; Huck, W. T. S. Chain-Growth Suzuki Polymerization of n-Type Fluorene Copolymers. *Macromolecules* **2011**, *44* (22), 9057−9061.
(12) Elmalem, E.; Biedermann, F.; Johnson, K.; Friend, R. H.; Huck, W. T. S. Synthesis and Photophysics of Fully pi-Conjugated Heterobis-Functionalized Polymeric Molecular Wires via Suzuki Chain-Growth Polymerization. *J. Am. Chem. Soc.* **2012**, *134* (42), 17769−17777.
(13) Tkachov, R.; Senkovskyy, V.; Beryozkina, T.; Boyko, K.; Bakulev, V.; Lederer, A.; Sahre, K.; Voit, B.; Kiriy, A. Palladium-Catalyzed Chain-Growth Polycondensation of AB-type Monomers: High Catalyst Turnover and Polymerization Rates. *Angew. Chem., Int. Ed.* **2014**, *53* (9), 2402−2407.
(14) Javier, A. E.; Varshney, S. R.; McCullough, R. D. Chain-Growth Synthesis of Polyfluorenes with Low Polydispersities, Block Copolymers of Fluorene, and End-Capped Polyfluorenes: Toward New Optoelectronic Materials. *Macromolecules* **2010**, *43* (7), 3233−3237.
(15) Fischer, C. S.; Baier, M. C.; Mecking, S. Enhanced Brightness Emission-Tuned Nanoparticles from Heterodifunctional Polyfluorene Building Blocks. *J. Am. Chem. Soc.* **2012**, *135* (3), 1148−1154.
(16) Fischer, C. S.; Jenewein, C.; Mecking, S. Conjugated Star Polymers from Multidirectional Suzuki−Miyaura Polymerization for Live Cell Imaging. *Macromolecules* **2015**, *48* (3), 483−491.
(17) Wen, H.; Ge, Z.; Liu, Y.; Yokozawa, T.; Lu, L.; Ouyang, X.; Tan, Z. Efficient synthesis of well-defined polycarbazoles via catalyst-transfer Kumada coupling polymerization. *Eur. Polym. J.* **2013**, *49* (11), 3740−3743.
(18) Stefan, M. C.; Javier, A. E.; Osaka, I.; McCullough, R. D. Grignard Metathesis Method (GRIM): Toward a Universal Method for the Synthesis of Conjugated Polymers. *Macromolecules* **2009**, *42* (1), 30−32.
(19) Heeger, A. J. Semiconducting polymers: the Third Generation. *Chem. Soc. Rev.* **2010**, *39* (7), 2354−2371.
(20) Kiriy, A.; Senkovskyy, V.; Sommer, M. Kumada Catalyst-Transfer Polycondensation: Mechanism, Opportunities, and Challenges. *Macromol. Rapid Commun.* **2011**, *32* (19), 1503−1517.
(21) Doubina, N.; Paniagua, S. A.; Soldatova, A. V.; Jen, A. K. Y.; Marder, S. R.; Luscombe, C. K. Steric Effects of the Initiator Substituent Position on the Externally Initiated Polymerization of 2-Bromo-5-iodo-3-hexylthiophene. *Macromolecules* **2011**, *44* (3), 512−520.
(22) Grisorio, R.; Suranna, G. P. Intramolecular catalyst transfer polymerisation of conjugated monomers: from lessons learned to future challenges. *Polym. Chem.* **2015**, *6* (45), 7781−7795.
(23) Yokozawa, T.; Ohta, Y. Transformation of Step-Growth Polymerization into Living Chain-Growth Polymerization. *Chem. Rev.* **2015**, *116* (4), 1950−1968.
(24) Koldemir, U.; Puniredd, S. R.; Wagner, M.; Tongay, S.; McCarley, T. D.; Kamenov, G. D.; Müllen, K.; Pisula, W.; Reynolds, J. R. End Capping Does Matter: Enhanced Order and Charge Transport in Conjugated Donor−Acceptor Polymers. *Macromolecules* **2015**, *48* (18), 6369−6377.
(25) He, M.; Qiu, F.; Lin, Z. Conjugated rod-coil and rod-rod block copolymers for photovoltaic applications. *J. Mater. Chem.* **2011**, *21* (43), 17039−17048.
(26) Yameen, B.; Zydziak, N.; Weidner, S. M.; Bruns, M.; Barner-Kowollik, C. Conducting Polymer/SWCNTs Modular Hybrid Materials via Diels-Alder Ligation. *Macromolecules* **2013**, *46* (7), 2606−2615.
(27) Bui, T.-T.; Goubard, F. Recent advances in small molecular, non-polymeric organic hole transporting materials for solid-state DSSC. *EPJ Photovoltaics* **2013**, *4*, 40402.
(28) Pron, A.; Gawrys, P.; Zagorska, M.; Djurado, D.; Demadrille, R. Electroactive materials for organic electronics: preparation strategies, structural aspects and characterization techniques. *Chem. Soc. Rev.* **2010**, *39* (7), 2577−2632.
(29) Moad, G.; Chen, M.; Haussler, M.; Postma, A.; Rizzardo, E.; Thang, S. H. Functional polymers for optoelectronic applications by RAFT polymerization. *Polym. Chem.* **2011**, *2* (3), 492−519.
(30) Li, J.; Grimsdale, A. C. Carbazole-based polymers for organic photovoltaic devices. *Chem. Soc. Rev.* **2010**, *39* (7), 2399−2410.
(31) Lellouche, J.-P.; Koner, R. R.; Ghosh, S. N-Substituted carbazole heterocycles and derivatives as multipurpose chemical species: at the interface of chemical engineering, polymer and materials science. *Rev. Chem. Eng.* **2013**, *29* (6), 413−437.
(32) Geissler, U.; Hallensleben, M. L.; Rienecker, A.; Rohde, N. Polyarylenes on the basis of alkylpyrrole and alkylcarbazole derivatives and their oligomeric model systems. *Polym. Adv. Technol.* **1997**, *8* (2), 87−92.
(33) Xu, F.; Kim, J.-H.; Kim, H. U.; Jang, J.-H.; Yook, K. S.; Lee, J. Y.; Hwang, D.-H. Synthesis of High-Triplet-Energy Host Polymer for Blue and White Electrophosphorescent Light-Emitting Diodes. *Macromolecules* **2014**, *47* (21), 7397−7406.
(34) Huang, J.; Niu, Y. H.; Yang, W.; Mo, Y. Q.; Yuan, M.; Cao, Y. Novel electroluminescent polymers derived from carbazole and benzothiadiazole. *Macromolecules* **2002**, *35* (16), 6080−6082.
(35) Li, Z. A.; Liu, Y.; Yu, G.; Wen, Y.; Guo, Y.; Ji, L.; Qin, J.; Li, Z. A New Carbazole-Constructed Hyperbranched Polymer: Convenient One-Pot Synthesis, Hole-Transporting Ability, and Field-Effect Transistor Properties. *Adv. Funct. Mater.* **2009**, *19* (16), 2677−2683.
(36) Liu, S.-J.; Lin, W.-P.; Yi, M.-D.; Xu, W.-J.; Tang, C.; Zhao, Q.; Ye, S.-H.; Liu, X.-M.; Huang, W. Conjugated polymers with cationic iridium(III) complexes in the side-chain for flash memory devices utilizing switchable through-space charge transfer. *J. Mater. Chem.* **2012**, *22* (43), 22964−22970.

DOI: 10.1021/acs.macromol.7b00144
Macromolecules 2017, 50, 1319−1330

(37) Luo, J.; Xie, G.; Gong, S.; Chen, T.; Yang, C. Creating a thermally activated delayed fluorescence channel in a single polymer system to enhance exciton utilization efficiency for bluish-green electroluminescence. *Chem. Commun.* **2016**, *52* (11), 2292−2295.
(38) Beouch, L.; Tran Van, F.; Stephan, O.; Vial, J. C.; Chevrot, C. Optical and electrochemical properties of soluble N-hexylcarbazole-co-3,4-ethylenedioxythiophene copolymers. *Synth. Met.* **2001**, *122* (2), 351−358.
(39) Lemasson, F.; Berton, N.; Tittmann, J.; Hennrich, F.; Kappes, M. M.; Mayor, M. Polymer Library Comprising Fluorene and Carbazole Homo- and Copolymers for Selective Single-Walled Carbon Nanotubes Extraction. *Macromolecules* **2012**, *45* (2), 713−722.
(40) Iraqi, A.; Wataru, I. 3,6-linked 9-alkyl-9H-carbazole main-chain polymers: Preparation and properties. *J. Polym. Sci., Part A: Polym. Chem.* **2004**, *42* (23), 6041−6051.
(41) Lee, R.-H.; Liu, J.-K.; Ho, J.-H.; Chang, J.-W.; Liu, B.-T.; Wang, H.-J.; Jeng, R.-J. Synthesis of quaternized ammonium iodide-containing conjugated polymer electrolytes and their application in dye-sensitized solar cells. *Polym. Int.* **2011**, *60* (3), 483−492.
(42) Vedarajan, R.; Hosono, Y.; Matsumi, N. π-Conjugated polycarbazole-boron complex as a colorimetric fluoride ion sensor. *Solid State Ionics* **2014**, *262*, 795−800.
(43) Zhang, Z.-B.; Motonaga, M.; Fujiki, M.; McKenna, C. E. The First Optically Active Polycarbazoles. *Macromolecules* **2003**, *36* (19), 6956−6958.
(44) Zhang, Z.-B.; Fujiki, M.; Tang, H.-Z.; Motonaga, M.; Torimitsu, K. The First High Molecular Weight Poly(N-alkyl-3,6-carbazole)s. *Macromolecules* **2002**, *35* (6), 1988−1990.
(45) Ostrauskaite, J.; Strohriegl, P. Formation of macrocycles in the synthesis of poly(N-(2-ethylhexyl)carbazol-3,6-diyl. *Macromol. Chem. Phys.* **2003**, *204* (14), 1713−1718.
(46) Xiao, X.; Fu, Y. Q.; Sun, M. H.; Li, L.; Bo, Z. S. Synthesis and characterization of conjugated triblock copolymers. *J. Polym. Sci., Part A: Polym. Chem.* **2007**, *45* (12), 2410−2424.
(47) Zhang, K.; Tao, Y.; Yang, C.; You, H.; Zou, Y.; Qin, J.; Ma, D. Synthesis and Properties of Carbazole Main Chain Copolymers with Oxadiazole Pendant toward Bipolar Polymer Host: Tuning the HOMO/LUMO Level and Triplet Energy. *Chem. Mater.* **2008**, *20* (23), 7324−7331.
(48) Schroot, R.; Schubert, U. S.; Jäger, M. Poly(N-alkyl-3,6-carbazole)s via Kumada catalyst transfer polymerization: Impact of Metal-Halogen exchange. *Macromolecules* **2016**, *49* (23), 8801−8811.
(49) Kun, H.; Yi, H.; Johnson, R. G.; Iraqi, A. Fluoro-protected carbazole main-chain polymers as a new class of stable blue emitting polymers. *Polym. Adv. Technol.* **2008**, *19* (4), 299−307.
(50) Smith, K.; James, D. M.; Mistry, A. G.; Bye, M. R.; Faulkner, D. J. A new method for bromination of carbazoles, β-carbolines and iminodibenzyls by use of N-bromosuccinimide and silica gel. *Tetrahedron* **1992**, *48* (36), 7479−7488.
(51) Li, Y.; Ding, J.; Day, M.; Tao, Y.; Lu, J.; D'Iorio, M. Synthesis and Properties of Random and Alternating Fluorene/Carbazole Copolymers for Use in Blue Light-Emitting Devices. *Chem. Mater.* **2004**, *16* (11), 2165−2173.
(52) Zhang, Y.; Gao, J.; Li, W.; Lee, H.; Lu, B. Z.; Senanayake, C. H. Synthesis of 8-Arylquinolines via One-Pot Pd-Catalyzed Borylation of Quinoline-8-yl Halides and Subsequent Suzuki−Miyaura Coupling. *J. Org. Chem.* **2011**, *76* (15), 6394−6400.
(53) Verswyvel, M.; Hoebers, C.; De Winter, J.; Gerbaux, P.; Koeckelberghs, G. Study of the Controlled Chain-Growth Polymerization of Poly(3,6-phenanthrene). *J. Polym. Sci., Part A: Polym. Chem.* **2013**, *51* (23), 5067−5074.
(54) Cantow, M. J. R. *Polymer Fractionation*, 1st ed.; Academic Press Inc.: New York, 1967.
(55) Lennox, A. J. J.; Lloyd-Jones, G. C. Selection of boron reagents for Suzuki-Miyaura coupling. *Chem. Soc. Rev.* **2014**, *43* (1), 412−443.
(56) Anderson, N. G. In *Practical Process Research and Development*, 2nd ed.; Academic Press: Oxford, 2012; Chapter 10, pp 261−287.
(57) Note that a similiar behavior was also found for other polymers to a much less extent, but this observation will not be further discussed.
(58) Coumont, L. S.; Veinot, J. G. C. Ni(COD)(2) coupling of 3,6-dibromocarbazoles as a route to all-carbazole shape persistent macrocycles. *Tetrahedron Lett.* **2015**, *56* (41), 5595−5598.
(59) Liu, S.-Y.; Li, H.-Y.; Shi, M.-M.; Jiang, H.; Hu, X.-L.; Li, W.-Q.; Fu, L.; Chen, H.-Z. Pd/C as a Clean and Effective Heterogeneous Catalyst for C−C Couplings toward Highly Pure Semiconducting Polymers. *Macromolecules* **2012**, *45* (22), 9004−9009.
(60) O'Keefe, D. F.; Dannock, M. C.; Marcuccio, S. M. Palladium catalysed coupling of halobenzenes with arylboronic acids: Rôle of the triphenylphosphine ligand. *Tetrahedron Lett.* **1992**, *33* (44), 6679−6680.
(61) Kong, K. C.; Cheng, C. H. Facile aryl-aryl exchange between the palladium center and phosphine ligands in palladium(II) complexes. *J. Am. Chem. Soc.* **1991**, *113* (16), 6313−6315.
(62) Pinto, R. M.; Olariu, R. I.; Lameiras, J.; Martins, F. T.; Dias, A. A.; Langley, G. J.; Rodrigues, P.; Maycock, C. D.; Santos, J. P.; Duarte, M. F.; Fernandez, M. T.; Costa, M. L. Study of selected benzyl azides by UV photoelectron spectroscopy and mass spectrometry. *J. Mol. Struct.* **2010**, *980* (1−3), 163−171.
(63) Li, Y.; Hoskins, J. N.; Sreerama, S. G.; Grayson, S. M. MALDI−TOF Mass Spectral Characterization of Polymers Containing an Azide Group: Evidence of Metastable Ions. *Macromolecules* **2010**, *43* (14), 6225−6228.

DOI: 10.1021/acs.macromol.7b00144
Macromolecules 2017, 50, 1319−1330

Publication P6

Block copolymer-type architecture with a central Ru^{II} sensitizer core: Conjugated poly(carbazole) for enhanced charge separation

R. Schroot, T. Schlotthauer, B. Dietzek, M. Jäger, U. S. Schubert, submitted.

Block copolymer-type architecture with a central Ru^{II} sensitizer core: Conjugated poly(carbazole) for enhanced charge separation

Robert Schroot, Tina Schlotthauer, Benjamin Dietzek, Michael Jäger,* Ulrich S. Schubert*

Abstract: Hierarchical macromolecules were prepared from a Ru(II) photosensitizer precursor. Following a modular chemistry-on-the-complex approach, only two coupling steps were required to attach the telechelic redox-active polymer chains *via* orthogonal end groups. The conjugated poly(3,6-carbazole) chain and styrenic poly(naphthalene diimide) segments act as electron donor and acceptor sites upon excitation of the interjacent Ru unit, as detailed by steady-state and time-resolved spectroscopy. The light-induced charge separation is completed within a few nanoseconds (>95%) and persists up to several tens of microseconds. The charge recombination is significantly reduced in comparison to conventional low-molecular photosystems (factor of 10) or to non-conjugated congeners (factor of 3), which reflects the higher charge mobility in conjugated polymers. In summary, the facile modular synthesis and the efficient long-lived charge separation demonstrate the feasibility for energy conversion.

The efficient conversion of photo into electrical or chemical bond energy can be achieved – among others – by molecular photosystems composed of functional building blocks.[1-6] The versatility of this approach relies on precisely tailored units for light absorption and charge separation, as demonstrated in molecular triads reaching impressive quantum efficiencies (up to 95%).[4] In these architectures, charge separation occurs after initial light absorption by the photosensitizer (**P**). In this regard, Ru(II) poly-pyridyl-type complexes often serve as versatile photosensitizer owing to their remarkable excited state properties.[7] Following the common oxidative quenching pathway, an electron is transferred from **P*** to the acceptor (**A**), while the donor (**D**) regenerates the photosensitizer by subsequent electron transfer and the fully charge separated (CS) state is obtained. In molecular model systems, the charges are reside on the single donor and acceptor sites and often inevitably recombine, before they can be harnessed, *e.g.*, by charge extraction (photovoltaics) or coupled catalytic processes (photosynthesis). In this regard, the incorporation of multiple donor/acceptor sites is attractive, but the convergent syntheses are often (prohibitively) elaborate in the case of low-molecular model systems. Alternatively, polymer chemistry offers an elegant route to tailored photo- and electrochemically active macromolecules,[8] which can provide charge percolation pathways, perform charge accumulation as well as a phase segregation of the donor/acceptor domains – as demonstrated by organic photovoltaics.[9-15] Numerous conceivable macromolecular photosystems are reported, *e.g*, Ru-decorated oligopeptides,[9-10] poly(styrene)s,[12] poly(acrylates)s,[13] poly(thiophene)s,[16] poly(fluorene)[15] or poly(fluorene-*co*-thiophene)[14]. Notably, the early examples comprise statistical assemblies, mainly due to the available polymerization techniques at that times. Hence, the progress in polymer science enables nowadays an *a priori* design and the preparation of well-defined functional macromolecules, which constitute of independently prepared functionalized building blocks,[8] *e.g.*, multi-donor ($\mathbf{D_n}$) and multi-acceptor ($\mathbf{A_m}$) polymers. Furthermore, such building blocks can be connected in a modular fashion by means of divergent syntheses to minimize the synthetic efforts substantially and to prepare linear $\mathbf{D_n–P–A_m}$ architectures for directional charge separation. The linear arrangement of the attached polymer chains around **P** ensures their maximal mutual distance, which is one important factor to minimize charge recombination between the charge–carrying sites. Recently, we reported the facile synthesis of telechelic poly(triarylamine) and poly(naphthalene diimide) by nitroxide-mediated polymerization (NMP), and their facile modular assembly was reported for various dyads ($\mathbf{D_n–P}$ or $\mathbf{P–A_m}$).[17-21] Notably, the efficient charge separation upon excitation was demonstrated.,[19, 22] revealing a remarkably long-lived component (2,400 ns) that is assigned to charge migration within the polymer.

In this contribution, the poly(triarylamine) block of the previous $\mathbf{D_n–P–A_m}$ architecture was replaced by a conjugated telechelic poly(3,6-*N*-alkylcarbazole), since conjugated polymers are known to feature higher charge charrier mobilities[23-29] and, thus, may prolong the CS life time. Notably, the desired triad can be readily prepared due to the chosen modular character of the chemistry-on-the-complex approach as outlined in Scheme 1. The individual synthesis of the poly(3,6-carbazole) (**pCarb**),[30] the poly(naphthalene diimide) (**pNDI**),[18] and the *bis*-functionalized Ru(II) precursor complex[18, 22] have been reported.

R. Schroot, T. Schlotthauer, Dr. M. Jäger, Prof. Dr. U. S. Schubert
Laboratory of Organic and Macromolecular Chemistry (IOMC)
Friedrich Schiller University Jena
Humboldtstraße 10, 07743 Jena, Germany
E-mail: michael.jager.iomc@uni-jena.de; ulrich.schubert@uni-jena.de

R. Schroot, T. Schlotthauer, Prof. Dr. Benjamin Dietzek,
Dr. M. Jäger, Prof. Dr. U. S. Schubert,
Center for Energy and Environmental Chemistry Jena (CEEC Jena)
Friedrich Schiller University Jena
Philosophenweg 7a, 07743 Jena, Germany

Prof. Dr. Benjamin Dietzek
Institute for Physical Chemistry and Abbe Center of Photonics (ACP)
Friedrich Schiller University Jena
Helmholtzweg 4, 07743 Jena, Germany
and
Leibniz Institute for Photonic Technology (IPHT)
Albert-Einstein-Straße 9, 07743 Jena, Germany

Supporting information for this article is given via a link at the end of the document.

Scheme 1. Modular assembly of the photosystem $\mathbf{D_n–P–A_m}$ (grey shaded) including the reference subsystems **P**, $\mathbf{D_n–P}$, $\mathbf{P–A_m}$ (black boxes) starting from building blocks: *Bis*-functionalized Ru-precursor (red) and telechelic polymers **pCarb** (blue) and **pNDI** (green). See right side for chemical structures.[a]

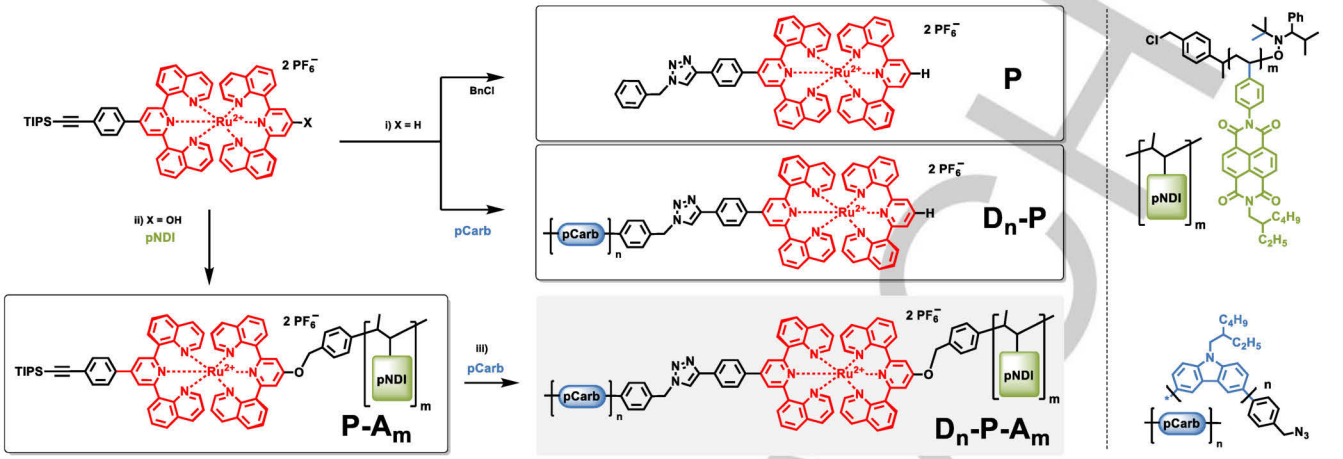

[a]reagents and conditions: i) CuBr, PMDETA, DMF, N_2, 80 °C, 101 h; ii) K_2CO_3, KI, DMF,N_2, 60 °C, 77 h; iii) (a) (n-Bu_4)NF×H_2O, THF, (b) CuBr, PMDETA, DMF, N_2, 80 °C, 96 h.

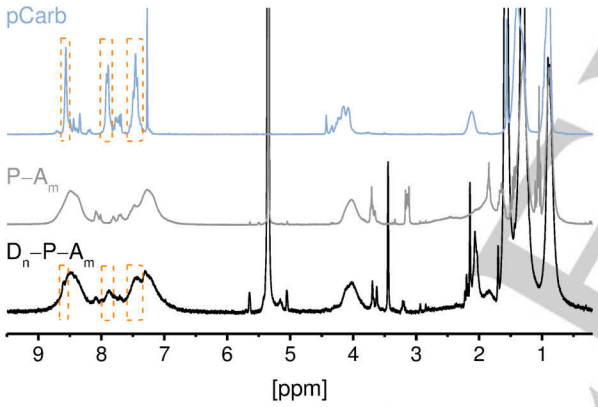

Figure 1. Proton NMR spectra of **pCarb**, $\mathbf{P–A_m}$ and $\mathbf{D_n–P–A_m}$ (300 MHz, $CDCl_3$ or CD_2Cl_2). The appearance of broad resonances of pCarb at approximately 7.4, 7.9 and 8.6 ppm (orange doted boxes) indicates the successful preparation of the triad $\mathbf{D_n–P–A_m}$.

The novel donor-dyad $\mathbf{D_n–P}$ was prepared from telechelic poly(3,6,-carbazole) *via* the copper(i) catalyzed azide-alkyne cycloaddition (CuAAC). The applied reagents, *i.e.* Cu(I)Br as catalyst, PMDETA as base and DMF as solvent are known to be efficient for the linkage of related azide decorated polymers with complexes.[18] However, longer reaction times and elevated temperatures were required as shown by SEC and TLC analysis. The purification was conveniently accomplished by preparative size-exclusion chromatography using a commercial resin (Toyopearl HW-55F). The successful linkage was confirmed by UV/vis SEC and MALDI-TOF mass spectrometry (Figure S8). The synthesis of the corresponding reference complex (**P**) was reported previously,[18] whereas the synthesis of the triad embarked from the *bis*-functionalized Ru(II) precursor (X=OH).[22] First, the precursor dyad $\mathbf{P–A_m}$ was prepared analogously to our established protocols.[18] The nucleophilic substitution of the hydroxyl group with benzyl-halide decorated poly(naphthalene diimide) afforded $\mathbf{P–A_m}$ in very good yields (75%). Next, the terminal alkyne group was quantitatively deprotected with (*n*-Bu_4)NF without the need of chromatographic purification. The final coupling step by CuAAC as described above gave the desired $\mathbf{D_n–P–A_m}$ triad. Notably, an excess of the donor polymer was used to account for residual macrocycles,[30] which cannot undergo coupling and are readily separated by preparative SEC. In contrast, the removal of unreacted acceptor dyad to obtain pure $\mathbf{D_n–P–A_m}$ was more challenging due to the marginal increase in molar mass of the triad *vs.* the dyad. This hypothesis is corroborated by the ^{1}H NMR spectra of **pCarb**, $\mathbf{P–A_m}$ and $\mathbf{D_n–P–A_m}$ (Figure 1), which reveal the characteristic but weak resonances of the poly(carbazole) in the final $\mathbf{D_n–P–A_m}$ triad.

The photophysical properties of the triad and the respective subsystems were investigated by steady-state and time-resolved spectroscopy. The light-induced electron transfer within the acceptor dyad $\mathbf{P–A_m}$ has been investigated previously,[18] hence we deliberately limit the discussion to the reference photosensitizer (**P**), the novel donor dyad ($\mathbf{D_n–P}$) and the final $\mathbf{D_n–P–A_m}$ triad. Figure 2 depicts the absorption spectra of the new compounds, which display the additive spectral features of the individual building blocks (Figure S14). The polymers dominate the absorption in the UV region, *i.e.*, poly(carbazole) (312 nm) and poly(naphthalene diimide) (360 and 380 nm), whereas the Ru(II) complex exclusively absorbs above 400 nm and stretching up to 600 nm. Note that these spectral features ensure the selective excitation of the photosensitizer by visible light, which benefits the analysis of the light-induced events with respect to less hierarchically and functionally defined polymer architectures (*vide supra*).[4] The steady state emission spectra are composed of Ru-based ^{3}MLCT emission (around 690 nm) and polymer-assigned emission below 650 nm (Figure S16), in agreement with reported data of poly(3,6-carbazoles)[31] and

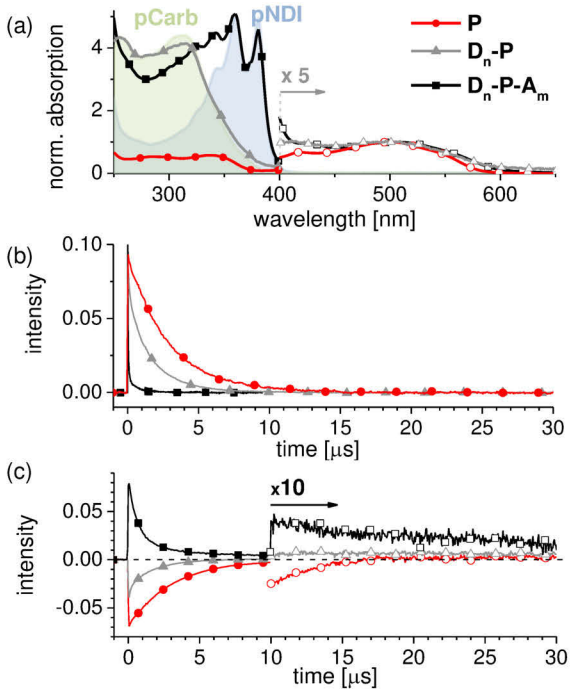

Figure 2. (a) Normalized absorption spectra of $\mathbf{D_n–P}$ (grey), $\mathbf{D_n–P–A_m}$ (black) and **P** (red) in CH_2Cl_2 (solid symbols). The colored-shaded area depicts the absorption spectra of the individual polymers **pCarb** and **pNDI**. Note the scaling (x5) of the ^{1}MLCT region (>400 nm) to assist visibility of Ru-based absorption (hollow symbols). (b) Time-resolved emission in purged CH_2Cl_2 (λ_{exc} = 500 nm, λ_{det} = 750 nm except for **P** with 700 nm). Note the significantly faster quenching of $\mathbf{D_n–P–A_m}$ *vs.* **P** or $\mathbf{D_n–P}$ (λ_{em} = 700 nm). The red-shifted emission detection was chosen to minimize polymer-based contribution (see text). (c) Transient absorption traces of **P'**, $\mathbf{D_n–P}$ (470 nm) and $\mathbf{D_n–P–A_m}$ (475 nm) indicating the formation of a long-lived charge separated state in the triad. Note, that scaling (x10) after 10 µs to assist visibility (hollow symbols).

poly(naphthalene diimide).[18-19] Upon comparison of the ^{3}MLCT emission of **P** *vs.* $\mathbf{D_n–P}$, a noticeable quenching (-25%) was observed (Figure S16), which is assigned to reductive quenching. The poly(3,6-carbazole) exhibits a formal redox potential of 0.22 V *vs.* $Fc^{+/0}$ (Figure S11), which gives a driving force estimate of +0.24 eV for reductive quenching (see SI Section 6 for details). Note, that this value represents a conservative upper bound estimate, as the (attractive) coulombic work term and the favorable entropic factors due to multiple donor sites are neglected. Hence, in view of the long excited state lifetimes, the minor reductive quenching pathway cannot be ruled out and the transient absorption data further supports this hypothesis (*vide infra*). Note, that ^{3}MLCT quenching by energy transfer is unlikely due the unfavorable energetics, as the emission of the poly(carbazole) occurs at higher energies (<650 nm).[31] More importantly, the triad $\mathbf{D_n–P–A_m}$ shows an almost quantitative ^{3}MLCT emission quenching by 96% (Figure S17), in excellent agreement with the oxidative quenching that has been previously identified for the $\mathbf{P–A_m}$ subsystem.[19] In order to facilitate the unambiguous identification of the charge separate states in the following section, the spectral signatures of the reduced poly(naphthalene diimide) ($\mathbf{pNDI^-}$) and the oxidized poly(carbazole) ($\mathbf{pCarb^+}$) were determined (see SI Section 7 for details). Next, time-resolved emission and transient absorption (TA) measurements were performed to detail the light-induced charge separation. Representative ^{3}MLCT emission traces of the triad and the references are displayed in Figure 2b. The photosensitizer **P** exhibits a mono-exponential decay with a lifetime of 2.9 µs, while the donor dyad $\mathbf{D_n–P}$ gives 1.7 µs. The formal decrease in lifetime (-41%) is in qualitative agreement with the decreased steady state emission intensity (-25%).[32] More importantly, the triad $\mathbf{D_n–P–A_m}$ features emission decay on a much shorter time scale (<10 ns, Figure S20), which suggests an almost quantitative oxidative quenching (>99%) based on the lifetimes data. In order to confirm these hypotheses, transient absorption (TA) spectra were recorded in the visible region (10 nm intervals) to identify the intermediately formed states. In the case of **P**, the TA traces decay with a lifetime similar to that obtained from emission measurements (Figure 2c), and the spectral domain shows several isosbestic points (Figure S21). Similarly, the TA signals of $\mathbf{D_n–P}$ decay with comparable lifetimes as determined from emission measurements, but the spectral domain revealed an additional component below 700 nm at short timescales (<30 ns). The origin is traced to polymer-based emission from the corresponding emission profiles (Figure S21b), in excellent agreement with the previously assigned polymer-based emission.[19] At longer time scales, the global fit gives a spectral signature that differs from the photosensitizer due to contributions by reductive quenching (Figure S25). In marked contrast, the triad $\mathbf{D_n–P–A_m}$ shows short-lived Ru emission but long-lived TA signals. The TA decay at 475 nm is best described by a biexponential kinetics with associated lifetimes of 0.7 µs (83%) and 7.2 µs (17%). The faster component is comparable to those of a related molecular triad (<200 ns) and, thus, is assigned to the corresponding initial charge-separated state. The slower recombination is reasonable in view of the unsaturated flexible linkage within the polymer. More importantly, the long-lived component exhibits the prolonged charge separation by a factor of 3 with respect to the poly(triarylamine)-based (**pTARA**) congener (2.4 µs).[22] In both cases the light-induced charge separation proceeds primarily *via* oxidative quenching to transfer an electron first to the acceptor chain and subsequently to regenerate the oxidized photosensitizers by secondary electron transfer from donor chain. Although the linkage pattern is reversed among both triads, which may influence the initial charge separation pathways,[33] the recombination depends largely on the (identical) distance of the charge-carrying units. Based on this assumption, the observed difference in recombination is interpreted in terms of the different nature of the donor chains. In the case of the **pTARA**-based triad, the redox active units are electronically decoupled through the saturated backbone and the charge migration follows a hoping mechanism. Instead, the **pCarb**-based triad consists of carbazole subunits with sizable electronic coupling. As a consequence, the hole can delocalize more readily,[34] which facilitates a more efficient spatial charge separation and consequently also the observed diminished recombination. A global analysis of the TA data was performed to retrieve any spectral differences, *i.e.*, the long-lived part (>100 ns) was fit to exclude polymer-based emission (Figure S24). Comparable lifetime values were obtained for both components, which validates previous analyses based on selected wavelengths. The components' spectra are virtually superimposing (Figure S25), which confirms that both decay channels belong to a fully charge separated state.

In conclusion, telechelic redox-active and conjugated polymers were utilized as versatile building blocks for the construction of $\mathbf{D_n–P–A_m}$ architectures,[8] which can be regarded as *block* copolymers with a single interjacent photosensitizer unit. The

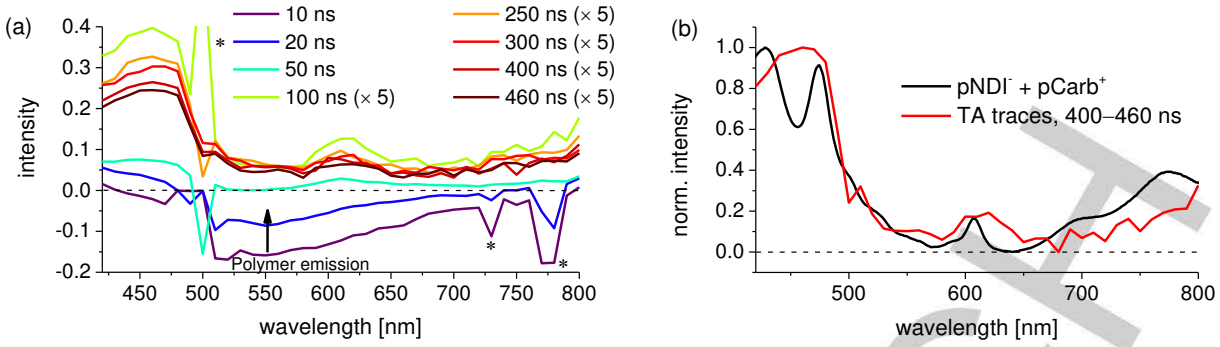

Figure 3. (a) Transient absorption data of $\mathbf{D_n–P–A_m}$ from 10 to 460 ns showing the formation of absorption features characteristic for the reduced **pNDI⁻** (470 and 605 nm) and the oxidized **pCarb⁺** (430 and above 600 nm) (purged solution, CH_2Cl_2, excitation at 500 nm). Note, that all spectra from 100 to 460 ns were scaled by the factor five to enhance the visibility of the spectral changes. (b) The combined absorption spectra of the reduced **pNDI⁻** and the oxidized **pCarb⁺** resemble the TA traces from 400 to 460 ns and indicate the formation of a charge separated state. Spectral artefacts from pulse and Raman scatter are marked with an asterisk. Spectral intervals are 10 nm.

modularity of the approach was ensured by the orthogonal linkage strategy and facile purification protocols, which enabled the successful design based on inherent optical and redox-chemical properties of the building blocks. Due to the optical transparency of the polymers in the visible light region, the selective excitation of the photosensitizer occurs and triggers light-induced energy and/or electron transfer. Efficient charge separation was observed, as unambiguously identified by transient absorption spectroscopy. The charge separated state features a long-lived component with a remarkably long life time (7 µs), which is assigned to secondary electron transfer steps within the polymers. The comparison of a non-conjugated poly(triarylamine) *vs.* conjugated poly(3,6-carbazole) donor chains revealed a lifetime enhancement by a factor of three, which indicates the utility of conjugated polymers to achieve long-lived light-induced charge separation. The presented approach combines simple and versatile syntheses with highest structural and photochemical control within the assembly, in particular of the interface between n- and p-conducting domains. In addition, these beneficial features may be utilized in phase-separating materials, in order to transduce the optical stimulus into a long-lived redox-chemical response.

Acknowledgements

Financial support by the Friedrich Schiller University Jena ("Nachwuchsförderung") and the Thüringer Ministerium für Wirtschaft, Wissenschaft und Digitale Gesellschaft (TMWWDG) is kindly acknowledged. The authors thank Annett Urbanek for MALDI-ToF measurements as well as Dr. Peter Bellstedt and the NMR platform of the IAAC/IOMC for help with the NMR measurements.

Keywords: Time-resolved spectroscopy • telechelic polymer • ruthenium(II) polypyridyl complex • electron transfer • donor acceptor system

[1] L. Hammarström, *Acc. Chem. Res.* **2015**, *48*, 840-850.
[2] V. Balzani, G. Bergamini, P. Ceroni, *Angew. Chem. Int. Ed.* **2015**, *54*, 11320-11337.
[3] J. J. Concepcion, R. L. House, J. M. Papanikolas, T. J. Meyer, *Proc. Natl. Acad. Sci. USA* **2012**, *109*, 15560-15564.
[4] J. H. Alstrum-Acevedo, M. K. Brennaman, T. J. Meyer, *Inorg. Chem.* **2005**, *44*, 6802-6827.
[5] V. Balzani, A. Credi, M. Venturi, *ChemSuSchem* **2008**, *1*, 26-58.
[6] V. Balzani, L. Moggi, M. F. Manfrin, F. Bolletta, M. Gleria, *Science* **1975**, *189*, 852-856.
[7] D. W. Thompson, A. Ito, T. J. Meyer, *Pure Appl. Chem.* **2013**, *85*, 1257-1305.
[8] R. Schroot, M. Jager, U. S. Schubert, *Chem. Soc. Rev.* **2017**, doi: 10.1039/C1036CS00811A.
[9] S. E. Bettis, D. M. Ryan, M. K. Gish, L. Alibabaei, T. J. Meyer, M. L. Waters, J. M. Papanikolas, *J. Phys. Chem. C* **2014**, *118*, 6029-6037.
[10] D. Ma, S. E. Bettis, K. Hanson, M. Minakova, L. Alibabaei, W. Fondrie, D. M. Ryan, G. A. Papoian, T. J. Meyer, M. L. Waters, J. M. Papanikolas, *J. Am. Chem. Soc.* **2013**, *135*, 5250-5253.
[11] Z. A. Morseth, L. Wang, E. Puodziukynaite, G. Leem, A. T. Gilligan, T. J. Meyer, K. S. Schanze, J. R. Reynolds, J. M. Papanikolas, *Acc. Chem. Res.* **2015**, *48*, 818-827.
[12] G. Leem, S. Keinan, J. Jiang, Z. Chen, T. Pho, Z. A. Morseth, Z. Hu, E. Puodziukynaite, Z. Fang, J. M. Papanikolas, J. R. Reynolds, K. S. Schanze, *Polym. Chem.* **2015**, *6*, 8184-8193.
[13] Z. Fang, A. Ito, H. Luo, D. L. Ashford, J. J. Concepcion, L. Alibabaei, T. J. Meyer, *Dalton Trans.* **2015**, *44*, 8640-8648.
[14] E. Puodziukynaite, L. Wang, K. S. Schanze, J. M. Papanikolas, J. R. Reynolds, *Polym. Chem.* **2014**, *5*, 2363-2369.
[15] G. Leem, Z. A. Morseth, E. Puodziukynaite, J. Jiang, Z. Fang, A. T. Gilligan, J. R. Reynolds, J. M. Papanikolas, K. S. Schanze, *J. Phys. Chem. C* **2014**, *118*, 28535-28541.
[16] L. Wang, E. Puodziukynaite, E. M. Grumstrup, A. C. Brown, S. Keinan, K. S. Schanze, J. R. Reynolds, J. M. Papanikolas, *J. Phys. Chem. Lett.* **2013**, *4*, 2269-2273.
[17] R. Schroot, T. Schlotthauer, M. Jäger, U. S. Schubert, *Macromol. Chem. Phys.* **2017**, 1600534-n/a.
[18] R. Schroot, T. Schlotthauer, U. S. Schubert, M. Jäger, *Macromolecules* **2016**, *49*, 2112-2123.
[19] J. Kübel, R. Schroot, M. Wächtler, U. S. Schubert, B. Dietzek, M. Jäger, *J. Phys. Chem. C* **2015**, *119*, 4742-4751.
[20] R. Schroot, U. S. Schubert, M. Jäger, *Macromolecules* **2015**, *48*, 1963-1971.
[21] R. Schroot, C. Friebe, E. Altuntas, S. Crotty, M. Jäger, U. S. Schubert, *Macromolecules* **2013**, *46*, 2039-2048.
[22] T. Schlotthauer, R. Schroot, S. Glover, L. Hammarström, M. Jäger, U. S. Schubert, *submitted* **2017**.
[23] E. M. Barea, G. Garcia-Belmonte, M. Sommer, S. Hüttner, H. J. Bolink, M. Thelakkat, *Thin Solid Films* **2010**, *518*, 3351-3354.
[24] J. Veres, S. D. Ogier, S. W. Leeming, D. C. Cupertino, S. Mohialdin Khaffaf, *Adv. Funct. Mater.* **2003**, *13*, 199-204.
[25] A. J. Heeger, *Chem. Soc. Rev.* **2010**, *39*, 2354-2371.
[26] C. Liao, F. Yan, *Polym. Rev.* **2013**, *53*, 352-406.

[27] J.-F. Morin, M. Leclerc, D. Adès, A. Siove, *Macromol. Rapid Commun.* **2005**, *26*, 761-778.
[28] Y. He, W. Hong, Y. Li, *J. Mater. Chem. C* **2014**, *2*, 8651-8661.
[29] X. Guo, M. Baumgarten, K. Muellen, *Prog. Polym. Sci.* **2013**, *38*, 1832-1908.
[30] R. Schroot, U. S. Schubert, M. Jäger, *Macromolecules* **2017**, *50*, 1319-1330.
[31] Y. C. Chen, G. S. Huang, C. C. Hsiao, S. A. Chen, *J. Am. Chem. Soc.* **2006**, *128*, 8549-8558.
[32] Note the unknown quantum yields of the photosensitzer and the donor dyad, which influence the observed steady state emission intensity in addition to the quenching pathways.
[33] Y. Luo, K. Barthelmes, M. Wächtler, A. Winter, U. S. Schubert, B. Dietzek, *Chem. Eur. J.* **2017**, doi: 10.1002/chem.201700413.
[34] H. Baessler, A. Koehler, *Unimolecular and Supramolecular Electronics I: Chemistry and Physics Meet at Metal-Molecule Interfaces* **2012**, *312*, 1-65.

Supporting Information

Block copolymer-type architecture with a central Ru^{II} sensitizer core: Conjugated poly(carbazole) for enhanced charge separation

Robert Schroot, Tina Schlotthauer, Benjamin Dietzek, Michael Jäger, Ulrich S. Schubert

R. Schroot, T. Schlotthauer, Dr. M. Jäger, Prof. Dr. U. S. Schubert
Laboratory of Organic and Macromolecular Chemistry (IOMC)
Friedrich Schiller University Jena
Humboldtstraße 10, 07743 Jena, Germany
E-mail: michael.jager.iomc@uni-jena.de; ulrich.schubert@uni-jena.de

R. Schroot, T. Schlotthauer, Prof. Dr. Benjamin Dietzek,
Dr. M. Jäger, Prof. Dr. U. S. Schubert,
Center for Energy and Environmental Chemistry Jena (CEEC Jena)
Friedrich Schiller University Jena
Philosophenweg 7a, 07743 Jena, Germany

Prof. Dr. Benjamin Dietzek
Institute for Physical Chemistry and Abbe Center of Photonics (ACP)
Friedrich Schiller University Jena
Helmholtzweg 4, 07743 Jena, Germany
and
Leibniz Institute for Photonic Technology (IPHT)
Albert-Einstein-Straße 9, 07743 Jena, Germany

Content

1. Instrumentation

NMR spectra were recorded on a 300 or 400 MHz NMR spectrometer (Bruker AVANCE or Fourier 300) in deuterated solvents at 300 K. Chemical shifts are reported in parts per million (ppm, δ scale) relative to the residual solvent signal.[1]

MALDI-TOF MS spectra were measured using an Ultraflex III TOF/TOF (Bruker Daltonics GmbH) equipped with a Nd:YAG laser and a collision cell. The spectra were recorded in the positive reflector or linear mode.

ESI-Q-TOF MS measurements were executed on a micrOTOF (Bruker Daltonics GmbH) mass spectrometer, which was equipped with an automatic syringe pump for sample injection. The pump was supplied from KD Scientific. It was operated in the positive ion mode. The standard electrospray ion (ESI) source was used to generate ions. Mixtures of dichloromethane and acetonitrile were used as solvent. The ESI-Q-TOF-MS instrument was calibrated in the m/z range 50 to 3,000 using an internal calibration standard (Tunemix solution), which was supplied from Agilent.
UV/Vis absorption spectra were measured on a Perkin-Elmer Lambda 45 UV/Vis spectrophotometer and emission as well as excitation spectra were recorded using a Jasco FP6500. Measurements were carried out using approx. 10^{-7} M solutions of aerated dichloromethane (spectroscopy grade) in 1 cm quartz cuvettes at 25 °C.

Electrochemical measurements were carried out on a Biologic VMP 3 potentiostat with a standard three-electrode configuration using a glassy-carbon-disk working electrode, a platinum-rod auxiliary electrode and an $Ag/AgNO_3$ reference electrode. Scan rates were varied from 100 to 1,000 mV/s. The experiments were carried out in CH_2Cl_2 containing tetra-*n*-butylammonium hexafluorophosphate (0.1 M). Ferrocene was added as internal standard at the end of each experiment.

The nanosecond (ns) transient absorption and emission spectra were collected on a setup consisting of a Nd: YAG laser system (355 nm, pulse duration ca. 5 ns, repetition rate 10 Hz) pumping a Continuum Surelite OPO Plus, which is used to modulate the excitation pulse wavelength (500 nm). The probe light is provided by a 75 W xenon arc lamp. Spherical concave mirrors are used to focus the probe beam into the samples and then send the beam to the monochromator (Acton, Princeton Instruments). The probe light is detected by a Hamamatsu R928 photomultiplier. The signal is amplified and processed by a commercially available detection system (Pascher Instruments AB). Freshly prepared samples with an optical density (ca. 0.1) at the excitation wavelength (500 nm) were used. Oxygen-free solutions were prepared by vigorous N_2-sparging. All measurements were performed in 1 cm path length fluorescence cuvettes. A spectral band of 20 nm around the pump wavelength is omitted from the data analysis due to pump-scatter in this spectral range.

Flash column chromatography was carried out on a Biotage Isolera One System using Biotage SNAP Cartridges KP-Sil. The Biotage Initiator Sixty Microwave synthesizer was used for microwave reactions.
Preparative size exclusion chromatography was either performed by using Bio-Beads (S-X1, dichloromethane) or Toyopearl (HW-55F, CH_2Cl_2/MeOH 95/5).

Analytical size exclusion chromatography was performed on the following systems:
1. Shimadzu system (controller: SCL-10A VP, degasser: DGU-14A, pump: LC-10AD VP, auto sampler: SIL-10AD VP, oven: Techlab, UV detector: SPD-10AD VP, RI detector: RID-10A, eluent: chloroform/iso-propanol/triethylamine [94:2:4], flow rate: 1 mL/min, temperature: 40 °C, column: PSS SDV pre/lin S column).

2. Shimadzu system (controller: SCL-10A VP, degasser: DGU-14A, pump: LC-10AD VP, auto sampler: SIL-10AD VP, oven: CTO-10A VP, UV detector: SPD-10MA VP, RI detector: RID-10A, eluent: DMAc + 0.08% NH_4PF_6, flow rate: 1 mL/min, temperature: 40 °C, column: Phenomenex Phenogel guard/10^5 Å/10^3 Å)

2. Experimental part

All reagents were purchased from ABCR, Acros Organics, Alfa Aesar, Apollo Scientific, Sigma-Aldrich or TCI chemicals and were used without further purification unless otherwise noted. Dry pyridine and dry *N*-*N*-dimethylformamide (DMF) were commercially available. THF was distilled from sodium/benzophenone. All solvents were degassed before use. *N*-(2-Ethyl-hexyl)-*N*'-(vinylphenyl)-naphthalene-1,4,5,8-dicarboxydiimide (**2**),[2] 3,6-dibromocarbazole,[3] 3,6-dibromo-9-ethylhexyl-9H-carbazole, 3-bromo-9-(2-ethylhexyl)-6-(4,4,5,5-tetramethyl-1,3,2-dioxaborolan-2-yl)-9H-carbazole (**1**),[4] 2-(4-(azidomethyl)phenyl)-4,4,5,5-tetramethyl-1,3,2-dioxaborolane (**4**),[5] [Ru(dqp-ph-tr-bn)(dqp)][PF_6]$_2$,[2] [Ru(dqp)$_2$][PF_6]$_2$[6] and [Ru(dqp-ph-C≡C-TIPS)(dqp-OH)][PF_6]$_2$[7] were prepared as described previously. Dqp is 2,6-di(quinolin-8-yl)pyridine, dqp-OH is 4-hydroxy-2,6-di(quinolin-8-yl)pyridine, dqp-ph-C≡C-TIPS is 4-(4-(triisopropylsilyl)ethynylphenyl)-2,6-di(quinolin-8-yl)pyridine, dqp-ph-tr-bn is 4-(4-(1-benzyl-1H-1,2,3-triazol-4-yl)phenyl)-2,6-di(quinolin-8-yl)pyridine), PMDETA is *N,N,N′,N″,N″*-pentamethyldiethylenetriamine.

The monomer **1** was prepared in a three-step synthesis from carbazole in good yields (≈ 60%) according to literature procedures.[3-4] The subsequent polymerization and end functionalization leading to the polymer **pCarb** was adopted from our previously reported protocol.[4] The successful end functionalization was verified by NMR spectroscopy (Figure S1). The also formed macrocycles were not removed after the polymerization as these compounds are indifferent in the functionalization with the ruthenium complex and can be readily removed afterwards (*see text*).
1,4,5,8-Naphthalenetetracarboxylic dianhydride was utilized as starting material for the preparation of the NDI-based monomer **2**. The two step synthesis gave the compound in good yields (≈ 60%) as reported previously.[2] The monomer was polymerized with the functional initiator CMSt-TIPNO (N-tert-Butyl-O-[1-[4-(chloromethyl)phenyl]ethyl]-N-(2-methyl-1-phenyl)hydroxylamine) to yield polymer **pNDI**. The isolated polymer featured a narrow molar mass distribution (Đ = 1.12). The proton resonances of the reactive chloromethyl group of the initiator can be seen in the NMR spectrum as broad signal at approximately 4.5 ppm.

pCarb. A nitrogen filled Schlenk tube was charged with **1** (0.225 g, 0.47 mmol), dry THF (15 mL) and a purged aqueous solution of K_2CO_3 (0.95 mL, 4 M). Subsequently [Pd(P^tBu_3)$_2$] (0.012 g, 0.02 mmol) was added as solution in THF (2.00 mL) and the resulting yellow mixture was stirred at room temperature for six hours. Then 2-(4-(azidomethyl)phenyl)-4,4,5,5-tetramethyl-1,3,2-dioxaborolane (**4**) (0.120 g, 0.47 mmol) was added as solution in dry THF (1.00 mL). After stirring overnight the mixture was precipitated in MeOH, filtered and the off-white solid was washed with MeOH as well as water and dried (0.080 g). SEC ($CHCl_3$/IPA/NEt_3 94/2/4, PS calibration): M_n = 3,300 g/mol, Đ = 1.59. ^{1}H NMR (300 MHz, $CDCl_3$): δ 8.95–8.14 (br), 8.14–7.61 (br), 7.61–7.23 (br), 4.52–4.39 (br), 4.52–3.83 (br), 2.44–1.92 (br), 1.52–1.13 (br), 1.13–0.42 (br).

pNDI. A glass tube equipped with a septum and an external overhead flushing with nitrogen was used for the polymerization. The reaction vessel was charged with **2** (0.500 g, 1.040 mmol), *N*-(*tert*-butyl)-O-(1-(4-(chloromethyl)phenyl)ethyl)-*N*-(2-methyl-1-phenylpropyl)hydroxylamine (CMSt-TIPNO) (0.019 g, 0.052 mmol) and anisole (4.0 mL).The mixture was purged with nitrogen for 20 min and placed in a pre-heated oil bath (120 °C). After 17 h the reaction mixture was diluted with CH_2Cl_2 and precipitated in cold MeOH. Subsequently, unreacted monomer was removed by preparative SEC (Bio-Beads S-X1, CH_2Cl_2). The polymer was obtained as yellow solid after precipitation in MeOH. Yield: 0.400 g. SEC ($CHCl_3$/IPA/NEt_3 94/2/4, PS calibration): M_n = 7,300 g/mol, Đ = 1.12. ^{1}H NMR (300 MHz, $CDCl_3$): δ 9.24–7.91 (br), 7.91–6.51 (br), 4.70–4.42 (br), 4.34–3.56 (br), 3.13–1.70 (br), 1.50–1.02 (br), 1.02–0.42 (br).

[Ru(dqp)(dqp-ph-tr-pCarb)][PF_6]$_2$ (D_n–P). A vial was charged with **pCarb** (9.00 mg, 2.14 μmol, 1 eq.) as well as [Ru(dqp)(dqp-ph-C≡CH)][PF_6]$_2$ (4.29 mg, 4.29 μmol, 2 eq.), sealed, evacuated and flushed with nitrogen. Then dry DMF (1.00 mL), CuBr (0.62 mg, 4.29 μmol, 2 eq.) as solution in DMF

(0.17 ml) and PMDETA as solution in DMF (0.02 mL, 0.24 M, 2 eq.) were added. The mixture was stirred for 24 h at RT before the temperature was increased to 60 °C as no conversion was detected by UV/Vis-SEC. After additional 24 h the temperature was increased to 80 °C and stirring was continued for 53 h until no further conversion was detected. The reaction mixture was precipitated in an aqueous solution of NH_4PF_6. Then CH_2Cl_2 was added and the aqueous phase was extracted. The combined organic extracts were dried over Na_2SO_4, filtered and concentrated under reduced pressure. The crude product was purified by preparative SEC using the Toyopearl HW-50F resin (2 mg (pure product) + 3 mg (product + minor impurities of the starting complex)). ^{1}H NMR (400 MHz, CD_2Cl_2): δ 8.75–8.30 (br, **pCarb**), 8.30−7.95 (br, Ru), 7.95−7.80 (br, **pCarb**), 7.80−7.62 (br, Ru), 7.62−7.31 (br, **pCarb** + Ru), 7.31–6.87 (br, **pCarb** + Ru), 4.34–3.88 (br, **pCarb**), 2.37–1.93 (br, **pCarb**), 1.52–1.0(br, **pCarb**) 0.97–0.88 (br, **pCarb**).

[Ru(dqp-O-pNDI)(dqp-ph-C≡C-TIPS)][PF_6]$_2$ (P–A$_m$). A vial was charged with **pNDI** (0.070 g, 0.008 mmol, 1 eq.), K_2CO_3 (0.001 g, 0.032 mmol, 4 eq.), KI (0.003 g, 0.016 mmol, 2 eq.) and [Ru(dqp-ph-C≡CH)(dqpOH)][PF_6]$_2$ (0.018 g, 0.014 mmol, 1.7 eq.), sealed and placed under a nitrogen atmosphere. Dry DMF (1.0 mL) was added and the resulting solution was heated to 60 °C. The reaction progress was monitored by TLC (aluminum oxide, CH_2Cl_2/MeOH 95/5) and analytical size exclusion chromatography (DMAc + 0.08% NH_4PF_6, diode array detection). The reaction was continued until no further conversion was monitored by TLC (77 h). The mixture was diluted with a minimum amount of THF and precipitated into aqueous NH_4PF_6 solution. The red precipitate was re-dissolved in CH_2Cl_2 and water. The layers were separated and the aqueous phase was further extracted with CH_2Cl_2 (3×). The combined organic batches were washed with brine, dried over Na_2SO_4 and concentrated under reduced pressure. Preparative size-exclusion chromatography (Toyopearl HW-55F, CH_2Cl_2/MeOH 95/5) gave the dyad **D2** as red solid (0.060 g, 75%). ^{1}H NMR (300 MHz, CD_2Cl_2): δ 9.11–8.17 (br, **pNDI**), 8.11 (br, Ru), 8.08 (br, Ru), 7.91 (br, Ru), 7.71 (br, Ru), 7.63–6.47 (br, **pNDI**), 5.61–5.48 (br, linker), 4.38–3.73 (br, **pNDI**), 3.17–1.56 (br, **pNDI**), 1.56–1.03(br, **pNDI**), 1.19 (s, TIPS), 1.03–0.34 (br, **pNDI**).

Deprotection: A vial was charged with **D2** (0.058 g, 0.058 mmol) and THF (3 mL) and the resulting solution was cooled to 0 °C. Then tetra-*n*-butylammonium fluoride (0.002 g, 0.007 mmol, 1.2 eq.) was added as solution in THF (0.150 mL) and the reaction mixture was stirred for 30 minutes. Subsequently the reaction was quenched with water and the mixture was precipitated in an aqueous NH_4PF_6 solution. The aqueous phase was extracted with CH_2Cl_2. The combined organic extracts were concentrated under reduced pressure. The red solid was used without further purification (0.058 g, 100%). ^{1}H NMR (300 MHz, CD_2Cl_2): δ 9.04–8.15 (br, **pNDI**), 8.06 (br, Ru), 8.02 (br, Ru), 7.82 (br, Ru), 7.71 (br, Ru), 7.48 (br, Ru), 7.63–6.58 (br, **pNDI**), 5.59–5.46 (br, linker), 4.42–3.77 (br, **pNDI**), 3.04–1.55 (br, **pNDI**), 1.55–1.12 (br, **pNDI**), 1.00–0.59 (br, **pNDI**).

[Ru(dqp-O-pNDI)(dqp-ph-C≡C-tr-pCarb)][PF_6]$_2$ (D$_n$–P–A$_m$). A vial was charged with **D2-depro** (0.015 g, 0.0015 mmol, 1 eq.) and **pCarb** (0.019 g, 0.0045 mmol, 3 eq.), sealed and place under a nitrogen atmosphere. Then dry DMF (1.5 mL), a solution of copper(I) bromide (0.0004 g, 0.003 mmol, 2 eq.) in DMF (0.160 mL) and a solution of PMDETA (0.013 mL, 2 eq., 0.24 M in DMF) were added. The reaction mixture was heated to 80 °C for 96 h. After cooling to room temperature, the solution precipitated in an aqueous NH_4PF_6 solution and the aqueous layer was extracted with CH_2Cl_2 (4 ×). The combined organic phases were dried over Na_2SO_4 and concentrated under reduced pressure. Purification by preparative size-exclusion chromatography (Toyopearl HW-55F) gave the product as red solid (0.004 g, 19% + 0.010 g, 48% (with minor impurities of the dyad after first purification run) ^{1}H NMR (300 MHz, CD_2Cl_2): δ 8.88–8.15 (br, **pCarb** + **pNDI**), 8.06 (br, Ru), 7.85 (br, Ru + **pCarb**), 7.66 (br, Ru), 7.43 (br, Ru), 7.61–6.60 (br, **pCarb** + **pNDI**), 5.17–5.07 (br, linker), 4.48–3.71 (br, **pCarb** + **pNDI**), 3.08–1.71 (br, **pNDI**), 1.42–1.01 (br, **pCarb** + **pNDI**), 1.01–0.54 (br, **pCarb** + **pNDI**).

3. NMR data

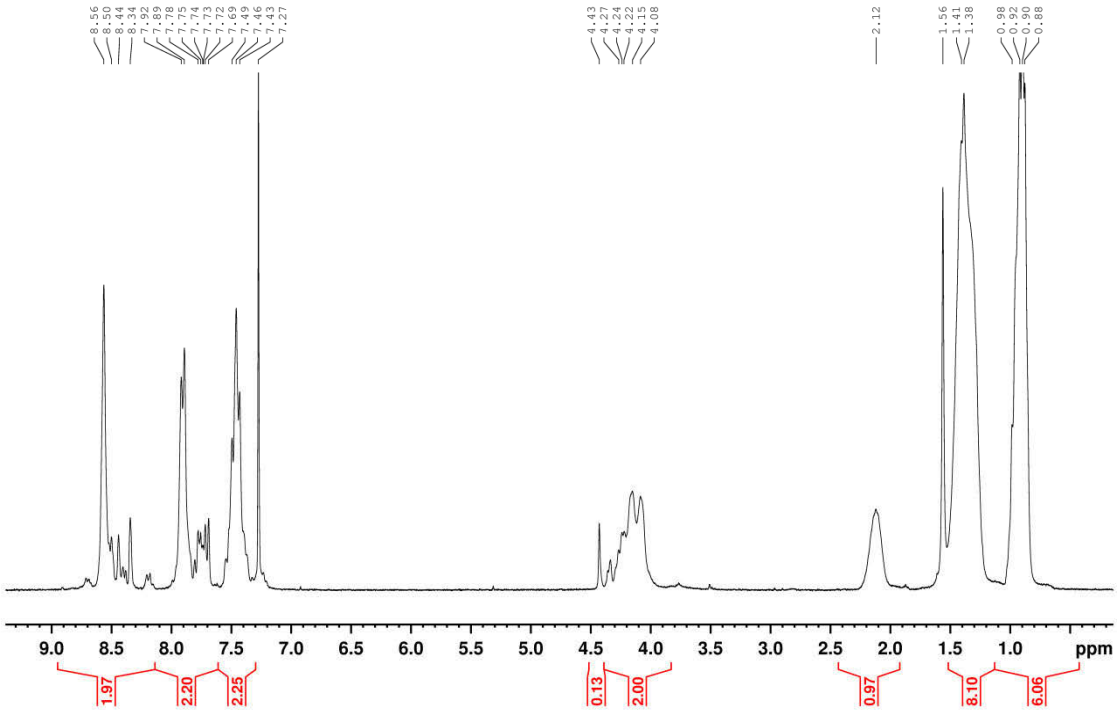

Figure S1. ^{1}H NMR spectrum (300 MHz, $CDCl_3$) of **pCarb**. The degree of polymerization (DP = 15) was estimated by comparison of the azide resonance (4.4 ppm, 0.13H) and the signal of the methylene group at 4.2 ppm (2H).

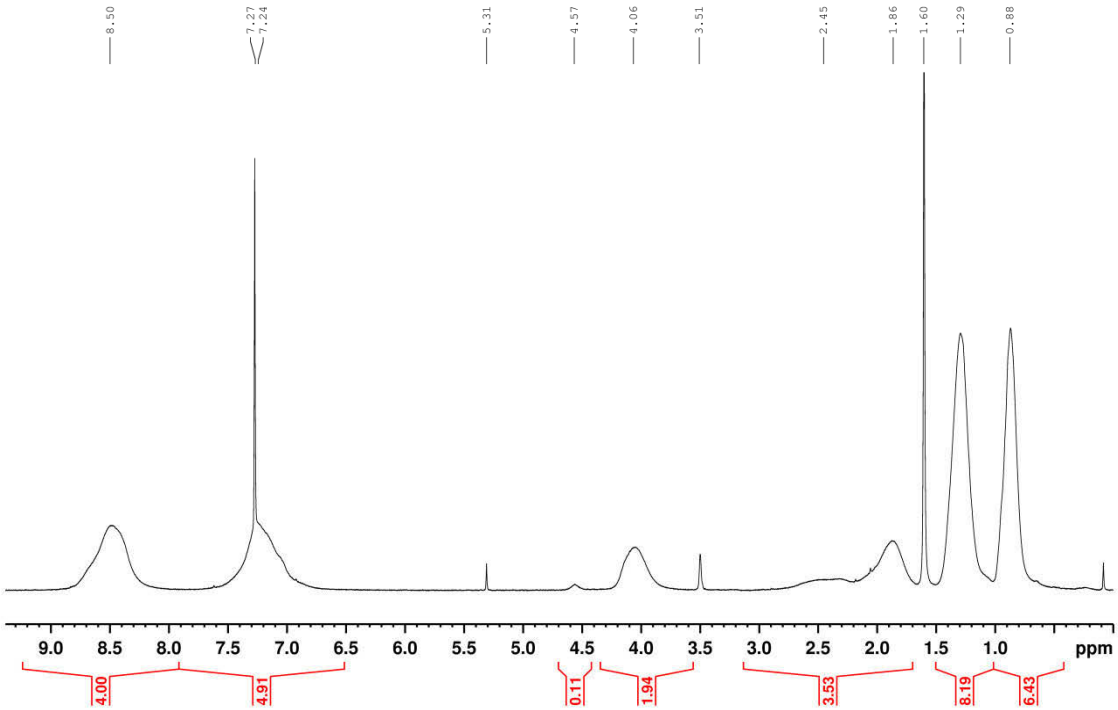

Figure S2. ^{1}H NMR Spectrum (300 MHz, $CDCl_3$) of **pNDI**. The degree of polymerization (DP = 18) was estimated by comparison of the chloromethyl resonance (4.6 ppm, 0.11H) and the signal of the NDI core at 4.2 ppm (4H).

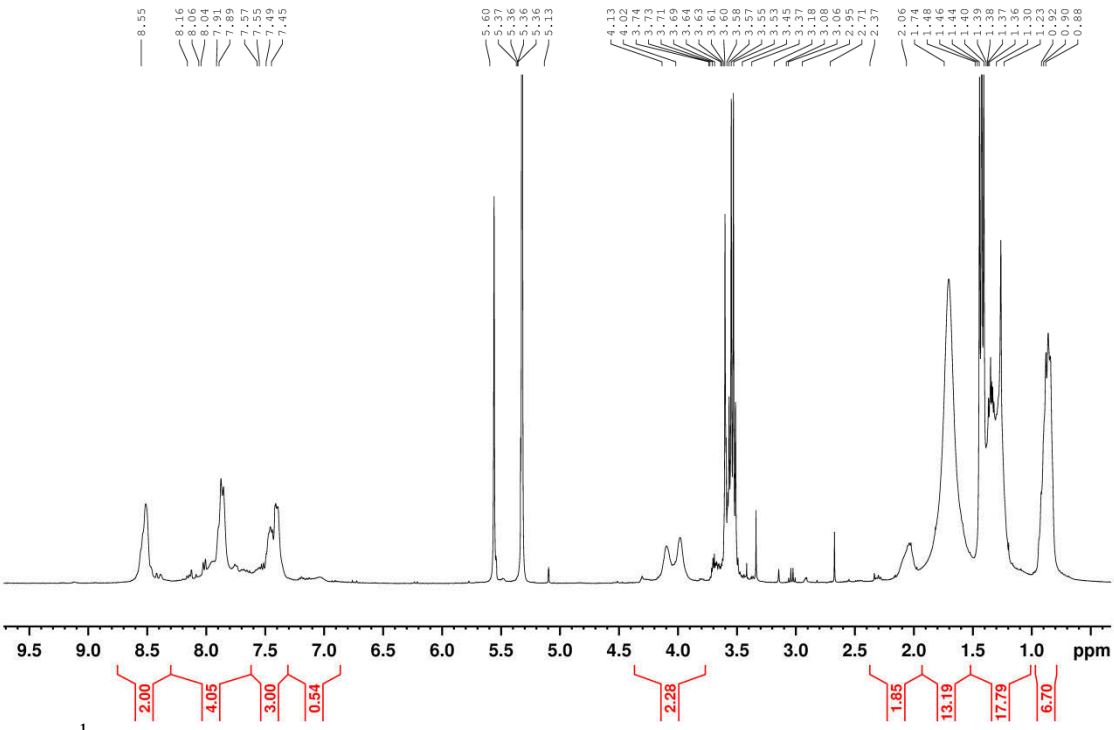

Figure S3. ^{1}H NMR spectrum (400 MHz, CD_2Cl_2) of $\mathbf{D_n}$**–P**.

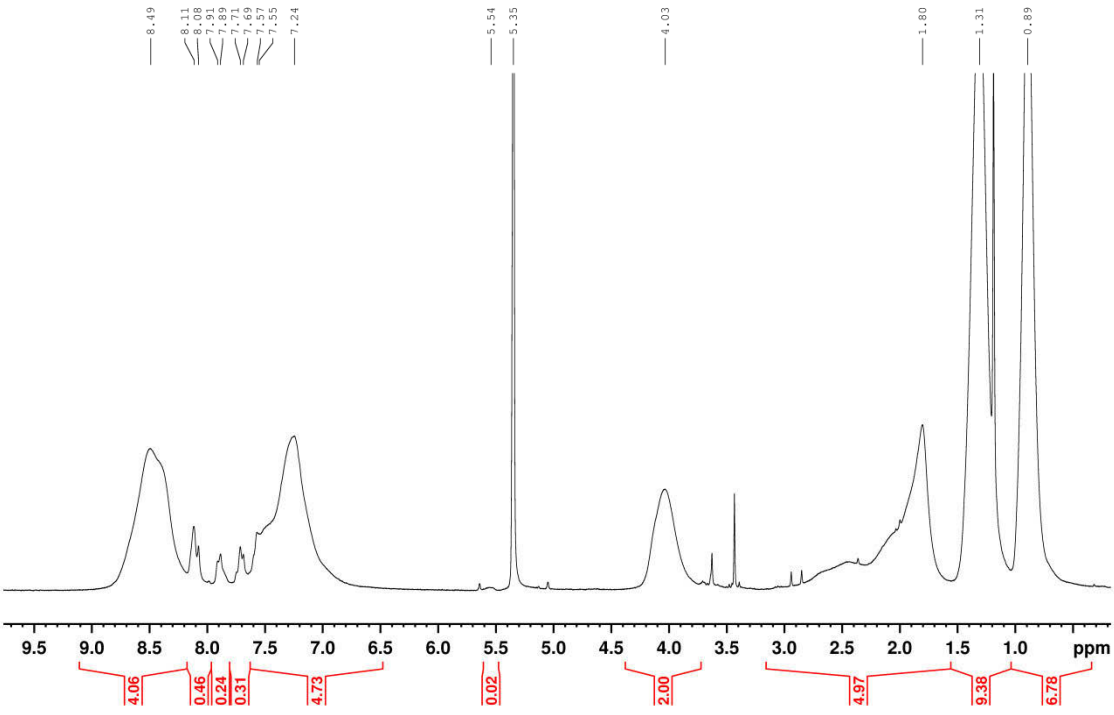

Figure S4. ^{1}H NMR spectrum (300 MHz, CD_2Cl_2) of **P–**$\mathbf{A_m}$.

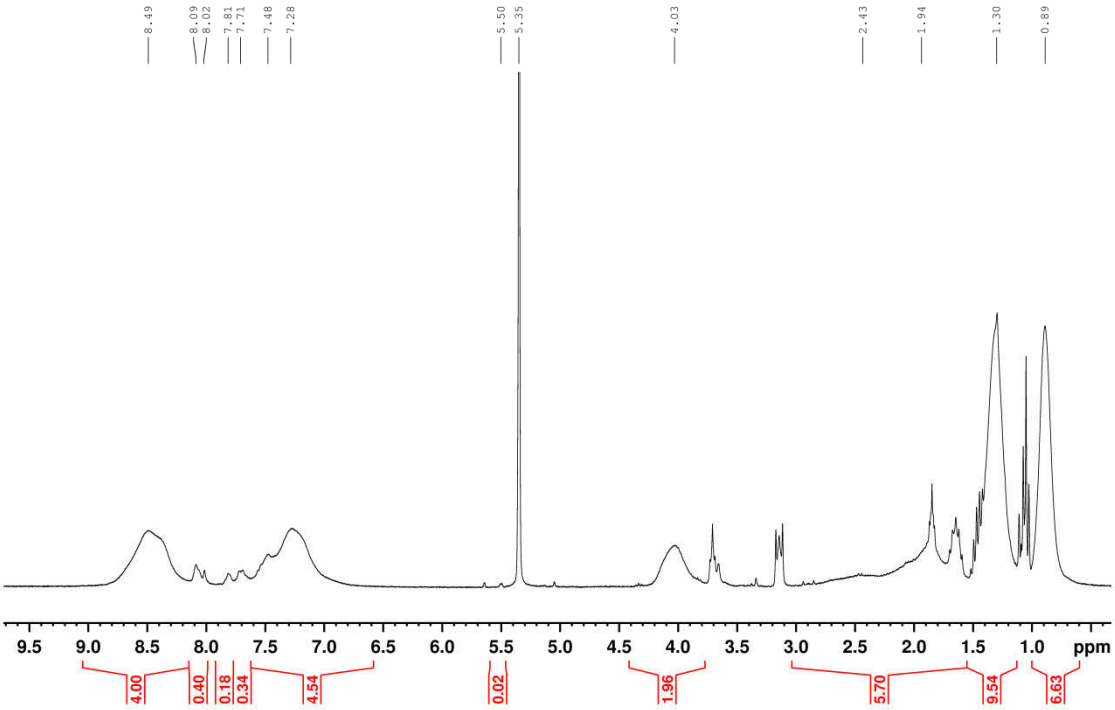

Figure S5. ^{1}H NMR spectrum (300 MHz, CD_2Cl_2) of deprotected **P–A$_m$**.

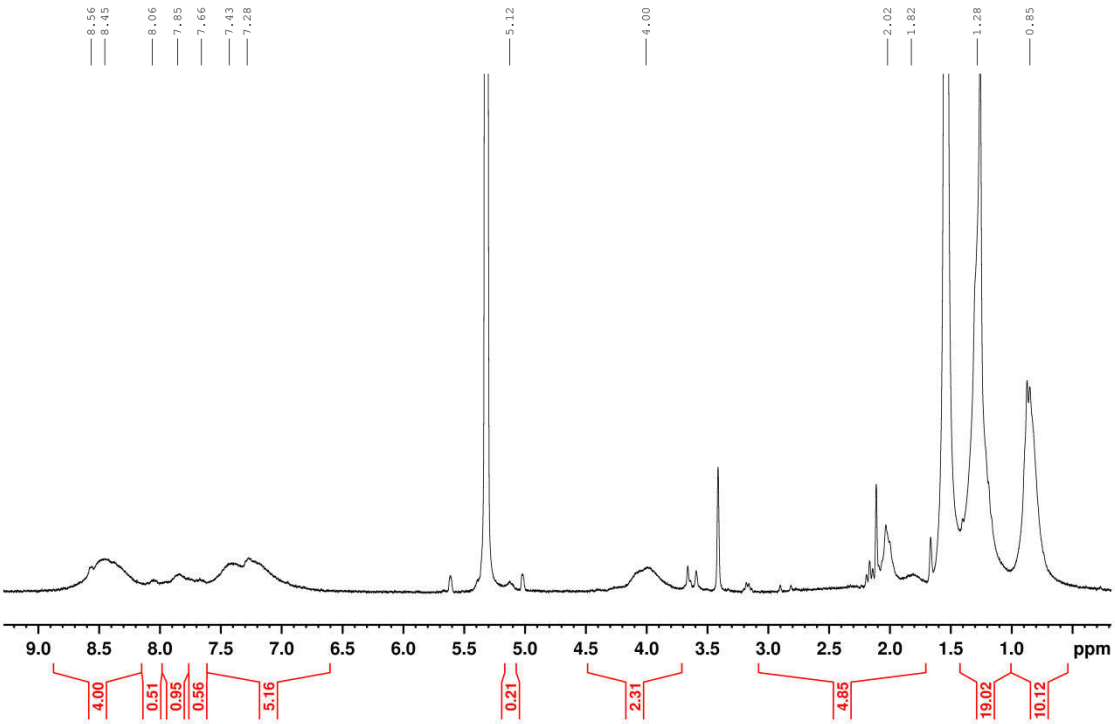

Figure S6. ^{1}H NMR spectrum (300 MHz, CD_2Cl_2) of **D$_n$–P–A$_m$**.

4. Mass spectra

We were not able to measure a useful mass spectrum of **pCarb** assigned to the known side and fragmentation reactions of azides during the ionization process.[8-9] Due to the small amount of isolated compound $\mathbf{D_n–P–A_m}$ and our hitherto gained experience with these kind of block copolymers, the recording of a MALDI-TOF mass spectrum was not tried to avoid a wasting of substance.

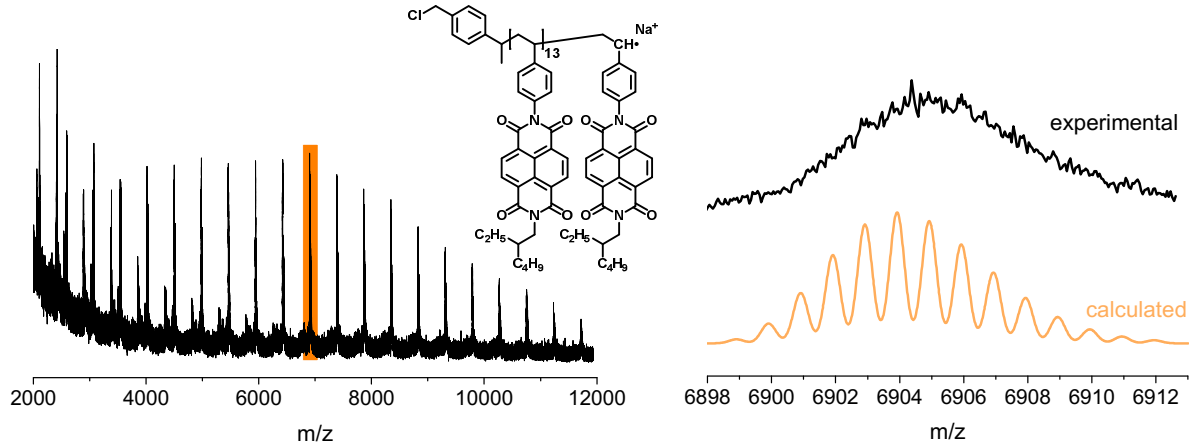

Figure S7. Left: MALDI-TOF mass spectrum of **pNDI**. Right: Experimental and calculated isotopic pattern of the highlighted signal with proposed structure of the fragment.

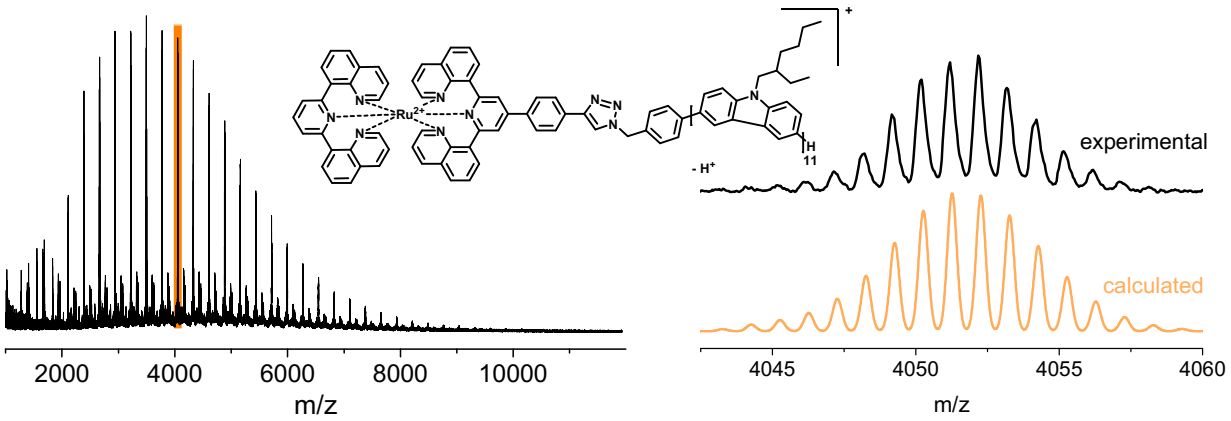

Figure S8. Left: MALDI-TOF mass spectrum of $\mathbf{D_n–P}$. Right: Experimental and calculated isotopic pattern of the highlighted signal with proposed structure of the fragment.

5. SEC data

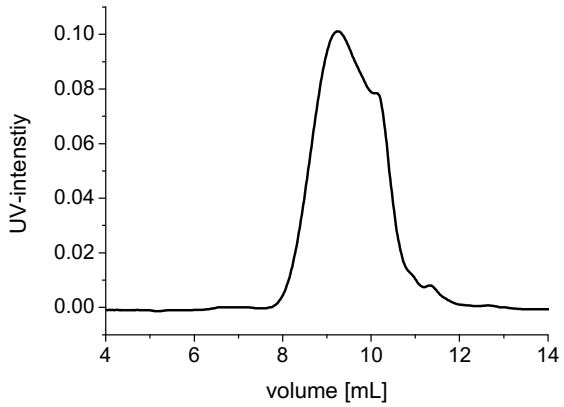

Figure S9. SEC elugram of **pCarb** (eluent: Chloroform/iso-propanol/triethylamine [94:2:4]).

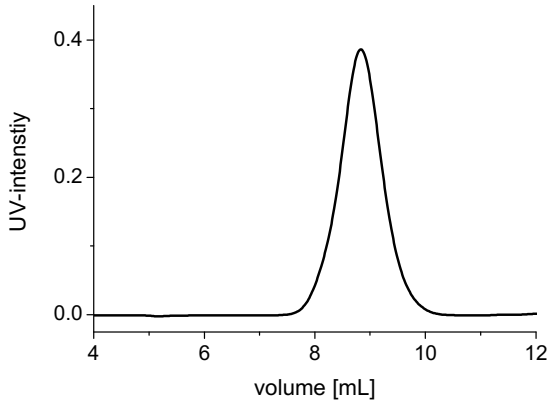

Figure S10. SEC elugram of **pNDI** (eluent: Chloroform/iso-propanol/triethylamine [94:2:4]).

6. Electrochemistry

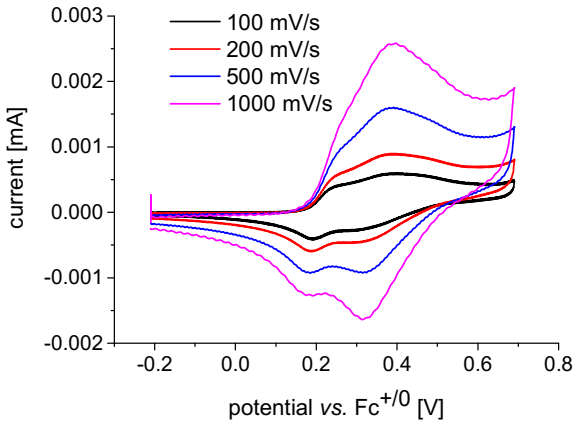

Figure S11. Cyclic voltammetry of **pCarb** (in CH_2Cl_2 containing 0.1 M $TBAPF_6$, potentials *vs.* ferrocene) at given scan rates. Note the formal redox potential at low scan rates of 0.22 V.

Driving force estimation for reductive quenching: The emission energy of the photosensitizer unit in **D_n–P** was calculated as 1.77 eV (λ_{em} = 700 nm, Figure S16) applying the correction as reported previously.[10] The redox potential of **pCarb** is taken as +0.22 V (Figure S11), while the Ru subunit in **D_n–P** was taken from the related poly(naphthalene diimide)-dyad featuring the identical substitution pattern with a formal ligand reduction at −1.79 V *vs.* $Fc^{+/0}$.[2] The calculated Ru excited state oxidation potential is −0.02 V, so that the formal driving force for reductive quenching is +0.24 V. This value represents a conservative upper bound estimate, as the (attractive) coulombic work term (the electron is transferred to the Ru^{II} ion), and favorable entropic factors due to the multiple donor sites are neglected. The results are in line with a previous report on the **pTARA**-based dyad, whose redox potential is anodically shifted (by +150 mV to +0.38 V) and shows no sign of reductive quenching.[11]

7. Spectroelectrochemistry and Redox-titration

The **pNDI**$^-$ was recorded in DMF, in order to estimate the extent of spectral changes, which may arise from the polymer-bound diimide subunits. Indeed, identical maxima at 475 nm and 610 nm were observed for **pNDI**$^-$ (Figure S12), so that subsequent measurements were performed in dichloromethane. The redox titration of poly(carbazole) revealed a decrease of the UV absorption bands (<360 nm) and new bands at 430 nm and above 600 nm for **pCarb**$^+$ (Figure S13).

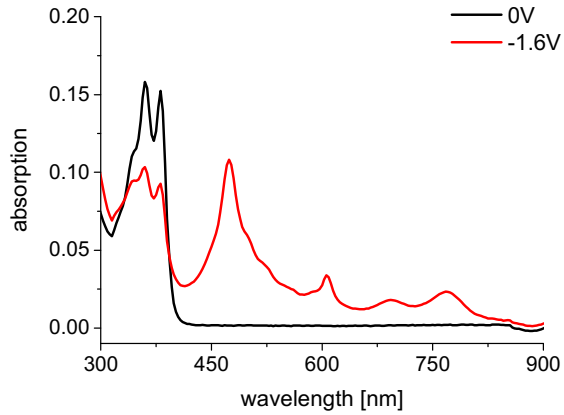

Figure S12. Spectroelectrochemical data of a **pNDI** showing characteristic reduction peaks at 475 and 610 nm (RE: Ag/AgCl/H_2O, CE: Pt, WE: Pt-Grid, 0.1M $TBAPF_6$ in DMF).

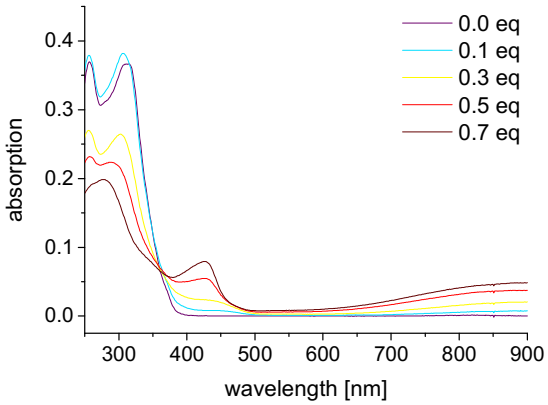

Figure S13. Redox titration of polymer **pCarb** with $SbCl_5$ solution (in aerated CH_2Cl_2, RT) showing the evolution of new absorption bands at 430 nm and above 600 nm.

8. Photophysical characterization

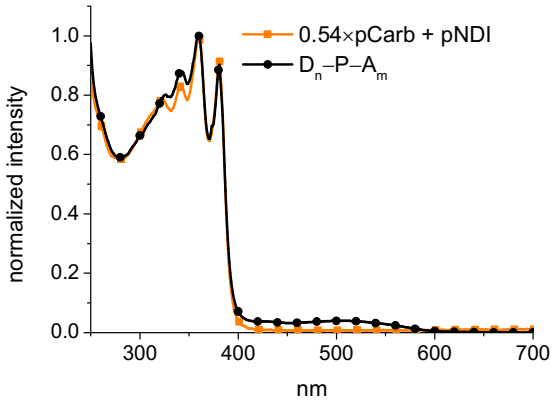

Figure S14. Absorption spectra of $\mathbf{D_n–P–A_m}$ in comparison to the linear combination of **pCarb** and **pNDI** to illustrate the accumulating contributions of both polymers (aerated CH_2Cl_2, RT).

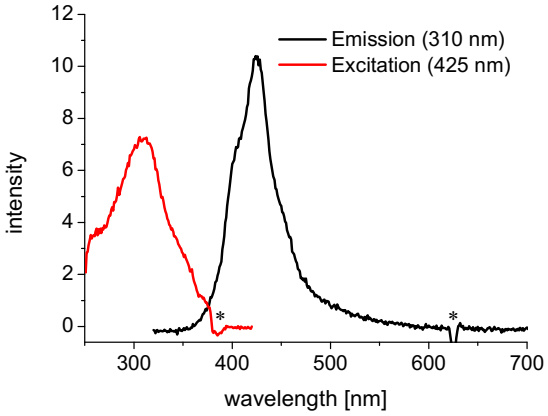

Figure S15. Non-corrected steady-state emission spectrum of **pCarb** after excitation at 310 nm (black) and respective excitation spectrum (red, emission wavelength 425 nm, aerated CH_2Cl_2, RT). Artefacts are marked with an asterisk.

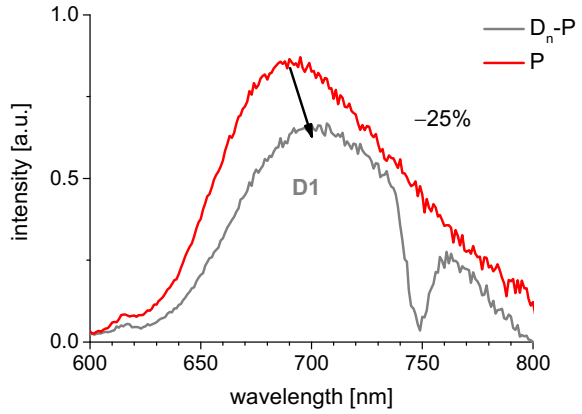

Figure S16. Corrected emission data of $\mathbf{D_n–P}$ and the suitable reference complex (aerated CH_2Cl_2, RT, iso-absorbing solutions at excitation wavelength (500 nm). The dyad $\mathbf{D_n–P}$ features a decreased Ru(II) emission. Spectral artefact from background correction due to Raman bands of the solvent (750 nm).

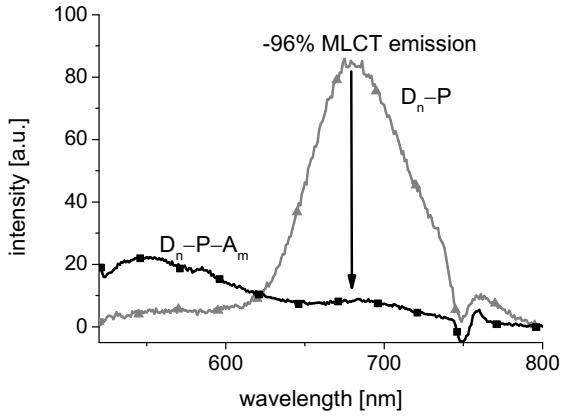

Figure S17. Non-corrected steady-state emission spectra of $\mathbf{D_n–P}$ and $\mathbf{D_n–P–A_m}$ after excitation at 500 nm (^{1}MLCT band) demonstrate efficient emission quenching in $\mathbf{D_n–P–A_m}$.

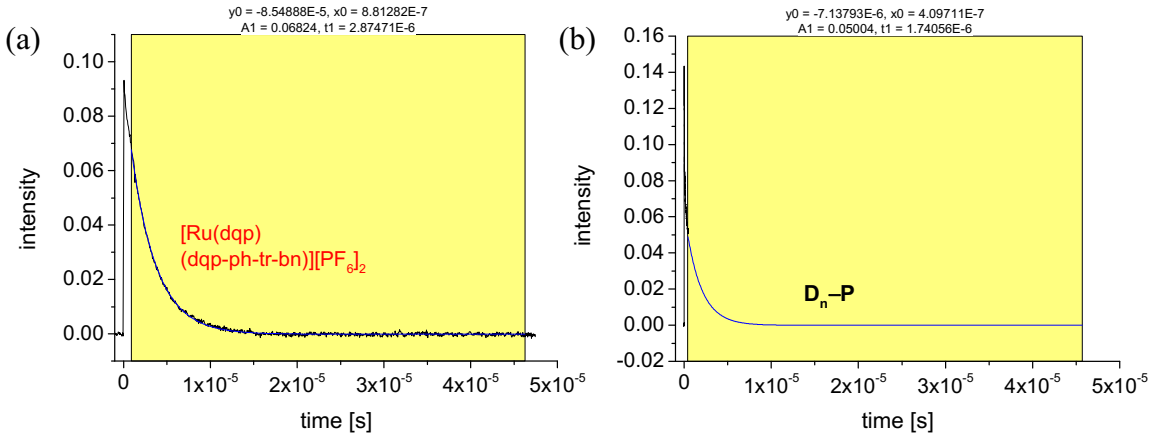

Figure S18. Emission decay and respective fits to determine the excited state life-time (t_1) of **P** (a, λ_{em} = 700 nm) and $\mathbf{D_n–P}$ (b, λ_{em} = 750 nm to minimize residual polymer based emission). Measurements in N_2-purged CH_2Cl_2, optical density approx. 0.1 at 500 nm, laser pulse at 500 nm.

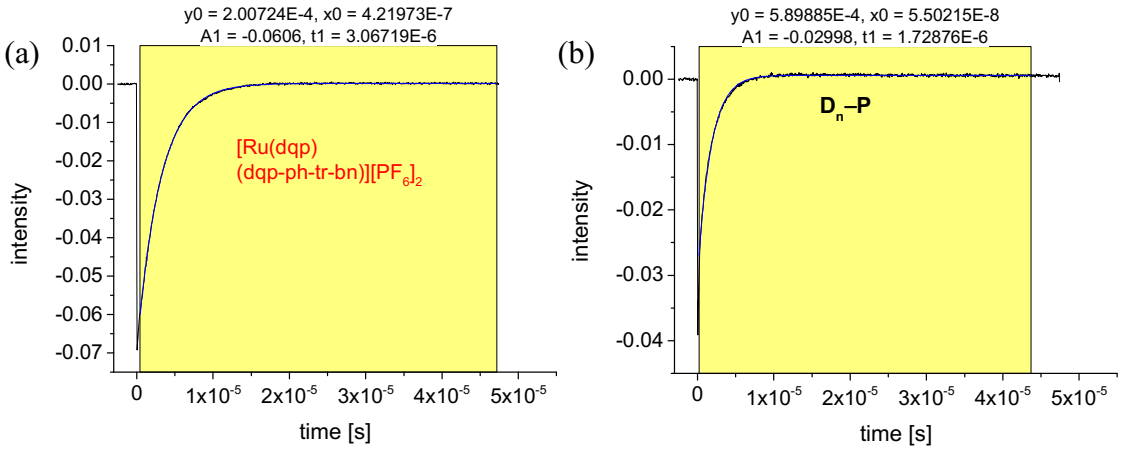

Figure S19. TA ^{1}MLCT bleach decay and respective fits to determine the excited state life-time (t_1) of **P** (a) and **D_n–P** (b). Measurements in N_2-purged CH_2Cl_2, optical density approx. 0.1 at 500 nm, laser pulse at 500 nm, trace at 470 nm.

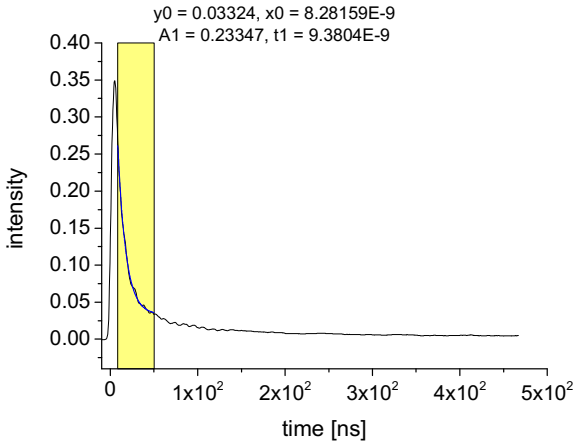

Figure S20. Emission decay trace of **D_n–P–A_m** at 750 nm to determine the life time of the residual Ru(II) ^{3}MLCT emission. Measurements in purged CH_2Cl_2, optical density approx. 0.1 at 500 nm, laser pulse at 500 nm.

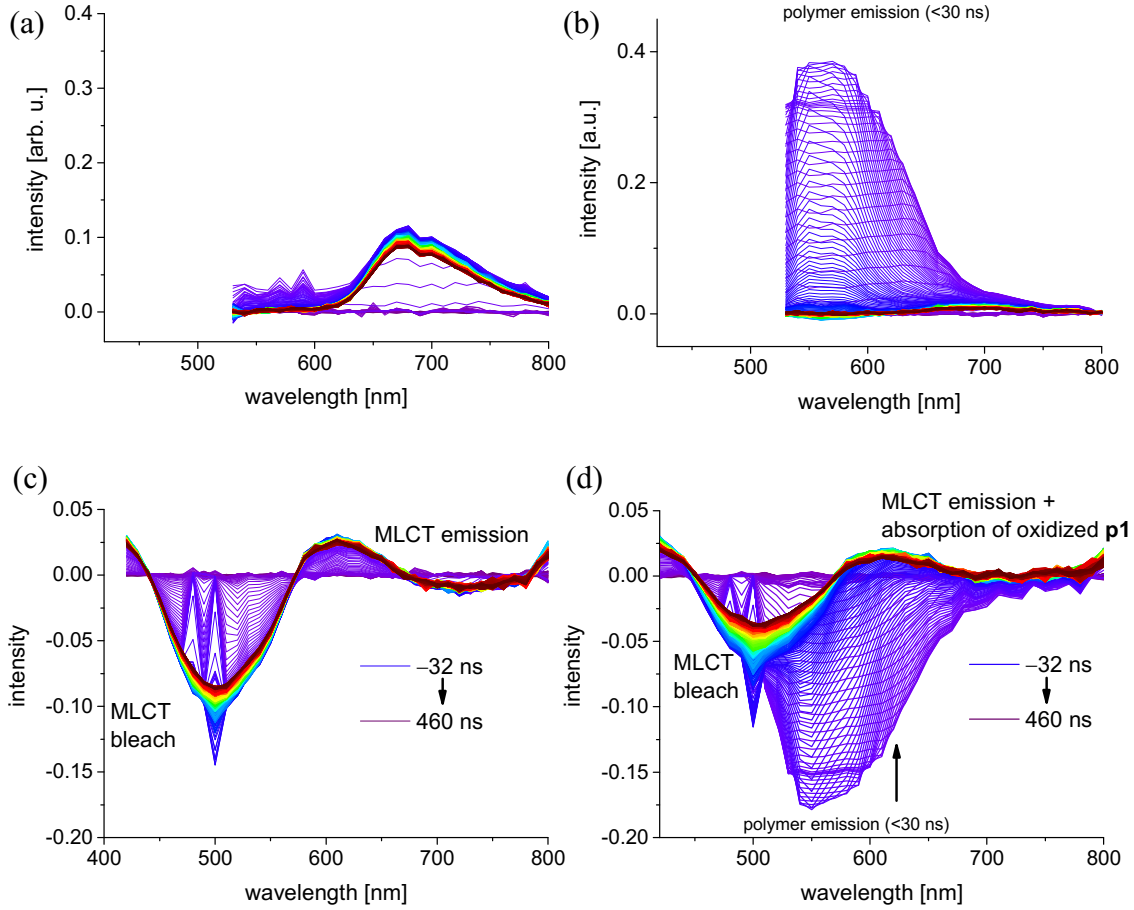

Figure S21. Comparison of emission (a and b) and transient absorption data (c and d) of **P** (a and c) and **D_n–P** (b and d) showing polymer emission as well as an additional absorption above 600 nm due to a the linkage of the Ru(II) complex to the polymer **pCarb** (purged CH_2Cl_2, optical density approx. 0.1 at 500 nm, laser pulse at 500 nm). After the decay of the polymer emission (<30 ns), the TA profile of **D_n–P** features bathochromically shifted isosbestic points (in comparison to the reference complex) and positive TA signals >650 nm. This observation parallels the positive spectral contributions of **pCarb**$^+$ around 430 nm, and isosbestic point).

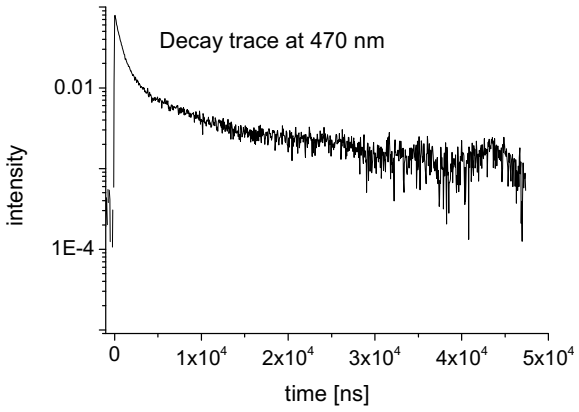

Figure S22. TA decay trace of **D_n–P–A_m** at 475 nm after excitation with a laser pulse at 500 nm. The multiexponential decay is indicated by the not-linear behavior despite the logarithmic y-axis (purged CH_2Cl_2, optical density approx. 0.1 at 500 nm).

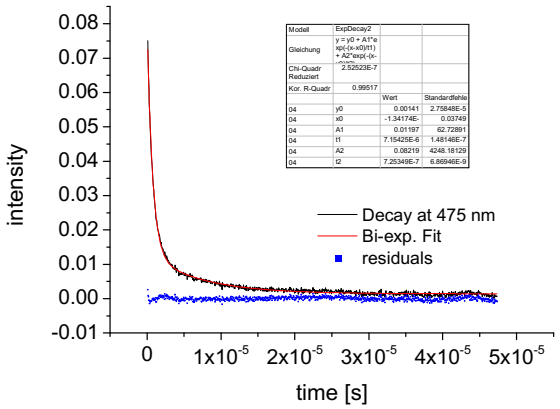

Figure S23. Bi-exponential fit of the TA decay curve at 475 nm for $\mathbf{D_n–P–A_m}$ to determine the live-times of the underlying processes (purged CH_2Cl_2, optical density approx. 0.1 at 500 nm, laser pulse at 500 nm).

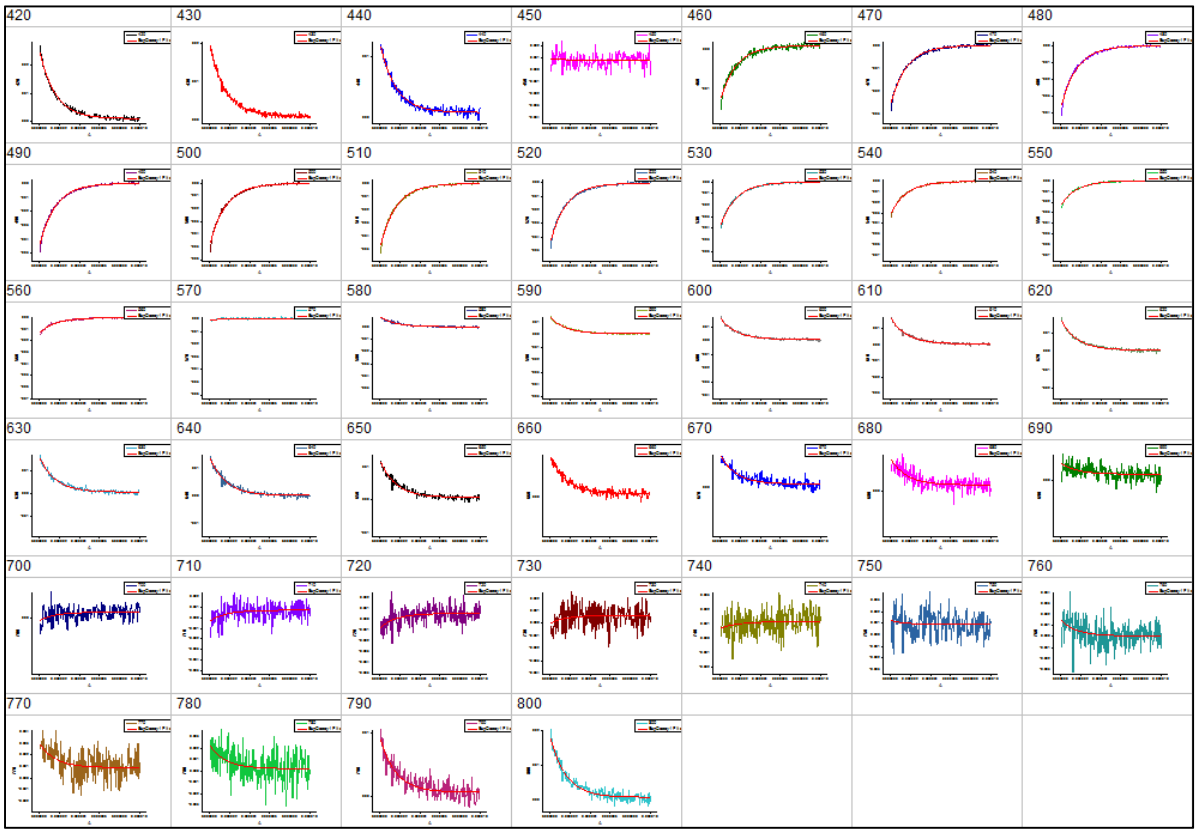

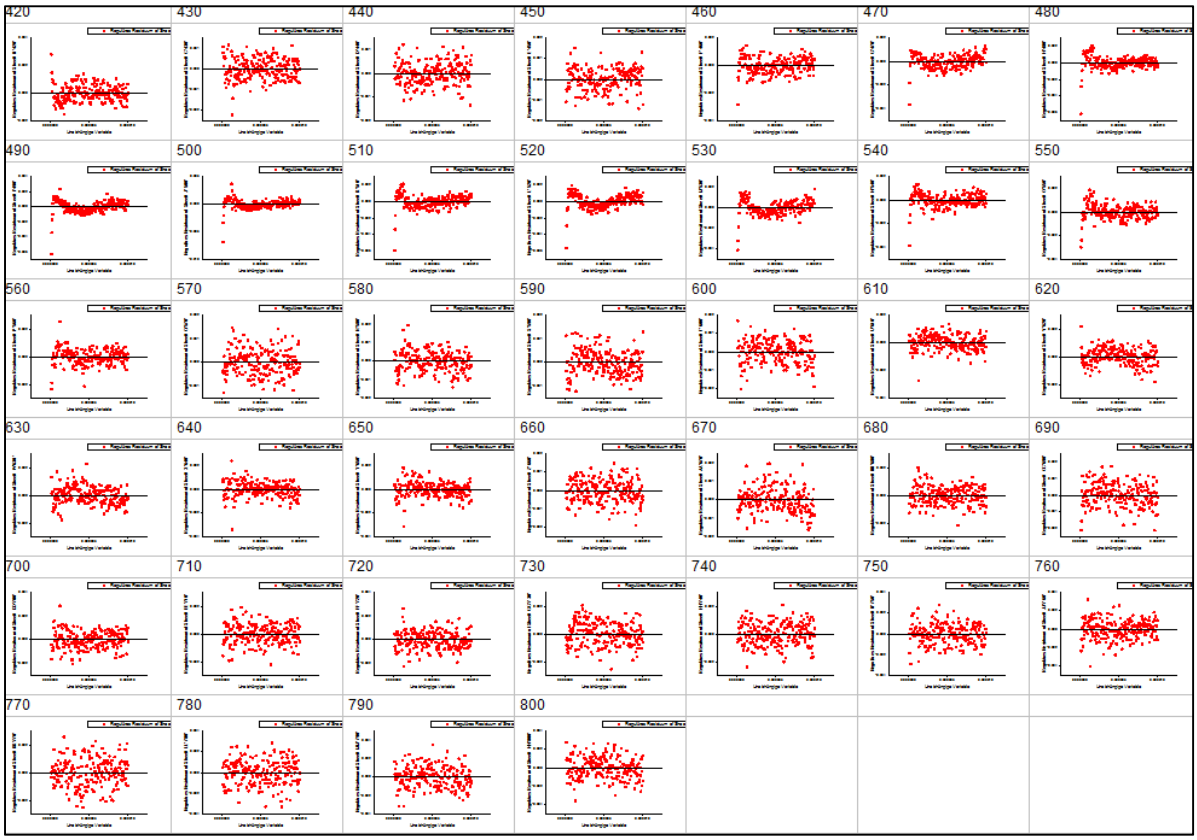

Figure S24. Global biexponential decay fit of $\mathbf{D_n–P–A_m}$. (Top) TA data and fit curve and (bottom) residuals. See Figure S25 for spectral profiles of the two components (0.7 µs and 6.8 µs).

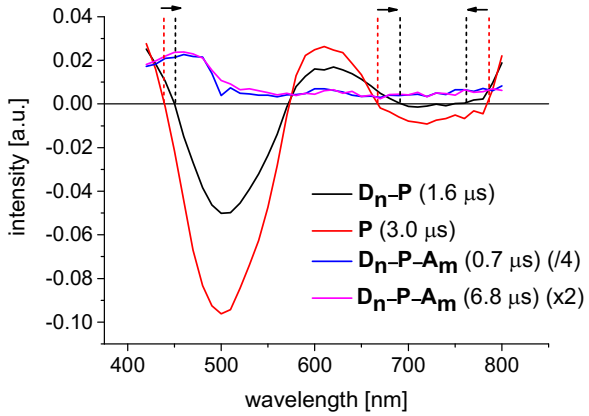

Figure S25. Comparison of TA profiles obtained from the global fit of the TA data with associated lifetimes: **P** (red, 3.0 µs), $\mathbf{D_n–P}$ (black, 1.6 µs) and $\mathbf{D_n–P–A_m}$ with first (blue, 0.7 µs) and second component (magenta, 6.8 µs). Note the same spectral feature of the two components $\mathbf{D_n–P–A_m}$. Note the indicative shifts of isosbestic points for $\mathbf{D_n–P}$ *vs.* **P** marked by dashed lines and arrows. The changes resemble the charge-separated state ($\mathbf{D_n^+–Ru^-}$), *i.e.* the positive TA contribution from $\mathbf{pCarb^+}$ (see Figure S13) leading to bathochromic shifts around 450 and 700 nm, but a hypsochromic shift at 750 nm.

9. References

[1] G. R. Fulmer, A. J. M. Miller, N. H. Sherden, H. E. Gottlieb, A. Nudelman, B. M. Stoltz, J. E. Bercaw, K. I. Goldberg, *Organometallics* **2010**, *29*, 2176-2179.

[2] R. Schroot, T. Schlotthauer, U. S. Schubert, M. Jäger, *Macromolecules* **2016**, *49*, 2112-2123.

[3] K. Smith, D. M. James, A. G. Mistry, M. R. Bye, D. J. Faulkner, *Tetrahedron* **1992**, *48*, 7479-7488.

[4] R. Schroot, U. S. Schubert, M. Jäger, *Macromolecules* **2017**, *50*, 1319-1330.

[5] J. K. Lee, S. Ko, Z. Bao, *Macromol. Rapid Commun.* **2012**, *33*, 938-942.
[6] M. Abrahamsson, M. Jäger, R. J. Kumar, T. Österman, P. Persson, H.-C. Becker, O. Johansson, L. Hammarström, *J. Am. Chem. Soc.* **2008**, *130*, 15533-15542.
[7] T. Schlotthauer, S. Glover, R. Schroot, U. S. Schubert, L. Hammarström, M. Jäger, *submitted* **2017**.
[8] R. M. Pinto, R. I. Olariu, J. Lameiras, F. T. Martins, A. A. Dias, G. J. Langley, P. Rodrigues, C. D. Maycock, J. P. Santos, M. F. Duarte, M. T. Fernandez, M. L. Costa, *J. Mol. Struct.* **2010**, *980*, 163-171.
[9] Y. Li, J. N. Hoskins, S. G. Sreerama, S. M. Grayson, *Macromolecules* **2010**, *43*, 6225-6228.
[10] T. Schlotthauer, B. Suchland, H. Görls, G. A. Parada, L. Hammarström, U. S. Schubert, M. Jäger, *Inorg. Chem.* **2016**, *55*, 5405-5416.
[11] J. Kübel, R. Schroot, M. Wächtler, U. S. Schubert, B. Dietzek, M. Jäger, *J. Phys. Chem. C* **2015**, *119*, 4742-4751.

Published Publication P6

Extending Long-lived Charge Separation Between Donor and Acceptor Blocks in Novel Copolymer Architectures Featuring a Sensitizer Core

R. Schroot, T. Schlotthauer, B. Dietzek, M. Jäger, U. S. Schubert, *Chem. Eur. J.* **2017**, *23*, 16484-16490.

The paper as well as the supporting information (free of charge) are available online under: doi.org/10.1002/chem.201704180

ChemPubSoc Europe

DOI: 10.1002/chem.201704180

CHEMISTRY
A European Journal
Full Paper

Donor–Acceptor Systems | *Hot Paper*

Extending Long-lived Charge Separation Between Donor and Acceptor Blocks in Novel Copolymer Architectures Featuring a Sensitizer Core

Robert Schroot,[a, b] Tina Schlotthauer,[a, b] Benjamin Dietzek,[b, c] Michael Jäger,*[a, b] and Ulrich S. Schubert*[a, b]

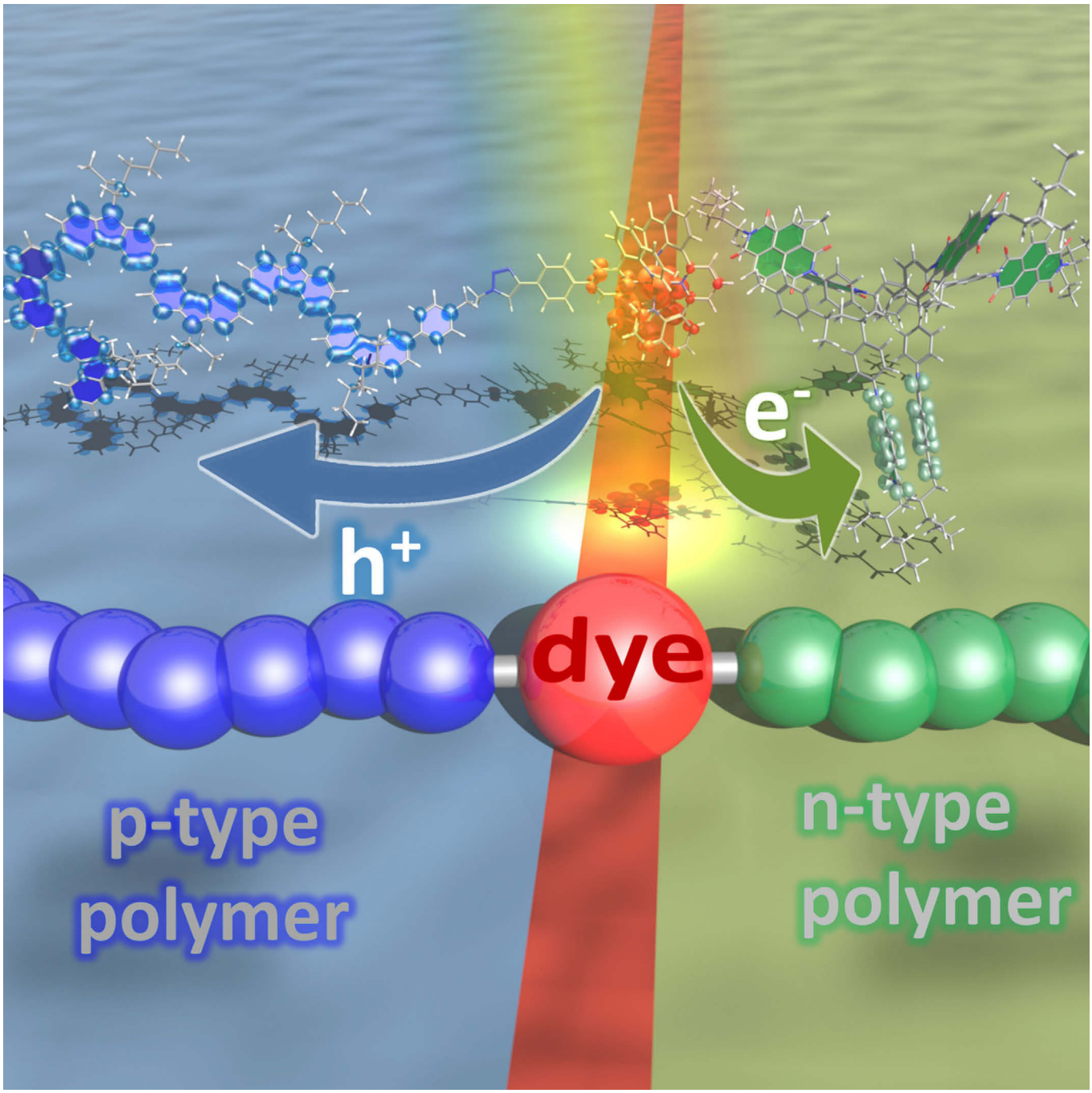

Abstract: A bifunctional Ru^{II} photosensitizer unit was decorated with one n- and one p-type polymer chain to form precisely controlled hierarchical copolymer-type architectures for light-induced charge separation. The applied modular chemistry-on-the-complex strategy benefits from separately prepared building blocks and their orthogonal linkage in the two final assembly steps. Upon visible light absorption, electron transfer is initiated between the conjugated poly(3,6-carbazole) chain and the styrenic poly(naphthalene diimide) segments. Steady-state and time-resolved spectroscopy show complete charge separation within a few nanoseconds (>95% efficiency) persisting several tens of microseconds. The recombination is significantly reduced in comparison to low-molecular model systems or to non-conjugated congeners, reflecting the higher charge mobility in conjugated polymers. In summary, the modularity of the presented approach is expected to serve as a versatile platform to tailor the interface between the charge transport domains in a systematic fashion.

Introduction

The efficient interconversion of photoenergy into electrical or chemical bond energy can be achieved, among other ways, by molecular photosystems composed of functional building blocks.[1–6] The versatility of this approach relies on precisely tailored units for light absorption and charge separation, as demonstrated in molecular triads reaching impressive quantum efficiencies (up to 95%).[2] After photon absorption by the photosensitizer (**P**), electron transfer steps occur to the attached donor (**D**) and/or acceptor (**A**) sites and the individual rates are controlled by the nature of the linkage (bridge).[7–11] Very long charge-separated (CS) lifetimes exceeding the microsecond timescale can be achieved,[12] for example, to harness the generated electrochemical potential in photovoltaic or by coupled catalytic processes. In this regard, Ru^{II} polypyridyl-type complexes often serve as versatile photosensitizer owing to their remarkable excited state properties.[13] In molecular **D–P–A** systems, the charges reside ultimately on the single donor and acceptor sites and often inevitably recombine, before they can be harnessed. Hence, the incorporation of multiple donor/acceptor sites is attractive, but the convergent syntheses are often (prohibitively) elaborate in the case of low-molecular model systems.

[a] *R. Schroot, T. Schlotthauer, Dr. M. Jäger, Prof. Dr. U. S. Schubert*
Laboratory of Organic and Macromolecular Chemistry (IOMC)
Friedrich Schiller University Jena
Humboldtstraße 10, 07743 Jena (Germany)
E-mail: michael.jager.iomc@uni-jena.de
ulrich.schubert@uni-jena.de

[b] *R. Schroot, T. Schlotthauer, Prof. Dr. B. Dietzek, Dr. M. Jäger, Prof. Dr. U. S. Schubert*
Center for Energy and Environmental Chemistry Jena (CEEC Jena)
Friedrich Schiller University Jena
Philosophenweg 7a, 07743 Jena (Germany)

[c] *Prof. Dr. B. Dietzek*
Institute for Physical Chemistry and Abbe Center of Photonics (ACP)
Friedrich Schiller University Jena
Helmholtzweg 4, 07743 Jena (Germany)
and
Leibniz Institute for Photonic Technology (IPHT)
Albert-Einstein-Straße 9, 07743 Jena (Germany)

Supporting information and the ORCID identification number(s) for the author(s) of this article can be found under https://doi.org/10.1002/chem.201704180.

Alternatively, polymer chemistry offers an elegant route to tailored photo- and electrochemically active macromolecules,[14] which a priori provide charge percolation pathways, can perform charge accumulation as well as a phase segregation of the donor/acceptor domains—in close resemblance of modern organic photovoltaics.[15–21] The versatility to design and construct macromolecular photosystems is evident from the reports on Ru-decorated oligopeptides,[15,16] poly(styrene)s,[18] poly(acrylates)s,[19] poly(thiophene)s,[22] poly(fluorene)[21] or poly(fluorene-*co*-thiophene).[20] Notably, most of the early examples comprised statistical assemblies and/or grafted macromolecules, mainly due to the available polymerization techniques (and their limitations) at that time. As a consequence, most of the aforementioned macromolecules are devoid of charge percolation pathways, despite their simple preparation. In order to diminish unfruitful recombination of the photo-generated charges, the (macro)molecular assembly must sustain charge transport, for example, to reach external electrodes or catalytically active sites. The recent advances in polymer science enables an a priori design and the facile preparation of well-defined functional macromolecules from photo- and redox-active building blocks. In other words, functionalized polymers can be tailored and prepared (e.g., multi-donor ($\mathbf{D_n}$) and multi-acceptor ($\mathbf{A_m}$) polymers) with the desired optoelectronic properties.[14] More importantly, such building blocks can be interconnected afterwards through the chain end's functional group in a modular fashion, leading to advanced architectures. In addition, such divergent syntheses further minimize substantially the synthetic efforts, which permits the systematic exploration of $\mathbf{D_n}$–**P**–$\mathbf{A_m}$ architectures. Recently, we reported the facile synthesis of telechelic poly(triarylamine) and poly(naphthalene diimide) by nitroxide-mediated polymerization (NMP), and their facile modular assembly was reported for various dyads ($\mathbf{D_n}$–**P** or **P**–$\mathbf{A_m}$).[23–27] Notably, the efficient charge separation upon excitation was demonstrated,[25,28] revealing a remarkably long-lived component (2,400 ns) that is tentatively assigned to charge migration within the polymer.

In this contribution, the poly(triarylamine) block of the previous $\mathbf{D_n}$–**P**–$\mathbf{A_m}$ architecture was replaced by a conjugated telechelic poly(3,6-*N*-alkylcarbazole), since conjugated polymers are known to feature higher charge charrier mobilities[29–35] and, thus, may prolong the CS life time.

Results and Discussion

Synthesis and characterization

The desired triad can be readily prepared due to the chosen modular character of the-chemistry-on-the-complex approach as outlined in Scheme 1. The individual syntheses of the poly(3,6-carbazole) (**pCarb**),[36] the poly(naphthalene diimide) (**pNDI**),[24] and the bis-functionalized Ru^{II} precursor complex[24,28] have been reported. The novel donor dyad $\mathbf{D_n}$–**P** was prepared from telechelic poly(3,6,-carbazole) via the copper(I) catalyzed azide–alkyne cycloaddition (CuAAC). The applied reagents, that is, $Cu^{I}Br$ as catalyst, PMDETA as base and DMF as solvent are known to be efficient for the linkage of related azide-decorated polymers with complexes.[24] However, longer reaction times and elevated temperatures were required as shown by analytical size-exclusion chromatography (SEC) and TLC analysis. The purification was conveniently accomplished by preparative SEC using a commercial resin (Toyopearl HW-55F). The successful linkage was confirmed by UV/Vis SEC analysis and MALDI-TOF mass spectrometry (Figure S8). The synthesis of the corresponding reference complex (**P**) was reported previously,[24] whereas the synthesis of the triad embarked from the bis-functionalized Ru^{II} precursor (X = OH).[28] First, the precursor dyad $\mathbf{P–A_m}$ was prepared analogously to our established protocols.[24] The nucleophilic substitution of the hydroxyl group with benzyl-halide decorated poly(naphthalene diimide) afforded $\mathbf{P–A_m}$ in very good yields (75%). Next, the terminal alkyne group was quantitatively deprotected with (nBu$_4$)NF without the need of chromatographic purification. The final coupling step by CuAAC as described above gave the desired $\mathbf{D_n–P–A_m}$ triad. Notably, an excess of the donor polymer was used to account for residual macrocycles,[36] which cannot undergo coupling and are readily separated by preparative SEC. In contrast, the removal of unreacted acceptor dyad to obtain pure $\mathbf{D_n–P–A_m}$ was more challenging due to the marginal increase in molar mass of the triad versus the dyad. This hypothesis is corroborated by the ^{1}H NMR spectra of **pCarb**, $\mathbf{P–A_m}$ and $\mathbf{D_n–P–A_m}$ (Figure 1), which reveal the characteristic but weak resonances of the poly(carbazole) in the final $\mathbf{D_n–P–A_m}$ triad. Although no MS data could be obtained to confirm the covalent linkage, the comprehensive 3D SEC analysis strongly suggests the covalent linkage. As expected, the elution profiles feature mono-modal distributions with decreased elution times due to the increased size (hydrodynamic volume) of the compounds, and the associated UV/Vis spectra correspond to the building blocks (see Supporting Information Section 5 for explanation and Figures S11–S15).

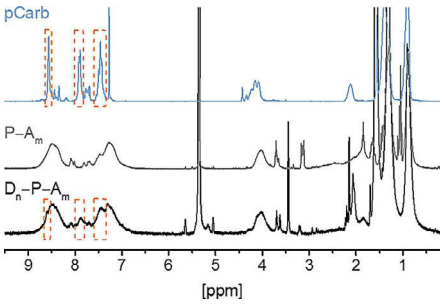

Figure 1. Proton NMR spectra of **pCarb**, $\mathbf{P–A_m}$ and $\mathbf{D_n–P–A_m}$ (300 MHz, $CDCl_3$ or CD_2Cl_2). The appearance of broad resonances of pCarb at approximately 7.4, 7.9 and 8.6 ppm (orange doted boxes) indicates the successful preparation of the triad $\mathbf{D_n–P–A_m}$. Note residual solvent signals in the aliphatic region of the triad.

Steady-state spectroscopy

The photophysical properties of the triad and the respective subsystems were investigated by steady-state and time-resolved spectroscopy. The light-induced electron transfer within the acceptor dyad $\mathbf{P–A_m}$ has been established previously,[24,25] hence we deliberately limit the discussion to the reference photosensitizer (**P**), the novel donor dyad ($\mathbf{D_n–P}$) and the final $\mathbf{D_n–P–A_m}$ triad. Figure 2 depicts the absorption spectra of the new compounds, which display the additive spectral features

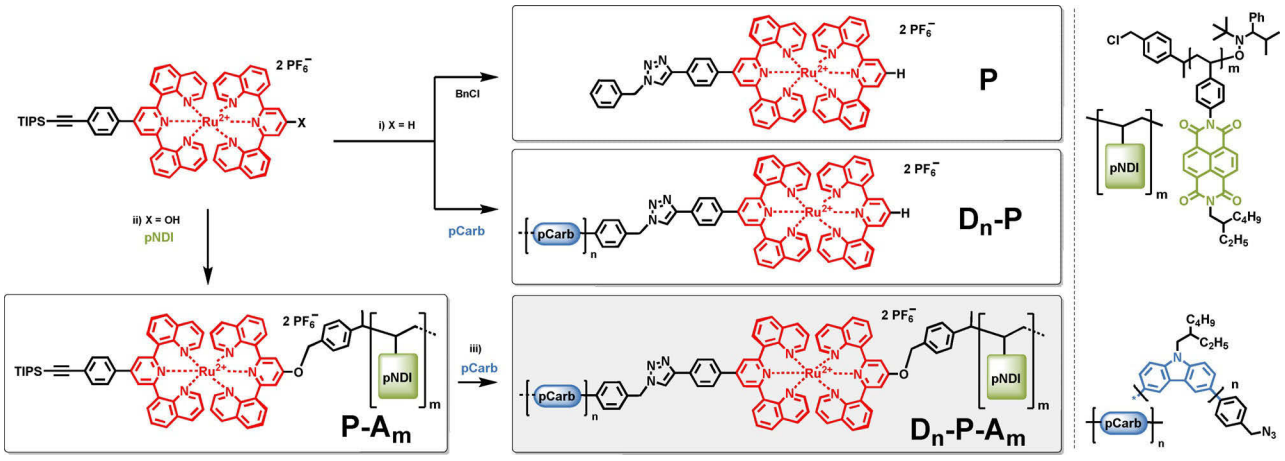

Scheme 1. Modular assembly of the photosystem $\mathbf{D_n–P–A_m}$ (grey shaded) including the reference subsystems **P**, $\mathbf{D_n–P}$, and $\mathbf{P–A_m}$ (black boxes) starting from building blocks: Bis-functionalized Ru-precursor (red) and telechelic polymers **pCarb** (blue) and **pNDI** (green). See right side for chemical structures. Reagents and conditions: i) CuBr, PMDETA, DMF, N_2, 80 °C, 101 h; ii) K_2CO_3, KI, DMF, N_2, 60 °C, 77 h; iii) (a) (nBu$_4$)NF·H_2O, THF, (b) CuBr, PMDETA, DMF, N_2, 80 °C, 96 h.

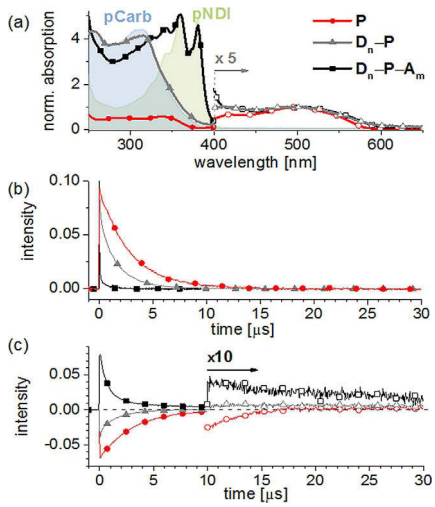

Figure 2. (a) Normalized absorption spectra of $\mathbf{D_n}$–**P** (grey), $\mathbf{D_n}$–**P**–$\mathbf{A_m}$ (black) and **P** (red) in CH_2Cl_2 (solid symbols). The colored-shaded area depicts the absorption spectra of the individual polymers **pCarb** and **pNDI**. Note the scaling (×5) of the ^{1}MLCT region (>400 nm) to assist visibility of Ru-based absorption (hollow symbols). (b) Time-resolved emission in purged CH_2Cl_2 (λ_{exc} = 500 nm, λ_{det} = 750 nm except for **P** with 700 nm). Note the significantly faster quenching of $\mathbf{D_n}$–**P**–$\mathbf{A_m}$ vs. **P** or $\mathbf{D_n}$–**P** (λ_{em} = 700 nm). The red-shifted emission detection was chosen to minimize polymer-based contribution (see text). (c) Transient absorption traces of **P**′, $\mathbf{D_n}$–**P** (470 nm) and $\mathbf{D_n}$–**P**–$\mathbf{A_m}$ (475 nm) indicating the formation of a long-lived charge separated state in the triad. Note, that scaling (×10) after 10 µs to assist visibility (hollow symbols).

of the individual building blocks (Figure S19). The polymers dominate the absorption in the UV region, that is, poly(carbazole) (312 nm) and poly(naphthalene diimide) (360 and 380 nm), whereas the Ru^{II} complex exclusively absorbs above 400 nm and stretching up to 600 nm. Note that these spectral features ensure the selective excitation of the photosensitizer by visible light, which benefits the analysis of the light-induced events with respect to less hierarchically and functionally defined polymer architectures (vide supra).[2] The steady state emission spectra are composed of Ru-based ^{3}MLCT emission (around 690 nm) and polymer-assigned emission below 650 nm (Figure S21), in agreement with reported data of poly(3,6-carbazoles)[37] and poly(naphthalene diimide).[24,25] Upon comparison of the ^{3}MLCT emission of **P** versus $\mathbf{D_n}$–**P**, a noticeable quenching (−25%) was observed (Figure S21), which is assigned to reductive quenching. The poly(3,6-carbazole) exhibits a formal redox potential of 0.22 V vs. $Fc^{+/0}$ (Figure S16), which gives a driving force estimate of +0.24 eV for reductive quenching (see Supporting Information Section 6 for details). Note, that this value represents a conservative upper bound estimate, as the (attractive) coulombic work term and the favorable entropic factors due to multiple donor sites are neglected. Hence, in view of the long excited state lifetimes, the minor reductive quenching pathway cannot be ruled out and the transient absorption data further supports this hypothesis (vide infra). Note, that ^{3}MLCT quenching by energy transfer is unlikely due the unfavorable energetics, as the emission of the poly(carbazole) occurs at higher energies (<650 nm).[37] More importantly, the triad $\mathbf{D_n}$–**P**–$\mathbf{A_m}$ shows an almost quantitative ^{3}MLCT emission quenching by 96% (Figure S22), in excellent agreement with the oxidative quenching that has been previously identified for the **P**–$\mathbf{A_m}$ subsystem.[25] In order to facilitate the unambiguous identification of the charge-separated states in the following section, the spectral signatures of the reduced poly(naphthalene diimide) ($\mathbf{pNDI^-}$) and the oxidized poly(carbazole) ($\mathbf{pCarb^+}$) were determined (see Supporting Information Section 7 for details).

Time-resolved measurements

Next, time-resolved emission and transient absorption (TA) measurements were performed to detail the light-induced charge separation. Representative ^{3}MLCT emission traces of the triad and the references are displayed in Figure 2b. The photosensitizer **P** exhibits a mono-exponential decay with a lifetime of 2.9 µs, while the donor dyad $\mathbf{D_n}$–**P** gives 1.7 µs. The formal decrease in lifetime (−41%) is in qualitative agreement with the decreased steady state emission intensity (−25%).[38] More importantly, the triad $\mathbf{D_n}$–**P**–$\mathbf{A_m}$ features an emission decay on a much shorter time scale (<10 ns, Figure S25), which suggests an almost quantitative oxidative quenching (>99%) based on the lifetimes data. In order to confirm these hypotheses, transient absorption (TA) spectra were recorded in the visible region (10 nm intervals) to identify the intermediately formed states (Figure 3). In the case of **P**, the TA traces decay with a lifetime similar to that obtained from emission measurements (Figure 2c), and the spectral domain shows several isosbestic points (Figure S26). Similarly, the TA signals of $\mathbf{D_n}$–**P** decay with

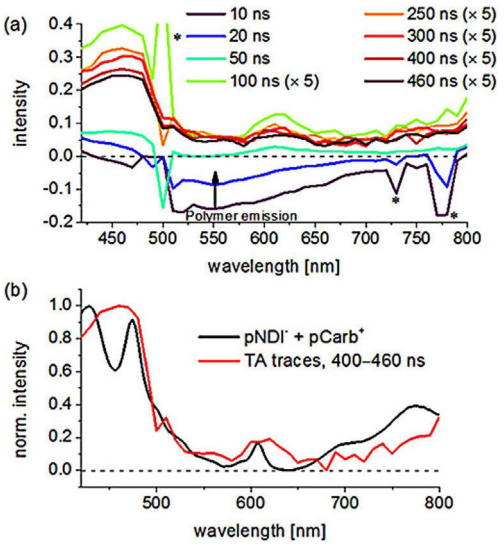

Figure 3. (a) Transient absorption data of $\mathbf{D_n}$–**P**–$\mathbf{A_m}$ from 10 to 460 ns showing the formation of absorption features characteristic for the reduced $\mathbf{pNDI^-}$ (470 and 605 nm) and the oxidized $\mathbf{pCarb^+}$ (430 and above 600 nm) (purged solution, CH_2Cl_2, excitation at 500 nm). Note, that all spectra from 100 to 460 ns were scaled by the factor five to enhance the visibility of the spectral changes. (b) The combined absorption spectra of the reduced $\mathbf{pNDI^-}$ and the oxidized $\mathbf{pCarb^+}$ (see Supporting Information Section 7) resemble the TA traces from 400 to 460 ns and indicate the formation of a charge separated state. Spectral artefacts from pulse and Raman scatter are marked with an asterisk. Spectral intervals are 10 nm.

comparable lifetimes as determined from emission measurements, but the spectral domain revealed an additional component below 700 nm at short timescales (< 30 ns). The origin is traced to polymer-based emission from the corresponding emission profiles (Figure S26a), in excellent agreement with the previously assigned polymer-based emission.[25] At longer time scales, the global fit gives a spectral signature that differs from the photosensitizer due to contributions by reductive quenching. In marked contrast, the triad $\mathbf{D_n–P–A_m}$ shows short-lived Ru emission but long-lived TA signals. The TA decay at 475 nm is best described by a biexponential kinetics with associated lifetimes of 0.7 μs (83%) and 7.2 μs (17%). The faster component is comparable to those of a related molecular triad (< 200 ns) and, thus, is assigned to the corresponding initial charge-separated state. The slower recombination is reasonable in view of the unsaturated flexible linkage to the polymer. More importantly, the long-lived component exhibits the prolonged charge separation by a factor of 3 with respect to the poly(triarylamine)-based (**pTARA**) congener (2.4 μs).[28] In both cases the light-induced charge separation proceeds primarily via oxidative quenching to transfer an electron first to the acceptor chain and subsequently to regenerate the active photosensitizers by secondary electron transfer from the donor chain. Although the linkage pattern is reversed among both triads, which may affect the kinetics of initial oxidative quenching,[39] the recombination of the fully charge separated state depends on the overall distance of the oxidized donor and reduced acceptor units, which would be the same again for both triads. Based on this hypothesis, the observed difference in recombination is interpreted in terms of the different nature of the donor chains. In the case of the **pTARA**-based triad, the redox active units are electronically decoupled through the saturated backbone and the charge migration follows a hoping mechanism. Instead, the **pCarb**-based triad consists of carbazole subunits with sizable electronic coupling. As a consequence, the hole may delocalize more readily,[40] which would facilitate a more efficient spatial charge separation and consequently also the observed diminished recombination rates.

Global analysis

Global fits of the corresponding TA data were performed to discern possible spectral differences and to summarize the transient absorption data (Figure 4). Note, that only the long-lived parts (> 100 ns) were used to exclude contributions from polymer-based emission (< 30 ns, Figure S26). As a consequence, the obtained lifetimes vary slightly but generally reproduce the previous values from selected wavelengths. The photosensitizer **P** features four isosbestic points due to the ^{1}MLCT bleach, positive ^{3}MLCT absorptions and ^{3}MLCT emission. Upon decoration with the donor chain, the $\mathbf{D_n–P}$ dyad features systematic changes of the isosbestic points. The bathochromic shifts around 450 and 700 nm, and the hypsochromic shift at 750 nm are attributed to the interactions between the donor chain and excited photosensitizer. Polymer-based emission should by ceased (vide supra) and, thus, reductive quenching may occur to generate $\mathbf{pCarb^+}$ and $\mathbf{P^-}$. The oxidized polymer

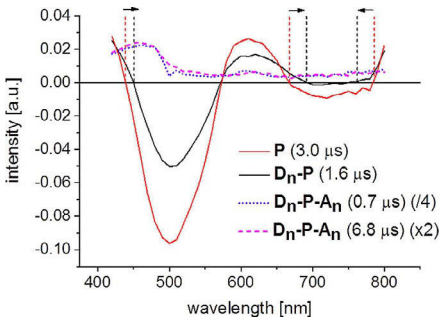

Figure 4. Comparison of TA profiles obtained from the global fit of the TA data with associated lifetimes: P (red, 3.0 μs), $\mathbf{D_n–P}$ (black, 1.6 μs) and $\mathbf{D_n–P–A_m}$ with first (blue, 0.7 μs) and second component (magenta, 6.8 μs). Note the same spectral feature of the two components $\mathbf{D_n–P–A_m}$. Note the indicative shifts of isosbestic points for $\mathbf{D_n–P}$ vs. P marked by dashed lines and arrows.

features positive TA contributions in the NIR region according to the redox titration data (Figure S18), while the reduced Ru complex formally re-populated the ^{1}MLCT bleach. Both features are qualitatively present in the spectral profile. In conjunction with the shorter emission lifetime versus **P**, reductive quenching for $\mathbf{D_n–P}$ on the microsecond time scale cannot be excluded. Finally, the $\mathbf{D_n–P–A}$ shows markedly different spectral components from the previous cases, due to very efficient electron transfer steps to form the fully charge separated state. Both components display identical spectra, which corroborates the previous assignment of long-lived charge separation. However, a further analysis at this stage is precluded, as the repeat units are spectroscopically invariant. In order to confirm charge percolation, we currently pursue the attachment of a distal reporter unit with distinct optical signature. Nevertheless, charge transport within organic semiconductors is well known,[40] and the prolonged CS lifetime between site-isolated poly(triarylamine) versus conjugated poly(carbazole) qualitatively agrees with the anticipated higher charge mobility.

Conclusion

Telechelic redox-active and conjugated polymers were utilized as building blocks to demonstrate the facile assembly to $\mathbf{D_n–P–A_m}$ architectures,[14] which can be regarded as block copolymers with a single interjacent photosensitizer unit. The modularity of the approach was ensured by the orthogonal linkage and the facile purification protocols, which enabled the successful design based on inherent optical and redox-chemical properties of the building blocks. Despite the small scale of prepared material necessary to conduct this study, the modularity and the divergent synthesis permits the scaling for each building block (polymer) independently, and to apply the optimal conditions for the coupling step–which is a strategic advantage over grafting approaches or statistical copolymers leading inevitably to defect sites. Hence, novel functional macromolecules were designed and prepared, which feature optical transparency of the polymers in the visible light region and, thus, the selective excitation of the photosensitizer occurs to assure quantitative light-induced electron transfer. Efficient

charge separation was observed, as unambiguously identified by transient absorption spectroscopy. The charge separated state features a long-lived component with a remarkably long life time component (7 μs), which is assigned to the possibility of charge transfer to other sites. The comparison of a non-conjugated poly(triarylamine) versus conjugated poly(3,6-carbazole) donor chains revealed a lifetime enhancement by a factor of three, which indicates the utility of conjugated polymers to achieve long-lived light-induced charge separation.

In summary, this novel approach towards polymer-based photosystems relies on the divergent preparation of the building blocks, and their versatile post-polymerization linkage through a modern chemistry-on-the-complex approach. As a consequence, libraries of $\mathbf{D_n–P–A_m}$ structures can be readily designed and prepared to independently optimize charge separation and charge transport. Further opportunities include the construction of redox cascades on a molecular level for directional charge transfer,[26] as well as phase separation using hydrophilic/hydrophobic substitution patterns.[23] Hence, the presented method is expected to serve as a versatile platform also for related fields to tailor (photo-)electroactive organo-based materials, for example, OFETs, OLEDs, or to transduce the optical stimulus into a long-lived redox-chemical and or redox-mechanical response.

Experimental Section

Instrumental details, further experimental details, as well as analytical, electrochemical and spectroscopic data can be found in the Supporting Information.

[Ru(dqp)(dqp-ph-trz-pCarb)][PF_6]$_2$ (D_n–P). A vial was charged with **pCarb** (9.00 mg, 2.14 μmol, 1 equiv.) as well as [Ru(dqp)(dqp-ph-C≡C-TIPS)][PF_6]$_2$ (4.29 mg, 4.29 μmol, 2 equiv.), sealed, evacuated and flushed with nitrogen. Then dry DMF (1.00 mL), CuBr (0.62 mg, 4.29 μmol, 2 equiv.) as solution in DMF (0.17 mL) and PMDETA as solution in DMF (0.02 mL, 0.24 M, 2 equiv.) were added. The mixture was stirred for 24 h at RT before the temperature was increased to 60 °C as no conversion was detected by UV/Vis-SEC. After additional 24 h the temperature was increased to 80 °C and stirring was continued for 53 h until no further conversion was detected. The reaction mixture was precipitated in an aqueous solution of NH_4PF_6. Then CH_2Cl_2 was added and the aqueous phase was extracted. The combined organic extracts were dried over Na_2SO_4, filtered and concentrated under reduced pressure. The crude product was purified by preparative SEC using the Toyopearl HW-50F resin (2 mg (pure product) + 3 mg (product + minor impurities of the starting complex)). ^{1}H NMR (400 MHz, CD_2Cl_2): δ = 8.75–8.30 (br, pCarb), 8.30–7.95 (br, Ru), 7.95–7.80 (br, pCarb), 7.80–7.62 (br, Ru), 7.62–7.31 (br, pCarb + Ru), 7.31–6.87 (br, pCarb + Ru), 4.34–3.88 (br, pCarb), 2.37–1.93 (br, pCarb), 1.52–1.0 (br, pCarb) 0.97–0.88 (br, pCarb).

[Ru(dqp-*O*-pNDI)(dqp-ph-C≡C-TIPS)][PF_6]$_2$ ($P–A_m$). A vial was charged with **pNDI** (0.070 g, 0.008 mmol, 1 equiv.), K_2CO_3 (0.001 g, 0.032 mmol, 4 equiv.), KI (0.003 g, 0.016 mmol, 2 equiv.) and [Ru(dqp-ph-C≡CH)(dqpOH)][PF_6]$_2$ (0.018 g, 0.014 mmol, 1.7 equiv.), sealed and placed under a nitrogen atmosphere. Dry DMF (1.0 mL) was added and the resulting solution was heated to 60 °C. The reaction progress was monitored by TLC (aluminum oxide, CH_2Cl_2/MeOH 95:5) and analytical size exclusion chromatography (DMAc + 0.08% NH_4PF_6, diode array detection). The reaction was continued until no further conversion was monitored by TLC (77 h). The mixture was diluted with a minimum amount of THF and precipitated into aqueous NH_4PF_6 solution. The red precipitate was re-dissolved in CH_2Cl_2 and water. The layers were separated and the aqueous phase was further extracted with CH_2Cl_2 (3×). The combined organic batches were washed with brine, dried over Na_2SO_4 and concentrated under reduced pressure. Preparative size-exclusion chromatography (Toyopearl HW-55F, CH_2Cl_2/MeOH 95:5) gave the dyad **D2** as red solid (0.060 g, 75%). ^{1}H NMR (300 MHz, CD_2Cl_2): δ 9.11–8.17 (br, pNDI), 8.11 (br, Ru), 8.08 (br, Ru), 7.91 (br, Ru), 7.71 (br, Ru), 7.63–6.47 (br, pNDI), 5.61–5.48 (br, linker), 4.38–3.73 (br, pNDI), 3.17–1.56 (br, pNDI), 1.56–1.03(br, pNDI), 1.19 (s, TIPS), 1.03–0.34 (br, pNDI).

Deprotection. A vial was charged with **D2** (0.058 g, 0.058 mmol) and THF (3 mL) and the resulting solution was cooled to 0 °C. Then tetra-*n*-butylammonium fluoride (0.002 g, 0.007 mmol, 1.2 equiv.) was added as solution in THF (0.150 mL) and the reaction mixture was stirred for 30 minutes. Subsequently the reaction was quenched with water and the mixture was precipitated in an aqueous NH_4PF_6 solution. The aqueous phase was extracted with CH_2Cl_2. The combined organic extracts were concentrated under reduced pressure. The red solid was used without further purification (0.058 g, 100%). ^{1}H NMR (300 MHz, CD_2Cl_2): δ 9.04–8.15 (br, pNDI), 8.06 (br, Ru), 8.02 (br, Ru), 7.82 (br, Ru), 7.71 (br, Ru), 7.48 (br, Ru), 7.63–6.58 (br, pNDI), 5.59–5.46 (br, linker), 4.42–3.77 (br, pNDI), 3.04–1.55 (br, pNDI), 1.55–1.12 (br, pNDI), 1.00–0.59 (br, pNDI).

[Ru(dqp-*O*-pNDI)(dqp-ph-trz-pCarb)][PF_6]$_2$ (D_n–P–A_m). A vial was charged with **P–A_m** (0.015 g, 0.0015 mmol, 1 equiv.) and **pCarb** (0.019 g, 0.0045 mmol, 3 equiv.), sealed and place under a nitrogen atmosphere. Then dry DMF (1.5 mL), a solution of copper(I) bromide (0.0004 g, 0.003 mmol, 2 equiv.) in DMF (0.160 mL) and a solution of PMDETA (0.013 mL, 2 equiv., 0.24 M in DMF) were added. The reaction mixture was heated to 80 °C for 96 h. After cooling to room temperature, the solution was precipitated in an aqueous NH_4PF_6 solution and the aqueous layer was extracted with CH_2Cl_2 (4×). The combined organic phases were dried over Na_2SO_4 and concentrated under reduced pressure. Purification by preparative size-exclusion chromatography (Toyopearl HW-55F) gave the product as red solid (0.004 g, 19% + 0.010 g, 48% (with minor impurities of the dyad after first purification run) ^{1}H NMR (300 MHz, CD_2Cl_2): δ = 8.88–8.15 (br, pCarb + pNDI), 8.06 (br, Ru), 7.85 (br, Ru + pCarb), 7.66 (br, Ru), 7.43 (br, Ru), 7.61–6.60 (br, pCarb + pNDI), 5.17–5.07 (br, linker), 4.48–3.71 (br, pCarb + pNDI), 3.08–1.71 (br, pNDI), 1.42–1.01 (br, pCarb + pNDI), 1.01–0.54 (br, pCarb + pNDI).

Acknowledgements

Financial support by the Friedrich Schiller University Jena ("Nachwuchsförderung") and the Thüringer Ministerium für Wirtschaft, Wissenschaft und Digitale Gesellschaft (TMWWDG) is kindly acknowledged. The authors thank Annett Urbanek for MALDI-ToF measurements as well as Dr. Peter Bellstedt and the NMR platform of the IAAC/IOMC for help with the NMR measurements.

Conflict of interest

The authors declare no conflict of interest.

Keywords: complex chemistry · donor–acceptor systems · electron transfer · ruthenium · time-resolved spectroscopy

[1] V. Balzani, L. Moggi, M. F. Manfrin, F. Bolletta, M. Gleria, *Science* **1975**, *189*, 852 – 856.
[2] J. H. Alstrum-Acevedo, M. K. Brennaman, T. J. Meyer, *Inorg. Chem.* **2005**, *44*, 6802 – 6827.
[3] V. Balzani, A. Credi, M. Venturi, *ChemSuSchem* **2008**, *1*, 26 – 58.
[4] J. J. Concepcion, R. L. House, J. M. Papanikolas, T. J. Meyer, *Proc. Natl. Acad. Sci. USA* **2012**, *109*, 15560 – 15564.
[5] V. Balzani, G. Bergamini, P. Ceroni, *Angew. Chem. Int. Ed.* **2015**, *54*, 11320 – 11337; *Angew. Chem.* **2015**, *127*, 11474 – 11492.
[6] L. Hammarström, *Acc. Chem. Res.* **2015**, *48*, 840 – 850.
[7] N. S. Hush, *Coord. Chem. Rev.* **1985**, *64*, 135 – 157.
[8] B. Albinsson, J. Martensson, *J. Photochem. Photobiol., C* **2008**, 9, 138 – 155.
[9] M. Gilbert, B. Albinsson, *Chem. Soc. Rev.* **2015**, *44*, 845 – 862.
[10] M. Natali, S. Campagna, F. Scandola, *Chem. Soc. Rev.* **2014**, *43*, 4005 – 4018.
[11] O. S. Wenger, *Coord. Chem. Rev.* **2009**, *253*, 1439 – 1457.
[12] H. Imahori, D. M. Guldi, K. Tamaki, Y. Yoshida, C. P. Luo, Y. Sakata, S. Fukuzumi, *J. Am. Chem. Soc.* **2001**, *123*, 6617 – 6628.
[13] D. W. Thompson, A. Ito, T. J. Meyer, *Pure Appl. Chem.* **2013**, *85*, 1257 – 1305.
[14] R. Schroot, M. Jager, U. S. Schubert, *Chem. Soc. Rev.* **2017**, DOI: 10.1039/C1036CS00811A.
[15] S. E. Bettis, D. M. Ryan, M. K. Gish, L. Alibabaei, T. J. Meyer, M. L. Waters, J. M. Papanikolas, *J. Phys. Chem. C* **2014**, *118*, 6029 – 6037.
[16] D. Ma, S. E. Bettis, K. Hanson, M. Minakova, L. Alibabaei, W. Fondrie, D. M. Ryan, G. A. Papoian, T. J. Meyer, M. L. Waters, J. M. Papanikolas, *J. Am. Chem. Soc.* **2013**, *135*, 5250 – 5253.
[17] Z. A. Morseth, L. Wang, E. Puodziukynaite, G. Leem, A. T. Gilligan, T. J. Meyer, K. S. Schanze, J. R. Reynolds, J. M. Papanikolas, *Acc. Chem. Res.* **2015**, *48*, 818 – 827.
[18] G. Leem, S. Keinan, J. Jiang, Z. Chen, T. Pho, Z. A. Morseth, Z. Hu, E. Puodziukynaite, Z. Fang, J. M. Papanikolas, J. R. Reynolds, K. S. Schanze, *Polym. Chem.* **2015**, *6*, 8184 – 8193.
[19] Z. Fang, A. Ito, H. Luo, D. L. Ashford, J. J. Concepcion, L. Alibabaei, T. J. Meyer, *Dalton Trans.* **2015**, *44*, 8640 – 8648.
[20] E. Puodziukynaite, L. Wang, K. S. Schanze, J. M. Papanikolas, J. R. Reynolds, *Polym. Chem.* **2014**, *5*, 2363 – 2369.
[21] G. Leem, Z. A. Morseth, E. Puodziukynaite, J. Jiang, Z. Fang, A. T. Gilligan, J. R. Reynolds, J. M. Papanikolas, K. S. Schanze, *J. Phys. Chem. C* **2014**, *118*, 28535 – 28541.
[22] L. Wang, E. Puodziukynaite, E. M. Grumstrup, A. C. Brown, S. Keinan, K. S. Schanze, J. R. Reynolds, J. M. Papanikolas, *J. Phys. Chem. Lett.* **2013**, *4*, 2269 – 2273.
[23] R. Schroot, T. Schlotthauer, M. Jäger, U. S. Schubert, *Macromol. Chem. Phys.* **2017**, 1600534-n/a.
[24] R. Schroot, T. Schlotthauer, U. S. Schubert, M. Jäger, *Macromolecules* **2016**, *49*, 2112 – 2123.
[25] J. Kübel, R. Schroot, M. Wächtler, U. S. Schubert, B. Dietzek, M. Jäger, *J. Phys. Chem. C* **2015**, *119*, 4742 – 4751.
[26] R. Schroot, U. S. Schubert, M. Jäger, *Macromolecules* **2015**, *48*, 1963 – 1971.
[27] R. Schroot, C. Friebe, E. Altuntas, S. Crotty, M. Jäger, U. S. Schubert, *Macromolecules* **2013**, *46*, 2039 – 2048.
[28] T. Schlotthauer, R. Schroot, S. Glover, L. Hammarström, M. Jäger, U. S. Schubert, *PCCP*, DOI: 10.1039/C7CP05593E.
[29] E. M. Barea, G. Garcia-Belmonte, M. Sommer, S. Hüttner, H. J. Bolink, M. Thelakkat, *Thin Solid Films* **2010**, *518*, 3351 – 3354.
[30] J. Veres, S. D. Ogier, S. W. Leeming, D. C. Cupertino, S. Mohialdin Khaffaf, *Adv. Funct. Mater.* **2003**, *13*, 199 – 204.
[31] A. J. Heeger, *Chem. Soc. Rev.* **2010**, *39*, 2354 – 2371.
[32] C. Liao, F. Yan, *Polym. Rev.* **2013**, *53*, 352 – 406.
[33] J.-F. Morin, M. Leclerc, D. Adès, A. Siove, *Macromol. Rapid Commun.* **2005**, *26*, 761 – 778.
[34] Y. He, W. Hong, Y. Li, *J. Mater. Chem. C* **2014**, *2*, 8651 – 8661.
[35] X. Guo, M. Baumgarten, K. Muellen, *Prog. Polym. Sci.* **2013**, *38*, 1832 – 1908.
[36] R. Schroot, U. S. Schubert, M. Jäger, *Macromolecules* **2017**, *50*, 1319 – 1330.
[37] Y. C. Chen, G. S. Huang, C. C. Hsiao, S. A. Chen, *J. Am. Chem. Soc.* **2006**, *128*, 8549 – 8558.
[38] Note the unknown quantum yields of the photosensitzer and the donor dyad, which influence the observed steady state emission intensity in addition to the quenching pathways.
[39] Y. Luo, K. Barthelmes, M. Wächtler, A. Winter, U. S. Schubert, B. Dietzek, *Chem. Eur. J.* **2017**, *23*, 4917 – 4922.
[40] H. Baessler, A. Koehler in *Unimolecular and Supramolecular Electronics I: Chemistry and Physics Meet at Metal-Molecule Interfaces* Springer-Verlag Berlin Heidelberg, **2012**, 312, 1 – 65.

Manuscript received: September 6, 2017
Accepted manuscript online: September 8, 2017
Version of record online: November 2, 2017

Publication P7

A *multi*donor-photosensitizer-*multi*acceptor triad for long-lived directional charge separation

T. Schlotthauer, R. Schroot, S. Glover, L. Hammarström, M. Jäger, U. S. Schubert, submitted.

Chemical Science

ARTICLE

A *multi*donor-Photosensitizer-*multi*acceptor triad for Long-Lived Directional Charge Separation

Received 00th January 20xx,
Accepted 00th January 20xx

DOI: 10.1039/x0xx00000x

www.rsc.org/

Tina Schlotthauer,[a] Robert Schroot,[a] Starla Glover,[b] Leif Hammarström,[b] Michael Jäger,[a,c,*] and Ulrich S. Schubert[a,c,*]

The modular assembly of a directional photoredox-active *multi*donor-photosensitizer-*multi*acceptor (D_n–P–A_m) architecture is presented. The triad assembly features a central Ru(II) sensitizer equipped with pendant polymer chains consisting of multiple triarylamine and naphthalene diimide units, respectively. Upon excitation, the efficient formation (>96%) of the charge separation (CS) was observed featuring similar CS lifetimes (400 ns) as related molecular triads. In contrast, a significant additional longer-lived CS component (2,400 ns, 30%) is observed indicating secondary charge transfer within the polymer chains.

Introduction

The efficient conversion of light energy into a redox-chemical potential is a longstanding academic and technological goal. On a molecular level, a multitude of sophisticated photosystems have been designed and synthesized relying on individual photo- and redox-active building blocks.[1-6] Such assemblies perform the light absorption with a photosensitizer (**P**) and charge storage on electron donor (**D**) and acceptor (**A**) sites. The linkage pattern (bridge) between the units dictates the rates of energy and electron transfer steps, and can be tuned by the degree of electronic communication and the mutual spatial orientation. In view of these tasks, electron-rich or electron-deficient aromatics serve as the donor or acceptor sites, while Ru^{II} polypyridyl-type complexes are versatile photosensitizer. In this regard, Ru^{II} complexes based on the 2,6-di(quinolin-8-yl)pyridine) dqp) ligand platform combine advantageous photophysical and geometrical properties,[7] and were shown to yield long-live charge separation (<200 ns) with excellent quantum efficiencies (up to 95%) in molecular D–P–A triads.[4] For many applications, the translocation of the generated charges is desired and formally implies multiple sites, where the need of linear iterative syntheses leads to prohibitively elaborate efforts. In this regards, modern polymerization techniques provide powerful methodologies to connect multiple functional units in a simple and defined manner, specifically allowing for a controlled degree of polymerization, low dispersity, and end group fidelity. Hence, these synthetic tools enable fascinating opportunities to prepare photoredox-active macromolecular architectures in facile manner,[8] particularly for energy conversion.[4, 9] Seminal architectures comprise Ru^{II}–decorated oligopeptides[10-12], polystyrenes,[13, 14] or PPMA[15] as structural backbone, or P3HT,[16] poly(fluorene)[17] or poly(fluorene-*co*-thiophene)[18] as photo- and/or redoxactive polymer. Early studies embarked on free radical polymerizations and/or grafting strategies to prepare statistical polymers, which demonstrated efficient light harvesting by energy transfer and long-lived charge separation. Recently, the advancements in synthetic polymer chemistry enabled the preparation of hierarchically controlled architectures, aiming at a directional character of the charge separation, *e.g.*, to provide a percolation pathway for charge transport in analogy to organic semiconductors.[19] Figure 1 depicts representative reference assemblies used in this study to detail and discern light-induced events in the first polymer-based $\mathbf{D_n–P–A_m}$ triad. This novel architecture features separate electron- and hole-transporting chains, which are attached to one central photosensitizer unit in a precise fashion. The selected linkage pattern adopts an axial geometry, in order to maximize the spatial separation of the charge-carrying units and, thus, is expected to minimize charge recombination.

Results and Discussion

Modular syntheses and analytical characterization.

In this contribution, we extended the modular synthesis strategy from the reported donor dyads ($\mathbf{D_n}$–**P**)[20] and acceptor dyads (**P**–$\mathbf{A_m}$)[21, 22] to present the first example of a covalently

[a] *Laboratory of Organic and Macromolecular Chemistry (IOMC), Friedrich Schiller University Jena, Humboldtstraße 10, 07743 Jena, Germany.*
[b] *Department of Chemistry – Ångström Laboratory, Uppsala University, Box 523, SE75120 Uppsala, Sweden.*
[c] *Center for Energy and Environmental Chemistry Jena (CEEC Jena), Friedrich Schiller University Jena, Philosophenweg 7a, 07743 Jena.*
* corresponding authors.
Electronic Supplementary Information (ESI) available: Synthetic procedures as well as additional characterization data (NMR, MS, SEC, UV/vis data). See DOI: 10.1039/x0xx00000x

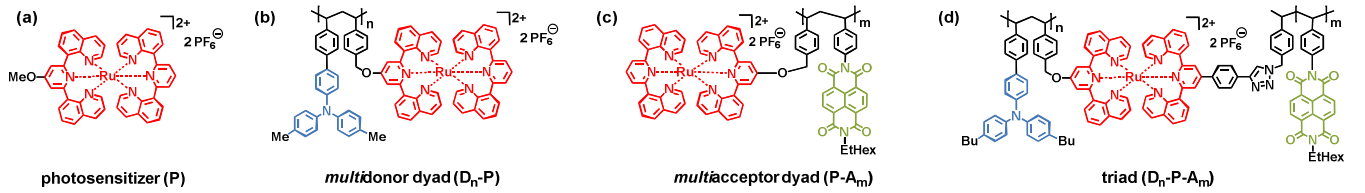

Figure 1. Molecular representation of the triad including reference subsystems investigated by time-resolved spectroscopy: (a) Photosensitizer core (**P**), (b) multidonor-photosensitizer dyad (**D_n–P**), (c) photosensitizer-multiacceptor dyad (**P–A_m**), and (d) multidonor-photosensitizer-multiacceptor triad (**D_n–P–A_m**). See ref. [21] and [20] for syntheses and steady state properties.

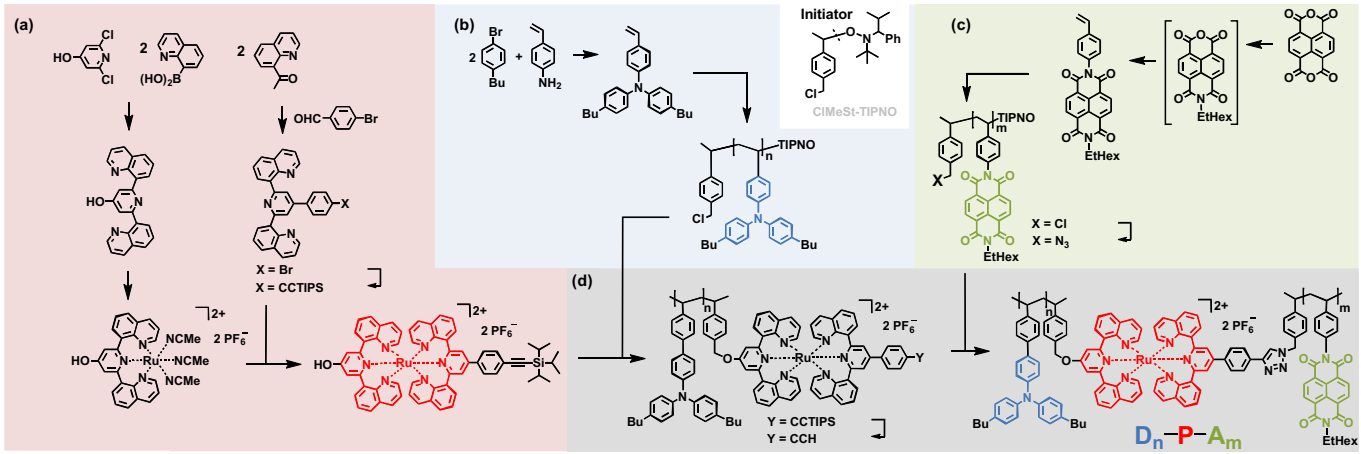

Scheme 1. Modular assembly strategy from building blocks. Syntheses of building blocks (colored boxes, a–c): (a) the *bis*-functionalized ruthenium photosensitizer, (b) the benzyl-chloride decorated poly(triarylamine) and (c) the azide-decorated poly(naphthalene diimide). Modular assembly (grey box, d) *via* Williamson ether synthesis and CuAAC reagents. Note the divergent character with at most five linear steps from commercially available starting reagents. For Reagents and conditions see SI.

linked multidonor-photosensitizer-multiacceptor (**D_n–P–A_m**) triad with precise internal architecture. The donor and acceptor blocks were selected due to their transparency in the visible region and their matching redox potentials with respect to light-induced electron transfer from the photosensitizer. In order to assist the readability throughout this manuscript, the functional building blocks will be color-coded, i.e., the photosensitizer in red, the electron donors in blue and electron acceptors in green, respectively. The preparation relies on the divergent synthesis of the individual functional building blocks and two subsequent orthogonal conjugation steps to modularly assemble the final **D_n–P–A_m** triad (Scheme 1). The bis-functionalized RuII complex is readily prepared via stepwise coordination of the two ligands (Scheme 1a),[23] which bear the desired hydroxyl or tri-isopropylsilyl (TIPS)-protected alkyne groups. The telechelic donor and acceptor polymers were prepared via nitroxide-mediated polymerization (NMP) from the styrenic triarylamine (Scheme 1b) or styrenic naphthalene diimide (Scheme 1c),[20, 22] which originate from vinyl aniline via the Hartwig-Buchwald coupling or stepwise condensation of naphthalene tetracarboxylic dianhydride.[20, 21] Noteworthy, the desired polymer end group is already introduced via the commercially available NMP initiator. In addition, the terminal benzyl chloride unit is readily converted to the corresponding azide group after polymerization. Further experimental details and analytical characterization are provided in the Supporting Information (Figure S2–S21). In summary, the divergently prepared building blocks are equipped with orthogonal functional groups to assist the modular assembly of the triad, the redox-active polymers poly(triarylamine) (**pTARA**) and poly(naphthalene diimide) (**pNDI**). Next, the **D_n–P–A_m** triad was prepared by Williamson ether synthesis to connect the pTARA-chain, followed by copper(I) catalyzed azide-alkyne cycloaddition (CuAAC) to attach the pNDI-chain (Scheme 1d). It should be noted, that the former polymer-analogous reactions required potassium iodide to facilitate efficient etherification via benzyl halide.[22] The covalent linkage of the donor dyad was confirmed by 1H NMR spectroscopy via the characteristic benzylic protons at the linkage position. (Figure S10). Size-exclusion chromatography (SEC) monitored by UV/vis further corroborates the covalent linkage, as shown by the characteristic polymer and Ru^{II} signatures at the same elution time (Figure S20).[22] Next, the silyl group was quantitatively cleaved by TBAF to release the free alkyne group, which served for the final CuAAC reaction with the azide-decorated pNDI-chain. The course of the reaction was easily monitored by UV/vis SEC and continued until no further conversion was observed. Notably, prolonged heating at elevated temperatures (80 °C) was necessary to obtain **D_n–P–A_m** applying our previously optimized protocol,[22] which stresses the necessity and utility of this highly efficient coupling strategy for such polymer-analogous reactions.[24, 25] The purification was readily achieved by the preparative SEC using

Toyopearl beads. Figure 2a highlights the excellent separation, i.e., the desired triad elutes first as judged by the characteristic absorption of **pTARA** (300 nm, grey shaded area) and **pNDI** (360 nm, black line). The 1H NMR spectrum of $\mathbf{D_n–P–A_m}$ features the three building blocks (Figure 2b, bottom), i.e., the typical broad resonances of the aromatic protons of the NDI units (8.3 to 9.0 ppm and 7.0 to 7.5 ppm) and of the TARA units (6.3 to 7.0 ppm), as well as the minor signals arising from the single ruthenium unit (7.5 to 8.3 ppm). All attempts to obtain reliable mass spectrometry data failed, which is attributed to the challenges to record mass spectra of block copolymers, particularly in case of the cationic charge of the Ru^{II} fragment.

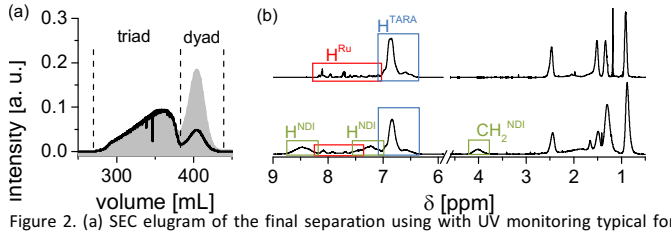

Figure 2. (a) SEC elugram of the final separation using with UV monitoring typical for pNDI (360 nm, black curve) and for pTARA (300 nm, grey shaded area). (b) ^{1}H NMR spectra (600 MHz, CD_2Cl_2) of the dyad (top) and triad (bottom) with assigned characteristic protons. See Scheme 1 for corresponding molecular representations of the dyad and the triad.

Optical and electrochemical properties.

In the following paragraph, the essential photophysical and electrochemical properties of the triad and related reference systems (Figure 1) will be presented. The absorption spectrum of the triad resembles those of the individual components (Figure 3), *i.e.*, identical maxima as **pTARA** (310 nm, blue-shaded), **pNDI** (360 and 386 nm, green-shaded), and the central $[Ru(dqp)_2]^{2+}$ unit (500 nm) as detailed previously,[21] indicating that no major perturbations in electronic character are introduced by linking of the triad. Hence the subsystems **P**, $\mathbf{D_n–P}$ and $\mathbf{P–A_m}$ (Figure 1a-c) are ideal reference systems for thermodynamic and kinetic analysis. The steady state emission spectrum of **P** displays the typical ^{3}MLCT-based emission around 700 nm,[23] whereas both reference dyads $\mathbf{D_n–P}$ and $\mathbf{P–A_m}$ feature a second component (<650 nm) that has been previously assigned to polymer-based emission.[21, 22] The donor dyad $\mathbf{D_n–P}$ shows a slightly lowered ^{3}MLCT emission intensity than **P**, which is reasonable in view of the unfavorable energetics for reductive quenching by the pTARA.[21] In contrast, the triad displays almost quantitative Ru emission quenching (96%), in line with the reported $\mathbf{P–A_m}$ dyad,[21] which indicates similar electron transfer to the **pNDI** fragment for $\mathbf{D_n–P–A_m}$ (*vide infra*). In line with steady state emission data, the electrochemical data are consistent with the postulated quenching pathways for the triad. The driving forces for electron transfer can be estimated from the formal excited state potential of the photosensitizer with respect to the redox potential of the polymers. The calculated driving forces suggest primarily oxidative quenching (ΔG = -0.25 eV) with possible secondary electron transfer to regenerate the photosensitizer (-0.25 eV), whereas the reductive quenching pathway is unfavorable (+0.20 eV) as detailed previously.[21]

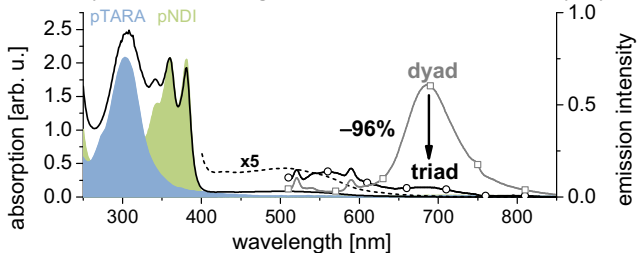

Figure 3. Absorption spectra of the polymeric building blocks pTARA (blue-shaded area) and pNDI (green-shaded area) and the triad (black curve). Note the amplified signal (x5, dashed line) to illustrate the weak absorption band of the single Ru photosensitizer unit (400–600 nm). Steady-state emission spectra of the precursor dyad (grey line, rectangles) and the triad (black line, circles). Note polymer-based emission (<650 nm) and the ^{3}MLCT emission (around 700 nm), the latter revealing strong quenching (-96%) between dyad and triad after subtracting residual polymer-based emission.

Next, the spectroelectrochemical features of the redox-active subunits will be briefly recalled (Figure S23),[21, 26] which are essential for the interpretation of the transient absorption data. The oxidized donor ($\mathbf{pTARA^+}$) exhibits a strong absorption around 690 nm, and the reduced acceptor ($\mathbf{pNDI^–}$) displays characteristic maxima at 475 and 610 nm. The oxidized photosensitizer (Ru^{III}) features a decrease of the ^{1}MLCT band (around 500 nm) and broad absorptions above 700 nm.

The time-resolved emission and transient absorption measurements (Figure 4) were performed to investigate the light–induced events of the triad in detail, including the reference systems shown in Figure 1. The observed emission lifetime of **P** (760 ns in DCM) is considerably shorter than that reported in MeCN (3,000 ns),[23] in line with the solvents effects leading to an analogously decreased lifetime of $[Ru(bpy)3]^{2+}$ (bpy is 2,2'-bipyridine).[27] The $\mathbf{D_n–P}$ dyad reveals a slightly shorter emission lifetime (660 ns) (Figure S24), in agreement with the steady state emission data. An additional short-lived component on the time-scale of the excitation pulse (ca. 10 ns) is observed in the dyad, which is absent in the case of the pristine photosensitizer unit. This distinct feature is assigned to polymer-based emission (*vide infra*), which stretched out to the ^{3}MLCT region as confirmed by the steady state emission data. A similarly short-lived emission (<10 ns) is detected for the $\mathbf{P–A_m}$ dyad (Figure S24d), but without any detectable long-lived ^{3}MLCT emission. These findings parallel our previous time-correlated single photon counting (TCSPC) data that showed efficient ^{3}MLCT emission quenching within 10 ns (90%).[21] In order to clarify the contribution by polymer-based emission (<650 nm) for the $\mathbf{D_n–P–A_m}$ triad, time-correlated single photon counting (TCSPC) measurements were performed using suitable filters for the polymer-based region (band pass, 450–650 nm) and the ^{3}MLCT region (long pass, >715 nm, Figure S26). The polymer-based region is best described by a mono-exponential decay with a lifetime of 3 ns (Figure S27), while the fit of the ^{3}MLCT region requires a second more long-lived component (49 ns, 22%), which may be explained by slow electron transfer due to the unsaturated flexible linkage.

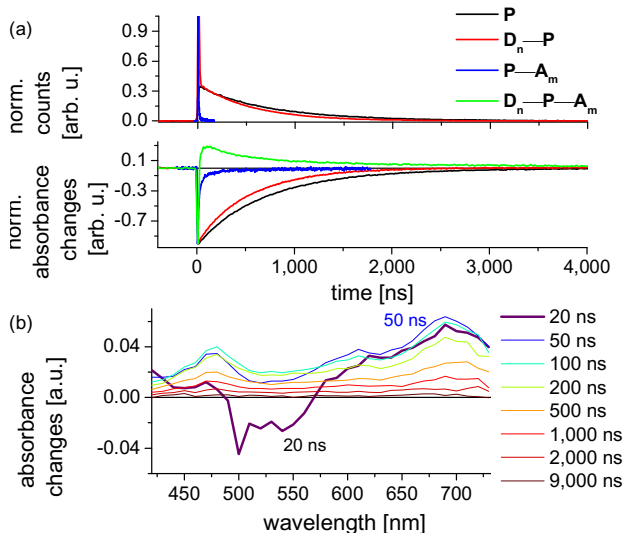

Figure 4. (a) Time-resolved emission (top) and transient absorption traces (bottom) in de-aerated DCM upon excitation at 532 nm (except for **D_n–P–A_m** at 500 nm). Emission recorded at 700 nm (except **P–A_m** at 690 nm), all transient absorption traces taken at 500 nm. Note the biexponential decay in the case of **D_n–P–A_m** with time constants of 430 and 2,400 ns (see Figure S31). (b) TA data showing the rapid formation of a charge-separated state and slow subsequent recombination. Note the fast ^{1}MLCT recovery, as well as the positive TA signatures of $pNDI^-$ (475 and 610 nm) and $pTARA^+$ (690 nm) in accordance with the spectroelectrochemical data (Figure S23).

Transient absorption (TA) spectra were recorded between 400 and 730 nm (Figure 4 and Figure S28-S30) to identify and follow the (intermediate) states by virtue of their characteristic spectroelectrochemical signatures. Upon excitation, the reference complex (**P**) shows the typical ^{1}MLCT bleach and ^{3}MLCT absorptions at longer wavelengths, which are partially overlapped by stimulated emission (Figure S28). The spectral decay is characterized by several isosbestic points and follows mono-exponential kinetics (730 ns), which is in satisfying agreement with the emission lifetime. The TA data of the **D_n–P** dyad shows a generally similar behavior (Figure S29), except for an unusual negative TA contribution at short time scales (<20 ns) and longer wavelengths (>550 nm, Figure S29b). In comparison to **P**, the isosbestic point at 435 nm is preserved, while the ones at 575 or 655 nm are absent. The TA recovery of **D_n–P** was followed at 470 nm and is best described by a mono-exponential decay (530 ns), although including a second component enhances the fit at early times (Figure S29). Hence, a biexponential global fit of the TA data was performed to verify this hypothesis. The spectral profile of the long-lived component (520 ns) matches perfectly that of **P**, including the identical isosbestic points, while the short-lived component (6 ns) resembles that of the polymer-based emission. In analogy, **P–A_m** also shows a short-lived polymer-based TA feature at similarly short times and comparable wavelengths (Figure S30). In line with our previous study that showed fast initial charge separation (<1.6 ns),[21] a weak NDI^- signature was observed (Figure S30b). As judged from absent build-up of the corresponding TA signatures, the charge recombination seems faster than charge separation, so that the TA recovery is completed within 100 ns (Figure 4a).[21] In marked contrast, the **D_n–P–A_m** triad shows the immediate formation of the fully charge separated (CS) state, as identified by the concomitant ^{1}MLCT recovery and the evolving positive TA signatures of $pNDI^-$ and $pTARA^+$ (Figure 4b). More importantly, the TA signal decays orders of magnitude slower than in the reference dyad, following biexponential kinetics (Figure S31). The associated lifetimes are 430 ns (70%) and 2,400 ns (30%). The faster component is comparable to that of related molecular triads showing mono-exponential recombination (140–200 ns),[28] whereas the second component is more long-lived by one order of magnitude. This observation and is tentatively assigned to the possibility of secondary charge transfer steps owing to the *multi*-donor and/or *multi*-acceptor character. A more detailed analysis will be reported in due course, more importantly, these first results demonstrate the effective and long-lived charge separation in the polymer-based triad.

Conclusion

An efficient divergent modular synthesis was utilized to prepare a *multi*donor-photosensitizer-*multi*acceptor triad (**D_n–P–A_m**), *i.e.*, only five linear synthetic steps from commercially available materials and facile purification. The functional building blocks were selected according to their photophysical and electrochemical properties (**P**, **D_n**, and **A_m**). Hence, the photosensitizer unit is exclusively excited in the visible light region and undergoes electron transfer steps. Detailed steady state and time-resolved spectroscopy of the triad and the related subsystems confirmed the effective initial charge separation and, more importantly, featuring a diminished component of recombination by one order of magnitude with respect to a molecular model triad. The flexibility and ease of the presented modular synthesis in conjunction with the enhanced charge separation will increase the feasibility of using polymer-based photosystems for energy conversion and/or to provide local redox gradients to power molecular machines.

Acknowledgements

Financial support by the Carl-Zeiss-Foundation, the Friedrich Schiller University Jena (“Nachwuchsförderung”) and the Thüringer Ministerium für Wirtschaft, Wissenschaft und Digitale Gesellschaft (TMWWDG), and the Swedish Research Council (grant no. 2012 - 3926) is kindly acknowledged. The authors thank Annett Urbanek for MALDI-ToF measurements as well as Dr. Peter Bellstedt and the NMR platform of the IAAC/IOMC for help with the NMR measurements.

References

1. L. Hammarström, *Acc. Chem. Res.*, 2015, **48**, 840-850.
2. V. Balzani, G. Bergamini and P. Ceroni, *Angew. Chem. Int. Ed.*, 2015, **54**, 11320-11337.
3. J. J. Concepcion, R. L. House, J. M. Papanikolas and T. J. Meyer, *Proc. Natl. Acad. Sci. USA*, 2012, **109**, 15560-15564.
4. J. H. Alstrum-Acevedo, M. K. Brennaman and T. J. Meyer, *Inorg. Chem.*, 2005, **44**, 6802-6827.

5. V. Balzani, A. Credi and M. Venturi, *ChemSuschem*, 2008, **1**, 26-58.
6. V. Balzani, L. Moggi, M. F. Manfrin, F. Bolletta and M. Gleria, *Science*, 1975, **189**, 852-856.
7. L. Hammarström and O. Johansson, *Coord. Chem. Rev.*, 2010, **254**, 2546-2559.
8. R. Schroot, M. Jäger and U. S. Schubert, *Chem. Soc. Rev.*, 2017, DOI: 10.1039/c1036cs00811a.
9. Z. A. Morseth, L. Wang, E. Puodziukynaite, G. Leem, A. T. Gilligan, T. J. Meyer, K. S. Schanze, J. R. Reynolds and J. M. Papanikolas, *Acc. Chem. Res.*, 2015, **48**, 818-827.
10. D. M. Ryan, M. K. Coggins, J. J. Concepcion, D. L. Ashford, Z. Fang, L. Alibabaei, D. Ma, T. J. Meyer and M. L. Waters, *Inorg. Chem.*, 2014, **53**, 8120-8128.
11. S. E. Bettis, D. M. Ryan, M. K. Gish, L. Alibabaei, T. J. Meyer, M. L. Waters and J. M. Papanikolas, *J. Phys. Chem. C*, 2014, **118**, 6029-6037.
12. D. Ma, S. E. Bettis, K. Hanson, M. Minakova, L. Alibabaei, W. Fondrie, D. M. Ryan, G. A. Papoian, T. J. Meyer, M. L. Waters and J. M. Papanikolas, *J. Am. Chem. Soc.*, 2013, **135**, 5250-5253.
13. G. Leem, S. Keinan, J. Jiang, Z. Chen, T. Pho, Z. A. Morseth, Z. Hu, E. Puodziukynaite, Z. Fang, J. M. Papanikolas, J. R. Reynolds and K. S. Schanze, *Polym. Chem.*, 2015, **6**, 8184-8193.
14. Z. Fang, A. Ito, S. Keinan, Z. Chen, Z. Watson, J. Rochette, Y. Kanai, D. Taylor, K. S. Schanze and T. J. Meyer, *Inorg. Chem.*, 2013, **52**, 8511-8520.
15. Z. Fang, A. Ito, H. Luo, D. L. Ashford, J. J. Concepcion, L. Alibabaei and T. J. Meyer, *Dalton Trans.*, 2015, **44**, 8640-8648.
16. L. Wang, E. Puodziukynaite, E. M. Grumstrup, A. C. Brown, S. Keinan, K. S. Schanze, J. R. Reynolds and J. M. Papanikolas, *J. Phys. Chem. Lett.*, 2013, **4**, 2269-2273.
17. G. Leem, Z. A. Morseth, E. Puodziukynaite, J. Jiang, Z. Fang, A. T. Gilligan, J. R. Reynolds, J. M. Papanikolas and K. S. Schanze, *J. Phys. Chem. C*, 2014, **118**, 28535-28541.
18. E. Puodziukynaite, L. Wang, K. S. Schanze, J. M. Papanikolas and J. R. Reynolds, *Polym. Chem.*, 2014, **5**, 2363-2369.
19. H. Baessler and A. Koehler, *Unimolecular and Supramolecular Electronics I: Chemistry and Physics Meet at Metal-Molecule Interfaces*, 2012, **312**, 1-65.
20. R. Schroot, C. Friebe, E. Altuntas, S. Crotty, M. Jäger and U. S. Schubert, *Macromolecules*, 2013, **46**, 2039-2048.
21. J. Kübel, R. Schroot, M. Wächtler, U. S. Schubert, B. Dietzek and M. Jäger, *J. Phys. Chem. C*, 2015, **119**, 4742-4751.
22. R. Schroot, T. Schlotthauer, U. S. Schubert and M. Jäger, *Macromolecules*, 2016, **49**, 2112-2123.
23. M. Jäger, R. J. Kumar, H. Görls, J. Bergquist and O. Johansson, *Inorg. Chem.*, 2009, **48**, 3228-3238.
24. U. Mansfeld, C. Pietsch, R. Hoogenboom, C. R. Becer and U. S. Schubert, *Polym. Chem.*, 2010, **1**, 1560-1598.
25. C.-H. Wong and S. C. Zimmerman, *Chem. Commun.*, 2013, **49**, 1679-1695.
26. R. Schroot, U. S. Schubert and M. Jäger, *Macromolecules*, 2015, **48**, 1963-1971.
27. J. V. Caspar and T. J. Meyer, *J. Am. Chem. Soc.*, 1983, **105**, 5583-5590.
28. R. J. Kumar, S. Karlsson, D. Streich, A. R. Jensen, M. Jäger, H.-C. Becker, J. Bergquist, O. Johansson and L. Hammarström, *Chem. Eur. J.*, 2010, **16**, 2830-2842.
29. J. Kübel, R. Schroot, M. Wächtler, U. S. Schubert, B. Dietzek and M. Jäger, *J. Phys. Chem. C*, 2015, **119**, 4742-4751.

Supporting Information

A *multi*donor-Photosensitizer-*multi*acceptor triad for Long-Lived Directional Charge Separation

Tina Schlotthauer,[a] Robert Schroot,[a] Starla Glover,[b] Leif Hammarström,[b] Michael Jäger,[a,c,] and Ulrich S. Schubert[a,c,*]*

[a] Laboratory of Organic and Macromolecular Chemistry (IOMC), Friedrich Schiller University Jena, Humboldtstraße 10, 07743 Jena, Germany

[b] Department of Chemistry - Ångström Laboratory, Uppsala University, Box 523, SE75120 Uppsala, Sweden

[c] Center for Energy and Environmental Chemistry Jena (CEEC Jena), Friedrich Schiller University Jena, Philosophenweg 7a, 07743 Jena

Content

1. Instrumentation

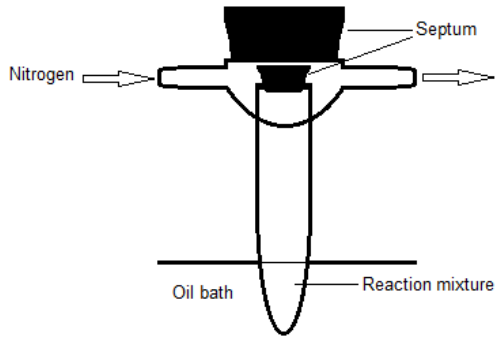

Figure S1. Reaction vessel used for the polymerization.

NMR spectra were recorded on a 300 or 600 MHz NMR spectrometer (Bruker AVANCE or Fourier 300) in deuterated solvents at 300 K. Chemical shifts are reported in parts per million (ppm, δ scale) relative to the residual solvent signal.[1]

MALDI-TOF MS spectra were measured using an Ultraflex III TOF/TOF (Bruker Daltonics GmbH) equipped with a Nd:YAG laser and a collision cell. The spectra were recorded in the positive reflector or linear mode.

ESI-Q-TOF MS measurements were executed on a micrOTOF (Bruker Daltonics GmbH) mass spectrometer, which was equipped with an automatic syringe pump for sample injection. The pump was supplied from KD Scientific. It was operated in the positive ion mode. The standard electrospray ion (ESI) source was used to generate ions. Mixtures of dichloromethane and acetonitrile were used as solvent. The ESI-Q-TOF-MS instrument was calibrated in the m/z range 50 to 3,000 using an internal calibration standard (Tunemix solution), which was supplied from Agilent.

UV/Vis absorption spectra were measured on a Perkin-Elmer Lambda 45 UV/Vis spectrophotometer and emission as well as excitation spectra were recorded using a Jasco FP6500. Measurements were carried out using approx. 10^{-7} M solutions of aerated dichloromethane (spectroscopy grade) in 1 cm quartz cuvettes at 25 °C.

Flash column chromatography was carried out on a Biotage Isolera One System using Biotage SNAP Cartridges KP-Sil. The Biotage Initiator Sixty Microwave synthesizer was used for microwave reactions.

Preparative size exclusion chromatography was either performed by using Bio-Beads (S-X1, dichloromethane) or Toyopearl (HW-55F, CH_2Cl_2/MeOH 95/5).

Analytical size exclusion chromatography was performed on the following systems:
SEC1. Shimadzu system (controller: SCL-10A VP, degasser: DGU-14A, pump: LC-10AD VP, auto sampler: SIL-10AD VP, oven: Techlab, UV detector: SPD-10AD VP, RI detector: RID-10A, eluent: chloroform/iso-propanol/triethylamine [94:2:4], flow rate: 1 mL/min, temperature: 40 °C, column: PSS SDV pre/lin S column).

SEC2. Shimadzu system (controller: SCL-10A VP, degasser: DGU-14A, pump: LC-10AD VP, auto sampler: SIL-10AD VP, oven: CTO-10A VP, UV detector: SPD-10MA VP, RI detector: RID-10A, eluent: DMAc + 0.08% NH_4PF_6, flow rate: 1 mL/min, temperature: 40 °C, column: Phenomenex Phenogel guard/10^5 Å/10^3 Å)

Time-correlated single photon counting was performed on a Edinburgh Instrument (EPL405), equipped a Hamamatsu MCP-photomultiplier (R3809U-51) for detection of single photons as described previously. The laser's pulse energy was (ca. 15 pJ, 77 ps pulses) and attenuated to a count rate of ca. 1% or less of the excitation frequency. Specific measurements were performed with 470 nm excitation with a repition rate of 20 μs applying using a long pass filter (715 nm) or 3C1 Russian Filter which transmits light at λ_{max} 540 with FWHM ca. 100 nm. The IRF has not been deconvoluted from the traces.

Time-resolved flash photolysis measurements were made with a frequency tripled Q-switched Nd:YAG laser (from Quantel, brilliantB) where 355 nm pulses with a 7 ns duration were directed through an OPO tuned to output of 500 or 532 nm at ca. 10-20 mJ/pulse. Analyzing light was supplied by a pulsed 150 W xenon lamp in a flash photolysis spectrometer (Applied Photophysics, LKS.80). Light that passed through the sample was sent through a monochrometer set to a bandwidth of 7 nm prior to reaching the 5 stage P928 photomultiplier tube (Hamamatsu). The signal was digitized using an Agilent Technologies Infiniium digital oscilloscope (600 MHz). Transient absorption traces were generated within the Applied Photophysics LKS software package where rates for each sample condition were determined from 24–64 laser shots. All emission measurements were performed in 1 × 1 cm quartz cuvettes in DCM.

2. Syntheses

All reagents were purchased from ABCR, Acros Organics, Alfa Aesar, Apollo Scientific, Sigma-Aldrich or TCI chemicals and were used without further purification unless otherwise noted. Dry pyridine and dry *N*-*N*-dimethylformamide (DMF) were commercially available. THF was distilled from sodium/benzophenone. All solvents were degassed before use. *N*-*N*-bis(4-butylphenyl)-(4-vinyl)aniline (**1**),[2] *N*-(2-Ethyl-hexyl)-*N*'-(vinylphenyl)-naphthalene-1,4,5,8-dicarboxydiimide (**2**),[3] [Ru(dqp-OH)$(CH_3CN)_3$][PF_6]$_2$,[4] 4-bromophenyl-2,6-di(quinolin-8-yl)pyridine[5], **P**,[4] $\mathbf{D_n}$**–P**,[2] and **P–**$\mathbf{A_m}$[3] were prepared as previously described. Dqp-OH is 4-hydroxy-2,6-di(quinolin-8-yl)pyridine), PMDETA is *N,N,N′,N″,N″*-pentamethyldiethylenetriamine.

*Note: The labeling of the prepared polymers (p) is based on the used monomers (**1** or **2**), the end group (prefix Cl or N_3) and the degree of polymerization as subscripted number. The availability of functional end group was verified by MALDI-TOF MS and by ^{1}H NMR. The resonances of the two protons next to the chlorine appear at a characteristic broad signal at approximately 4.4 or 4.6 ppm, respectively. Noteworthy, the integral of these signals is used to determine the degree of polymerization and, more importantly, chemical shift of this signal is sensitive and acts as sensor for further functionalization reactions.*

4-(4-(Triisopropylsilyl)ethinyl)phenyl-2,6-di(quinolin-8-yl)pyridine (dqp-ph-C≡C-TIPS). A flask was charged with 4-bromophenyl-2,6-di(quinolin-8-yl)pyridine (0.700 g, 1.433 mmol), $Pd(PPh_3)_4$ (0.099 g, 0.086 mmol) and copper(I) iodide (0.016 g, 0.086 mmol), sealed and placed under a nitrogen atmosphere. Then dry THF (50 mL), dry triethylamine (25 mL) and triisopropylsilylacetylene (0.6 mL,

2.674 mmol) were added via a syringe and the mixture was heated to 60 °C for 16 h until the TLC (CH_2Cl_2/MeOH 99/1, silica) showed full conversion. The reaction mixture was allowed to cool to room temperature and was filtered over Celite. The solvents were removed under reduced pressure and the residual crude product was purified by flash column chromatography (silica, eluent: CH_2Cl_2/EtOAc 90/10 followed by CH_2Cl_2/MeOH 99/1). The combined product-containing fractions were dried in vacuo to yield the product as off-white solid. (0.695 g, 85%). ^{1}H NMR (250 MHz, $CDCl_3$): δ 9.08–8.93 (m, 2H), 8.37–8.19 (m, 6H), 7.90 (d, *J* = 8.1 Hz, 2H), 7.78 (d, *J* = 7.7 Hz, 2H), 7.68 (t, *J* = 7.7 Hz, 2H), 7.60 (d, *J* = 7.7 Hz, 2H), 7.46 (dd, *J* = 8.1, 4.0 Hz, 2H), 1.15 (s, 21H). ^{13}C NMR (63 MHz, $CDCl_3$): δ 157.5, 150.5, 146.4, 146.2, 139.5, 139.4, 136.5, 132.7, 131.7, 128.8, 128.7, 127.5, 126.8, 123.9, 123.8, 121.1, 107.0, 92.1, 18.8, 11.5. MS (MALDI-ToF, DCTB) m/z: 590.39 ($[C40H39N3Si+H]^+$). HR-ESI ($[C40H39N3Si+H]^+$) m/z: calc: 590.2986, found: 590.2964, Error: 3.7 ppm.

pTARA. A glass tube equipped with a septum and an external overhead flushing with nitrogen was used for the polymerization (Figure S1). The reaction vessel was charged with **1** (0.940 g, 2.451 mmol), *N*-(*tert*-butyl)-*O*-(1-(4-(chloromethyl)phenyl)ethyl)-*N*-(2-methyl-1-phenylpropyl)hydroxylamine (CMSt-TIPNO) (0.046 g, 0.123 mmol) and anisole (2.4 mL).The mixture was purged with nitrogen for 20 min and placed in a pre-heated oil bath (120 °C). After 23 h the reaction mixture was diluted with CH_2Cl_2 and precipitated in cold MeOH. Subsequently, unreacted monomer was removed by preparative SEC (Bio-Beads S-X1, CH_2Cl_2). The polymer was obtained as yellow solid after precipitation in MeOH. Yield: 0.465 g. SEC ($CHCl_3$/IPA/NEt_3 94/2/4, PS calibration): M_n = 4,600 g/mol, Đ = 1.06. ^{1}H NMR (300 MHz, $CDCl_3$): δ 7.56 – 7.06 (br), 7.06 – 6.13 (br), 4.60 – 4.21 (br), 2.72 – 2.65 (br), 2.65 – 1.78 (br), 1.78 – 1.42 (br). 1.42 – 1.18 (br), 1.18 – 0.74 (br), 0.74 – 0.11 (br).

pNDI (Cl-decorated). The reaction vessel was charged with **2** (0.500 g, 1.040 mmol), *N*-(*tert*-butyl)-*O*-(1-(4-(chloromethyl)phenyl)ethyl)-*N*-(2-methyl-1-phenylpropyl)hydroxylamine (CMSt-TIPNO) (0.019 g, 0.052 mmol) and anisole (4.0 mL).The mixture was purged with nitrogen for 20 min and placed in a pre-heated oil bath (120 °C). After 17 h the reaction mixture was diluted with CH_2Cl_2 and precipitated in cold MeOH. Subsequently, unreacted monomer was removed by preparative SEC (Bio-Beads S-X1, CH_2Cl_2). The polymer was obtained as yellow solid after precipitation in MeOH. Yield: 0.400 g. SEC ($CHCl_3$/IPA/NEt_3 94/2/4, PS calibration): M_n = 6,400 g/mol, Đ = 1.11. ^{1}H NMR (300 MHz, $CDCl_3$): δ 9.04 – 7.98 (br), 7.78 – 6.67 (br), 4.72 – 4.42 (br), 4.34 – 3.60 (br), 2.91 – 1.72 (br), 1.52 – 1.04 (br). 1.04 – 0.45 (br).

pNDI (azide-decorated). *Safety advice: Sodium azide is very toxic, personal protection precautions should be taken. Heavy metal azides are explosive. Do not use metal spatula.* A glass vial was charged with **pNDI (Cl-decorated)** (0.150 g, 0.024 mmol, 1 eq.) and sodium azide (0.005 g, 0.071 mmol, 3 eq.), capped and placed under a nitrogen atmosphere. Dry DMF (4.5 mL) was added and the reaction mixture was immersed in an oil bath at 60 °C at which the polymer dissolved. After 48 h CH_2Cl_2 and water were added to the formed suspension and the layers were separated. The aqueous layer was extracted two times with CH_2Cl_2. The combined organic layers were three times washed with brine and dried over Na_2SO_4. After removal of the solvent under reduced pressure, a yellow solid was obtained. Yield: 0.135 g. SEC ($CHCl_3$/IPA/NEt_3 94/2/4, PS calibration): M_n = 6,300 g/mol, Đ = 1.08. ^{1}H NMR (300 MHz, $CDCl_3$): δ 9.04 – 7.98 (br), 7.78 – 6.66 (br), 4.56 – 4.22 (br), 4.23 – 3.60 (br), 2.83 – 1.65 (br), 1.51 – 1.05 (br), 1.05 – 0.45 (br).
Note: The quantitative substitution was verified by a shift of the methylene proton resonances in the proton NMR of pNDI (azide-decorated). *(from 4.6 ppm to 4.3 ppm).*

[Ru(dqp-OH)(dqp-ph-C≡C-TIPS)][PF_6]$_2$. A flask was charged with [Ru(dqp-OH)(CH_3CN)$_3$][PF_6]$_2$ (0.450 g, 0.521 mmol), dqp-ph-C≡C-TIPS (0.307 g, 0.521 mmol) and dry DMF (10 mL) under nitrogen. Subsequently the reaction mixture was heated to 140 °C for 48 h. After cooling to room temperature the solution was precipitated in an aqueous NH_4PF_6 solution, filtered and re-dissolved in CH_3CN. The crude product was purified by column chromatography on silica using a mixture of $CH_3CN/H_2O/KNO_{3(aq)}$ (40/4/1) as eluent. Afterwards on anion exchange was performed by precipitation in an aqueous NH_4PF_6 solution. Finally, diffusion controlled crystallization (diethyl ether into acetonitrile solution) gave the desired complex as red solid (0.350 g, 51%). ^{1}H NMR (600 MHz, CD_3CN): δ 9.15 (br, OH), 8.13 (m, 4H), 8.06 (m, 6H), 7.93 (d, *J* = 8.5 Hz, 2H), 7.86 (dd, *J* = 1.1 Hz, 7.5 Hz, 2H), 7.71 (dd, *J* = 1.1 Hz, 7.3 Hz, 2H), 7.67 (m, 6H), 7.45 (m, 4H), 7.37 (s, 2H), 7.07 (m, 4H), 1.16 (m, 21H). ^{13}C NMR (150 MHz, CD_3CN): δ 166.2, 159.6, 159.5, 158.5, 158.2, 149.1, 147.6 (2×), 138.4, 138.3, 137.1, 134.3, 133.7, 133.6, 132.9, 132.6, 131.5 (2×), 128.6, 127.7, 127.6, 127.5, 126.1, 125.9, 122.9, 116.7, 107.2, 94.2, 18.9, 12.0. HR-ESI-ToF-MS: $[C_{63}H_{54}N_6ORuSi]^{2+}$ m/z: calculated: 520.158, found: 520.1599, error: 1.9 ppm.

[Ru(dqp-O-pTARA)(dqp-ph-C≡C-TIPS)][PF_6]$_2$. A vial was charged with **pTARA** (0.400 g, 0.087 mmol) and anisole (1.5 mL). Then [Ru(dqp-OH)(dqp-ph-C≡C-TIPS)][PF_6]$_2$ (0.231 g, 0.174 mmol), KI (0.029 g, 0.174 mmol), K_2CO_3 (0.024 g, 0.174 mmol) and DMF (1.5 mL) were added. Subsequently, the vial was capped and immersed in a preheated oil bath at 60 °C. The reaction progress was monitored by UV/vis SEC and TLC (aluminium oxide, CH_2Cl_2/MeOH 95/5). After 89 h no further conversion was detected and the reaction mixture was cooled to room temperature. An aqueous solution of NH_4PF_6 was added and the suspension was extracted with CH_2Cl_2 (3 ×). The organic extracts were dried over Na_2SO_4 and concentrated under reduced pressure. The desired dyad was isolated by preparative SEC (Toyopearl HW-55F, CH_2Cl_2/MeOH 95/5) as red solid (0.250 g, 48%). ^{1}H NMR (600 MHz, CD_2Cl_2): δ 8.17 (br, Ru), 8.10 (br, Ru), 7.96 (br, Ru), 7.73 (br, Ru), 7.60 (br, Ru), 7.53 (br, Ru), 7.39 (br, Ru), 7.26 (br, Ru), 7.05 – 5.81 (br, p1$_{15}$), 5.46 (br, linker), 5.24 (br, linker), 2.64 – 2.34 (br, (br, p1$_{15}$), 2.34 – 1.85 (br, p1$_{15}$), 1.85 – 1.43 (br, p1$_{15}$). 1.43 – 1.22 (br, p1$_{15}$), 1.22 – 1.15 (br, TIPS), 1.00 – 0.72 (br, p1$_{15}$).

[Ru(dqp-O-pTARA)(dqp-ph-C≡C-H)][PF_6]$_2$. A vial was charged with [Ru(dqp-O-pTARA)(dqp-ph-C≡C-TIPS)][PF_6]$_2$ (0.230 g, 0.038 mmol) under nitrogen. Then dry THF (5.0 mL) was added and the resulting solution was cooled with an ice bath. Subsequently, a solution of (*n*-Bu_4)NF (0.040 g, 0.143 mmol) in THF (0.265 mL) was added and the mixture was stirred for 0.5 h at 0 °C. Afterwards, water was added and the solution was extracted with CH_2Cl_2. The organic extracts were dried over Na_2SO_4 and concentrated under reduced pressure. The red solid was washed with CH_3CN and was dried (0.230 g, 100%). ^{1}H NMR (300 MHz, CD_2Cl_2): δ 8.04 (br, Ru), 7.99 (br, Ru), 7.79 (br, Ru), 7.65 (br, Ru), 7.51 (br, Ru), 7.33 (br, Ru), 7.14 (br, Ru), 7.04 – 6.30 (br, p1$_{15}$), 5.14 (br, linker), 2.63 – 2.28 (br, p1$_{15}$), 2.25 – 1.62 (br, p1$_{15}$), 1.62 – 1.39 (br, p1$_{15}$). 1.39 – 1.18 (br, p1$_{15}$), 0.97 – 0.74 (br, p1$_{15}$).

[Ru(dqp-O-pTARA)(dqp-ph-tr-pNDI)][PF_6]$_2$ (D_n–A–P_m). A vial was charged with [Ru(dqp-O-pTARA)(dqp-ph-C≡C-H)][PF_6]$_2$ (0.014 g, 0.003 mmol, 1 eq.) and pNDI (azide-decorated) (0.030 g, 0.005 mmol, 2 eq.) under nitrogen. Then dry DMF (1.0 mL), solution of CuBr (0.001 g, 0.010 mmol, 4 eq.) in DMF (0.2 mL) and PMDETA (0.24 M in DMF, 0.04 mL, 4 eq.) were added. The mixture was heated to 80 °C for 96 h. The mixture was precipitated in aqueous NH_4PF_6 and the red solid was extracted with CH_2Cl_2. After drying over Na_2SO_4, the desired triad **T1** was purified by preparative size-exclusion chromatography (Toyopearl HW-55F, CH_2Cl_2/MeOH 95/5, two runs) and was isolated as light red solid (0.017 g, 58%). ^{1}H NMR (300 MHz, CD_2Cl_2): δ 8.84 − 8.17 (br, p2$_{17}$), 8.08 (br, Ru), 7.91

(br, Ru), 7.68 (br, Ru), 7.64 − 7.04 (br, Ru + $p2_{17}$), 7.04 – 6.29 (br, $p1_{15}$), 5.57 (br, linker), 5.20 (br, linker), 4.32 − 3.58 (br, $p2_{17}$), 2.96 – 2.29 (br, $p1_{15}$), 2.29 – 1.59 (br, $p1_{15}$ + $p2_{17}$), 1.59 – 1.44 (br, $p1_{15}$). 1.39 – 1.04 (br, $p1_{15}$ + $p2_{17}$), 1.04 – 0.46 (br, $p1_{15}$ + $p2_{17}$).

3. NMR spectroscopy

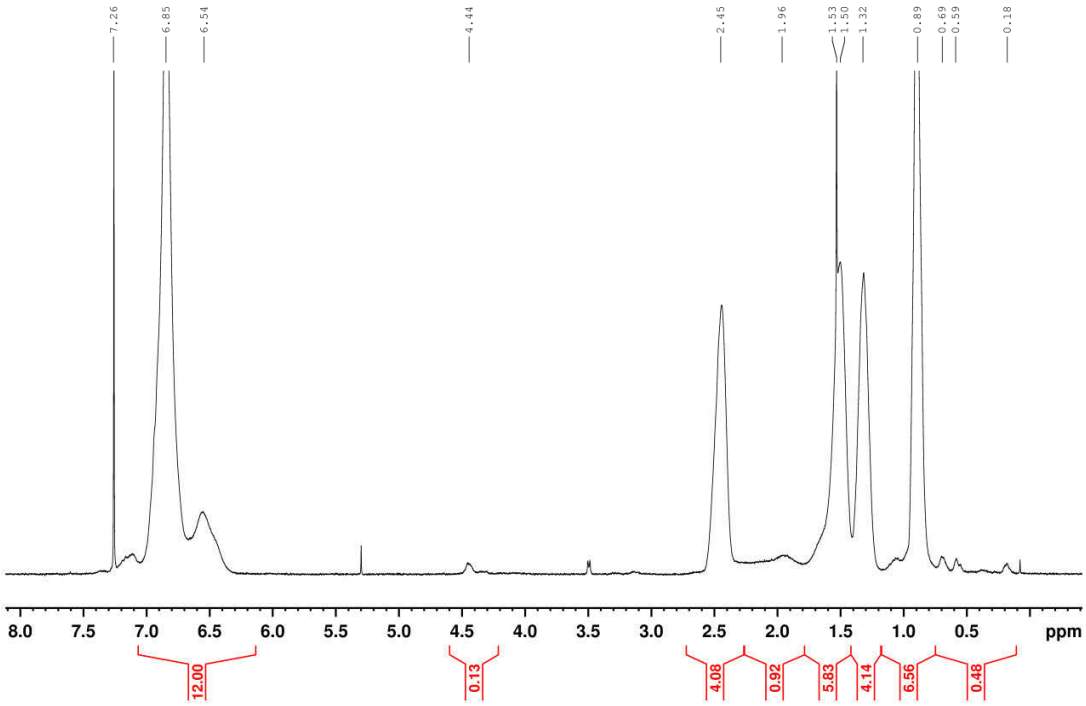

Figure S2. ^{1}H NMR spectrum (300 MHz, $CDCl_3$) of **pTARA**.

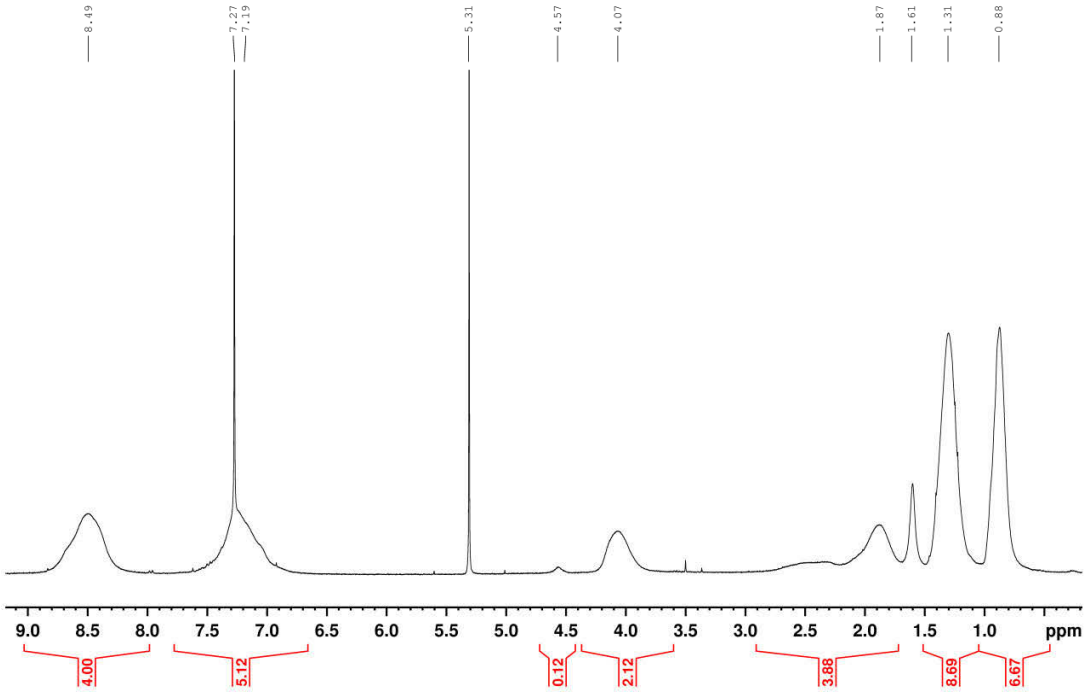

Figure S3. ^{1}H NMR spectrum (300 MHz, $CDCl_3$) of **pNDI (Cl-decorated)**. Note the chloromethyl group at 4.57 ppm.

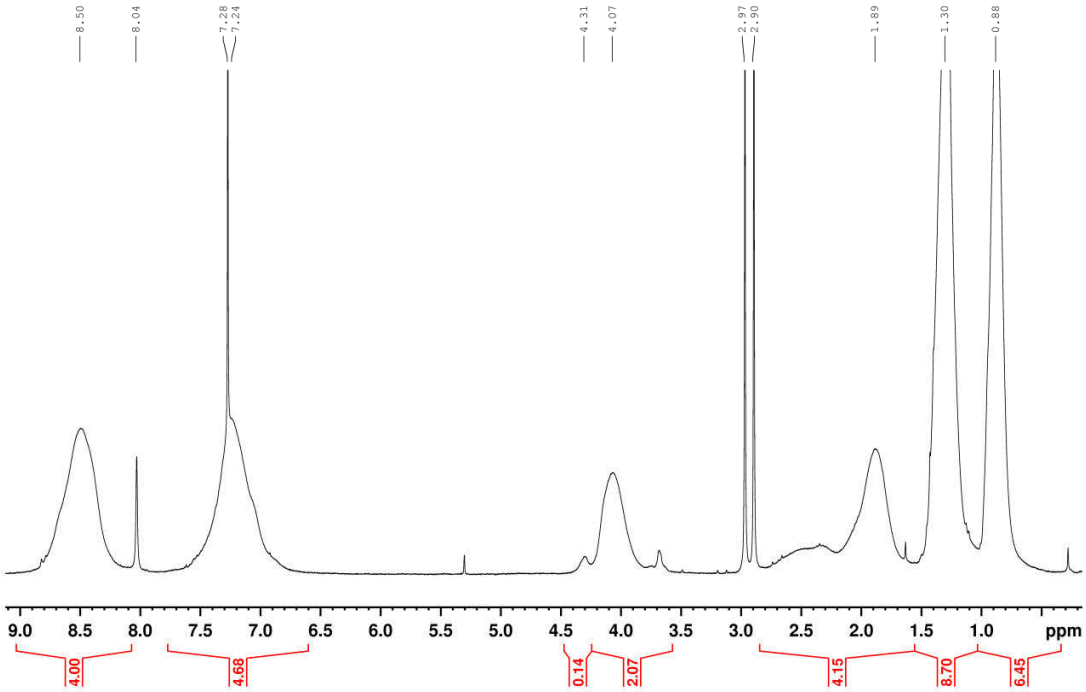

Figure S4. ^{1}H NMR spectrum (300 MHz, $CDCl_3$) of **pNDI (azide-decorated)**.

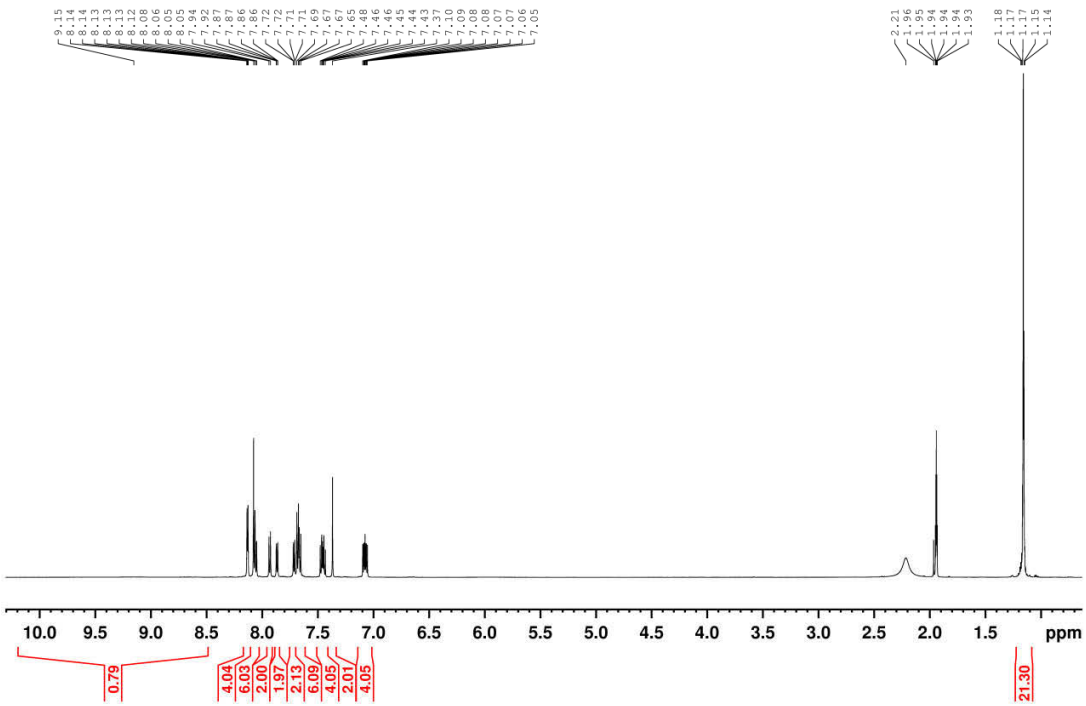

Figure S5. ^{1}H NMR spectrum (600 MHz, CD_3CN) of $[Ru(dqp\text{-}OH)(dqp\text{-}ph\text{-}C{\equiv}C\text{-}TIPS)][PF_6]_2$.

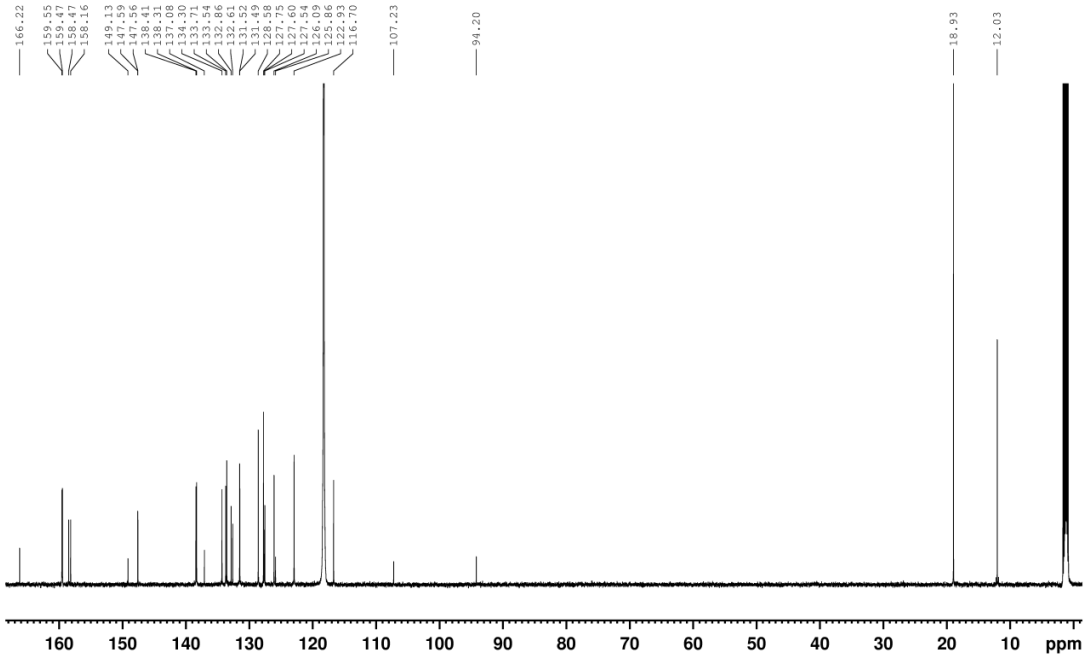

Figure S6. ^{13}C NMR spectrum (150 MHz, CD_3CN) of $[Ru(dqp\text{-}OH)(dqp\text{-}ph\text{-}C{\equiv}C\text{-}TIPS)][PF_6]_2$.

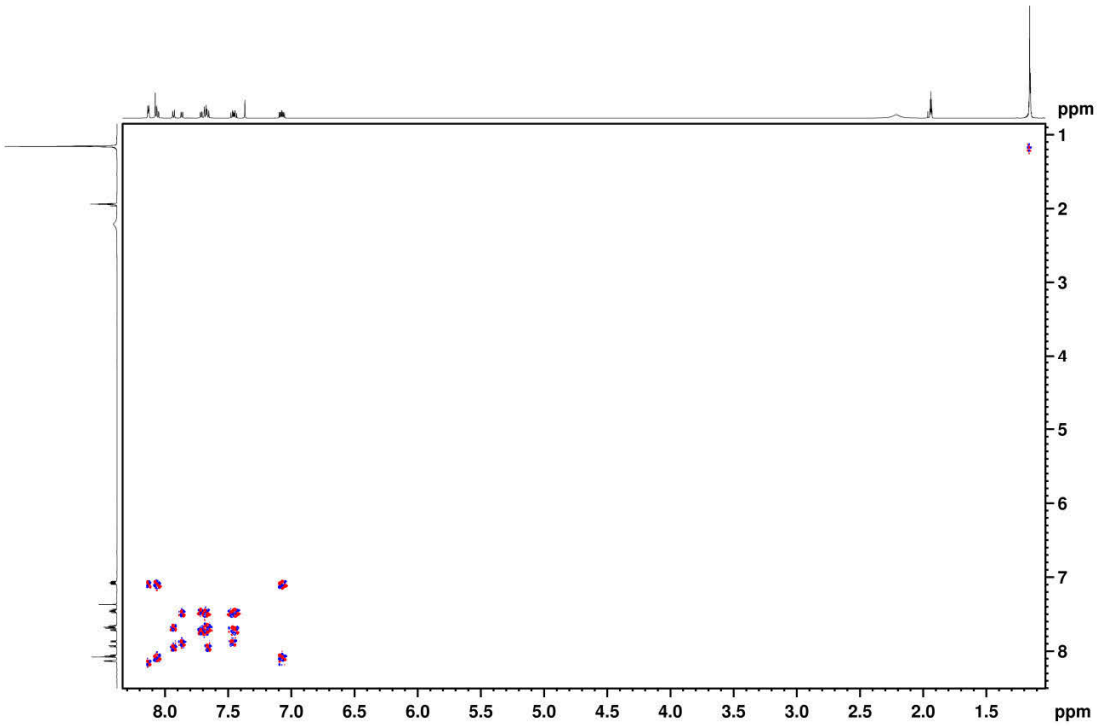

Figure S7. H,H COSY spectrum of [Ru(dqp-OH)(dqp-ph-C≡C-TIPS)][PF_6]$_2$.

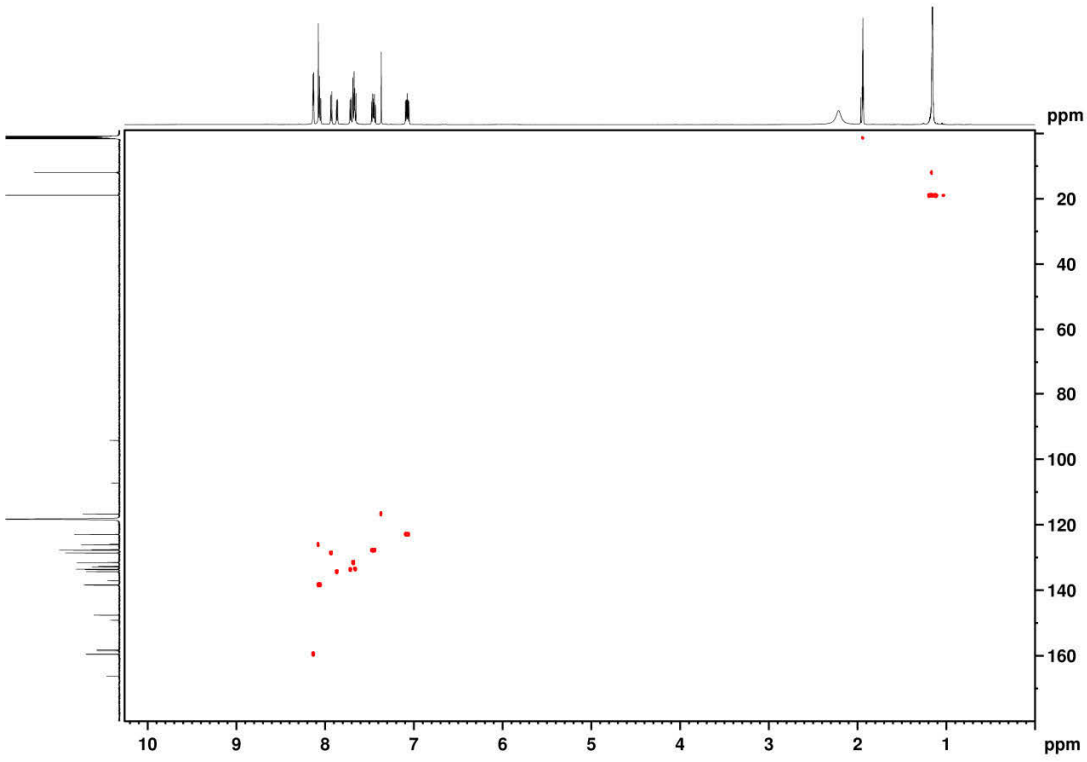

Figure S8. HSQC spectrum of [Ru(dqp-OH)(dqp-ph-C≡C-TIPS)][PF_6]$_2$.

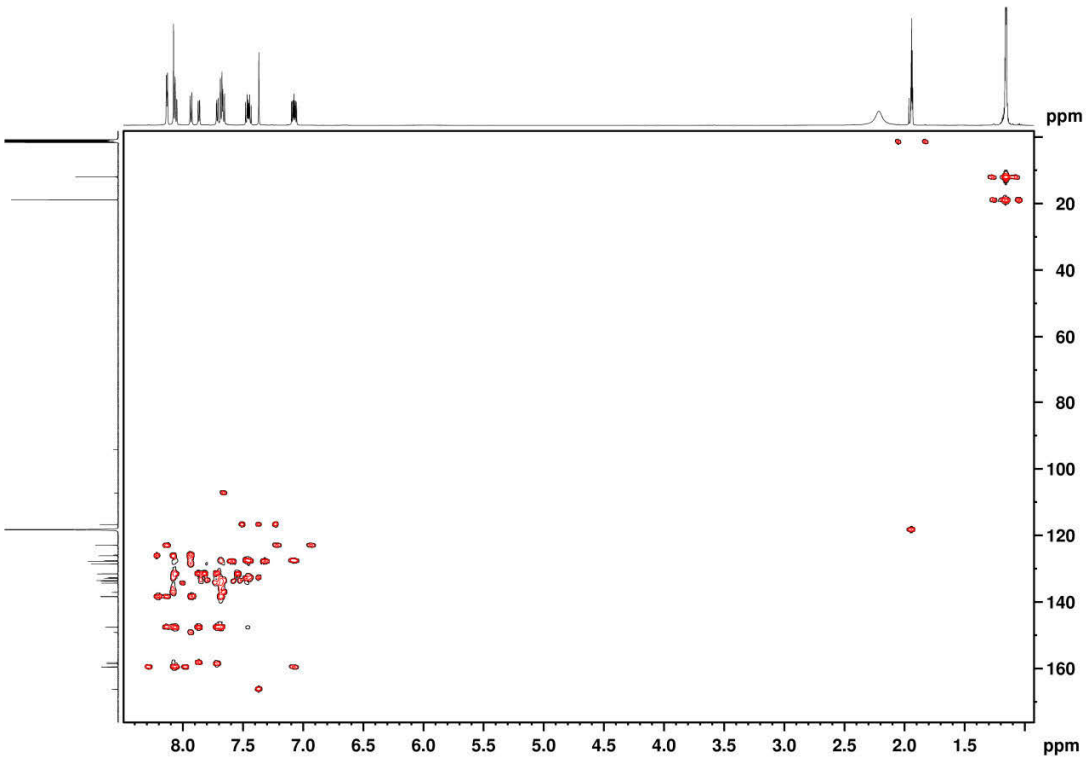

Figure S9. HMBC spectrum of [Ru(dqp-OH)(dqp-ph-C≡C-TIPS)][PF_6]$_2$.

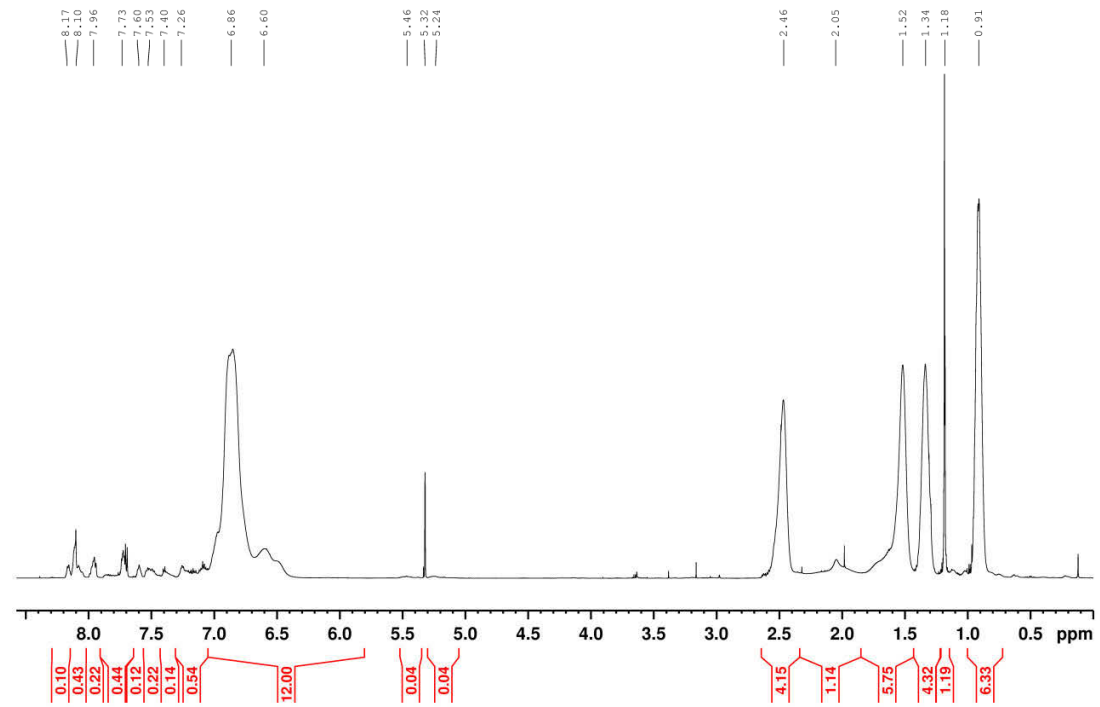

Figure S10. ^{1}H NMR spectrum (300 MHz, CD_2Cl_2) of [Ru(dqp-O-pTARA)(dqp-ph-C≡C-TIPS)][PF_6]$_2$. Note the downfield shift of the methylene group upon linkage (from 4.57 in Figure S3) to 5.5 ppm.

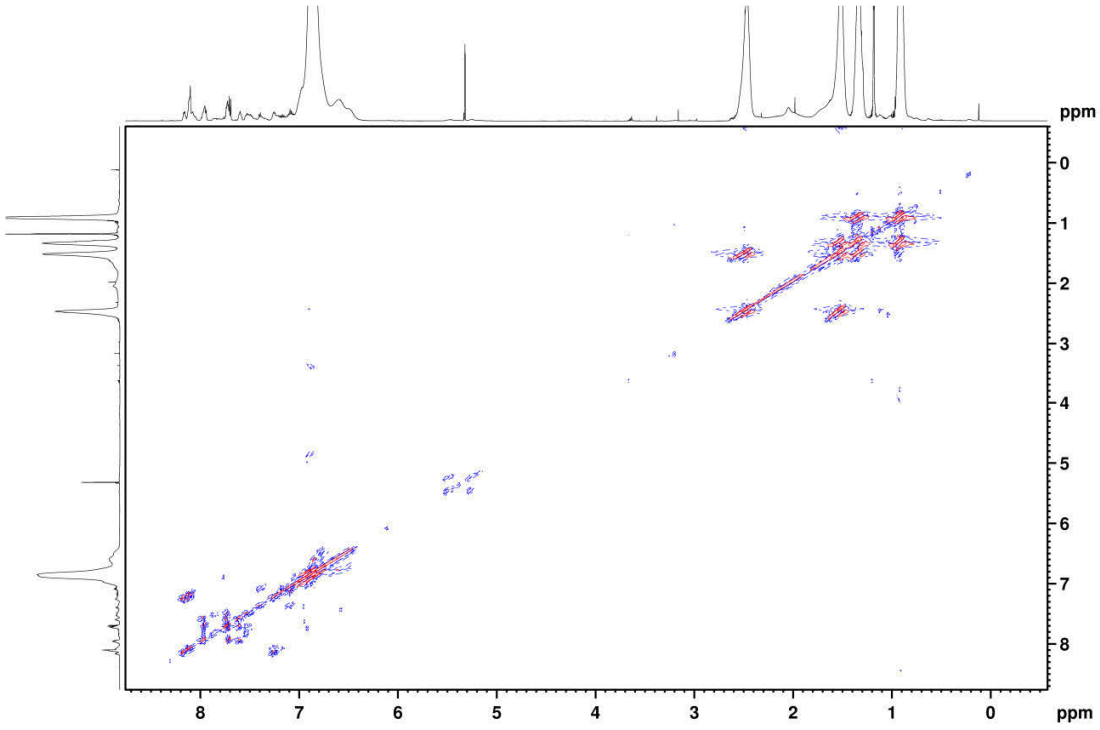

Figure S11. H,H COSY spectrum of [Ru(dqp-O-pTARA)(dqp-ph-C≡C-TIPS)][PF_6]$_2$.

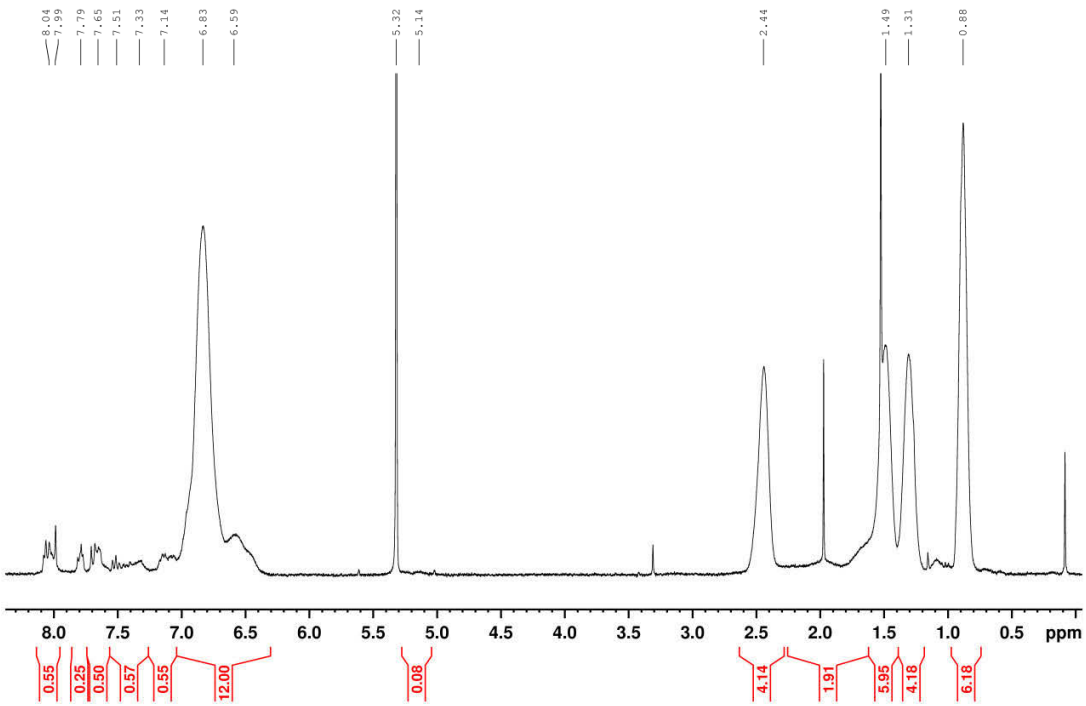

Figure S12. ^{1}H NMR spectrum (300 MHz, CD_2Cl_2) of [Ru(dqp-O-pTARA)(dqp-ph-C≡CH)][PF_6]$_2$.

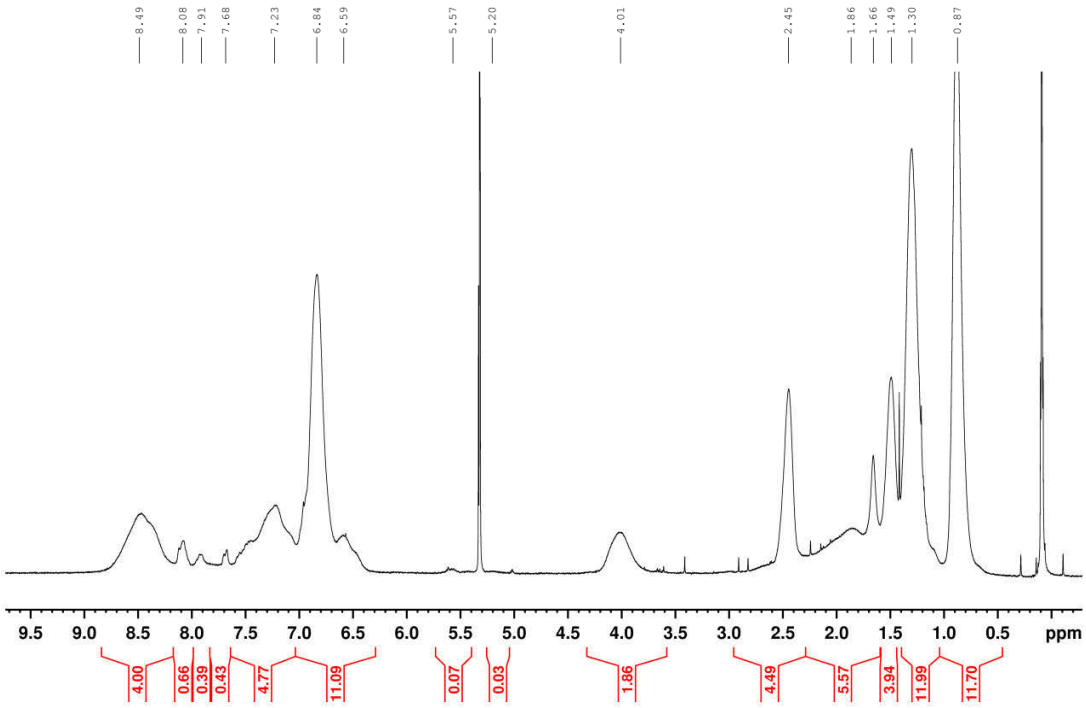

Figure S13. ^{1}H NMR spectrum (300 MHz, CD_2Cl_2) of [Ru(dqp-O-pTARA)(dqp-ph-trz-pNDI)][PF_6]$_2$ (D_n–P–A_m).

4. Mass spectrometry

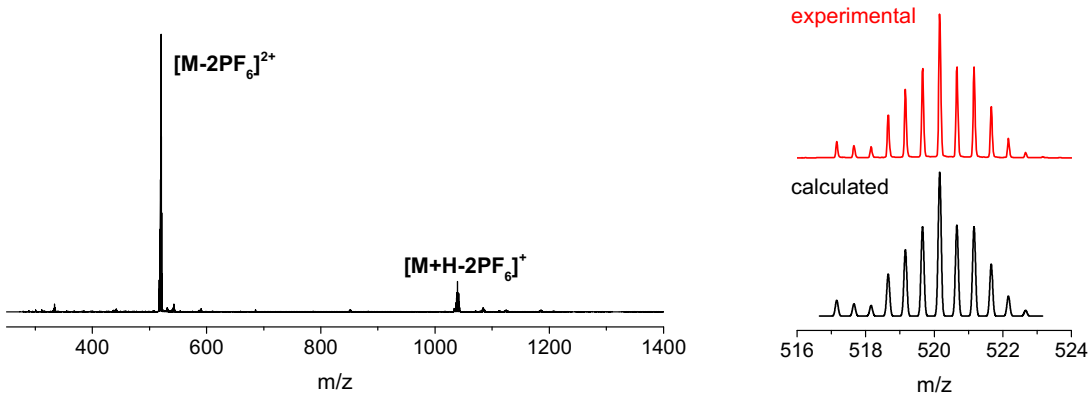

Figure S14. ESI TOF MS data of [Ru(dqp-OH)(dqp-ph-C≡C-TIPS)][PF_6]$_2$ and (right) comparison of measured and calculated isotope pattern.

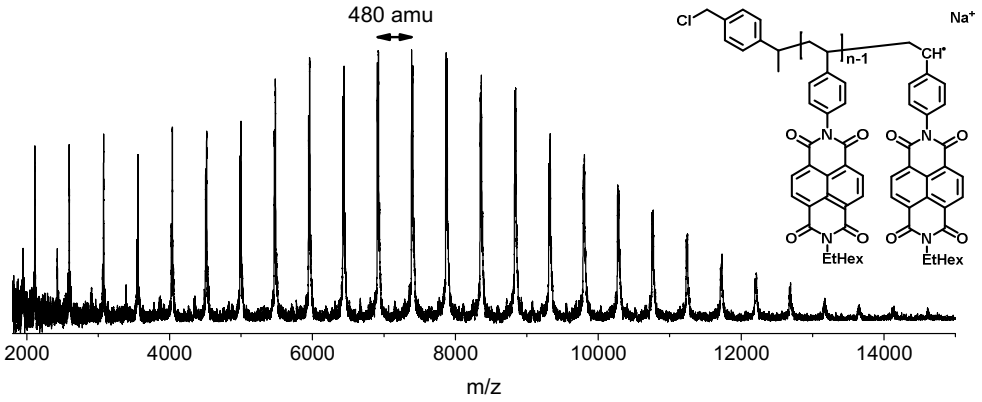

Figure S15. MALDI TOF mass spectrum of **pNDI (Cl-decorated)** (matrix: HABA + NaTFA) with proposed structure of the main series.

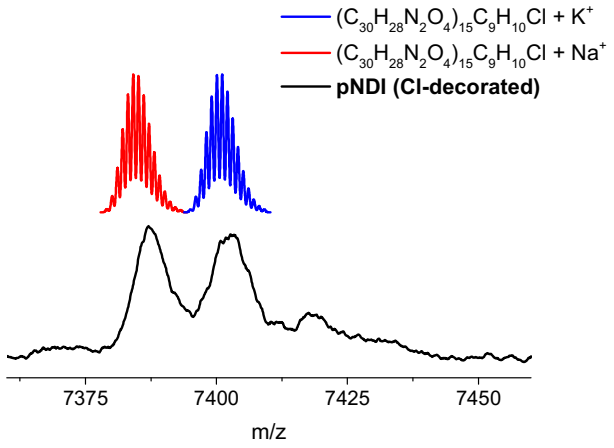

Figure S16. Theoretical (top) isotopic patterns to fit the experimental (bottom) data of the signal corresponding to a DP = 15 (matrix: HABA + NaTFA).

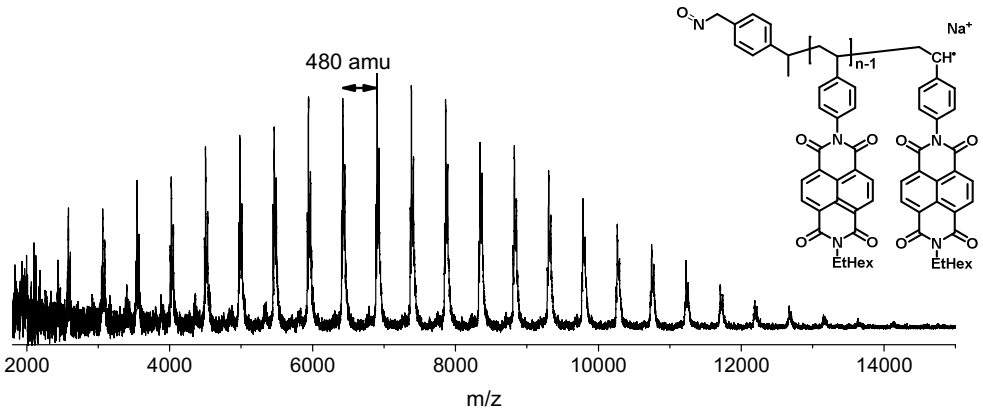

Figure S17. MALDI TOF mass spectrum of **pNDI (azide-decorated)** (matrix: HABA + NaTFA) with proposed structure of the main series.

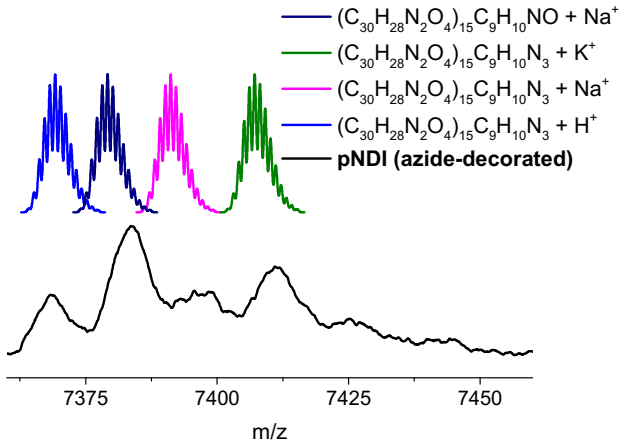

Figure S18. Theoretical (top) isotopic patterns to fit the experimental (bottom) data of the signal corresponding to a DP = 15 (matrix: HABA + NaTFA).

5. Size exclusion chromatography

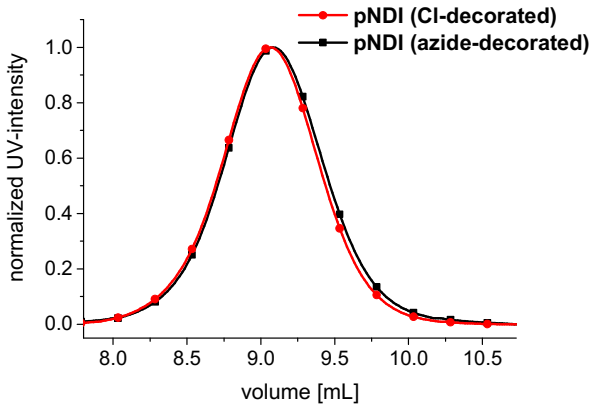

Figure S19. SEC elugrams of **pNDI (Cl-decorated and azide-decorated)** showing the absence of degradation during the functionalization (UV: 340 nm detection wavelength, $CHCl_3$, *iso*-propanol, triethylamine 94/2/4).

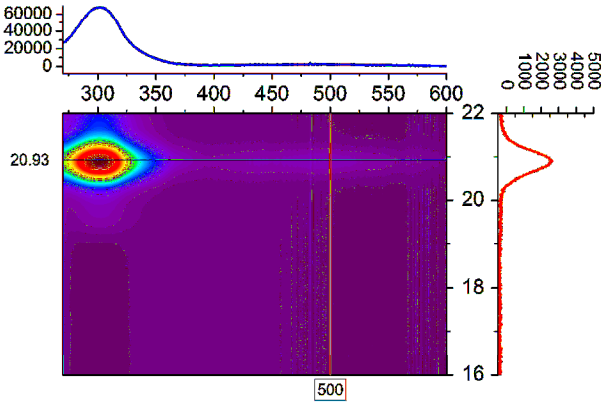

Figure S20. 3D SEC data (wavelength vs elution time, DMAc + 0.08% NH4PF6) of [Ru(dqp-O-pTARA)(dqp-ph-C≡C-TIPS)][PF_6]$_2$ with projections: (top) UV trace at 20.03 mL; (right) chromatogram at 500 nm in a.u..

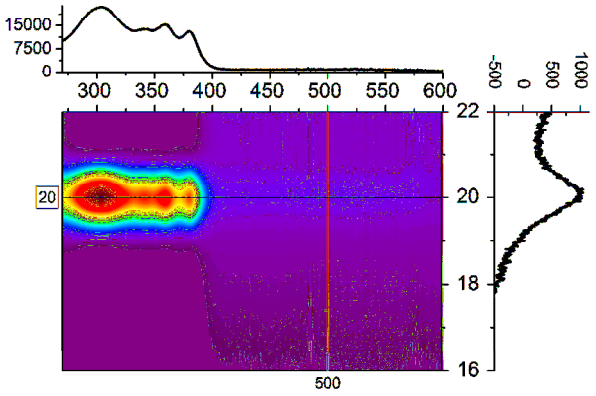

Figure S21. 3D SEC data (wavelength vs elution time, DMAc + 0.08% NH4PF6) of [Ru(dqp-O-pTARA)(dqp-ph-C≡C-trz-pNDI)][PF_6]$_2$ **(D_n–P–A_m)** with projections: (top) UV trace at 20.03 mL; (right) chromatogram at 500 nm in a.u..

6. Steady state optical data

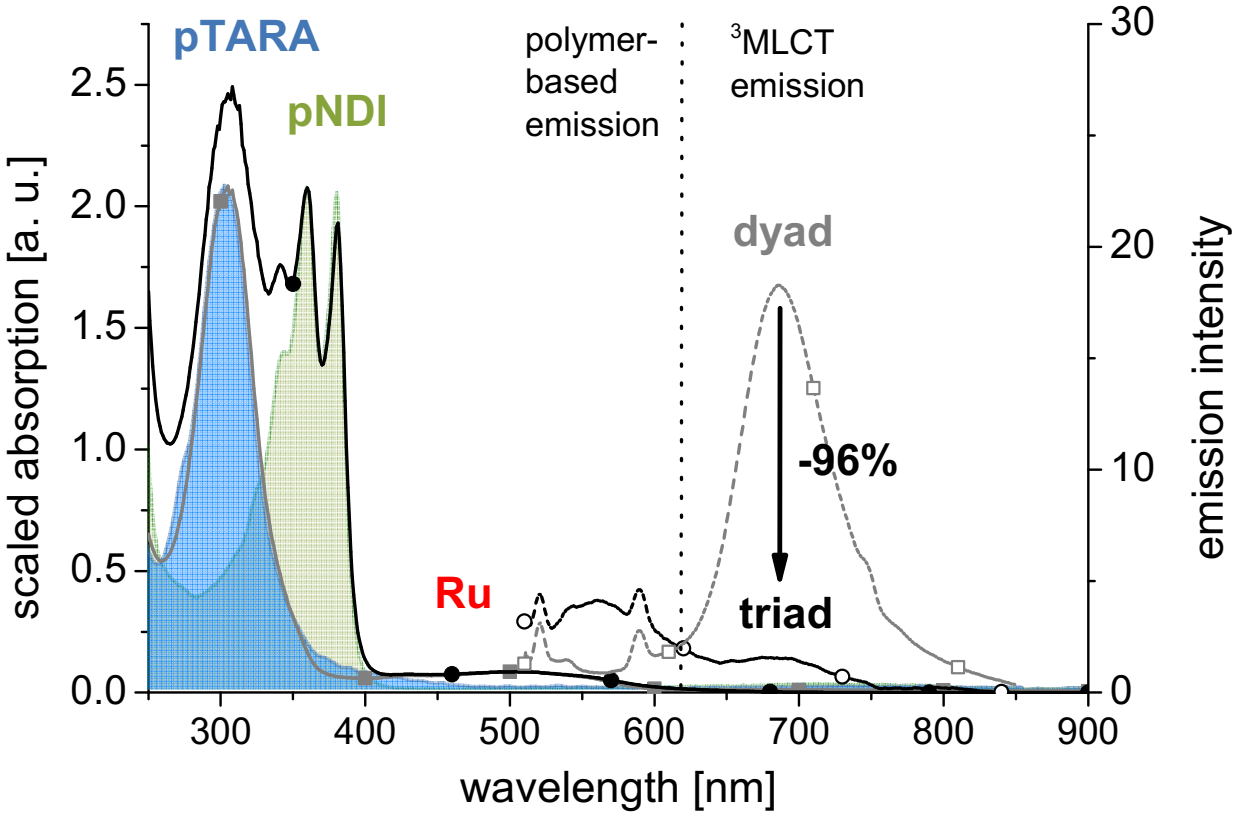

Figure S22. Enlarged version: Absorption spectra (left axis) of the triad (black curve, circles), including its precursor dyad (grey curve, rectangles) and the polymeric building blocks pTARA (blue-shaded area) and pNDI (green-shaded area). Note the absorption band of the single Ru photosensitizer unit (400–600 nm). Steady-state emission spectra (right axis) of the precursor dyad (grey dashed line, rectangles) and the triad (black dashed line, circles). Note polymer-based emission (<650 nm) and the ^{3}MLCT emission (around 700 nm), the latter one quenched by 96% comparing dyad and triad (subtracting residual polymer-based emission). All measurements were performed in aerated DCM solution, asterisk denotes Raman artefacts.

7. Spectroelectrochemical data

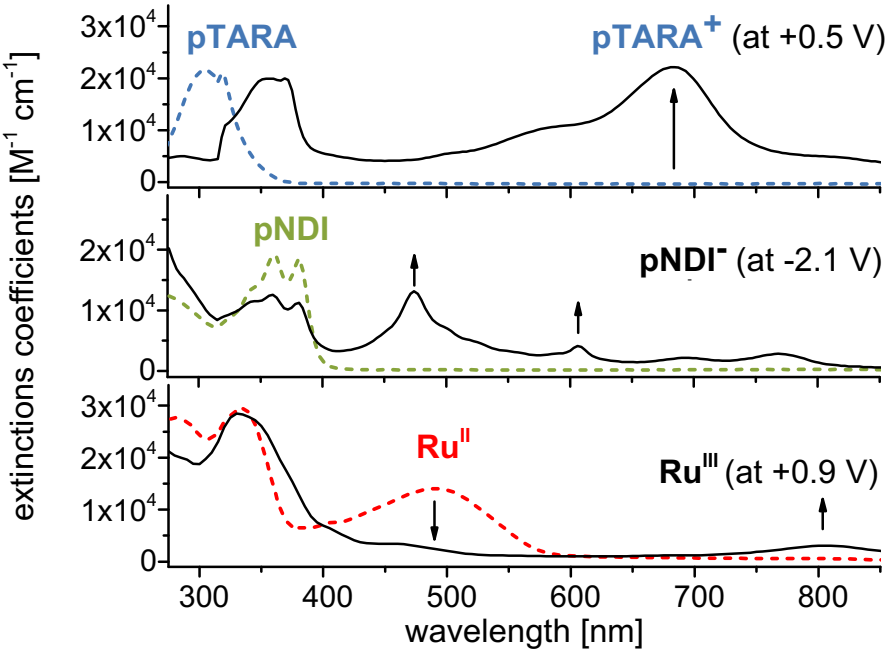

Figure S23. Spectro-electrochemical data (in 0.1 M $^{n}Bu_4NPF_6$ in CH_2Cl_2, potentials *vs.* $Fc^{+/0}$) of the pTARA block (top), the pNDI block (middle), and the Ru reference complex (bottom). Spectroelectrochemical data taken from refs. [3,6]

8. Time-resolved data

8.1. Emission data

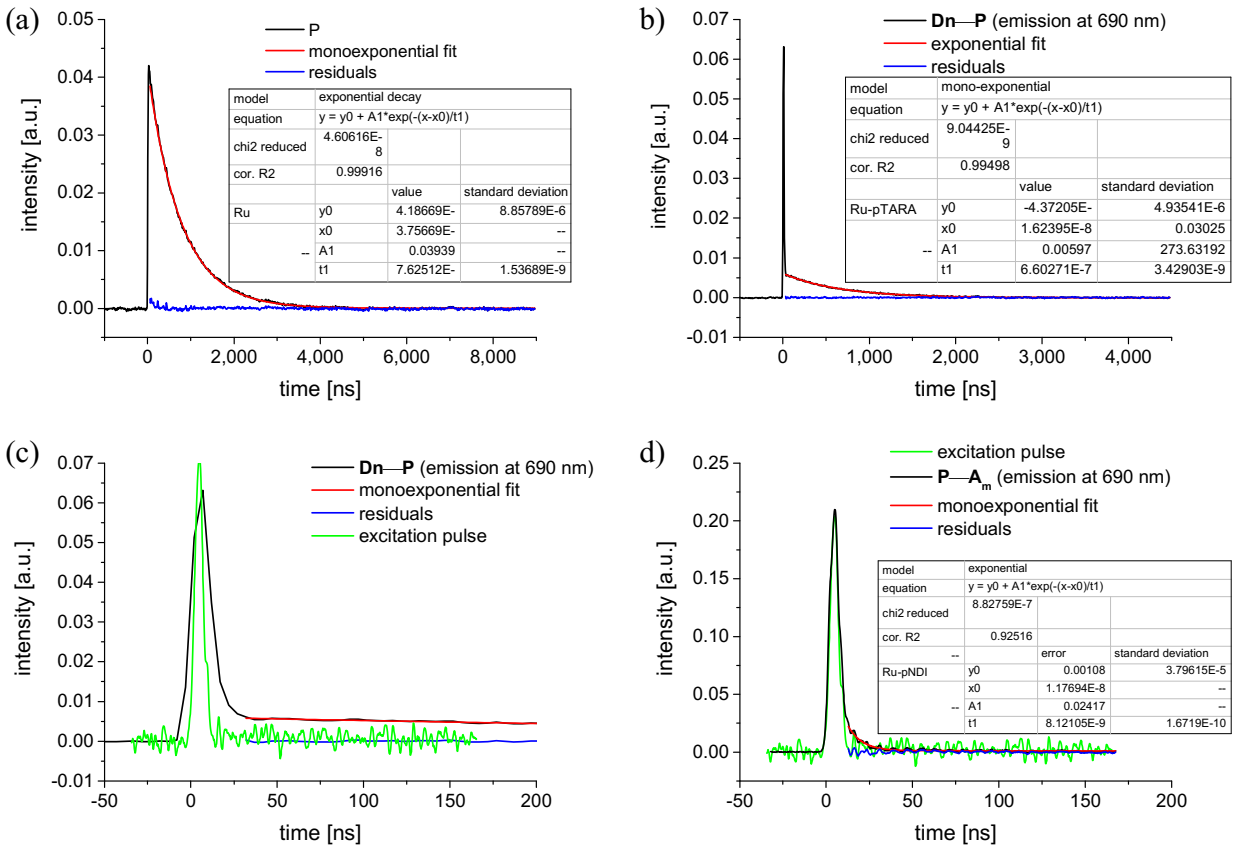

Figure S24. Emission data and respective fits for the reference systems: (a) Photosensitizer (**P**), (b) donor dyad ($\mathbf{D_n–P}$) with zoom of the pulse region (c), and (d) acceptor dyad ($\mathbf{P–A_m}$) including pulse (green). Excitation pulse width (approximately 10 ns) determined from Raman scatter of a pure DCM sample.

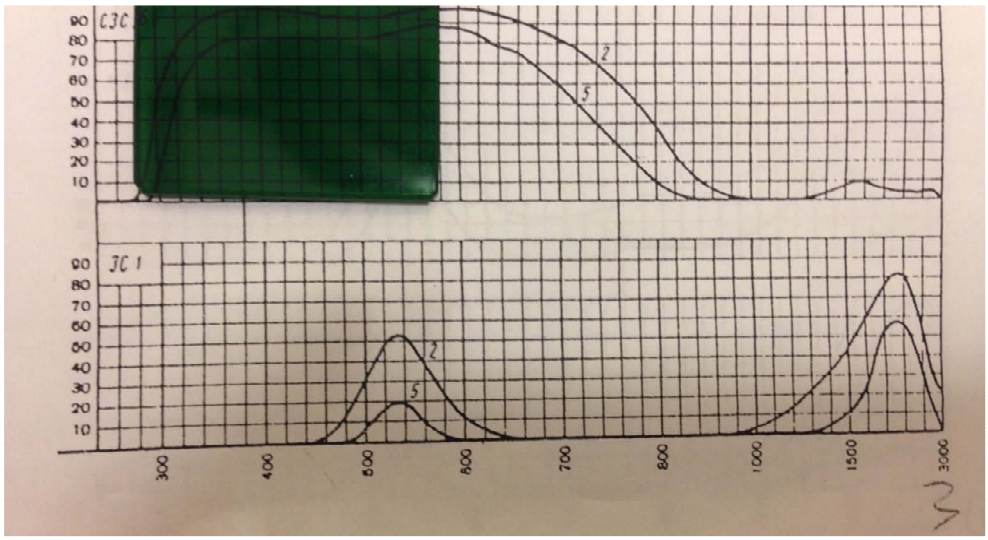

Figure S25. Transmission properties of band pass filter (3C1) used in TCSPC measurements (λ_{max} = 540 nm with FWHM ca. 100 nm. Note that blocked transmission above 650 nm, which is typical for the ^{3}MLCT emission.

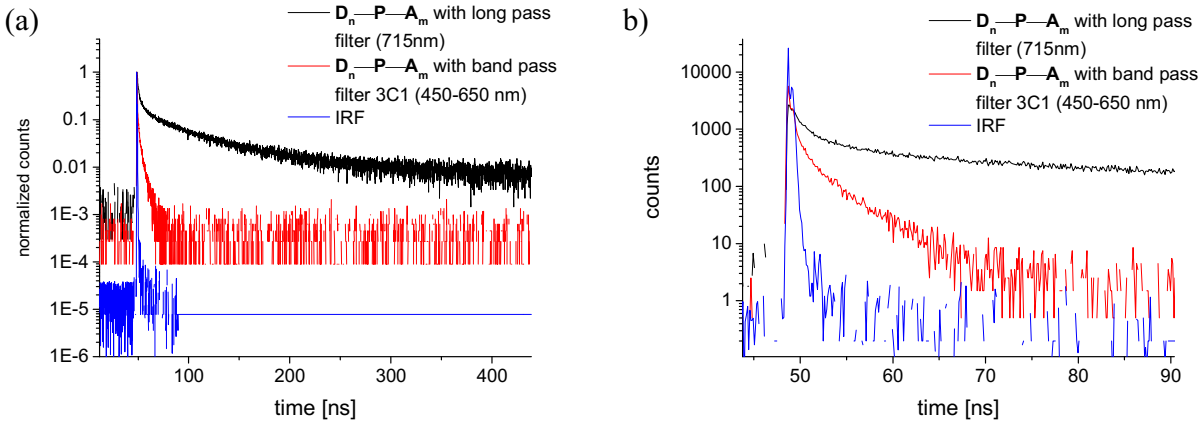

Figure S26. Normalized time-correlated single photon counting data of **D_n–P–A_m** (a) and expansion of pulse region (b). Instrument response function (IRF, blue), with long pass filter (>715 nm, black) and with band pass filter (3C1, 450-650 nm, red). See Figure S25 for transmission characteristics of 3C1 filter.

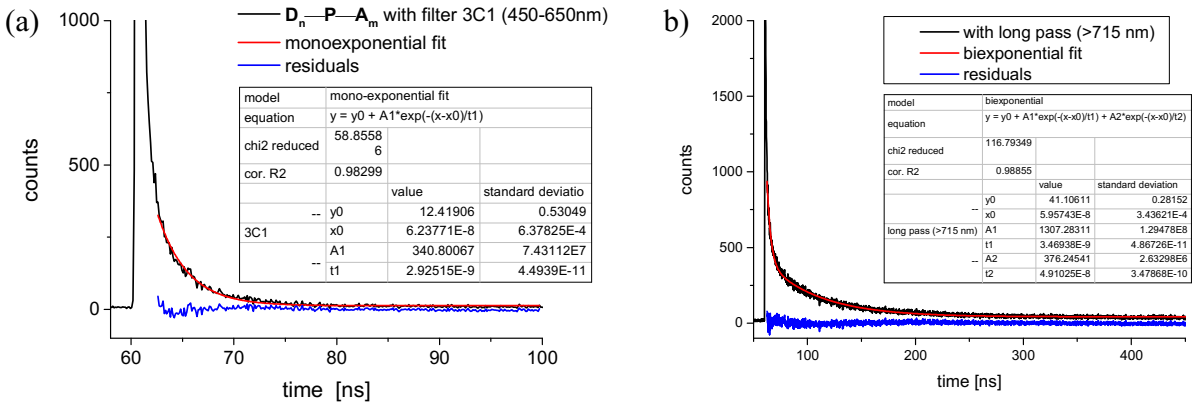

Figure S27. TCSPC data and fits of **D_n–P–A_m** using (a) the band pass filter 3C1 (450–650 nm), and (b) the long pass filter (>715 nm).

8.2. Transient absorption data

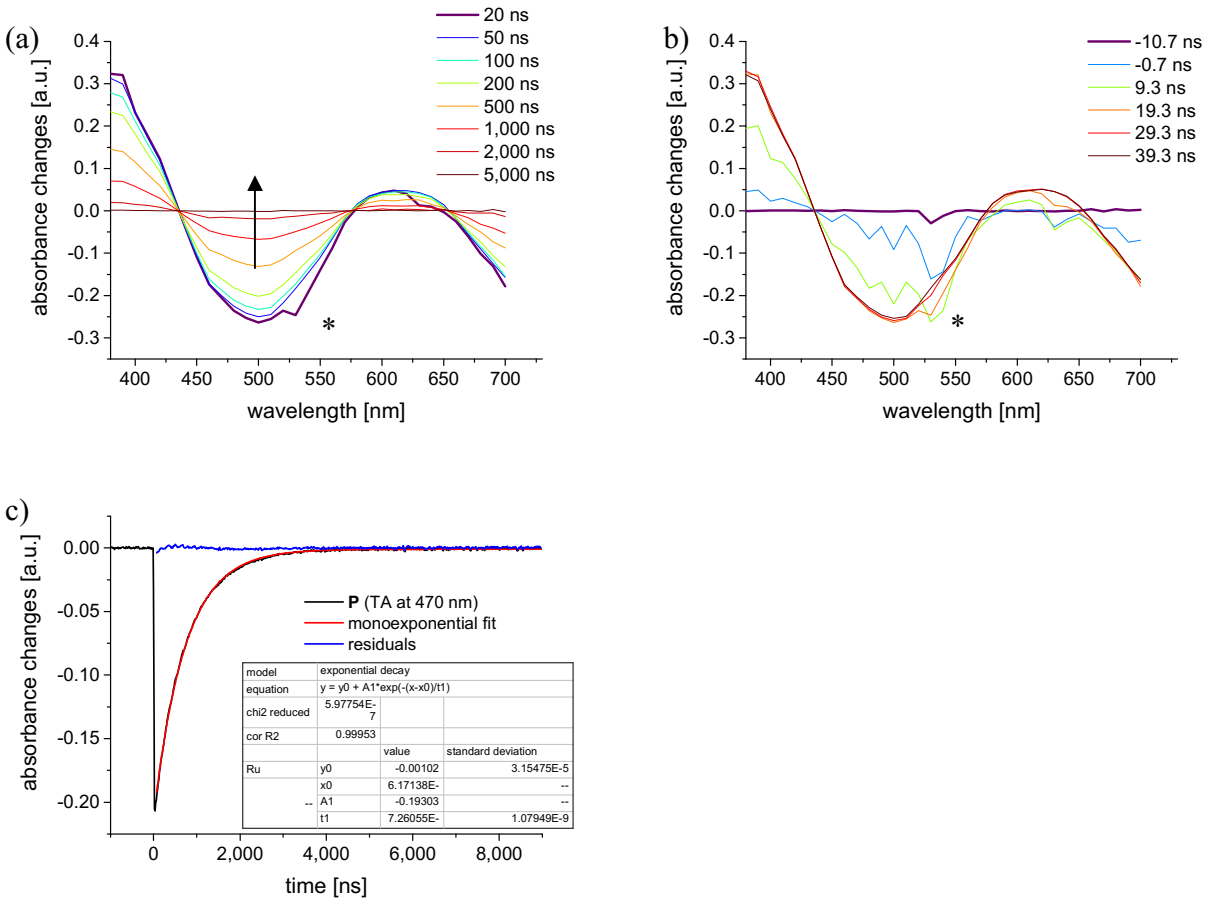

Figure S28. Transient absorption data of **P**: (a) Spectral recovery at selected times with zoom of pulse region (b). Note the isosbestic points around 435 and 575 nm. Asterisk denotes excitation pulse artefacts due to Rayleigh scatter. (c) Decay profile with fit at 470 nm.

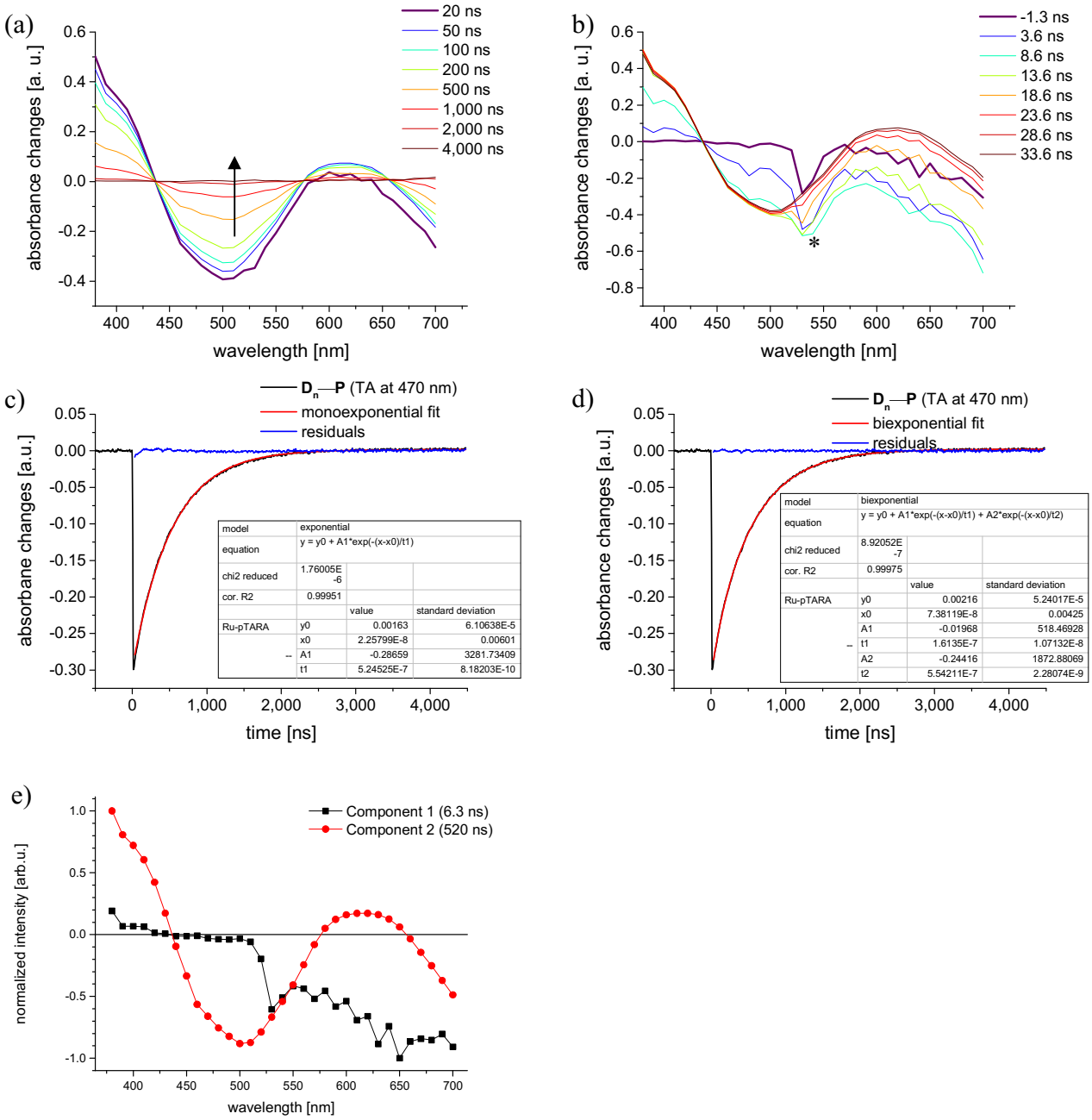

Figure S29. Transient absorption data of $\mathbf{D_n}$**–P**: (a) Spectral recovery at selected times with zoom of pulse region (b). Note the preserved isosbestic point around 435 nm but clear deviation at 575 nm with respect to Ru (Figure S28), as well as weaker TA signals between 575 and 650 nm assigned to additional polymer-based emission (see text). Asterisk denotes excitation pulse artefacts including

Rayleigh scatter. (c) Decay profile with fit at 470 nm including biexponential decay (d). Global fit (>= 18.6 ns) with biexponential kinetics with corresponding amplitudes (scaled for comparison). Component 1 (black curve) shows similar spectral signatures as polymer-based emission from steady state data with comparable lifetimes (6.3 ns) as observed in TCSPC with band pass filter (Figure S27), while component 2 (red curve) resembles **P** in terms for its spectrum and lifetime (520 ns, Figure S28).

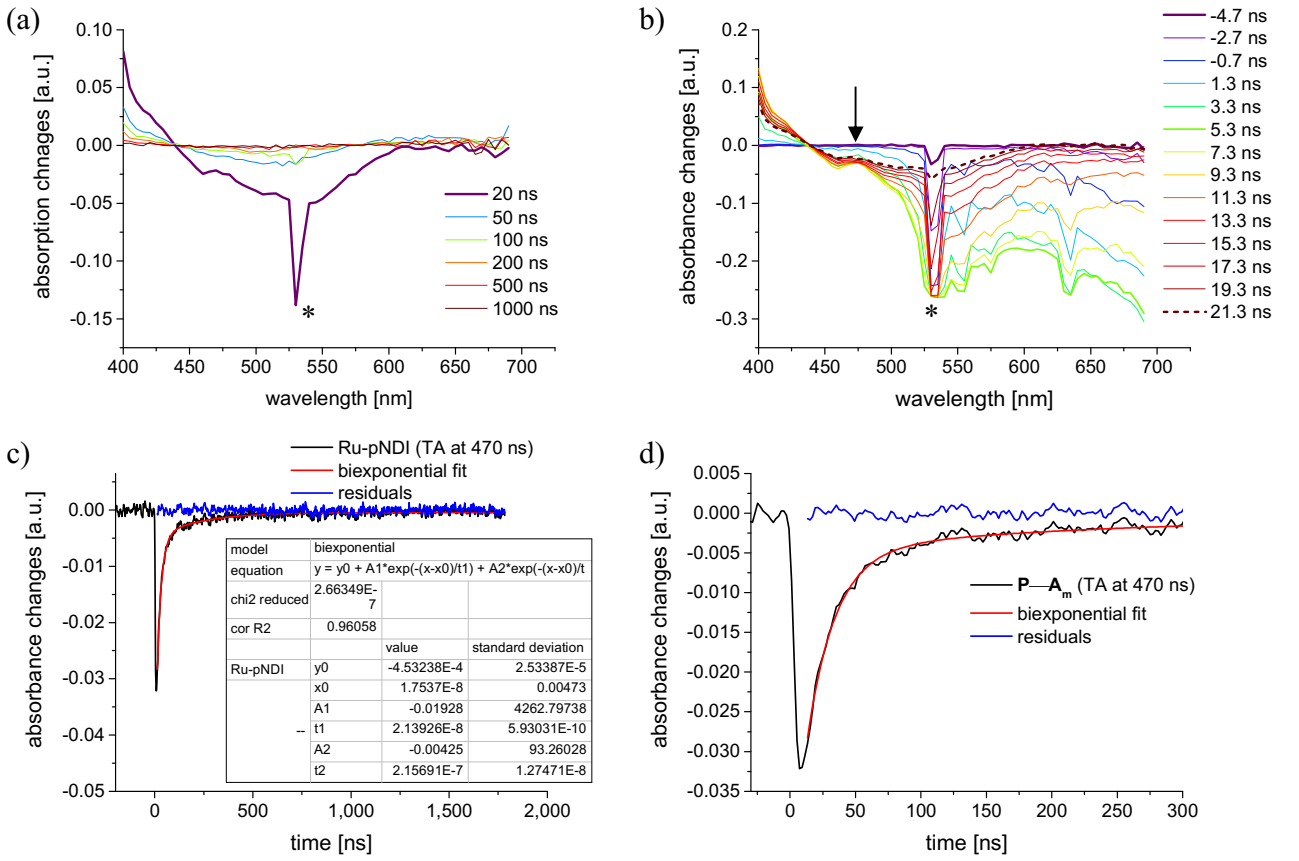

Figure S30. Transient absorption data of **P–A$_m$**: (a) Spectral recovery at selected times with zoom of pulse region (b). Note the preserved isosbestic point around 435 nm but clear deviation at 575 nm with respect to Ru (Figure S28), as well as the more negative TA signals between 575 and 650 nm assigned to additional polymer-based emission (see text). Note the very weak TA features of pNDI$^-$ (475 nm) developing and decaying with excitation time window (maximal after 5.3 ns). After 21.3 ns, the typical ^{3}MLCT without polymer-emission is observed. Asterisk denotes excitation pulse artefacts including Rayleigh scatter. (c) Decay profile with fit at 470 nm and zoom to pulse region (d), corroborating the charge separation and rapid charge recombination.

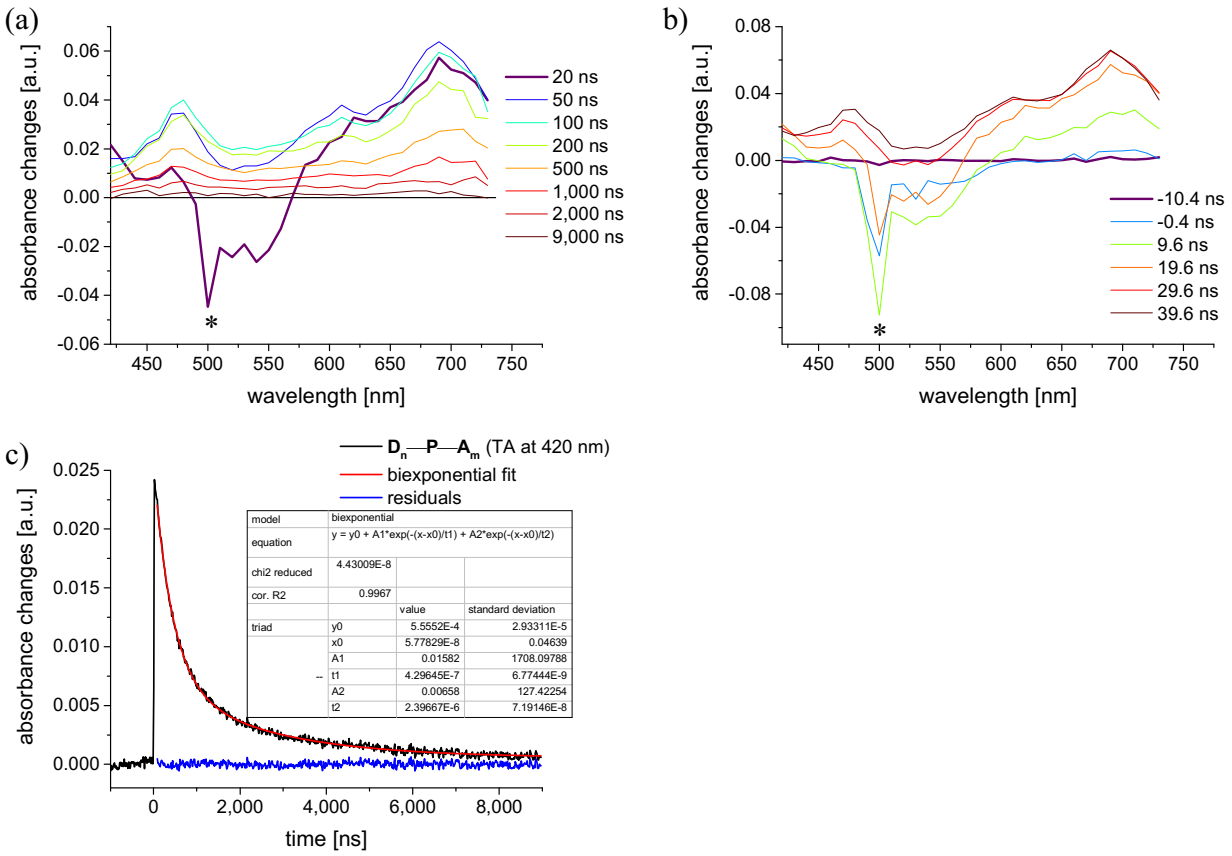

Figure S31. Transient absorption data of $\mathbf{D_n–P–A_m}$: (a) Spectral recovery at selected times with zoom of pulse region (b). Asterisk denotes excitation pulse artefacts due to Rayleigh scatter.Note the rapid formation of positive TA signals with characteristic signatures of $pNDI^{-}$ (475 and 610 nm) and $pTARA^{+}$ (690 nm) in accordance to the spectroelectrochemical data. (c) Decay profile (at 420 nm) and biexponential fit with time constants of 430 ns (70%) and 2,400 ns (30%).

References

(1) Fulmer, G. R.; Miller, A. J. M.; Sherden, N. H.; Gottlieb, H. E.; Nudelman, A.; Stoltz, B. M.; Bercaw, J. E.; Goldberg, K. I. *Organometallics* **2010**, *29*, 2176.

(2) Schroot, R.; Friebe, C.; Altuntas, E.; Crotty, S.; Jäger, M.; Schubert, U. S. *Macromolecules* **2013**, *46*, 2039.

(3) Kübel, J.; Schroot, R.; Wächtler, M.; Schubert, U. S.; Dietzek, B.; Jäger, M. *The Journal of Physical Chemistry C* **2015**, *119*, 4742.

(4) Jäger, M.; Kumar, R. J.; Görls, H.; Bergquist, J.; Johansson, O. *Inorg. Chem.* **2009**, *48*, 3228.

(5) Jäger, M.; Eriksson, L.; Bergquist, J.; Johansson, O. *J. Org. Chem.* **2007**, *72*, 10227.

(6) Schroot, R.; Schubert, U. S.; Jäger, M. *Macromolecules* **2015**, *48*, 1963.

Published Publication P7

A multidonor–photosensitizer–multiacceptor triad for long-lived directional charge separation

T. Schlotthauer, R. Schroot, S. Glover, L. Hammarström, M. Jäger, U. S. Schubert,
Phys. Chem. Chem. Phys. **2017**, *19*, 28572-28578.

The paper as well as the supporting information (free of charge) are available online under: doi.org/10.1039/c7cp05593e

PCCP

PAPER

Cite this: *Phys. Chem. Chem. Phys.*, 2017, **19**, 28572

A multidonor–photosensitizer–multiacceptor triad for long-lived directional charge separation†

Tina Schlotthauer,[a] Robert Schroot,[a] Starla Glover,[b] Leif Hammarström,[b] Michael Jäger *[ac] and Ulrich S. Schubert *[ac]

Received 16th August 2017,
Accepted 10th October 2017

DOI: 10.1039/c7cp05593e

rsc.li/pccp

The modular assembly of a directional photoredox-active multidonor–photosensitizer–multiacceptor (D_n–P–A_m) architecture is presented. The triad assembly features a central Ru(II) sensitizer equipped with pendant polymer chains consisting of multiple triarylamine (pTARA) and naphthalene diimide (pNDI) units, respectively. Upon excitation, the efficient formation (>96%) of charge separation (CS) was observed featuring similar CS lifetimes (400 ns) as related molecular triads. In contrast, a significant additional longer-lived CS component (2400 ns, 30%) is observed indicating multiple contributing pathways.

The efficient conversion of light energy into a redox-chemical potential is a longstanding goal. On a molecular level, a multitude of artificial photosystems have been designed from individual photo- and redox-active building blocks.[1–7] These subunits perform the elementary steps of light absorption (by photosensitizer, P) and charge storage (by electron donor, D; electron acceptor, A) to generate a photo-induced charge separation. Within such assemblies, the individual (photo)-redox potentials dictate the thermodynamic driving forces for electron transfer, while the linkage pattern (bridge) between the units control the kinetics, which can be tuned in terms of electronic communication and the mutual distances.[8–11] Among other photosensitizers, polypyridyl-type Ru^{II} complexes display remarkable photophysical properties,[12–14] particularly $[Ru(bpy)_3]^{2+}$-based (bpy is 2,2′-bipyridine) complexes. Recently, $[Ru(dqp)_2]^{2+}$-type (dqp is 2,6-di(quinolin-8-yl)pyridine) complexes have emerged due to their advantageous combination of photophysical properties and axial symmetry, as well as enhanced photostability in comparison to $[Ru(bpy)_3]^{2+}$.[15,16] Typical electron donor units are based on electron-rich aromatics (*e.g.*, phenothiazine, triarylamines), while electron-deficient heterocycles (*e.g.*, methyl viologen, aromatic diimides) or quinones often serve as electron acceptors.[17–20] Numerous advanced molecular systems (triads, D–P–A; tetrades *etc.*) have been devised, that feature high molecular symmetry, adjusted redox potentials, and distinct spectroscopic signatures to elucidate the charge separation events. Noteworthy, extraordinary long-lived charge separation with excellent quantum yield has been achieved.[17–20] However, charge migration and storage – as desired for device application – implies formally multiple units, leading to increasingly elaborative syntheses, which impedes the practical value despite the powerful design principles. In this context, polymer chemistry offers not only appealing opportunities to connect multiple units, but also to further exploit the macromolecule's architecture (Fig. 1).[2,21] The capability to apply some of the principles in the design of macromolecular architectures is exemplified for light harvesting,[2,21] *e.g.*, using Ru^{II}-decorated oligopeptides[22–24] or polystyrene (PS),[25,26] poly(propylmethacrylate) (PPMA),[27] poly(3-hexylthiophene) (P3HT),[28] poly(fluorene)[29] or poly(fluorene-*co*-thiophene).[30] The seminal studies utilized statistical polymers *via* free radical polymerizations and/or grafting strategies, *e.g.*, to randomly embed D–P–A subunits within a P_n polymer chain (Fig. 1a). Efficient light harvesting and long-lived charge separation was demonstrated, although the generated charges are trapped locally due to the absent percolation pathway as a consequence of the random incorporation. In this regard, the reactive chain terminus offers an elegant opportunity to design directional macromolecular architectures. For example, a single viologen acceptor was appended to the P_n chain terminus, leading to approximately 30% emission quenching assigned to energy transfer and subsequent charge separation.[26] Similarly, an inverted architecture was devised with a single sensitizer coupled to a multi-acceptor chain, which displayed quantitative charge separation.[31,32] The immobilization of polymer-based dyads onto semiconductor interfaces (Fig. 1b and c), in analogy to dye sensitized solar cells,[33] was also reported. Due to the rapid interfacial electron injection and the semi-conductors band structure, long-lived charge separation up to hundreds

[a] *Laboratory of Organic and Macromolecular Chemistry (IOMC), Friedrich Schiller University Jena, Humboldtstraße 10, 07743 Jena, Germany. E-mail: michael.jager.iomc@uni-jena.de, Ulrich.schubert@uni-jena.de*
[b] *Department of Chemistry – Ångström Laboratory, Uppsala University, Box 523, SE75120 Uppsala, Sweden*
[c] *Center for Energy and Environmental Chemistry Jena (CEEC Jena), Friedrich Schiller University Jena, Philosophenweg 7a, 07743 Jena, Germany*

† Electronic supplementary information (ESI) available: Synthetic procedures as well as additional characterization data (NMR, MS, SEC, UV/vis data). See DOI: 10.1039/c7cp05593e

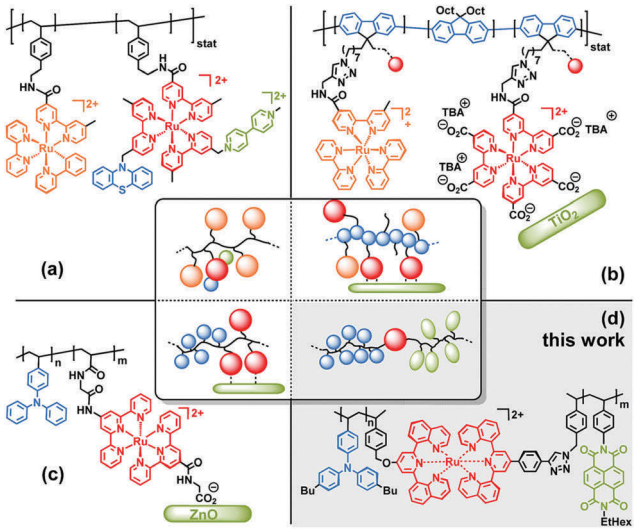

Fig. 1 Illustrative examples of macromolecular Ru-based photosystems composed of photosensitizer (in orange/red), electron donors (in blue) and electron acceptors (in green). Typical polypyridyl-type ligands based on bpy (a and b), tpy (c), and dqp (this work) framework, electron donors based on aromatic amines (a: phenothiazine; c and d: triarylamines) or polyfluorene (b), electron acceptors (a: methyl viologen, d: naphthalene diimide) or inorganic semiconductors (b: TiO_2, c: ZnO). Polymer backbones based on styrene (a and d), acrylates (c) or conjugated fluorene (b), forming statistical copolymers (a and b) or block-copolymers (c and d). See text for further details.

of microseconds was observed (Fig. 1b).[30] The progress in polymer chemistry further enabled the utilization of conjugated polymers, which were shown to act as electron donors in charge separation.[29,30] From a hierarchical perspective, the immobilized block-copolymer depicted in Fig. 1c features a multi-donor triarylamine polymer corona on a multi-acceptor ZnO particle with interjacently embedded photoactive Ru^{II} units. Notably, the detailed analysis required substantial molecular modelling to interpret the multiexponential decay data, which arises from the conformational freedom of the flexible polymer as well as defects due to incomplete grafting and/or chain-end functionalization.

In this contribution, a novel fully polymer-based architecture is explored (Fig. 1d and Scheme 1). The D_n–P–A_m triad consists of a single bifunctional photosensitizer, which can be selectively excited in the visible light region. The two functional groups were used to selectively attach precisely one multi-donor and one multi-acceptor chain. Triarylamine and naphthalene diimide units were selected as versatile donor and acceptor units, respectively, which are, *e.g.*, investigated in self-assembled naphthalene diimide (NDI) stacks for electron transport.[34,35] Hence, the resulting block-copolymer-type D_n–P–A_m architecture assures a percolation pathway for charge transport, in analogy to typical transport mechanisms in organic semiconductors.[36] The linkage pattern around the central Ru sensitizer unit adopts an axial geometry, in order to maximize the spatial separation of the charge-carrying units and, thus, is expected to minimize charge recombination. In addition, the synthesis relies on a modular chemistry-on-the-complex strategy including optimized purification protocols.

Modular syntheses and analytical characterization

The synthesis from donor dyads (D_n–P)[37] and acceptor dyads (P–A_m)[31,32] was extended to prepare a novel covalently linked multidonor–photosensitizer–multiacceptor (D_n–P–A_m) triad. Hence, the essential aspects in the design and preparation will be briefly recalled. In order to assist the readability throughout this manuscript, the functional building blocks and the corresponding properties are color-coded, *i.e.*, the photosensitizer in red, the electron donors in blue and electron acceptors in green, respectively. The donor and acceptor units were selected due to their transparency in the visible region, suitable redox potentials with respect to light-induced electron transfer, and

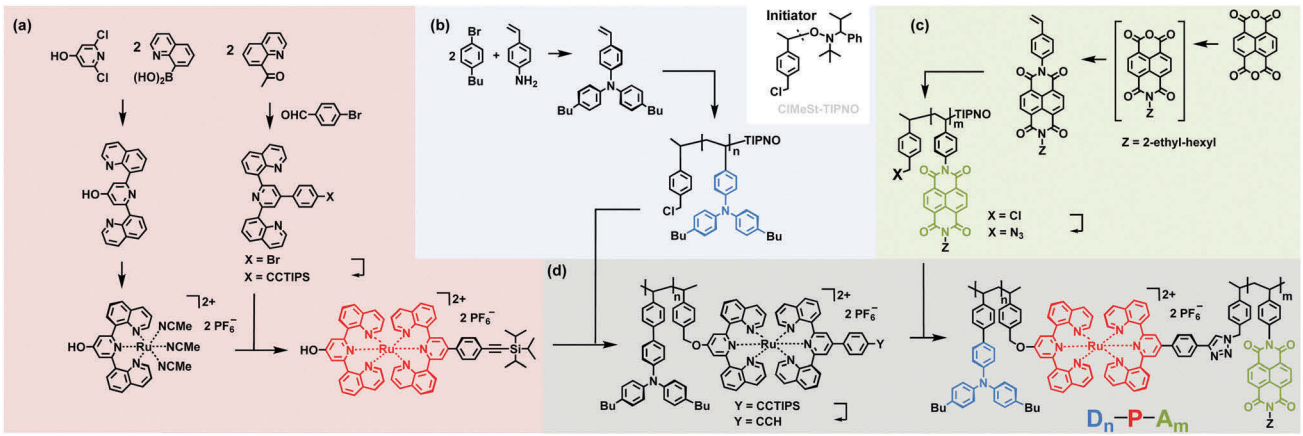

Scheme 1 Modular assembly strategy from building blocks. Syntheses of building blocks (colored boxes, a–c): (a) the bis-functionalized ruthenium photosensitizer, (b) the benzyl-chloride decorated poly(triarylamine) and (c) the azide-decorated poly(naphthalene diimide). Modular assembly (grey box, d) *via* Williamson ether synthesis and CuAAC reagents. Note the divergent character with at most five linear steps from commercially available starting reagents. For reagents and conditions see ESI.†

distinguishable spectroscopic signatures in the reduced/oxidized form. Following a divergent synthesis approach with at most five linear steps (Scheme 1), the chosen chemistry-on-the-complex approach and the developed purification protocols permits the quantitative functionalization by independently prepared polymers. The bis-functionalized Ru^{II} complex is readily prepared *via* stepwise coordination of the two ligands (Scheme 1a),[38] which bear the desired hydroxyl or tri-isopropylsilyl (TIPS)-protected alkyne groups. The telechelic donor and acceptor polymers were prepared *via* nitroxide-mediated polymerization (NMP) from the styrenic triarylamine (Scheme 1b) or styrenic naphthalene diimide (Scheme 1c),[32,37] which originate from vinyl aniline *via* the Hartwig–Buchwald coupling or stepwise condensation of naphthalene tetracarboxylic dianhydride.[31,37] Noteworthy, the desired polymer end group is already introduced *via* the commercially available NMP initiator. In addition, the terminal benzyl chloride unit is readily converted to the corresponding azide group after polymerization. Further experimental details and analytical characterization are provided in the ESI† (Fig. S2–S21). In summary, the divergently prepared building blocks are equipped with orthogonal functional groups to assist the modular assembly of the triad, the redox-active polymers poly(triarylamine) (pTARA) and poly(naphthalene diimide) (pNDI). Next, the D_n–P–A_m triad was prepared by Williamson ether synthesis to connect the pTARA-chain, followed by copper(I) catalyzed azide–alkyne cycloaddition (CuAAC) to attach the pNDI-chain (Scheme 1d). It should be noted, that the former polymer-analogous reactions required potassium iodide to facilitate efficient etherification *via* benzyl halide.[32] The covalent linkage of the donor dyad was confirmed by ^{1}H NMR spectroscopy *via* the characteristic benzylic protons at the linkage position (Fig. S10, ESI†). Size-exclusion chromatography (SEC) monitored by UV/vis further corroborates the covalent linkage, as shown by the characteristic polymer and Ru^{II} signatures at the same elution time (Fig. S20, ESI†).[32] Next, the silyl group was quantitatively cleaved by TBAF to release the free alkyne group, which served for the final CuAAC reaction with the azide-decorated pNDI-chain. The course of the reaction was easily monitored by UV/vis SEC and continued until no further conversion was observed. Notably, prolonged heating at elevated temperatures (80 °C) was necessary to obtain D_n–P–A_m applying our previously optimized protocol,[32] which stresses the necessity and utility of this highly efficient coupling strategy for such polymer-analogous reactions.[39,40] The purification was readily achieved by the preparative SEC using Toyopearl beads. Fig. 2a highlights the excellent separation, *i.e.*, the desired triad elutes first as judged by the characteristic absorption of pTARA (300 nm, grey shaded area) and pNDI (360 nm, black line). The ^{1}H NMR spectrum of D_n–P–A_m features the three building blocks (Fig. 2b, bottom), *i.e.*, the typical broad resonances of the aromatic protons of the NDI units (8.3 to 9.0 ppm and 7.0 to 7.5 ppm) and of the TARA units (6.3 to 7.0 ppm), as well as the minor signals arising from the single ruthenium unit (7.5 to 8.3 ppm). All attempts to obtain reliable mass spectrometry data failed, which is attributed to the challenges to record mass spectra of block copolymers, particularly in case of the cationic charge of the Ru^{II} fragment.

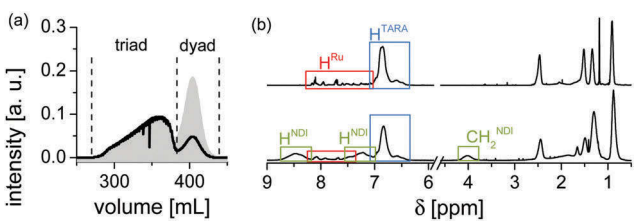

Fig. 2 (a) SEC elugram of the final separation using with UV monitoring typical for pNDI (360 nm, black curve) and for pTARA (300 nm, grey shaded area). (b) ^{1}H NMR spectra (600 MHz, CD_2Cl_2) of the dyad (top) and triad (bottom) with assigned characteristic protons. See Scheme 1 for corresponding molecular representations of the dyad and the triad.

Optical and electrochemical properties

In the following paragraph, the essential photophysical and electrochemical properties of the triad and related reference systems (Fig. 4) will be presented. The absorption spectrum of the triad resembles those of the individual components (Fig. 3), *i.e.*, identical maxima as pTARA (310 nm, blue-shaded), pNDI (360 and 386 nm, green-shaded), and the central $[Ru(dqp)_2]^{2+}$ unit (500 nm) as detailed previously,[31] indicating that no major perturbations in electronic character are introduced by linking of the triad. Hence the subsystems P, D_n–P and P–A_m (Fig. 4a–c) are ideal reference systems for thermodynamic and kinetic analysis. The steady state emission spectrum of P displays the typical ^{3}MLCT-based emission around 700 nm,[38] whereas both reference dyads D_n–P and P–A_m feature a second component (<650 nm) that has been previously assigned to polymer-based emission.[31,32] The donor dyad D_n–P shows a slightly lowered ^{3}MLCT emission intensity than P, which is reasonable in view of the unfavorable energetics for reductive quenching by the pTARA.[31] In contrast, the triad displays almost quantitative Ru emission quenching (96%), as detailed for the P–A_m dyad,[31] which indicates similar electron transfer to the pNDI fragment for D_n–P–A_m (*vide infra*). In line with steady state emission data, the electrochemical data are consistent with the postulated quenching pathways for the triad. The driving forces for

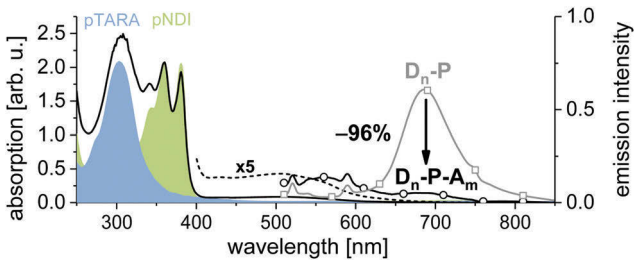

Fig. 3 Absorption spectra of the polymeric building blocks pTARA (blue-shaded area) and pNDI (green-shaded area) and the triad (black curve). Note the amplified signal (×5, dashed line) to illustrate the weak absorption band of the single Ru photosensitizer unit (400–600 nm). Steady-state emission spectra of the precursor dyad (grey line, rectangles) and the triad (black line, circles). Note polymer-based emission (<650 nm) and the ^{3}MLCT emission (around 700 nm), the latter revealing strong quenching (−96%) between dyad (D_n–P) and triad after subtracting residual polymer-based emission.

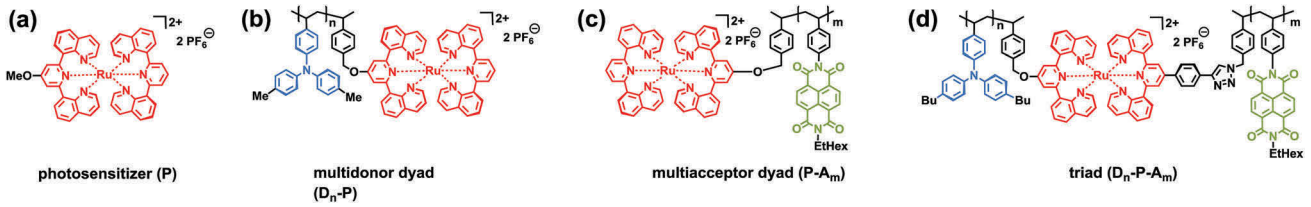

Fig. 4 Molecular representation of the triad including reference subsystems investigated by time-resolved spectroscopy: (a) photosensitizer core (P), (b) multidonor–photosensitizer dyad (D_n–P), (c) photosensitizer–multiacceptor dyad (P–A_m), and (d) multidonor–photosensitizer–multiacceptor triad (D_n–P–A_m). See ref. 31 and 37 for syntheses and steady state properties.

electron transfer can be estimated from the formal excited state potential of the photosensitizer with respect to the redox potential of the polymers. The calculated driving forces suggest primary oxidative quenching (ΔG = −0.25 eV) with secondary electron transfer to regenerate the photosensitizer (−0.25 eV), whereas the reductive quenching pathway is unfavorable (+0.20 eV) as detailed previously.[31] Next, the spectroelectrochemical features of the redox-active subunits will be briefly recalled (Fig. S23, ESI†),[31,41] which are essential for the interpretation of the transient absorption data. The oxidized donor ($pTARA^+$) exhibits a strong absorption around 690 nm, and the reduced acceptor ($pNDI^-$) displays characteristic maxima at 475 and 610 nm. The oxidized photosensitizer (Ru^{III}) features a decrease of the ^{1}MLCT band (around 500 nm) and broad absorptions above 700 nm.

The time-resolved emission and transient absorption measurements (Fig. 5) were performed to investigate the light–induced events of the triad in detail, including the reference systems shown in Fig. 4. The observed emission lifetime of P (760 ns in DCM) is considerably shorter than that reported in MeCN (3000 ns),[38] in line with the solvent effects leading to an analogously decreased lifetime of $[Ru(bpy)_3]^{2+}$ (bpy is 2,2′-bipyridine).[42] The D_n–P dyad reveals a slightly shorter emission lifetime (660 ns) (Fig. S24, ESI†), in agreement with the steady state emission data. An additional short-lived component on the time-scale of the excitation pulse (*ca.* 10 ns) is observed in the dyad, which is absent in the case of the pristine photosensitizer unit. This distinct feature is assigned to polymer-based emission (*vide infra*), which stretched out to the ^{3}MLCT region as confirmed by the steady state emission data. A similarly short-lived emission (<10 ns) is detected for the P–A_m dyad (Fig. S24d, ESI†), but without any detectable long-lived ^{3}MLCT emission. These findings parallel our previous time-correlated single photon counting (TCSPC) data that showed efficient ^{3}MLCT emission quenching within 10 ns (90%).[31] In order to clarify the contribution by polymer-based emission (<650 nm) for the D_n–P–A_m triad, time-correlated single photon counting (TCSPC) measurements were performed using suitable filters for the polymer-based region (band pass, 450–650 nm) and the ^{3}MLCT region (long pass, >715 nm, Fig. S26, ESI†). Although the polymer-based emission is reasonably well described by a mono-exponential decay (τ = 3 ns, Fig. S27, ESI†), adding a second decay component improved the fit (Table S1, ESI†). Likewise, the fit of the ^{3}MLCT region requires a second more long-lived component (49 ns, 22%). This finding parallels the observed multiexponential emission decay in a Ru-NDI dyad with flexible linkage, assigned to several conformers with different mutual distances and orientations and, thus, electron transfer rates.[43] A similar scenario is conceivable for the unsaturated polymer backbone, which gives rise to an even more complicate ensemble of geometries.[44] A Stern–Vollmer analysis using the donor D_n–P subunit and unbound NDI-based acceptors revealed the diffusional quenching pathway (Fig. S28, ESI†) and, thus, further corroborates the successful linkage of the covalent D_n–P–A_m triad.

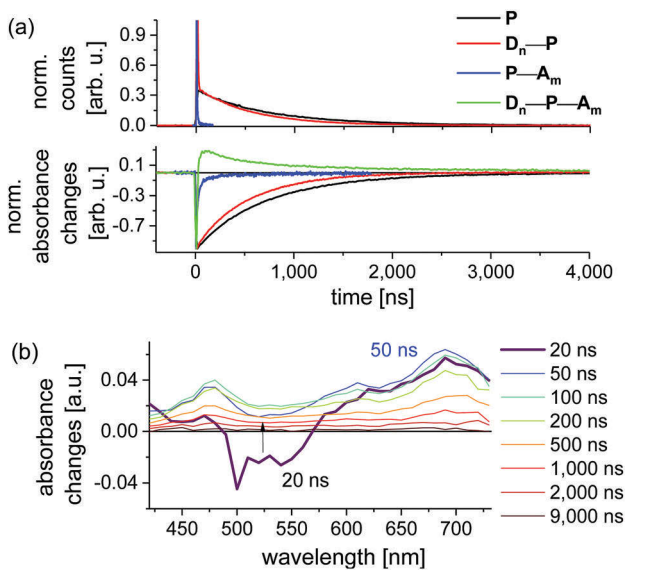

Fig. 5 (a) Time-resolved emission (top) and transient absorption traces (bottom) in de-aerated DCM upon excitation at 532 nm (except for D_n–P–A_m at 500 nm). Emission recorded at 700 nm (except P–A_m at 690 nm), all transient absorption traces taken at 500 nm. Note the biexponential decay in the case of D_n–P–A_m with time constants of 430 and 2400 ns (see Fig. S32, ESI†). (b) TA data showing the rapid formation of a charge-separated state and slow subsequent recombination. Note the fast ^{1}MLCT recovery, as well as the positive TA signatures of $pNDI^-$ (475 and 610 nm) and $pTARA^+$ (690 nm) in accordance with the spectroelectrochemical data (Fig. S23, ESI†).

Transient absorption (TA) spectra were recorded between 400 and 730 nm (Fig. 5 and Fig. S29–S32, ESI†) to identify and follow the (intermediate) states by virtue of their spectroelectrochemical signatures. Upon excitation, the reference complex (P) shows the typical ^{1}MLCT bleach and ^{3}MLCT absorptions at longer wavelengths, which are partially overlapped by stimulated emission (Fig. S29, ESI†). The spectral decay is characterized by several isosbestic points and follows mono-exponential kinetics (730 ns), which is in satisfying agreement with the emission lifetime. The TA data of the D_n–P dyad shows a generally similar

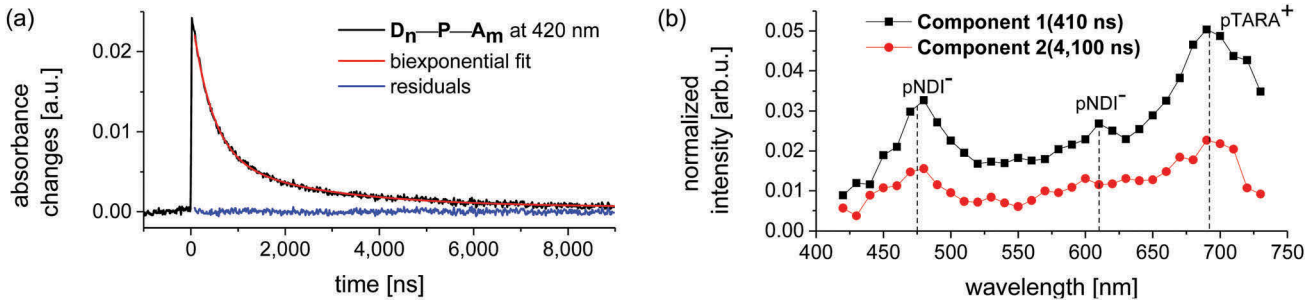

Fig. 6 Transient absorption data of D_n–P–A_m: (a) spectral recovery at 420 nm with biexponential fit. (b) Spectral signatures derived from global analysis (>100 ns) applying biexponential kinetics. Dashed lines visualize typical absorptions of the reduced pNDI (475 and 610 nm) and oxidized pTARA (690 nm). Note the similar spectral signatures of component 1 (black curve) and 2 (red curve) indicative for the fully charge separated state D_n^+–P–A_m^-.

behavior (Fig. S30, ESI†), except for an unusually strong negative TA contribution at short time scales (<20 ns) and higher wavelengths (>550 nm, Fig. S30b, ESI†). In comparison to P, the isosbestic point at 435 nm is preserved, while the ones at 575 or 655 nm are absent. The TA recovery of D_n–P was followed at 470 nm and is best described by a mono-exponential decay (530 ns), although including a second component enhances the fit at early times (Fig. S30, ESI†). Hence, a biexponential global fit of the TA data was performed to verify this hypothesis. The spectral profile of the long-lived component (520 ns) matches perfectly that of pristine P, including the identical isosbestic points, while the spectrum of the short-lived component (6 ns) resembles that of the polymer-based emission. A similar short-lived polymer-based TA feature was also found for P–A_m (Fig. S31, ESI†). In contrast, the long-lived ^{3}MLCT-based TA signal is absent, in line with our previous study that revealed fast initial charge separation (<1.6 ns).[31] In fact, a weak NDI^- signature was observed on the time scale of the excitation pulse (Fig. S31b, ESI†). As judged from absent build-up of the corresponding TA signatures, the charge recombination seems faster than charge separation, so that the TA recovery is completed within 100 ns (Fig. 5a).[31] In marked contrast, the D_n–P–A_m triad shows the immediate formation of the fully charge separated (CS) state, as identified by the concomitant ^{1}MLCT recovery and the evolving positive TA signatures of $pNDI^-$ and $pTARA^+$ (Fig. 5b). More importantly, the TA signal decays orders of magnitude slower than in the reference dyad, following multiexponential kinetics (Fig. S32, ESI†). The associated lifetimes of a biexponential fit are 430 ns (71%) and 2400 ns (29%). Performing the global fit of the 2D TA data revealed identical spectral profiles of the two components, which are characteristic for the fully charge separated state (Fig. 6). Notably, the charge separation persists even longer than observed for $[Ru(dqp)_2]^{2+}$-based related molecular triads (140–200 ns).[45] A further assignment, *e.g.*, as reported for an extremely long-lived molecular tetrades with distinct spectroscopic signatures,[17] is precluded due to the invariant spectral signatures of the repeating units. In addition, the ensemble of conformations is also unknown (*vide supra*) but can be estimated from extensive molecular modelling in analogy to the polymer-based light harvesting and electron transfer studies as reported by Papanikolas *et al.*[7,46] In general, the back-folding of the flexible polymer chain leads to shorter formal electron transfer distances than the one set by the sensitizer and the first repeat unit along the attached chain. Hence, multiple electron transfer pathways can exist explaining the observed multiexponential emission decay. Notably, the emission decay within a few nanoseconds confirms efficient charge separation, while the timescale of recombination is two orders of magnitude longer. The multi-exponential character of the emission and recombination indicates multiple pathways, which are practically indistinguishable due to the identical signatures of the repeating units, yet long-lived charge separation is observed within the polymer assembly. Although such spectroscopic properties seem unfavorable in terms of a full spectroscopic analysis, the simple modular preparation and the resemblance of organic semiconductors may open promising routes to tune subsequent charge transport.[36]

Conclusions

An efficient divergent modular synthesis was established to prepare a multidonor–photosensitizer–multiacceptor triad (D_n–P–A_m), *i.e.*, only five linear synthetic steps from commercially available materials and facile purification. The functional building blocks were selected according to their photophysical and electrochemical properties (P, D_n, and A_m), and were connected in a modular fashion. After selective excitation of the photosensitizer in the visible light region, quantitative charge separation was observed. Detailed steady state and time-resolved spectroscopy of the triad and the related subsystems confirmed long-lived charge separation, despite the unsaturated flexible linkage pattern among the units that is usually avoided in model systems. Multiexponential decay was observed, in line with the conformational freedom and ensemble of electron transfer pathways. Nevertheless, the advantages and the future perspective to utilize such triad assembly originate from the synthetic advance in polymer chemistry,[47] *e.g.*, to assure an internal redox-cascade by block-copolymer,[41] to incorporate phase-forming substituents[48] to achieve self-organization for energy conversion,[35] to embed conjugated organic semiconductors,[49] and/or to provide local redox gradients to power molecular machines.

Conflicts of interest

There are no conflicts to declare.

Acknowledgements

Financial support by the Carl-Zeiss-Foundation, the Friedrich Schiller University Jena ("Nachwuchsförderung") and the Thüringer Ministerium für Wirtschaft, Wissenschaft und Digitale Gesellschaft (TMWWDG), and the Swedish Research Council (grant no. 2012-3926) is kindly acknowledged. The authors thank Annett Urbanek for MALDI-ToF measurements as well as Dr Peter Bellstedt and the NMR platform of the IAAC/IOMC for help with the NMR measurements.

References

1 V. Balzani, G. Bergamini and P. Ceroni, *Angew. Chem., Int. Ed.*, 2015, **54**, 11320–11337.
2 J. H. Alstrum-Acevedo, M. K. Brennaman and T. J. Meyer, *Inorg. Chem.*, 2005, **44**, 6802–6827.
3 J. J. Concepcion, R. L. House, J. M. Papanikolas and T. J. Meyer, *Proc. Natl. Acad. Sci. U. S. A.*, 2012, **109**, 15560–15564.
4 L. Hammarström, *Acc. Chem. Res.*, 2015, **48**, 840–850.
5 V. Balzani, A. Credi and M. Venturi, *ChemSuSchem*, 2008, **1**, 26–58.
6 V. Balzani, L. Moggi, M. F. Manfrin, F. Bolletta and M. Gleria, *Science*, 1975, **189**, 852–856.
7 Z. A. Morseth, T. V. Pho, A. T. Gilligan, R. J. Dillon, K. S. Schanze, J. R. Reynolds and J. M. Papanikolas, *J. Phys. Chem. B*, 2016, **120**, 7937–7948.
8 N. S. Hush, *Coord. Chem. Rev.*, 1985, **64**, 135–157.
9 B. Albinsson and J. Martensson, *J. Photochem. Photobiol., C*, 2008, **9**, 138–155.
10 O. S. Wenger, *Coord. Chem. Rev.*, 2009, **253**, 1439–1457.
11 M. Natali, S. Campagna and F. Scandola, *Chem. Soc. Rev.*, 2014, **43**, 4005–4018.
12 S. Campagna, F. Puntoriero, F. Nastasi, G. Bergamini and V. Balzani, in *Photochemistry and Photophysics of Coordination Compounds I*, ed. V. Balzani and S. Campagna, Springer-Verlag Berlin, Berlin, 2007, vol. 280, pp. 117–214.
13 A. Juris, V. Balzani, F. Barigelletti, S. Campagna, P. Belser and A. von Zelewsky, *Coord. Chem. Rev.*, 1988, **84**, 85–277.
14 D. W. Thompson, A. Ito and T. J. Meyer, *Pure Appl. Chem.*, 2013, **85**, 1257–1305.
15 L. Hammarström and O. Johansson, *Coord. Chem. Rev.*, 2010, **254**, 2546–2559.
16 M. Abrahamsson, M. Jäger, R. J. Kumar, T. Österman, P. Persson, H.-C. Becker, O. Johansson and L. Hammarström, *J. Am. Chem. Soc.*, 2008, **130**, 15533–15542.
17 H. Imahori, D. M. Guldi, K. Tamaki, Y. Yoshida, C. P. Luo, Y. Sakata and S. Fukuzumi, *J. Am. Chem. Soc.*, 2001, **123**, 6617–6628.
18 J. Hankache and O. S. Wenger, *Chem. Commun.*, 2011, **47**, 10145–10147.
19 M. H. V. Huynh, D. M. Dattelbaum and T. J. Meyer, *Coord. Chem. Rev.*, 2005, **249**, 457–483.
20 J. Hankache, M. Niemi, H. Lemmetyinen and O. S. Wenger, *Inorg. Chem.*, 2012, **51**, 6333–6344.
21 Z. A. Morseth, L. Wang, E. Puodziukynaite, G. Leem, A. T. Gilligan, T. J. Meyer, K. S. Schanze, J. R. Reynolds and J. M. Papanikolas, *Acc. Chem. Res.*, 2015, **48**, 818–827.
22 D. M. Ryan, M. K. Coggins, J. J. Concepcion, D. L. Ashford, Z. Fang, L. Alibabaei, D. Ma, T. J. Meyer and M. L. Waters, *Inorg. Chem.*, 2014, **53**, 8120–8128.
23 S. E. Bettis, D. M. Ryan, M. K. Gish, L. Alibabaei, T. J. Meyer, M. L. Waters and J. M. Papanikolas, *J. Phys. Chem. C*, 2014, **118**, 6029–6037.
24 D. Ma, S. E. Bettis, K. Hanson, M. Minakova, L. Alibabaei, W. Fondrie, D. M. Ryan, G. A. Papoian, T. J. Meyer, M. L. Waters and J. M. Papanikolas, *J. Am. Chem. Soc.*, 2013, **135**, 5250–5253.
25 G. Leem, S. Keinan, J. Jiang, Z. Chen, T. Pho, Z. A. Morseth, Z. Hu, E. Puodziukynaite, Z. Fang, J. M. Papanikolas, J. R. Reynolds and K. S. Schanze, *Polym. Chem.*, 2015, **6**, 8184–8193.
26 Z. Fang, A. Ito, S. Keinan, Z. Chen, Z. Watson, J. Rochette, Y. Kanai, D. Taylor, K. S. Schanze and T. J. Meyer, *Inorg. Chem.*, 2013, **52**, 8511–8520.
27 Z. Fang, A. Ito, H. Luo, D. L. Ashford, J. J. Concepcion, L. Alibabaei and T. J. Meyer, *Dalton Trans.*, 2015, **44**, 8640–8648.
28 L. Wang, E. Puodziukynaite, E. M. Grumstrup, A. C. Brown, S. Keinan, K. S. Schanze, J. R. Reynolds and J. M. Papanikolas, *J. Phys. Chem. Lett.*, 2013, **4**, 2269–2273.
29 G. Leem, Z. A. Morseth, E. Puodziukynaite, J. Jiang, Z. Fang, A. T. Gilligan, J. R. Reynolds, J. M. Papanikolas and K. S. Schanze, *J. Phys. Chem. C*, 2014, **118**, 28535–28541.
30 E. Puodziukynaite, L. Wang, K. S. Schanze, J. M. Papanikolas and J. R. Reynolds, *Polym. Chem.*, 2014, **5**, 2363–2369.
31 J. Kübel, R. Schroot, M. Wächtler, U. S. Schubert, B. Dietzek and M. Jäger, *J. Phys. Chem. C*, 2015, **119**, 4742–4751.
32 R. Schroot, T. Schlotthauer, U. S. Schubert and M. Jäger, *Macromolecules*, 2016, **49**, 2112–2123.
33 B. E. Hardin, H. J. Snaith and M. D. McGehee, *Nat. Photonics*, 2012, **6**, 162–169.
34 A. L. Sisson, N. Sakai, N. Banerji, A. Furstenberg, E. Vauthey and S. Matile, *Angew. Chem., Int. Ed.*, 2008, **47**, 3727–3729.
35 O. Yushchenko, D. Villamaina, N. Sakai, S. Matile and E. Vauthey, *J. Phys. Chem. C*, 2015, **119**, 14999–15008.
36 H. Baessler and A. Koehler, *Topics in Current Chemsitry*, Springer Verlag, Berlin Heidelberg, 2012, vol. 312, pp. 1–66.
37 R. Schroot, C. Friebe, E. Altuntas, S. Crotty, M. Jäger and U. S. Schubert, *Macromolecules*, 2013, **46**, 2039–2048.
38 M. Jäger, R. J. Kumar, H. Görls, J. Bergquist and O. Johansson, *Inorg. Chem.*, 2009, **48**, 3228–3238.
39 U. Mansfeld, C. Pietsch, R. Hoogenboom, C. R. Becer and U. S. Schubert, *Polym. Chem.*, 2010, **1**, 1560–1598.
40 C.-H. Wong and S. C. Zimmerman, *Chem. Commun.*, 2013, **49**, 1679–1695.
41 R. Schroot, U. S. Schubert and M. Jäger, *Macromolecules*, 2015, **48**, 1963–1971.
42 J. V. Caspar and T. J. Meyer, *J. Am. Chem. Soc.*, 1983, **105**, 5583–5590.
43 D. W. Dixon, N. B. Thornton, V. Steullet and T. Netzel, *Inorg. Chem.*, 1999, **38**, 5526–5534.

44 Adding a third component further improved the fit (see Table S1 (ESI†) for comparison).
45 R. J. Kumar, S. Karlsson, D. Streich, A. R. Jensen, M. Jäger, H.-C. Becker, J. Bergquist, O. Johansson and L. Hammarström, *Chem. – Eur. J.*, 2010, **16**, 2830–2842.
46 C. N. Fleming, K. A. Maxwell, J. M. DeSimone, T. J. Meyer and J. M. Papanikolas, *J. Am. Chem. Soc.*, 2001, **123**, 10336–10347.
47 R. Schroot, M. Jäger and U. S. Schubert, *Chem. Soc. Rev.*, 2017, **46**, 2754–2798.
48 R. Schroot, T. Schlotthauer, M. Jäger and U. S. Schubert, *Macromol. Chem. Phys.*, 2017, **218**, DOI: 10.1002/macp.201600534.
49 R. Schroot, T. Schlotthauer, B. Dietzek, M. Jäger and U. S. Schubert, *Chem. – Eur. J.*, 2017, DOI: 10.1002/chem.201704180.

